Organised by:

THE HONG KONG INSTITUTION OF ENGINEERS 香港工程師學會
Geotechnical Division 岩土分部

Supporting Organisations:

HKGES HONG KONG GEOTECHNICAL SOCIETY 香港岩土工程學會
A Member Society of International Society for Soil Mechanics and Geotechnical Engineering
Since 2003

THE HONG KONG INSTITUTION OF ENGINEERS 香港工程師學會
Civil Division 土木分部

THE HONG KONG INSTITUTION OF ENGINEERS 香港工程師學會
Structural Division 結構分部

THE HONG KONG INSTITUTION OF ENGINEERS 香港工程師學會
Environmental Division 環境分部

The HKIE Geotechnical Division 43rd Annual Seminar 2023

Towards a Smart Green-Resilient Geo-Future for World-class City Development

AECOM

Delivering a better world

At AECOM, we envision a world where infrastructure creates opportunity for everyone. By harnessing the power of digital technology and innovation, and connecting our technical experts around the world, we deliver tailored sustainable solutions and transformative outcomes for our clients, communities and planet.

AECOM is ranked No. 1 by *Fortune* magazine's list of the World's Most Admired Companies in its industry for a third year in 2023.

aecom.com

C M WONG & ASSOCIATES LTD
黃志明建築工程師有限公司

11/F Universal Trade Centre
3-5A Arbuthnot Road, Hong Kong
Tel: (852)2522-1068
Fax: (852)2526-3111
www.cmwal.com
cmwal@cmwal.com

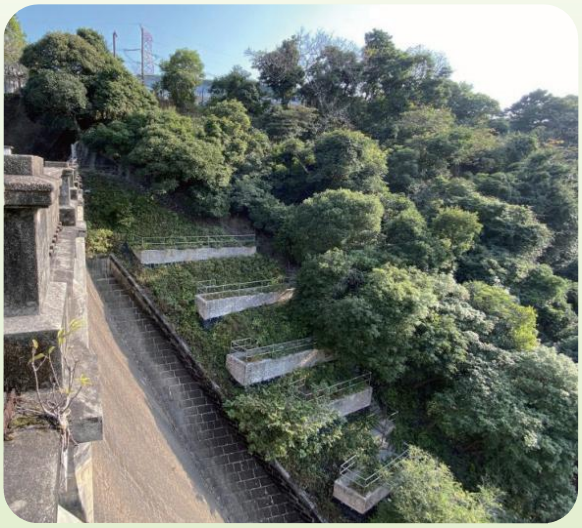

C M Wong & Associates Ltd is a Hong Kong based consulting engineer in providing a full range of professional services including feasibility studies, planning, design and supervision in relation to building and infrastructure projects. Our clients include various Hong Kong Government departments, institutions and major developers.

We adopt a flexible approach to suit clients' needs. We are also renowned for providing innovative engineering solutions for challenging projects especially for those with difficult ground conditions.

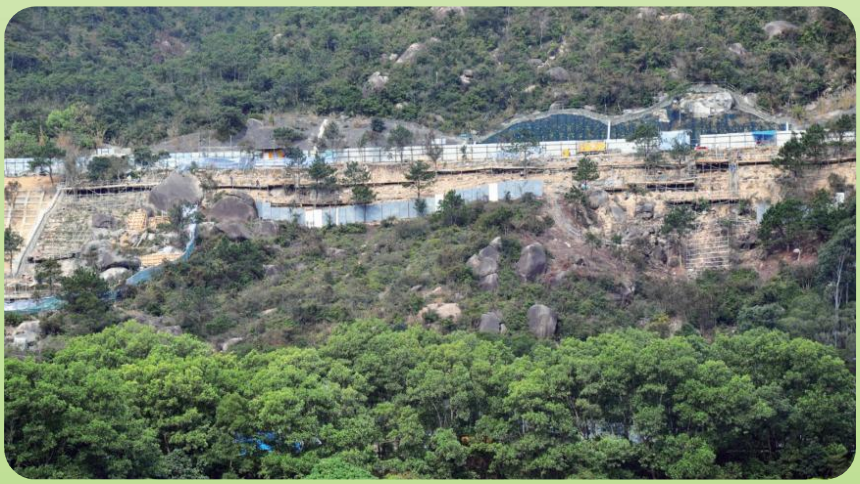

ISO 9001 : 2015
Certificate No.: CC 801

ISO 14001 : 2015
Certificate No.: CC 5408

ISO 45001 : 2018
Certificate No.: CC 7033

ARUP

Shaping a digitally enabled sustainable future

Combining our domain knowledge with advanced technology, Arup is taking a digital-based approach to develop geotechnical designs that enable sustainable, strategic infrastructure and building projects, shaping a greener, smarter and more resilient Hong Kong.

Image

Residential Development at STTL609, To Shek, Shatin

www.arup.com

asia infrastructure solutions

DELIVERING THE FUTURE

Asia Infrastructure Solutions (AIS) is a leader in delivering sustainable design, engineering, project & programme management, cost management, business advisory and consultancy solutions for the infrastructure, buildings and environmental markets.

AIS is established by Global Infrastructure Solutions Inc. (GISI) and its founding members who bring over 90 years of project experience in Asia. Operating in more than 90 countries, the company employs over 12,500 people globally and serves the clients through three platforms: Construction Services, Engineering and Consulting Services, and Global Impact and Sustainability Services,. We have a strong and diversified team and with a long track record in the infrastructure, building and environmental markets delivering the future for the built and natural environment. We inherited our professional and technical expertise and capabilities from the Arcadis Design & Engineering / Hyder Consulting / Acer Consultants / Freeman Fox in Hong Kong.

AIS shapes our growing communities by offering our global ground and underground engineering expertise with diversified knowledge in reclamation, road, tunnel, rail and other civil engineering projects. We also have been appointed as the Independent Design Checkers for complex, multi-discipline infrastructure works in Hong Kong. Our specialist skills are exhibited through our global and local projects such as Singapore Deep Tunnel Sewerage System, Trunk Road T2 and Cha Kwo Ling Tunnel, Hopewell Centre Development, Site Formation and Infrastructure Works for Housing Developments at Pok Fu Lam, Integrated Waste Management Facilities, and Relocation of Diamond Hill Fresh Water and Salt Water Service Reservoirs to Caverns. Our involvement covers all stages of project delivery from investigation and study, through conceptual phase and detailed design phase, to supervising the construction of the projects whilst deploying the latest digital tools managing geotechnical risks for clients.

Connect with us : +852 3619 9400 info-hk@asiainfrasolutions.com www.asiainfrasolutions.com

Engineering a better *future*

Aurecon is a design, engineering and advisory company.
We live our purpose of bringing ideas to life by imagining and co-creating with our clients a better future for people and the planet. We bring vital engineering experience, technical capability, and design expertise to our projects.

- Central Kowloon Route – Central Tunnel
- Tseung Kwan O - Lam Tin Tunnel
- Lok Ma Chau Loop Site Formation
- Anderson Road Quarry Site Formation
- Liantang Lung Shan Tunnel
- AAHK APM and BHS Tunnel
- AAHK North Runway Modification
- MTR Hung Shui Kiu Station
- MTR Tsim Sha Tsui Station Entrance A1

aurecongroup.com

aurecon
Bringing ideas to life

中国地质工程集团有限公司
CHINA GEO-ENGINEERING CORPORATION

我們的主要業務包括：
Our Business includes:

- 基礎工程
  Foundation Works
- 斜坡及擋土牆長遠防治山泥傾瀉工程
  Construction of Landslip Preventive and Mitigation Works to Slopes and Retaining Walls
- 道路及渠務工程
  Roads and Drainage
- 水務工程
  Waterworks
- 地盤平整工程
  Site Formation

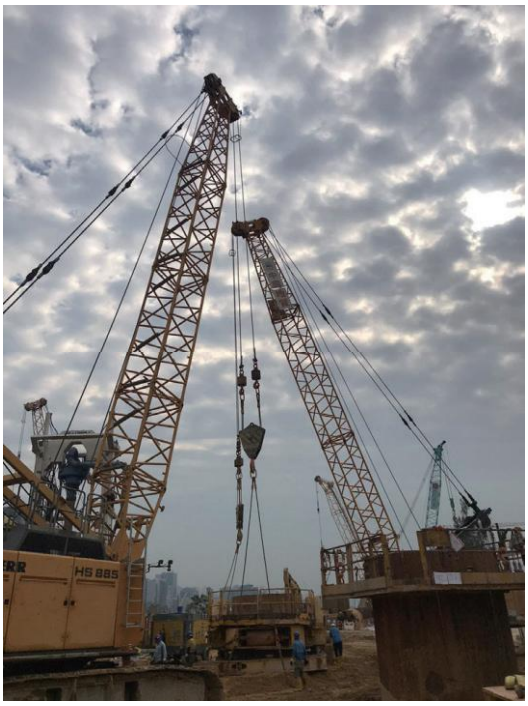

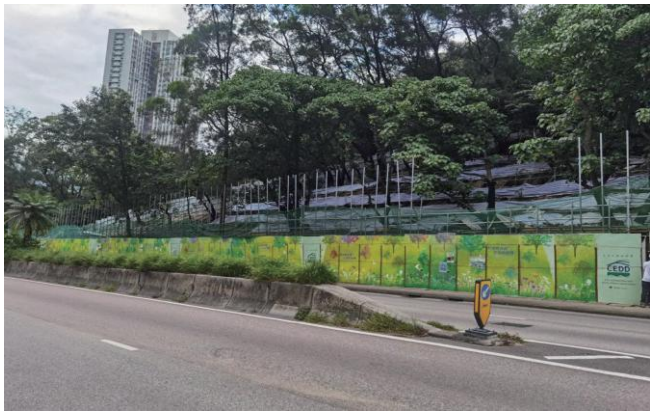

香港灣仔港灣道 30 號新鴻基中心 24 樓 2421－25 室
Rm. 2421-25, 24/F., Sun Hung Kai Centre, 30 Harbour Road, Wanchai, Hong Kong
TEL : (852) 2511 9001 FAX : (852) 2580 0697

FUGRO

UNLOCKING **INSIGHTS** FROM **GEO-DATA** FOR A **SAFE** AND **LIVEABLE** WORLD

For more information visit
fugro.com

Fraser Construction Co., Ltd.
科正建築有限公司

Slope Stabilization / Site Formation / Piling

Specialist Contractor

Address: Rm 1122, 11/F, Pacific Link Tower (South Mark),
11 Yip Hing Street, Wong Chuk Hang,
Hong Kong

Website: www.fraserconstruction.com.hk

Email: info@fraserconstruction.com.hk

Tel: 2770 0122 **Fax: 2580 0470**

Gammon

安全
SAFETY

卓越
EXCELLENCE

誠信
INTEGRITY

Gammon Construction is a leading construction and engineering services group committed to finding innovative solutions for our customers. Headquartered in Hong Kong for over 65 years, we have built a distinguished reputation for delivering high quality and complex projects throughout Hong Kong, Mainland China and Southeast Asia. We are fully committed to building for a better quality of life and living environment in a safe and sustainable manner.

www.gammonconstruction.com

G & E ENGINEERING
Since 1984

Sustainable development, carbon credit and climate change mitigation encompassing innovation and technology have been widely implemented. What is lacking awareness is perhaps the contribution of geosynthetic towards these goals. A great many research have shown 25 - 90% reduction in carbon emission on construction designed with geosynthetic. Geogrid reinforced fill consumes less timber, concrete and steel, geomembrane and geosynthetic clay liner replace quarry clay, geotextile and geocomposite reduce use of granular material. Transportation fuel becomes less demanding, natural resources are better preserved and water loss are controlled. Talk to us on applications and merits.

Concrete Canvas – Slope Work
Kardoorie Farm, March 2020

Flexible Barrier – Shum Wat Natural Terrain Lantau, May 2018

HDPE geomembrane – Landfill Gas Barrier
TKO Development, December 2019

Geocomposite – Retaining Wall Drainage, Police Facilities
Kong Nga Po, March 2021

Geogrid - Reinforced Fill Slope
HKZMB, October 2017

Reinforcement Geosynthetic Geotextile –
3rd Runway Concourse, January 2022

G & E ENGINEERING Since 1984

G and E Company Limited
14/F, Kiu Yin Commercial Building,
361-363 Lockhart Road, Wanchai, Hong Kong
Tel: 2570 0103 Fax: 2570 0089
e-mail: info@g-and-e.com www.g-and-e.com

igs

ISO 9001 : 2015 UKAS MANAGEMENT SYSTEMS 0273

VSL INTRAFOR

INTRAFOR, YOUR GROUND ENGINEERING SPECIALIST

TUEN MUN - CHEK LAP KOK LINK

Intrafor is a specialized contractor in foundation engineering, retaining structures, ground improvement, horizontal directional drilling and coring. We provide turnkey solutions for geotechnical challenges across the entire construction spectrum. We have contributed to the most complex and ambitious projects in the world. Are you based in Hong Kong? We'd love to know more about your project! Please get in touch with us to discuss your needs.

Intrafor Hong Kong Ltd
20/F Eight Commercial Tower • 8 Sun Yip Street, Chai Wan, Hong Kong
Tel. 2590 2288 • www.intrafor.com

盼記建設有限公司
Pan Kee Construction Limited



PAN KEE CONSTRUCTION LIMITED (盼記建設有限公司), as a construction company main business engaged on slope improvement works in Hong Kong, was established in 2013. Our goal is to develop a safer environment for living with professions and sincere.

License

Relevant Government departments or public organizations	Registration and qualification	Category
Buildings Department	Registered Specialist Contractor	Site Formation Category
Construction Industry Council	Registered Subcontractor	General civil works with specialty in geotechnical works
Bureau	Approved Suppliers of Materials and Specialist Contractors for Public Works	Landslip Preventive/Remedial Works to Slopes/Retaining Walls

Nature	Certification
Quality Management System	ISO 9001:2015
Environmental Management System	ISO14001:2015
Occupational Health and Safety Management System	ISO45001:2018

We have the following current contracts on hand

8/LANDS/21	Upgrading/Improvement Works to Lands Department Slopes in the Southern Region
HKHA Contract No. 20219053	Term Contract for Slope Maintenance & Improvement Works for Region C (2022 – 2025)
GE/2020/10	Landslip Prevention and Mitigation Programme, 2017, Package F, Landslip Prevention and Mitigation Works

Contact

Tel 2818 6811
Fax 2818 6899
Email info@pankee.com.hk

Unit 7, 3/F., Block 2, Tak Fung Industrial Centre, No. 168, Texaco Road, Tsuen Wan, N.T
Tel: 2818 6811 Fax: 2818 6899

ISO 9001:2015 Certificate No:Q1948
ISO 14001:2015 Certificate No:E1115
ISO 45001:2018 Certificate No:S961

MTR

caring for life's journeys

VIBRO 惠保

新創建集團成員
Member of NWS Holdings

COMMITTED
PROFESSIONAL
UNITED

New Acute Hospital at Kai Tak Development Area

Road Improvement Works in West Kowloon Reclamation Development

WWW.VIBRO.COM.HK

HONG KONG

INNOVATE
OUR FUTURE

Laying smart groundworks for Hong Kong's sustainable future

Whether it be a smart building or even a resilient city, a strong foundation is vital for whatever that relies on it. Incorporating our innovative digital solutions that scale up the overall efficiency and quality, our geotechnical experts are committed to be the masterminds behind the strong foundations of future-proof infrastructures and buildings, shaping our world-class built environment for the city to thrive.

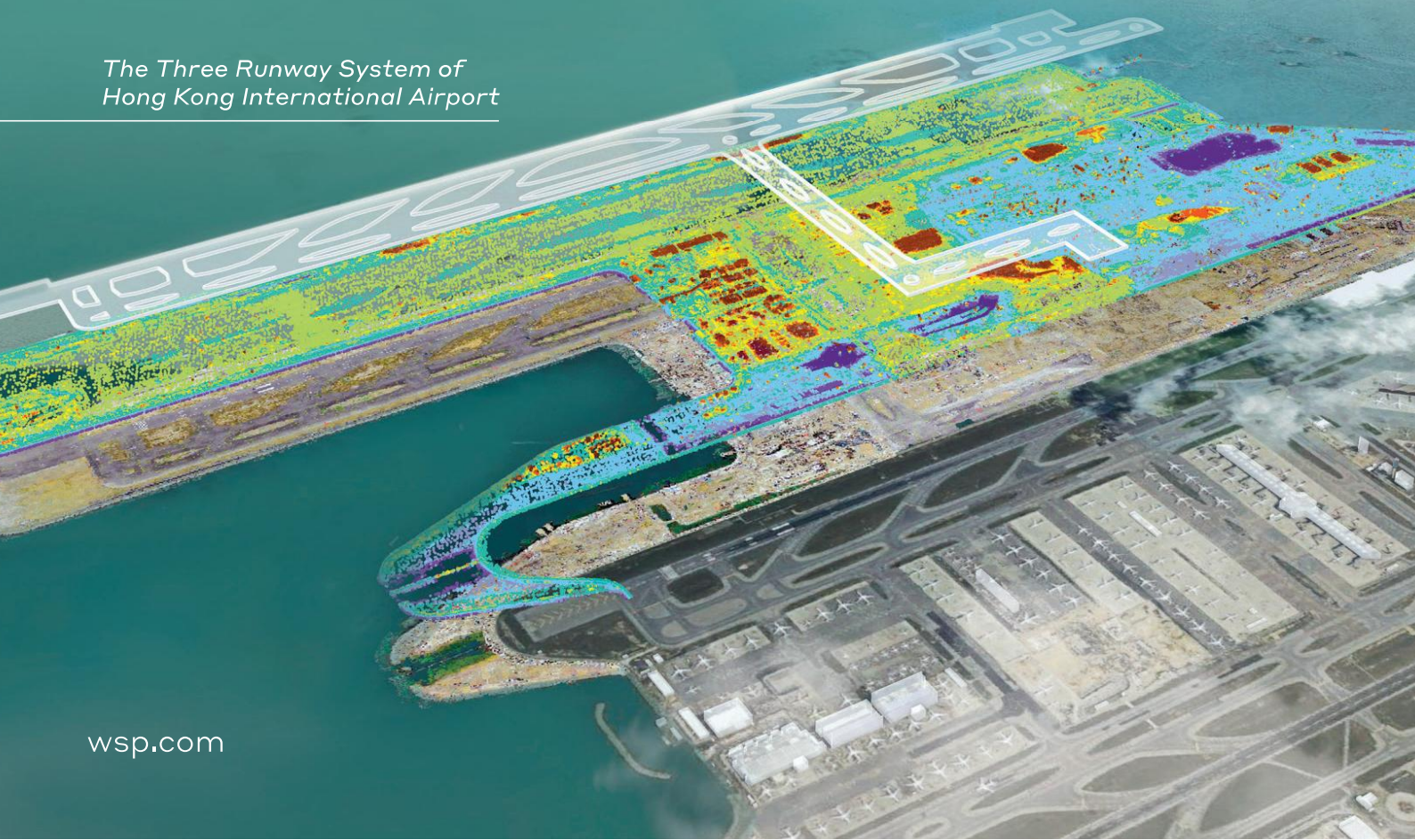

The Three Runway System of Hong Kong International Airport

wsp.com

迪時建築運輸有限公司
Dix Construction & Transportation Ltd.

Congratulations

to

The HKIE Geotechnical Division 43rd Annual Seminar
Towards a Smart-Green-Resilient
Geo-Future for World-class City Development

Government Approved Contractor
Road and Drainage / Site Formation /Landslip Preventive Remedial Works to Slope Retaining Walls category

Address: 22/F., Supreme Commercial Building, 368 King's Road, North Point, H.K.
Tel.: 2426 1877 Fax.: 2426 5777 E-mail: dix@dix.com.hk

ISO 14001 : 2015 Certificate No: CC8446
ISO 9001 : 2015 Certificate No: CC592

UX DEBRIS FLOW BARRIER

BRUGG Geobrugg
Safety is our nature

UX - 160 , 4M HIGH

The debris flow barrier is part of the UX system and it was erected for the first time in Hong Kong in 2015.

Marketing Manager:
Thomas Mok
Tel: 2893 0444
Mobile: 9887 0410
Email: fog@fong-on.com.hk

CE European Technical Approval
www.eota.eu

Creating Value
for Corporate Sustainability
企業長青 創建新價值

www.pyengineering.com

泰昇集團
TYSAN GROUP

泰昇地基工程有限公司
TYSAN FOUNDATION LIMITED

泰昇地基土力工程有限公司
TYSAN FOUNDATION GEOTECHNICAL LIMITED

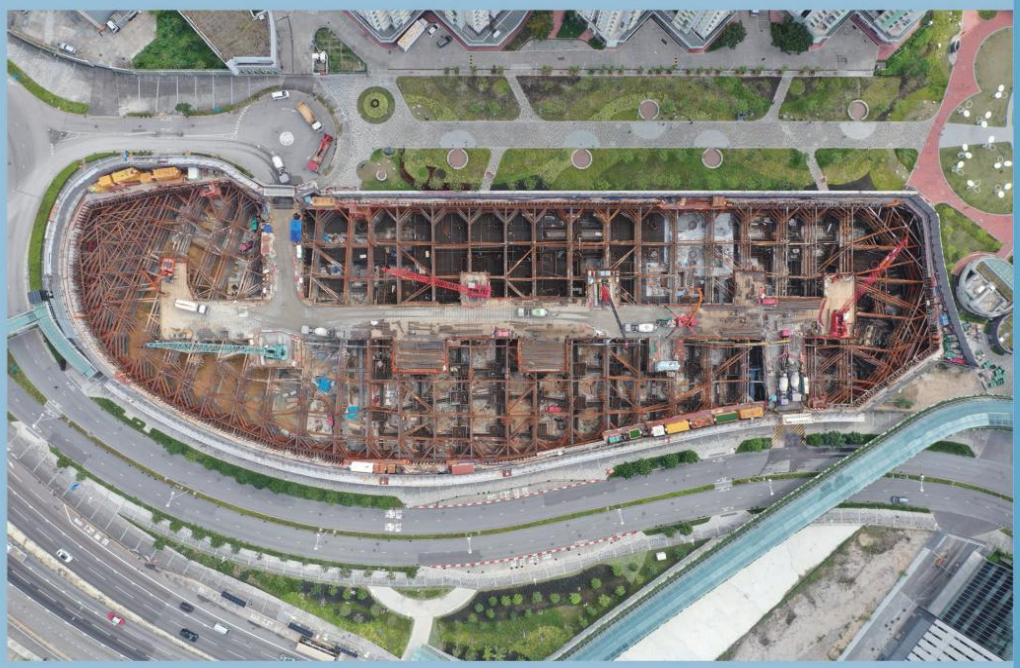

泰昇地基工程有限公司
泰昇地基土力工程有限公司

業務覆蓋香港及澳門，專注地基工程，主要提供設計及建造服務，包括地盤勘察、海陸鑽孔樁／打樁、迷你樁、鑽孔工程、地腳、樁帽及地庫工程、地盤平整、泥釘及斜坡之防護工程。

Tysan Foundation Limited
Tysan Foundation Geotechnical Limited

spcialise in foundation works with businesses covering Hong Kong and Macau area. We provide services on design and construction which include site investigation, land & marine bored/driven piling, mini-piling, preboring work, footing, pile cap & basement construction, site formation, soil nail and slope protection work.

香港黃竹坑香葉道2號
One Island South 20樓
20/F One Island South, 2 Heung Yip Road,
Wong Chuk Hang, Hong Kong.
電話 Tel: (852) 2882 3632
傳真 Fax: (852) 2808 0565
網址 Website: http://www.tysan.com

Proceedings of the 43rd Annual Seminar
Geotechnical Division, The Hong Kong Institution of Engineers

Towards a Smart-Green-Resilient Geo-Future for World-class City Development

19 May 2023
Hong Kong

Organised by:
Geotechnical Division, The Hong Kong Institution of Engineers

Supported by:
The Hong Kong Geotechnical Society
Civil Division, The Hong Kong Institution of Engineers
Environmental Division, The Hong Kong Institution of Engineers
Structural Division, The Hong Kong Institution of Engineers

ORGANISING COMMITTEE

Chairman
Ir Terence Yau

Members
Ir Ray Chan
Ir Dr Tony Chen
Ir Tony Ho
Ir Roy Hung
Ir Joanne Ko
Ir Kenneth Lai
Ir Alvin Lam
Ir Dr S W Lee
Ir Dr Andy Leung
Ir Clifford Phung
Ir Grace Tam
Ir Dr Gavin Toh
Ir Victon Wong

Published by:
Geotechnical Division
The Hong Kong Institution of Engineers
9/F., Island Beverley, 1 Great George Street, Causeway Bay, Hong Kong

Tel: 2895 4446 Fax: 2577 7791
Prepared in Hong Kong

FOREWORD

It is my great pleasure to welcome you all to the 43rd Annual Seminar of the Hong Kong Institution of Engineers (HKIE) Geotechnical Division. This year's seminar is themed "Towards a Smart-Green-Resilient Geo-Future for World-class City Development", and it promises to be an exciting and informative event.

As we gather, both in-person at the Hong Kong Convention and Exhibition Centre and virtually online, we are reminded of the critical role that geotechnical engineering plays in the development of Hong Kong. With heightened expectations for green growth and sustainable development, we are in a prime position to build Hong Kong into a world-class, smart, and resilient city.

Geotechnical engineering has been at the forefront of innovation and technology in laying the groundwork for the provision of land and infrastructure in Hong Kong. We have seen significant progress, including the six new major rail link and road projects announced in the 2022 Policy Address. This progress is a testament to the collaborative efforts of the government, academia, practitioners, and industrial partners, who are working together to tackle climate change and carbon neutrality, and to reinforce Hong Kong as one of the most liveable cities.

As geotechnical engineers, we have overcome geographical constraints of very limited natural, developable land, and have enhanced our economy and living quality. We are proud of the progress we have made, and we are committed to seizing future opportunities and shaping the new future of Hong Kong.

This year's seminar provides a platform for policy makers, practitioners, and academia to share their insights and brainstorm ideas. It is an opportunity to learn from each other and to explore new possibilities. We are confident that the discussions and presentations at this seminar will contribute to the growth and development of Hong Kong, as we continue to build towards a smart, green, and resilient geo-future.

Before I conclude, I would like to express my sincere appreciation to the organizing committee led by Ir Terence Yau, all our sponsors, speakers, and participants who have made this seminar possible. Your support and contributions are invaluable, and we are grateful for your commitment to the geotechnical engineering community.

We hope you have a productive and enjoyable experience, and we look forward to the discussions and insights that will emerge from this event. Thank you.

Ir Dr Johnny Cheuk
Chairman, Geotechnical Division
Hong Kong Institution of Engineers (2022/23 Session)

ACKNOWLEDGEMENTS

The Organising Committee would like to acknowledge the support of the following sponsors for their generous support of the Seminar:-

AECOM Asia Company Limited
Asia Infrastructure Solution Limited
Aurecon Hong Kong Limited
C M Wong & Associates Limited
China Geo-engineering Corporation
Dix Construction & Transportation Limited
Fong On Geotechnic Limited
Fraser Construction Company Limited
Fugro Geotechnical Services Limited
G and E Company Limited
Gammon Construction Limited
Intrafor Hong Kong Limited
Kin Wing Engineering Company Limited
Lambeth Associates Limited
MTR Corporation Limited
Ove Arup & Partners (Hong Kong) Limited
Pan Kee Construction Limited
Paul Y Engineering Group Limited
Tysan Foundation Limited
Vibro (H.K.) Limited
WSP (Asia) Limited

TABLE OF CONTENTS

Mechanical method for turning Hong Kong soils into construction materials including sand

Z.Q. Yue
Department of Civil Engineering, Faculty of Engineering, The University of Hong Kong

ABSTRACT

Sand is the most exploited raw solid material in the world. It can be used for construction of buildings, roads, railways, bridges, tunnels and beaches. According to United Nations' reports in 2019 and 2022, the world is facing a shortage crisis of sand, as one of the greatest sustainability challenges of the 21st century. Such sand shortage crisis around the world has affected the use of sand in Hong Kong since Hong Kong does not produce any sand. This paper presents a newly invented method for turning Hong Kong soils into construction materials including sand. The local completely decomposed granitic soil and volcanic soil in Hong Kong can be mechanically turned into the materials of gravel, sand, silt and clay. The gravel, sand and silt are siliceous solid particles and mainly quartz mineral particles. The clay is mainly kaolinite mineral. These materials with known and narrow particle size ranges can be used as the raw solid materials in construction and other industry. The method presented in this paper can offer a new sustainable and environmental-friendly and economic solution to the world' sand shortage crisis.

1 INTRODUCTION

1.1 CDG and CDV soils in Hong Kong

Hong Kong soils are dominantly the completely decomposed granitic (CDG) soils and the completely decomposed volcanic (CDV) soils (GEO, 2017; Yue, 2013). The residual soils and colluvial soils also come from the CDG or CDV soils. The CDG or CDV soils are in-situ weathered soils and also called saprolitic soils. They are derived from in-situ chemical weathering of igneous rocks and retain the original texture, fabric and structure of the parent igneous rock. Residual soils are the in-situ soils derived from the CDG and CDV soils and do not contain any traces of the original texture, fabric and structure of the parent rock. Colluvial soils (or colluvium) are formed by slipping, flowing or rolling of saprolitic soils, residual soils and/or rock stones down slopes under the action of gravity and rainfall water. Public fill mainly is the excavated soil due to construction activities on ground.

Hong Kong soils are nature mixtures of siliceous mineral particles, clay mineral particles, and water. The siliceous mineral particles mainly include quartz mineral particles and generally have the particle sizes greater than 0.002 (or 0.0008) mm. They are further divided into gravel, sand, and silt with the particle sizes respectively between 63 mm and 2 mm, between 2 mm and 0.063 mm, and between 0.063 mm and 0.002 mm. They are the preserved minerals of the parent granitic or volcanic rocks. The clay mainly includes the clay mineral of kalinite and generally have the particle sizes smaller than 0.002 mm. The clay minerals are the weathering products of the parent granitic or volcanic rocks, where the weathering has chemically decomposed the feldspar and biotite minerals of the parent rocks into clay minerals. The quartz mineral is the only siliceous minerals that can resist the weathering.

1.2 Objective of this paper

According to United Nations' reports (UNEP, 2019; UNEP, 2022), the world is facing a shortage crisis of sand, as one of the greatest sustainability challenges of the 21st century. Such sand shortage crisis around the world has affected the use of sand in Hong Kong since Hong Kong does not produce any sand. This paper presents a newly invented mechanical method to convert the Hong Kong soil into the quality materials of siliceous mineral particles (or sand/sand/silt) and clay mineral particles (clay) (Yue, 2021). The test results demonstrate that these individual materials have high economic values for use in construction, other industries and agriculture in Hong Kong and other regions (Song et al. 2023; Ma et al. 2023). They further discover that the Hong Kong soil is a non-metallic ore of siliceous sand and clay minerals.

2 MECHANICAL METHOD

2.1 Brief

The mechanical method is a mechanical process of washing and sieving the general soil. It has four main steps. The first step washes the general soil into clean natural sand and soil slurry. The second step washes and sieves the soil slurry into clean fine sand and mud slurry. The third step washes and sieves the mud slurry into silt and clay slurry. The fourth step cycles the used water from the clay slurry and obtains clay material.

The method can convert the general soil into the particles of siliceous minerals and the particles of clay minerals. We have demonstrated that the engineering method is cost-effective, sustainable and environmental-friendly and produces an insignificant amount of carbon dioxide CO_2 and other green-house gases.

2.2 Step I for converting soil into clean sand and soil slurry

The Step I uses a rotary snail-type mixture to mix and wash the soil with water (Plate 1). Once the soil is mixed with water, the heavy and large particles are automatically settled at the bottom of the snail container. The light and small particles are suspended in the water and make the water become the soil slurry. The soil slurry usually contains the particles of clay, silt, and fine sand. The heavy and large particles include gravels, sands, and some fine particles of clay and silt.

Plate 1: Step I for mixing and washing soil with water

The soil slurry in the upper portion of the snail container is then poured into a large bucket. Then more water is added into the snail container for further mixing and washing. New soil slurry appears in the upper portion of the snail container again and is poured into the bucket. This adding water, washing the soil, and pouring soil slurry operation is repeated until both the new heavy and large particles and the new soil slurry becomes relative clean (Plate 2).

Plate 2: Results of clean sand and soil slurry from Step I of mixing and washing soil with water

2.3 Step II for converting soil slurry into clean fine sand and mud slurry

The soil slurry portion obtained from Step I contains mainly silt and clay and some fine sands. The Step II is to separate the fine sand from the silt and clay materials in the soil slurry. The soil slurry is poured out of the container on a steel sieve with the aperture of 0.063 mm (or other sizes) (Plate 3). The soil slurry on the sieve is stirred and washed with additional water. The fine sand is staying on the sieve and the silt and clay become the mud slurry that is leaking through the sieve into the bucket. This stirring washing and sieving operation is completed when both the fine sand on the sieve and the leaking water become clean. As a result, the clean fine sand is obtained and collected from the sieve. The mud slurry is collected for the Step III treatment.

Plate 3: Step II for washing and sieving soil slurry into fine sand and mud slurry with water

2.4 Step III for converting mud slurry into clean silt and clay slurry

The Step III is similar to the Step II. Instead of using the steel sieve, the Step III uses the nylon filter cloth with aperture of 0.002 mm (or other sizes) as the sieve. The mud slurry on the sieve is stirred and washed with additional water. The silt is staying on the sieve and the clay slurry is leaking through the sieve into the bucket (Plate 4). This washing and sieving operation is completed when both the silt on the sieve and the leaking water become clean. As a result, the clean silt is obtained and collected from the sieve. The clay slurry is collected for recycle of the used water and clay material in Step IV.

Plate 4: Step III for washing and sieving mud slurry into silt and clay slurry with water

2.5 Step IV for recycle of used water from clay slurry and obtain clay material

The clay slurry has the density of 1.0470 to 1.0054 g/cm3. It can contain water of the weight 20 to 200 times more than the weight of clay material. We have found that it is statically placed in a container, the clay slurry can experience gravity-induced sedimentation. Clean water appears at upper container and clay material consolidates in lower container (Plate 5).

Plate 5: Step IV for recycling water from clay slurry and obtain clay material

After 16 hours of the static sedimentation, more than 85% of the water in the original clay slurry would present at the upper container. The clay slurry can become highly saturated soft clay with density of 1.4 g/cm3. Other methods can also be used for dewatering the soft clay. The water can be recycled for re-use in the proposed washing and sieving method.

The recycled water has been tested for its purity with Cary 100 UV-Visible Spectrophotometer. The test results show the quality of the recycled water is high. The water can have the clay content less than 3.33 ppm.,

2.6 The use of electric power

The use of electric power for the Steps I, II and III can be illustrated with the following test examples. For a CDV soil from Yuen Lang, the electric power used for the Steps I, II and III are respectively about 2, 7 and 29 kwh for ton of the soil. For a CDG soil from Happy Valley, the electric power used for the Step III is about 27 kwh for one ton of the soil. The static sedimentation method used in Step IV does not use any electric power. The transportation and uplifting of soil, water, soil slurry, mud slurry and clay slurry are manually carried at present. Some electric power is needed if automatic conveyor belt is used to do the transportation and uplifting of these materials.

3 THE PRODUCTS OF MATERIALS WITH KNOWN PARTICULAR SIZES

3.1 General

The mechanical method has been used to convert the local soils in Hong Kong and other soils from Shenzhen and other places of Mainland China into quality materials of gravels, sand, silt and clay. Some examples are given below for the illustration.

3.2 The products of CDG soil

Plate 6 presents the photographs of the CDG soil from Happy Valley and its converted sand with gravel, silt and clay. Figure 1 shows the three curves of the particle size distribution (PSD) of the CDG soil, the CDV soil and the public fill. The weight percentages of gravel, sand, silt and clay are 11%, 37%, 4% and 48%, respectively. The gravel and sand in Plate 6 are further sieved into 12 individual particle sizes as shown in Plate 7. The three corresponding PSD curves of the gravel and sand are shown in Figure 2. The gravel and sand are well graded.

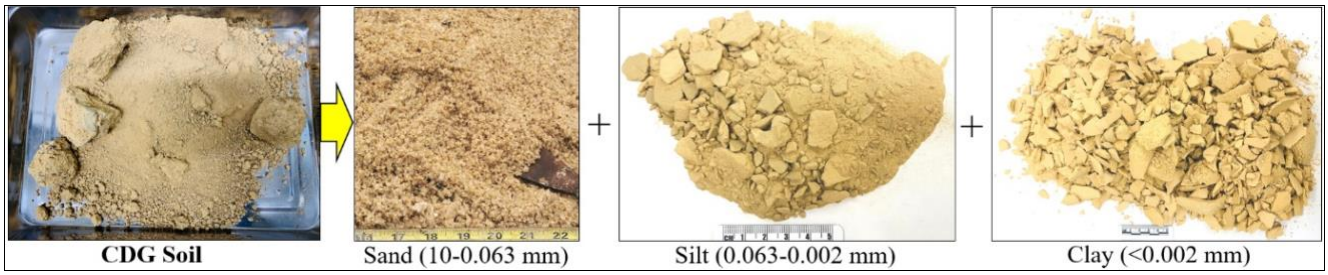

Plate 6: Products of sand, silt and clay converted from a typical CDG soil from Happy Valley, Hong Kong

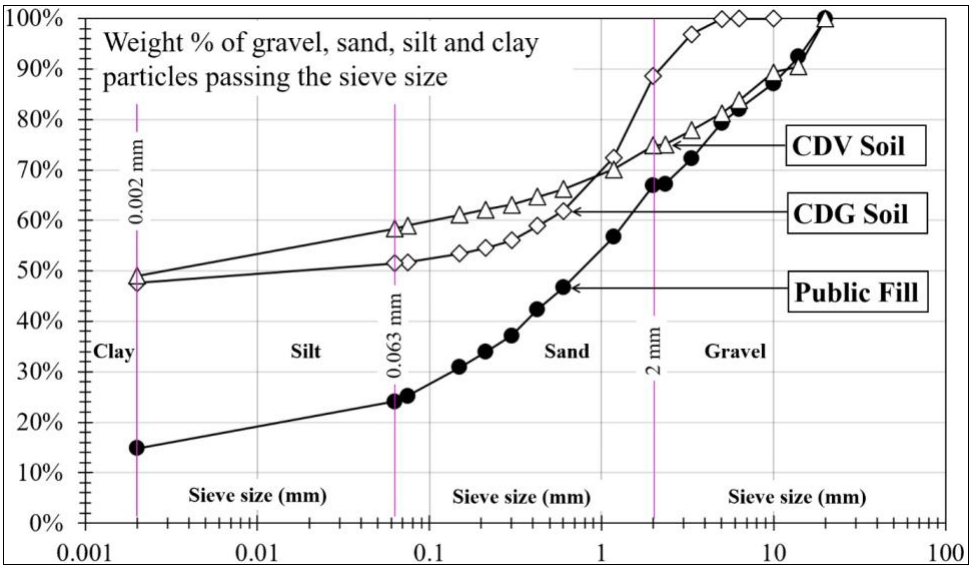

Figure 1: Particle size distribution (weight percentages) of the sand, silt and clay converted from the CDG soil, CDG soil and public fill soil in Plate 6, Plate 11 and Plate 13, respectively

Plate 7: The 12 individual particle sizes of the CDG sand in Plate 6 by dry sieve method

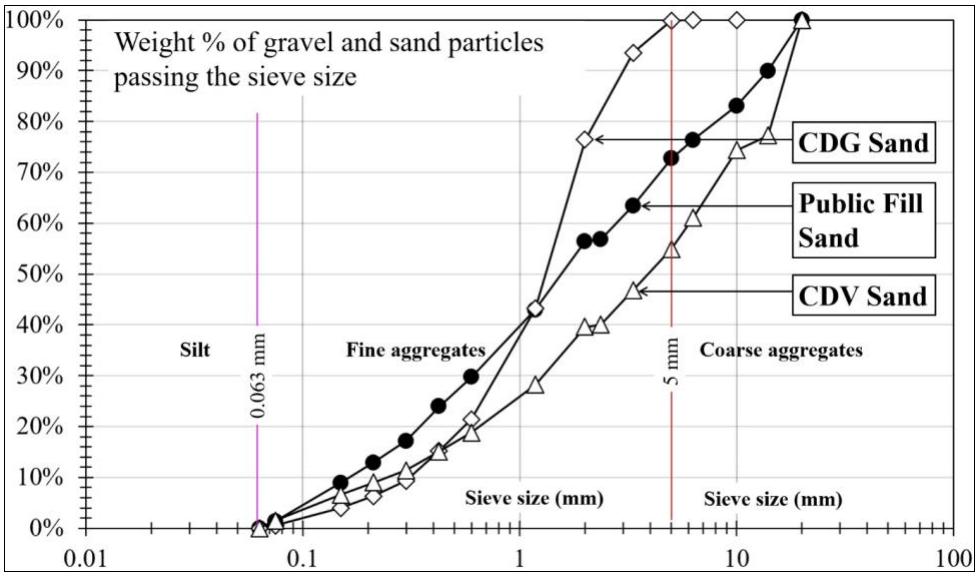

Figure 2: Particle size distribution (weight percentages) of the sand converted from the CDG soil, CDG soil and public fill soil in Plate 8, Plate 12 and Plate 14, respectively

The Leica M205C stereomicroscope is further used to observe the particles of the sand, silt and clay. Plate 8 shows the nine stereomicroscopic images for the nine sub-groups of sand particles. The images clearly illustrate that the sand is dominantly quartz particles plus few feldspars. Furthermore, the Step III method can be further applied to wash and sieve the silt and clay into different size sub-groups.

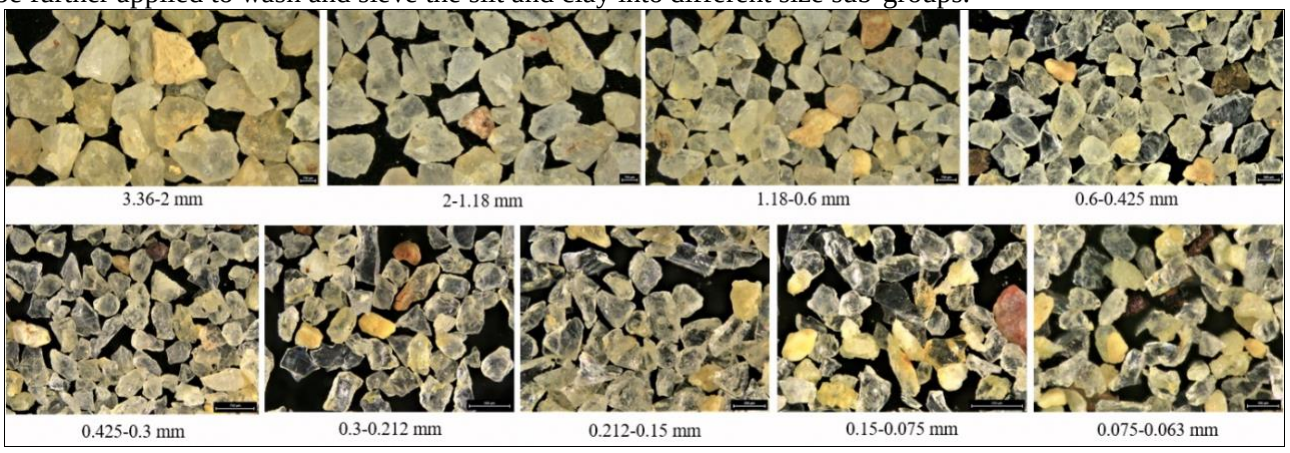

Plate 8: Stereomicroscopic images of the sand converted from the CDG soil in Plate 6 and Plate 7

Plate 9 shows the twelve stereomicroscopic images for the twelve sub-groups of silt particles with the particle sizes from 0.063 mm to 0.002 mm. The images clearly illustrate that the silt is also dominantly quartz particles plus few feldspars.

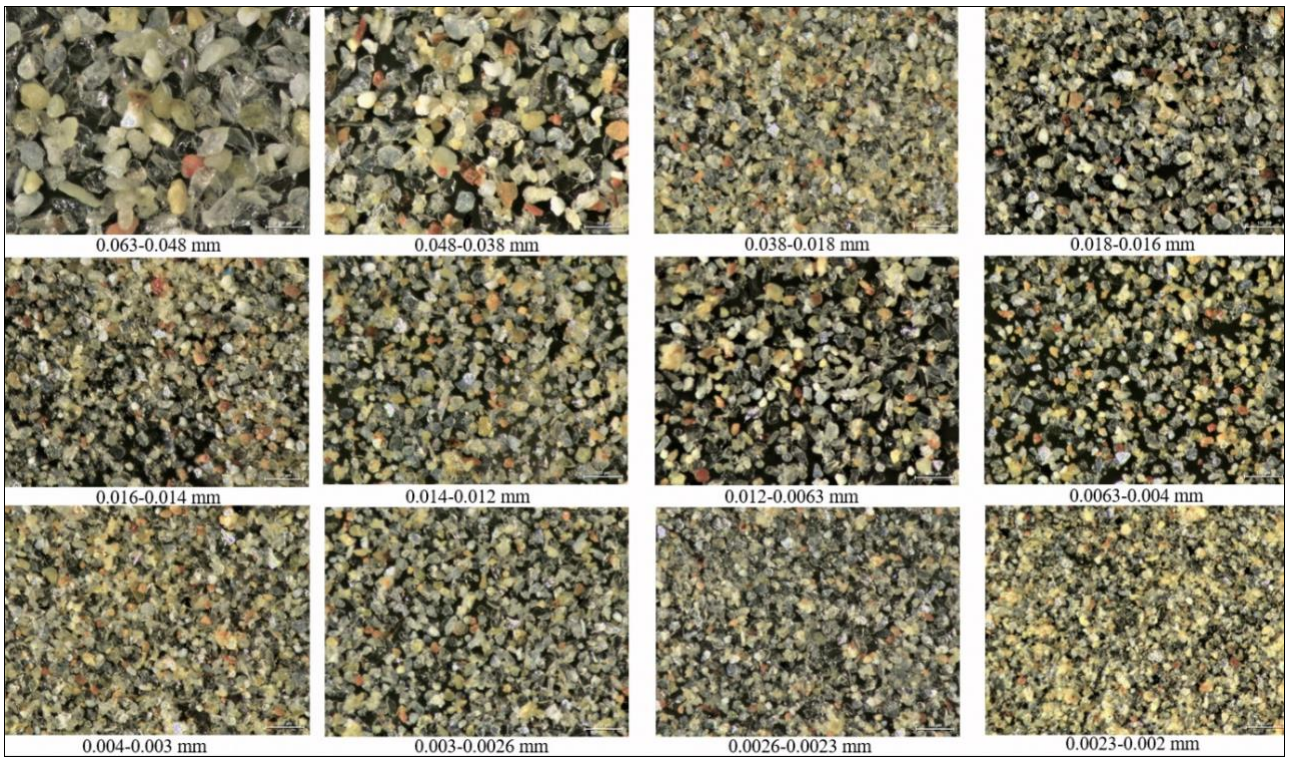

Plate 9: Stereomicroscopic images of the silt converted from the CDG soil in Plate 6

Plate 10 shows the seven stereomicroscopic images for the further sub-groups of clay particles with the particle sizes smaller than 0.002 mm. The first four images with the particle sizes from 0.002 mm to 0.001 mm in Plate 10 clearly illustrate that the particles are the combinations of siliceous mineral particles and the clay mineral particles. The image for the size from 0.001 mm to 0.0008 mm in Plate 10 shows that the clay mineral particles are more than the siliceous mineral particles. The image for the particle size smaller than 0.0008 mm in Plate 10 shows that the particles are dominantly clay mineral particles.

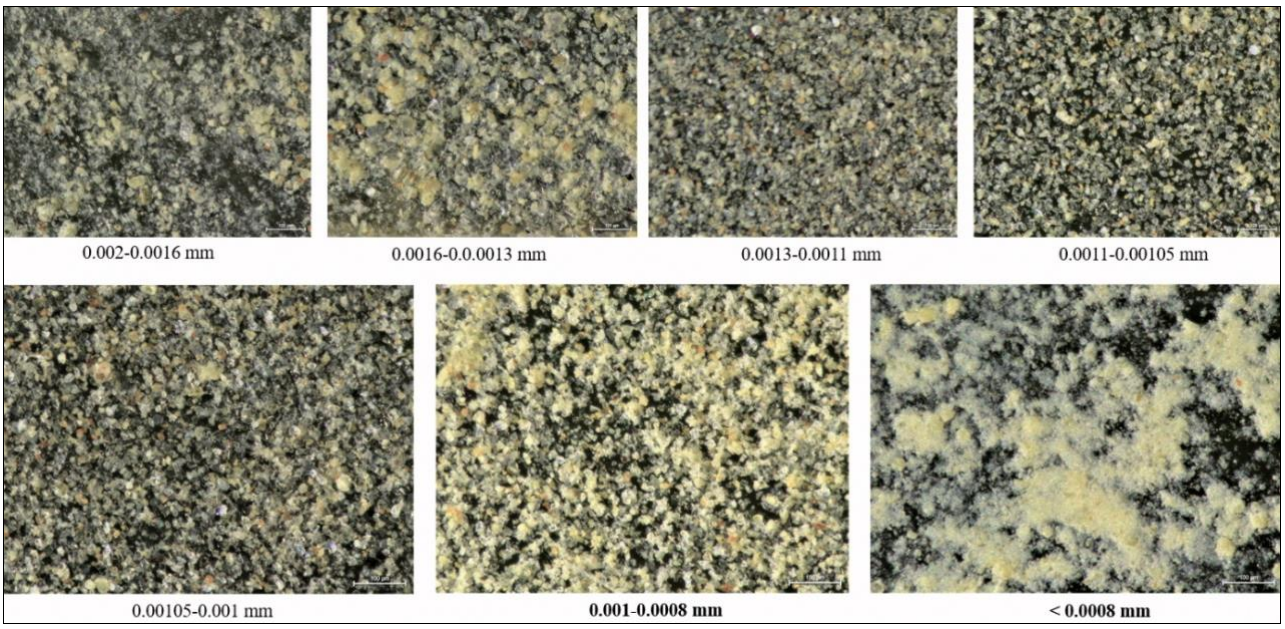

Plate 10: Stereomicroscopic images of the silt and clay converted from the CDG soil in Plate 6

3.3 The products of CDV soil

Plate 11 presents the photographs of the CDV soil from Shum Wan Road and its converted sand with gravel, silt and clay. Figure 1 shows the particle size distribution (PSD) of the CDV soil. The weight percentages of gravel, sand, silt and clay are 25%, 17%, 7% and 49%, respectively. The gravel and sand in Plate 11 are further sieved into 14 individual particle sizes as shown in Plate 12. The PSD of the gravel and sand is shown in Figure 2. The gravel and sand are well graded.

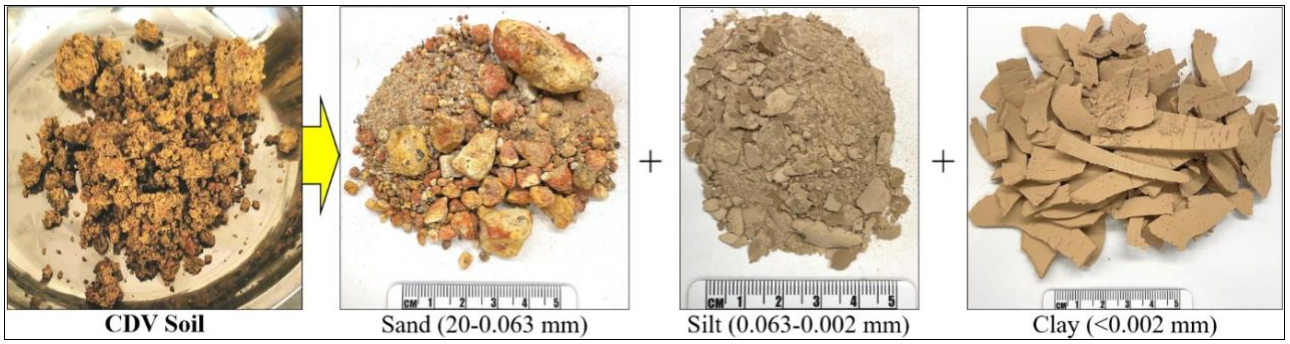

Plate 11: Products of sand, silt and clay converted from a typical CDV soil from Shum Wan Road, Hong Kong

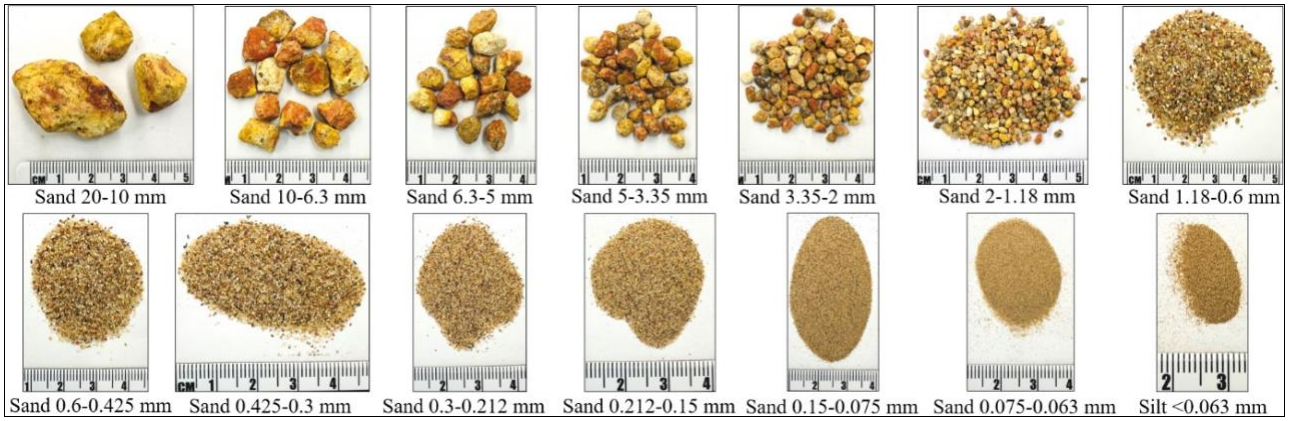

Plate 12: The 14 individual particle sizes of the CDV sand in Plate 11 by dry sieve method

3.4 The products of public fill soil

Plate 13 presents the photographs of the public fill soil from Tuen Mun Area 38 Fill Bank and its converted sand with gravel, silt and clay. Figure 1 shows the particle size distribution (PSD) of the public fill soil. The weight percentages of gravel, sand, silt and clay are 33%, 42%, 9% and 15%, respectively. The gravel and sand in Plate 13 are further sieved into 13 individual particle sizes as shown in Plate 14. The PSD of the gravel and sand is shown in Figure 2. The gravel and sand are well graded.

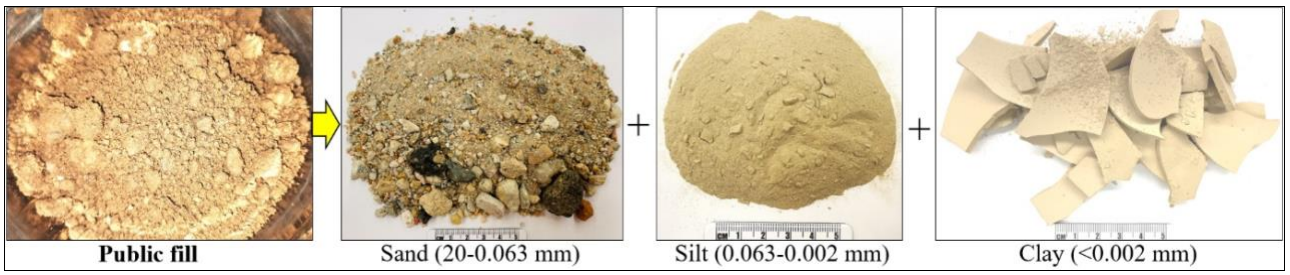

Plate 13: Products of sand, silt and clay converted from a typical public fill soil from Tuen Mun Area 38 Fill Bank, Hong Kong

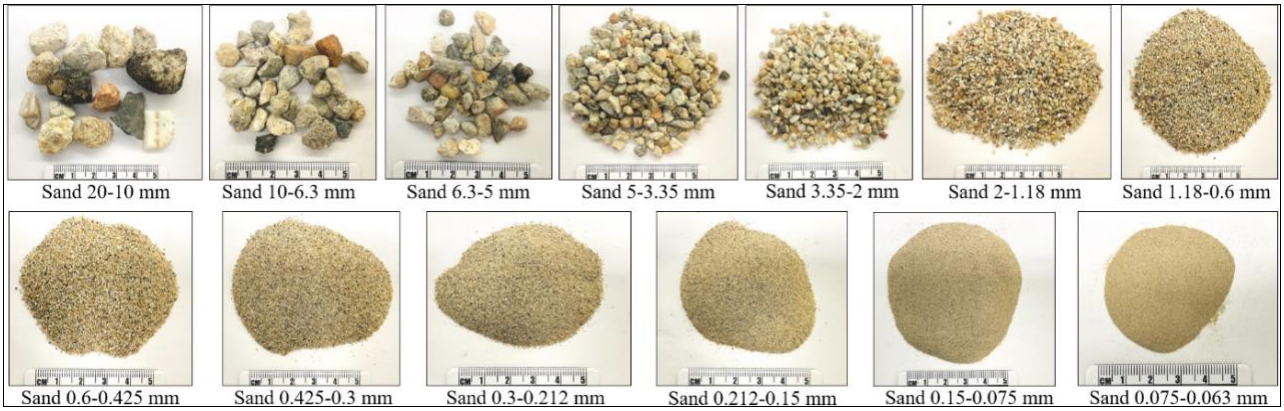

Plate 14 The 13 individual particle sizes of the sand in Plate 13 by dry sieve method

4 CONCLUSIONS AND RECOMMENDATIONS

4.1 Conclusions

Hong Kong soils and public fill are nature mixtures of siliceous mineral particles, clay mineral particles, and water. The invented engineering method can cost-effectively, sustainably and environmental-friendly convert the local soils into individual particles of gravel, sand and silt and clay. The gravel, sand and silt are solid particles of siliceous minerals and mainly quartz minerals. The clay is mainly the clay mineral kaolinite. Hence, Hong Kong soils (CDG and CDV) are non-metallic ore of siliceous minerals and clay mineral.

To convert one ton of the CDG or CDV soils into one ton of gravel, sand, silt and clay, the total electric power can be respectively about 2, 7 and 29 kwh. The total is 38 kwh. Since the price for one kwh is HK$1.214, the electric costs are respectively about HK$3, 8 and 35 for producing gravel and sand, fine sand, silt and clay. The total electric cost is HK$46. The value of the one ton of gravel, sand, silt and clay materials is much more than HK$46.

4.2 Recommendations

Figure 3 shows the conceptual design of the automatic mass production line for massively converting local soil (public fill) into gravel, sand, silt and clay. A conveyor belt system is used to transport and uplift the soil and gravel/sand/silt for washing, rinsing and storage piling. A sinkhole, channel and pipe system is used to transport and pump the water, soil slurry, mud slurry and clay slurry.

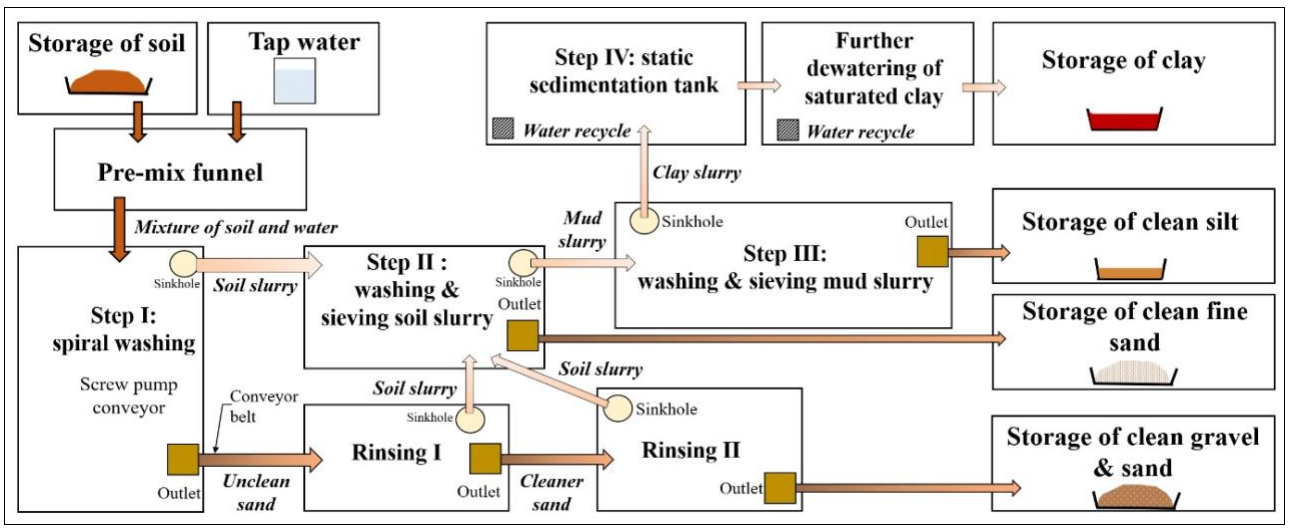

Figure 3: Automatic mass production line for converting local soil (public fill) into gravel, sand, silt and clay

The gavel and sand and silt can replace the imported marine sand for land reclamation. The gravel can be used as coarse aggregate and the sand can be used as fine aggregate for production of concrete. The silt can be used to replace the carbon-intensive cement content for production of concrete. The method can be applied to a range of engineering applications and offer an innovative and environmentally friendly solution to supply useful construction materials for use in the local construction industry. The clay can have many uses in construction and material industries and agriculture.

ACKNOWLEDGEMENTS

The author thanks the financial support (Project Nos. HKU 17207518 and R5037-18) from the Research Grants Council of the Hong Kong Special Administrative Region, China. The author thank Mr. Junqi Feng and other engineers in Soils & Materials Engineering Co., Ltd. in Hong Kong for using their stereomicroscopic facilities.

REFERENCES

GEO, 2017. *Guide to Rock and Soil Descriptions* (Geoguide 3), Geotechnical Engineering Office (GEO), Civil Engineering and Development Department of The Government of HKSAR, Hong Kong. P.171.

Ma, S.N., Song, Y., Liu, J.W., Yue, Z.Q. 2023. Extended wet sieving method for determining complete particle size distribution of general soil. *Journal of Rock Mechanics and Geotechnical Engineering*, in press.

Song, Y., Ma, S.N., Liu, J.W., Yue, Z.Q. 2023. Laboratory investigation of CDG soil as source of fine aggregates for Portland cement concrete. *Construction and Building Materials*, 367(2023) 130226: 1-21.

UNEP. 2019. *Sand and Sustainability: Finding new solutions for environmental governance of global sand resources*. GRID-Geneva, United Nations Environment Programme (UNEP), Geneva, Switzerland, ISBN No.: 978-92-807, pp.56.

UNEP. 2022. *Sand and Sustainability: 10 strategic recommendations to avert a crisis*. GRID-Geneva, United Nations Environment Programme (UNEP), Geneva, Switzerland, ISBN No.: 978-92-807-3932-9, pp.90.

Yue, Z.Q. 2013. Social benefits of landslide prevention and mitigation in Hong Kong, China, in *Progress of Geo-Disaster Mitigation Technology in Asia*, Springer, ISBN 9783642291074_3: 55-75.

Yue, Z.Q. 2021. *A Method for Preparing Construction and Industrial Materials*, Patent No.: HK30049139, Patents Registry, Intellectual Property Department, HKSAR Government, Hong Kong.

BIM Application in Geotechnical Works for Masterplanning and Construction Monitoring

Penny KC Choy, Terrence YK Tse & Ricky HT Wong
WSP Limited, Hong Kong

ABSTRACT

Implementation of geotechnical data to Building Information Modelling (BIM) can improve the master planning of building development and facilitate monitoring of site construction. At the early stage of design development, application of BIM embedding the site geology, building master layout and associated engineering design elements (i.e., foundations and ELS works, etc.) helps the illustration of different options of building massing, especially for a development with significant geotechnical content (i.e., hillside site, near MTRC tunnel). It can be studied quickly to come up with the most cost-efficient scheme of building plan and information including a balance of optimum choice of volume of soil/rock excavation, extent of formation works, amount of material input, etc.

BIM can also help engineers to review the construction sequence for complex geotechnical work including phasing of different kinds of works such as pile foundation construction, site formation and ELS works. Nowadays, creation of the 4D (and 5D) modelling allows the programme to be optimized (and construction cost forecast) and facilitates better understanding of the construction sequence. Simulation for construction method in geotechnical works is developed to allow the construction method to be rehearsed virtually so that the engineers and workers can understand it more before execution.

This paper discusses the aforesaid BIM applications in geotechnical works for different building projects including institutional developments. The use of BIM results in better design communication within the design team, as well as with the owners and other stakeholders.

1 INTRODUCTION

In the construction industry, Building Information Modelling (BIM) in an approach of collaborative design is not only commonly used nowadays in the architectural, civil, structural and building services fields, but is also applied in geotechnical works. It can be used to create and manage digital models of the geology such as subsurface soil and rock conditions of a site, as well as the associated geotechnical structures and foundations. BIM can also be used to simulate the geotechnical works sequence, identify site constraints and facilitates construction site management.

Recently the authors have been working on some building development projects that illustrate the beauty of BIM applications in geotechnical works. The following sections describe the use of BIM in masterplanning and construction monitoring resulting in increased efficiency of design, reduction of construction cost, improvement of sustainability and enhancement of collaboration and communication among engineers, contractors and owners.

2 MASTER PLANNING IN GEOTECHNICAL WORKS

Master planning in geotechnical works involves development of a comprehensive plan to manage the geotechnical aspects of construction works such as site formation works, foundation works and ELS works. BIM is applied in geotechnical works at the early stage of master planning to evaluate site conditions, assess potential risks and develop design solutions to address these risks.

2.1 Identification of Potential Risks

By incorporating the data obtained from desk study, site reconnaissance and ground investigation into the BIM, the designers can enhance their visualization of underground constraints, take good control of the design process, have clear understanding of ground behavior and react faster to potential issues on site. The BIM as shown below demonstration the underground constraints such as MTR tunnels and geotechnical features for the entire project team to have a holistic picture for deriving a master plan for the project.

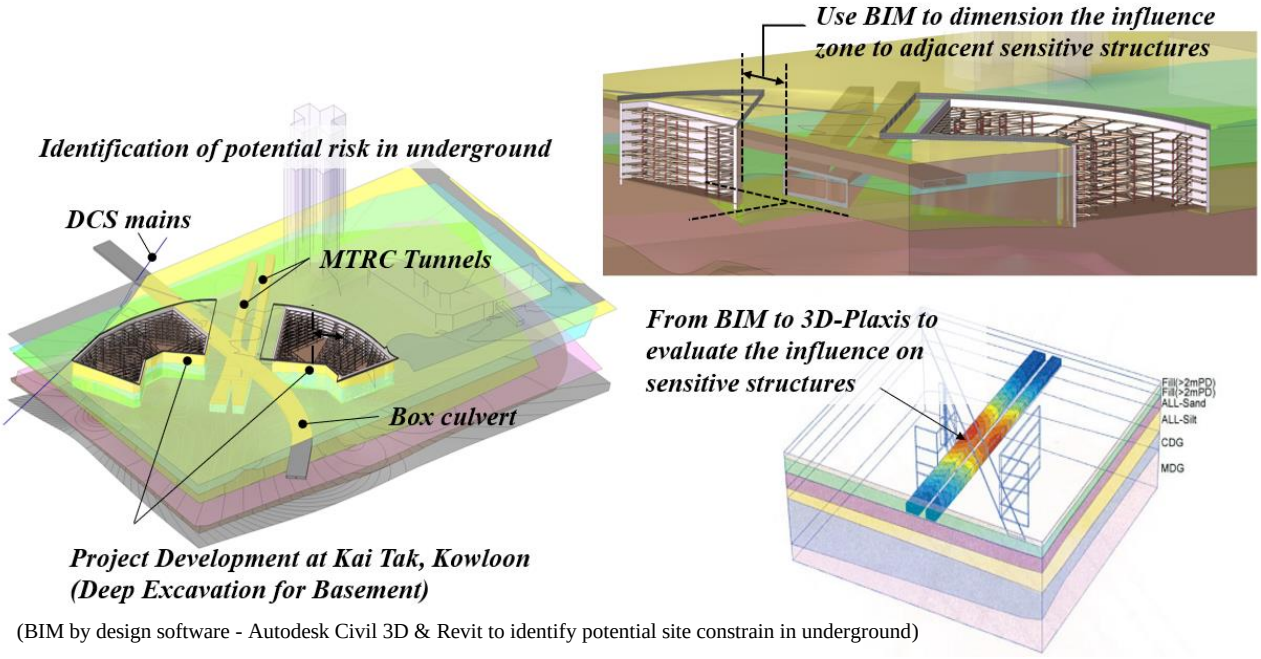

Figure 1: Visualization of potential risks at early design stage for commercial development at Kai Tak

2.2 Efficiency and Accuracy of Formation Layout

Designing the master layout for a building development is time consuming, especially in utilization of underground space. To reduce cost and time implications of a master layout, cutting and filling can be formed strategically to minimize the amount of excavation and material needed for grading (or backfilling). Moreover, identification of soil & rock conditions is also dictating the layout of basement. In the past, a number of 2D sections would be necessary to identify the soil & rock conditions and take advantage of natural topography for master layout design but that approach is not efficient.

Today we have BIM as a strategic tool to optimize the cut and fill analysis process. This can help (i) to identify areas where excavation and filling can be minimized without compromising the integrity of the site; (ii) to reduce the construction time in excavation of hard material and (iii) to reduce carbon emissions

Comparisons of bulk excavation volume for master plan layout design with and without BIM at the early stage of development of several projects are shown below:

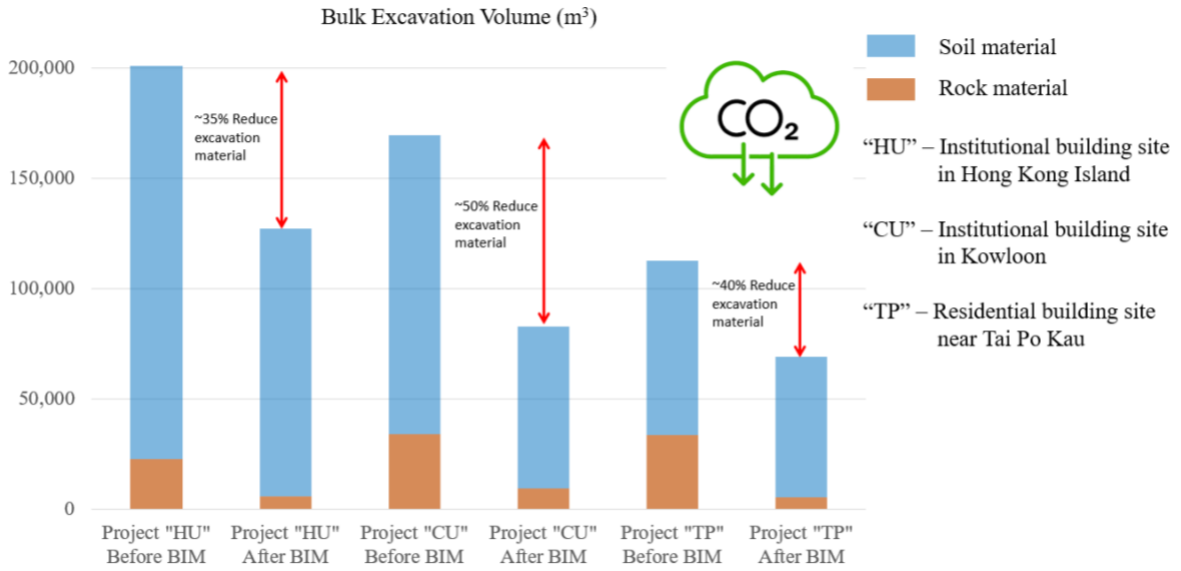

Figure 2a: Reduce bulk excavation after review master plan layout in BIM

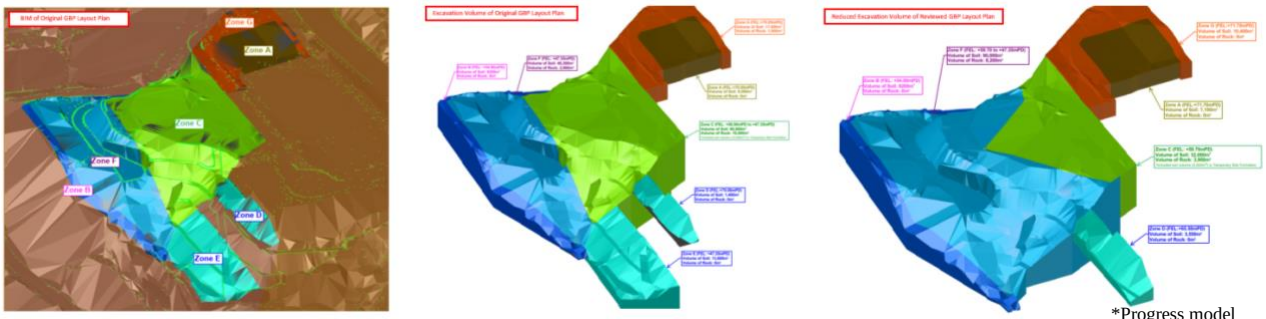

*Progress model

Figure 2b: Cut & Fill analysis by 3D modeling for institutional building development in Hong Kong Island
(BIM by design software - Autodesk Civil 3D & Revit to minimize cut & fill during planning stage)

2.3 Management of Geotechnical Data

Good management of geotechnical data can help to improve the assessment quality of potential hazards associated with site geology such as fault zone and sinkholes. BIM is a digital process that can be used for foundation design and geology analysis to improve the accuracy, speed and efficiency of the design scheme selection. For example, the model can help to identify areas of site with poor soil/ rock condition, such as data of fault material encountered in GI records and help to determine the appropriate foundation plan strategy.

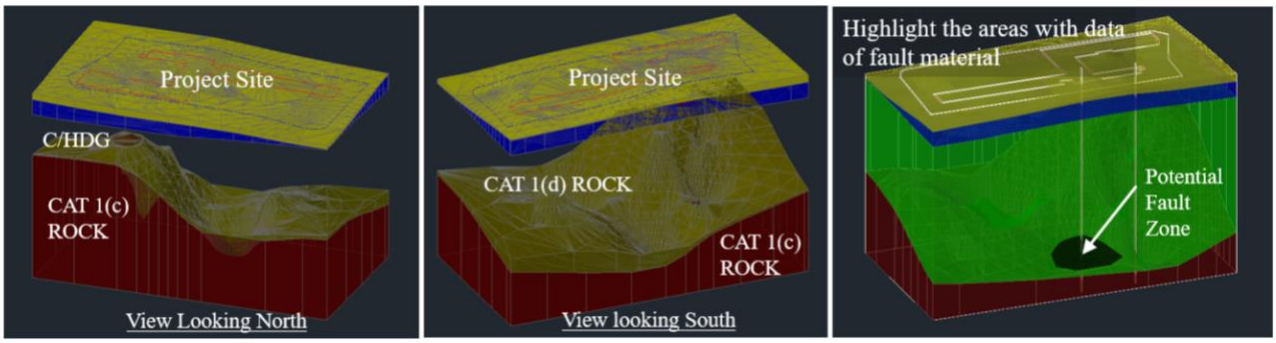

Figure 3: BIM involves creating a 3D model of site geology for hospital development at a Kowloon site to identify potential fault zone
(BIM by design software - Autodesk Civil 3D to identify potential fault zone for pilling design and review building layout)

Moreover, it can help to improve the efficiency of design such as clashing analysis, quantifying design elements, and creation of design sections, etc.

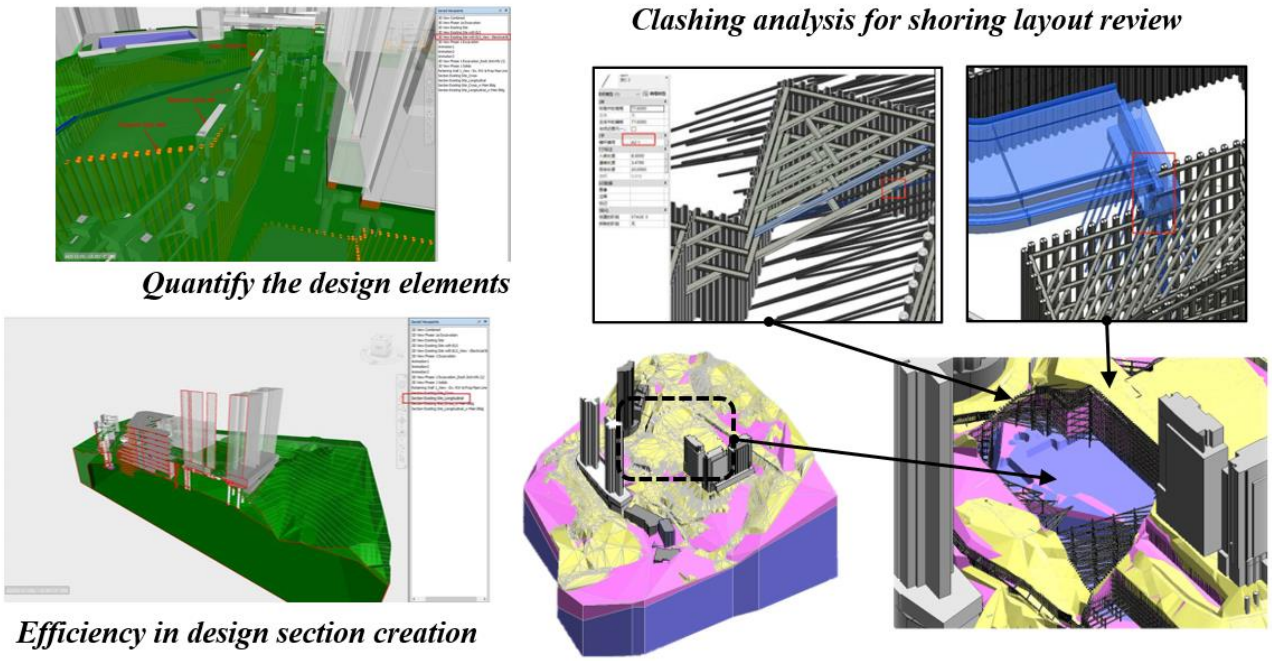

Figure 4a: BIM involvement in detail design stage for institutional building development in Hong Kong Island

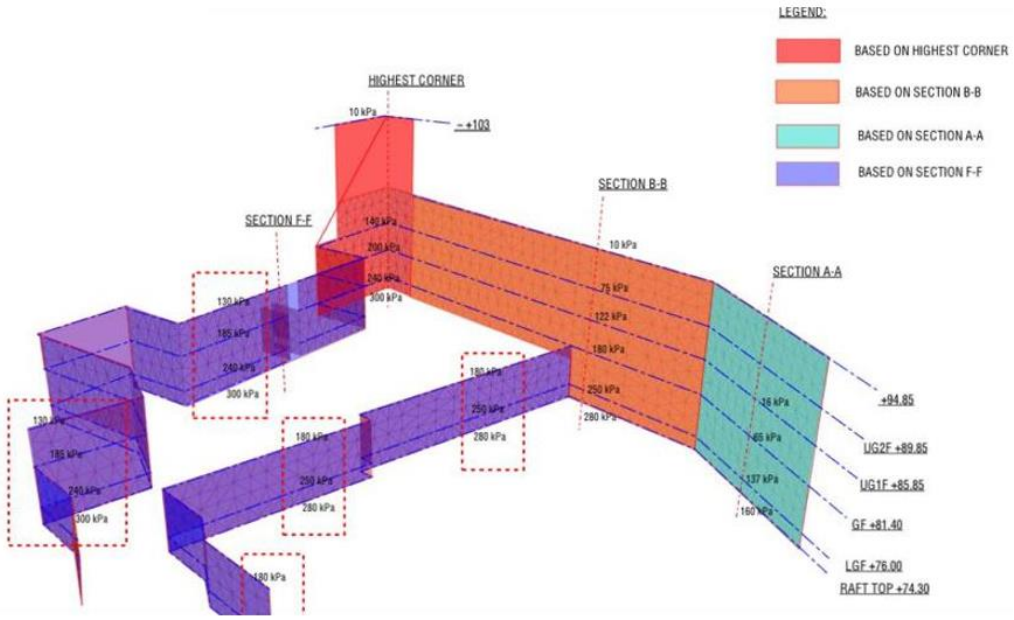

Figure 4b: BIM involvement in detail design for building soil load

3 CONSTRUCTION SITE MONITORING

3.1 Construction Monitoring

One of the key benefits of BIM for construction monitoring is that it enables the engineer to track progress against a detailed construction schedule. This can help to identify potential delays or bottlenecks early on, so that corrective actions can be taken before the project falls behind schedule. By integrating the models with survey data (i.e., drone with lidar scanner) and tracking material deliveries on site, BIM can help the engineer

to optimize the site formation (or foundation and ELS works) programme, estimate construction cost and understand better the construction status.

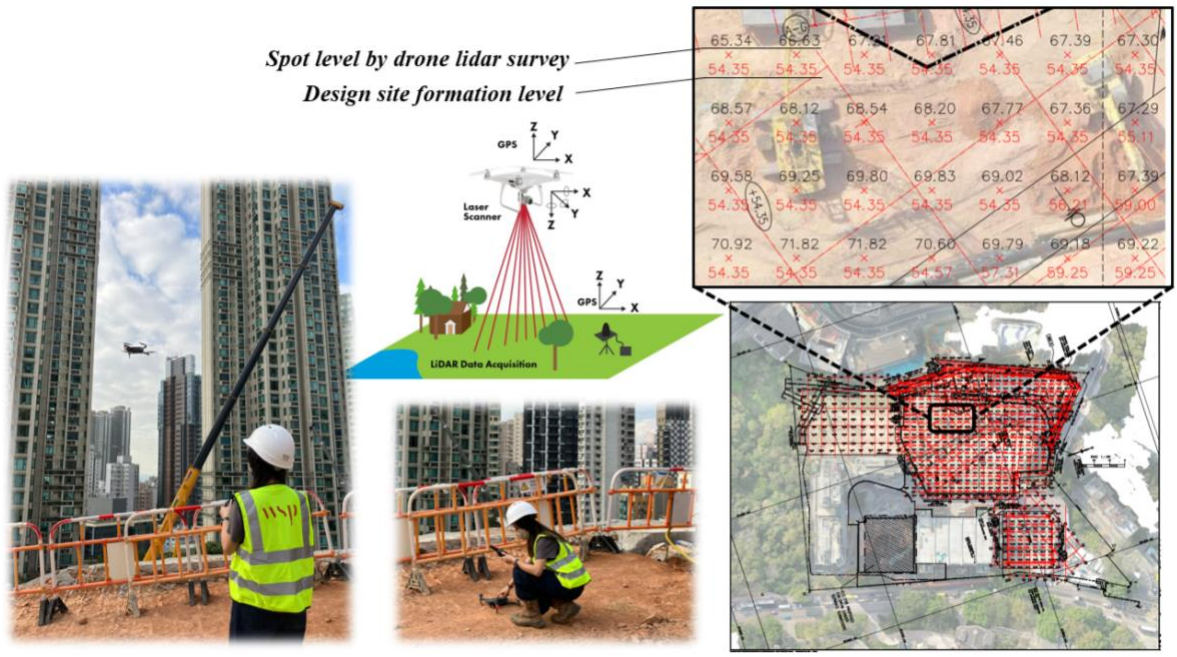

Figure 5a: Site staff using drone lidar survey data integrated to BIM for construction monitoring

Figure 5b: BIM technology to track the construction progress and cost status

Nowadays, creation of the 4D (and 5D) modelling, as shown in the above figures, is one of the BIM uses to improve communication and collaboration among project stakeholders.

3.2 Simulation for Works Sequence

BIM can also be used to optimize construction process by providing a detailed, step-by-step works sequence. For example, it can be used to identify potential conflicts between different elements of construction, such as installation of ground anchor and strut removal sequence and help to find solutions for these conflicts before construction begins. In addition, it is possible to reduce waste, minimize downtime and improve safety on the construction site.

The simulation of construction method in geotechnical works is developed to rehearse construction sequence digitally, which allows the engineers and workers to understand it more before the work begins.

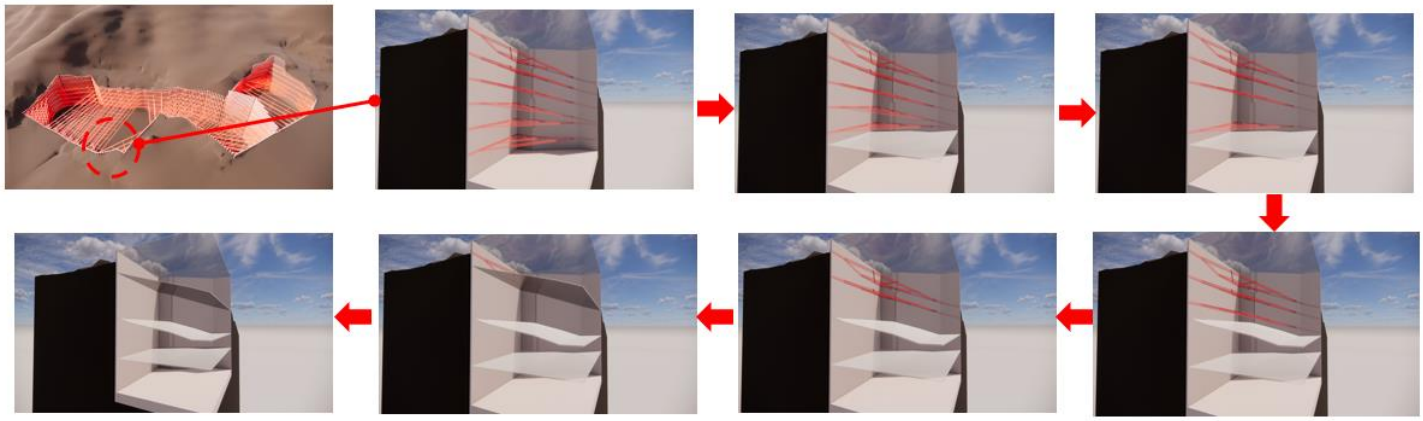

Figure 6: BIM involvement in detail design for strut removal sequence
(BIM by design software - Autodesk Navisworks to model ELS de-structing sequence with permanent structure)

4 CONCLUSIONS

Using Building Information Modelling (BIM) in geotechnical works can result in several benefits including:

1. Enhancement in the efficiency and accuracy for master planning, especially in sub-structure design

2. Visualization of the geotechnical conditions and structures, which can help to identify potential issues and design solutions

3. Better management of geotechnical data and improvement of the quality and consistency of the design, Thus resulting with more cost-effective design and improved sustainability

4. Powerful construction monitoring for improving construction efficiency, reducing costs, and helping the projects to be completed on time and to a high standard

5. Improved communication and collaboration among engineers, contractors and owner.

Down the road, it is expected that BIM technology will continue to evolve and become more sophisticated. This will provide geotechnical engineers with even more powerful tools for creating accurate, efficient, and collaborative designs, and will help to enhance innovation and progress in the field of geotechnical engineering.

ACKNOWLEDGEMENTS

The authors wish to thank the clients, The University of Hong Kong for permission to publish this paper and to acknowledge the assistance & encouragement of their colleagues in WSP Limited for preparation of this paper.

Potential of Early-age Thermal Cracking in High-strength Concrete Bored Piles

Tzu-Han Wen & Terry Y.P. Yuen
Department of Civil Engineering, National Yang Ming Chiao Tung University, Taiwan
Victor Li
Victor Li & Associates Ltd., Hong Kong

ABSTRACT

Field measurements were carried out using optical fiber on a 3m diameter bored pile constructed using Grade 60 concrete for a foundation project in Hong Kong. Sensors placed inside sonic pipes at about 35cm from the edge of the instrumented bored pile were used to monitor the pile's field temperature and strain changes for approximately 380 hours after concreting casting. The data obtained from the instrumented pile were utilized to validate the theoretical model presented in this paper, which can rigorously evaluate the coupled mechanical-thermal responses of the bored pile. To assess the potential for early thermal cracking, a transient coupled thermal-mechanical response analysis was performed for the 3m diameter instrumented bored pile, incorporating the heat of the hydration curve by CIRIA Report C766. The simulated temporal evolution and spatial temperature distribution agreed well with the field measurements, which showed a peak of 67°C 33 hours after casting. According to the theoretical model, the predicted maximum temperature rise can reach nearly 85°C at the pile center. Large horizontal thermal gradients were observed across the pile's cross-sections, leading to potential vertical crack development in the pile. Based on the analysis results, the estimated maximum crack width is 0.06 mm, which satisfies the serviceability limit.

1 INTRODUCTION

The use of high-strength concrete (HSC) with a compressive strength of $f_c = 60$ MPa for deep foundations of high-rise buildings is gaining popularity worldwide (Kou et al. 2018; Larisch 2011; Voort et al. 2008). In Hong Kong, foundation works are usually awarded under design-and-build contracts to contractors. Where feasible, larger bored piles with diameters of 2.5m, 3m, or even 3.2m are preferred if practicable to reduce the total number of bored piles and hence the foundation cost. It is increasingly popular amongst foundation contractors to adopt HSC for foundation design as it can further reduce the foundation costs by lowering the reinforcement content and have the added benefit of making the handling of lighter reinforcement cages easier during construction.

The mix proportioning of HSC is characterized by a very low water-cement/binder ratio (e.g., w/b < 0.4) and higher cement content compared to normal strength concrete (NC) (Larisch 2011). Reactive pozzolans such as silica fume, pulverized fuel ash, and ground granulated blast-furnace slagcan also be blended with cement to reduce porosity and densify the HSC microstructure through pozzolanic reactions during hydration (McCarthy & Dyer 2019). HSC can deliver many practical benefits for mass concrete placements, such as reduced member

size and self-weight, lesser required lap-splice/bond lengths, higher elastic modulus, lower shrinkage and creep, high workability/self-compacting ability with good consistency if mixed with optimal proportions of super-plasticizers and viscosity modifiers (Claisse 2016), good resistance to chemical ingressions, and higher durability than NC.

Although HSC with a lower water-cement ratio would normally produce lower heat of hydration than NC (Smeplass & Maage 1990), intended hydration acceleration to achieve high early strength by adding a high dosage of silica fumes can lead to higher heat of hydration than NC in the first 12 hours (Shi et al. 2015). It has been reported in the literature that the maximum adiabatic temperature rise in HSC can be 54.2^{o}C, which is about 10^{o}C higher than that in NC with temperature rises of 44.5^{o}C (Do et al. 2020). At this elevated temperature level, no harm would be inflicted on the integrity of the concrete element if it can deform under a uniform thermal strain. Unfortunately, the thermal gradient is always present in reality when the concrete pile foundation is exposed to the ambient environment of soil. Tensile stress can develop in the element under non-uniform thermal strain induced by the coupled thermal gradient and deformation restraint (ACI 2012; Kim 2010; Bamforth 2007). Thermal cracks can eventually develop when the tensile strength is exceeded. Once cracking occurs, HSC elements would be deprived of most of the abovementioned advantages, such as resistance to chemical ingressions and durability. Furthermore, the structural capacity of the foundation or piles would be degraded as the concrete strength can soften significantly with the development of lateral cracking (Vecchio & Collins 1986). For a deep foundation constructed using tremie concrete and buried deep in the soil, the problems associated with thermal cracking may be difficult to detect even with detailed and comprehensive inspection of the structural integrity based on conventional techniques such as Cross-hole sonic logging and Pile Integrity Testing (Larisch 2011) . Hence, it is always desirable to prevent thermal cracking in the first place.

As Kwan & Ng (2004) discussed, sub-vertical thermal cracks may be caused within large-diameter columns due to internal restraints to thermal movement. Figure 1 shows examples of sub-vertical cracks observed from concrete cores of large-diameter bored piles in Hong Kong that were constructed using Grade C45 NC. Such defects were likely to be attributed to thermal cracking. It will be interesting to investigate whether the thermal cracking problem will become more severe for bored piles constructed using HSC.

Figure 1: Examples of subvertical crack observed on concrete cores of bored piles

The main goal of the paper is present a preliminary study to analyze the potential for thermal cracking in HSC piles due to the heat generated during hydration. To achieve this, a thermal-mechanical finite element (FE) model is developed based on field data of temperature monitoring of a bored pile constructed using Grade C60 HSC. The model is developed using the ABAQUS finite element package and includes simulation of heat generation during early-stage hydration and strength development, as well as analysis of temperature evolutions, temperature distributions, and maximum tensile stress in the pile. The simulation results will help determine the potential for thermal cracking in HSC piles and formulate strategies for preventing such cracking.

2 FIELD MEASUREMENTS IN A BORED PILE

A research study on the thermal cracking of bored piles constructed using HSC has recently been initiated and funded by Victor Li & Associates Ltd. As part of the research program, field works had been carried out by a research team at the Hong Kong Polytechnical University under the auspices of PolyU Technology Consultancy Co. Ltd. (PTCCL). The temperature and strain profiles along two bored piles constructed using Grade 60 HSC were monitored using optical fiber fixed onto the reinforcement cage. In addition, an optic fiber and one conventional temperature sensor were also placed inside one of the steel pipes installed for sonic logging test (hereafter called sonic pipe) for one of the bored piles. The monitoring results and further details of this field study are presented in PTCCL (2022).

In this paper, only the results of temperature monitoring obtained from the optical fiber and conventional temperature sensor installed in one of the bored piles will be presented and compared with the theoretical predictions. The bored pile had a shaft diameter of 3m and was constructed using C60 HSC. Figure 2 shows the details of the bored pile. The concreted pile had a length of 16.17 meters, with its top level at a depth of about 10m below ground. The minimum concrete cover to the steel reinforcement was 75mm. The pile was surrounded by completely decomposed granite (CDG) and embedded into the bedrock with a socket diameter of 2.8m and a bellout diameter of 4.95m. The pile bore above the concreted pile was backfilled by soils to ground level. The sonic pipe housing the optical fiber was located about 35cm from the edge of the bored pile, and the conventional temperature sensor was placed at a depth of about 19.5m below ground.

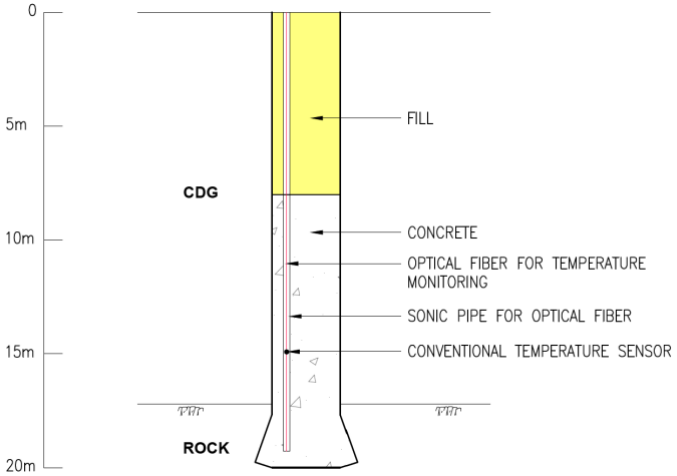

Figure 2: Details of the bored pile

3 FINITE ELEMENT MODEL

3.1 Fluctuation of soil temperature with depth

The early cracking risk of concrete construction is affected not only by the mechanical (e.g., strength, stiffness, and creep) and thermal properties (e.g., hydration heat generation, thermal conductivity, and specific heat capacity) of concrete but also by the deformation restraints and the ambient conditions.

Furthermore, the soil temperature would be different from the air temperature T_a and changing with the soil depth. For Hong Kong, the soil temperature T_s at the current day number n and the soil depth x can be modelled by the following empirical equation proposed by Chow et al. (2011):

$$T_s(n,x) = a_1 \exp(-a_2 x) T_a + b_1 \exp(-b_2 x) \sin\left(\frac{2\pi}{365} n + b_3 x + b_4\right) + c_1 \left(-\frac{2}{\pi}\right) \tan^{-1}(c_2 x) + d_1 \quad (1)$$

Under the assumed condition of $T_a = 18°\text{C}$ and $n = 14$ day, the numerical coefficients of Eq. (1) are given in Table 1 (Chow et al. 2011).

Table 1: Coefficients of Eq. (1)

a_1	a_2	b_1	b_2	b_3	b_4	c_1	c_2	d_1
0.4041	1.4284	4.687	0.2223	–0.3465	–2.0866	15.3297	–2.7204	11.4603

3.2 Thermal analysis of the bored pile

A 3D numerical model of the above HSC (C60) bored pile was established using the program ABAQUS (2020) for thermal analysis, as shown in Figure 3. The pile is modelled as a cylinder with a shaft diameter of 3m and embedded in bedrock approximately 2 meters deep with a bellout. The reinforcement bars in the bored piles are also incorporated in the model. The binder content is taken to be 430 kg/m^3 with 10% fly ash. The estimated mechanical and thermal properties of materials, such as the pile, surrounding soil, and bedrock, are listed in Table 2. The model is meshed with three-dimensional 8-node linear heat transfer brick elements, as illustrated in Figure 3.

The average daily air temperature was assumed to be $T_a = 18°\text{C}$, and the placing temperature was 5°C above the mean ambient temperature. Based on the binder content and assumed placing temperature at 22°C, the generated hydration heat per unit mass Q(t) over 100 hours in the concrete pile is estimated according to Bamfoth (2018) and plotted in Figure 4. The hydration heat generation is modeled as the body heat flux $\dot{\text{Q}}(\text{t})$, plotted in Figure 4, to the pile. In the numerical model, the body heat flux $\dot{\text{Q}}_v(\text{t})$ is expressed as the heat per unit volume per unit time, thus

$$\dot{\text{Q}}_v(\text{t}) = \dot{\text{Q}}(\text{t})\rho \quad (2)$$

where ρ is the concrete density.

Table 2: Estimated mechanical and thermal properties of the materials

	Concrete (C60)	Bedrock	Soil/backfill
Young's modulus, E(GPa)	39	40	0.3
Poisson's ratio, ν	0.2	0.25	0.25
Bulk density (kg/m^3)	2400	2600	2080
Specific heat J/(kg °C)	1050	770	1483
Thermal conductivity W/(m °C)	2	3.2	3.34
Thermal expansion coefficient (10^{-6}/ °C)	10	24	14
References	CEN 2004; Bamfoth 2018	Lumb 1983; Cho et al 2009; Robertson 1988	Hamdhan & Clarke 2010; GEO 2006; Wypych 2021

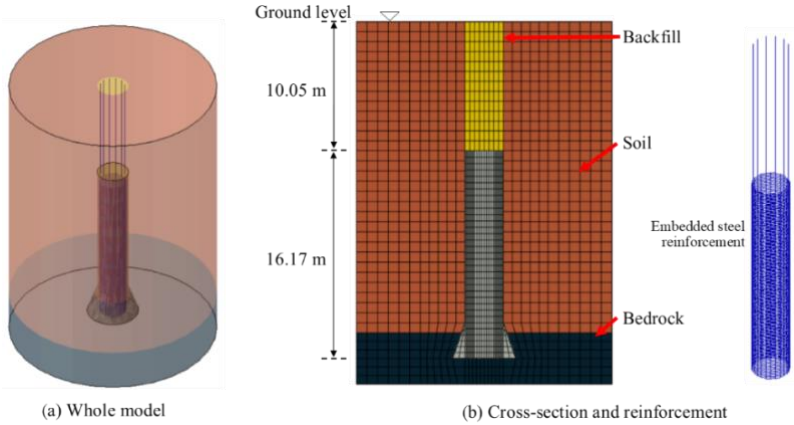

Figure 3: Numerical model of the bored pile

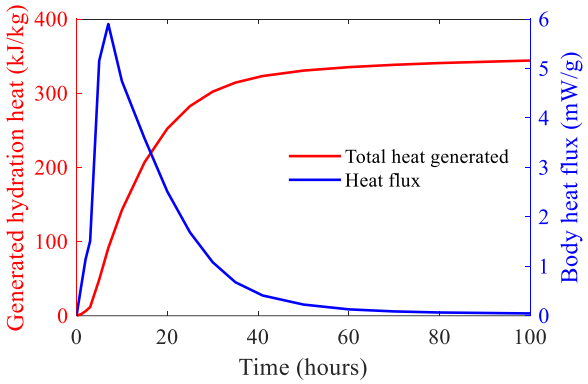

Figure 4: Generated hydration heat and heat flux in the concrete pile (per kg of binder)

3.3 Coupled Temp-Displacement Analysis

To accurately analyze the stress in concrete, it is crucial to consider the temperature distribution as it directly affects stress. Therefore, a fully coupled thermal-stress analysis using ABAQUS/Standard is necessary. The heat generated during hydration induces thermal stress in concrete, which can result in cracks. Reinforcements are used to prevent the propagation of these cracks. To account for this, simultaneous thermal and mechanical solutions are required. A backward-difference scheme is employed to integrate the temperatures, while the

nonlinear coupled system for fully coupled temperature-displacement analysis is solved using Newton's method, as recommended by ABAQUS (2020).

3.4 Results of coupled thermal-mechanical analysis of the bored pile

The temperature profiles along the pile length at different locations of the pile shaft were extracted from the simulations and compared with field data. Figure 5 illustrates the pile's simulated temperature evolutions (plotted in solid curves) at different locations with the same level as the conventional temperature sensor. The predicted results at point TWL2, located at a distance of 38cm from the pile edge, show a good agreement with the in-situ measurements (plotted as a dashed line) measured from the conventional temperature sensor at the position of the sonic pipe. The simulated temperatures at position TWL2 and the center reached their highest values of 66°C and 84°C, respectively, at about 60 and 84 hours. The numerical simulation results along the pile's concrete portion at the position TWL2 are also compared to the in-situ data obtained from the optical fiber placed within the sonic pipe, as presented in Figure 6. According to Figure 6, the temperature tended to fluctuate significantly along the backfilled soil and more uniformly along the length of the pile. The simulation results showed a resonably good agreement with the in-situ data.

The simulated evolutions of temperature distributions within the pile shaft over 15 days are shown in Figure 7(a). Within the first 12 hours, the temperature distributions in the pile were around 48°C. After 24 hours, the temperature in the pile's core increased to just over 70°C. On the third day, the temperature reached its peak, exceeding 80°C. Moreover, the temperature was higher closer to the pile's center, which can be attributed to the lower radial gradient of temperature and hence a slower rate of dissipation of hydration heat near the pile center.

Following the peak temperature, the pile gradually cooled down. However, it can be observed from Figure 7(a) that the temperature at the bottom of the pile was higher than in other regions due to the bell-out of the pile influencing heat dissipation. By the 15th day, the temperature near the bell-out could reach almost 57°C.

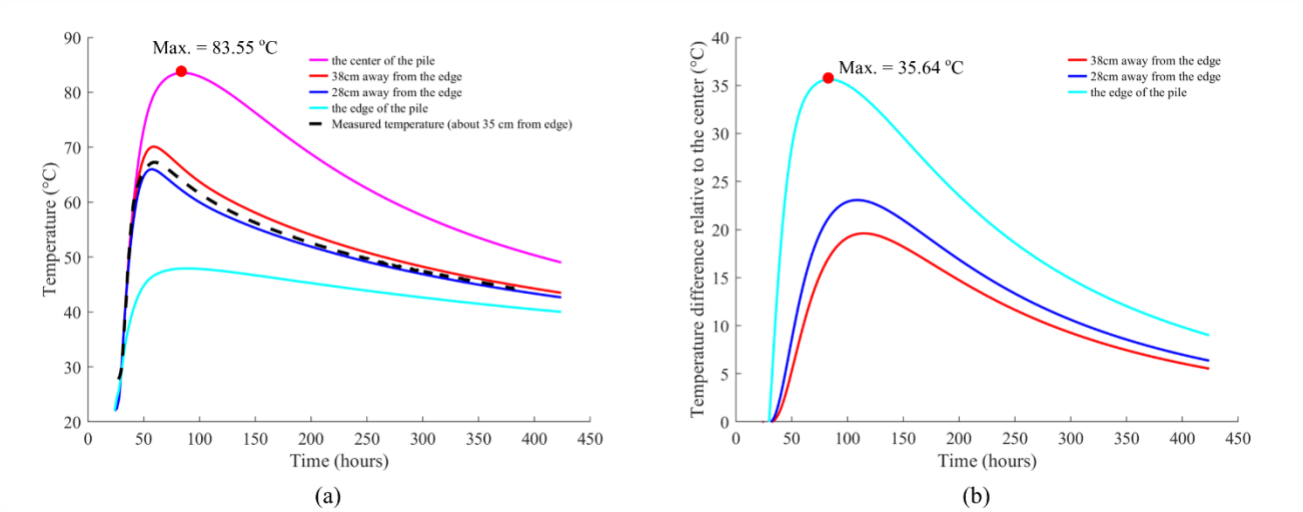

Figure 5: (a) Comparisons of the simulation (solid-lines) and in-situ measured temperature (dashed-line) evolutions of the pile at different locations at the same level of conventional temperature sensor; (b) Temperature differences relative the pile center's temperature at different locations.

During the hydration process, the stress in the steel reinforcement was induced by the increasing temperature due to thermal effects and deformation restraints. Figure 7(b) shows that the induced stress in the steel reinforcement near the pile head was the highest among the pile. On the first day, the maximum stress was 7.35 MPa, and when the temperature peaked, it also reached its highest value of 20.14 MPa. As the pile cooled, the maximum stress reduced to 8.44 MPa at 10 days.

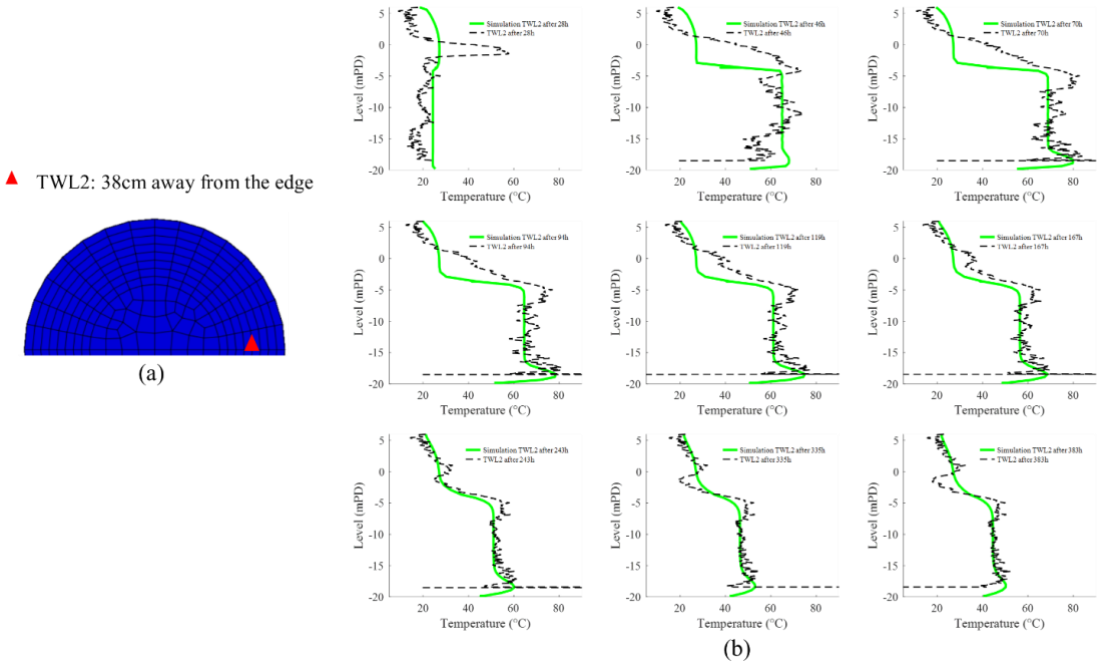

Figure 6: (a) The record location TWL2; (b) comparisons of the simulated and measured temperature distributions at different hours after concreting.

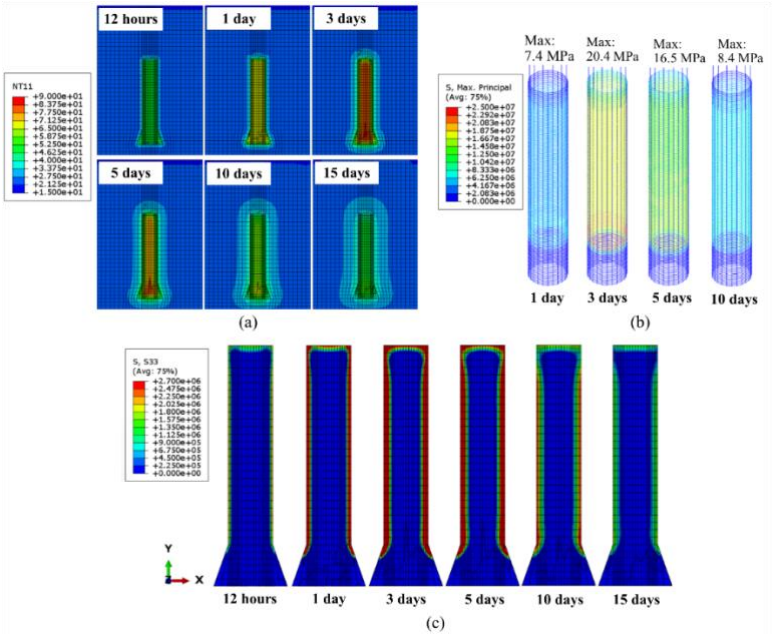

Figure 7(a): Simulated temperature distributions in the pile and surrounding soil and rock over 15 days (unit: ºC); (b) Simulated max. tensile stress in the steel reinforcement of the pile (unit: Pa) ; (c) Simulated radial stress in the concrete (unit: Pa)

3.5 Internal restraint of the bored pile

In the absence of a specific methodoloy for assessing the reinforcement needed to control the crack width of concrete in bored piles, the method proposed in CIRIA Report C766 may be adopted as an approximation for this particular case history. According to CIRIA Report C766 (Bamfoth 2018), when the internal restraint dominates the design of reinforcement for control of cracking, the restrained strain may be estimated by:

$$\varepsilon_r = K_{c1} \times \Delta T \times \alpha_c \times R_1 \quad (3)$$

where $K_{c1} = 0.65$; $R_1 = 0.42$; $\Delta T =$ the difference in temperature between the center and the surface. In this case, the maximum temperature difference was 35.64℃ (Figure 5(b)); $\alpha_c = 10^{-5}/℃$, which is the coefficient of thermal expansion. Then, the restrained strain is equal to $\varepsilon_r = 9.73 \times 10^{-5}$. The crack-inducing strain is calculated by:

$$\varepsilon_{cr} = \varepsilon_r - 0.5\varepsilon_{ctu} \quad (4)$$

where $\varepsilon_{ctu} =$ tensile strain capacity. The tensile strain capacity ε_{ctu} is calculated using the expressions:

$$\varepsilon_{ctu}(t) = 1.08\frac{f_{ctu}(t)}{E_{cm}(t)} \quad (5)$$

with the tensile strength $f_{ctu}(t)$ and elastic modulus $E_{cm}(t)$ derived from BS EN 1992-1-1:

$$E_{cm}(t) = (\frac{f_{cm}(t)}{f_{cm}})^{0.3}E_{cm} \quad (6)$$

$$f_{ctu}(t) = (\beta_{cc}(t))^{\alpha} \cdot f_{ctu} \quad (7)$$

where E_{cm} and f_{cm} are the values determined at the age of 28 days, and $\alpha = 1$ for $t < 28$. According to BS EN 1992-1-1, for concrete strength C60, E_{cm} and f_{cm} are 39 GPa and 68 MPa, respectively. $f_{cm}(t)$ and $E_{cm}(t)$ are the values at an age of *t* days. $f_{cm}(t)$ is estimated from:

$$f_{cm}(t) = \beta_{cc}(t)f_{cm} \quad (8)$$

$$\beta_{cc}(t) = \exp\{s[1 - (\frac{28}{t})^{1/2}]\} \quad (9)$$

where *t* is the age of the concrete in days; *s* is a coefficient that depends on the type of cement. According to the results presented in Figure 5, the maximum temperature difference occurred at 84 hours, while the hydration heat began to release (setting) at about 24 hours. Therefore, the age of the concrete *t* is about 60 hours or 2.5 days. The coefficient *s* depends on the different strength classes of cement. For the calculation, *s* was taken as 0.20 (Bamfoth 2018). Then, $f_{ctm}(2.5) = 2.75$ MPa and $\varepsilon_{ctu}(2.5) = 8.77 \times 10^{-5}$ that result in the crack-inducing strain $\varepsilon_{cr} = 5.34 \times 10^{-5}$. To control the crack spacing, the areas of circular links, setting aside the requirement for providing the required shear capacity for resisting the lateral loads on the bored pile, should be sufficient such that steel yielding will not happen even when a crack occurs. BS EN 1992-1-1 defines the

minimum area of reinforcement $A_{s,min}$ according to the equation:

$$A_{s,min}\sigma_s = k_c k f_{ct,eff} A_{ct} \quad (10)$$

where $A_{s,min}(\mathrm{mm}^2/m)$ is the minimum area of horizontal reinforcing steel per unit meter within the tensile zone; $A_{ct} = 1.11\ \mathrm{m}^2/\mathrm{m}$ is the area of concrete per unit meter within the tensile zone; $\sigma_s =$ absolute value of the maximum stress permitted in the reinforcement after the formation of a crack, and it could be taken as the yield strength of the steel, f_{yk}; $f_{ct,eff} =$ tensile strength of the concrete effective at the time when the cracks may first be expected to occur. For internal restraint dominant, the coefficients, k_c and k, are 0.5 and 1.0, respectively.

For the bored pile, the yield strength of the steel was assumed as 500MPa. The tensile strength of the concrete effective $f_{ct,eff}$ was taken as $f_{ctm}(2.5) = 2.75$ MPa. Based on the FE model, the area of concrete within the tensile zone at 2.5 days is equal to $4.257\mathrm{m}^2$, which is the red and green regions illustrated in Figure 8. The minimum area of reinforcement for thermal crack control can be calculated by Eq. (10) is $0.0031\ \mathrm{mm}^2/\mathrm{m}$. Since the maximum elastic tensile stress $\sigma_{max,t} = 6.8$ MPa (Figure 8) exceeds the effective tensile strength at 2.5 days, $f_{ctm}(2.5) = 2.75$ MPa, cracks would occur in the pile and the crack opening direction would follow the maximum principal strain direction, which aligns with the maximum temperature gradient direction (Figure 8). Hence, vertical cracks can potentially develop in the pile, similar to the example shown in Figure 1.

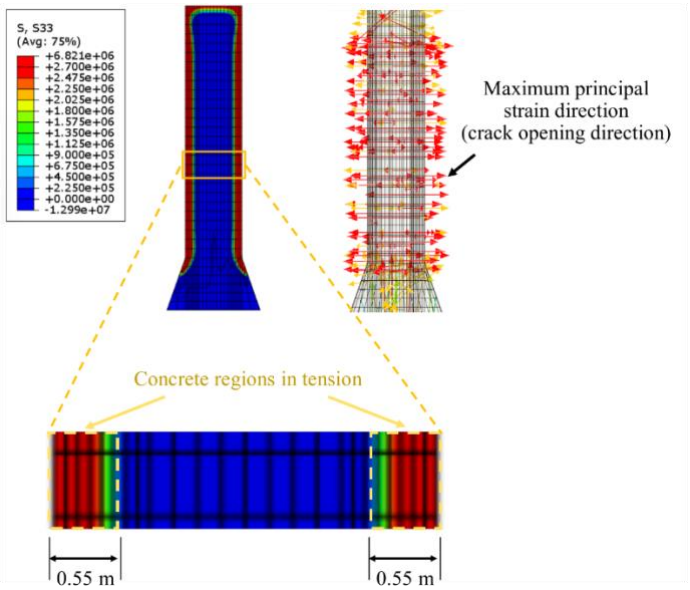

Figure 8: The concrete area within the tensile zone at 2.5 days.

To assess the effects of the vertical cracks, the maximum crack spacing, $S_{r,max}$, is calculated as follows:

$$S_{r,max} = 3.4c + 0.425\frac{k_1 k_2 \phi}{\rho_{ct,eff}} \quad (11)$$

where $c = 75mm$, which is the cover to the reinforcement controlling the cracking; k_1 is a coefficient that

takes account of the bond properties of the reinforcement; BS EN 1992-1-1 recommends a value of 0.8 for high bond bars; $k_2 =$ a coefficient that takes account of the distribution of strain. For direct tension, $k_2 = 1.0$. The bar diameter is $\phi = 16$ mm; $\rho_{ct,eff} = A_s/A_{c,eff} = 0.0065$ is the ratio of the area of reinforcement to the effective area of concrete with the provided horizontal reinforcing steel (i.e. circular links) (T16@150 mm) per unit meter $A_s = 0.0027\ \mathrm{m}^2/m$; $A_{c,eff} = 0.415\ \mathrm{m}^2/\mathrm{m}$ is the effective area of concrete in tension around the reinforcement to a depth of $h_{c,ef} = \min[D_a/2,\ 2.5(c + \phi/2)] = 0.2075$ mm with the pile diameter $D_a =$ 3 m and the concrete cover $c = 75$ mm. Therefore, the maximum crack spacing calculated by the Eq. (11) is 1.098 m. BS EN 1992-1-1 gives the equation for the estimated surface crack width as follows:

$$\omega_k = S_{r,max} \cdot \varepsilon_{cr} \tag{12}$$

Hence, the potential crack width for the bored pile is 0.06 mm, less than the limiting crack width for the serviceability limit state (Bamfoth 2018) for this particular case study, as summarized in Table 3.

Table 3: Limiting crack widths (Bamfoth 2018)

Limit state	Limiting crack width (mm)	Position of assessment
Durability	0.3	Recognizing that cracks taper from the surface to the reinforcement, if the cover is greater than that required for durability, the allowable crack width may be estimated at the specified depth of cover required for durability.
Serviceability	0.05 – 0.2	Through cracks will vary in width to a lesser extent than flexural cracks.
Appearance	0.3 or greater	At the surface.

4 DISCUSSIONS AND CONCLUSIONS

A rigorous coupled thermal-mechanical finite element model was successfully developed to analyze the thermal stress in large-diameter Grade C60 HSC bored pile, and verified by temperature measurements obtained by optical fiber and conventional temperature senor in field tests. The simulated time evolution of the temperature distributions in the piles matched reasonably well with the field measurements. The simulation also obtained the stress history in the steel reinforcement caused by the coupled thermal gradient and deformation restraint, which identified the potential locations of thermal crack development.

The field tests measured the temperature developments near the pile edge, which were adequately captured by the simulation. The simulation showed that the highest temperature of nearly 85°C occurred in the pile center. While the vertical temperature variation along the pile is not high, significant horizontal temperature gradients occur across the cross-sections of the pile. Under the combined actions of the internal deformation restraint and

horizontal temperature gradients, radial tensile stress would develop and can possibly lead to vertical cracks in the pile.

According to the simulation results, the tension zone occurs closer to the pile edge. This may explain why such thermal cracks are not usually detected and hence overlooked by practitioners because proof drilling of concrete is normally carried out near the pile center to avoid intersecting the reinforcement bars of bored piles.

The numerical modelling presented in this paper has demonstrated that tools are available for assessing the potential of vertical cracking occurring due to thermal effects. To mitigate the possible effects of vertical cracks on the performance of bored piles, the steel content of circular links should be increased to control the spacing and hence the crack width. More research is needed to establish simpler and more practical rules for reinforced concrete design of bored piles for controlling the effects of thermal cracking that are expected to occur for large diameter bored piles, particularly for piles constructed using HSC.

ACKNOWLEDGEMENTS

The authors would like to express their gratitude for the funding support by the Ministry of Science and Technology, R.O.C. under Grand Number 111-2221-E-A49 -016-. We sincerely thank the research team from the Department of Civil & Environmental Engineering, Polytechnic University of Hong Kong, for completing the field study under the supervision of Dr. Andy Leung and Professor J.H. Yin.

REFERENCES

ABAQUS Inc. (ABAQUS) 2020. *ABAQUS Analysis User's Manual*.

ACI Committee 207 (ACI). 2012. *ACI PRC-207.1-05: Guide to Mass Concrete*.

Bamforth, P.B. 2007. *Early-Age Thermal Crack Control in Concrete*. CIRIA Report C660, London.

Bamforth, P.B. 2018. *Control of Cracking Caused by Restrained Deformation in Concrete*. CIRIA Report C766, London.

CEN. 2004. *Eurocode 2: Design of Concrete Structures. Part 1: General Rules and Rules for Buildings (EN 1992–1-1:2004)*. European Committee for Standardization, Brussels.

Cho, W.J., Kwon, S., & Choi, W. 2009. The thermal conductivity for granite with various water contents. *Engineering Geology* 107 (3–4): 167–71.

Chow, T.T., Long, H., Mok, H.Y. & Li, K.W. 2011. Estimation of soil temperature profile in Hong Kong from climatic variables. *Energy and Buildings* 43 (12): 3568–75.

Claisse, P. A. 2016. Admixtures for concrete. *Civil Engineering Materials*, 251–58. Elsevier.

Do, T.A., Hoang, T.T., Bui-Tien, T., Hoang, H.V., Do, T.D. and Nguyen, P.A. 2020. Evaluation of heat of hydration, temperature evolution and thermal cracking risk in high-strength concrete at early ages. *Case Studies in Thermal Engineering*, 21 (October): 100658.

Geotechnical Engineering Office (GEO). 2006. *GEO Publication No. 1/2006: Foundation Design and Construction*.

Hamdhan, I.N., Clarke, B.G. 2010. Determination of thermal conductivity of coarse and fine sand soils. *Proc. World Geothermal Congress 2010*, Bali, Indonesia, 25-29.

Kim, S.G. 2010. *Effect of Heat Generation from Cement Hydration on Mass Concrete Placement*. MSc Thesis, Iowa State University.

Kou, H.L., Diao, W.Z., Liu, T., Yang, D.L. & Horpibulsuk, S. 2018. Field performance of open-ended prestressed high-strength concrete pipe piles jacked into clay. *Sensors*, 18(12).

Kwan, A.K.H. and Ng, I.Y.T. (2004). `Avoiding early thermal cracking in concrete structures: to insulate or not to insolute?", Hong Kong Engineer, Feb Issue, 15-16.

Larisch, M.D. 2011. Experience with high strength concrete for the foundation of a high rise building. *9th Symposium on High Performance Concrete*. Rotorua, New Zealand.

Lumb, P. 1983. Engineering properties of fresh and decomposed igneous rocks from Hong Kong. *Engineering Geology*, 19: 81–94.

McCarthy, M.J., and Dyer, T.D. 2019. Pozzolanas and pozzolanic zaterials. *Lea's Chemistry of Cement and Concrete*, 363–467. Elsevier.

PolyU Technology & Consultancy Company Ltd. (PTCCL). 2022. *Temperature Monitoring of Two Concrete Piles Using Distributed Fibre Optic Sensors*.

Robertson, E. C. 1988. *Thermal Properties of Rocks*. Open File Report 88-441, U. S. Geol. Survey, Reston, Va.

Shi, C., Wang, D., Wu, L. & Wu, Z. 2015. The hydration and microstructure of ultra high-strength concrete with cement–silica fume–slag binder. *Cement and Concrete Composites* 61 (August): 44–52.

Smeplass, S. & Maage, M. 1990. Heat of hydration of high-strength concretes. *ACI Symposium Paper* 121: 433–56.

Vecchio, F. J. & Collins, M.P. 1986. The modified compression-field theory for reinforced concrete elements subjected to shear. *ACI Journal*. 19(16): 219–23.

Voort, T.V., Suleiman, M.T. & Sritharan, S. 2008. *Design and Performance Verification of Ultra-high Performance Concrete Piles for Deep Foundations*. Centre for Transportation Research and Education, Iowa State University.

Wypych, G. 2021. Fillers – origin, chemical composition, properties, and morphology. *Handbook of Fillers*, 13–302. Elsevier.

Recent Developments of Drilling Techniques for Construction of Foundation Works

Jukka Ahonen
Mincon Nordic Oy, Finland
Victor Li
Victor Li & Associates Ltd., Hong Kong

ABSTRACT

The sinking of a drillhole into the ground (or overburden drilling) for installation of pipe piles for shoring works and cased excavation for construction of pile foundations is an important type of geotechnical works. The Odex system, which was the dominant technique for overburden drilling in Hong Kong some 20 years ago and notorious for causing problems such as ground subsidence and sinkhole formation, is seldom used nowadays. There have been significant developments in the technology of overburden drilling since the introduction of the Odex system. In this paper, the problems associated with the traditional techniques of overburden drilling are discussed. Two pieces of recently introduced equipment which can mitigate or eliminate the problems caused by conventional equipment are described. They include the Spiral Flush pilot bit which can reduce the likelihood of air leakage and an entirely different system named the Airless Flushing system which uses water instead of compressed air as the flushing medium for removal of cuttings. A case study which demonstrates the benefits of the Spiral Flush drillbit will also be described.

1 INTRODUCTION

Geotechnical works often involve overburden drilling which is the formation of a circular drillhole in the ground such as for installation of pipe piles as embedded walls for shoring works or cased excavation for construction of king posts and pile foundations. Overburden drilling is conventionally conducted with the help of a steel casing and an assembly of equipment placed inside the casing comprising the drill rod, a down-the-hole (DTH) hammer and a drillbit connected to the hammer. The compressed air will lift and drop the piston of the DTH hammer to produce percussive action of the drillbit. The combined percussive and rotatory action of the drillbit will cause the soils, rocks or hard obstructions below the casing toe to be broken up. The cuttings produced by the drillbit will then be air-lifted and removed by the compressed air, hopefully through a path confined entirely within the steel casing.

There are inherent problems associated with drillbits operated by compressed air. The compressed air may leak outside the steel casing, causing overbreaks to be formed around the casing and below the casing toe. Further air leakage may be exacerbated by these overbreaks. The end results are that ground subsidence and formation of sinkhole are frequently found to occur next to the drillhole, particularly for deep overburden drilling. If there are existing buildings close to the drilling operation, excessive building settlements may also be induced.

In this paper, problems associated with conventional techniques of overburden drilling are discussed. Recent developments which can mitigate some of the adverse effects will be described, including a recently developed pilot bit named the Spiral Flush system which can better control the leakage of compressed air and a new technique called the **A**ir**l**ess **F**lushing (ALF) system which uses water instead of compressed air as the flushing medium for removal of cuttings.

2 CONVENTIONAL TECHNIQUES

The Odex system (which stands for **o**verburden **d**rilling **ex**centric) used to be the most popular technique for overburden drilling in Hong Kong. The Odex drillbit comprises a pilot bit and an excentric reamer. During overburden drilling, the drill rod will rotate in one direction. When the assembly of reamer and pilot bit has protruded entirely outside the casing toe, the excentric reamer will swing out to form a hole larger than the external diameter of the steel casing. The oversized drillhole enables the casing to be advanced in phase with the drillbit. When drilling is completed, the drill rod will rotate in an opposite direction and the excentric reamer will retract to become smaller in size than the inner diameter of the steel casing allowing the drillbit to be retrieved from within the steel casing.

In the past, the Odex system had often led to problems of ground subsidence, sinkhole formation and building settlement and/or tilting for geotechnical projects in Hong Kong. Figure 1 presents two examples of such problems reported by Li et al (2018) caused by overburden drilling using the Odex system. Figure 1(a) shows a masonry wall with more than 0.5m of settlement observed during construction of mini-piles in front of the wall using 219mm diameter steel casing. Figure 1(b) is an example of sinkhole formed during construction of rock-socketed H-piles using 610mm diameter steel casing. It is therefore not surprising that the Odex system is now seldom permitted for geotechnical projects in Hong Kong.

(a) (b)

Figure 1: (a) Settlement of masonry wall and (b) formation of sinkhole (Li et al. 2018)

There are two main problems associated with the Odex system. The first problem concerns the use of compressed air for removal of cuttings from the drillhole. The second problem arises from the Odex drillbit protruding entirely outside the toe of steel casing during overburden drilling.

The first problem also occurs to a differing degree for other drilling systems operated by compressed air. The air pressure required to overcome hydrostatic water pressure will be about 100 kPa (or 1 bar) for every 10m depth of water. For deep overburden drilling, say, to a depth of 50m or more which is not uncommon for socketed H-pies in Hong Kong, the air pressure required to overcome the water pressure alone will be 500 kPa (or 5 bars). The air pressure needed to both overcome the water pressure and flush out the cuttings will be even higher. For this reason, air compressors capable of generating an air pressure of 10 to 15 bars are commonly used for overburden drilling in Hong Kong.

Under a high air pressure, high velocity air/water jets will be formed at the flushing holes in the drillbit in a manner similar to that shown in Figure 2. Such air/water jets can easily cause overbreaks to be formed in soft soils. Overbreaks can also occur in dense soils if subjected to prolonged water jetting when blockage occurs in the steel casing making advance of drilling very slow. When overbreaks develop into progressively larger soil cavities with time, ground subsidence may happen due to loss of ground and a sinkhole will eventually occur if collapse of a large soil cavity occurs.

Figure 2: Water jet created by high pressure at outlet holes of drillbit

There have been improvements made to the design of drillbit by foundation equipment companies since the introduction of the Odex system. For instance, a revised design with a smaller retractable reamer is used in the Super Maxbit system (MMC 2004). However, the reamer will still protrude beyond the casing toe during overburden drilling and hence will suffer from a similar albeit lesser drawback as the Odex system.

To prevent the drillbit from protruding beyond the casing toe, the ring bit system has been developed by various manufacturers to be used in conjunction a pilot bit. Figure 3 shows an example of a ring bit used for installation of interlocking pipe piles. A ring bit is a sacrificial ring-shaped rotary drillbit fixed onto the steel casing by welding. The outer diameter of the ring bit is slightly larger than the outer diameter of steel casing to create a slightly oversized drillhole to allow the casing to advance smoothly in phase with the drillbit. For installation of interlocking pipe piles, the size of the ring bit needs to be sufficiently large to accommodate the interlocking joints within the drillhole.

Another drillbit called the pilot bit will be placed inside the steel casing. When the drill rod rotates in a specified direction, the pilot bit will engage the ring bit such that both drillbits will rotate in phase for forming the drillhole. After completion of drilling, the rotation of the drill rod is reversed to disengage the pilot bit with the ring bit to allow the pilot bit to be retrieved from within the steel casing. With this setup, the task of creating an oversized drillhole will now be undertaken mainly by the ring bit as compared with retractable reamer in the Odex system. There is now no need for the pilot bit to protrude extensively beyond the casing toe. Such a drilling system is commonly called the “concentric method” in Hong Kong.

Figure 3: Example of a ring bit

There are also a variety of pilot bits developed by different manufacturers for the concentric method of overburden drilling. Examples of such systems include Rotex Symmetrix, Robit, Bulroc, Stabotec, Elemex and etc. They differ in the layout of contact surfaces at the end face of the pilot bit, the design return paths for compressed air and the extent of protrusion beyond the casing toe. Figure 4(b) and (c) show the end view of the pilot bit/ring bit assembly for two conventional overburden drilling systems in the market, named Design 1 and Design 2 in this paper. The tungsten carbide inserts on the drillbits are not shown for clarity. The majority of pilot bits in the market have the flushing air discharged from the flushing holes in a vertical or subvertical direction as shown in Figure 4(a). The air/water jets created by the flushing air can have significant erosion power to cause overbreaks to be formed if the air pressure is not properly controlled during drilling. Although there must be flushing channels provided at the pilot bit for the flushing air to return to the steel casing, leakage of flushing air can occur through the easier alternative paths if there are overbreaks outside the steel casing. Such uncontrolled leakage of flushing air can cause the overbreaks to become even larger and more extensive.

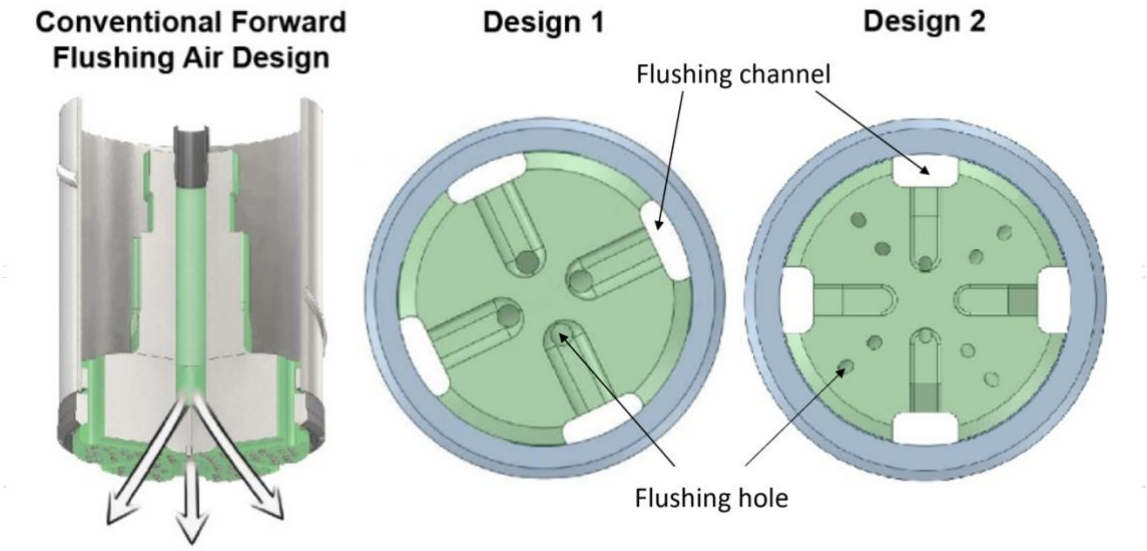

(a) Direction of flushing air (b) Design 1 (c) Design 2

Figure 4: Details of some conventional drillbits in the market

3. RECENT DEVELOPMENTS

Two recent developments for overburden drilling are now discussed, including the Spiral Flush pilot bit which has a different design for the return path for the flushing air and the ALF system which utilize water as the flushing medium.

3.1 Spiral Flush pilot bit

The Spiral Flush pilot bit recently introduced to the market have two distinct features. First, the Spiral Flush pilot bit is practically flush with the ring bit. This can reduce the chance of the flushing air leakage out of the steel casing. Second, the flushing air design is such that the flushing holes are placed in a radial direction at the pilot bit. This will avoid direct impact of the air/water jets onto the materials to be excavated and allow the flushing air to return to the casing more easily in a shortest possible path to reduce the chance of air leakage.

Figure 5(a) shows the anticipated return paths of flushing air to the steel casing and Figure 5(b) a schematic view of the end face of a Spiral Flush pilot bit/ring bit assembly.

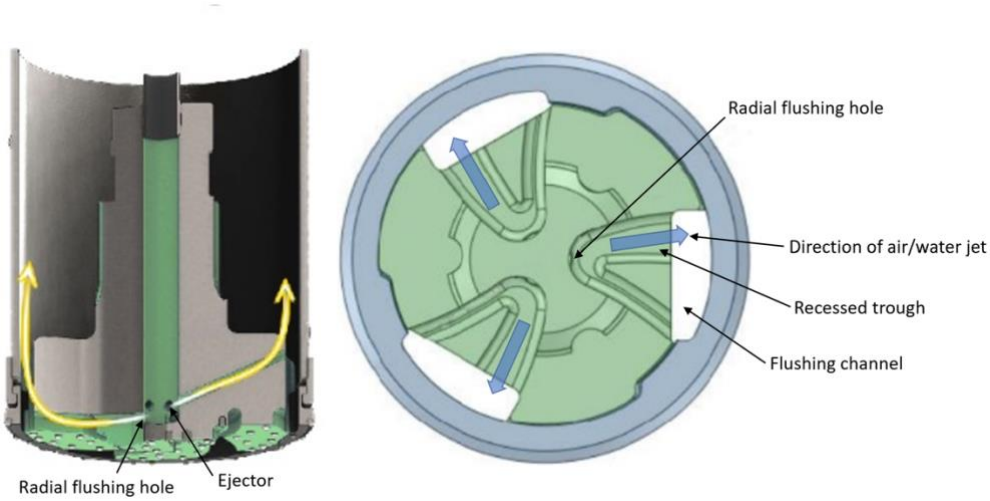

(a) (b)

Figure 5: Details of Spiral Flush bit (a) direction of flushing air; (b) end face of pilot bit/ring bit assembly

As indicated in Figure 5(a), there are two groups of release holes for the compressed air, including the flushing holes and the ejectors. The radial flushing holes are located at the bottom of the pilot bit. The radial air/water jet created by the flushing holes will flush the cuttings along the recessed trough or groove provided at the end face of the pilot bit toward the flushing channels. The cuttings will then be removed by air lifting from within steel casing. The ejectors are upward inclined holes located on the pilot bit at a higher level inside the flushing channel. The compressed air supplied to the pilot bit will be partially discharged through ejectors to create a vacuum in the flushing channel. This will enable the flushing water mixed with the cuttings to enter the flushing channels more easily and become subsequently removed by air lifting inside the steel casing.

Figure 6 presents photographs of the prototype Spiral Flush pilot bit, giving a better indication of the flushing holes, the ejectors and the recessed trough between flushing holes and the flushing channel.

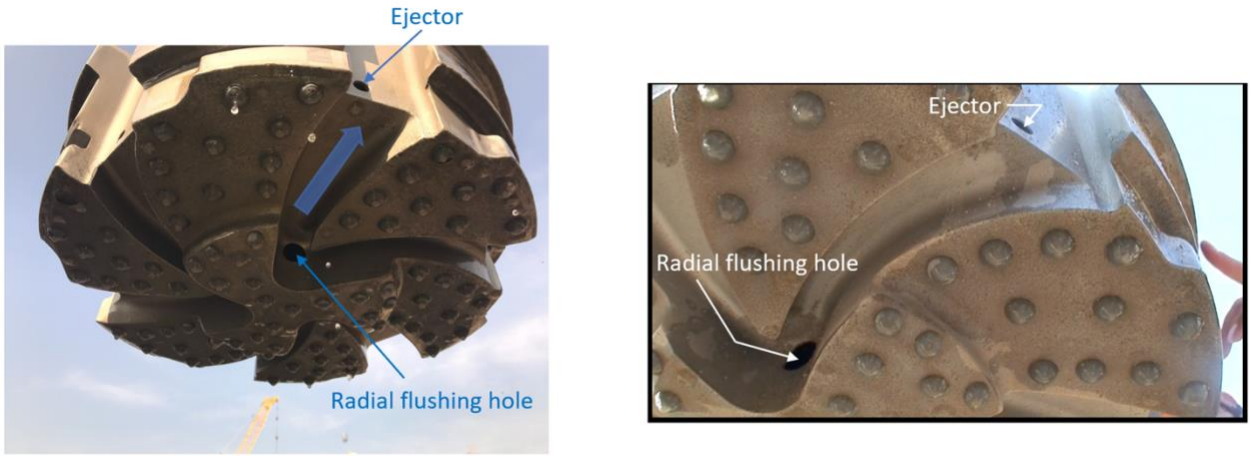

(a) (b)

Figure 6: Photographs of Spiral Flush pilot bit (a) overall view; (b) close-up view showing the horizontal nozzle for compressed air

The major problems associated with overburden drilling operated by compressed air are the potential of air leakage and the likelihood of overbreak. To assess whether the Spiral Flush pilot bit will lead to a better performance than conventional pilot bits, computational fluid dynamics (CFD) analyses have been conducted

by ECE (2019) using the program Ansys Fluent to simulate the release of compressed air into the pilot bit. The program is a general-purpose software for modelling fluid flow, heat and mass transfer, Three performance indicators are used for evaluation, including the amount of mass flow penetrating the soils, the velocity of the soil medium and the induced pressure below the pilot bit. Three pilot bits are considered, including the Spiral Flush and two other pilot bits named Design 1 and Design 2 shown earlier in Figure 5(b) and 5(c) respectively. The ease with which air can penetrate through a soil medium can be characterized by the intrinsic permeability of soil to air, or simply air permeability of soil, k_a. It has the SI unit of m^2. The meaning and measurement of air permeability are discussed in Grant & Groenevelt (2008). In the study by ECE (2019), simulations have been performed for two different air permeabilities. In this paper, the results are presented only for an air permeability of 10^{-5} cm^2 which corresponds to well sorted sand or sand and gravel according to classification by Bear (1972). The analyses were conducted based on an air flow rate of 66 m^3/min.

Table 1: Amount of mass flow penetrating the soil

Type of pilot bit	Mass flow to soil (%)
Spiral Flush	8.8
Design 1	54.0
Design 2	44.5

Table 1 summarizes the percentages of air by mass penetrating the soils for the three pilot bits studied. It can be observed that the mass flow of air to soils for Design 1 and Design 2 are higher than that of the Spiral Flush pilot bit by 6.1 and 5 times respectively. This suggests that leakage of air to soil tends to be higher for conventional design with flushing air discharged in the vertical direction for soils of the same air permeability.

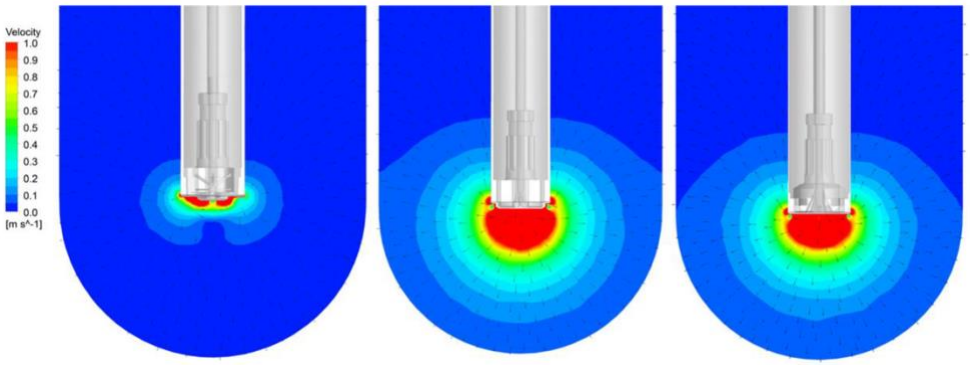

(a) Spiral Flush (b) Design 1 (c) Design 2

Figure 7: Velocity contour and normalized velocity vectors of the soil domain

Figure 7 shows the velocity contour and velocity vectors in the soil domain obtained from the simulation study. As expected, the velocity of the soil domain is higher for Design 1 and Design 2 as the soils are impinged directly by the vertical or subvertical air/water jets for such pilot bits whereas the soils are less disturbed by the radial air/water jets created by the Spiral Flush pilot bit.

Figure 8 shows the results for soil pressure at the bottom of the pilot bits. The soil pressure for Design 2 is less than that of Design 1 because compressed air is spread over 10 flushing holes for the latter and only 4 for the former. Hence, a lower contact pressure is expected. In comparison, the Spiral Flush pilot bit will induce significantly less soil pressure than the two other pilot bits and this can be attributed to the difference in the direction of air jet for Spiral Flush pilot bit. The trend for induced pressure is similar to that of velocity shown in Figure 7, being highest for Design 1 and much lower than for the Spiral Flush pilot bit.

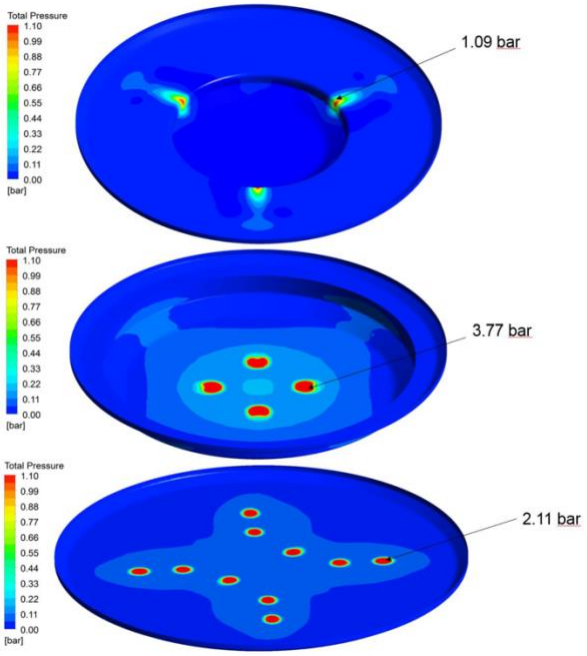

Figure 8: Pressure contours at the interface of soil domain and the pilot bit

According to the simulation study, the three performance indicators suggest that the Spiral Flush pilot bit should offer benefits over conventional pilot bits due to the difference in the direction of flushing in the equipment design. With similar operating conditions and soil types, the Spiral Flush pilot bit tends to have lower air loss to the soils and induce lower velocity and pressure on the soil domain. The end results are that air leakage and soil overbreaks should be less likely for the Spiral Flush pilot bit from a theoretical standpoint.

Figure 9: A large-sized Spiral Flush pilot bit

Field trials using the Spiral Flush pilot bit have been conducted in Hong Kong, including the trial report by Li et al. (2018) and another trial conducted for a public works project. The feedbacks from contractors are that the Spiral Flush pilot bit tend to cause less ground disturbance than conventional pilot bits.

The Spiral Flush system is now widely in Finland, Scandinavia, Middle Europe and North America. This is also a demand for a larger Spiral Flush pilot bit for forming large drillholes for which conventional drillbits are likely to cause significant problems. Figure 9 shows a large-sized Spiral Flush pilot bit that can fit in a 1.524m diameter steel casing.

3.2 Overburden drilling using Airless Flushing

Due to the inherent problems associated with compressed air for overburden drilling, alternative drilling techniques using water as the flushing medium have been developed in the past. Examples of such drilling systems are discussed in Li et al. (2018). Unfortunately, such techniques are still not common in Hong Kong. This may be attributed to the unwillingness of foundation contractors or subcontractors to change or that there is no such requirement specified by the Engineer or the client in the foundation contract of banning compressed air for overburden drilling.

A new technique for overburden drilling, named the ALF system, has recently been developed by the first author. Similar to some existing systems, the ALF system utilizes compressed air for operating the DTH hammer and water for flushing of cuttings.

Figure 10 shows details of the ALF system. The compressed air is fed through a central hollow drill rod for operating the DTH hammer. There are swivels with a bladder near the end of the steel casing. Two pressure lines connected to the upper swivel are provided, one supplying flushing water to the pilot bit for removal of cuttings and the other supplying pressured air or water to activate the bladder. When activated, the bladder will seal the steel casing so that the compressed air released by the DTH hammer can only return to ground from inside the steel casing.

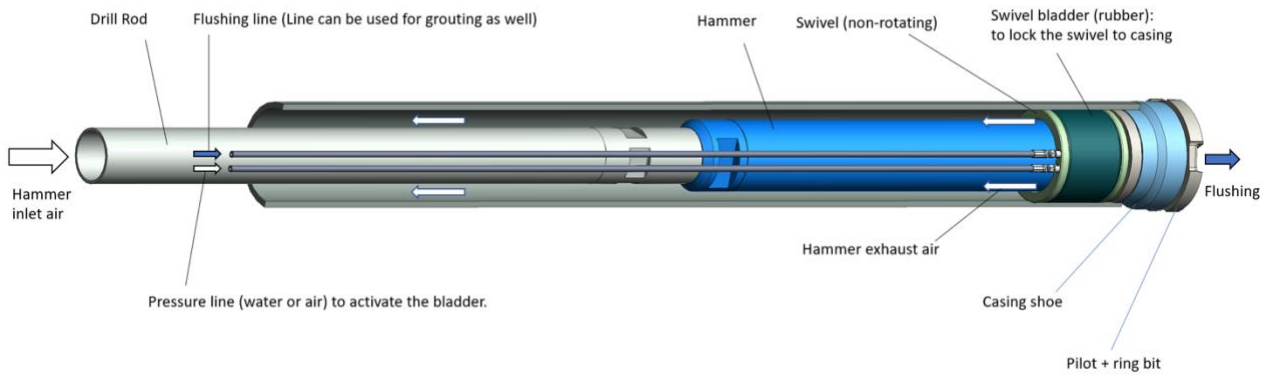

Figure 10: Details of ALF system

During overburden drilling, the ring bit will form a small annular gap or thin zone of weakened soil outside the steel casing. The pressurized flushing water supplied to the pilot bit will mix with the cuttings to form a slurry with suspended particles. The slurry will percolate through the void space outside the steel casing to the ground surface as shown in Figure 11.

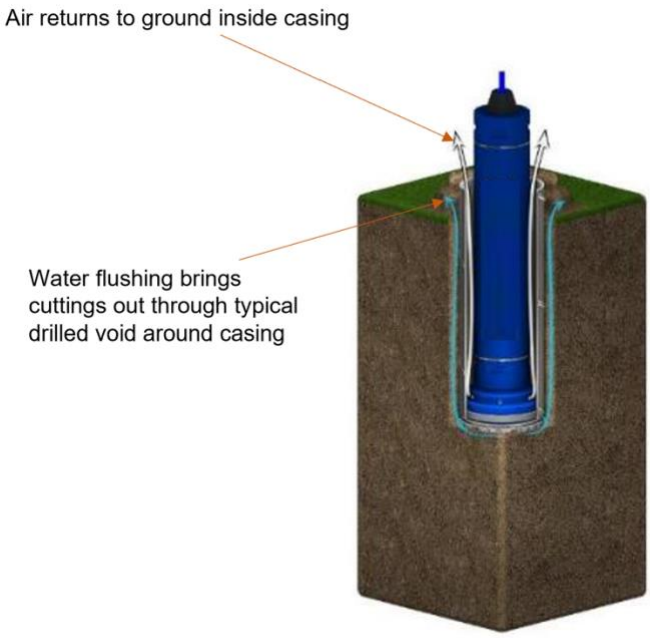

Figure 11: Flow paths of cuttings in ALF system

Figure 12 shows photographs of typical overburden drilling using the ALF system. The slurry containing the suspended particles of the cuttings escapes to the ground through the drilled void outside the steel casing as shown in Figure 12(a) while the compressed air is exhausted through the inside of the steel casing as shown in Figure 12(b).

Figure 12: Flow paths of air and water during drilling using the ALF system

When drilling is stopped, the suspended particles in the slurry will settle and fill up the voids outside the steel casing. When drilling is resumed after temporary suspension of works, flushing using water only will be carried out for a suitable period of time to re-create a water flow path in the filled-up voids outside the steel casing before re-commencement of overburden drilling.

To a certain extent, there exists a self-healing process when carrying out overburden drilling using the ALF system. Voids or overbreaks which are created during overburden drilling will initially provide drainage paths for discharge of the slurry. Such void space will later be filled in part or in full by the cuttings, thus reducing the chance of such voids from developing into large soil cavities or consequent ground subsidence.

If it is desired to strengthen the soils or to fill up the voids if any outside the steel casing upon completion of drilling, grout can be used in lieu of water for carrying out the final stage of airless flushing.

4 CASE STUDY

Although the Spiral Flush pilot bit has only been used in limited number of trials in Hong Kong to date, it is popular in Finland and many other parts of the world for overburden drilling for projects close to or abutting sensitive receivers such as old buildings vulnerable to damage caused by settlement. To eliminate the adverse effects of using compressed air as the flushing medium, the ALF system can be adopted to further reduce the risk of ground settlement caused by overburden drilling.

A case study involving the use of Spiral Flush pilot bit is now described. The project was an office building in Helsinki, Finland, completed in 2019. The development has a three-level carpark basement. The soil profile at the site is characterized by very compact till with a sloping bedrock varying from a depth of 6 to 10m below ground. The site is abutted by two old buildings, one of which was built in 1928 supported by a raft footing and the other was built in 1962 supported by driven concrete piles.

Pipe piles of 610mm diameter and 711mm diameter were used as the embedded wall for supporting the basement excavation. It was of prime importance to prevent settlement of the adjacent old buildings. To achieve this objective, the measures taken included:

(a) Installation of jet grout columns along the two sides of the site along the old buildings prior to installation of pipe piles;
(b) Use of Spiral Flush pilot bit for installation of pipe piles as an added precautionary measure to minimize ground loss or disturbance during overburden drilling;
(c) Use of interlocking joints for connecting pipe piles to prevent loss of ground between pipe piles during excavation. The interlocking joints were formed using the male and female connectors;
(d) Sealant was placed in female connector before installation. The sealant will then cut off the water flow in the interlocking joint during and after excavation;
(e) Grouting was carried out to seal the annular voids created by the ring bit in the rock socket and in soils outside the pipe pile.

The installation procedures of interlocking pipe piles using the Spiral Flush pilot bit for this project were similar to those discussed by Li et al. (2018), except that a slightly different design had been adopted for the female connectors. To enable grouting to be carried out after drilling, a special female connector as shown in Figure 13 was used. The female connector has two ribs which will form a channel for grouting when the two ribs are welded onto the casing. A non-return valve was provided to seal the end of female connector. When cement grout was fed into the channel of the female connector, the grout would emerge from the non-return value in a bottom-up manner to gradually fill up the annual voids in the rock socket and in soils.

The grouting operation was found to be very successful as the annular voids were observed to be fully filled during excavation. Figure 14 shows a photograph of the hardened cement grout observed in granite of the rock socket exposed during excavation.

The excavation and lateral support works for the project had been completed successfully in a water-tight manner and without causing any settlement of the adjacent old buildings. Figure 15 shows a photograph of the pipe piles which had been installed using the Spiral Flush pilot bit.

Figure 13: Joint details (a) interlocking joints; (b) Female joint welded onto casing with non-return value at its end; (b) 3-D diagram of female joint and non-return valve

Figure 14: Grout observed in the rock socket during rock excavation

3 DISCUSSIONS AND CONCLUSIONS

In Hong Kong, geotechnical designers are not as familiar as they should with foundation construction and equipment. As a result, the construction procedures or equipment specified in the drawings or specifications may not necessarily be appropriate for ensuring that the adverse effects associated with overburden drilling are kept to a minimum.

Geotechnical works in Hong Kong are also highly competitive. The works are usually subcontracted by the main contractor to various sub-contractors of different trades and often on a lump-sum or fixed rate basis for them to share the risks. To win the contract, the main contractor and/or the sub-contractors may sometimes take risk in order to keep the bidding competitive. Even if the right equipment has been specified by the Engineer, it is not uncommon for contractors to only keep limited sets of the specified equipment on site for display purpose and actually use cheaper counterfeit or copycat equipment, which may have doubtful performance, for construction in order to keep the costs down.

Figure 15: Pipe piles installed using Spiral Flush pilot bit adjacent to the 1962 old building

Improved construction equipment such as those described in this paper has been available in the market for some time. The costs of remedial works are often much higher than those of using the right equipment and adopting the appropriate procedures for construction. If our goals are to advance the practice of overburden drilling, geotechnical engineers, including those working in regulatory authorities, should be more acquainted with the new developments of foundation equipment so as to stipulate and only approve the suitable techniques for construction. Efforts should also be made by the Engineer to ensure that once an appropriate equipment or construction procedures have been specified or approved, contractors/sub-contractors should be discouraged from cutting corners to risk causing unwanted effects during construction.

More trials of overburden drilling using newer and safer techniques should be conducted by contractors or specified/encouraged by the Engineer to build up a wealth of experience for the selection of the right drilling equipment for different ground conditions in Hong Kong.

ACKNOWLEDGEMENTS

The authors are grateful to Mr. Falco Chu of Unicon Ltd. for his assistance in preparing this paper.

REFERENCES

Bear, J. 1972. *Dynamics of Fluids in Porous Media*. Dover Publication, Inc.

Elomatic Consulting & Engineering (ECE) 2019. *Mincon CFD Study – Simulation Report*.

Grant, C.D. & Groenevelt, P.H. 2008. Chapter 61 – Air Permeability. In M.R. Carter & E.G. Gregorich (ed.) *Soil Sampling and Methods of Analysis*. CRC Press.

Li, V., Ho, A. & Lo, C. 2018. A field trial for interlocking pipe piles. *Proc. HKIE Geotechnical Division Annual Seminar*. 82-90.

Mitsubishi Materials Corporation (MMC) 2023. *Super Maxbit/Super Maxbit G-Model – Operation Manual* (http://www.mitsubishicarbide.com/application/files/2615/5926/8509/RT14A_SMB_Operation_Manual_201905.pdf, accessed on 4 April 2023)

MACHINE LEARNING-BASED CONE PENETRATION TEST (CPT) DATA INTERPRETATION

Boyu Wang, Kelvin Tse, Clifford Phung

WSP (Asia) Limited

Abstract: Ground investigations (GI) are essential prior to the design of construction projects. Among the different GI tasks, classifying soils into groups with similar properties is a fundamental geotechnical engineering process. Currently, experienced geotechnical engineers manually conduct soil classification using empirical tables based on laboratory or in-situ tests, which is labor-intensive and time-consuming. This study presents a machine learning (ML)-based approach to inferring soil types based on Cone Penetration Test (CPT) data. To identify an appropriate classification model, three classic algorithms, including Support Vector Machine (SVM), Artificial Neural Network (ANN), and Random Forest (RF), were built and validated on data collected from a reclamation project (The Project). Four important attributes from CPTs, including tip resistance q_c, sleeve friction f_s, pore-pressure u_2, and depth d, were used as input features, and six soil types in The Project were applied as labels. The different models were compared based on their prediction performance and required learning time. The best results for both targets were obtained using the RF classifier, achieving over 90% accuracy.

Keywords: Cone Penetration Test, Machine Learning, Soil Classification

1. INTRODUCTION

Classifying soils into groups with similar properties is a fundamental engineering task during the preliminary stages of a construction project. However, during the feasibility stage, project-specific soil properties are not yet determined without investing in project-specific ground investigations (GI), which can be high-risk and costly. As investigating subsoil conditions using a combination of field and laboratory tests is inevitably associated with high costs, this process is often designed to be minimal. In recent years, the Cone Penetration Test (CPT) has become a popular and cost-effective tool for investigating subsoil conditions [8,10,11].

In a CPT, a cone with a specific diameter is pushed vertically into the ground at a constant rate, as shown in **Figure 1**. Based on the different measured data, such as tip resistance (q_c) and sleeve friction (f_s), various soil behavior charts have been developed to identify soil strata and behavior types. Additionally, various empirical correlations have been published to interpret CPT data quickly and easily (including parameter determination). CPTs are mainly performed to determine subsoil conditions, such as soil type and stratification, and to estimate shear strength parameters (e.g., effective friction angle ϕ', cohesion c, etc.). However, determining soil strata from CPT data requires manual processing using soil behavior type charts provided by Robertson [10,11], as shown in **Figure 2**, which is a time-consuming and error-prone task.

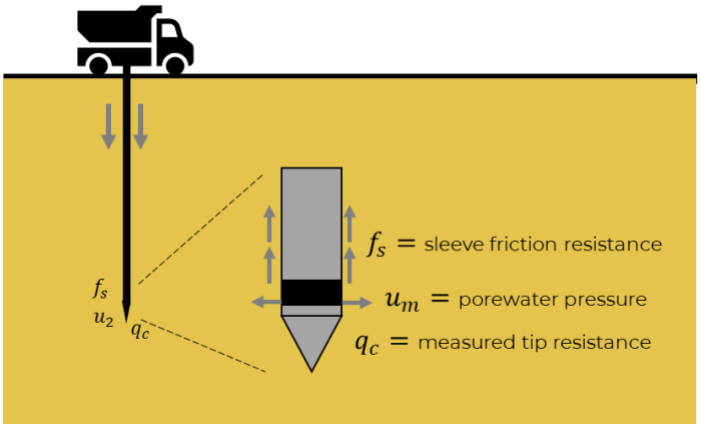

Figure 1. Overview of the CPT

There have been some research efforts to improve the accuracy and efficiency of CPT data interpretation. Wang et al. [12-15,17] focused on predicting soil stratification with limited data. For instance, Wang et al. [14] developed a Bayesian approach to explicitly model the uncertainty of the chart-based interpretation. Building on this work, Wang et al. [15] extended the Bayesian approach from one dimension (1D) to two dimensions (2D) and proposed a subsurface soil stratification and zonation method in a 2D vertical cross section. Zhao et al. [17] combined Markov Chain Monte Carlo with Bayesian Compressive Sensing (BCS) to achieve fast non-parametric simulation of 2D multi-layer CPT data. Shi and Wang [12,13] leveraged prior geological knowledge to construct three-dimensional (3D) subsurface geological models.

Meanwhile, with the rise of machine learning (ML), big data-driven approaches have also emerged as a promising trend. Over the last decade, the application of ML algorithms in civil engineering has gained more interest as it could play a key role in reducing costs and time needed for data analysis and prediction [6,8]. Machine learning techniques have been employed in previous studies to classify soils based on CPT data and to accurately estimate soil and design parameters [5, 9, 16]. In contrast to previous studies, the present investigation is based on an extensive dataset of 700 CPT tests that were conducted under similar soil and environmental conditions in Hong Kong. Three classic ML models were evaluated in terms of accuracy and learning time. The results demonstrate that the ML approaches can achieve over 90% accuracy in predicting soil type and significantly reduce the inference time for engineers.

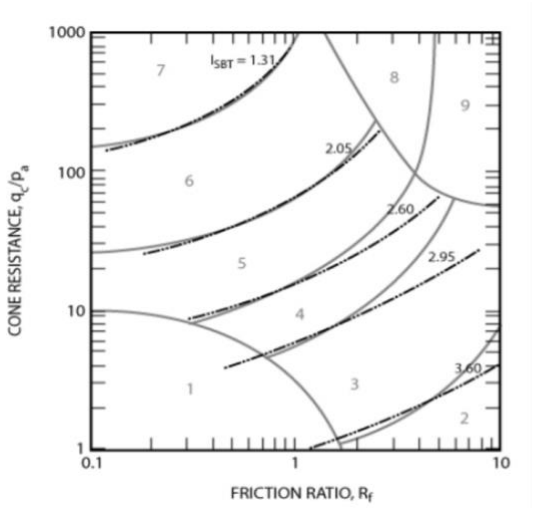

1. Sensitive fine-grained
2. Clay – organic soil
3. Clays: clay to silty clay
4. Silt mixtures: clayey silt & silty clay
5. Sand mixtures: silty sand to sandy silt
6. Sands: clean sands to silty sands
7. Dense sand to gravelly sand
8. Stiff sand to clayey sand *
9. Stiff fine-grained *

Figure 2. Soil behavior type charts provided by Robertson [10,11].

2. DATASET

The dataset consisting of 700 CPTs used for this study was collected from The Project. In total eight types of soil were considered including Marine Deposit (MD), Dumped Mud (DM), Dumped Sand (DS), Alluvium Sand (ALL-s), Intermediate Alluvium Clay (ALL-c(int)), Unweathered Alluvium Clay (ALL-c(unw)), Paleosol Alluvium Clay (ALL-c(pal)) and Grade V soil. As the soil properties of MD and DM are quite similar, this study did not differentiate the two classes purposely. The same strategy also applied to the soil types of DS and ALL-s. The soil strata information was obtained based on adjacent boreholes.

In this study, four crucial parameters obtained from CPTs - namely, tip resistance q_c, sleeve friction f_s, pore pressure u_2, and depth d - have been utilized as input features for predictive modeling. To ensure data quality, any rows with missing or null entries were removed since the sample size was sufficiently large. The dataset was then split into two subsets for training and validation using the scikit-learn tool "train_test_split" [7], which randomly divides the samples. In this study, 100 CPTs were used for training and the remaining 600 CPTs were used for validation. A sample of the CPT data is presented in **Figure 3**.

To ensure that each input feature contributes equally to the training and prediction process, the "StandardScaler" module was used to scale the features. This scaling process rescaled the features to lie between -1 and +1 while keeping the median at the same level, thereby avoiding any bias. Additionally, the uneven distribution

of data between the classes can pose challenges for many ML algorithms in making accurate predictions. In this study, a data resampling strategy was employed to address this issue. Specifically, an oversampling algorithm was used to fill the underrepresented classes with synthetic data generated from the available data, while overrepresented classes were removed to balance the dataset. Throughout this process, statistical parameters such as the mean and median of the data were kept at the same level, ensuring that the resampled data was representative of the original dataset.

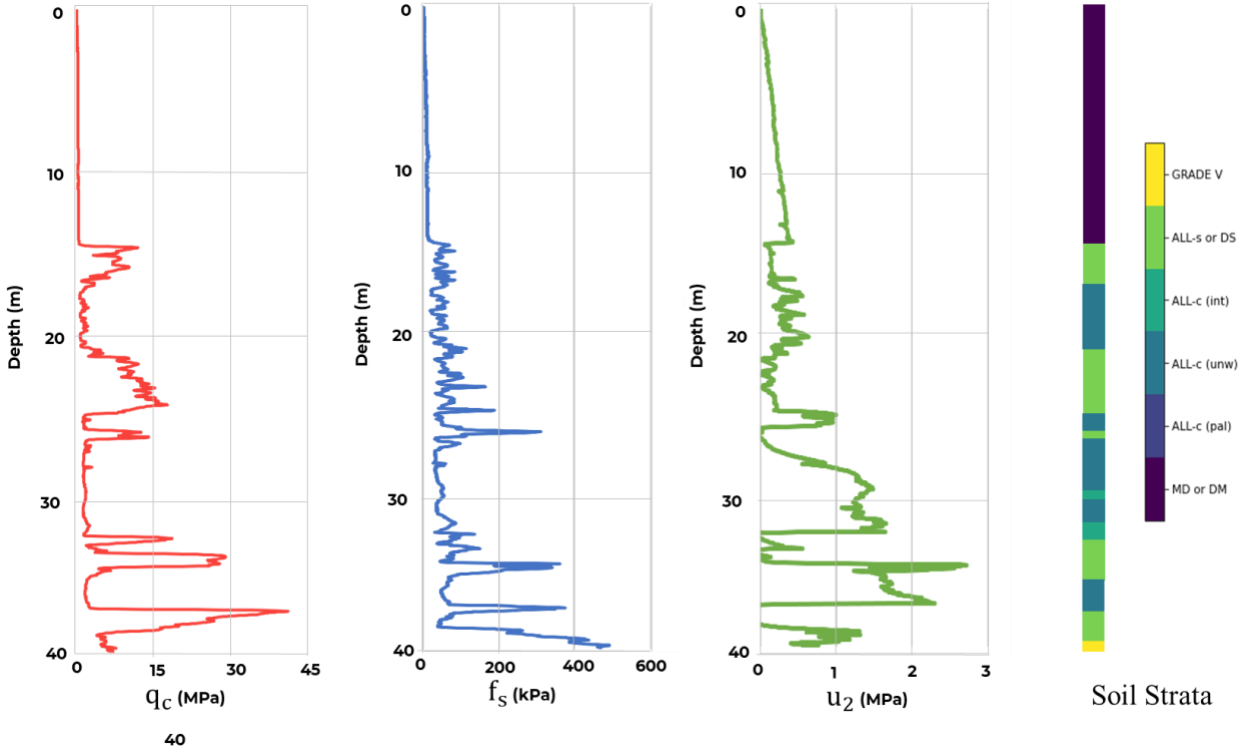

Figure 3. An example of measured data from a CPT (tip resistance q_c, sleeve friction f_s as well as pore-pressure u_2) and the corresponding soil strata.

3. MACHINE LEARNING MODELS

To efficiently interpret the collected CPT data, learning-based method is utilized in this study. ML has emerged as a popular tool for analyzing large datasets in various scientific fields. Unlike traditional computing algorithms that compute results based on input and predefined solutions, ML models learn from input features and their corresponding outputs (targets) to find solutions, regardless of the specific algorithm used [1]. This study evaluates three distinct ML algorithms - the Support Vector Machine (SVM) [3], Artificial Neural Network (ANN) [4], and Random Forest (RF) [2] - each with their own unique function principles, which are briefly described in the following subsections.

3.1 Support Vector Machine

The Support Vector Machine (SVM) is a supervised learning algorithm that can be used for classification, regression, and outlier detection [3]. For classification and regression tasks, the SVM algorithm aims to find separating hyperplanes in a high or infinite-dimensional space with the largest margin. A larger margin corresponds to a lower generalization error of the model. An example of a linear SVM is depicted in **Figure 4(a)**, where the samples on the boundaries are referred as support vectors. In this study, radial kernel function was used for the employed SVM model to achieve higher prediction accuracy.

3.2 Artificial Neural Network

The Artificial Neural Network (ANN) is inspired by the function principle of the human brain (as shown in **Figure 4(b)**) and is composed of three distinct types of layers: the input layer, where input features are inputted into the model; the hidden layer(s), where information from the input layer is combined with weights; and the output layer, where results are computed [4]. In this study, the backpropagation algorithm is used to train the neural network iteratively. During training, the model's output is compared with the real targets of the training set to calculate the error and update the weights in the hidden layers. This process continues until a minimum error is reached or the incremental improvement between iterations becomes negligible.

The ANN model was constructed using the MLPClassifier module of the scikit-learn library [7]. The best combination of hyperparameters was determined using grid search techniques, where a range of values for each parameter was defined. To ensure reasonable training time, the number of hidden layers was restricted to a maximum of three, with a maximum of 10 neurons per layer.

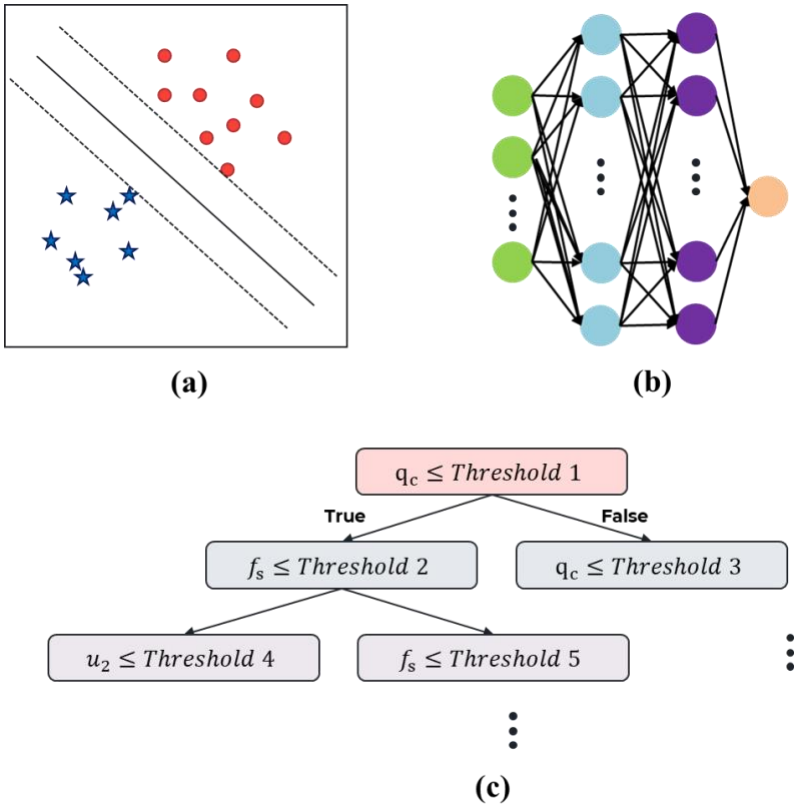

Figure 4. ML algorithm visualization. (a) SVM. (b) ANN. (c) RF.

3.3 Random Forest

The Random Forest (RF) is an ensemble of decision trees, where each decision tree is a non-parametric supervised learning method that summarizes decision rules from a series of data with features and labels [2]. Decision trees are capable of solving classification and regression problems by presenting the rules in a comprehensible tree structure that allows for the identification of each input feature's contribution to the model. As depicted in **Figure 4(c)**, decision trees consist of nodes responsible for different decision-making steps.

In this study, the RF classifier was implemented using the ensemble learning module of scikit-learn. Similar to the ANN models, the best set of hyperparameters was determined through cross-validation. Learning and validation curves were used to analyze the RF models and visualize bias and variance, which indicate susceptibility to overfitting or underfitting. To obtain a robust model, bias and variance should be kept low. Variance is represented by the difference between training and validation accuracy. High variance results in a model that is not able to generalize well, leading to much higher training accuracy than validation accuracy. High bias, on the other hand, indicates that

the data are too complex for the model. One of the primary hyperparameters that governed bias and variance in an RF model was the maximum size of each tree ("max_depth") in the forest.

3.4 Post Processing

To enhance the consistency of prediction results from machine learning (ML) models, a smoothing technique has been developed. For each predicted label at a specific position, the k neighboring labels are examined. If the most frequent labels above and below the query position are the same, and the predicted label is different from the frequent label, the frequent label will be assigned to the query position. This approach helps to eliminate noise and improve the robustness of the prediction results.

4. TRAINING, VALIDATION & TESTING

In this section, the performance of the three built ML models on the prepared dataset are reported. The experiment settings are described in detail.

4.1 Experiment Procedure

Following data pre-processing, the construction of a ML model can be broken down into three distinct stages. The first stage is the training phase, where the ML algorithm learns from the training data through an iterative process that continues until a desired minimum error or maximum accuracy, or a predetermined maximum number of iterations, is achieved. The second stage is the validation phase, where the model's generalization properties, such as overfitting and underfitting, are analyzed. Overfitting occurs when the model fits the training data better than the validation data, while underfitting indicates that the model is too simplistic for the given data. To mitigate any issues related to data distribution, validation is commonly performed using cross-validation (CV) techniques such as k-fold cross validation, which involves splitting the training data into k subsets for training and testing. Through CV, learning and validation curves can be plotted to assess model performance. The third stage is the testing phase, where the model, with optimized hyperparameters, is evaluated on unseen data from the test dataset.

4.2 Experiment Configurations

All models were built on a DELL Precision 5570 (CPU: 12th Gen Intel (R) Core (TM) i7-12800H (20CPUs) ~2.4 GHz, RAM: 32 GB, GPU: NVIDIA RTX A1000 Laptop GPU) using the Anaconda python environment. The ML algorithms used are part of the open-source-software library of scikit-learn.

4.3 Evaluation Metrics

To assess the robustness and efficiency of the classification models, a confusion matrix was used to visualize their performance. The overall classification accuracy (OA) was then utilized to quantitatively evaluate the performance of the CPT data-based soil classification. In addition to OA, three other classification metrics, namely precision, recall, and F1-score, were applied to comprehensively evaluate performance. The definitions of these evaluation metrics are presented below.

A confusion matrix (CM) is a summary of a classifier's prediction results that provides a visual representation of its performance. **Table 1** illustrates the contents of a confusion matrix, where true positive (TP) indicates a positive prediction that correctly matches the actual positive state. False negative (FN) represents a negative prediction that should have been positive, while false positive (FP) indicates a positive prediction that should have been negative. True negative (TN) represents a correct negative prediction. The confusion matrix not only provides a visual representation of the model's performance but also facilitates the identification of confusion between similar classes for error analysis.

Table 1. Schema of a confusion matrix for the evaluation of results

		Actual	
		Positive	Negative
Predicted	Positive	True Positive (TP)	False Positive (FP)
	Negative	False Negative (FN)	True Negative (TN)

The overall segmentation accuracy (OA) is the rate of accurately predicted labels out of the total number of data samples (**Eq. (1)**). However, OA alone is insufficient for evaluating a classifier's performance. Therefore, three additional classification metrics, including precision, recall, and F1-score, were used to quantitatively assess the performance of the classification models. Precision measures the accuracy of positive predictions (**Eq. (2)**), while recall refers to the ratio of positive data samples that are correctly predicted by the classifier (**Eq. (3)**). The F1-score represents the harmonic mean of precision and recall (**Eq. (4)**), integrating the precision and recall values into a single metric.

$$\text{Accuracy} = \frac{\text{TP} + \text{TN}}{\text{TP} + \text{TN} + \text{FP} + \text{FN}} \quad \textbf{Eq.(1)}$$

$$\text{Precision} = \frac{\text{TP}}{\text{TP} + \text{FP}} \quad \textbf{Eq.(2)}$$

$$\text{Recall} = \frac{\text{TP}}{\text{TP} + \text{FN}} \quad \textbf{Eq.(3)}$$

$$\text{F1} - \text{score} = \frac{2 * \text{Recall} * \text{Precision}}{\text{Recall} + \text{Precision}} \quad \textbf{Eq.(4)}$$

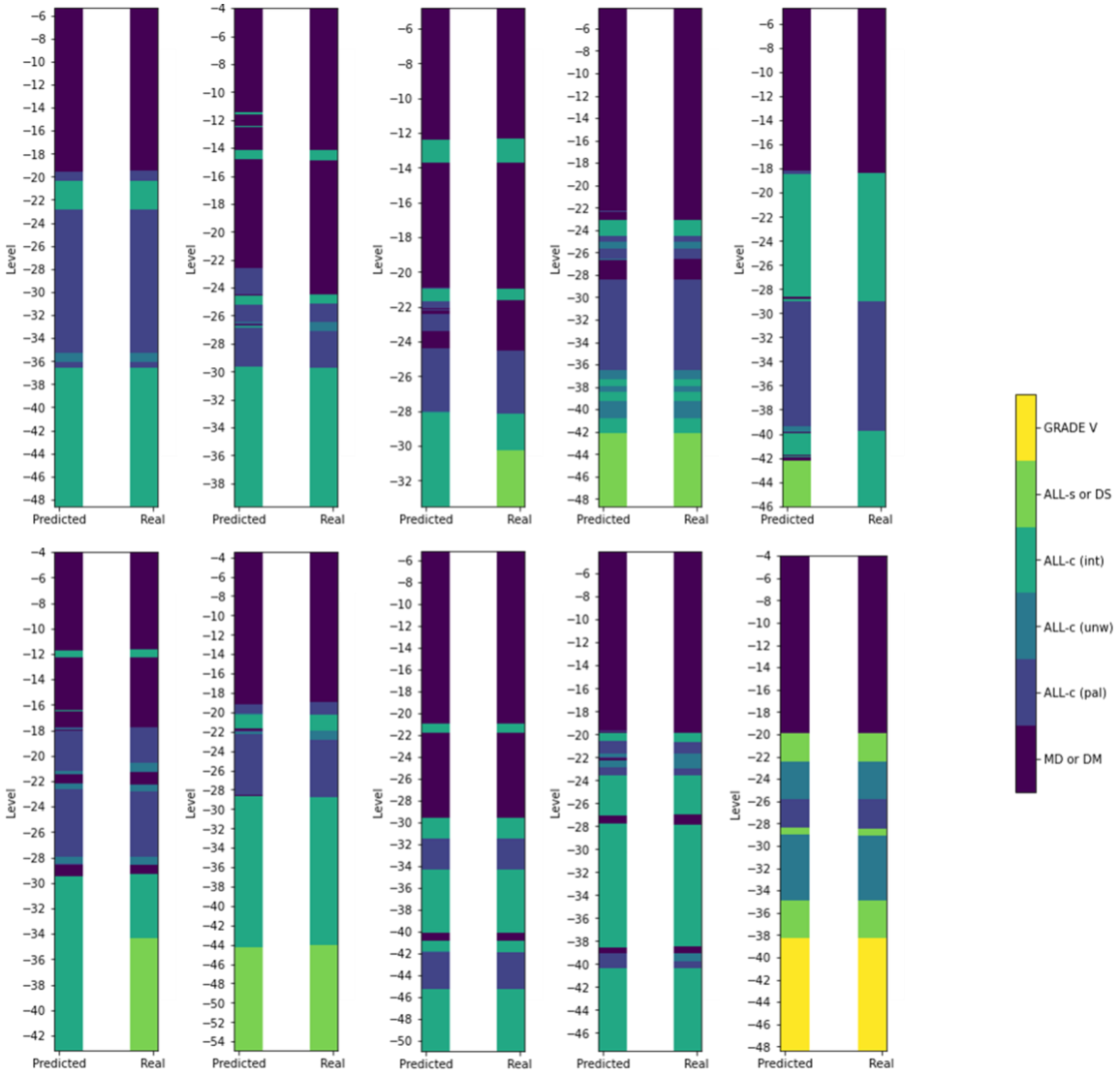

Figure 5. Comparison between the soil classification obtained from RF and the actual soil classification from adjacent boreholes in The Project

5. RESULTS

The RF algorithm achieved the best performance across all classification targets and feature sets, exhibiting high accuracy (92%) and minimal training time as shown in **Table 2**. In addition to the RF model, the SVM model was found to be unsuitable for this type of task and data, as it took significantly longer to train than the other two models and produced the worst overall accuracy of 81%. The three-layer ANN model was easier to train and performed better in determining soil classes from CPT data, achieving an accuracy of 85%.

Figure 5 displays a selection of comparison samples between the soil classification obtained from the RF model and the actual soil classification obtained from adjacent boreholes in The Project. It can be observed that the soil types in most positions were predicted correctly using the RF model with excellent consistency.

Table 2. Model performance reports

Algorithms	Training Time (s)	Accuracy	Recall	Precision	F1-score
SVM	565	0.81	0.81	0.78	0.78
ANN	89	0.85	0.85	0.86	0.85
RF	71	0.92	0.92	0.92	0.92

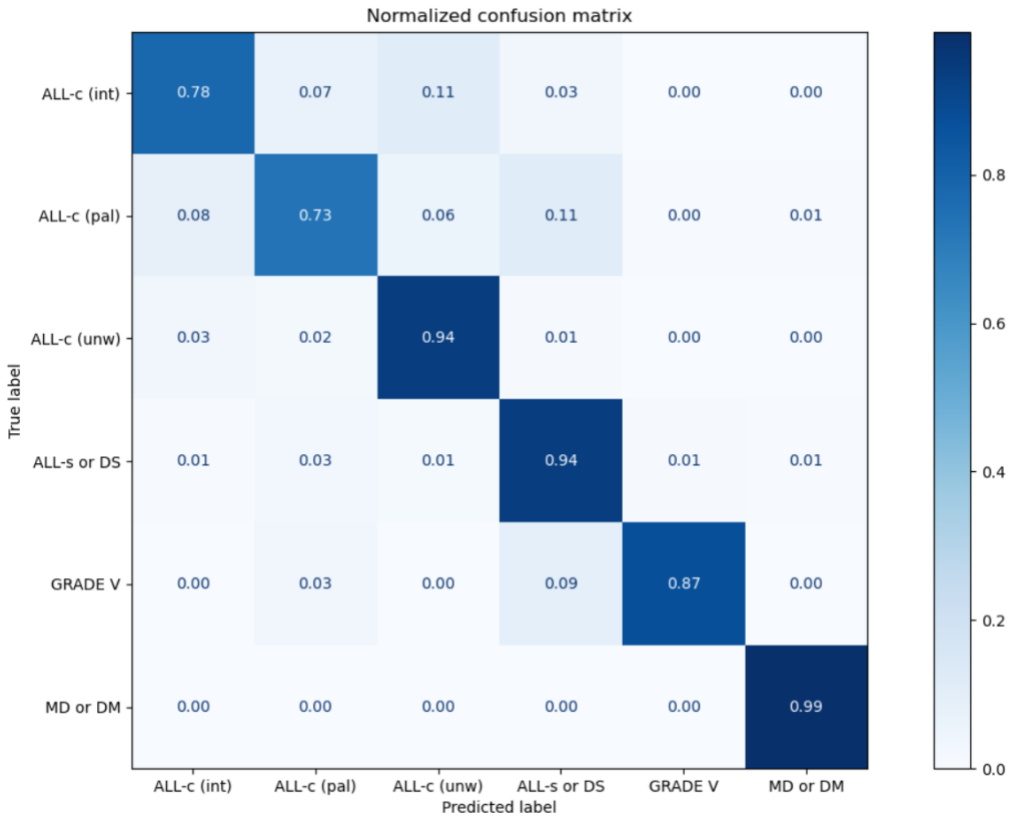

Figure 6. Confusion matrix visualization for the testing results of the RF model.

The confusion matrix for the RF model is presented in **Figure 6**. The results show that more than 94% of soil samples of types "ALL-c (unw)", "ALL-s or DS", and "MD or DM" were correctly predicted. The model exhibited less confidence in recognizing soil type "ALL-C (pal)", which was often classified as "ALL-s or DS", "ALL-c (unw)", or "ALL-c (int)". Similarly, "ALL-c (int)" could sometimes be misclassified as either of the other two "ALL-c" soil types.

Despite the possibility of misclassification, the ML methods offer a clear advantage over traditional workflows that rely on engineer judgement in CPT data interpretation, as illustrated in **Figure 7**. Using a machine learning approach, the analysis of 600 CPTs can be completed within half an hour, while the manual process can only handle less than 50 CPTs within the same time frame. ML can be used as a preprocessing tool to speed up the overall workflow without sacrificing accuracy.

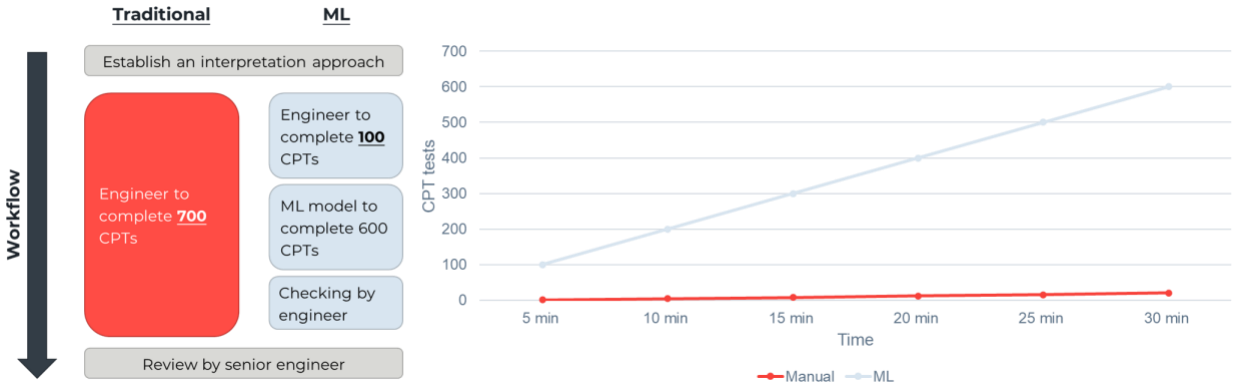

Figure 7. Efficiency comparison between the ML approach and the traditional interpretation process.

5. CONCLUSION & DISCUSSION

This paper has demonstrated that ML algorithms can accurately classify soils based on measured CPT data. The best results in terms of prediction accuracy and learning time were achieved using a RF classifier. However, it should be noted that more advanced neural networks, such as deep neural networks (DNN), may lead to even better results. These investigations are part of ongoing research.

Compared to traditional manual processes, ML methods can significantly expedite the CPT data interpretation process. It may serve as a useful tool within geotechnical engineering software packages to obtain fast and reliable soil classifications without relying on third-party solutions.

Since ML model training requires massive amounts of data, the authors propose that the relevant Hong Kong Government department(s) could take the lead to coordinate with local engineering firms and developers / clients to create a centralized GI inventory. Prior to submitting the data to the Government, the submitting party would be responsible for checking the data format and cleansing the data. Additionally, a cloud-based data management system could be utilized to facilitate better data sharing and access. With a rich and comprehensive dataset, ML models can produce more accurate results. Moreover, larger and more reliable deep learning models can be used to perform sophisticated GI data analysis tasks, such as constructing three-dimensional subsurface geological models.

REFERENCES

1. Alpaydin, E. (2020). Introduction to machine learning. *MIT press*.
2. Breiman, L. (2001). Random forests. *Machine learning*, 45, 5-32.
3. Hearst, M. A., Dumais, S. T., Osuna, E., Platt, J., & Scholkopf, B. (1998). Support vector machines. *IEEE Intelligent Systems and Their Applications*, 13(4), 18-28.
4. Hornik, K., Stinchcombe, M., & White, H. (1989). Multilayer feedforward networks are universal approximators. *Neural Networks*, 2(5), 359-366.
5. Kurup, P. U., & Griffin, E. P. (2006). Prediction of soil composition from CPT data using general regression neural network. *Journal of Computing in Civil Engineering*, 20(4), 281-289.
6. Padarian, J., Minasny, B., & McBratney, A. B. (2020). Machine learning and soil sciences: a review aided by machine learning tools, *Soil*, 6, 35–52.
7. Pedregosa, F., Varoquaux, G., Gramfort, A., Michel, V., Thirion, B., Grisel, O., & Duchesnay, E. (2011). Scikit-learn: Machine learning in Python. *The Journal of Machine Learning Research*, 12, 2825-2830.
8. Rauter, S., & Tschuchnigg, F. (2021). CPT data interpretation employing different machine learning techniques. *Geosciences*, 11(7), 265.
9. Reale, C., Gavin, K., Librić, L., & Jurić-Kaćunić, D. (2018). Automatic classification of fine-grained soils using CPT measurements and Artificial Neural Networks. *Advanced Engineering Informatics*, 36, 207-215.

10. Robertson, P. K. (2009). Interpretation of cone penetration tests—a unified approach. *Canadian Geotechnical Journal*, 46(11), 1337-1355.
11. Robertson, P. K. (2016). Cone penetration test (CPT)-based soil behaviour type (SBT) classification system—an update. *Canadian Geotechnical Journal*, 53(12), 1910-1927.
12. Shi, C., & Wang, Y. (2022). Data-driven construction of Three-dimensional subsurface geological models from limited Site-specific boreholes and prior geological knowledge for underground digital twin. *Tunnelling and Underground Space Technology*, 126, 104493.
13. Shi, C., & Wang, Y. (2022). Machine learning of three-dimensional subsurface geological model for a reclamation site in Hong Kong. *Bulletin of Engineering Geology and the Environment*, 81(12), 1-18.
14. Wang, Y., Huang, K., & Cao, Z. (2013). Probabilistic identification of underground soil stratification using cone penetration tests. *Canadian Geotechnical Journal*, 50(7), 766-776.
15. Wang, Y., Hu, Y., & Zhao, T. (2020). Cone penetration test (CPT)-based subsurface soil classification and zonation in two-dimensional vertical cross section using Bayesian compressive sampling. *Canadian Geotechnical Journal*, 57(7), 947-958.
16. Zhang, W., Wu, C., Zhong, H., Li, Y., & Wang, L. (2021). Prediction of undrained shear strength using extreme gradient boosting and random forest based on Bayesian optimization. *Geoscience Frontiers*, 12(1), 469-477.
17. Zhao, T., Xu, L., & Wang, Y. (2020). Fast non-parametric simulation of 2D multi-layer cone penetration test (CPT) data without pre-stratification using Markov Chain Monte Carlo simulation. *Engineering Geology*, 273, 105670.

A Complete Digital Solution to Site Formation, ELS System and Foundations Design

Keith Leung, Simon Lam, Derek So, Jasper Lee, Allen Tao & Ryan Yan
AECOM Asia Company Limited

ABSTRACT

Conventionally, geotechnical designs are carried out on a few representative critical sections. It is probably due to its simplicity as everything is kept in the two-dimensional manner. On the one hand, this approach has been proven to be satisfactory from engineering performance perspective. On the other hand, this approach might have hindered a cost-saving design optimisation. With the increasing computational power as well as growing trend to embrace digital transformation, BIM adoption and design automation, more digital solutions/tools are available in the market. This has opened the gate for a holistic review for design optimisation.

This paper presents some more efficient digital solutions applicable to common geotechnical designs with the help of a few design examples as demonstration. The information flow from planning, design, engineering analysis and drawings preparation is discussed. In particular, the authors focus on how issues of compatibility and interoperability among various digital solutions, which has long been an obstacle for seamless and efficient design workflow, could be resolved.

INTRODUCTION

1.1 Background

In coherent with the final call for Net Zero Carbon Emissions in the 27th Conference of the Parties to the United Nations Framework Convention on Climate Change (COP27) held in November 2022, the need for a complete digital solution to various geotechnical design, including site formation, Excavation and Lateral Support (ELS) system and foundations, is overwhelming as this could facilitate a systemic optimisation of the design scheme and therefore reduce the emissions of greenhouse gases from the perspective of materials consumption and construction programming. It is expected that such savings could be enormous for mega civil engineering projects in Hong Kong's near future.

Site formation design is the process of preparing land supply suitable for development by shaping and levelling the ground. Key elements in site formation design include design of optimal site layout for the built asset as well as designing the grading and drainage systems to ensure proper water flow and prevent erosion. A well-designed site could reduce the risk of damage or failure and facilitate efficient use of resources for environmental-friendliness and sustainability. In addition, it adds value to the project by maximising the use of available space and optimising the functionality of the infrastructure.

ELS system design involves excavation in soil or rock to create the space for development. It involves the design of a support system that prevents sides of the excavation from collapsing or moving excessively, which causes safety hazards and damage to adjacent buildings and structures. This involves determining the size and shape of the excavation, as well as the depth and slope of the sides and selecting the appropriate support system, which typically includes pile walls, shoring and/or bracing. A poorly designed or constructed excavation could lead to

safety hazards, structural damage, and undesirable project delays and, therefore an ELS system design is usually a crucial element in civil engineering projects.

Foundation design is another critical element of civil engineering projects involving the construction of built assets such as buildings, bridges, highways, and other infrastructures. It involves the design of a stable supporting system counteracting the weight of the built asset and resisting other external forces such as wind, earthquakes and soil pressure. In particular, selecting an appropriate foundation type, which could be shallow foundations such as spread footings or mat foundations, or deep foundations such as piles or barrette, is the prime objective in foundation design. This continues with determining the size and shape of the foundation, as well as the depth and strength required to support the built asset. A well-designed foundation ensures the safety, stability and serviceability of the built asset and prevents undesirable structural damage and unnecessary repairs in future.

In the past few years, digital transformation has been proven to help in many ways in civil engineering projects, including site formation, ELS system and foundations design. For example, digital transformation has helped to improved accuracy and efficiency of the design with digital technologies such as BIM software, digital models, and other simulation tools. These technologies help engineers to visualise and analyse complex data and scenarios, enable them to make more informed decisions and optimise designs. In addition, it enhances collaboration and facilitates communication among project stakeholders, including designers, contractors, and clients, which, in turn, helps streamline the design and construction process, reducing the risk of errors and delays. Moreover, cost savings could be done with digital transformation, which helps reduce costs in civil engineering projects by improving efficiency, reducing errors, and optimising designs.

Overall, digital transformation plays a significant role in improving the efficiency, safety, and sustainability of civil engineering projects. By leveraging digital technologies, engineers could make better-informed decisions, reduce risks and costs, and enhance the overall success of the project. The digital solutions presented in this paper mainly focus on improving design efficiency and quality of design works, which, in turns, enable better design optioneering and reducing wastage due to design errors.

1.2 Objectives

This paper presents some recently developed digital workflows which are applicable to site formations, ELS system and foundations design. These workflows often involve designs and visualisation in the three-dimensional space contrary to the traditional two-dimensional sections, bringing about numerous advantages to the efficiency and effectiveness of the design process. First, design changes, which are inevitable in almost all engineering design journeys, could be more efficiently incorporated into the digital workflows. Second and more importantly, engineering designs carried out in the three-dimensional space would offer a more promising design optimisation, which answer the need for net zero carbon emissions via the use of less construction materials and thus the reduction of construction wastes and energy consumptions, without compromising the safety margin of the engineering designs. Due to limitation of this paper, only the three major geotechnical designs, namely site formations, ELS system and foundations design, will be discussed.

2 SITE FORMATIONS DESIGN

2.1 Conventional Design Approach

Conventional site formations design is usually done in a sequential approach, where engineering geologists and geotechnical engineers appraise the ground conditions and site constraints, prepare conceptual and/or schematic design for the key built assets, carry out detailed design to determine the extent of slopes and retaining structures to be formed and consider other provisions for the site (e.g., slope furniture, drainage, maintenance access, etc.). By assessing the existing ground conditions of the site, critical locations will be identified for different zones of the site. Design on the slopes and retaining structures could then be carried out based on two-dimensional sections at these critical locations.

2.2 Problem Statement

Commonly in site formation design, the most difficult task is to determine the location and extent of slopes and retaining structures to be formed in consideration of the topography and subsurface ground conditions of the site, which requires accurate interpretation of subsurface ground conditions by the engineering geologist. Ideally, with sufficient ground investigation coverage within the site, ground conditions could be interpreted for the construction of ground models and site formation design could be carried out according to the two-dimensional representative sections at critical locations. However, it is not always the case as existing ground information is insufficient to build an accurate ground model.

When the interaction with existing topography comes into the design works, it appears that the adoption of representative sections might only well answer the question of stability of the slopes and/or retaining structures but when it comes to the designed extent of slopes and/or retaining structures, the combination of topography and subsurface ground conditions might make it difficult to determine, especially for site where natural terrain is involved due the complex configuration of the ground profile. In some more extreme cases where soil-rock interface is encountered, determination of slope extent might be even more time-consuming as the design slope angle of the formed slope might not be the same for soil slopes and rock slopes.

Moreover, as site formation is designed to address various constraints such as required formation level, road alignment, site issues etc., the sequential design process would need to be repeated each time when theses constraints are changed or updated. This often lengthens the time required to deliver a design in its final form.

2.3 Digital Solutions

2.3.1 Computation Design with 3D Terrain Models and 3D Ground Models

With increasing computing power and the government's policy of open data for smart city, territory-wide LiDAR data could be used to generate three-dimensional terrain model to facilitate the site formation design. From the large amount of information obtained from ground investigation and laboratory tests, three-dimensional ground model could be generated with simulation tools such as Leapfrog to allow better interpretation and representation of the ground conditions with these geological information visualised in three-dimensional space.

Based on the three-dimensional terrain model generated, together with the footprint or alignment of the built asset, level difference between the existing ground level and desired formation level could be obtained from the software straightforwardly. From this site formation model, design works for slopes, retaining walls and other provisions are made more precisely with ease (GEO, 1984; GEO 1993). Furthermore, compared to the conventional design approach where most of the design are performed only on several critical sections, higher level of design optimisation could be carried out using this model, reducing the repetitive labour intensity when site constraints and design requirements are updated or changed.

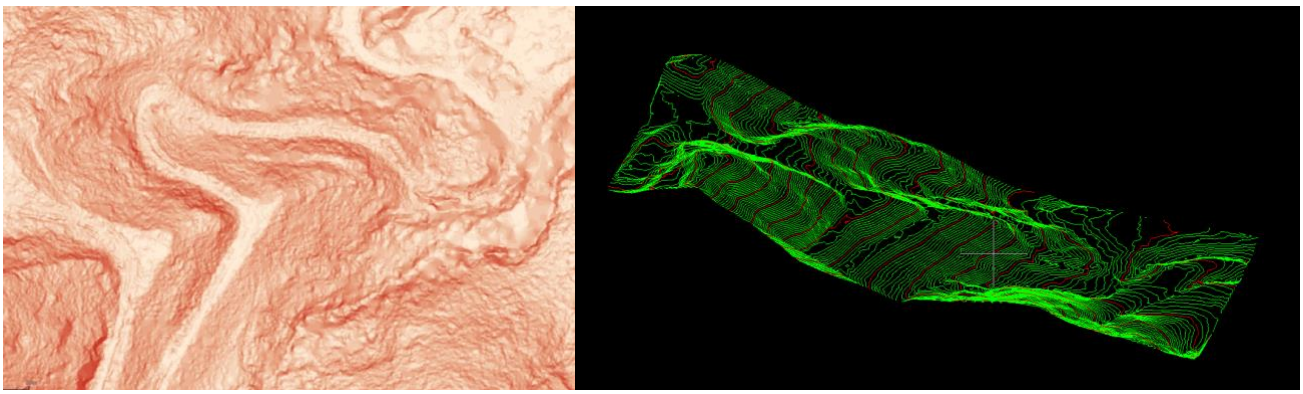

Figure 1: 3D terrain model generated from LiDAR data

Similarly, three-dimensional ground model could now be generated with the interpreted ground conditions and be readily used in association with other BIM software which could build up the slope using "templates". The "templates" is a set of customised design criteria that make use of the information from the terrain models and ground models to generate the required slopes. With proper "templates" defining the required slope angle in soil and in rock, an accurate extent of slope could be generated without much effort compared to conventional design approach where manual interpretation is done exhaustively section by section.

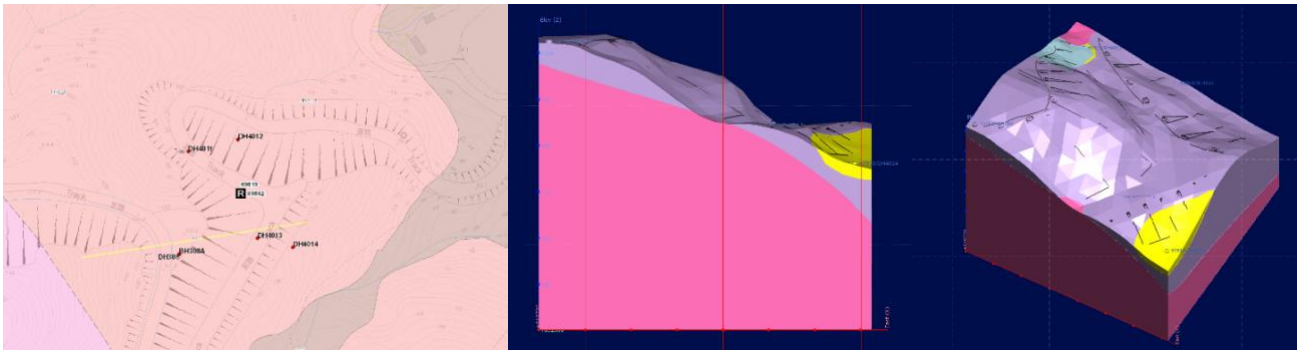

Figure 2: 3D ground models generated from interpreted ground conditions in Leapfrog

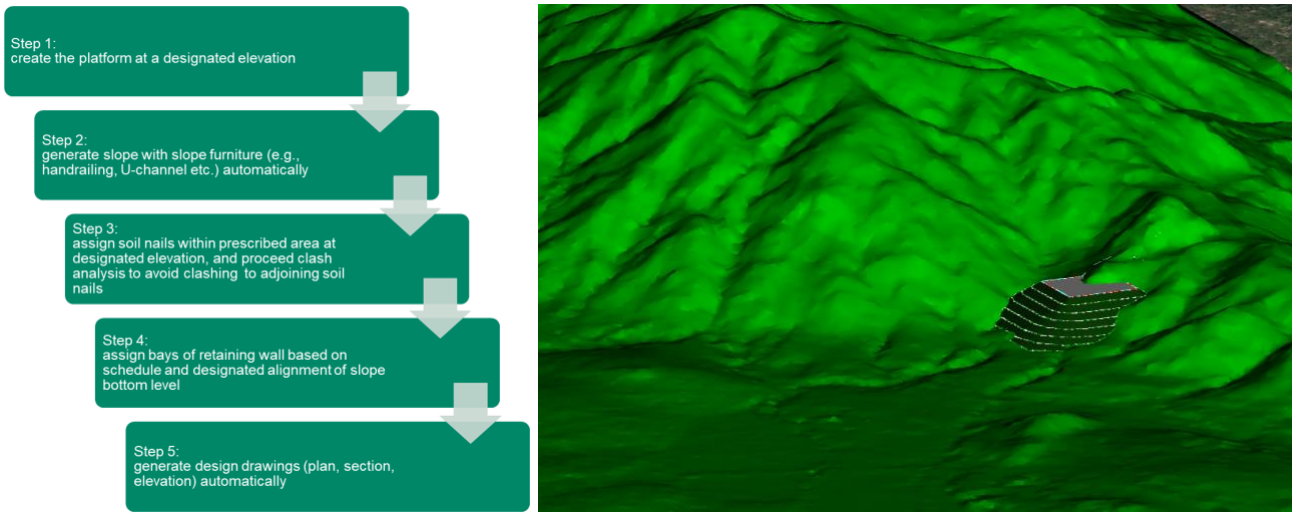

Figure 3: Site formation design using 3D terrain models and ground models in OpenRoads

2.3.2 Parametric Design of Other Provisions

Digital tools with three-dimensional site modelling could also be used in the designs of some other relevant provisions. For instance, with the slope stability assessment based on the representative design sections, the required soil nails could be directly generated from the results of the slope stability assessment and be "placed" on the slope in the digital model with corresponding length, orientation and inclination as specified. Alternatively, in some more complex terrain models where local adjustment is required, we can modify the soil nail layout to the designated location which make more sense and re-generate the digital model of the soil nails based on the coordinates of the soil nails in the revised layout (see **Figure 4**). Clash analysis could thus be carried out efficiently from the model to check if there is any conflicts with other soil nails, underground utilities and/or building and strcutures (GEO, 2008). For any subsequent update on the future ground profile or other design requirements, taking advantage of digital models, soil nails could be redistributed in the software swiftly without the need of intensive and time-consuming labour works.

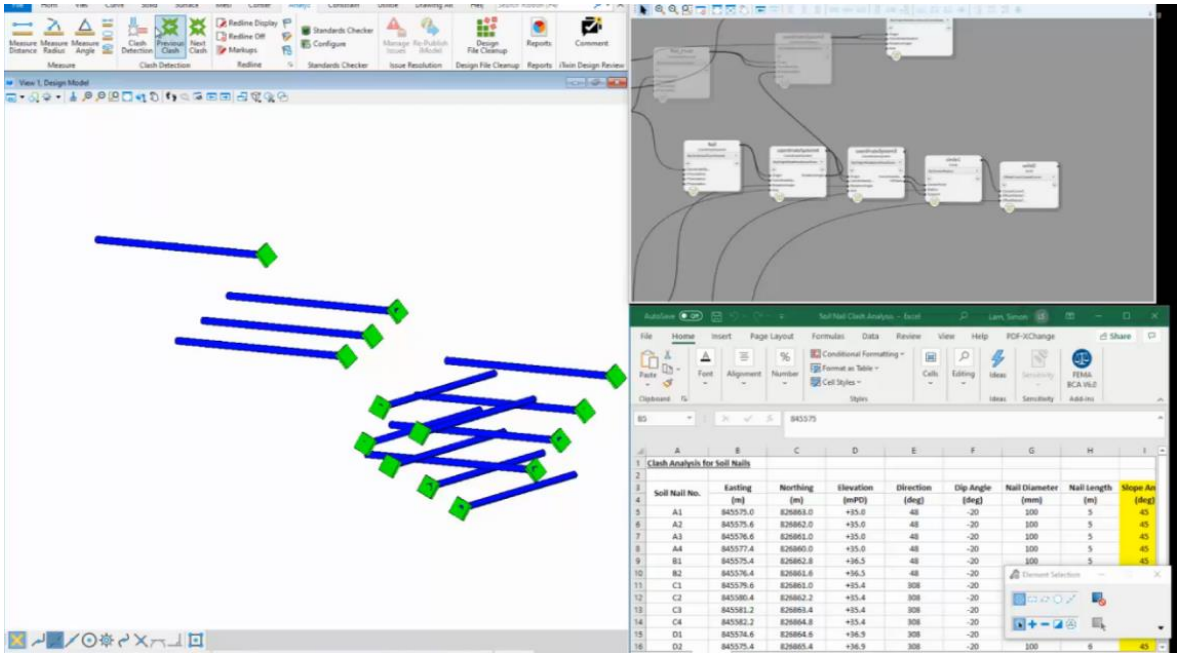

Figure 4: Constructing soil nails in digital models using OpenRoads Generative Components

The power of this digital tools is not only confined to constructing soil nails; with proper design of the algorithm, parametric design for other provision including maintenance access and drainage (using size and type of drainage as an input) could also be allowed, greatly reducing the processing time especially for large scale projects.

2.3.3 Quantitative Design Optimisation

One of the major benefits in adopting BIM software is that making use of the digial models and parametric modelling, designers could quickly work out different design options and evaluate their impact on the overall performance. It is also able to couple with other energy analysis tools to evaluate energy consumption and identify area of improvement in great details. Cost estimation could also be generated for various design options with schedules and summaries obtained from the digital models (see **Figure 5**). Not only the cost could be estimated, materials optimisation by analysing the geometry and structural requirements allows designers to identify opportunities to reduce material waste and minimise the environmental impact of construction. Overall, the digital models help designers optimise the designs by providing quantitative information they need to make informed decisions to assess the cost, environmental impact and other performance indicators that could justify the preferred option, quantitatively over intuitively.

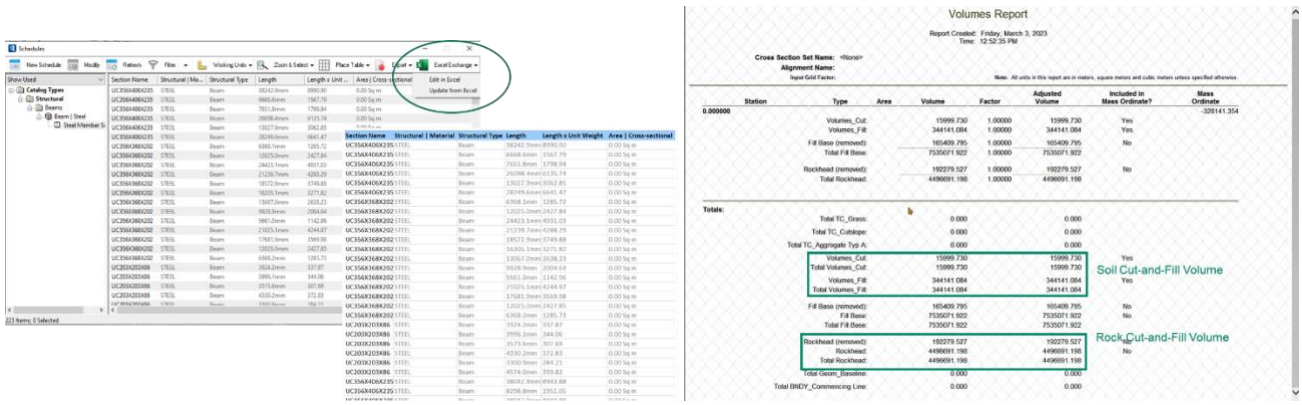

Figure 5: Quantities of materials and volumes of earthworks for site formation design in OpenBuildings and OpenRoads

3 EXCAVATION AND LATERAL SUPPORT (ELS) SYSTEM DESIGN

3.1 Conventional Design Approach

Similar to site formation designs, engineering geologists and geotechnical engineers appraise the ground conditions and site constraints and propose feasible schemes for the ELS systems with respect to the proposed/required final excavation profile. After considering the pros and cons of various schemes, high degree of collaboration between geotechnical engineers and structural engineers is often required in typical ELS system designs due to the iterative modelling of behaviour of soil-structure interactions to ensure the stability and serviceability of the ELS system.

Nevertheless, during construction stage where more information is revealed, the actual ground conditions, for instance the thickness of the soil stratum and/or the groundwater regime, may deviate from the expected ground conditions and site monitoring system, together with regular design review, are required to ensure stability of the ELS system.

3.2 Problem Statement

Commonly in ELS system design, the most difficult task is to fine-tune and optimise the ELS system without compromising the safety margin. Repetitive works are usually handled by the geotechnical engineers and structural engineers manually and the prolonged involvement of designers is rather time consuming and error-prone, especially for the changes (e.g., extent, layout, excavation level of the system) are required in the last minute.

While construction of the ELS system is always tied with that of permanent works, the tight construction programme of ELS system normally could not accommodate sufficient time for design review when the unforeseen conditions are encountered during construction stage. Subsequently, a more efficient workflow with the support from digital solutions which reduces the processing time for the iterative design and enhances accuracy and correctness of the ELS design is warranted.

3.3 Digital Solutions

The enhanced workflow make uses of digital solutions such as three-dimensional terrain models and ground models generated from LiDAR data and interpreted ground conditions (similar to **Section 2.3.1** above), BIM approach and design automation with programming scripts (e.g., Microsoft Excel VBA, Python scripts) reduce the reliance of manual input as happened in conventional design approach. Apart from the enhancements similar to those discussed in **Section 2**, with the growth of geotechnical analysis software like Plaxis, design automation is enabled through Python scripts, which acts as a communicator between Plaxis and other conventional design tools in form of Microsoft Excel files.

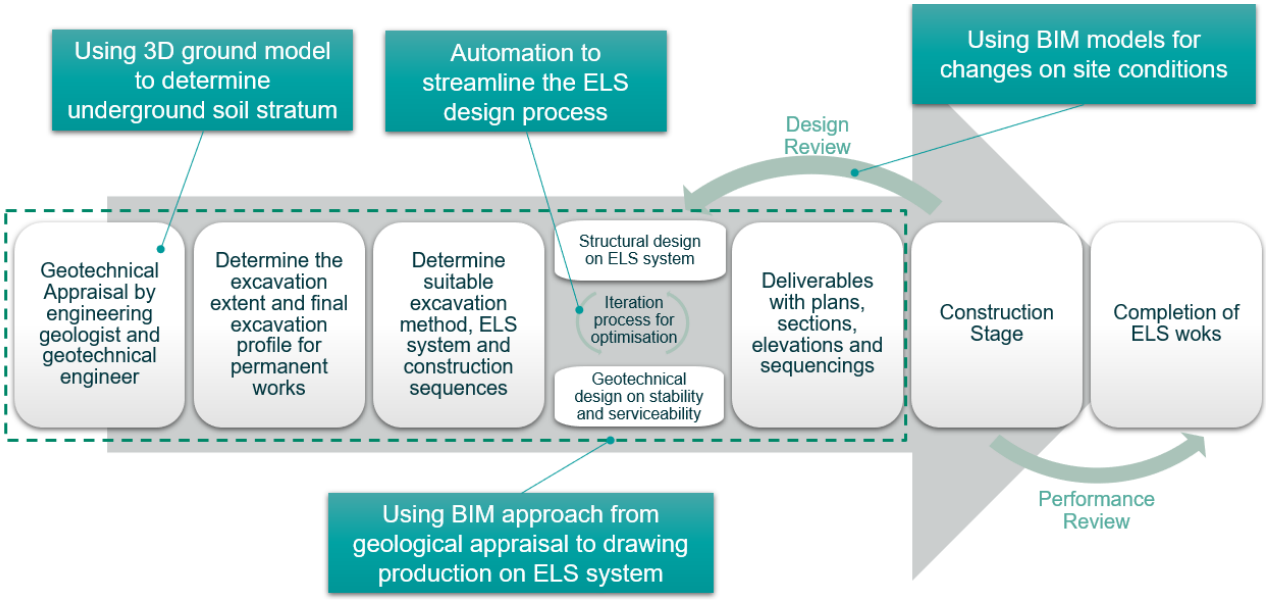

Figure 6: Enhanced workflow using digital solutions

3.3.1 Generative Design

The ELS design process typically involves preliminary design of the layout of the pile wall system with or without shoring layout, depending on whether it is a cantilever wall system or a strutted wall system. It has long been a controversial issue whether a reasonable ELS layout could be generated from artificial intelligence (A.I.) to facilitate the design work. Whilst there is still not a reliable and robust A.I. system available due to unpredictability associated with the black box algorithm, an alternative generative design approach using programming technique has been explored.

Unlike working with A.I. where sufficient training based on preceding cases and verification is required, the experience and good practices of previous ELS system designs have been reviewed and consolidated into algorithm, which imitates how the designer "thinks" in reality and is coded with programming scripts in Microsoft Excel VBA. With the logic behind the algorithm, it takes the setting-out coordinates of the ELS system and maximum strut spacing as input and calculates the paired coordinates necessary to define the primary struts, secondary struts and corner struts of the system. The paired coordinates are then imported into other BIM software to generate the three-dimensional models of the ELS system. **Figure 7** presents a shoring layout generated automatically from the algorithm programmed in Microsoft Excel VBA. The paired coordinate, together with the strut sizing, is then passed to BIM model using OpenBuildings Generative Component. Summary of strutting layout, including the size and length of each strut, could then be generated for design option comparison.

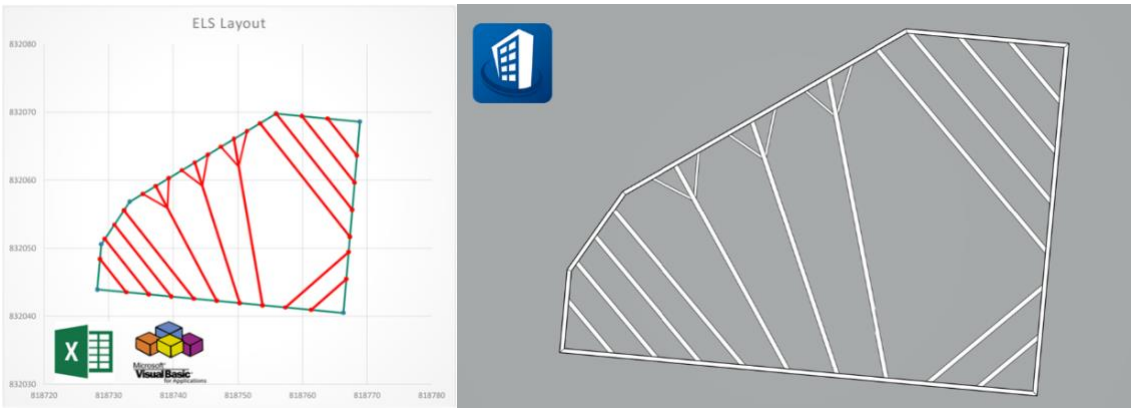

Figure 7: ELS layout generated by algorithm using Microsoft Excel VBA and OpenBuildings Generative Component

3.3.2 Automated Design

In order to minimise the need of manual input for the geotechnical analysis, which could be labour intensive and time consuming, Python scripts has been developed to connect the analysis with the design tools to streamline the conventional design approach with the use of standardised spreadsheet (see **Figure 8**).

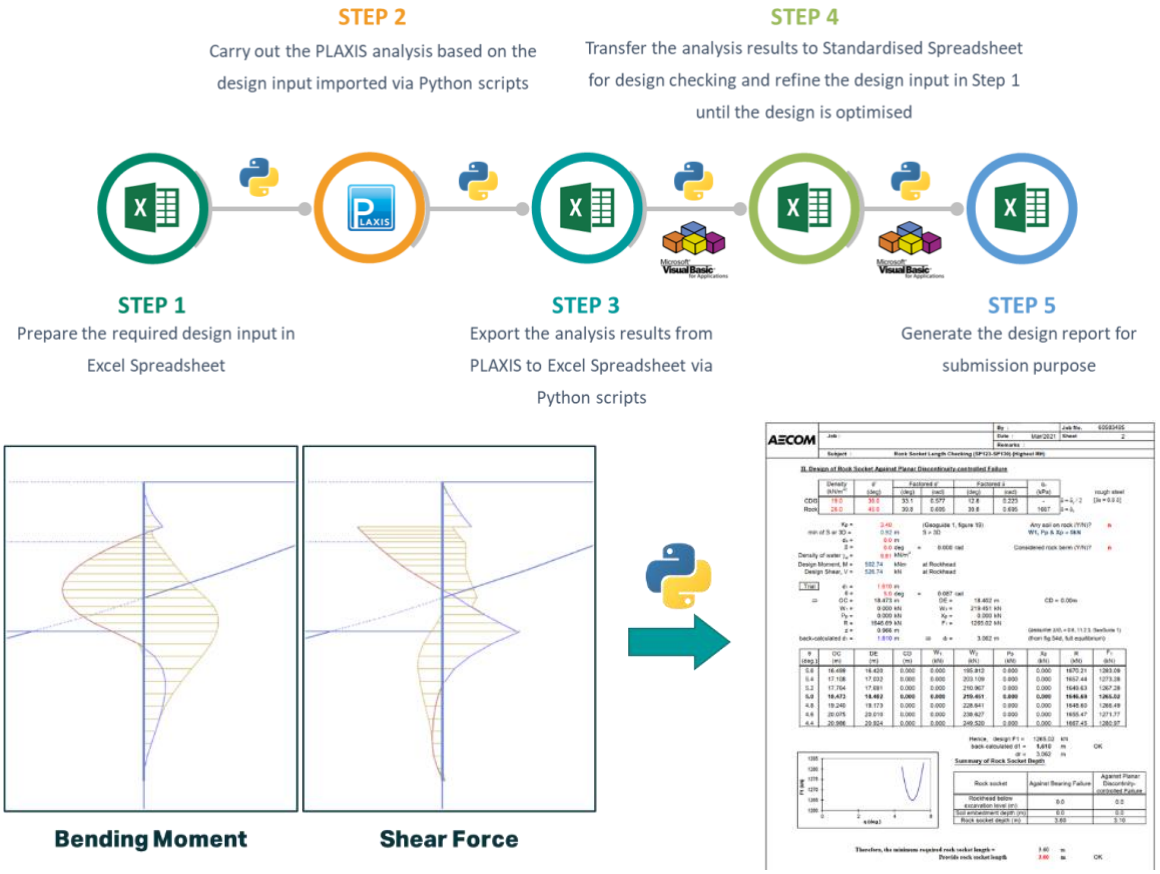

Figure 8: Proposed data flow using programming scripts for ELS designs

Configuration, properties, modelling sequence and results are extracted from the geotechnical analysis software by Python scripts developed and summarised in table format which is readily connected with other standardised spreadsheets in Microsoft Excel. Should the capacity of the ELS system be exceeded, modification of input

parameters could be done in Microsoft Excel and the information would be re-imported into the geotechnical analysis software by Python scripts directly, improving the consistency of the entire ELS system design.

Upon completion of the iterative design, the three-dimensional BIM model could be regenerated/updated with the paired coordinate adopted in the revised design models such that it is always synchronised with each other.

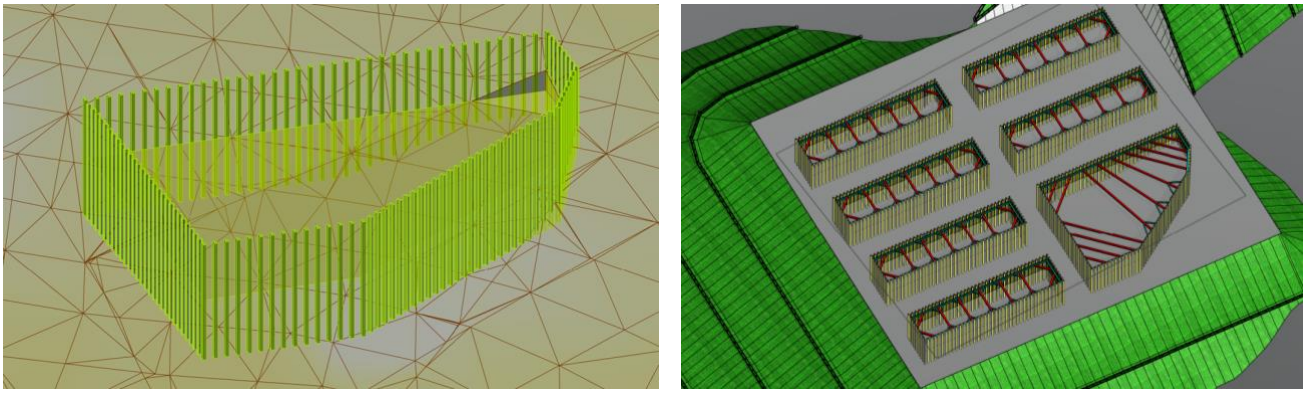

Figure 9: 3D BIM models to facilitate changes/reviews based on site conditions in OpenBuildings

4 FOUNDATIONS DESIGN

4.1 Conventional Design Approach

In the conventional design approach, the sequential update of foundation designs from engineering geologists to geotechnical engineers and to draughtsmen may take up considerable time. This typically involves updating the interpreted rockhead contour generated from commercial software Surfer or other similar software with the information obtained from pre-drilling works, updating the interpreted rockhead level of the piles at the location of the piles and updating the design checking (e.g., structural capacity of the piles, bearing capacity of the piles, soil/rock cone stability, stepping effect due to interaction among piles) and drawings in accordance with the updated interpreted rockhead level.

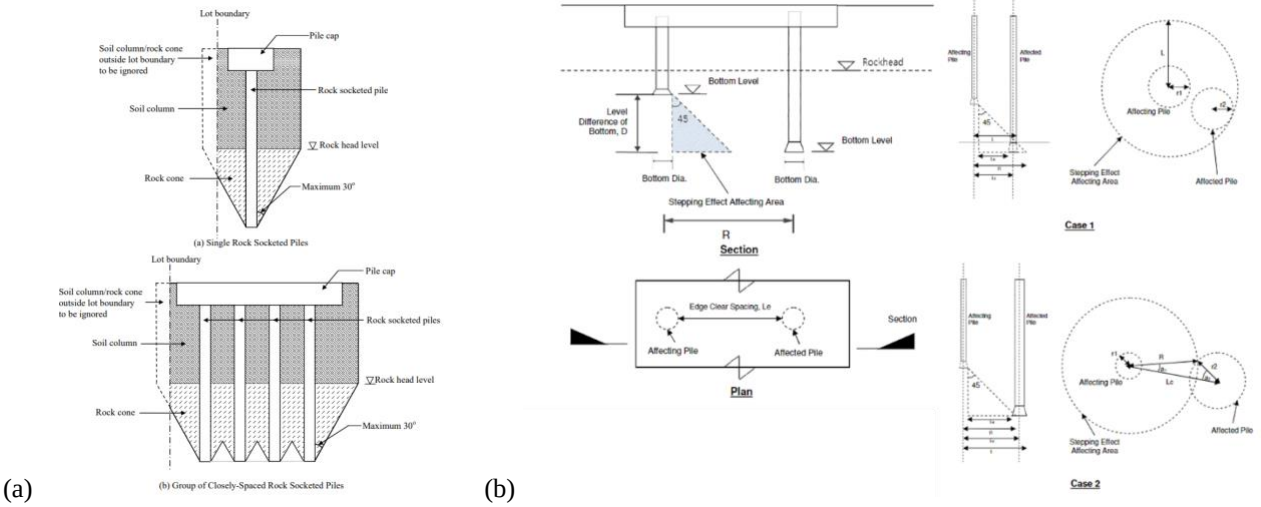

(a) (b)

Figure 10: (a) Design illustration of evaluation of soil/rock cone (extracted from CoP for Foundations, 2017 (BD, 2017))
(b) Design illustration of assessment of stepping effect

4.2 Problem Statement

Unless extensive ground investigation is carried out in the design stage, sufficiently fulfil the requirements for pre-drilling works of foundations, it is inevitable to carry out design verification based on pre-drilling works, of which the results come in batches usually. Based on the results of pre-drilling works, the interpreted rockhead contour and the associated foundation design is to be updated to reflect the latest known ground condition.

Once the interpreted rockhead contour is updated by the engineering geologists, the proposed termination depth might be increased or decreased and the design checking, especially those related to geometry in three-dimensional space, would need to be revisited to ensure validity of the foundation design. Very often this process is repeated frequently as the result comes back in a piecemeal manner, making it difficult to maintain the consistency between versions of foundation design and various documents (e.g., design calculations, design sections, elevations, and schedules, etc.). Apparently, this calls for a more efficient workflow with the support from digital solutions which reduces the processing time and enhances accuracy and quality of the foundation designs.

4.3 Digital Solutions

With a detailed review on the workflow on how we carry out foundation designs, we have considered the possibility of use of digital solutions to enhance the workflow and handle the repetitive tasks. It covers from the most straightforward use of three-dimensional representation of the interpreted rockhead, especially important in the location where complex geology is anticipated, the use of "virtual elements" for geometry related design checking, and the use of BIM software to produce construction drawings.

4.3.1 Evaluation of Soil/Rock Cone

As mentioned in **Section 4.1**, one of the most time-consuming tasks in foundation designs is to work out the spatial relationships among the piles (GEO, 2011). This is particularly difficult for closely-spaced piles as the combined effect of the pile group would generate a more complex geometry for the analysis (see **Figure 10(a)**). Although this could be simplified to two-dimensional planner problem, over-simplification may result in unnecessary long piles which reduce constructability on site. To properly address this, a new approach making use of the three-dimensional model with the introduction of "virtual element" is proposed to quickly obtain the volume of the soil and rock column directly from the model for further analysis.

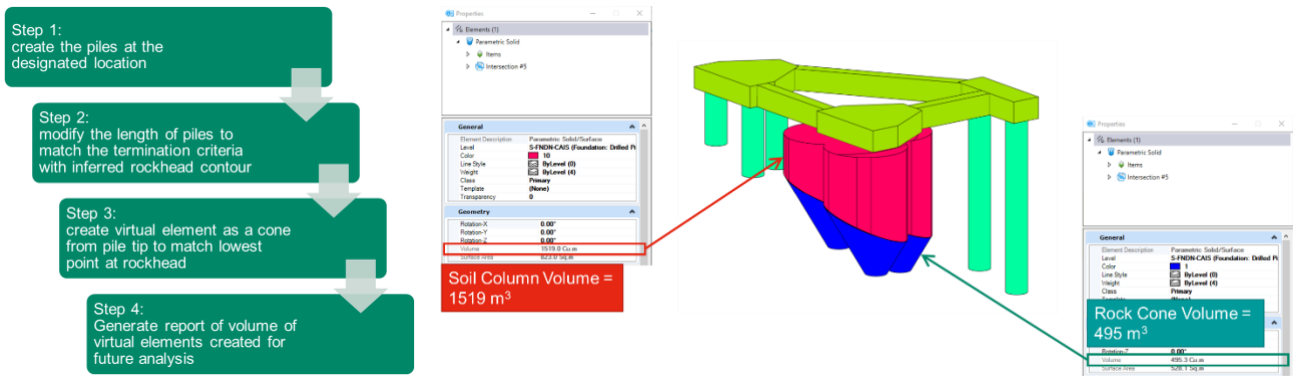

Figure 11: Evaluation of soil/rock cone with the use of "virtual elements"

4.3.2 Assessment of Stepping Effect

One should notice that the assessment of stepping effect involves the interactions among piles, which, in turn, require iterative checking in three-dimensional space and conventional checking in two-dimensional manner may take much longer time to determine the critical case, especially for closely-spaced piles. Every time when

the foundation layout is revised, the assessment of stepping effect must be updated accordingly and the original critical case may have been shifted as a result of the changes.

Similar to soil/rock cone checking mentioned in the previous section, the use of "virtual elements" could be introduced to represent the load spread of piles and simple clash analysis could be adopted to check if the deeper piles would be subject to the lateral load induced by the shallower piles. This resolves the spatial relationship directly from the design model in three-dimensional space and thus enhances the efficiency of design checking.

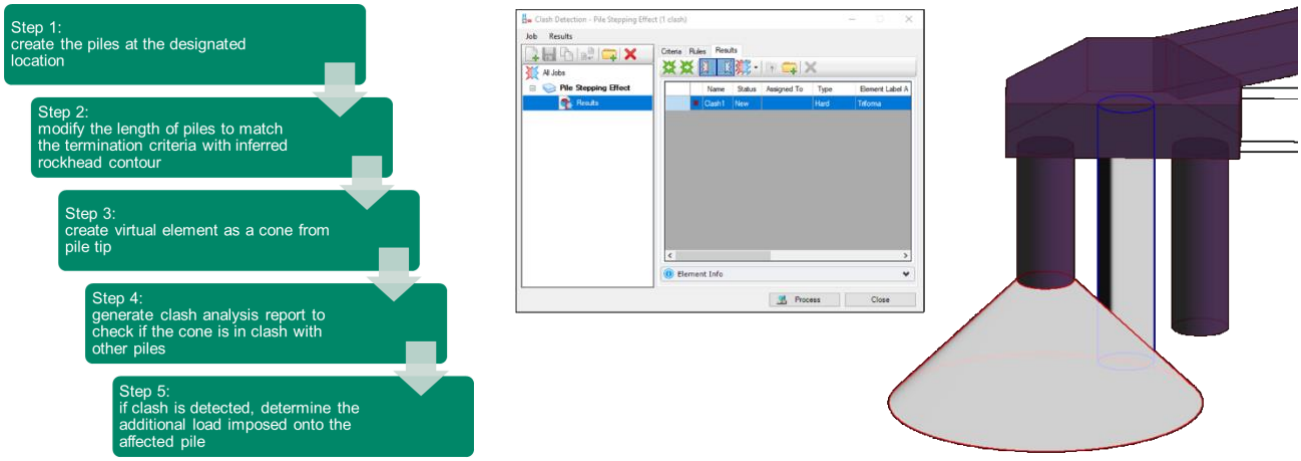

Figure 12: Assessment of stepping effect with the use of "virtual elements"

5 DISCUSSIONS

Currently there is still no one-off software available in the market and, therefore, the use of a combination of software is still needed to complete the engineering designs and we will need to solve the issues associated with the compatibility of the software. While it is possible to develop a new one-off software to cater for the need of engineering designs, the time and cost for the development could be huge. A more practical way to deal with the compatibility of the software adopted is making use of an intermediate data file, which is commonly readable by various software (e.g., Microsoft Excel file), and programming scripts (e.g., VBA scripts, Python scripts) to connect the input and output among the software. This does not only resolve the compatibility issues among software that we adopted in the engineering designs, but also allows design automation, either completely or partially, which highly enhances the quality and efficiency of the design process. More importantly, it allows us to move on the journey of digital transformation from visualisation to design works.

The illustrative examples from **Section 2** to **Section 4** have shown that digital solutions developed so far enables compatible design of multiple systems, which, in turn, allows design review and optimisation to a higher level of a project. With this new digital solution, focus of compatibility of the systems is not only on clash analysis in spatial aspects but also the overall cost-effectiveness of the projects with better flow of information among the design analysis and evaluation tools.

Although the digital workflows discussed in this paper open the possibility to automate major geotechnical designs, making use of digital tools commonly available in the current market, this may not be exhaustive and is subject to change with future advancement in technology. With more support from industrial practitioners, it is expected that the advancement of digital solutions would be even more readily compared to the past few years and rapid development of new solutions is anticipated in the near future. More all-rounded digital solutions would be devised to accommodate a more comprehensive digital workflow, which could further enhance user-friendliness and efficiency of the design process.

Unavoidably, during the development of the digital solutions, it comes to our attention whether digital solutions, especially design automation done by the computers, could replace our engineers. Despite we have tried our

best to accommodate the "good practices" in engineering designs in the digital solutions, it appears that engineering judgement and experience is still required to ensure the design generated by the digital solutions is a safe and robust design. In many of the cases, the digital solutions developed offer us some reasonable schemes supporting the feasibility of design automation; in some more complicated cases, it appears that the constructability, buildability, cost effectiveness and/or sustainability of the generated engineering solutions may not be fully optimised. Therefore, despite the digital solutions have significantly streamlined the conventional workflow, not until the digital solutions are proven to be robust enough to incorporate these factors in the engineering solutions, judgement from professionals is still essential.

Design optimisation is another major benefit that could be brought forward by digital solutions. Unlike the old days where only limited options could be developed due to limited resources and tight design programme, more design options with fine-tuning by parametric design could be carried out using digital solutions developed to allow qualitative option comparisons. Quantity of the proposed works could be taken from the design models readily with the programming scripts to fit into the bill of quantity for cost estimate. In future, there stands an opportunity to further connect the design models with tools to assess constructability, buildability and/or sustainability (e.g., BES(E) tools, BEAM+ assessment, etc.) to allow for a more holistic and comprehensive design option comparison (Penny et al., 2021).

6 CONCLUDING REMARKS

With the advanced development of digital solutions, digitalisation in engineering has migrated to the next level in recent years. This paper discussed some efficient digital solutions developed for common geotechnical designs including site formation, ELS, and foundations and suggested how this could facilitate our design works, in particular for design optimisation, which aims to enhance cost-effectiveness, constructability and sustainability of the engineering solutions. Various conventional design approaches were reviewed in consideration of available digital tools for enhancement. Although there is still no one-stop solution that could carry out all design works in one suite, it is still possible to completely digitalise the workflow to reduce the processing time, especially for design optimisation using parameter design and for design changes due to site constraints and/or observations. Before a well-proven one-stop solution is available for the engineering design works, the feasibility of adapting "connectors" for data flow using programming scripting in common format (e.g., Microsoft Excel file) has been explored and it is proven to be successful in many cases. Not only can the "connectors" help to interrelate the input and output among software for design and visualisation purpose; it can also transfer relevant information from the design models directly to other design and/or evaluation tools for seamless design and design optimisation. Whilst design optimisation using digital solutions is made possible with the boosted-up of design efficiency, further study on enhancement of digital solutions with the potential of emerging digital technologies is always welcomed.

REFERENCES

BD (2017). Code of Practice for Foundations. Buildings Department, Hong Kong.

GEO (1984). Geotechnical Manual for Slopes (2nd Edition). Geotechnical Engineering Office, Hong Kong.

GEO (1993). Geoguide 1: Guide to Retaining Wall Design (2nd Edition). Geotechnical Engineering Office, Hong Kong.

GEO (2008). Geoguide 7: Guide to Soil Nail Design and Construction. Geotechnical Engineering Office. Hong Kong.

GEO (2011). GEO Publication No. 1/2006: Foundation Design and Construction. Geotechnical Engineering Office, Hong Kong.

Penny, James A., Leung, Rupert K.Y., & Leung, Keith P.W. (2021, January). Design Review and Implementation of Buildability Evaluation System for Public Engineering Works Projects. Hong Kong Engineer, 15-17.

Smart Logging – An Innovative Approach for Generation of Digital Subsurface Data

Anthony C.T. So

Development Bureau, the Government of the Hong Kong Special Administrative Region

Louis N.Y. Wong

Department of Earth Sciences, The University of Hong Kong

Tony Y.K. Ho

Development Bureau, the Government of the Hong Kong Special Administrative Region

ABSTRACT

Ground investigation (GI) to collect subsurface data is one of the crucial parts of engineering projects. With the rapid development of digital technology, 3-D and BIM applications have widely been adopted in these projects. To meet the current demand for real-time generation and dissemination of digital subsurface data, it is necessary to explore ways to enhance the production of the GI data to support these applications.

Traditionally, project engineers or engineering geologists make use of the data in the GI records to produce geological models, by hand or using Computer Aided Design (CAD). Recently, computer software to extract digital AGS data to form 3-D ground models becomes more important. The requirement for preparing the AGS disks was introduced to GI term contracts administered by the Geotechnical Engineering Office (GEO) of the Civil Engineering and Development Department (CEDD) in 1993. Most Government contracts have also adopted similar requirements for AGS data. The reports and the corresponding AGS disks are kept in the Geotechnical Information Unit (GIU) of the Civil Engineering Library (CEL). Currently, over 210,000 sets of GI data in AGS format are kept in the CEL.

It takes some time after completion of GI fieldwork before project engineers or engineering geologists can obtain the GI logs under the current arrangement. Since most engineering projects have very tight programmes, there is a need to explore ways to streamline this procedure. In addition, during production of geological logs, the logs done by logging geologists and other site staff need to be transferred to digital format and such work involves substantial resources and time, and sometimes may introduce unnecessary errors.

To tackle the above issues, a 'Smart Logging' approach which makes use of mobile handheld devices for inputting and uploading GI data to establish geological models in a real-time manner is proposed. Under this arrangement, geologists and site staff can use a mobile handheld device to input geological and other GI data. Project engineers or engineering geologists are able to download the GI data to establish or refine their geological models as soon as the logging is completed. This greatly improves the efficiency of the study works. In addition, an artificial Intelligence (AI) tool has recently been developed and can be integrated into the Smart Logging app. Such AI tool can provide a useful check of the GI logs done by field personnel to reduce human errors. A feasibility study has recently been conducted and the result is promising.

This paper presents the principle, methodology and way forward of this innovative Smart Logging approach for generation of digital subsurface data.

Keywords: Smart Logging, ground investigation, digital subsurface data, artificial Intelligent

1. INTRODUCTION

In line with the initiative of Construction 2.0 as steered by the Development Bureau, the construction industry has been making continuous efforts to adopt digitalization and advanced technologies in different construction projects, for example, Building Information Modelling (BIM), Geographic Information System (GIS), remote sensing, Internet of Things (IOT), Artificial Intelligence (AI) and robotics, etc. Going digitalization with the use of innovative technology is no doubt the direction in enhancing the efficiency and effectiveness of construction projects.

GI to collect subsurface data is one of the crucial parts of engineering projects. With the rapid development of digital technology, 3-D geological models and BIM applications have widely been adopted in these projects. Many construction projects have very tight schedules. To meet the current demand for real-time generation and dissemination of digital subsurface data, it is necessary to explore ways to enhance the production of the digital GI data to support these applications.

2. HISTORY OF DIGITAL SUB-SURFACE DATA (AGS) IN HONG KONG

GI industry has a very long history in Hong Kong. There were no standards for GI fieldwork and geological logging in the past. In 1987 and 1988, the GEO published Geoguide 2 – Guide to Site Investigation and Geoguide 3 – Guide to Rock and Soil Descriptions respectively which provide comprehensive guidelines for GI fieldwork and geological descriptions. Such guides have been adopted by the construction industry and are still being used with only minor revisions after more than 3 decades.

In the past, GI data including geological descriptions and test results were produced by geologists and field technicians in hard copy format. Using these data digitally for study was not possible unless inputting the entire dataset to the computer system manually. Such works are time consuming and can easily introduce human errors. There was also no standardized data format for such data and correlation of the GI data among different projects was different. In 1993, the GEO introduced AGS data format, which is a standardized digital format published by the Association of Geotechnical and Geo-environmental Specialists (AGS), to the GI term contracts (Figure 1). Most Government GI contracts have also adopted similar requirements for AGS data. The current specification in Hong Kong is based on AGS Version 4 with some modifications.

When completing GI works for Government projects, contractors need to submit the final fieldwork reports in hard copy together with the corresponding AGS disks. The reports and AGS disks are kept in the Geotechnical Information Unit (GIU) of the Civil Engineering Library (CEL) of the (CEDD). The GIU, which was established in 1983, forms part of the Civil Engineering Library (CEL) and houses a comprehensive collection of geotechnical data throughout the Hong Kong SAR. Since 1993, about 210,000 sets of GI Data have been stored in different types of storage media and kept in the Geotechnical Information Unit (GIU) (Figure 2) (Lai et al., 2019). All AGS data have been transferred to a central server for better data storage and management.

```
SAMP_TYPE","BLK","Block sample"
SAMP_TYPE","C","Core Sample"
SAMP_TYPE","D","Small disturbed sample"
SAMP_TYPE","LB","Large bulk disturbed sample (for earthworks testing)"
SAMP_TYPE","M","Mazier type smaple"
SAMP_TYPE","P","Piston sample"
SAMP_TYPE","SPTLS","Standard penetration test liner sample"
SAMP_TYPE","U","Undisturbed sample - open drive"
SAMP_TYPE","W","Water sample"
GRAD_TYPE","HY","Hydrometer"
GRAD_TYPE","WS","Wet sieve"
ROCK_PLTF","A","Axial"
ROCK_PLTF","D","Diametral"
ROCK_PLTF","L","Parallel to planes of weakness"
ROCK_PLTF","P","Perpendicular to planes of weakness"
ROCK_PLTF","I","Irregular lump"
ROCK_PLTF","B","Block"
TRIG_TYPE","CD","Consolidated drained (single stage)"
TRIG_TYPE","CDM","Consolidated drained (multi-stage)"
TRIG_TYPE","CU","Consolidated undrained with pwp measurement (single stage)"
TRIG_TYPE","CUM","Consolidated undrained with pwp measurement (multi-stage)"
TRIG_TYPE","UU","Unconsolidated quick undrained (single stage)"
TRIG_TYPE","UUM","Unconsolidated quick undrained (multi-stage)"

**UNIT"
*UNIT_UNIT","*UNIT_DESC"
cm3","cubic centimetres"
dd/mm/yyyy","day month year"
deg","degree (angle)"
degC","degree Celsius"
hhmmss","hours minutes seconds"
kN/m2","kiloNewtons per square metre"
kPa","kiloPascals"
l/m","litres per minute"
m","metre"
m/s","metres per second"
m2/MN","square metres per MegaNewton"
m2/yr","square metres per year"
Mg/m3","Megagrams per cubic metre"
mm","millimetres"
mm/min","millimetres per minute"
mm/s","millimetres per second"
GPa","GigaPascals"
%","percentage"
mV","milliVolts"
ppm","parts per million"
g/l","grams per litre"
Ohm m","Ohm metre"

**SAMP"
*HOLE_ID","*SAMP_TOP","*SAMP_REF","*SAMP_TYPE","*SAMP_DIA","*SAMP_BASE","*SAMP_DESC","*SAMP_UBLO","*SAMP_REM","*SAMP_DATE","*SAMP_
<UNITS>","m","","","mm","m","","","","dd/mm/yyyy","hhmmss","kPa","m","degC","kPa","l/m","",""
FB-PH04","37.20","","C","83","37.92","","","","","","","","","","","",""
FB-PH04","38.10","","C","83","38.15","","","","","","","","","","","",""
FB-PH04","35.20","","C","83","35.37","","","","","","","","","","","",""
HCB-PH03","28.22","","C","83","28.34","","","","","","","","","","","",""
```


Figure 1 - Example of AGS Data

GI Report & AGS Floppy Disk

GI Report & AGS CD-ROM

AGS Disk – DVD-ROM

Figure 2 - GI Reports and AGS Disks Produced in Different Periods

3. ISSUES OF PRODUCTION OF DIGITAL SUB-SURFACE DATA

Obtaining GI data for conducting design of construction works is critical to engineering projects. For many years, there have been grave concerns from the project engineers about the timing of submission of GI reports due to the tight project schedule. However, it normally takes some time after completion of GI fieldwork before project engineers or engineering geologists can obtain the GI logs under the current arrangement. As such, there is a need to explore ways to streamline this procedure. In addition, the geological logs done by logging geologists and other site staff are recorded manually and in hard copy format. During production of GI reports, such records need to be transferred to digital format and such work involves substantial resources and time, and sometimes may introduce unnecessary errors during data transfer.

4. SMART LOGGING – A NEW APPROACH TO GENERATE DIGITAL GI DATA

4.1 Proposed Workflow

To tackle the above issues, a 'Smart Logging' approach which makes use of a mobile handheld device for inputting and uploading GI data to produce geological logs in a real-time manner is proposed. Under this arrangement, geologists and site staff can use mobile handheld devices such as mobile phones or tablets to input geological and other GI data such as field test results and field installation details. The GI data are converted to AGS format immediately after completion of the fieldwork. The data will then be sent to the computer server or cloud for storage. At the same time, project engineers or engineering geologists can access the server or cloud to download the GI data to establish or refine their geological models as soon as the logging is completed. If project engineers or engineering geologists consider that the GI data are not sufficient, they can order additional GI immediately (Figure 3). This would avoid the likelihood of delaying the work as the GI contractors may have demobilized and additional time is required to re-mobile to site if the additional GI is not ordered timely. Hence, this can greatly improve the efficiency of the workflow and save cost for additional mobilization or re-mobilization. In some situations, further access permission and traffic arrangement would be required if additional GI is not ordered timely. Such administrative work will not only induce extra cost, but more importantly, affect the progress of the projects. In addition to fast generation of GI logs, since the GI data are already in AGS format, users can integrate these data with the existing AGS data obtained from the GIU to establish geological models in a fast manner (Figure 4).

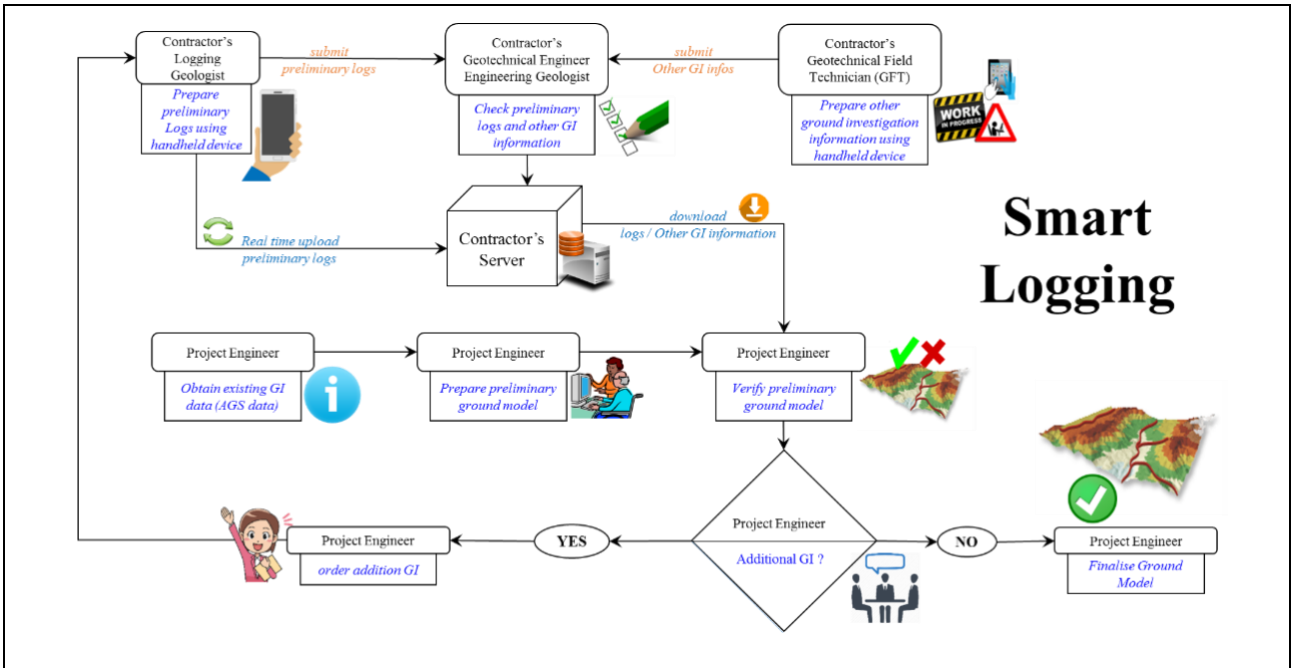

Figure 3 - General Workflow of Smart Logging

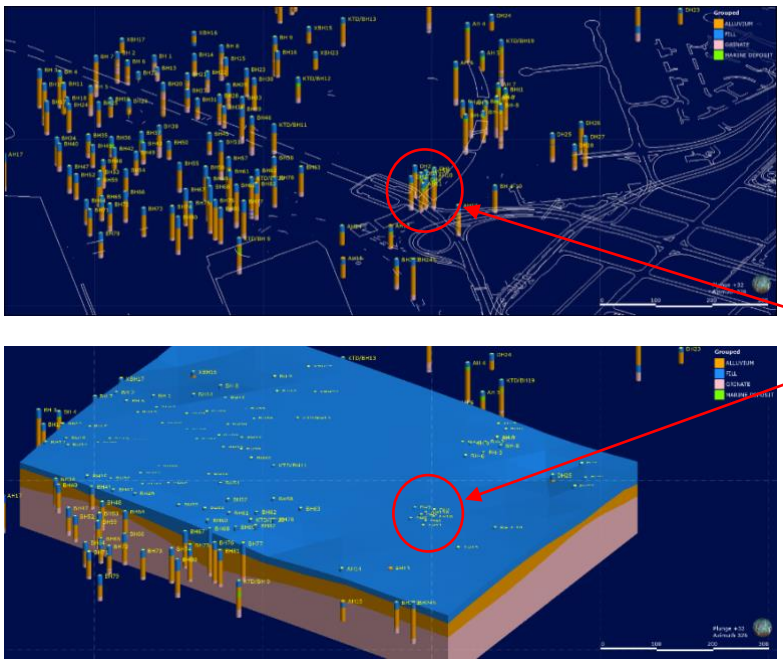

1. Use AGS data of existing boreholes from the GIU to establish a general geological model
2. Add AGS data generate from Smart Logging to refine the geological model

Figure 4 - Digital Model Generated from AGS Data using Smart Logging

4.2 Feasibility Study

Riding on the aforementioned workflow, a beta version of the Smart Logging app has been developed. A feasibility study has been conducted to evaluate the functionality and practicality of this app. This study was participated by selected groups of GI contractors and consultants (Figure 5). The study included assessment of the capability of the mobile app to generate AGS data which is important to the users to establish digital geological models. The mobile app developed in the study was able to run on the two most common mobile operating systems i.e. iOS and Android. This app was a preliminary version and could only record geological information such as weathering grade and geological descriptions according to Geoguide 3. Nevertheless, it is considered that this app was sufficient to test the concept and identify the advantages and disadvantages of the Smart Logging approach. Promising results have been obtained from the feasibility study and the Smart Logging approach is proven to have great potential to expedite the generation of digital GI data and geological models.

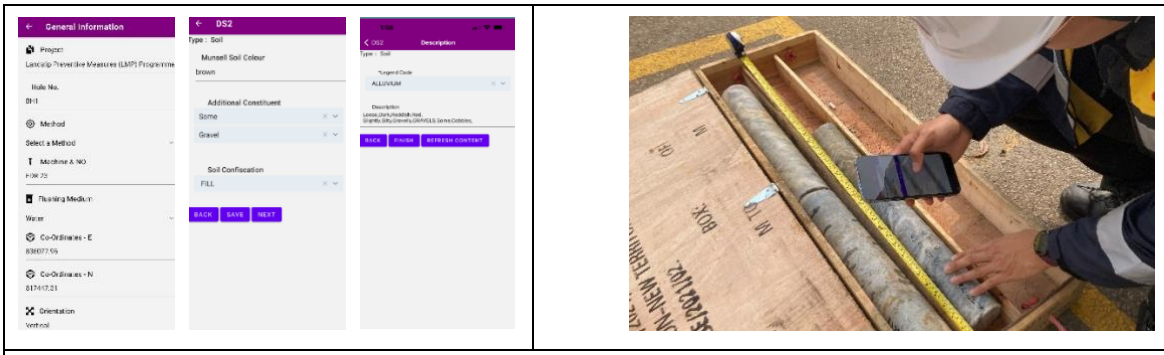

Figure 5 – Beta Version of Smart Logging App used in the Feasibility Study

4.3 Pilot Contracts

To further evaluate the practicality of the proposed approach under actual working environment, pilot contracts will be launched to adopt the Smart Logging app for real applications. In the pilot contracts, a full version of the Smart Logging app which is capable of recording geological descriptions, field test results and field installations will be developed. Similar to the app used in the feasibility study, this mobile app will be able to run on the latest version of two mobile operating systems (mobile OS), i.e. iOS and Android. It will support the input of borehole and other GI data by geologists and field technicians on site. The input GI data will be stored in the mobile phones or tablets when it is not accessible to the internet or under offline mode. When internet is available, the data can be upload to the system. In addition, the system would provide a function to identify locations of GI stations. After inputting of GI data is completed, it will generate a standard GI log in accordance with the relevant guideline and allow authorized users to download. It will also generate the geological descriptions and other GI data in AGS Version 4 format.

It is believed that the experience gained in these pilot contracts will further enhance this Smart Logging app before full implementation.

4.4 Challenges

Although this approach has many merits, it is relatively new in Hong Kong and several hurdles are yet to be overcome. During the feasibility study, useful feedbacks from the frontline users had been collected. The participants reported that they sometimes encountered difficulties in using the mobile app in adverse weather conditions. In addition, logging using a handheld device is new and the logging geologists and field technicians need time to adapt to this new approach including hardware, software and workflow. Longer time to complete the logs at the beginning is inevitable. However, in the long run, this approach could substantial reduce resources spent on manual inputting and checking and avoid unnecessary errors.

4.5 Classification of Rocks using Artificial Intelligence

To aid the classification of rock types for geotechnical engineering purposes, the University of Hong Kong (HKU) have recently explored the use of convolutional neural network (CNN) deep learning models to classify some common Hong Kong rock types - coarse ash tuff, fine ash tuff, coarse-grained granite, medium-grained granite, and fine-grained granite. A large rock image database containing more than 17,000 rock images subsampled from core box images either cropped from the pdf files of GI reports or original camera captured photographs in JPEG format was developed. After manual labelling of the images, a multi-stage strategy of model training, validation and testing of five landmark CNNs was conducted. The performance of MobileNet V2 was found to be the most satisfactory in classifying the above rock types with an average prediction accuracy of around 90%. In addition, the HKU research team has recently proposed a new CNN called HKUDES_Net (Zhou et. al., 2023), which contains several salient features, including dynamic expansion, Swish activation, and squeeze and excitation to provide better perceived mineral and texture patterns in the rock images, hence giving better prediction performance for seven types of Hong Kong rock (Figure 6). The on-going research is to develop a mobile application, with a user-friendly interface for automatic classification of common types of Hong Kong igneous rock and decomposition grades, and for the determination of fracture state indices based on user's uploaded rock corebox photographs. With proper interfacing, this mobile application may become a module of the Smart Logging to provide a useful check of the GI logs done by the field personnel to reduce human errors in the future.

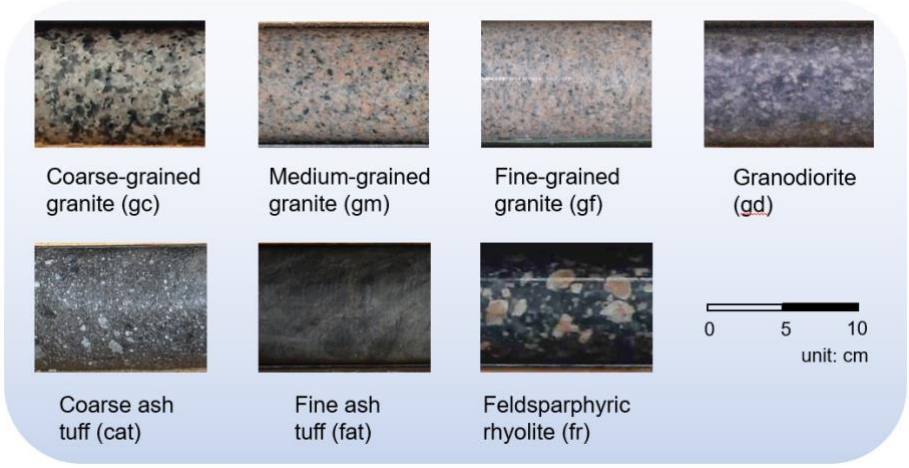

(a)

precision	recall	f1-score	generalization gap	accuracy gap
90.9%	**90.4%**	**90.5%**	**0.03**	**2.38%**

(b)

Figure 6 – Classification of Rocks using Artificial Intelligence (a) examples of rock images for training HKUDES_Net, (b) prediction performance of HKUDES_Net (Zhou et al., 2023)

5 WAY FORWARD

From the generation of the idea of Smart Logging through the feasibility study and pilot contracts, we are progressively enhancing this approach with input from different stakeholders at different stages. With the rapid development of computer software and hardware, it is believed that the issues encountered would be addressed adequately. After the experience gained from the pilot contracts and the corresponding enhancement works made, it is intended that this approach will be implemented in future Government works contracts.

In addition to enhancement to the GI logging using Smart Logging, Measuring-While-Drilling (MWD) which records the drilling machine parameters during the drilling process can also provide additional quantitative information on sub-surface conditions (BSI, 2016). With the rapid increase in the use of innovative technology, digital sensors and IoT can provide powerful means to monitor site works effectively. Drilling parameters such as penetration rates, hydraulic pressure, rotation torque and rotation speed can be obtained in a real-time manner. These data give useful and objective information on the sub-surface geological conditions. MWD can also more accurately record fractures and no recovery zones which are extremely useful for conducting geotechnical studies especially in marble areas and determination of founding levels of piles. With the availability of such parameters, in-depth analysis can be conducted to give a better understanding of ground conditions. Moreover, real-time monitoring allows observation and documentation of operational conditions of the equipment and quality control during construction. The MWD has been used for blast holes drilling in "The Relocation of Sha Tin Sewage Treatment Works to Caverns" and encouraging results were obtained (Leung & Ko, 2022). It is considered that the MWD can also be adopted in the drilling for GI works in Hong Kong. With the Smart Logging and MWD techniques, it can significantly uplift the performance of the GI works and the digital capability of the GI industry.

6 CONCLUSION

To meet the current demand for digital GI data, it is no doubt that the Smart Logging approach can provide a convenient, effective and efficient means to generate digital sub-surface information. Although it is still at a preliminary stage, it is believed that the technical problems arisen would be resolved and site personnel would gradually adapt to this approach. Despite the development and implementation of the Smart Logging approach still remains challenging at this moment, it is certain that this digital approach will greatly facilitate construction projects.

REFERENCES

Lai, A.C.S., So, A.C.T. & Mok, S.C. (2019). AGS Data – Subsurface Data in Digital Format in Hong Kong. Proceedings of the HKIE Geotechnical Division 39th Annual Seminar: Transformation in Geotechnical Engineering – Technology, Digital and Innovation, 78-83.

Leung, S & E.M.Y. Ko (2022). Active Site Supervision to Enhance Drilling & Blasting, Proceedings of the HKIE Geotechnical Division 42nd Annual Seminar: A New Era of Metropolis and Infrastructure Developments in Hong Kong, Challenges and Opportunities to Geotechnical Engineering, 208-223

BSI (2016): BS EN ISO 22476-15:2016, Geotechnical Investigation and Testing – Field Testing Part 15: Measuring While Drilling, British Standards Publication.

Zhou, Y., Wong, L. N. Y., & Tse, K. K. C. (2023). Novel Rock Image Classification: The Proposal and Implementation of HKUDES_Net. Rock Mechanics and Rock Engineering, 56(5), 3859.

Effects of Soil-Structure Interaction on Wall Deflections and Surface Settlements During Deep Excavations

L.W. Wong
SMEC Asia Limited, Hong Kong

ABSTRACT

Ground movements due to excavations may cause damages to structures. While wall deflections could be adequately predicted, accurate estimations of ground movements are usually far from field observations. It has been identified that the behaviour of soil at small strain plays a key role in predicting the surface settlements. Presented herein is a study on a well-documented excavation case history in soft ground located in Taipei Basin. Two-dimensional finite element analyses adopting the hardening soil with small-strain stiffness to simulate the nonlinear stress-strain relationship of soils have been conducted. Various interface reduction factors have been adopted to simulate the soil-structure interaction. The effect of water pressures on the performance of excavations was studied. The analyzed results show that the hardening soil with small-strain stiffness model could reliably predict the wall deflections and the surface settlements simultaneously. The interface reduction factor would be the key parameter for exploring the ground movements due to deep excavations.

Keywords: Soil-structure Interaction, Hardening-Soil Model, Small Strain, Ground Movements

1 INTRODUCTION

The prediction by numerical analysis on surface settlements next to excavations has been the challenge of the researchers and the practicing profession. Jardine et al. (1986) and Burland (1989) pointed out that as soil displays non-linear behavior and the stiffness of soils at small strain is very high, the small-strain behaviour of soil plays an important role on predicting the ground surface settlements induced by excavation.

In order to investigate the importance of the nonlinear behavior of soil on predicting the ground surface settlements, Kung & Ou (2006) conducted numerical analysis on a case history using various soil models. Amongst the models adopted in the analysis, they found that good predictions on surface settlements could be obtained by using the Modified Pseudo-Plasticity model (Kung, 2003) and by the Three-Surface Kinematic Hardening model (Stallebrass & Taylor 1997). These 2 soil models consider high initial stiffness of soil and nonlinear behavior at small strain. The other soil models, the Modified Cam-clay model (Roscoe & Burland 1968) and the Original Hyperbolic model (Kondner & Zelasko 1963; Duncan & Chang 1970), cannot properly predict the surface settlements. Kung & Ou (2006) confirmed the importance of behavior of soil at small strain on the prediction of excavation behaviour.

The Modified Pseudo-Plasticity model and the Three-Surface Kinematic Hardening model are in-house programs of the research or the academic institutes and are not readily available by the practicing professionals. On the other hand, the Hardening-Soil with small-strain Stiffness model (HSS) developed by Benz (2006) and introduced in the PLAXIS program (PLAXIS 2013) is commercially available. Since the HSS model simulates the nonlinear stress-strain-strength relationship of soils, it is expected that the HSS model could be applicable for predicting the behavior of surface settlements induced by excavations.

In this paper the excavation case history on Taipei National Enterprise Centre (TNEC) is adopted for the numerical analysis using the HSS soil model. The study results demonstrate that the Hardening-Soil with Small Strain stiffness (HSS) model is capable for predicting both the wall deflections and the surface settlements simultaneously.

2 CASE STUDIED

The Taipei National Enterprise Center (TNEC), depicted in Figure 1, is a well-documented excavation case history presented by Ou et al. (1998, 2000b), Kung & Ou (2006), Kung et al. (2009) and Ou (2016). The main observation section on the southeast of the excavation pit comprised an inclinometer in wall and 4 inclinometers in ground. The array of the settlement markers deployed next to the inclinometers SI1 to SI4 comprised 21 markers spacing at 1 m to 3 m. The array was extended to 49 m behind the south wall.

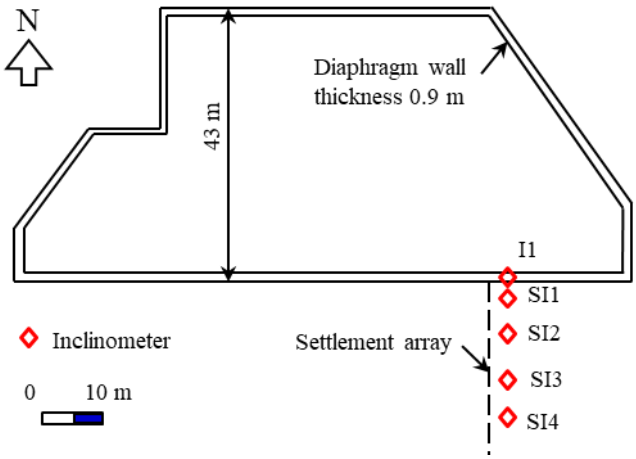

Figure 1: Instrumentation layout of the Taipei National Enterprise Center (TNEC) excavation

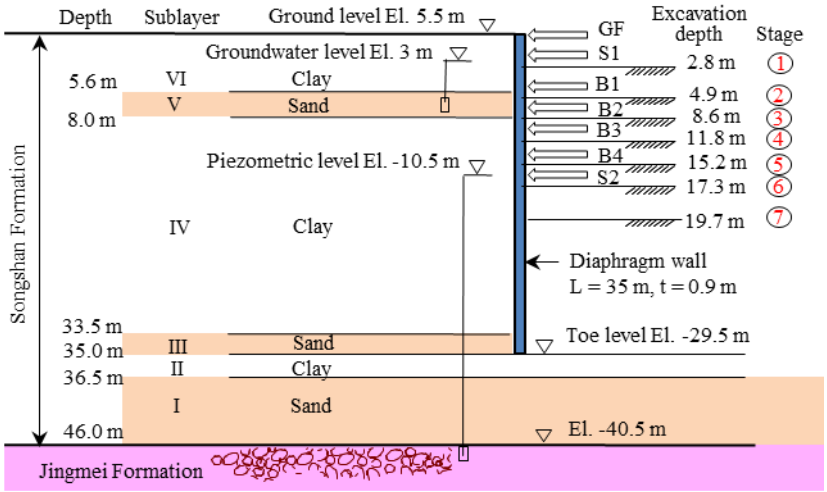

Figure 2: Soil profile of the TNEC case and excavation scheme

2.1 Ground conditions

The TNEC building is located in the K1 Geological Zone (MAA 1987) in the eastern portion of the Taipei Basin. A representative excavation model is shown in Figure 2. The excavation was carried out to a depth of 19.7 m in 7 stages. The pit was retained by diaphragm wall of 0.9 in thickness and 35 m in length. Excavation for the foundation was constructed by the top-down method. The diaphragm wall was supported by the ground floor (GF) slab and 4 levels of basement floor slabs (B1 to B4) of 150 mm in thickness. Temporary steel struts were erected at the upper and the lower levels (S1 & S2). Excavation commenced in January 1992 and the foundation slab at 19.7 m depth was cast in November 1992.

As depicted in the soil profile shown in Figure 2, the Songshan Formation of 46 m in thickness comprises six alternating sand (SM) and clay (CL) layers. Sublayers I, III, and V are sandy soils and Sublayers II, IV, and VI are clayey soils. The properties of the six sublayers in the Songshan Formation have been well

discussed in literature (Moh and Ou 1979; MAA 1987; Moh et al. 1989). Underlying the Songshan Formation is a water-rich gravelly (GM) Jingmei Formation, which is a competent formation with very high stiffness.

2.2 Undrained shears strengths for clay sublayers

An advanced study was conducted by Geotechnical Engineering Specialty Consultant engaged by the Department of Rapid Transit Systems of Taipei City Government in the very early stage of the metro construction. This Designated Task studied the characteristics of the soils in the Taipei Basin to provide the basic information required for the design and construction of metro facilities (Chin et al. 1994 and 2007; Chin & Liu 1997; Hu et al. 1996). This was a research project so it was carried out under stringent supervision. Soil samples of high quality were obtained and tested with great care. The test results are therefore more reliable than those normally obtained. Figure 3 presents the results of the CK_0UC tests conducted on the specimens recovered from borehole R-1 that Chin et al. (1994) reported. Borehole R-1 was located in the K1 Geological Zone in Taipei Basin. Kung et al. (2009) and Ou et al. (2000a) presented the results of undrained shear strength, s_u, for the K1 Geological Zone in the Taipei Basin. The s_u values were determined from consolidated triaxial undrained compression and extension tests conducted on specimens recovered from the clayey Sublayer IV. The specimens were saturated and K_0-consolidated to the in-situ effective stress states. The undrained shear strengths to the vertical effective stresses, the s_u/σ'_v ratio, for the compression tests is 0.29. For the extension tests, the s_u/σ'_v ratio is 0.21. The variation in undrained shear strengths for the compression tests that Ou et al. (2000a) and Kung et al. (2009) reported are presented in Figure 3. Compared with the CK_0UC tests reported by Chin et al. (1994), the s_u values obtained by Ou et al. (2000a) and by Kung et al. (2009) are lower. The lower s_u values would likely be attributable to sampling disturbance. Although the specimens were consolidated to the in-situ horizontal stress, such process could not fully compensate the effect due to sample disturbance.

In this study, the Author has proposed the undrained shear strengths of the sublayers IV and II clayey soils in the K1 Geological Zone of the Songshan Formation could be expressed by the empirical equation:

$$s_u = 60 + 4.8\ (D - 15) \text{ in kPa} \qquad (1)$$

where D is the depth in metre and s_u is the undrained shear strength in kPa.

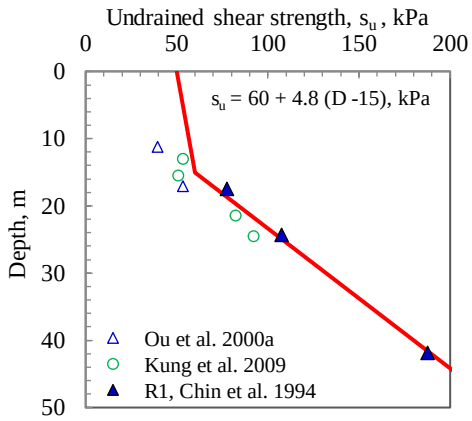

Figure 3: Undrained shear strengths of clays obtained by CK_0UC triaxial tests

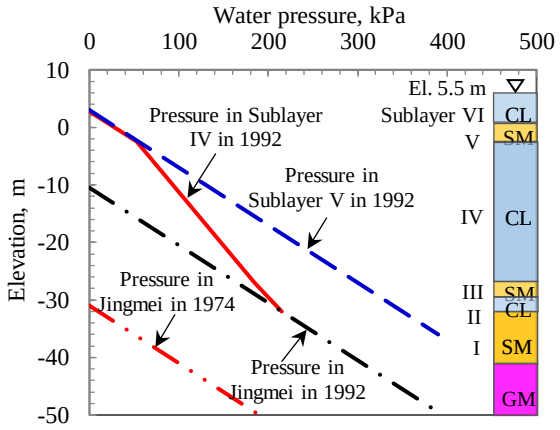

Figure 4: Groundwater pressures on the outer face of the diaphragm walls

2.3 Groundwater conditions

The piezometric level in the Jingmei Formation was lowered to a level near the bottom of the Songshan Formation in the 1970s due to excessive extraction of groundwater to supply water to the city, leading to significant reductions in water pressures in the Songshan Formation and substantial ground settlements as a result. The piezometric level in the Jingmei Formation did not recover till 1974 although pumping had been banned since 1968. The subsoils in the Songshan Formation in the Taipei Basin are thus substantially over-

consolidated. This is particularly true for the clayey Sublayer II because the underlying sandy Sublayer I is so permeable that the piezometric level in Sublayer I essentially dropped by the same magnitudes as those in the Jingmei Formation. Based on monitoring records at the deep well at Sun Yet Sin Memorial Hall, located at 1.2 km south of the TNEC project site, Hwang and Moh (2022) reported that the piezometric level in the Jingmei Formation in the eastern portion of the Taipei Basin was around El. -10.5 m in 1992. In the central portion of the Taipei Basin, the piezometric level in Jingmei Formation recovered to El. 0 m in 2017.

Ou et al. (2000b) reported that the groundwater level in the Songshan Formation at TNEC was located at 2 m depth prior to excavation. The piezometric level of El. 3.0 m for the sublayers V is adopted for the numerical analysis in this study. The distributions of the water pressures outside the diaphragm wall at TNEC in 1992 are presented in Figure 4. For sublayer I and Jingmei Formation, the piezometric level of El. -10.5 m in 1992 is adopted. The water pressures for sublayers II to IV are interpolated between sublayers V and I. Inside the pit, the piezometric levels were maintained at a depth of 1 m below the excavation levels in each stage have been adopted in the analysis.

3 NUMERICAL SIMULATION

3.1 Finite element mesh

The section for the numerical analysis is depicted in Figure 5. The width of the excavation is 40 m. Because of symmetry in geometry, only half of the section is analyzed as depicted in Figure 5. The excavation is carried out to a depth of 19.7 m in the analysis. The lateral extent of the finite element model reaches a distance of 140 m from the central axis of the excavation trench. The ground model is 60 m in depth and the diaphragm wall is located at a distance of 20 m from the axis of the trench.

The Jingmei Formation is a competent formation with very high stiffness and is frequently assumed to be the base of the numerical models. However, the base of the finite element model in this study is placed at a depth of 60 m to include a 14 m layer of the Jingmei Formation to ensure that the contribution of this formation to ground movements is accounted for.

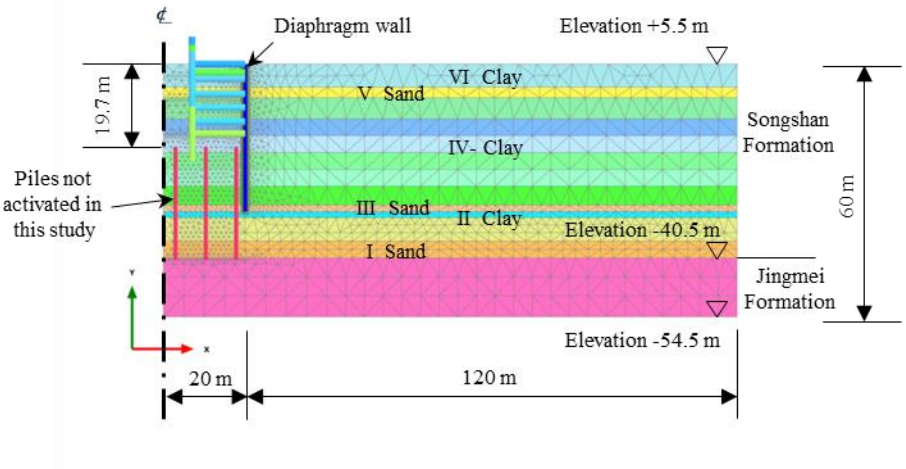

Figure 5: Finite element mesh for the analytical section for 7 stages of excavation

3.2 Nonlinearity of soil behavior - Hardening-soil with small-strain stiffness model

The PLAXIS-2D finite element software developed by PLAXIS BV (2013) has become a very popular tool in geotechnical analysis and design. The Hardening-Soil with Small-strain stiffness (HSS) constitutive soil model is an extension of the Hardening-Soil model (Benz 2006, Schanz & Vermeer 1998; Schanz et al. 1999) introduced in the PLAXIS program and is adopted herein to simulate the non-linear stress-strain relationship of soils under loading and unloading conditions. In the HSS model, the parameters adopted to define the hyperbolic stress-strain relationship are as follows:

- E^{ref}_{50} is the reference secant stiffness from standard triaxial drained test,
- E^{ref}_{oed} is the reference tangent stiffness for oedometer primary loading,
- E^{ref}_{ur} is the reference unloading-reloading stiffness from standard triaxial drained test,
- m is the exponential factor for stress-level dependency of stiffness,
- R_f is the failure ratio, $R_f = q_f / q_a$,
- q_a is the asymptotic value of the shear strength and q_f is the failure strength,
- G^{ref}_0 is the reference shear modulus at the level of very small strains,
- $\gamma_{0.7}$ is the reference shearing strain to define the behavior of degradation of moduli when G^{ref}_0 is reduced to 0.7 G^{ref}_0.

In this study, the stiffness values of soils are related to the undrained shear strengths for clays and the N values for sands as expressed in the empirical Equations 2 to 6:

$$E^{ref}_{50} = 150\ s_u \text{ (for clayey soils)} \quad (2)$$
$$E^{ref}_{50} = 2\ N \text{ (in MPa for sandy soils)} \quad (3)$$
$$E^{ref}_{oed} = E^{ref}_{50} \quad (4)$$
$$E^{ref}_{ur} = 5\ E^{ref}_{50} \quad (5)$$
$$G^{ref}_0 = E^{ref}_{ur} \quad (6)$$

in which s_u is the undrained shear strengths of clayey soils and N is the blow-counts obtained in standard penetration tests for sandy soils. The parameters adopted in this study are summarized in Table 1. The effective shear strength parameters, i.e., the c' and ϕ' values, for the silty sand strata, are determined from laboratory tests conducted on thin-wall tube specimens. For the clayey layers, c' = s_u and $\phi' = 0^o$ is assumed in the analyses. The dilation angle, ψ', of 2^o, 0^o, and 3^o are adopted for the sandy, the clayey, and the gravelly soils respectively. The R_f equals 0.9 is adopted. The unload-reload Poisson's ratio, υ_{ur}, of 0.2 is used as suggested by Benz (2006) and Schanz et al. (1999). Although the HSS soil model is an effective stress model and adopting the $\phi' = 0^o$ for the clayey soils loses its compression hardening function and stress-dependent stiffness, parametric studies using both the effective and the total stress models show that the computed wall deflections and settlements are essentially the same. The total stress model for clay is adopted in this study.

Table 1: Soil parameters for the HSS model adopted in the PLAXIS analyses

Mid depth m	Soil type	Unit weight γ' kN/m^3	N value	Undrained shear strength s_u, kPa	Effective cohesion c' kPa	Effective friction angle ϕ', deg	Dilation angle ψ' deg	Reference stiffness, MPa		Initial shear moduli G^{ref}_0, MPa
								Secant stiffness E^{ref}_{50}	Unload-reload stiffness E^{ref}_{ur}, MPa	
2.8	CL	18.3	3	52				7.8	39	39
7	SM	18.9	5		0	31	2	10	50	50
11	CL	18.2	3	57				8.6	43	43
15.5	CL	18.2	4	62				9.4	47	47
19.5	CL	18.2	4	82				12.2	61	61
23.5	CL	18.2	7	101				15.1	76	76
27	CL	18.2	8	118				17.6	88	88
31	CL	18.2	5	137				20.5	103	103
34.5	SM	19.6	14		0	31	2	28	140	140
35	CL	19.1	10	163				24.5	122	122
39.3	SM	19.6	24		0	32	2	48	240	240
44	SM	19.6	20		0	32	2	40	200	200
53	GM	20.6	>100		0	35	3	300	1500	1500

3.3 Determination of small-strain stiffness

The parameters for the small-strain stiffness, i.e., the G^{ref}_0 and the $\gamma_{0.7}$, have been determined from the laboratory tests. Kung et al. (2009) presented the results of small-strain triaxial tests and bender element tests conducted on undisturbed specimens recovered from clayey Sublayer IV of the Songshan Formation. The specimens were saturated and K_0-consolidated to the in-situ effective stress states. The K_0 values applied for

consolidation ranged from 0.5 to 0.55. After completing the K_0-consolidation, but prior to the shearing tests, bender element tests were carried out to measure the shear moduli of the clay specimens. Compression and extension undrained triaxial shearing tests were then conducted. The undrained shear strengths profile obtained is presented in Figure 3. Based on the results of the bender element tests, Kung et al. (2009) obtained the G_{max}/s_u ratios ranging from 738 to 788, with an average ratio of 759 for the axial compression tests, where G_{max} is the initial shear modulus. For the axial extension tests, the G_{max}/s_u ratios ranged from 614 to 751, with an average of 671. In this study, the $G^{ref}_0 = 750\ s_u$ is adopted.

Chin et al. (2007) presents the CK_0UDSS test results that depicted in Figure 6. Santos & Correia (2001) recommended that the stress-strain curve for small-strains can be described as:

$$G / G_0 = 1 / (1+ 0.385\ \gamma / \gamma_{0.7}) \quad (7)$$

where G_0 is the maximum small-strain shear modulus. The modulus degradation curves with the threshold $\gamma_{0.7}$ values ranging from $0.8x10^{-4}$ to 10^{-3} are shown in Figure 7. The degradation of the shear moduli with shear strain interpreted from the direct simple shear test is presented Figure 7, showing that the Taipei clay would have the $\gamma_{0.7}$ value of 5×10^{-4}. In this study, a $\gamma_{0.7}$ value of 4×10^{-4} has been adopted.

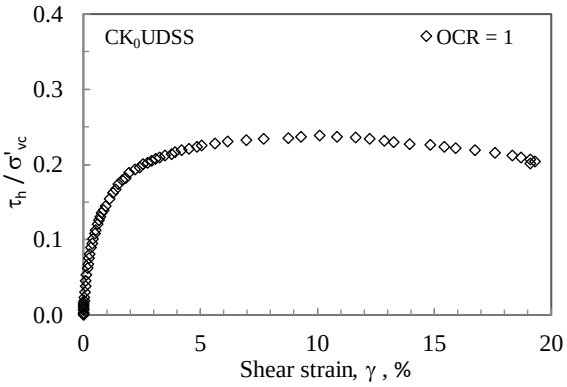

Figure 6: Stress-strain curve of Taipei clay under CK_0UDSS test (After Chin et al. 2007)

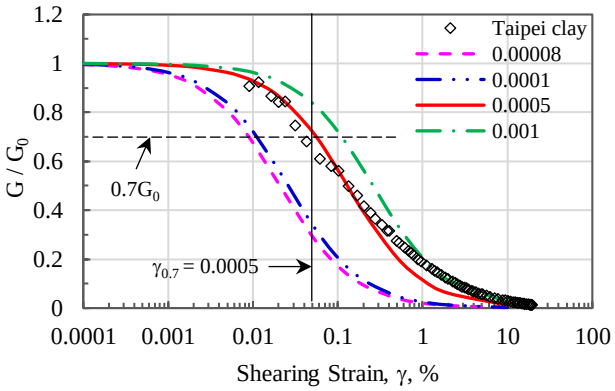

Figure 7: Degradation of shear moduli with shearing strain

3.4 Modeling of the retaining structures

The excavation scheme and the retaining structures are depicted in Figure 2. The diaphragm wall is simulated by plate element and an E_c value of 25,000 MPa is adopted for concrete with a characteristic compressive strength of 28 MPa. The estimated flexural rigidity (denoted as E_cI_c where I_c is the moment of inertia) and the axial stiffness (denoted as E_cA_c where A_c is the sectional area) of the diaphragm wall of 0.9 m in thickness are 1,067 MN-m and 15,810 MN/m respectively. These values have already been reduced from their original values by 30 % to account for tensile cracks and creeping of concrete during excavation.

The excavation was supported by 5 levels of floor slabs, namely, the ground level floor (GF) and the 4 basement floors (B1 to B4) of 150 mm in thickness and 2 levels of steel struts. During the top-down construction, openings were provided on the floor slabs for transportation of excavated materials and for delivery of construction materials such as reinforcement bars, concrete and the steel struts. In addition to the concrete creeping effect, the axial stiffnesses of the floor slabs have been further reduced by 30 % for the openings. For the combining effect of creeping and the presence of opening, a reduction factor of 0.5 is adopted. The axial stiffness of 1,988 MN/m is adopted for the slabs GF and B1 to B4 in the numerical analysis. The level S1 struts were erected at the depths of 2 m prior to the construction of the GF slab.

Table 2: Strut properties

Strut level	Depth m	Strut type	Area A_s, cm^2	Stiffness E_sA_s/s, MN/m	Design preload, kN/m	Strut spacing s, m
S1	2.0	1H300x300x10x15	118.5	714	231	2.0
S2	16.5	1H400x400x13x21	218.7	1,319	346	

The slabs and the struts are represented by fixed-end anchors. The properties for the steel struts are presented in Table 2. The steel is assumed to be an elastic material with a Young's modulus (E_s) of 210 GPa.

3.5 Modeling of soil-structure interface

The contact between the soil and the wall structure is a critical issue to be considered in deep excavations. A frictional contact model is applied at the soil-wall interface to investigate its influence on the wall deflection and on the surface settlement behavior. In the PLAXIS software, an elastic-plastic model following the Mohr-Coulomb criterion is used to describe the interfaces for the soil-structure interaction. According to the Reference Manual (Bentley, 2022), the strength properties of the interface are related to the strength properties of a soil layer by a strength reduction factor, $R_{inter,}$ and are calculated by applying the following rules:

$$s_{u,i} = R_{inter}\, s_{u,\,soil} \quad (8)$$

$$\tan \phi_i = R_{inter} \tan \phi_{soil} \quad (9)$$

$$\psi_i = 0 \text{ for } R_{inter} < 1, \text{ otherwise } \psi_i = \psi_{soil} \quad (10)$$

where $s_{u,\,i}$, ϕ_i , ψ_i are the undrained shear strength, the friction angle and the dilation angle of the interface. It is noted that the interface stiffness is also linked to the R_{inter} value by the expressions:

$$G_i = R^2_{inter}\, G_{soil} \quad (11)$$

$$E_{oed,i} = 2\, G_i\, (1 - \nu_i) / (1 - 2\, \nu_i) \quad (12)$$

where the G_i is the shear moduli and the $E_{oed,i}$ is the compression moduli of the interface. The Poisson's ratio of the interface, ν_i , is 0.45. The R_{inter} value of 1 is the rigid mode and represents the rough interface.

In this study, various R_{inter} values have been adopted to assess the influence of soil-structure interaction. As summarized in Table 3, Case 1, Case 2 and Case 3 adopt the R_{inter} values of 1, 0.5 and 0.3 respectively.

4 RESULTS OF NUMERICAL ANALYSIS

4.1 Computed wall deflections

The computed wall deflection profiles for the TNEC case are presented in Figure 8. The analysis results are compared with those observed at inclinometers I-1 that Ou et al. (2000b) reported. Close matching of the computed profiles with those observed has been achieved for Case 3 adopting the $R_{inter} = 0.3$. In the final stage the computed maximum deflection, $\delta_{h\text{-}max}$, is 109.7 mm, which deviates from the observed 106.4 mm by only 3 %. The computed wall deflections and surface settlements for Case 1 to Case 3 are summarized in Table 3, showing a trend that the smaller R_{inter} value, the larger wall deflections would be computed. The $\delta_{h\text{-}max}$ values of 109.7mm and 98.7 mm are computed for the cases adopting the R_{inter} values of 0.3 and 1 respectively. Smooth interfaces ($R_{inter} < 1$) would give larger wall deflections than those for the rough interface.

Table 3: Computed wall deflections and surface settlements in the final stage

Case	Interface reduction R_{inter}	Wall deflection, mm		Wall settlement, mm			Surface settlement, mm		Settlement between wall & ground, mm
		Maximum $\delta_{h\text{-}max}$	At toe $\delta_{h\text{-}toe}$	At top	At toe	Short-ening	Maximum $\delta_{v\text{-}max}$	Next to wall	
Observed	-	106.4	11.4	-	-	-	74	40	-
1	1	98.7	7.4	5.0	4.4	0.6	57.0	4.1	-0.9
2	0.5	93.6	9.0	8.0	7.5	0.5	63.0	13.2	5.2
3	0.3	109.7	14.2	18.4	18.1	0.3	77.3	30.0	11.6

4.2 Computed lateral ground movements

Along the instrumented section at the southeast area of the excavation pit, the inclinometers in ground SI-1 to SI-4 were installed at the distances of 2 m to 22 m behind the diaphragm wall. Ou et al. (2000b) and Kung et al. (2009) reported the ground movement profiles observed at these inclinometers. Figure 9 presents the

computed ground movements in the final stage for Case 3 adopting the R_{inter} value of 0.3. The computed lateral ground movement profiles closely match with those observed at SI-1 to SI-4.

It is noted that inclinometers SI-3 and SI-4 were 30 m in length and were not embedded into the Jingmei Formation. The numerical analysis shows that the toe movements of 19 mm and 12 mm would occur at the toe levels of these inclinometers in the final stage. The lateral deflection profiles for SI-3 and SI-4 shown in Figure 9 are therefore adjusted by adding the computed toe movement values.

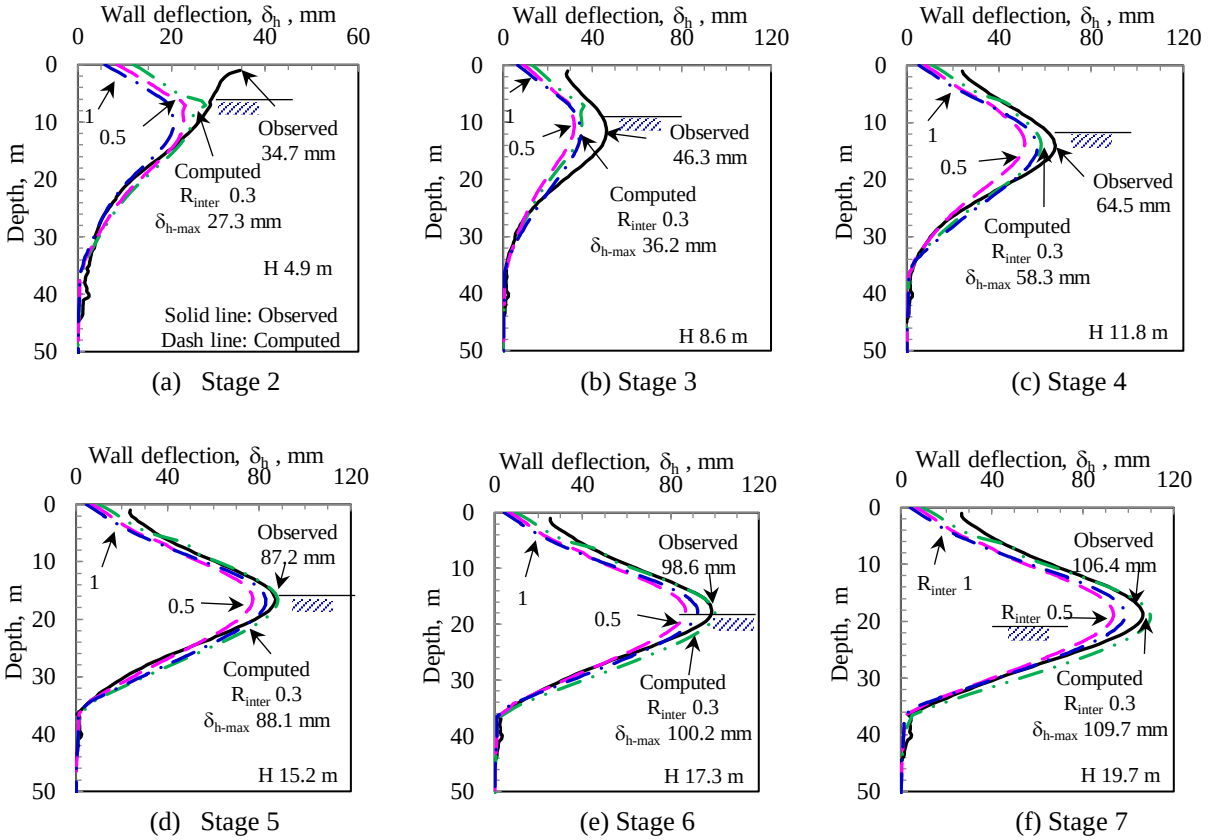

Figure 8: Computed and observed wall deflections for Stage 2 to Stage 7 – Case 1 to Case 3

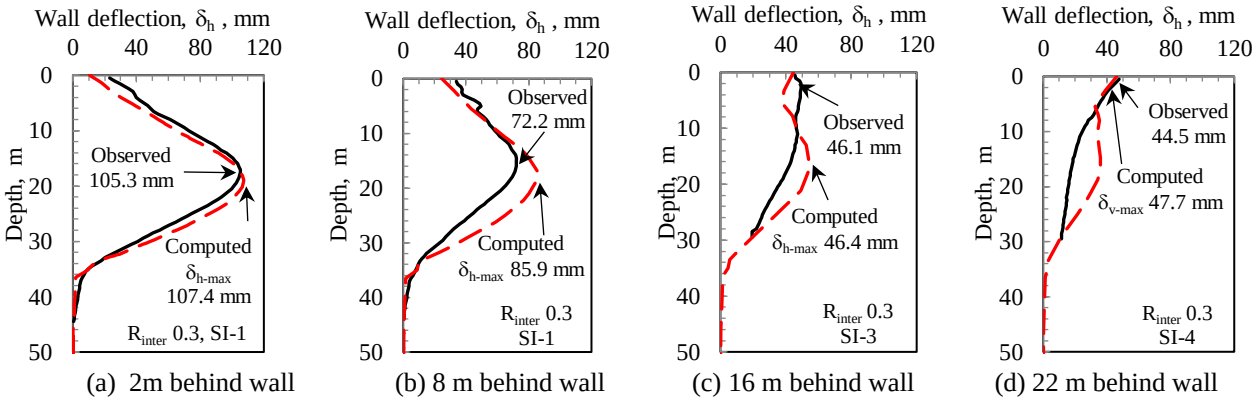

Figure 9: Computed and observed wall deflections in final stage at various distances behind wall - Case 3

4.3 Computed surface settlements

Figure 10 presents the computed surface settlements for Case 1 to Case 3 in Stage 2 to Stage 7. Compared with the observed settlements that Kung & Ou (2006) reported, close matching between the analyzed and the observed has been achieved in the final Stage for Case 3, which adopts the R_{inter} value of 0.3. In the final Stage

the computed maximum settlement, $\delta_{v\text{-}max}$, is 77.3 mm, which over-estimates the observed 74 mm by 4.5 %. Compared with the surface settlements predicted by other nonlinear soil models that Kung & Ou (2006) presented, the results obtained in this study by the HSS model is considered as satisfactory.

Table 3 shows that the computed $\delta_{v\text{-}max}$ in the final stage for Case 1 adopting the R_{inter} value of 1 is 57.0 mm, which deviates from the observed $\delta_{v\text{-}max}$ of 74 mm by 23 %. For Case 2 adopting the R_{inter} value of 0.5, the computed $\delta_{v\text{-}max}$ of 63.0 mm deviates from the observed 74 mm by 15 %. As summarized in Table 3, there is a trend that the smaller the R_{inter} value, or the smoother along the soil-wall interface, the larger surface settlements would occur.

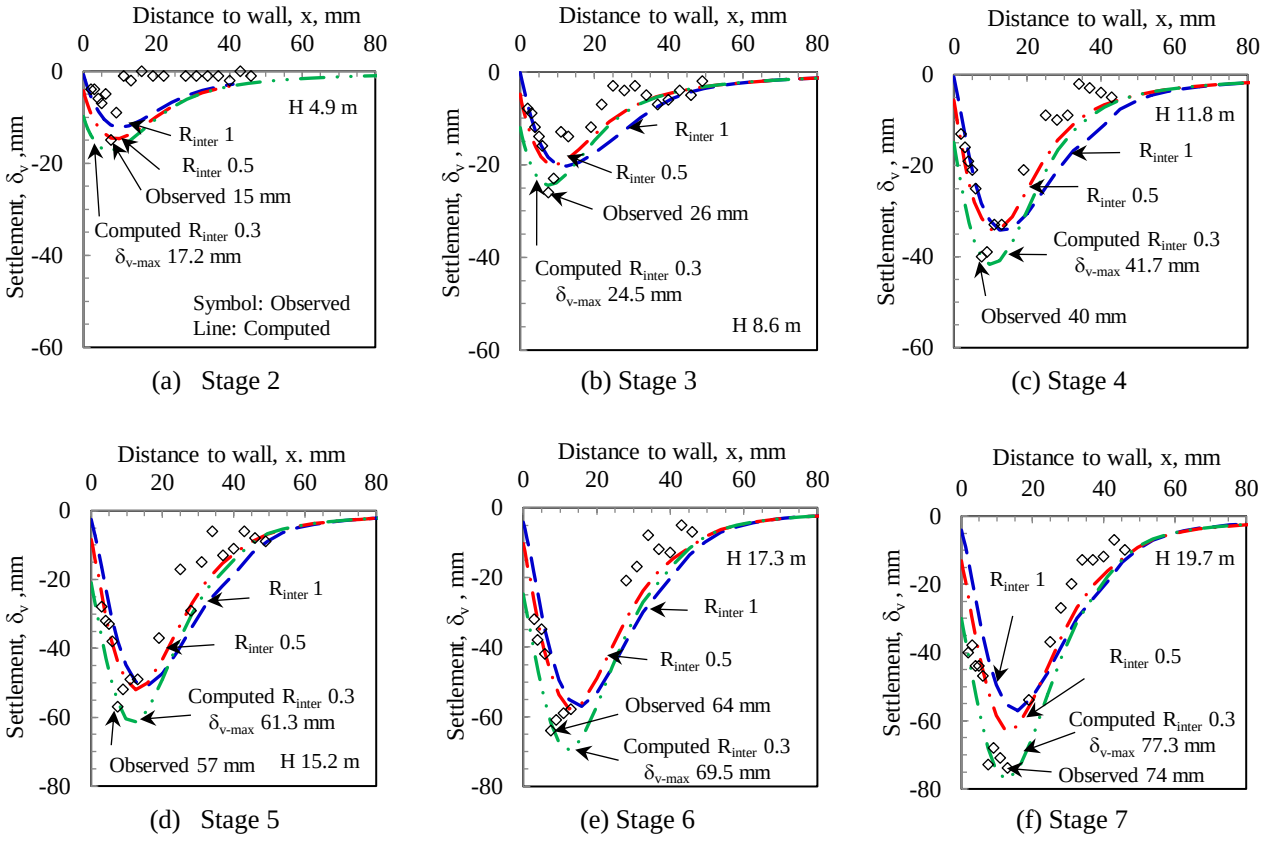

Figure 10: Computed and observed surface settlements in Stage 2 to Stage 7 – Case 1 to Case 3

4.4 Normalized settlement profiles

Figure 11 presents the normalized computed and observed settlement profiles in the final Stage for Case 1 to Case 3. The surface settlements, δ_v, are normalized with the maximum settlement, $\delta_{v\text{-}max}$. The distances to the wall, the x values, are normalized with the excavation depth, H. While close matching between the computed and the observed normalized profiles is achieved at the distance within 1H behind the wall, the computed results for these 3 cases would over-estimate the settlements at the distances between 1H and 2.5H. Case 3 would slightly over-estimate the surface settlements by $0.13\delta_{v\text{-}max}$ at the distance of 1.6H to the wall. For Case 2 and Case 1, the over-estimation would increase to $0.18\delta_{v\text{-}max}$ and $0.25\delta_{v\text{-}max}$ respectively at that distance.

Case 3 has the narrowest width of the settlement trough. Measuring at $0.2\delta_{v\text{-}max}$, the width of the normalized settlement trough is approximately 2.1H for Case 3. For Case 2 and Case 1, the widths of the troughs are approximately 2.3H and 2.4H respectively. Amongst these 3 cases, the shape of the settlement trough for Case 3 has the closest matching with that observed.

Figure 11 shows that at the distance immediately next to the wall at x = 0, the computed normalized settlements, $\delta_v/\delta_{v\text{-}max}$, for the cases adopting the R_{inter} values of 1, 0.5 and 0.3 are 0.07, 0.21 and 0.39 respectively. The numerical analysis in this study shows that the lower the R_{inter} value, the larger settlements

would occur next to the wall. The interface reduction factor, R_{inter}, would be the key parameter for assessing the surface settlements behind the retaining structures.

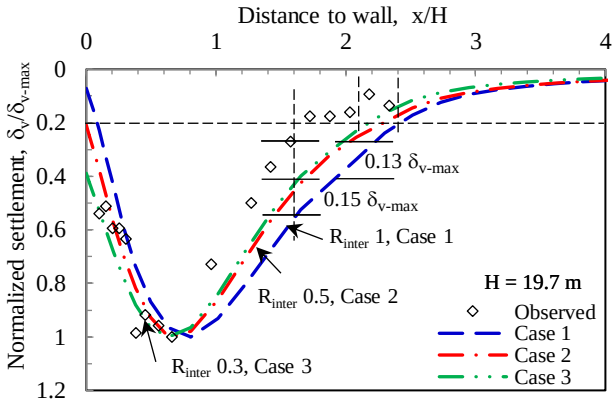

Figure 11: Normalized computed and observed surface settlements in final stage - Case 1 to Case 3

4.5 Settlements of the wall

The effect of soil-structure interface to wall and ground movements can be seen from the results of parametric studies presented in Table 3. There is the trend that the lower the R_{inter} values, the less shortening of the wall. Deducing from the wall top and the wall toe settlements, the wall shortening would be 0.6 mm with the rough interface (R_{inter} = 1). With the smooth interfaces, R_{inter} of 0.5 and 0.3, the wall shortening would be 0.5 mm and 0.4 mm respectively. This implies that the soil frictions acting along the wall would be largest for the rough interface and the soil frictions would be less for the smooth interfaces (R_{inter} < 1).

The relative settlements between the wall and the soil immediately behind can be deduced from the wall top settlements and the surface settlements next to the wall. With the rough interface R_{inter} of 1, the relative settlement between the wall and the ground would be 0.9 mm. With the smooth interface R_{inter} of 0.3, the relative settlement would be as large as 11.6 mm. The smooth interface would give the apparent "slippage" along the soil-wall interface.

4.6 Effect of water pressures

In addition to the groundwater pressures in 1992 that Case 3 adopted, the performance of excavation with the piezometric levels in Jingmei Formation in 2023 and in 1974 have been studied. The piezometric levels of El. 0 and El. -31 in Jingmei Formation for Case 4 and Case 5 respectively are analyzed. Table 4 summarized the piezometric levels adopted for Case 3 to Case 5. The R_{inter} value of 0.3 is adopted for these cases.

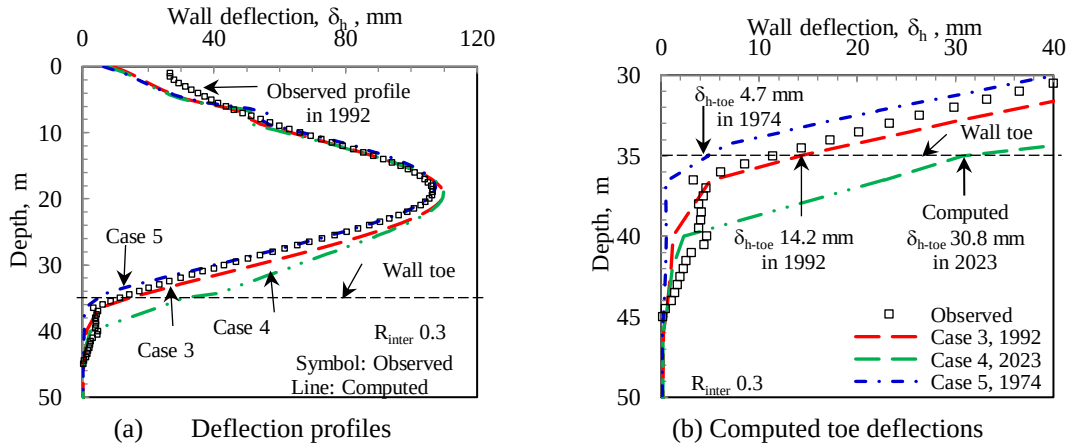

Figure 12: Wall deflections in the final stage with various piezometric levels in Jingmei Formation - Case 3 to Case 5

Table 4: Computed wall deflections for various piezometric levels in Jingmei Formation

Case	Piezometric level in Jingmei Formation, El. m	Year	Wall deflection, mm		Difference in deflection, mm	
			Maximum	At toe	Maximum	At toe
Observed	-10.5	1992	106.4	11.4	-	-
3	-10.5	1992	109.7	14.2	3.3	2.8
4	0	2023	109.8	30.8	3.4	19.4
5	-31.0	1974	107.3	4.7	0.9	-6.7

The computed wall deflections in the final stage for Case 3 to Case 5 are presented in Figure 12 and summarized in Table 4. The computed maximum wall deflections for Case 3 and Case 4 are within 3.4 mm of those observed. The groundwater pressure effect would be minimal to the maximum wall deflections.

The wall toe deflections are however sensitive to the groundwater pressures. Table 4 shows that the computed toe deflection, $\delta_{h\text{-}toe}$, would be as large as 30.8 mm for Case 4, which adopts the piezometric level in the Jingmei Formation at El. 0 m in 2023. Compared with the toe deflection of 11.4 mm observed in 1992, the computed $\delta_{h\text{-}toe}$ value for Case 4 would be 2.7 times of that occurred in 1992. For the scenario that the excavation would be conducted in 1974 with the piezometric level in the Jingmei Formation as low as El. -31 m in Case 5, the computed $\delta_{h\text{-}toe}$ is 4.7 mm, which would be 40 % of that occurred in 1992.

The effect of water pressures plays an important role on the performance of the deflections at the wall toe levels. The toe deflections as large as 30 mm would be crucial for interpreting the wall deflection profiles from inclinometers not embedded in competent stratum.

5 CONCLUSIONS

Two-dimensional numerical analysis on an excavation case history in soft ground has been conducted. The maximum excavation depth of 19.7 m was supported with diaphragm wall of 0.9 m in thickness and by top-down construction. The nonlinear Hardening-soil with small-strain stiffness (HSS) soil model is adopted. The following conclusions could be drawn:

(1) The nonlinear HSS soil model could reliably estimate the wall deflections, lateral ground movements behind the wall and the surface settlements simultaneously.
(2) The parametric study adopting various interface reduction factors shows that the performance of surface settlements behind the wall is intimately affected by the shear strengths developed along the soil-structure interface. The lower in the interface reduction factor, the larger wall deflections, wall settlements and surface settlements would be computed.
(3) The smooth interface would give the apparent “slippage” along the soil-wall interface. Such slippage would occur at the interface reduction factor around 0.3.
(4) The water pressure in the underlying water bearing strata is a key factor for assessing the wall performance especially at the toe level.

The set of stiffness parameters obtained from the small-strain triaxial tests and bender element tests have been verified by the TNEC excavation case history and could be the reference for studying other cases in the K1 Geological Zone of the Taipei Basin. The interface reduction factor would be the key parameter for exploring the ground movements due to deep excavations.

REFERENCES

Bentley (2022). *PLAXIS 2D-Reference Manual*. CONNECT Edition V22.02, Bentley Advancing Infrastructure, August 2022.

Benz, T. (2006). Small-strain stiffness of soils and its numerical consequence. *Dissertation of thesis*, the Institute of Geotechnics, University Stuttgart.

Burland, J.B. (1989). Ninth Lauritus Bjerrum Memorial Lecture: “Small is beautiful” - the stiffness of soils at small strain. *Canadian Geotechnical Journal*, Vol.26: 499-516.

Chin, C.T., Chen, J.R., Hu, I.C., Yao, D.H.C. & Chao, H.C. (2007), Engineering characteristics of Taipei clay. In T.S. Tan, K.K. Phoon, D.W. Hight & S. Leroueil (Eds), entitled*: Characterization and Engineering Properties of Natural Soils*, Taylor & Francis Group, v3:1755-1803.

Chin, C.T., Crooks, A.J.H. & Moh, Z.C. (1994). Geotechnical properties of the cohesive Sungshan deposits. *Geotechnical Engineering, J. Southeast Asian Geotechnical Society*, Taipei, Taiwan 25(2): 77-103. (in Chinese)

Chin, C.T. & Liu, C-C. (1997). Volumetric and undrained behaviors of Taipei silty clay. *J. Chinese Institute of Civil and Hydraulic Engineering*, Taipei, Taiwan 9(4): 665-678. (in Chinese)

Duncan, J.M. & Chang, C.Y. (1970). Nonlinear analysis of stress and strain in soils. *Journal of the Soil Mechanics and foundation Division*, ASCE, Vol.96, No. 5: 637-659.

Hwang, R. & Moh, Z.C. (2022). Groundwater drawdown and subsidence in the Taipei Basin. *Sino-Geotechnics*, No. 173/2022.9: 99-110. (in Chinese)

Hu. I.C., Chin, C.T. & Liu, C.J. (1996). Review of the geotechnical characteristics of the soil deposits in Taipei, *Sino-Geotechnics*, No. 54: 5-14. (in Chinese)

Jardine, R.J., Potts, D.M., Fourie, A.B. & Burland J.B. (1986). Studies on the influence of non-linear stress-strain characteristics in soil-structure interaction. *Geotechnique*, Vol. 36, No. 2: 377-396.

Kondner, R.L. & Zelasko, J.S. (1963). A hyperbolic stress-strain formulation of sands. *Proceedings of the 2nd Pan American Conference on Soil Mechanics and Foundation Engineering*. San Paulo, Brazil, 1963. Associacao Brasileira de Mecanica dos Solos, Vol 1: pp 289–324

Kung, T.C. (2003). Surface settlement induced by excavation with consideration of small-strain behavior of Taipei silty clay. *Ph.D. Dissertation*, National Taiwan University of Science and Technology, Taiwan.

Kung, T.C. & Ou, C.Y. (2006). Prediction of surface settlement caused by excavation. Taylor & Francis Group plc, London UK: 853-858.

Kung, G.T.C, Ou, C.Y. & Juang C.H. (2009). Modelling small-strain behavior of Taipei clays for finite element analysis of braced excavations. *Computers and Geotechnics* 36 (2009): 304-319.

MAA (1987) *Engineering properties of the soil deposits in the Taipei Basin*, Report No. 85043, Ret-Ser Engineering Agency and Taipei Public Works Department, Taipei. (in Chinese)

Moh, Z.C. & Ou C.D. (1979). Engineering characteristics of Taipei Silt. *Proc., 6th Asian Regional Conference on Soil Mechanics and Foundation Engineering*, Singapore, 1: 155-158.

Moh, Z.C., Chin, C.T., Liu, C.J. & Woo, S.M. (1989). Engineering correlation for soil deposits in Taipei. *J. Chinese Institution of Engineers*, 124(9): 798-808.

Ou, C.Y. (2016), Finite element analysis of deep excavation problems. 2015 TGS Geotechnical Lecture, *Journal of GeoEngineering*, Vol. 11, No.1: 1-12.

Ou, C.Y., Liao, J.T. & Lin, H.D. (1998), Performance of diaphragm wall constructed using top-down method, *Journal of Geotechnical and Geoenvironmental Engineering*, ASCE, Vol. 124, No.9: 798-808.

Ou, C.Y., Liao, J.T. & Cheng, W.L. (2000a), Building response and ground movements induced by a deep excavation, *Geotechnique*, Vol. 50, No. 3: 209-220.

Ou, C.Y., Shiau, B.Y. & Wang, I.W. (2000b), Three-dimensional deformation behavior of the Taipei National Enterprise Center (TNEC) excavation case history, *Canadian Geotechnical Journal*, Vol. 37(2): 438-448.

PLAXIS B.V. (2013). *PLAXIS Reference Manual*. PLAXIS, BV, Delft, the Netherlands.

Roscoe, K.H. & Burland, J.B. (1968). On the generalized stress-strain behavior of 'wet clay'. *Engineering Plasticity*, Cambridge University. 535-585.

Santos J.A. & Correia, A.G. (2001). Reference threshold shear strain of soil. Its application to obtain a unique strain-dependent shear modulus curve for soil. *In 15th Int. Conf. SMGE*, Volume 1, Istanbul,, A.A. Balkema. 267-270.

Schanz, T. & Vermeer, P.A. (1998). On the Stiffness of Sands. *Geotechnique*, 46, No. 1: 145-151.

Schanz, T., Vermeer, P.A. & Bonnier, P.G. (1999). The hardening soil model: formulation and verification. *Beyond 2000 in Computational Geotechnics*. Rotterdam, the Netherlands. 281-290.

Stallebrass, S.E. & Taylor, R.N. (1997). The development and evaluation of a constitutive model for the prediction of ground movements in over-consolidation clay. *Geotechnique*, 47(2): 235-253.

Performance of Buttress Wall in a Deep Excavation in Soft Ground

L.W. Wong
SMEC Asia Limited, Hong Kong

ABSTRACT

Diaphragm wall strengthened with buttress panels has frequently been adopted for reducing the wall deflections and the adjacent ground surface settlements caused by deep excavations. A case history on top-down construction with the excavation depth of 32 m is reviewed to study the effect of the buttresses on reduction in wall deflections. The excavation was supported by perimeter diaphragm walls of 1.5 m in thickness, 52 m in length and stiffened with buttresses spacing at 8.75 m. Two-Dimensional numerical analyses using the nonlinear Hardening-Soil with Small-Strain Stiffness constitutive soil model have been conducted. Five sets of wall stiffnesses with different interface reduction factors have been adopted to simulate buttresses with various spacing. Close matching between the computed wall deflections with those observed in the inclinometers validated the set of the soil stiffness parameters for the Hardening-Soil with Small-Strain Stiffness model. The effectiveness of the buttresses was assessed by comparing the computed wall deflections with and without the buttress panels.

Keywords: Excavation, Hardening Soil Model, Small Strain, Buttress, Ground Movements

1 INTRODUCTION

Ground movements caused by deep excavations have been one of the prime concerns for underground construction in urban areas. In order to minimize their adverse effects to structures nearby, strengthening measures have often been constructed in addition to the perimeter diaphragm walls. The use of jet grout slabs, cross-walls and buttress walls as the strengthening measures have been reported in the literature. Chuang et al. (2002) reported the use of buttresses to reduce the diaphragm wall deflections for a 32 m deep excavation. Ou et al. (2006) presented case records on excavation with cross-walls and buttresses in basement excavations.

In order to study the effectiveness of buttress walls in reducing ground movements, performance of the diaphragm wall strengthening with buttresses for a case history is critically reviewed. The case of Core Pacific City Shopping Complex (CPC) was previously reported by Chuang et al. (2002) and Hwang et al. (2007). As shown in Figures 1, the development comprised a 12-storey building complex and an 11-storey spherical shopping mall. The basement area was approximately 118 m along the north-south and the east-west directions as depicted in Figure 2. Excavation to a maximum depth of 31.7 m was carried out by using the top-down method of construction. The pit was retained by perimeter diaphragm walls and braced by floor slabs. Buttress panels were installed to reinforce the diaphragm walls at locations where there were existing buildings as a building protection measure.

Back-analyses have been conducted to evaluate the performance of the excavation by using the finite element computer code PLAXIS. The Hardening-Soil with small-strain Stiffness model (HSS), developed by Benz (2006) and introduced in the PLAXIS program (PLAXIS 2013), has been adopted to simulate the stress-strain-strength relationship of soils. Readings of inclinometers are available to compare with the results of the analyses. By matching the calculated wall deflection profiles with those observed, the soil parameters are validated. The effectiveness of buttresses in reducing wall deflections is assessed.

2 SUBSOIL CONDITIONS

2.1 Ground conditions

The project site for Core Pacific City is located in the K1 Zone (MAA 1987; Lee 1996) in the southeast part of the Taipei Basin. As depicted in Figure 3, at the surface lies the Songshan Formation which typically comprises six alternating sand and clay layers. At the ascending order Sublayers I, III and V are sandy soil (SM) and Sublayers II, IV and VI are clayey soil (CL) strata. The underlying Jingmei Formation, a gravelly soil (GM) stratum, is encountered at the depth about 49 m (Elevation -43.5 m). The ground levels range from El. 5.5 m to El. 6.1 m above the mean sea level. Table 1 summarized the soil parameters for the various sublayers. At this site, the Songshan Formation is dominant with the thick clayey Sublayer IV and Sublayer II, which are encountered at the depths between 8 m and 32 m and between 34 m and 47 m respectively. The sandy Sublayers V, III and I are encountered at the depths of 4 m, 32 m and at 47 m respectively.

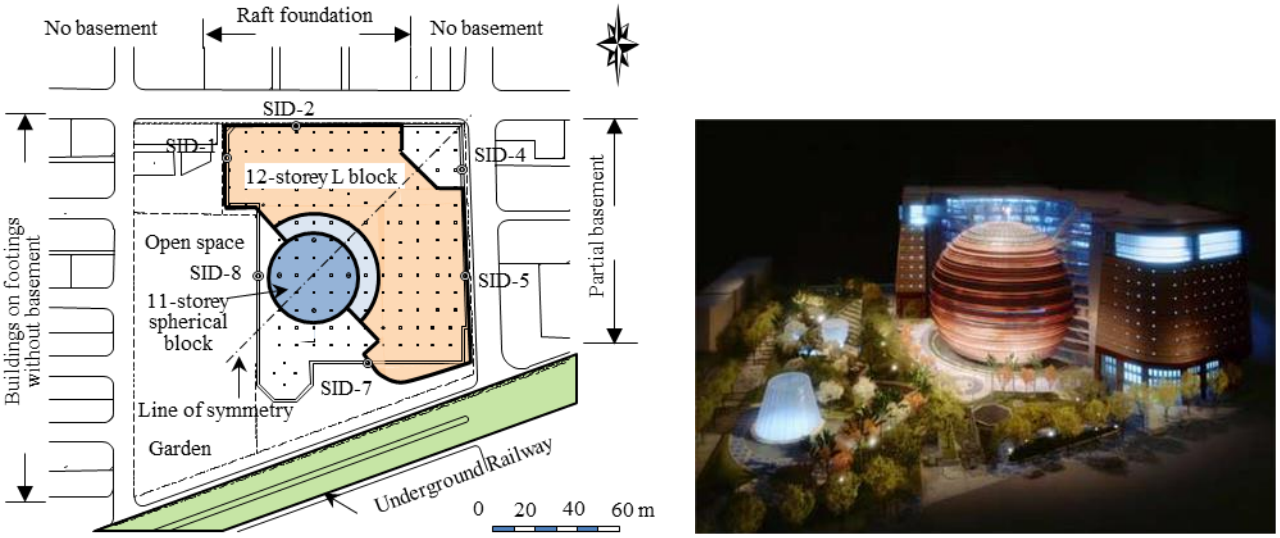

(a) Layout plan (b) Isometric View

Figure 1: General layout of Core Pacific City Shopping Complex (CPC)

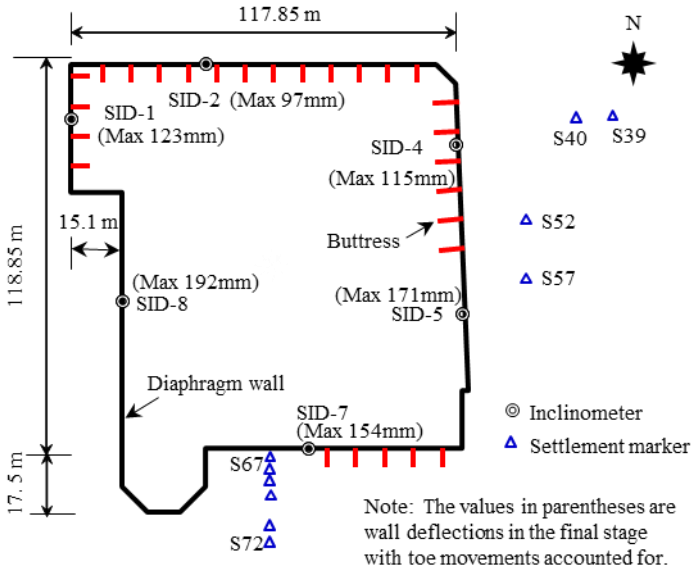

Figure 2: Layout of diaphragm wall and buttress wall (after Hwang et al. 2007)

A representative excavation model is shown in Figure 3. The excavation was carried out to a depth of 31.7 m in 9 stages. The pit was retained by diaphragm walls of 1.5 m in thickness and 52 m in length. Excavation for the foundation was constructed by the top-down method. The diaphragm wall was abutted by buttress panels of 1.5 m in thickness, 3.5 m to 3.7 m in breadth, 29.5 m in length and spacing at 8.75 m. The buttresses were installed and cast together with the diaphragm walls with reinforcement interlocked.

The excavation was conducted by top-down construction using the ground floor slab (GF) and 6 levels of basement floor slabs (B1 to B6) of 150 mm in thickness as the lateral supports. Temporary steel struts were erected at the openings at GF, B1 and B2 slabs. Excavation commenced in January 1999 and the foundation slab was cast in October 2000.

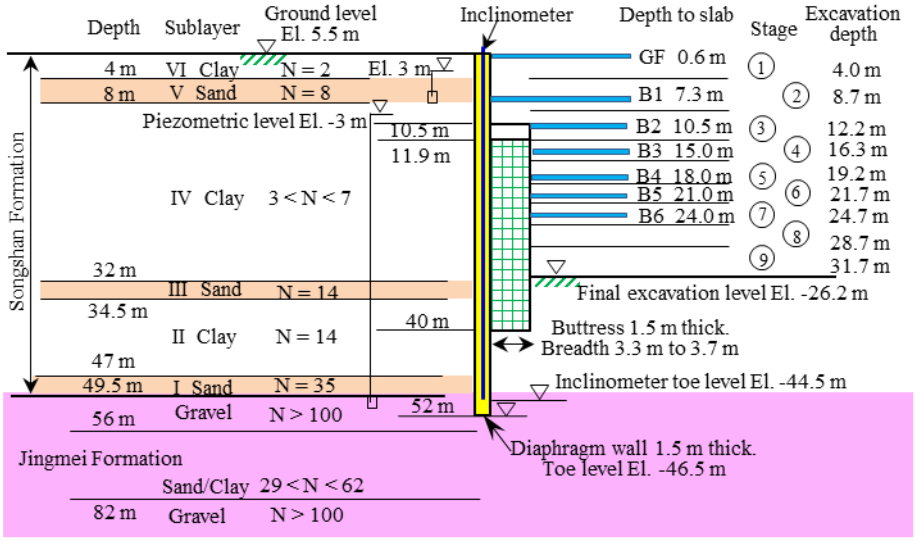

Figure 3: Soil profile of the CPC Case and excavation scheme

2.2 Undrained shear strengths

The properties of the six sublayers in the Songshan Formation have been well discussed in the literature (Moh and Ou 1979; MAA 1987). An advanced study was conducted by Geotechnical Engineering Specialty Consultant engaged by the Department of Rapid Transit Systems of Taipei City Government in the very early stage of the metro construction as a Designated Task to study the characteristics of Taipei clays (Chin et al., 1994 and 2007; Chin & Liu 1997; Hu et al., 1996). It was conducted in collaboration with a research team from Massachusetts Institute of Technology (MIT). Figure 4 presents the results of the CK_0UC tests conducted on the specimens recovered from borehole R-1 that Chin et al. (1994) reported. Borehole R-1 was located in the K1 Geological Zone in Taipei Basin.

Kung et al. (2009) presented the results of undrained shear strength, s_u, for an excavation case history located at 300 m north of the CPC project site. The s_u values were determined from consolidated triaxial undrained compression tests conducted on specimens recovered from the clayey Sublayer IV. The specimens were saturated and K_0-consolidated to the in-situ effective stress states. The variation in undrained shear strengths for the compression tests that Ou et al. (2000) and Kung et al. (2009) reported are presented in Figure 4. Compared with the CK_0UC tests reported by Chin et al. (1994), the s_u values obtained by Ou et al. (2000) and Kung et al. (2009) are lower, which would be attributable to sampling disturbance. Although the specimens were consolidated to the in-situ horizontal stress, such process could not fully compensate the effect due to sample disturbance. Based on the s_u profile presented in Figure 4, the s_u values varying from 50 kPa to 60 kPa can be obtained above a depth of 15 m. The Author has proposed in this study that the s_u values for the clay below 15 m depth can be expressed as follows:

$$s_u = 60 + 4.8\,(D-15) \tag{1}$$

where D is the depth in metre and s_u is the undrained shear strength in kPa.

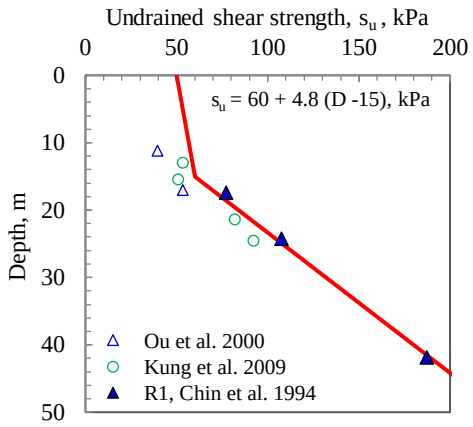

Figure 4: Undrained shear strengths of clays obtained by CK_0UC triaxial tests

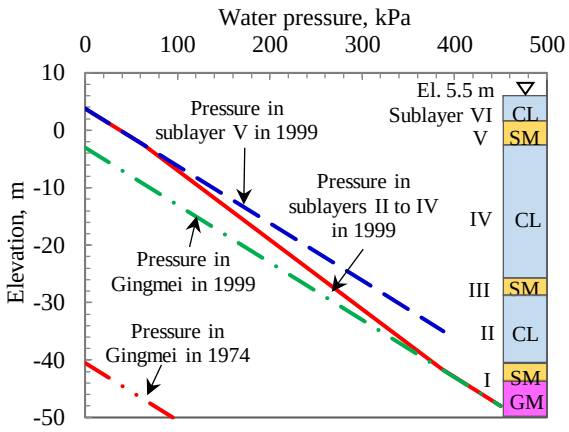

Figure 5: Groundwater pressures on the outer face of the diaphragm walls

2.3 Groundwater conditions

Piezometers monitoring was conducted prior to and during excavation for the CPC project site. The groundwater level in the Sublayer V sand was around El. 3 m. Due to excessive extraction of groundwater to supply water to the city, the piezometric levels in the Jingmei Formation were lowered to a level near the bottom of the Songshan Formation in the 1970s, leading to significant reductions in water pressures in the Songshan Formation and substantial ground settlements as a result. The piezometric levels in the Jingmei Formation did not recover till 1974 although pumping had been banned since 1968. The subsoils in the Songshan Formation in the Taipei Basin are thus substantially over-consolidated. This is particularly true for the clayey Sublayer II because the underlying sandy Sublayer I is so permeable that the piezometric levels in Sublayer I essentially dropped by the same magnitudes as those in the Jingmei Formation.

Based on monitoring records at the deep well at Sun Yet Sin Memorial Hall, located at 1 km south of the CPC project site, Hwang and Moh (2022) reported that the piezometric level in the Jingmei Formation in the eastern portion of the Taipei Basin was around El. -3 m in 1999. In the central portion of the Taipei Basin, the piezometric level in Jingmei Formation recovered to El. 0 m in 2017. The distributions of the water pressures outside the diaphragm wall at CPC in 1999 are presented in Figure 5. For the Sublayer I and Jingmei Formation, the piezometric level of El. -3 m in 1999 is adopted in numerical analysis. The water pressures for sublayers II to IV are interpolated between sublayers V and I. Inside the pit, the piezometric levels maintaining at a depth of 1m below the excavation levels in each stage have been adopted in the analysis.

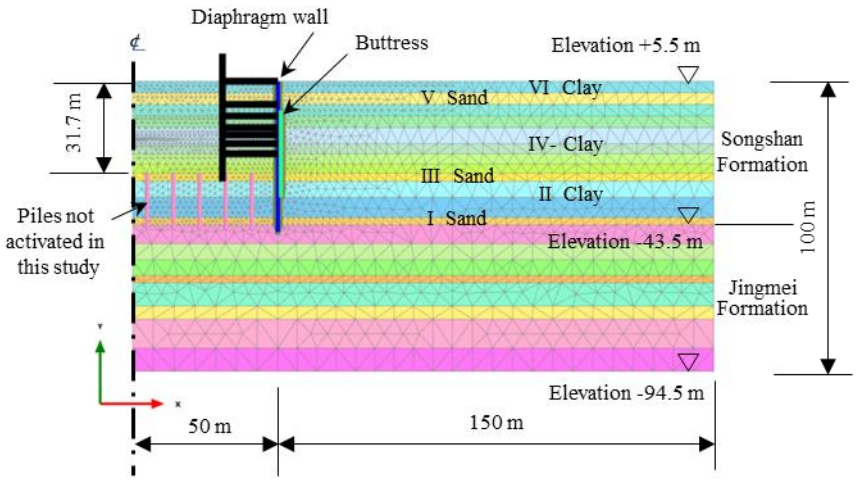

Figure 6: Finite element mesh for the analytical section for 9 stages of excavation

3 NUMERICAL SIMULATION

3.1 Finite element mesh

The section analyzed is depicted in Figure 6. The excavation is carried out to a depth of 31.7 m in 9 stages in the analysis. While the CPC project site had the widths of 100 m and 118 m along the east-west and the north-south directions respectively, a half-width of 50 m has been adopted in the model. The diaphragm wall is located at a distance of 50 m from the axis of the trench. Because of symmetry in geometry, only half of the section has been analyzed as depicted in Figure 6. The lateral extent of the finite element model behind the diaphragm wall is 150 m, which is 4.7 times of the final excavation depth of 31.7 m.

The Jingmei Formation underlying the Sungshan Formation is a water-rich gravelly stratum. This stratum is a competent formation with very high stiffness and is frequently assumed to be the base of the numerical analysis. Since there is presence of a sand and stiff clay stratum at the depths between 56 m and 82 m, the base of the finite element model in this study is placed at a depth of 100 m to include a 51 m layer of the Jingmei Formation to ensure that the contribution of this formation to ground movement is accounted for.

3.2 Nonlinearity of soil behavior - Hardening-soil with small-strain stiffness model

The PLAXIS-2D finite element software developed by PLAXIS BV (2013) has become a very popular tool in geotechnical analysis and design. The Hardening-Soil with Small-strain stiffness (HSS) constitutive soil model is an extension of the Hardening-Soil model (Benz 2006, Schanz & Vermeer 1998; Schanz et al. 1999) introduced in the PLAXIS program and is adopted herein to simulate the non-linear stress-strain relationship of soils under loading and unloading conditions. In the HSS model, the parameters adopted to define the hyperbolic stress-strain relationship are as follows:

- E^{ref}_{50} is the reference secant stiffness from standard triaxial drained test,
- E^{ref}_{oed} is the reference tangent stiffness for oedometer primary loading,
- E^{ref}_{ur} is the reference unloading-reloading stiffness from standard triaxial drained test,
- m is the exponential factor for stress-level dependency of stiffness,
- R_f is the failure ratio, $R_f = q_f / q_a$,
- q_a is the asymptotic value of the shear strength and q_f is the failure strength,
- G^{ref}_0 is the reference shear modulus at the level of very small strains,
- $\gamma_{0.7}$ is the reference shearing strain to define the behavior of degradation of moduli when G^{ref}_0 is reduced to 0.7 G^{ref}_0.

The stress-strain curves can be determined from laboratory tests such as the K_0-consolidated triaxial undrained compression and extension tests. In this study, the stiffness values of soils are related to the undrained shear strengths for clays and the N values for sands as expressed in the empirical Equations 2 to 6:

$$E^{ref}_{50} = 150\ s_u \text{ (for clayey soils)} \quad (2)$$

$$E^{ref}_{50} = 2\ N \text{ (in MPa for sandy soils)} \quad (3)$$

$$E^{ref}_{oed} = E^{ref}_{50} \quad (4)$$

$$E^{ref}_{ur} = 5\ E^{ref}_{50} \quad (5)$$

$$G^{ref}_0 = 1.07\ E^{ref}_{ur} \quad (6)$$

in which s_u is the undrained shear strengths of clayey soils and N is the blow-counts obtained in standard penetration tests for sandy soils. The parameters adopted in this study are summarized in Table 1. The empirical Equations (2) to (5) have been calibrated against a well-documented case history that Wong (2023) reported. The effective shear strength parameters, i.e., the c' and ϕ' values, for the silty sand strata, are determined from laboratory tests conducted on thin-wall tube specimens. For the clayey layers, c' = s_u and ϕ' = 0° is assumed in the analyses. The dilation angle, ψ', of 2°, 0°, and 3° are adopted for the sandy, the clayey, and the gravelly soils respectively. The R_f equals 0.9 is adopted. The unload-reload Poisson's ratio, υ_{ur}, of 0.2 is used as suggested by Benz (2006) and Schanz et al. (1999). Although the HSS soil model is an effective stress model and adopting the ϕ' = 0° for the clayey soils loses its compression hardening function and stress-

dependent stiffness, parametric studies using both the effective stress and the total stress models show that the computed wall deflections and surface settlements are essentially the same. The total stress input parameters for clay have been adopted in this study.

Table 1: Soil parameters for the HSS model adopted in the PLAXIS analyses

Mid depth m	Soil type	Unit weight γ' kN/m^3	N value	Undrained shear strength s_u, kPa	Effective cohesion c' kPa	Effective friction angle ϕ', deg	Dilation angle ψ' deg	Reference stiffness		Initial shear moduli G^{ref}_0, MPa
								Secant stiffness E^{ref}_{50}, MPa	Unload-reload E^{ref}_{ur}, MPa	
2	CL	19	2	50				7.5	38	40
6	SM	19	8	-	0	32	2	16	80	86
9.75	CL	18.4	3	57				8.6	43	46
13.75	CL	18.4		60				9.0	45	48
18.75	CL	18.4		78				11.7	59	63
23	CL	19	7	98				14.8	74	79
26.5	CL	19		115				17.3	86	92
30.25	CL	19		133				20	100	107
33.25	SM	19.3	14	-	0	32	2	28	140	150
33.75	CL	19.5	14	169				25	127	136
44	CL	19.5	14	199				30	149	160
48.25	SM	20.3	35	-	0	32	2	70	350	375
52.75	GM	21.9	>100		0	35	3	200	1,000	1,070
61.5	CL/SM	19.5	25	-	0	32	2	50	250	268
68.25	SM	21.6	50	-	0	33	2	100	500	535
73.5	CL/SM	19.9	29	-	0	32	2	58	290	310
79.75	SM	19.7	50	-	0	33	2	100	500	535
91	GM	21.9	>100		0	35	3	200	1,000	1,338

3.3 Determination of small-strain stiffness

The parameters for the small-strain stiffness, i.e., the G^{ref}_0 and the $\gamma_{0.7}$, have been determined from the laboratory tests. Kung et al. (2009) presented the results of small-strain triaxial tests and bender element tests conducted on undisturbed specimens recovered from clayey Sublayer IV of the Songshan Formation. The specimens were saturated and K_0-consolidated to the in-situ effective stress states. The K_0 values applied for consolidation ranged from 0.5 to 0.55. After completing the K_0-consolidation, but prior to the shearing tests, bender element tests were carried out to measure the shear moduli of the clay specimens. Compression and extension undrained triaxial shearing tests were then conducted. The undrained shear strengths profile obtained is presented in Figure 3. Based on the results of the bender element tests, Kung et al. (2009) obtained the G_{max}/s_u ratios ranging from 738 to 788, with an average ratio of 759 for the axial compression tests, where G_{max} is the initial shear modulus. For the axial extension tests, the G_{max}/s_u ratios ranged from 614 to 751, with an average of 671. In this study, the $G^{ref}_0 = 800\ s_u$ is adopted.

The reference shearing strain $\gamma_{0.7}$ value would range from 0.8×10^{-4} to 1×10^{-3}. Chin et al. (2007) presents the stress-strain curve of a CK_0UDSS test conducted on Taipei clay. Wong (2023) reported the degradation of the shear moduli with shear strain interpreted from this direct simple shear test, showing that the Taipei clay would have the threshold $\gamma_{0.7}$ value of 5×10^{-4}. In this study, a $\gamma_{0.7}$ value of 6×10^{-4} is adopted.

3.4 Modeling of the retaining structures

In the numerical model, the diaphragm walls are modelled as plate elements. The E value of 25,000 MPa is adopted for concrete with a characteristic compressive strength, i.e. f'_c value, of 28 MPa. Following the normal practice to account for the influence of cracking, creep and relaxation of concrete during excavation, the flexural stiffness, EI, (I = moment of inertia) and the axial stiffness, EA (A = sectional area) values, of the diaphragm walls and the buttress are reduced by 30 %. The diaphragm wall and the buttress are essentially the flange and the web of an integrated T-section respectively. For a spacing of 8.75 m, the buttresses increase the EA by 11.30 GN/m and the EI values by 67.72 GNm^2/m. As shown in Figure 2, there were several buttresses

on both sides of SID-2. The increase in the wall stiffnesses due to the buttresses spacing at 8.75 m can be fully accounted for. In consideration of the fact that SID-5 was 17.5 m away from the nearest buttress at the east wall and SID-7 was 8.75 m away at the south wall, a contribution factor, μ, of 25 % is applied to the former and 50 % to the latter due to the buttresses. Table 2 summarized the contribution factors adopted for the diaphragm walls and the buttresses located next to the inclinometers.

Table 2: Cases studied in numerical analysis

Case	Configuration of diaphragm wall, buttresses & inclinometer	Contribution factor, μ, %	Interface reduction, R_{inter}	Inclino -meter	Wall location	Excavation width, m
1	No buttress	0	0.52	SID-8	West	100
2	Inclinometer 17.5 m to buttress	25	0.6	SID-5	East	100
3	Inclinometer 8.75 m to buttress	50	0.8	SID-7	South	118
4	At centre of buttresses spaced 8.75 m	100	1	SID-2	North	118
5	At centre of buttresses spaced 4.38 m	200	1	-	-	118

3.5 Case analyzed

In order to study the effectiveness of the buttresses, 5 cases with the various buttresses spacing at various distances to the nearest panel have been analyzed. Case 1 has no buttress. Case 4 and Case 5 have the buttress panels spacing at 8.75 m and at 4.38 m respectively. The inclinometers for Case 2 and Case 3 are located at 8.75 m and at 17.5 m to the nearest panel respectively. The stiffness values adopted for the flanges and the webs for these 5 cases are summarized in Table 3.

Figure 2 shows that inclinometers SID-1, SID-2 and SID-4 are located at the distances ranging from 17 m to 38 m to the corners of the basement excavation. The wall deflections observed in these 3 inclinometers are compared with those computed by the 2-Dimensional analysis for Case 4 to assess the corner effect.

The pit was braced by 7 levels of floor slabs, namely, the ground level floor (GF) and 6 basement floor (B1 to B6) slabs during excavation and by the base slab at the end. The floor slabs were 150 mm in thickness and are represented by fixed-end anchors in the analyses. Openings such as elevator shafts and staircases were provided on the floor slabs for de-mucking soils and for delivering construction materials and steel struts.

In addition to the concrete creeping effect, the axial stiffnesses of the B3 to B6 floor slabs have been further reduced by 0.59 to account for the effects of the openings. Beneath the spherical block that shown in Figure 1, there were the permanent circular openings of 35 m in diameter at the GF and B2 floor slabs. The 0.41 reduction factor is adopted for these 2 floors. At the B1 floor, the permanent opening was 60 m x 70 m. This wide opening was supported with temporary steel struts of twin H400x400x13x21 spacing at 8.75 m along both directions. The reinforced concrete slab for B1 occupied only 20 % of the floor area and the reduction factor of 0.20 is adopted. The combined reduction in the slab stiffnesses are summarized in Table 4.

Table 3: Stiffnesses of diaphragm wall and buttress adopted in numerical analysis

Case	Wall location	Flange element		Web element			Combined T-section	
		0.7EA GN/m	0.7EI GNm^2/m	Contribution factor, μ, %	0.7EA GN/m	0.7EI GNm^2/m	0.7EA GN/m	0.7EI GNm^2/m
1	West	26.355	4.94	0	0	0	26.36	4.94
2	East	26.355	4.94	25	2.82	16.93	29.18	21.87
3	South	26.355	4.94	50	5.65	33.86	32.01	38.80
4	North	26.355	4.94	100	11.30	67.72	37.65	72.66
5	-	26.355	4.94	200	22.59	135.44	48.95	140.38

Table 4: Floor slab stiffnesses

Floor level	Slab thickness mm	Axial stiffness AE, MN/m	Reduction factor			Input axial stiffness MN/m
			Creep	Opening	Combined	
GF, B2	150	3750	0.7	0.41	0.285	1070
B1	150	3750	0.7	0.20	0.14	530
B3 to B6	150	3750	0.7	0.59	0.41	1540

3.6 Modelling of soil-structure interface

The interface between the soil and the wall structure is a critical issue to be considered in soil-structural interaction analyses of deep excavations. In the PLAXIS software, an elastic-plastic model following the Mohr-Coulomb criterion is used to simulate the interaction effects between the walls and the soil. According to the Reference Manual (Bentley, 2022), the strength properties of the interface are related to the strength properties of a soil layer by a strength reduction factor, R_{inter}. The interface is assumed to be rough with the full soil strength available with R_{inter} equals to 1. The stresses and strains developed along the soil-wall interface would be inversely proportional to the contact areas of the interface. In this study, the roughness of the soil-wall interface has been proportional to L_t, the unit length of a typical T-section with the buttresses spacing at 8.75 m. Let L_1 denotes the distance between the inclinometer and the buttress and L_2 denotes the breadth of the buttress, the unit length of the soil-wall interface on the buttress side, L_i, is $(L_1+L_2)/L_1$. The L_i values for Case 1 to Case 4 are compared with the L_t value. Table 5 summarizes the L_i/L_t ratios for Case 1 to Case 4 ranging from 1 to 0.54. The R_{inter} values ranging from 0.52 to 1 have been adopted in this study.

Table 5: Proportioning the strength reduction factors with the lengths of soil-wall interface

Case	Distance of inclino-meter to buttress, L_1, m	Breadth of buttress, L_2, m	Unit length of soil-wall interface, m		Ratio L_i/L_t	R_{inter} adopted
			$L_i = (L_1+L_2)/L_1$	T-section, L_t		
1	4.38	0	1	1.85	0.54	0.52
2	17.5	3.7	1.21	1.85	0.65	0.6
3	8.75	3.7	1.42	1.85	0.77	0.8
4	4.38	3.7	1.85	1.85	1	1

4 RESULTS OF NUMERICAL ANALYSIS

4.1 Computed wall deflections

Hwang et al. (2007) presented the wall deflection profiles observed at 6 inclinometers. The computed wall deflections for Case 1 and Case 2 in the final stage are presented in Figure 7. The matching between the computed maximum wall deflection, $\delta_{h\text{-}max}$, and that observed at SID-8 is close, with the difference of -1.5 mm for Case 1. For Case 2, the difference between the computed $\delta_{h\text{-}max}$ and that observed at SID-5 is 6.8 mm.

The computed wall deflections for Case 3 are presented in Figure 8, showing the consistence between the computed and the observed profiles in the various stages. The computed $\delta_{h\text{-}max}$ in the final stage of 149.7mm deviates from 154 mm that observed at SID-7 by 4.3 mm.

The computed $\delta_{h\text{-}max}$ values for Case 1 to Case 5 in the final stage are summarized in Table 6. The close matching between the computed and the observed wall deflections for Case 1 to Case 3 validates the R_{inter} values ranging from 0.52 to 0.8 adopted for these cases. The R_{inter} value of 0.52 for Case 1 would imply that the diaphragm wall without buttress could have a relatively smooth soil-wall interface. The $\delta_{h\text{-}max}$ values computed by the 2-dimensional analysis for Case 4 are 13 % to 44 % larger than those observed at inclinometers SID-1, SID-2 and SID-4, which are under the influence of the corner effect.

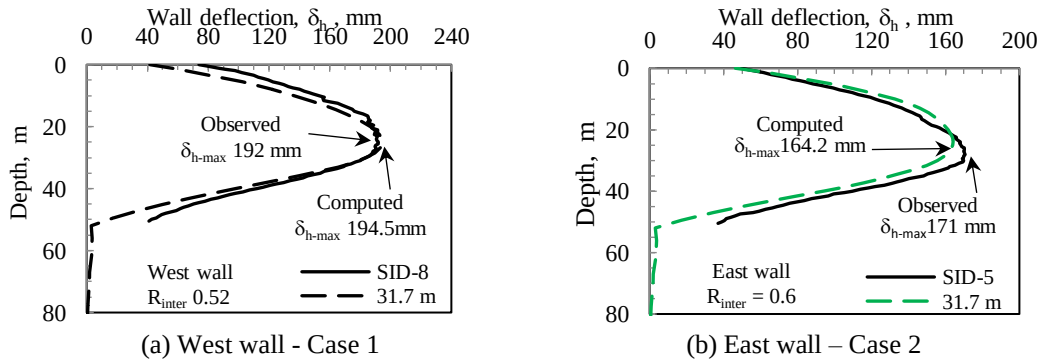

(a) West wall - Case 1 (b) East wall – Case 2

Figure 7: Computed and observed wall deflections for east wall and west wall in final stage – Case 1 and Case 2

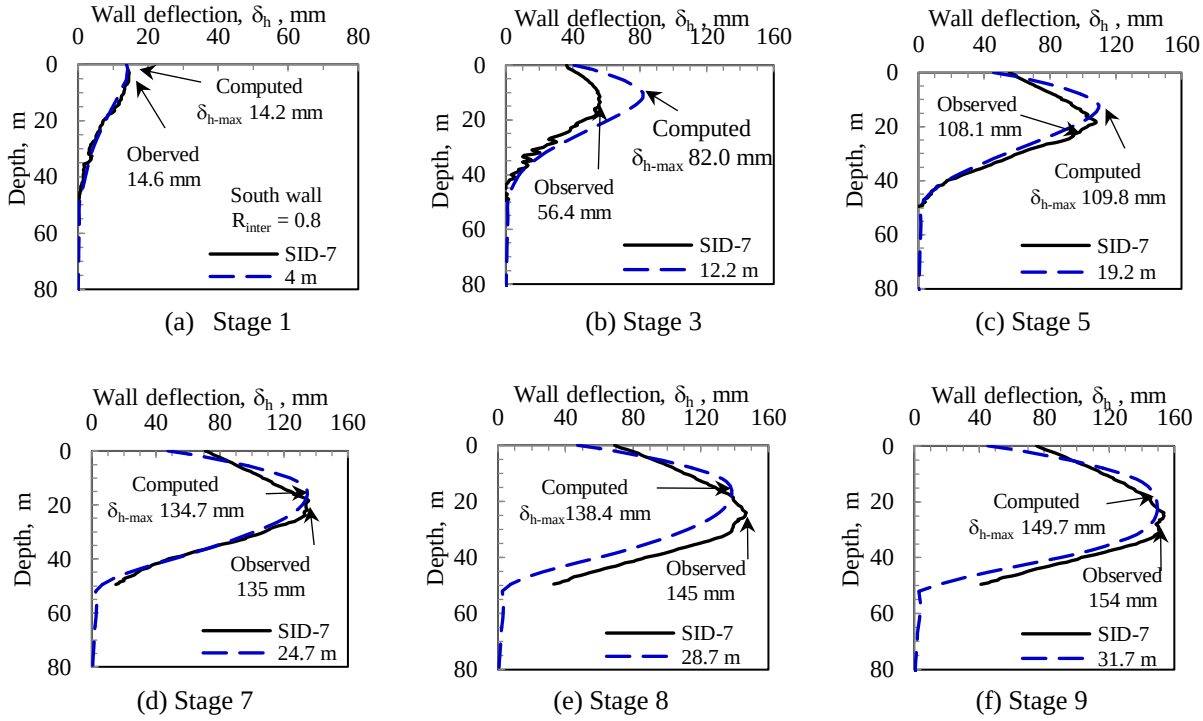

Figure 8: Computed and observed wall deflections at south wall – Case 3

Table 6: Computed wall deflections for various cases in final stage

Case	Analyzed section	Inclino -meter	Excavation width, m	Interface reduction, R_{inter}	Maximum wall deflection, $\delta_{h\text{-}max}$, mm		
					Observed	Computed	% difference
1	West	SID-8	100	0.52	192	194.5	1.3
2	East	SID-5	100	0.6	171	164.2	-4.0
3	South	SID-7	118	0.8	154	149.7	-2.8
4	North	SID-2	118	1	97	139.2	44
		SID-4	118	1	115	139.2	21
		SID-1	118	1	123	139.2	13
5	-	-	118	1	-	142.2	-

4.2 Effectiveness of buttresses

The computed wall deflections for Case 1 to Case 5 in the final stage are plotted in Figure 9 and summarized in Table 6. The family of deflection profiles shows that there is a trend of reduction in the radius of curvature of the wall at the buttress portion between the depths of 10.5 m and 40 m.

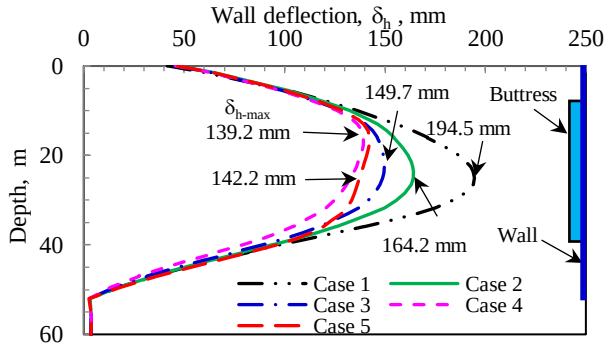

Figure 9: Computed wall deflections with various wall stiffnesses at excavation depth 31.7 m

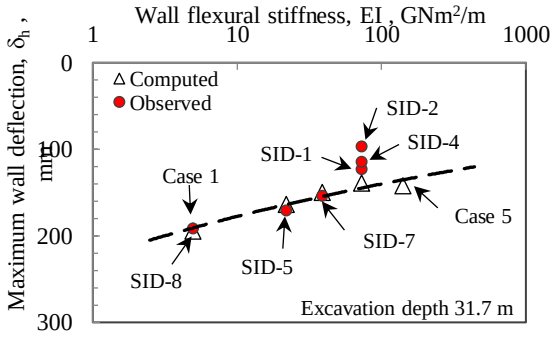

Figure 10: Relationship between wall deflections and wall stiffnesses

Figure 10 presents the variation in the $\delta_{h\text{-}max}$ values in the final stage with the various wall stiffnesses for Case 1 to Case 5, showing the trend of reduction in wall deflections with increase in wall stiffnesses. The computed maximum wall deflections for Case 1 to Case 3 agree with those observed. The $\delta_{h\text{-}max}$ values observed at SID-1, SID-2 and SID4, ranging from 97 m to 123 mm, are lower than the computed 139.2 mm for Case 4. The actual wall deflections at SID-1, SID-2 and SID4 being significantly lower than the trend line could be attributed to the corner effect.

4.3 Computed surface settlements

As depicted in Figure 2, the 4 settlement markers, S39, S40, S56 and S57 were located at the horizontal distances of 16 m to 52 m from the east wall. These markers were installed on the footings of the 4-storey buildings. The 6 settlement markers, S67 to S72, were installed on the ground surface at 2 m to 25 m from the south wall. Figure 11 presents the computed surface settlements behind the east wall for Case 2. Close matching between the analyzed and the observed settlements has been achieved in Stages 8 and 9. In Stage 9, the computed maximum settlement, $\delta_{v\text{-}max}$, of 136.2 mm is close to the observed 133 mm.

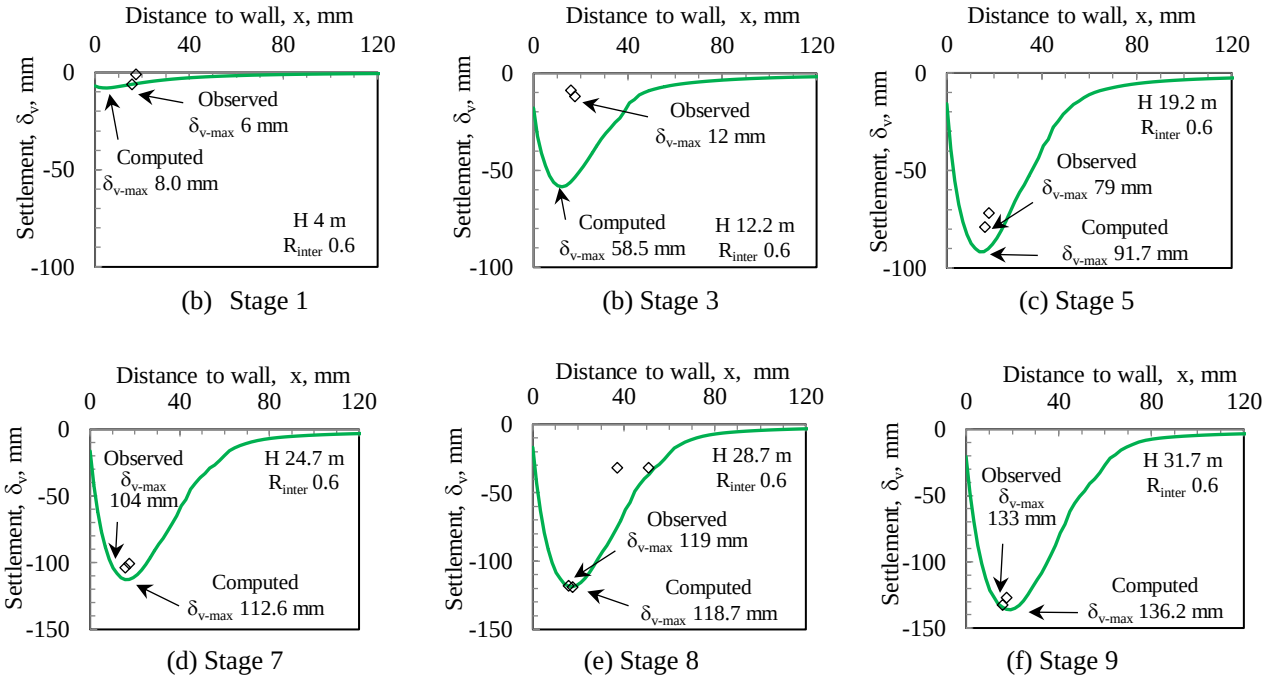

Figure 11: Computed and observed surface settlements behind east wall – Case 2

Figure 12 presents the computed $\delta_{v\text{-}max}$ values behind the south wall for Case 3. The observed settlements significantly exceed those computed in all stages. In Stage 9, the observed $\delta_{v\text{-}max}$ of 190 mm is 1.56 times of the computed value of 121.4 mm. With the observed $\delta_{h\text{-}max}$ of 154 mm at SID-7, the observed settlement to wall deflection ratio, $\delta_{v\text{-}max}/\delta_{h\text{-}max}$, is 1.23 on the south side. On the east side, the observed $\delta_{v\text{-}max}$ is 133 mm and the observed $\delta_{h\text{-}max}$ is 171 mm at SID-5 in the final stage, with the $\delta_{v\text{-}max}/\delta_{h\text{-}max}$ ratio of 0.78. On the south side, the $\delta_{v\text{-}max}/\delta_{h\text{-}max}$ ratio of 1.23 exceeding unity could be attributable to consolidation. Such consolidation effect to surface settlements is not modelled in this study.

Figure 1(a) shows that there is an underground railway aligned along the south side of the CPC project site. The distances of the railway tunnel to the south wall range from 15 m to 40 m. Hwang (2023) advised that the diaphragm wall for constructing the underground railway was approximately 40 m in length. The damming effect of that diaphragm wall blocked the seepage paths in the sandy Sublayers III and V. Groundwater recharging to the soil strata between the south wall and the railway tunnel via those 2 sandy sublayers was then disabled. Piezometers monitoring at 10 m horizontal distance behind the south wall showed that the piezometric level in Sublayer I was lowered from El. -4.2 m in January 1999 to El. -10.2 m in June 2000. The 6 m drawdown could contribute to the consolidation settlements.

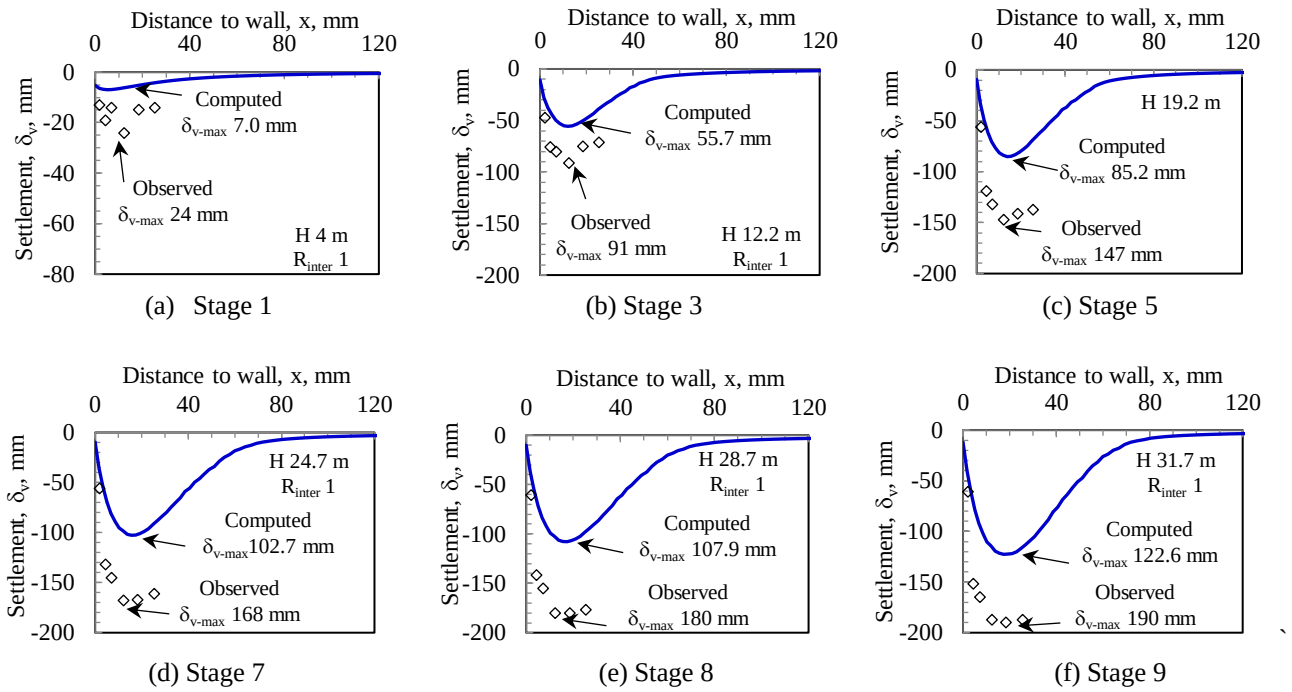

Figure 12: Computed and observed surface settlements behind south wall – Case 3

4.4 Normalized settlement profiles

Figure 13 presents the normalized computed and observed settlement profiles behind the south and the east walls in Stage 7 to Stage 9. The surface settlements, δ_v, are normalized with the maximum settlement, $\delta_{v\text{-}max}$ of and the distances to the wall, the x values, are normalized with the excavation depth, H, of each stage. Although the observed settlements behind the south wall are far larger than those computed, the shapes of the normalized profiles match with those computed within 1H behind the wall. In Stage 8, the normalized observed settlement profile behind the east wall matches with that computed within the distance 2H. The matching between the observed and the computed normalized settlement profiles shows that the numerical analysis using the HSS model could reliably predict the magnitude and the shape the surface settlements.

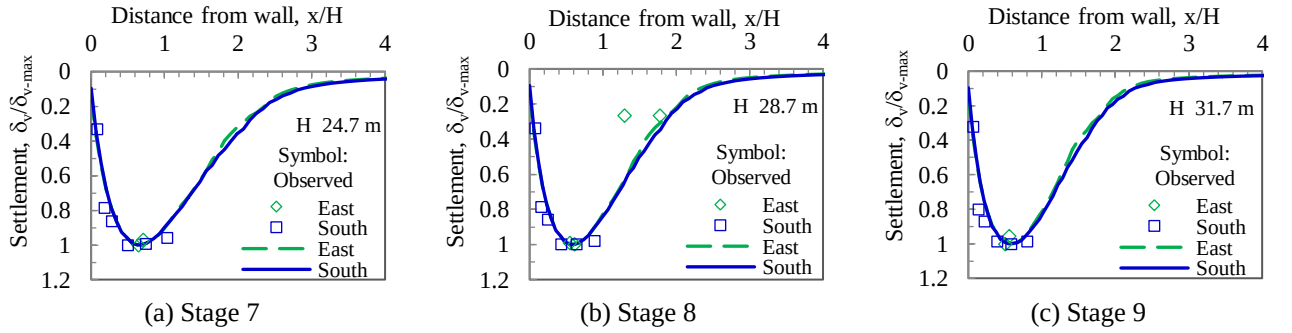

Figure 13: Normalized computed and observed surface settlements behind the south and the east walls

5 CONCLUSIONS

Two-dimensional numerical analysis on an excavation case history in soft ground has been conducted. The top-down construction for the maximum excavation depth of 31.7 m was supported by diaphragm wall with buttresses panels. The nonlinear Hardening-soil with small-strain stiffness (HSS) soil model is adopted. The following conclusions could be drawn:

(1) The HSS soil model could estimate the wall deflections and the surface settlements simultaneously.

(2) The presence of the buttress wall could affect the roughness along the soil-wall interface, which is one of the key parameters affecting the performance of wall deflections and surface settlements.
(3) The analysis confirms the trend of reduction in wall deflections with increasing in wall stiffnesses.

The set of the parameters for the small-strain stiffness adopted in this study has been interpreted from the laboratory tests and verified by an excavation case history. Close matching of the computed results with those observed in this case history further verifies the parameters.

REFERENCES

Bentley (2022). *PLAXIS 2D-Reference Manual*. CONNECT Edition V22.02, Bentley Advancing Infrastructure, August 2022.

Benz, T. (2006). Small-strain stiffness of soils and its numerical consequence. *Dissertation of thesis*, the Institute of Geotechnics, University Stuttgart.

Chen, Y.K, Huang, C.C & Wang, F.G. (1997). Grouted raft for building protection in excavation in soft clay. Proc.,7th Conf. on Current Research in Geotechnical Engineering, Taiwan, Vol. 1:593-600. (in Chinese)

Chin, C.T., Chen, J.R., Hu, I.C., Yao, D.H.C. & Chao, H.C. (2007), Engineering characteristics of Taipei clay. In T.S. Tan, K.K. Phoon, D.W. Hight & S. Leroueil (Eds), entitled*: Characterization and Engineering Properties of Natural Soils*, Taylor & Francis Group, v3:1755-1803.

Chin, C.T., Crooks, A.J.H. & Moh, Z. C. (1994). Geotechnical properties of the cohesive Sungshan deposits. *Geotechnical Engineering, J. Southeast Asian Geotechnical Society*, Taipei, Taiwan 25(2): 77-103. (in Chinese)

Chin, C.T. & Liu, C-C. (1997). Volumetric and undrained behaviors of Taipei silty clay. *J. Chinese Institute of Civil and Hydraulic Engineering*, Taipei, Taiwan 9(4): 665-678. (in Chinese)

Chuang, M.H., Chou, C.R., Su, T.C. & Wang, C.H. (2002). A case study of 32 m excavation in soft ground. Proc., Urban Underground Construction and Environmental Protection, Cross-Strait Geotechnical Conference, Shanghai, China. 171-180. (in Chinese)

Hwang, R. (2023). *Personal communication*.

Hwang, R., Moh, Z.C. & Hu, I-C. (2013). Effects of consolidation and specimen disturbance on strengths of Taipei Clays, *Geotechnical Engineering, J. of SEAGS & AGSSEA*, March, Bangkok, 44(1): 9-18.

Hwang, R., Moh, Z.C. & Wang, C.H. (2007). Performance of wall systems during excavation for Core Pacific City. *J. of GeoEngineering*, 2(2), Taipei, Taiwan. 53-60.

Hwang, R. & Moh, Z.C. (2022). Groundwater drawdown and subsidence in the Taipei Basin. *Sino-Geotechnics*, No. 173/2022.9: 99-110. (in Chinese)

Hu. I.C., Chin, C.T. & Liu, C.J. (1996). Review of the geotechnical characteristics of the soil deposits in Taipei, *Sino-Geotechnics*, No. 54: 5-14. (in Chinese)

Kung, G.T.C, Ou, C.Y. & Juang C.H. (2009). Modelling small-strain behavior of Taipei clays for finite element analysis of braced excavations. *Computers and Geotechnics* 36 (2009): 304-319.

Lee, S.H. (1996). Engineering geological zonation for the Taipei City. *Sino-Geotechnics*, (54): 25-34. (in Chinese)

MAA (1987) *Engineering properties of the soil deposits in the Taipei Basin*, Report No. 85043, Ret-Ser Engineering Agency and Taipei Public Works Department, Taipei. (in Chinese)

Moh, Z.C. & Ou C.D. (1979). Engineering characteristics of Taipei Silt. *Proc., 6th Asian Regional Conference on Soil Mechanics and Foundation Engineering*, Singapore, 1: 155-158.

Ou, C.Y., Liao, J.T. & Cheng, W.L. (2000), Building response and ground movements induced by a deep excavation, *Geotechnique*, Vol. 50, No. 3: 209-220.

Ou, C.Y., Lin, Y.L. & Hsieh, P.G. (2006). Case record of excavation with cross walls and buttress walls. J. of *GeoEngineering*, 1(2), Taipei, Taiwan. 63-73.

PLAXIS B.V. (2013). *PLAXIS Reference Manual*. PLAXIS, BV, Delft, the Netherlands.

Schanz, T. & Vermeer, P.A. (1998). On the Stiffness of Sands. *Geotechnique*, 46, No. 1: 145-151.

Schanz, T., Vermeer, P.A. & Bonnier, P.G. (1999). The hardening soil model: formulation and verification. *Beyond 2000 in Computational Geotechnics*. Rotterdam, the Netherlands. 281-290.

Wong, L.W. (2023). Effects of soil-structure interaction on wall deflections and surface settlements during deep excavations. *Proceedings, 43rd HKIE Geotechnical Division Annual Seminar*, Hong Kong, May 2023.

Deep Cement Mixing (DCM) method for reclamation of Tung Chung East Reclamation – Construction aspects

M.S. Kang
Build King Zens Engineering, Hong Kong
K. W. Cheung
AECOM, Hong Kong

ABSTRACT

Deep Cement Mixing (DCM) is an effective soil improvement technique widely used in geotechnical engineering. This technique involves the use of cement slurry to create cylindrical columns in the soil. These columns help to improve the strength, stiffness, and stability of the soil. DCM has been successfully applied in various projects, including marine infrastructure development. In the advanced work for Tung Chung New Town Extension (TCNTE) project, as a non-dredged construction scheme, deep cement mixing (DCM) method for ground improvement was used to strengthen very soft to soft marine sediment of clay to silty-clay materials in the project area for supporting seawalls and overlying fill material for ground formation. During the project, various types of DCM method and equipment were used according to the construction stage, purpose and site restraints in both marine and land work front. Different challenges were encountered and handled during the project such as low water, works near the noise sensitive area, severe barges interference by site congestion, low headroom and many others. Through the entire project, more than 6.2 million m^3 of volume of DCM was installed successfully which sets the record of world largest DCM application for a single contract.

1 OVERVIEW OF PROJECT

1.1 Project Introduction

The Tung Chung East (TCE) project is a reclamation project located in the Tung Chung New Town Extension (TCNTE), undertaken by the Civil Engineering and Development Department (CEDD). The project aims to create 130 hectares of new land adjacent to the existing residential area of Tung Chung new town.

Over the years, reclamation methods and ground treatment techniques have advanced significantly to meet technical requirements and social expectations. To promote sustainable reclamation method, the TCE reclamation project has adopted several measures, including non-dredged reclamation methods, specifically the deep cement mixing (DCM) method, and the use of construction and demolition (C&D) materials as the primary filling material. Given the pressing need for land, TCE reclamation is the first public works project in Hong Kong that has adopted the DCM method to expedite reclamation activities.

Table 1: Superficial deposits beneath the area of the proposed reclamation

Stratum	Soil Type	Thickness (m)	Description
Marine Deposits (MD)	Silts/ Clay	10 ~ 17	Very soft to soft MARINE DEPOSITS CLAY and SILT, locally granular.
Alluvium (ALL)	Interbedded Clays/ Silts & Sands	10 ~ 21	Medium dense to dense silty fine to coarse SAND / Sandy clayey SILT (occasionally very stiff), interbedded with fine to coarse GRAVEL of rhyolite and quartz with cobbles.

During the project, various types of DCM methods and equipment were used based on the construction stage, purpose, and site constraints in both the marine and land work front.

For the general soil profile, the soil underlying the proposed reclaimed area typically consists of deep layers of very soft Marine Deposit (MD) and Alluvium (ALL). These superficial deposits are, in turn, underlain by an in-situ weathered granite profile, encountered at approximately 36m below the seabed. The description and thickness of the superficial deposits are presented in Table 1.

1.2 Geotechnical properties of the soils to be treated by DCM

DCM method was utilized as a non-dredged construction scheme to improve the soft marine sediment consisting of clay to silty-clay materials in the project area, in order to support seawalls and overlying fill material for ground formation. This method involves treating the entire stratum of MD layer and a portion of the ALL layer within the column for each installation. The toe of the DCM column is terminated at the level of competent stratum (CS), which is defined as having a minimum 2m embedment depth in stratum with rolling average $q_c \geq 1.5$MPa, according to CPT results. This level is referred to as CS top level.

The water content of the original soil deposits, as measured with soil samples collected from the G.I, ranges from 70-110% for the upper 10m of MD and 15-45% for ALL layers. The bulk density of the alluvial layer is higher than that of the marine deposit layer, with an average value of 1.9tf/m^3 compared to the marine deposit layer's average value of 1.5tf/m^3.

Based on Atterberg limit test results, MD is classified as almost MH (Silt of High Plasticity) and ALL is classified as almost CL (Clay of Low Plasticity) according to the United Soil Classification System (USCS).

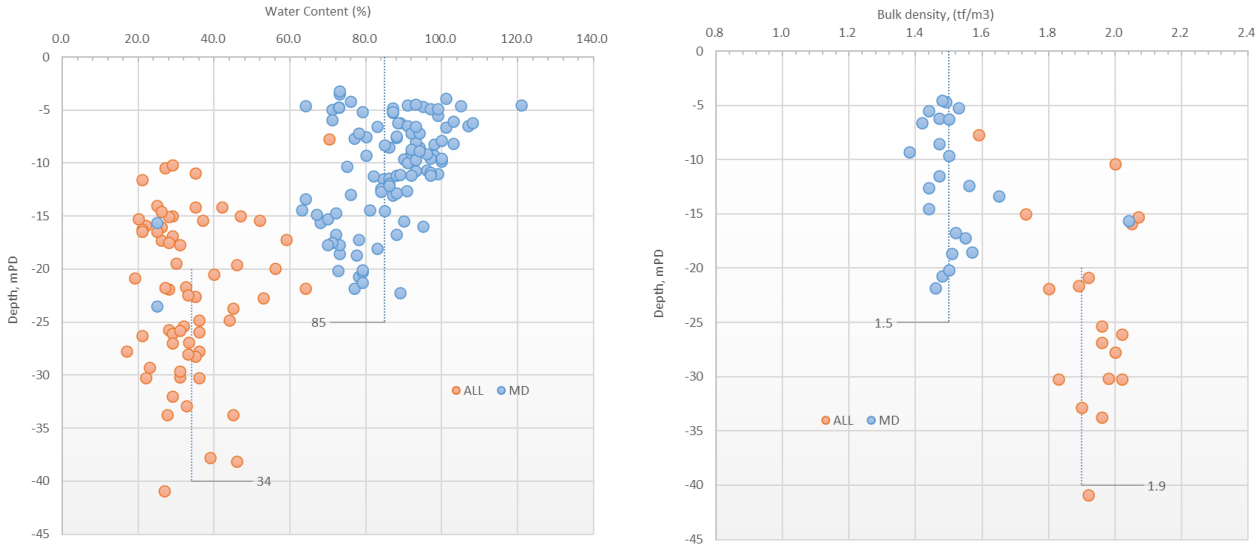

Figure 1: Water content of MD and ALL

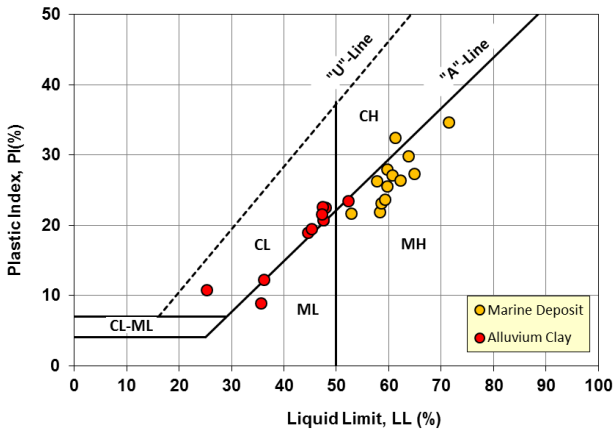

Figure 2: Atterberg limit

2 LABORATORY MIX TEST

2.1 Test Conditions

DCM is a ground treatment technique and the design is site specific. The mixing parameters, such as the dosage of binder and mixing time are tested and verified for individual soil layers to ensure consistency of DCM quality. The test is first carried out in laboratory under control environment. The objective of the laboratory mixing test is to establish the soil properties, its mixability and binder dosage etc. Test specimens for the laboratory mixing test were prepared in accordance with the Japanese standard laboratory procedure on the preparation and storing of test samples of soil for dry and wet mixing methods (JGS 0821-2009).

It is well-established that the strength of binder-stabilized soil using DCM is significantly influenced by the in-situ water content of the soils. The total water content in the treated soil mass, that is the in-situ water content plus the additional water in making of the slurry plus any additional water will make up the total water content in the end-product. This total water content to the binder ratio is found to be of relationship to the final strength of the DCM. Water content test is based on the procedures as recommended in Geoguide 3 (CEDD).

In the TCE project, there are two distinctive soil layers that are targeted for treatment using DCM. Soil samples from the MD and ALL layers were collected at the site using tube sampling, and the water content of the tested soils was controlled to represent those two soil layers in the mixing test. As the water content varies with depth and location across the site, the designer shall collect sufficient samples from different depth and location to provide reliable results.

To prepare the testing soils from the MD layers, the soils were screened by a sieve to remove larger size particles and mixed thoroughly in a soil box using portable hand-held mixing drills. The water content of the soils was controlled to the target water content, which was determined to be the average value of 85% in the original ground (refer to Figure 1).

On the other hand, the average water content of the ALL layers was found to be 34%, which is relatively low. It was often observed that the tamping of the mold with stiff binder-soil mixtures was not sufficient, resulting in failures to obtain proper test specimen conditions. A tailored made compact table, (Figure 3) standardize the compaction energy to ensure the samples are well compacted and to the same degree of compaction.

Furthermore, considering the practical limitation of DCM rig penetration capability and to ensure proper mixing, it is not uncommon to adopt water injection to assist penetration and disturb of stiff ALL layer and achieve the desired penetration. It is envisaged that this injected water would result in a increase in the water content of this layer. Therefore, the water content of the ALL soils used in the laboratory mixing test was determined to be the average value of 40.0%.

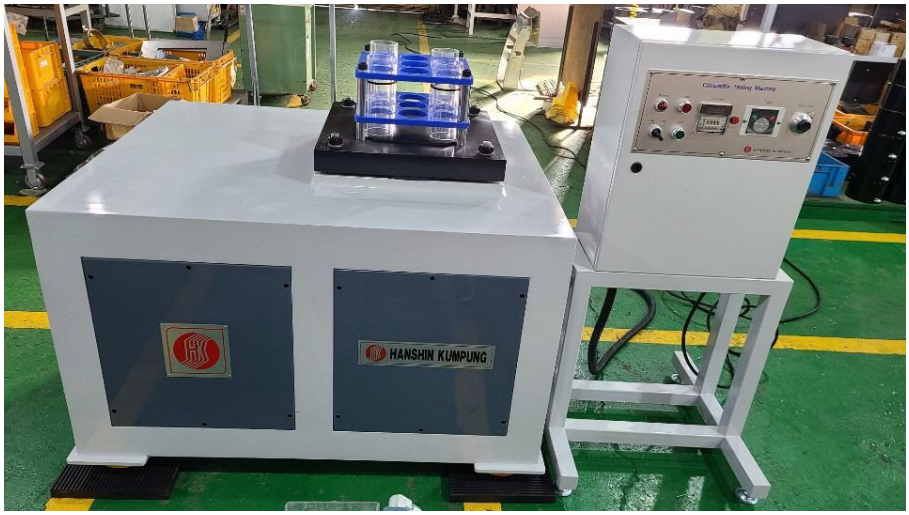

Figure 3: Compaction table for DCM laboratory mix test

2.2 UCS Strength Characteristics from the Laboratory Mix Test

The Unconfined Compressive Strength (UCS) test was conducted in accordance with ASTM D2166M-16 and the Interim Guidelines on Testing Unconfined Compressive Strength of Cement Stabilized Soil Cores in Hong Kong. Figure 4 illustrates the relationship between the dosage of binder cement and UCS, as determined through laboratory testing of MD and ALL soils stabilized with Portland Blast Furnace Cement (PBFC) and Ordinary Portland Cement (OPC), and tested after 28 days of curing. Although there were some variations in the test results for specimens tested under the same conditions, the overall trend indicates that UCS increases with an increasing amount of binder cement. Notably, the UCS values differ significantly between the MD and ALL layers, which strongly suggests that the water content of the soils may be a key factor influencing UCS under laboratory conditions, particularly when the degree of mixing is high enough for either soil type to avoid the effects of insufficient degree of mixing.

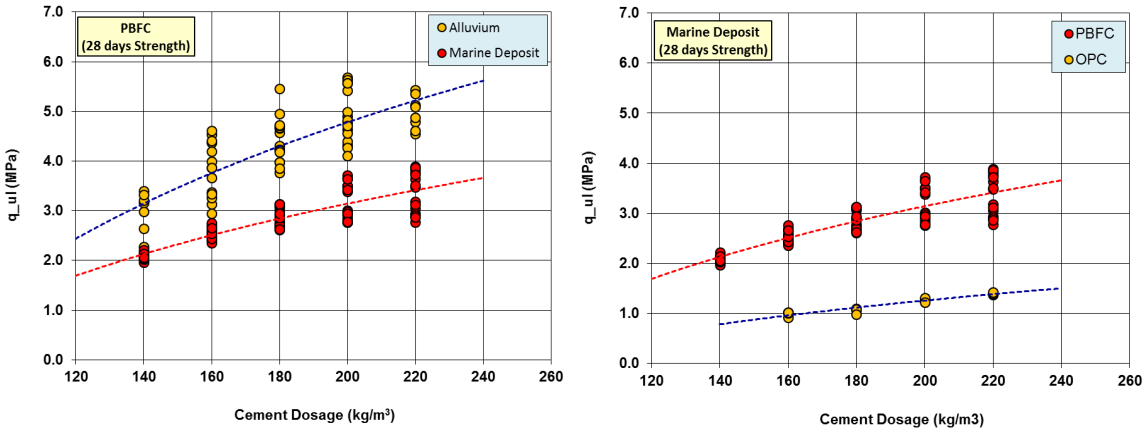

(a) UCS for MD and ALL (b) UCS for Biner Type

Figure 4: UCS at 28 days for MD and ALL using PBFC and OPC

As indicated by the results, the UCS of treated soils decreased with an increasing initial water content, regardless of the soil or cement type used. Of particular concern was the strength reduction of DCM in the upper soft soils within the MD layer. To further investigate this issue, additional UCS tests were conducted on MD soils with varying water content. Figure 5 illustrates the relationship between normalized unconfined compressive strength and initial water content of MD soils using two different binders of PBFC and OPC.
The results revealed that UCS decreased with increase of water content and that its decreasing rate is higher in case of using OPC compared to PBFC for the type of soils used in the test. Therefore, it is highly recommended that laboratory tests with various mixing conditions are needed for better planning of DCM before the field application.

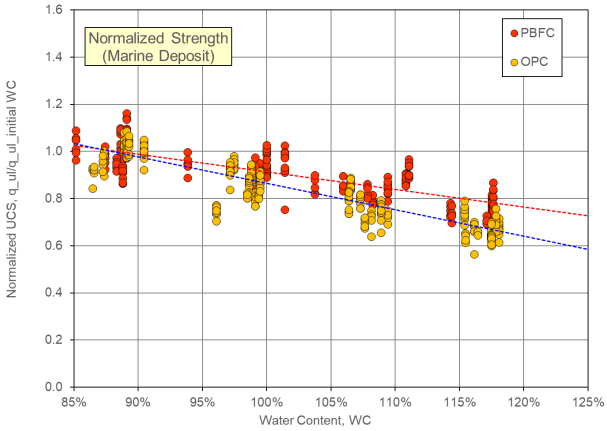

where, q_{ul} : UCS by laboratory test with increasing water content
$q_{ul\_initial\ WC}$: UCS by laboratory test at initial water content

Figure 5: Relationship between normalized UCS and water content of stabilized Marine Deposit (MD)

3 MARINE DCM

3.1 Mobilization of DCM Barges into the Site

The TCE reclamation project required the construction of a 4.9km long seawall, which was crucial to support the reclamation materials needed to form the new land. As the foundation of the seawall was designed with DCM walls and slabs, the DCM installation for the original ground under the seabed had to be conducted in marine conditions. Before starting marine DCM works, a sand blanket was laid on the original seabed along the footprint of the DCM foundation. This was done to provide a safe environment for water quality protection and to cut off direct exposure to seawater during DCM construction for the treatment of surface soils along the seabed. To achieve the target depth of DCM treatment, high-mast marine DCM barges, which were 52~53m above the water level, were selected. In total, six marine DCM barges with the same configuration were used for this task. All these DCM barges were equipped with multiple rigs that allowed the installation of three DCM clusters at the same time, as seen in Figure 6. The spacing between the rigs was adjustable to suit the design requirements.

Figure 6: Marine DCM barges used in TCE project

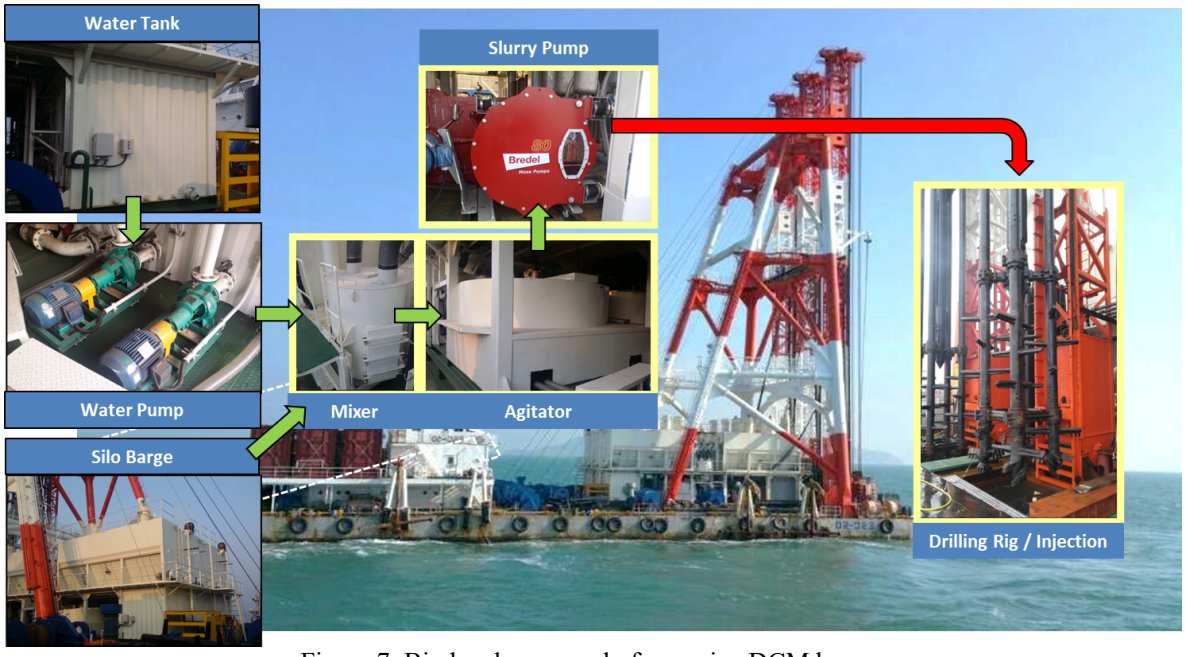

Figure 7: Binder slurry supply for marine DCM barges

Each DCM barge was equipped with 6 cement silos of 70~80 ton capacity each for the storage and supply of the dry binder to the mixing plant. In the mixing plant, a batch of the binder was weighed and dropped into the mixer where seawater was added proportionally at the predetermined water-binder ratio (normally 80-100%). This fresh mixture of binder slurry was then transferred to the agitator, and this process was repeated until the required volume of binder slurry was reached for one DCM cluster installation. The flow of binder slurry was controlled by the measurement of a flow meter attached to the slurry pump, ensuring accurate injection at the discharge outlet of the mixing blade system (Figure 7).

Due to the physical constraints of the site, the high-mast DCM barges had to pass under the existing Tuen Mun Chek Lap Kok (TMCLK) link viaduct during mobilization. To meet the height restrictions for passing under the TMCLK bridge, the barges had to be lowered with the rigs fitted at a height lower than 21m. Once they had passed under the bridge, the barges were reassembled.

Before mobilization, the rigs and leaders were dismantled, and the backstay tower (also known as the A-frame) was demounted and lifted onto a flat barge to be separately towed for assembly by a crane barge, as shown in Figure 8. For some of the DCM barges, due to their original barge layout, the backstay tower could not be lifted. In such cases, the front laying method was adopted, as shown in Figure 9.

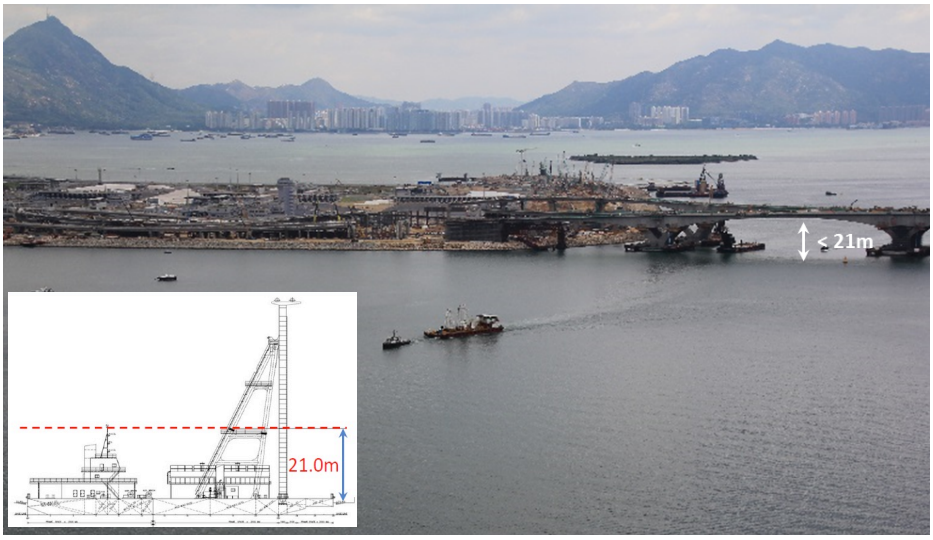

Figure 8: Towing of barges into the site passing under TM CLK Link

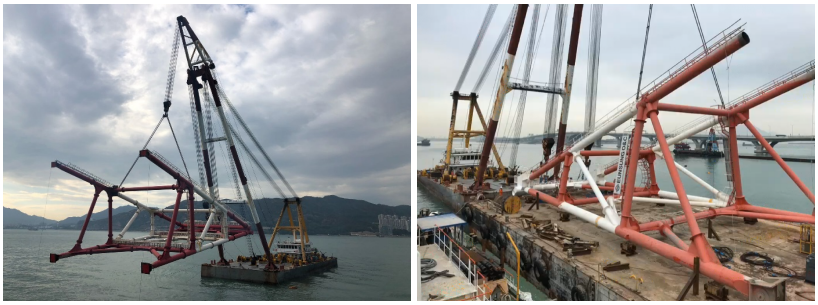

(a) Dismantling of back stay and placing on a flat barge for towing

(b) Front inclining of back stay

Figure 9: Dismantling and inclining of back stay for towing into the site

3.2 Marine DCM Works

During the marine DCM operation, certain site restrictions were in place, such as the need to work in close proximity to the existing residential areas. To comply with Environmental Permit, working hours were limited to 12 hours per day, from 7 am to 7 pm, and all necessary noise reduction devices and measures were prepared and equipped to minimize noise impact in the sound-sensitive area. The noise generated from the working barges was subdued and minimized to the best extent possible. The major sources of noise were covered by noise mats, including the Auger motors of each rig and the mixing plant used for preparing and supplying binder slurry. The generator engine rooms were enclosed by steel housing and panels to further reduce noise emissions.

Figure 10: Marine DCM barges on work close to residential area

In the DCM application, the 4-shafts DCM blade system consists of blades mounted on a steel rod shaft that are rotated to mix the soil and injected slurry and each cylindrical column per shaft has a diameter of 1.3 meters so that the dimensional area of treatment by each DCM cluster becomes 4.63m^3. The extent of a DCM cluster from the original seabed is varied in the range of 18~30m according to the required thickness of MD and ALL layer for improvement. The binder slurry can be injected from the bottom nozzle of the blade rods for penetration injection and from the top injection outlet for withdrawal injection.

Figure 11 shows the illustrated installation cycle diagram for a single cluster by marine DCM. After the DCM barge is positioned to the designated location, via Real-Time Kinematic GPS control, the DCM rig starts to penetrate down into the ground while the blades are rotating.

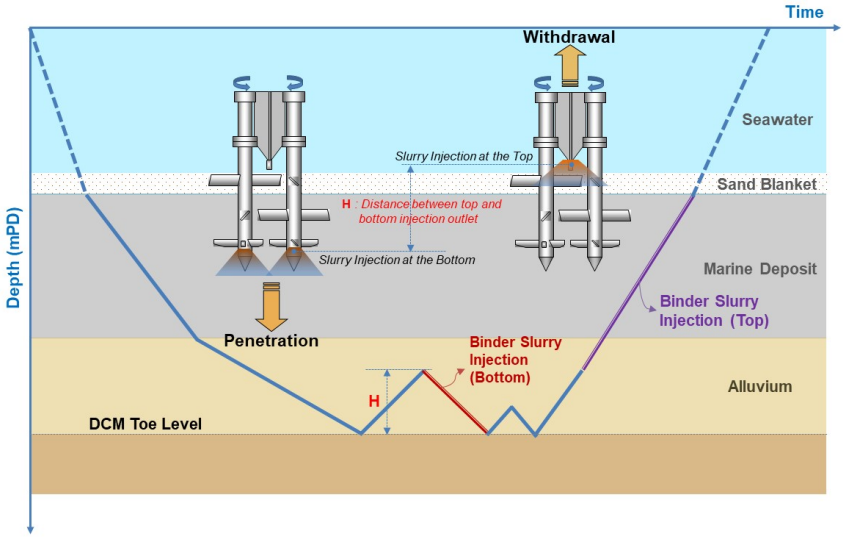

Figure 11: DCM installation cycle diagram

Once the penetration at the bottom end of the blade system (Zero-level) reaches to the design toe level, the blade system is then raised by "H" (the distance between top and bottom injection outlet points) as indicated in the Figure 11 so that this range of thickness is treated by "penetration injection". After the treatment of this portion of the cluster profile is completed, the outlet of binder injection switches from the bottom to the top so that the "withdrawal injection" is maintained to continue to treat the remaining part of soils up to the design top level of a DCM cluster.

The penetration rate of the mixing shaft may vary depending on the ground stiffness. The typical range of penetration rate is between 0.5m/sec to 1m/sec. The degree of mixing is dependent on the vertical movement of the mixing tools and the rotation speed of the blades. These two key parameters are presented in an index form, "Blade Rotation Number (BRN). BRN for DCM is defined in EuroCode 7, Execution of special geotechnical works, Deep mixing (EN 14679:2005) ;

BRN = (Total number of mixing blades) x ($Nu/Vu + Nd/Vd$)

Where, Nu : Rotation speed in rpm of the blades during withdrawal;
Vu : Mixing blade withdrawal velocity (m/min).
Nd : Rotation speed in rpm of the blades during insertion;
Vd : Mixing blade insertion velocity (m/min).

During the process of penetrating the ground with the DCM rig, the rotation of blades fully disturbs the original soil structure. The main purpose of this penetration is to confirm if the rig can reach to the design toe level, therefore until the design toe is confirmed, no binder slurry is injected. Through the penetration rotation, the soil is remolded and will improve the mixability of the soil with the cement slurry.

The resistance of the soil to the rotation of the blades at certain RPM can be estimated by measuring the current (Ampere) of the electric auger motors. This provides an indication of the ground stiffness encountered during the penetration of the DCM rig.

Figure 12 shows an example on the track record of DCM installation obtained from one of the DCM clusters by marine DCM. The rotational resistance of the auger motor is compared with CPT(Cone Penetration Test) values obtained from the original ground before DCM installation, it is understood that the trend of this resistance is well fit with the CPT results. This indicates that relatively accurate understanding of soil layer profiles can be obtained during the installation of DCM by the operator.

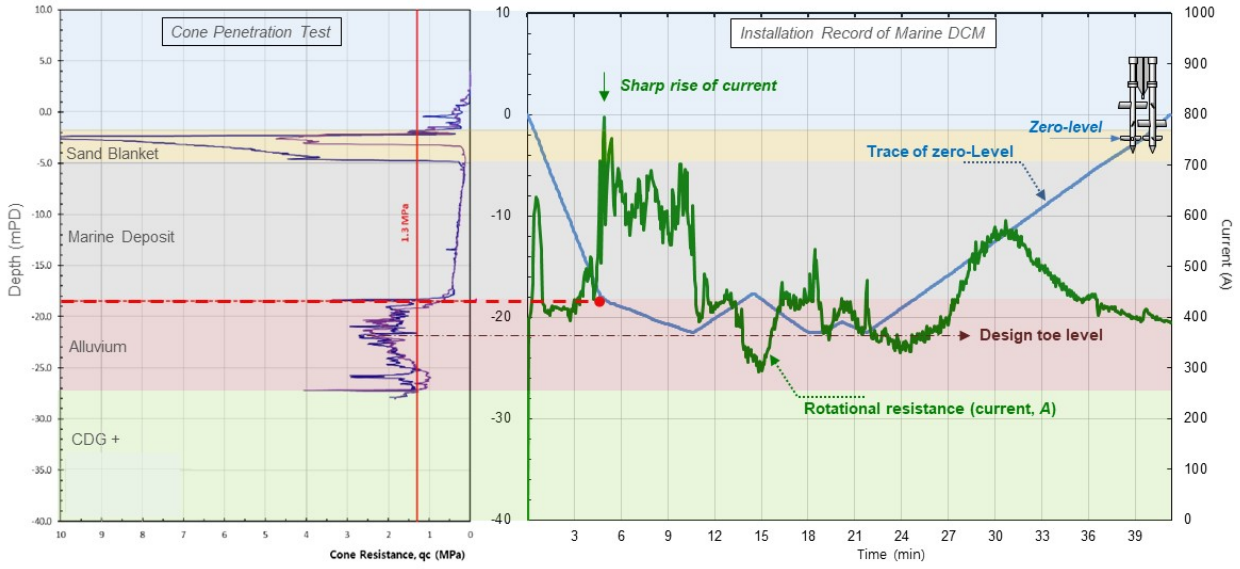

Figure 12: Example of installation record for DCM cluster

From Figure 12, it also can be seen that slightly before the bottom end of blades reaches the top of alluvial layer, the current started to build up with increase of resistance and the dramatical increase of current indicates

that the blades encountered the Alluvial layer. With such measurement, the DCM operator can estimate the ground condition so that the operator can correspond timely with appropriate controlling of rig penetration by regulating the RPM of auger motors or by handling the lifting of the rig by the main wire, or by water injection so that they can provide proper mixing condition for good quality of DCM treatment.

In addition, installation criteria were established in case the rig cannot reach the design toe level or it is interfered with during the penetration. The DCM operator can refer to the cycle record as illustrated in Figure 12 to make decisions based on such predetermined criteria.

4 LAND DCM

4.1 Land DCM Machines

Land DCM method was used to treat the soils at area where DCM barge could not access, due to shallow water. Around 47,000 clusters of DCM were installed using 17 land DCM machines, making it one of the largest land DCM installations for a single reclamation project.

The maximum reach of the land DCM was 31~32m from the ground level varying between +3 to +4mPD based on the site conditions. The land DCM machine has similar configuration as the marine DCM rig, that is a multi-auger system which combined four individual motors with a capacity of 110kW each, allowing the machine to construct DCM clusters with the same size as those used for marine DCM. The multi-auger system provided powerful rotational torque, allowing it to penetrate large depths and overcome complex ground formations with intermediate stiff layers or hard materials. This was the first attempt that four auger motors of large capacity were combined for a single cluster formation.

Due to the weight of the rig being over 35 tons, the base machine had to be sufficiently large for safe operation. The DCM rig of the land DCM was mounted to the leader of a crawler type pile driver, and the rig was lifted by the main winch with steel wire rope.

Unlike the marine DCM, the land DCM typically used the penetration injection method due to the complexity of attaching additional injection pipe and hose lines. It was also considered that this attachment could add excessive overburden weight to the rig, which was not beneficial for safe operation. Figure 13 shows the typical cycle diagram for the installation process by land DCM. After the rig is fully penetrated to the target depth of improvement, the rig is lifted to the designed top level of a DCM cluster to start the binder slurry injection at the bottom of the blade system. The rig is then lowered at the predetermined rate of penetration, RPM of blade rotation, and rate of slurry injection to form the DCM cluster.

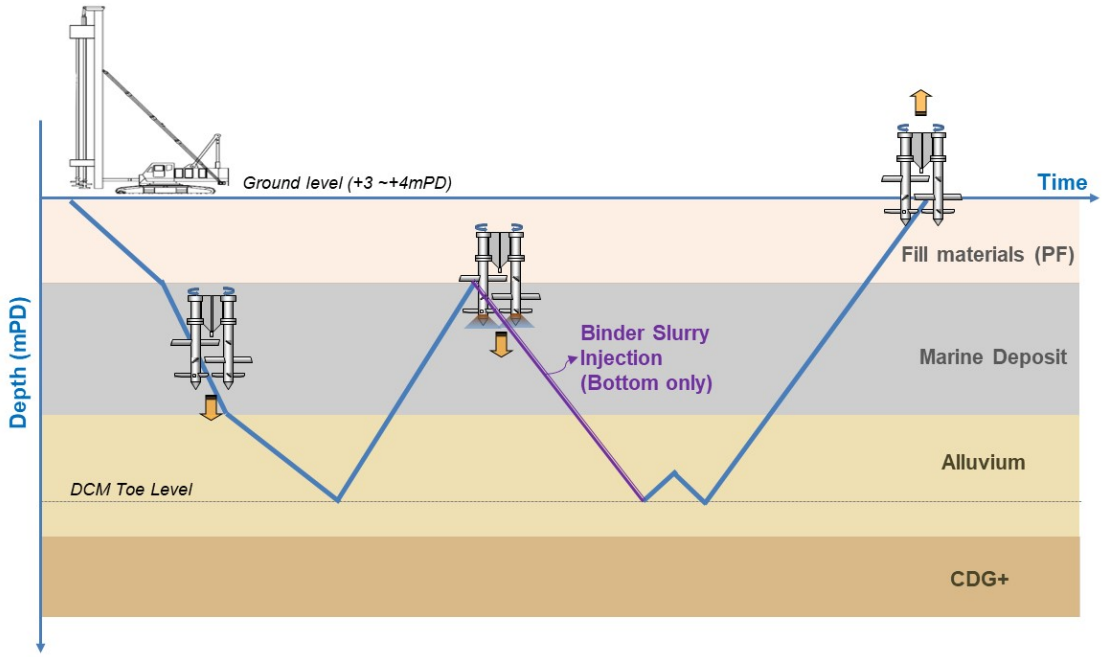

Figure 13: Cycle diagram for land DCM installation

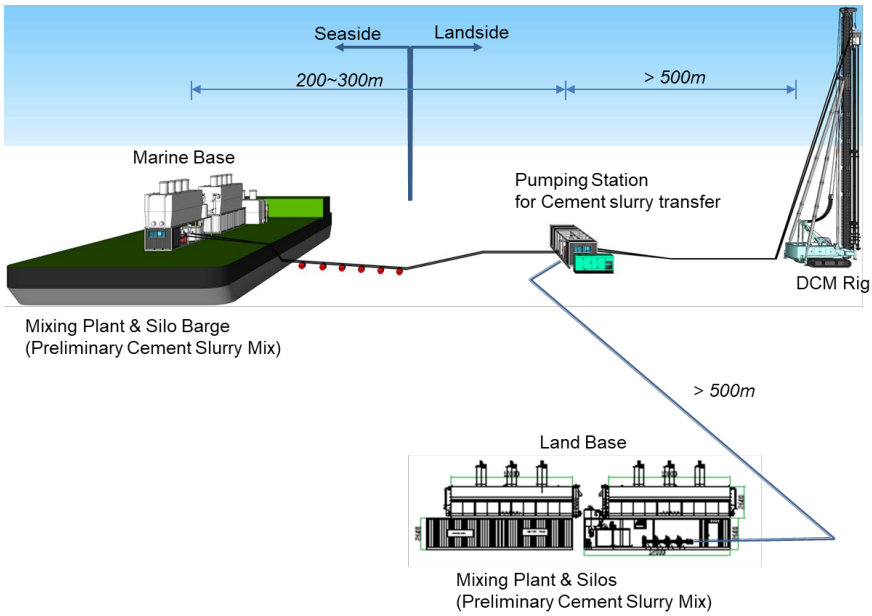

Figure 14: Arrangement of land DCM application

Unlike the DCM barge, there are separate cement silos, mixer plant and pumping stations set up remote from the DCM machine and this fixed location has to be selected considering site conditions such as interference to the other works nearby due to long term occupation of the plant facilities within the area, method for daily supply of cement/binder to the storage silos and maximum distance between the plant and the DCM machines. The mixer plant and silos can be facilitated on the marine barge or on the land as it is illustrated in Figure 14 and the pumping station is setup for the longer supply of binder slurry by relaying the pumping between the mixer plant and the DCM machine. When the supply of cement/binder is planned by marine transport, the area near to the vertical seawall is more advantageous for the plant facilities. The binder slurry that is prepared in the mixer plant is transferred by slurry pumps in the mixer plant or pumping station through high-pressure hoses that were extended up to 500m. However, for easier quality control and for preventing from clogging of high pressure due to long lead time by long pumping distance, it is preferred to keep the slurry pumping distance from the mixer plant to the DCM machine to within 300m.

Figure 15: Land DCM machines and its working on land

5 LOW HEADROOM DCM

Figure 16 illustrates a construction site located beneath the TM-CLKL viaducts, where the maximum allowable headroom is approximately 17m above mean sea level. This height restriction makes it impossible to employ standard DCM barges in this low headroom working condition. Initially, wire-mounted Cutter Soil Mixing (CSM) barges were planned for the area, but this approach posed significant challenges, including limited working space, the need for multiple working barges to complete the required volume of DCM within the allowed time, and safety concerns due to the operational status of the bridge.

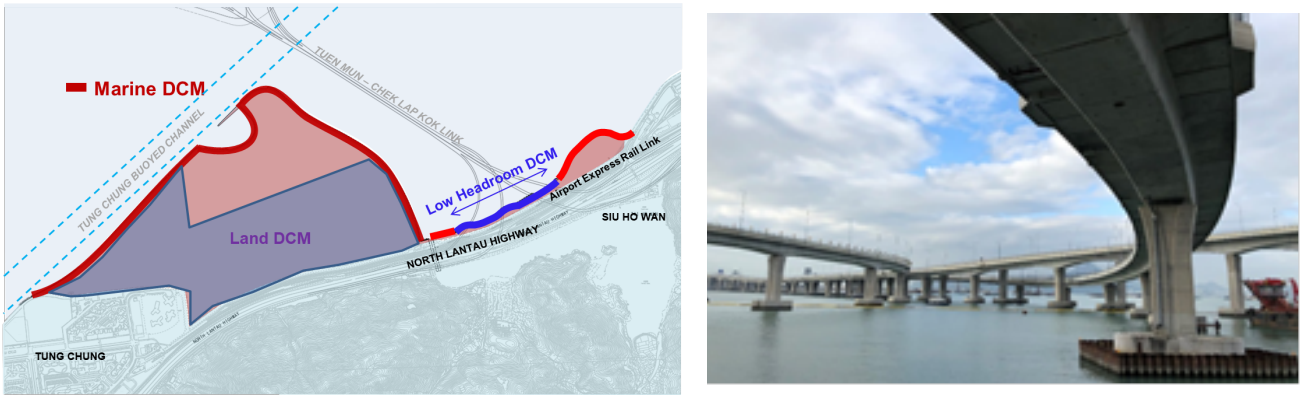

Figure 16: Area for low headroom DCM

To address these challenges, a proactive decision was taken in the middle of the project to develop a custom-made "low headroom DCM barge." This innovative barge featured a telescopic retractable rod design that was combined with a standard marine DCM application method. This solution enabled the barge to safely enter the low headroom area and install DCM treatment down to the design level by extending the rods up to four stages. This novel system represented a significant achievement for the project team, as it was the first of its kind and demonstrated their advanced technical capabilities.

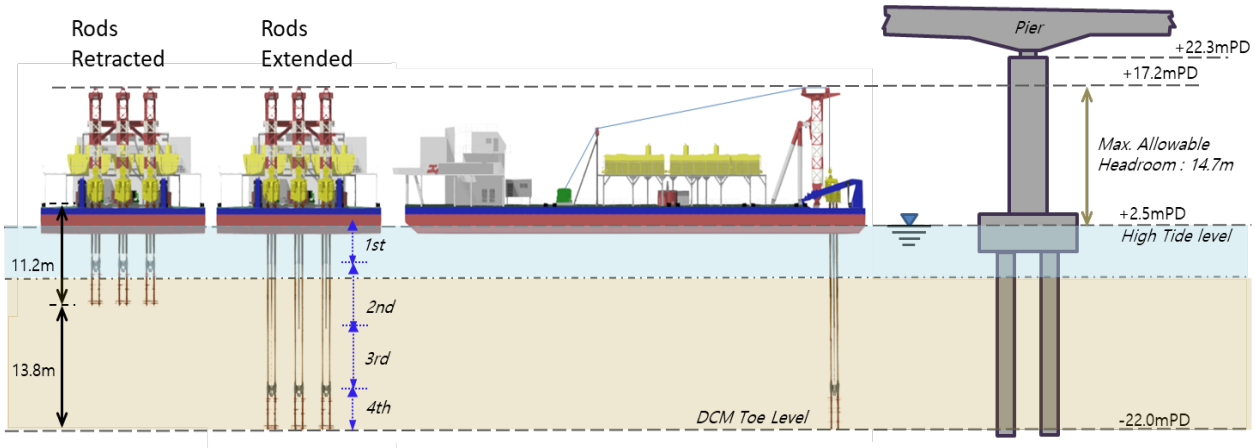

Figure 17: Low headroom DCM barge with 4 stage retractable rods

The new design not only overcame the stringent site conditions but also improved the overall productivity and flexibility of barge deployment. Unlike the conventional CSM system, which can only mount one set of wheels on a barge, the retractable telescopic design allows for up to three retractable rods to be equipped on one barge. This enables three DCM columns to be completed simultaneously, resulting in a significant increase in productivity, with a treated volume (per insertion) 170% of that achievable with conventional CSM machines. Furthermore, the total number of DCM installations required to build the same design foundation for seawalls was reduced.

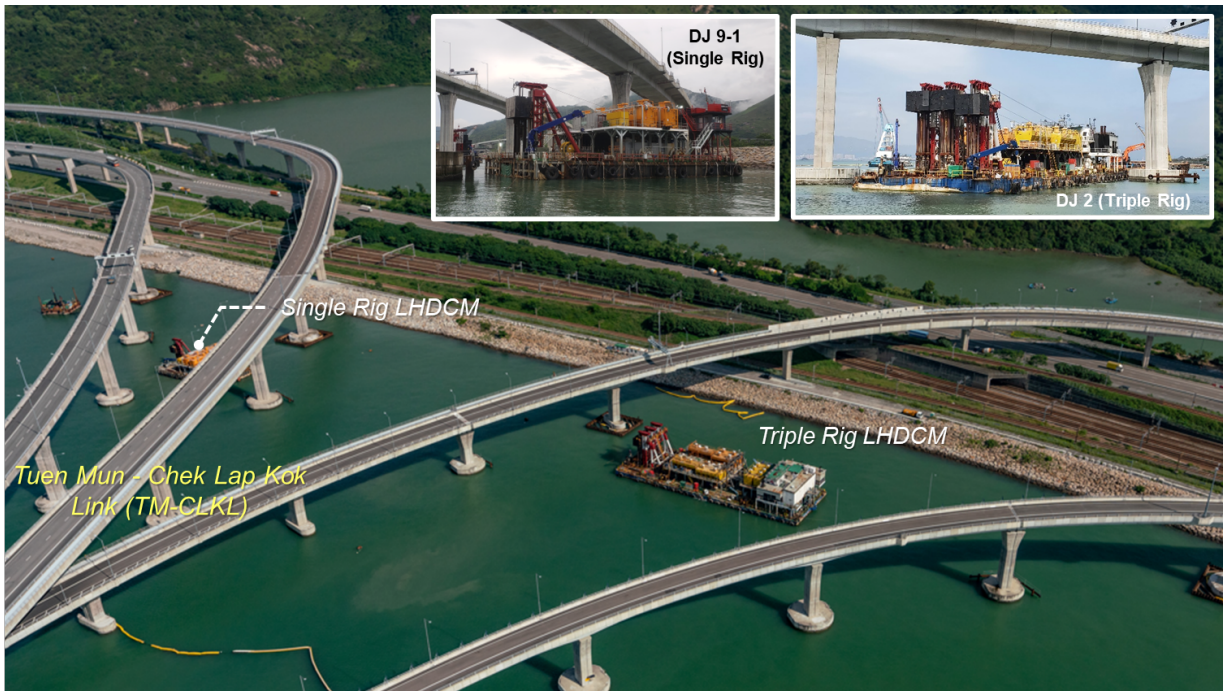

Figure 18: Two low headroom barges working under the TM-CLK Link

As a result of this innovative design, the number of working barges needed for the project was dramatically reduced from the anticipated seven barges to only two, while productivity was enhanced. The novel low headroom barge successfully completed ground treatment works in the extremely congested area in a timely manner, ultimately reducing the overall construction time by 35%. Additionally, as a result of this design, the potential risk of barge collisions was significantly reduced, and it had less effects on the environment of the adjacent water during construction.

6 OBSTRUCTIONS TO DCM

A limitation of DCM method is the ground obstructions, including cobbles and boulders. The mixing shaft is able to push individual obstruction sideway during the penetration through the rotation of the mixing blades. Modern DCM rigs, individual mixing shafts could be operated individually, that is they can rotate, not rotate or rotate in reversed direct. Through the operation of experienced DCM operator, individual obstruction in most cases could be push sideway to facilitate the continuous penetration and mixing action of the mixing shafts. When larger size obstructions or in case of thick layer of cobbles and gravels, the penetration capacity is limited. Repeated up and down motion of the mixing shaft may be able to assist the penetration.

Sometimes, additional water injection would be able to ease the penetration through obstruction. The pre-insertion test and site trial insertion is useful means for the operator to experience the ground response before carrying out permanent DCM works.

Other means of ground treatment method may be required, example jet grouting, depends on the design requirements and assessment of the toe levels actually achieved.

7 CONCLUSIONS

The Tung Chung East (TCE) reclamation project is the first public project to adopt sustainable method – DCM, and represents the large-scale reclamation utilizing a diverse array of deep cement mixing (DCM) techniques as non-dredging ground improvement method, including marine DCM, land DCM, and low headroom DCM. Prior to commencement of the main works, laboratory mix tests were conducted to evaluate the characteristics of the soils to be treated using DCM. These tests utilized soil samples extracted from the project site, and revealed significant variations in the unconfined compressive strength (UCS) characteristics

of the Marine Deposit and Alluvium layers, which were found to be influenced by binder types, dosages, and water content of the original soil.

The marine DCM works utilized high-mast marine DCM barges equipped with multiple rigs for seawall foundations, while the land DCM installation process employed more than 17 land DCM machines to improve the soft soils beneath the reclaimed land with public fills. A custom-made "Low Headroom DCM barge" was specifically designed to overcome site-specific constraints related to working under the viaduct of TM-CLK Link. This innovative solution utilized a four-stage retractable rod system, ultimately resulting in reduced construction time and enhanced worker safety.

The Tung Chung East reclamation project stands as a prime example of the successful implementation of deep cement mixing (DCM) in large-scale reclamation projects.

ACKNOWLEDGEMENTS

The authors thank the Civil Engineering and Development Department of HKSAR for the permission to publish this paper. Also thank to AECOM and Build King project team for the supports.

REFERENCES

U.S. Department of Transportation, Federal Highway Administration. 2013. Federal Highway Administration Design Manual: Deep Mixing for Embankment and Foundation Support, *Publication No. FHWA-HRT-13-046*.

US Department of Transportation, Federal Highway Administration. 2000. An introduction to the Deep Soil Mixing Methods as Used in Geotechnical Applications, *Publication No. FHWA-RD-99-138*.

M. Kitazume, M. Terashi, 2013. The Deep Mixing Method. *CRC Press/Balkema*. Taylor and Francis Group, London.

Hong Kong Institution of Engineers (Geotechnical Division). 2017. Interim Guidelines on Testing of Unconfined Compressive Strength of Cement Stabilised Soil Cores in Hong Kong.

Unconventional Excavation and Lateral Support System near Seashore in Lamma Power Station Extension

K.T. Hung & John Lai
The Hongkong Electric Company Limited
Michael W.L. Ng
AECOM Asia Company Limited

ABSTRACT

Nowadays in Hong Kong, the maritime construction is becoming more common for the infrastructure projects especially on the increasing demand of the land use for those residential and housing supply. Those civil infrastructure works would normally be completed in reclamation projects prior to the land grant to a private developer. For the developments under private and quasi-government sectors, the projects are required to execute under the land lease allocated conditions and controlled under Buildings Ordinance CAP123. The nature of this project in Lamma Power Station Extension (LMX) contains both characteristics in buildings and infrastructures, including reclamation and seawall construction. Under this circumstance, the excavation and lateral support would have considered the merits between both requirements and advancing to an out of conventional land construction method. The subjected site is situated at the southern-east of the LMX reclaimed platform facing to the incipient Lamma Island. The project required to construct a No. 5 C.W. Intake adjacent to the existing seawall. Under a fast-track programme, an Excavation and Lateral Support (ELS) system with submerged excavation was adopted for tow-in of the precast caisson chamber. This paper summaries the key features for the design and construction of the ELS for the project.

1 INTRODUCTION

1.1 Background

Hong Kong is being one of the most developed urban regions and global financial centre. An uninterrupted world-class electricity supply is one of the key attributed factors for this success. The Hongkong Electric Company Limited (HEC) provides a safe and highly reliable electricity for those financial centers / commercial & industrial buildings as well as those residential buildings in Hong Kong Island and Lamma Island through the century. In order to provide a clean, more sustainable and environmental friendly power supply, HEC has developed its own gas-fired combined-cycle unit that uses liquefied natural gas (LNG) since year 2006 at the newly reclaimed Island next to the operating Lamma Power Station. Committed to meet a long-term green energy need, this extends the LNG gas-fired stations to be further developed to achieve less carbon emission target. AECOM has been appointed to provide a design and supervision consultancy services for the No. 5 C.W. Intake Chamber which would supply seawater intake for cooling system of the newly constructed gas-fired station Unit L12 as well as future Unit L13.

1.2 Project Particular

The location for No. 5 C.W. Intake situated at the southern-east of the 22-hectare newly reclaimed platform, ***Plate 1***. A planned new intake chamber would be adopted as the current No. 4 C.W. Intake is reaching its capacity for the commissioned gas-fired stations Unit L9 to L11. The proposed new intake chamber was constructed and connected to the adjacent 3 nos. existing reserved intake culverts which were integrated as part of the existing vertical seawall back in earlier stage of reclamation. The marine deposit at the footprint of No. 5 C.W. Intake and the vertical seawall were dredged away and backfilled by layered rockfill and sand

filling upto the ground level of +5.5mPD between year 2001~2004 forming the current reclamation platform. Therefore, excavation to the formation of the new intake was required for the construction.

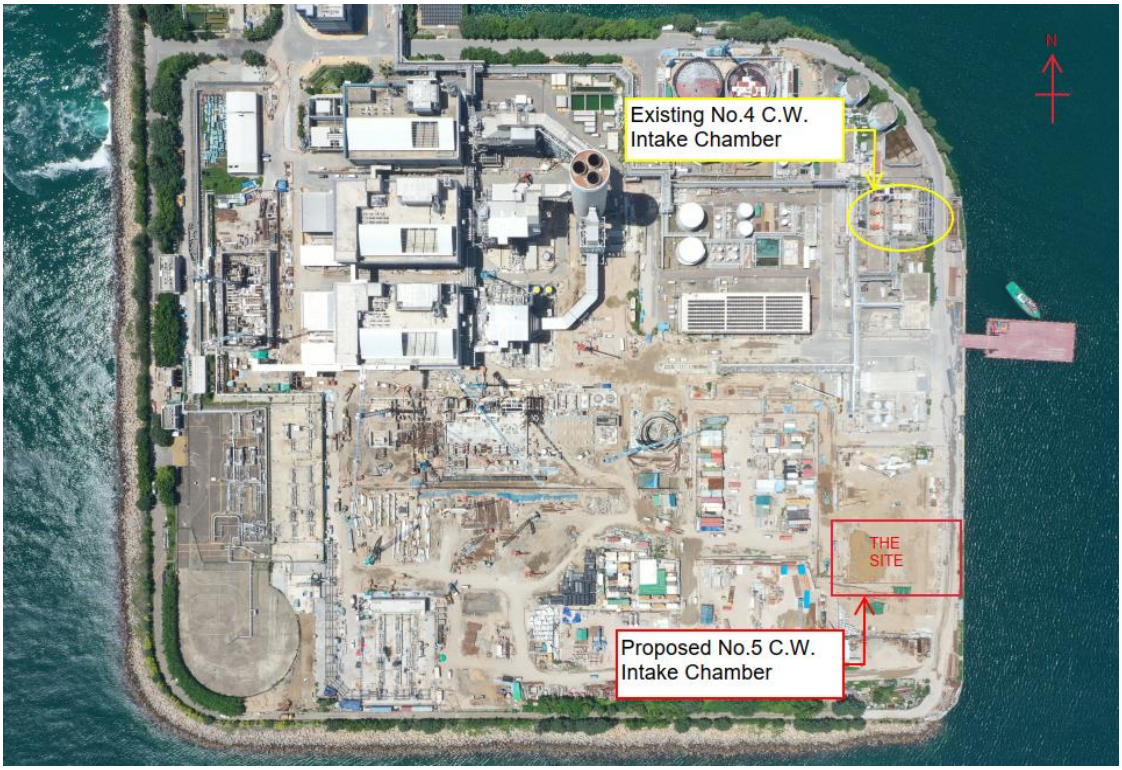

Plate 1: Site Layout Plan

2 DESIGN SCHEME AND OPTIONS

Based on the general arrangement, ***Figure 1 & 2***, the proposed intake chamber would be as deep as the invert level of the existing intake culvert and down to -7.5mPD. The plan size of the intake chamber would be 30m x 45m including the chamber for bar-screen and penstock, drum mesh screen, main reaction pump and discharge valve. Hence, the proposed excavation would be as large as 35m x 50m x 13m deep from the existing ground level. The construction sequence is always one of the most contributing factor for the design of Excavation and Lateral Support System and the options are discussed in the following sub-section.

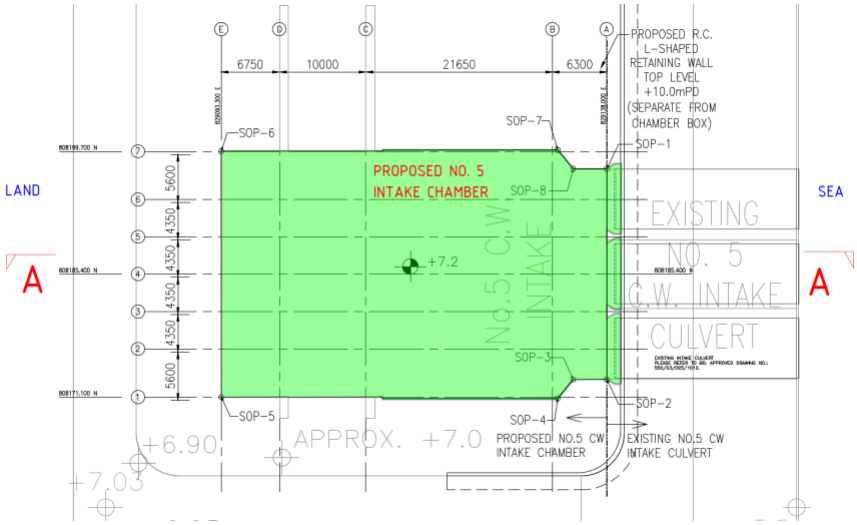

Figure 1: Layout for Proposed No. 5 Intake Chamber

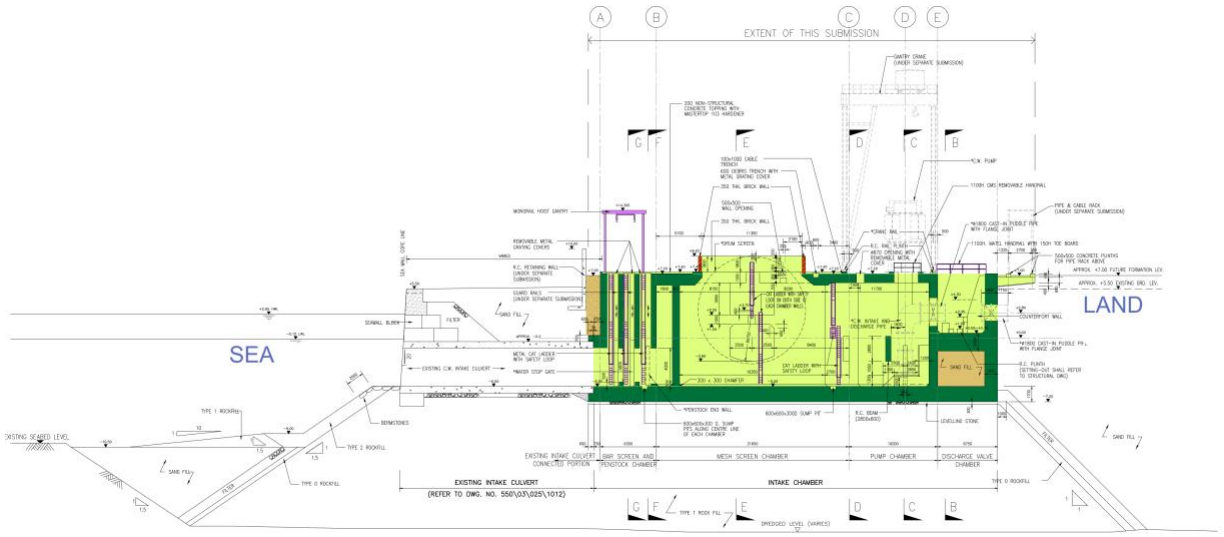

Figure 2: Section A-A for Proposed No. 5 Intake Chamber

2.1 Typical Land Base Option – Cast-in-situ

For the private developments in Hong Kong, it is very common to adopt vertical elements using sheet pile or pipe pile with cross flying strut for the ELS works. The curtain grouting might be necessary to provide an effective water cut-off for dewatering within the cofferdam using cast-in situ concrete construction method. When dealing with the situation near the seashore, sometime might need to adopt double hydraulic cut-off wall system to safe-guard the seepage conditions against the sea. It is always difficult and not environmentally welcome for grouting close to the seawall. In this project, the intake chamber required to form connection to the existing culvert, therefore an opening to the pre-installed ELS vertical elements was inevitable which would complicate the situation. Experiences told that it would be very time consuming to form successive water cutoff against the sea and might involve several stages of grouting and re-grouting works. Moreover, the flying struts would pose numerous restrictions to the subsequent in-situ reinforced concrete construction for the chamber. Therefore, this option was not pursued for this project.

2.2 Adopted Design Scheme

In order to meet the operation target for the new power generating unit, it was planned to have the on-site excavation as well as off-site precast construction working simultaneously and thereafter the permanent precast structure could be shipped from the Mainland China as a floating caisson. Hence, the ELS design had to consider the tow-in operation of the precast structure and the opening of the existing seawall. The time management, logistic, weather forecast with tidal effect shall be well planned throughout the design and construction stage. For the vertical element of ELS works, interlocking pipe pile was deployed to control the loss of fine material during the submerged excavation. While the lateral support, tie-back system was adopted to allow maneuvering of the tow-in operation for the precast structure installation. Once the lateral ties were installed layer by layer above the water level, further excavation was carried out under-water until reaching to the formation level of the structure. The general arrangement of the ELS works is shown in ***Figure 3.***

After the completion to the excavated formation, the existing seawall and intake culverts would be temporary removed in the remaining phase of construction. It was necessary to check the partial stability of the seawall during construction against the tidal effect. The seawall blocks and existing culverts were removed in stages and temporary stored for reinstatement after the installation of the precast intake chamber. When the opening of seawall was completed, the precast caisson would be tow-in to position. The backfilling and reinstatement works could be carried out concurrently with the culvert connection work as well as further construction of internal structural elements and M&E installations.

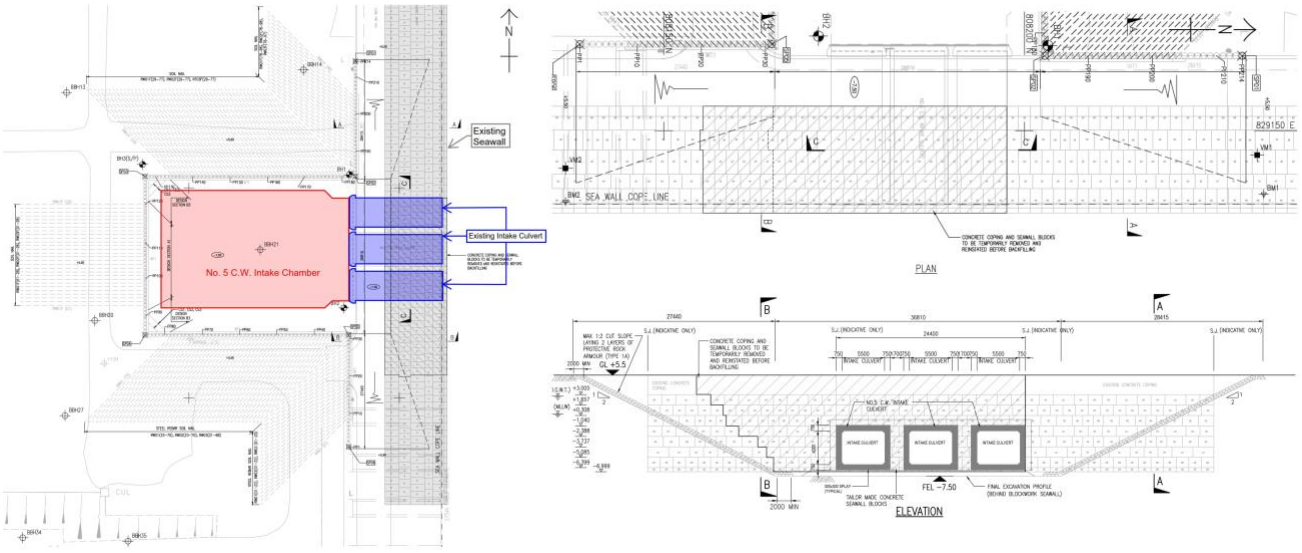

Figure 3: General Arrangement for the ELS Design Layout and Sewall Opening

Since the excavation was carried out in submerged conditions, the overall water pressure tended to be balanced at both retaining side and excavation side. Nevertheless, as the seawall would be opened up during the construction, the ELS works would therefore be subjected to the wave action and suctional force. Reference was therefore made to the nearest tide station in Chi Ma Wan from the Port Works Design Manuel (PWDM 2002) to allow the effect on tidal water level in the design, ***Figure 4***.

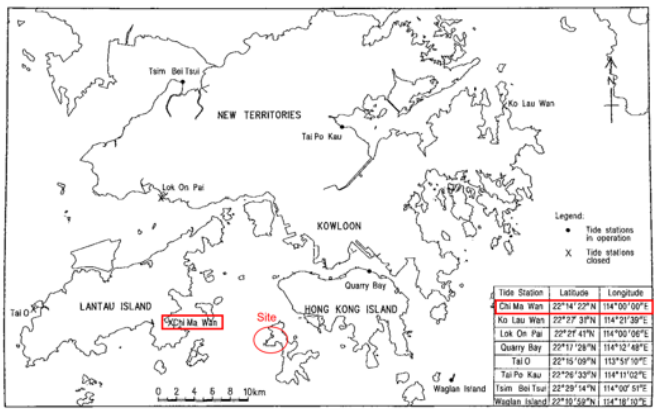

Table 2 Mean Sea Levels, Mean Higher High Water Levels and Mean Lower Low Water Levels

Location	Period of Data	Mean Sea Level (mPD)	Mean Higher High Water Level (mPD)	Mean Lower Low Water Level (mPD)
Chi Ma Wan	1981-1997	1.3	2.0	0.4
Ko Lau Wan	1983-1995	1.3	2.0	0.5
Lok On Pai	1982-1999	1.2	2.1	0.3
Quarry Bay/North Point	1981-1999	1.3	2.0	0.5
Tai O	1985-1997	1.2	2.1	0.2
Tai Po Kau	1981-1999	1.2	2.0	0.4
Tsim Bei Tsui	1983-1999	1.3	2.3	0.2
Waglan Island	1981-1999	1.3	2.0	0.6

Tidal Records of Nearest tide station

Figure 4: Reference on the Tidal Water Level near seashore, PWDM 2022

Based on the monitoring record and the G.I. from the Lamma Island Extension, which had been recorded more than 2 years covering the rainstorm periods, the highest measured ground water level was +1.7mPD. As the Site was relatively close and surrounded by the Sea, the ground water response and recharge on this reclaimed platform would likely be influenced by tidal fluctuation. As the excavation was designed to be carried out underwater, i.e. submerged excavation, therefore the following two scenarios of water level was considered:-

In **Case 1**, the design groundwater level at the retained side was +2.65mPD while at submerged excavation side was MLLW = +0.40mPD.

In **Case 2**, the design groundwater level at the retained side was +1.70mPD while at submerged excavation side was MSL = +1.30mPD.

While Case 1 was adopted for the structural capacity checking and Case 2 was adopted for estimating the wall deflection and ground movement in serviceability conditions.

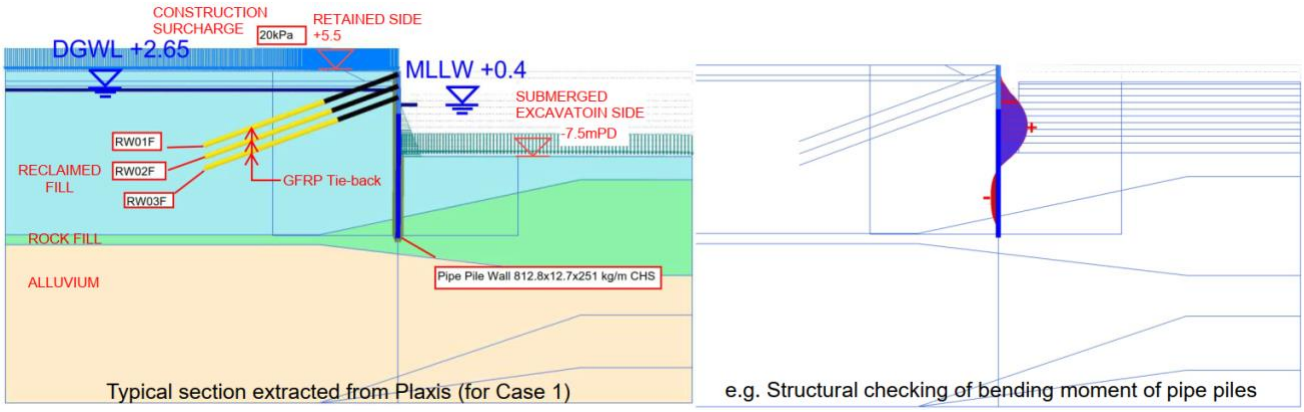

Figure 5: Design Condition Case 1 (for Structural Design Checking)

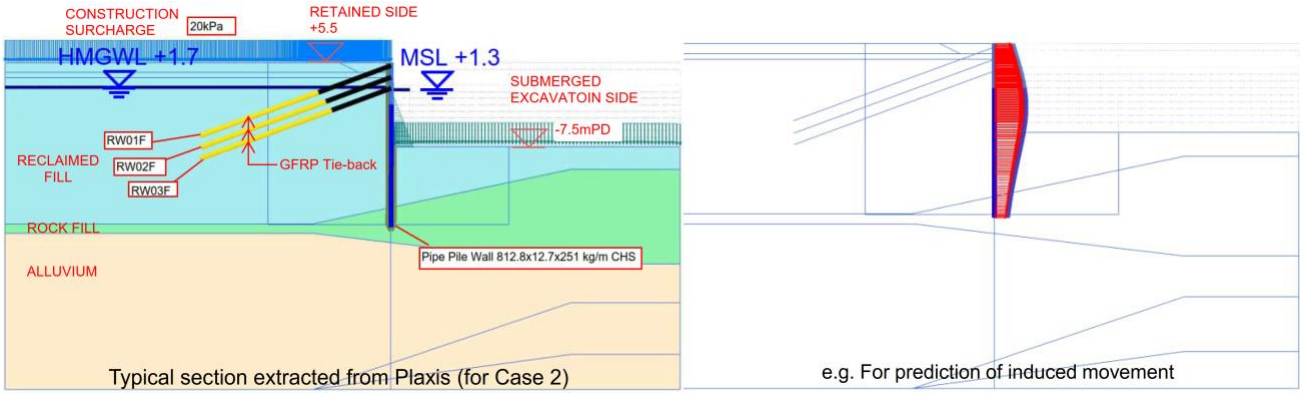

Figure 6: Design Condition Case 2 (for Serviceability Design Checking)

3 USE OF GLASS FIBRE REINFORCED POLYMER (GFRP) FOR TIE BACK SYSTEM

Glass fibre-reinforced polymer (GFRP) is a composite material made of glass fibres embedded in a polymeric resin matrix. This material composition results high strength primarily along the length of the bar in tension while it can be easily abraded or "consumed" by boring machinery. This unique "anisotropic" property offers many benefits in temporary construction. It has been widely adopted for diaphragm wall nowadays with soft eye opening for the receiving tunnel boring machine cutting through as well as tie-back system for excavation, ***Figure 7***.

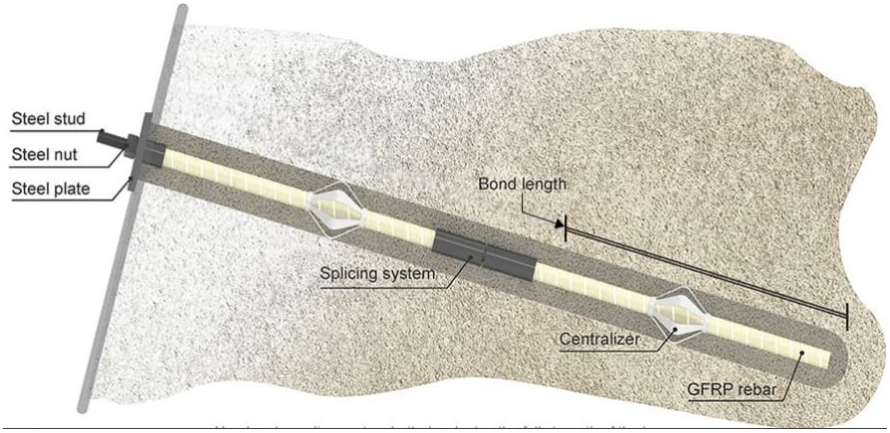

Figure 7: GFRP Tie-Back System

3.1 Project Benefits to be Adopted

The Lamma Power Station extension (LMX) had been planned and designed full house of the M&E installation. Adjacent to the No. 5 C.W. intake, there would be development for Chlorinators Areas, C.W. Pump Equipment Room, Crane Rail Foundation, 275kV cable Landing Point as well as other facilities for the coming LMX 12 to 13 which all require their foundation system. It was therefore proposed to adopt GFRP tie-back system within the future foundation footprint to enable further developments. The GFRP reinforcement is an alternative to the steel reinforcing bar. Its performance is much better when exposes to aggressive environment such as marine for which bare steel would have corrosion deterioration. Besides, it is non-magnetic and would not have electromagnetic interference problem against the plant and machinery operations. The high tensile strength performance helps to achieving the tension forces for the lateral support and stabilize the overall ground action. Also, the cuttability enhances its temporary usage, with strong action in main axis but can be easily machine bored and abraded away by excavation equipment later on.

3.2 Design Standard

There was no specific British Standard / Hong Kong Standard or Code of Practice addressing the design and the usage for reinforcement with GFRP bars. The American Concrete Institute Manual of Concrete Practice ACI 440.1R-06 was considered to provide the most up-to-date methodology for undertaking design of the reinforcement with Fibre Reinforced Polymer (FRP) and this code was adopted for the design of the GFRP bars. This ACI guide was based on the knowledge gained form worldwide experimental research, analytical works and field applications of GFRP.

The physical and mechanical properties of GFRP bars were dependent on the technology and processes employed by the manufacturer's making of the bars. For the tie-back system adopted in the ELS works, the following mechanical properties was used for the design and are summarized in the ***Table 1*** below for easy reference:-

Table 1: GFRP Mechanical Property adopted for Design, Dextra (2019)

Bar Dia. (mm)	Nominal Area (mm^2)	Guarantee Tensile Strength, f^*_{fu} (N/mm^2)	Ultimate Tensile Load (kN)	Tensile Modulus of Elasticity, E_f (GPa)	Ultimate Strain (%)
41	1339	>460 (672)	900.0	>40.8 (50)	>1.13% (1.48%)

For GFRP design, the ACI 440.1R-06 applied a "strength design approach" based on limit state design philosophy consistent with the relevant provisions in ACI 318-05 "Building Code Requirement for Structural Concrete". Whereas the soil nail and tie-back system would follow the recommendation given in Geoguide 7 which had been commonly adopted in Hong Kong practices. In comparison of the factor of safety, the onerous approach was adopted in the design to cater for the uncertainty.

The ACI 440.1R-06 recommended that GFRP bars were not be relied upon to resist compression. Justification calculations therefore ignore any contribution of GFRP bars in the compression stress block to the section. The tie-back system in Lamma Island was not required to resist compression. From the analysis, the tie-bars were all in tension at all stages of excavation process. The adopted of the tie-back system was mainly for the control of the wall deformation and hence the servicing settlement. Moreover, GFRP bars should be formed into the required shape during fabrication in factory and field bending was not allowed. The bending in GRFP bars for the tie-back system would not be required.

3.3 Testing and Verification

In section 11 of ACI440.1R-06 identifies two testing regimes with respect to the performance of GFRP bars:

- Product Certification of guaranteed and nominal values (denoted "C" in the "test regime" column in table 2 below). Product Certification was to be based on testing prior to the delivery of the product.
- Manufacturer's quality control tests / purchaser's quality assurance tests on the production lots of the bars incorporated into the specific works (denote "Q" in the "test regime" column in table 2 below).

The Quality Assurance / Quality Control (QA/QC) were based on testing of a minimum of five samples taken from each production lot of bars delivered to site. Test Certificates to show Product Certification for the specified properties were to be provided by the manufacturer prior to the works. QA/QC test certificates for the production lots were required for properties that were critical to the performance of GFRP bars in the specific application in the Tie-back System of Lamma Island. The properties of the GFRP reinforcing bars for 41mm dia. are specified in ***Table 2*** below:-

Table 2: Mechanical Property for testing or certification of GFRP, DEXTRA (2020)

Manufacturer recommendation

Ref	Property	Unit	Requirement	Standard Test Method	Test Regime
1	Nominal area	mm^2	1339	ACI440.3R-04/B.1	C
2	Fibre content	%	>55 (73)	ASTM D2584-08	C
3	Guaranteed tensile strength f*fu	N/mm^2	>460 (672)	ACI440.3R-04/B.2	C, Q
5	Ultimate tensile strain, ε*fu	%	>1.13 (1.48)	ACI440.3R-04/B.2	C, Q
6	Modulus of elasticity, ef	kN/mm^2	>40.8 (50)	ACI440.3R-04/B.2	C, Q
7	Transverse shear strength	N/mm^2	>115	ASTM D4475-02	C, Q
8	Bond strength (pull-out strength)	N/mm^2	>1.1 (3.0)	ACI440.3R-04/B.3	C, Q
9	Longitudinal wicking for void	Presence of voids	Report results only	ASTM D5117-09	C
10	Barcol Hardness	--	Report results only	ASTM D2583-07	C

During installation progress, 8 nos. of site trial with pull-out testing were carried out before working nail installation. Besides, 10 nos. of the working nail were selected for further performance testing. It was reviewed that both results from site trial and performance test were well agreed with the design assumption prior to the further excavation, ***Plate 2***.

Plate 2: Set up of Pull out test on Site

4 MARITIME DESIGN AND CONSTRUCTION

4.1 Design

The opening of the existing vertical seawall was located at the east of the reclaimed platform where the fetch length was shielded by the incipient Lamma Island. Therefore, the tidal effect would not be significant comparing to the shoreline facing to the South China Sea. The vertical seawall with pre-constructed intake culverts would be temporarily removed until the installation of the intake chamber. Hence, the temporary stability of seawall should be checked according to the Port Works Design Manual 2002, ***Figure 7***. Besides, protective rock armour was proposed to be laid over the excavation face with max. 1:2 temporary slope to resist wave wash.

Wave Fetch at the CW Intake

Return Period (yr)	Wave Height (m)	Wave Period (s)
10	1.09	2.86
50	1.54	3.21
100	1.78	3.37

Design Significant Wave Heights and Wave Periods

Case No.	Design Condition	Water Level: Return Period/Condition	Water Level: Still Sea Water Level (mPD)	Wave: Return Period/Condition	Wave: Hs (m)	Wave: Ts (s)
Case 1	Normal	2yr	2.65	Typhoon No.3	0.53	2.25
Case 2	Normal	MLLW	0.40	Typhoon No.3	0.53	2.25
Case 3	Extreme	10yr	2.65	100yr	1.78	3.37
Case 4	Extreme	100yr	2.65	10yr	1.09	2.86
Case 5	Extreme	50yr	2.65	50yr	1.54	3.21
Case 6	Extreme	MLLW	0.40	100yr	1.78	3.37

Environmental Load Combinations according to PWDM

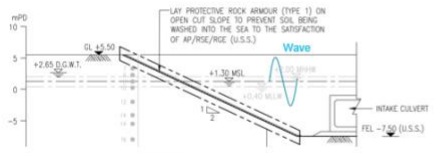

Anti-scouring Rock Armour Layer According to PWDM Against Wave Washes (Van der Meer Criteria)

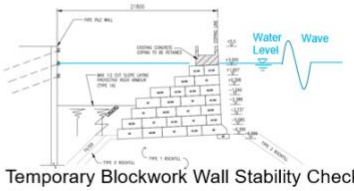

Temporary Blockwork Wall Stability Checks (Bearing, Sliding and Overturning)

Figure 7: Design Consideration with PWDM(2002).

4.2 Maritime Construction

Due to the limitation of loading capacity of the semi-submersible barge and to avoid future in-situ works to be affected by tidal action, only the bottom part of the chamber without internal walls was constructed on the semi-submersible barge in one of the pre-cast factory yards at Mainland China in Xinhui. The pre-cast portion of the intake chamber was of size approximate 30m x 45m x 10m in height. Careful planning was needed for the transportation of this huge structure including the weather forecast, geometry of the routing, suitable marine vessel and equipment. Since the construction involved the marine works within the Hongkong Waters, Marine Department Notice should be arranged prior to the construction works. It was planned to have 1 main tug, 2 auxiliary tugs, 1 crane barge and 1 semi-submersible barge for the installation of the precast caisson. The depth of the seabed nearby the site only have 6m ~ 8m and would not be suitable for the semi-submersible barge to be submerged for unloading the precast caisson. The South West Lamma Anchorage was selected as the sinking area with water depth of approximate 20 metres which met the sinking depth requirements for off-loading.

Figure 8: 15000DWT Semi-submersible Barge (ZHONG REN 1500)

The loading capacity of the semi-submersible barge could be reached upto 14387.50 ton and the deck submersion to a maximum of 6.0m, ***Figure 8***. That allowed the off-loading of the precast caisson at the designated sinking area by floatation. Suitable time window taking into account the high tide cycle and installation time was carefully planned to ensure there would be sufficient water depth for chamber floatation to facilitate the pulling in of the pre-cast chamber into position. The removed seawall blocks and intake culverts were temporary stored on barges such that these elements could be reinstated in the later stage after installation of the pre-cast chamber in position. Besides, some site safety and environmental precautionary measures were deployed for the marine operation including silt curtains, floating wave breaker against the sea front of predominant wave direction, monitoring of floating level marked on the pre-cast chamber, early alarm for loading/lifting winch operation, subscription of long weather forecast (over a month) and contingency plan for the barges to vacate in case of typhoon…etc. so as to minimize the risk throughout the delivery of the pre-cast chamber from the casting yard all the way to Lamma site for installation.

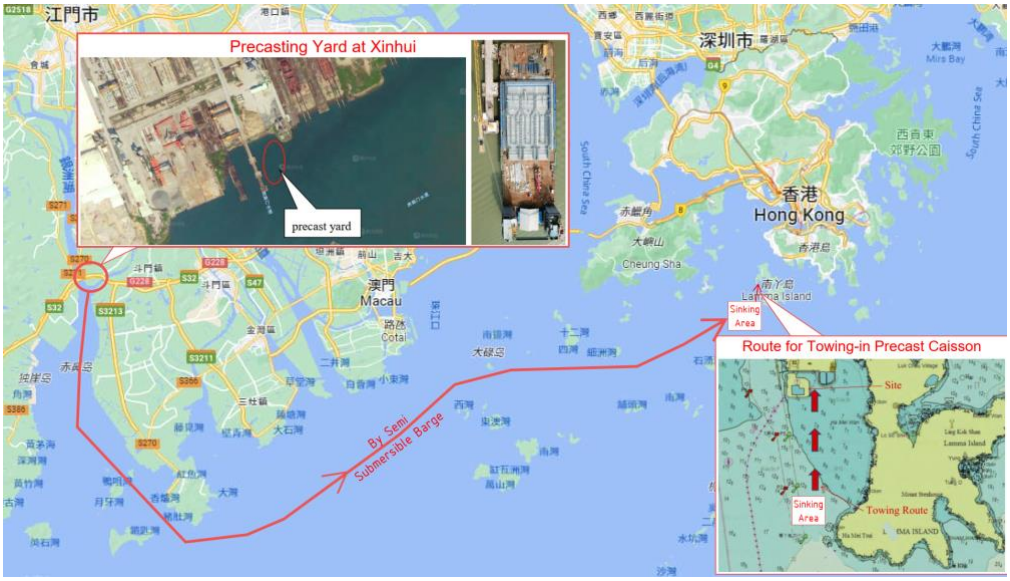

Figure 9: Transport Routing from Mainland to the Site

After the precast chamber had completed in the Mainland China, it would then deliver to the Sinking Area within the Hongkong Waters, ***Figure 9***. It was necessary to plan for the transportation date, to avoid the towing operation at bad weather from the forecast. The Intake Chamber would then be winched out with mooring cable and act as floating caisson by itself when reached to the sinking area. Finally, the precast intake chamber would be installed and offload onto position of the excavated formation level, ***Plate 3***.

Plate 3: The ELS with seawall opening for receiving the floating caisson

5 DESIGN TO SUIT STATUTORY REQUIREMENTS AND STANDARD

Unlike the government, railway and other civil infrastructure projects, this project was a private development and shall be controlled under the Buildings Ordinance. The following sub-sections discuss the approach to fulfill the relevant regulations and administrative requirements for the design of ELS works especially for those uncommon material.

5.1 GFRP

Under the regulation 54 of previous CAP123B, Building (Construction) Regulation published in 1990, the reinforcement for concrete should be hot rolled steel bars, cold reduced steel wire or steel fabric of suitable composition, manufacture, and chemical and physical properties. The proposed use of GFRP bars for soil nailing tie-back would constitute the standard and code commonly adopted for reinforcing bar as stipulated in CAP 123B not being applicable. Therefore, a specified form BA16 for the modification of and/or exemption from the provisions of the regulation was required to submitted to the Buildings Authority. Currently, the regulation CAP123B had been obsoleted and replaced by newly enforced CAP123Q in 2021 which regulates the use of material in a performance base. This would promote the use of new material under the Buildings Ordinance including GFRP.

Safety Factors

ACI 440.1R-06 applied limit state philosophy whereas the guaranteed tensile strength by the manufacturer was the initial properties that did not include the effects of long-term exposure to the environment. Therefore, a reduction factor that specific to the use of FRP in order to take into account the impact of environmental and the exposure conditions. This factor was time dependent and hence would be more onerous for longer design life periods. Since the factor developed in the logarithm relationship to the design life and hence the factors were significant even after relatively short periods. In the case of the tie-back system of Lamma Power Station, the approximately design life would be 18 months (1.5 years), and hence the application factor the Environment factor CE (for concrete exposed to earth and weather) was 0.70 [Refer to ACI 440.1R-06 Table 7.1]. Besides, a strength reduction factor Φ from 0.55 to 0.65 was recommended by the ACI 440.1R-06 in design for the account of the GFRP bars exhibited low modulus of elasticity and ductility. Since the design of the tie-back system was subjected to the axial tension loading in principle and its temporary use for less than 1.5 years, the FoS of 2.0 (i.e equivalent to 0.5 reduction) was taken for the global factor of safety in design of the tensile capacity correlated to the adopted guarantee tensile strength.

Bond Resistance between GFRP and grout

The requirements for development length and splices in GFRP bars were addressed in ACI440.1R-06 section 11. The design methodology was based on experimental testing, mostly of spiral wrap and helical lug patterned bars. No notable difference in bond with concrete was found for these alternative bars. The bond strength between concrete(grout) and GFRP rebar was tested by the manufacturer in accordance with ACI440.3R-04. Based on the testing results, the maximum bond stress could be as high as 7.1MPa. However, based on experimental data, ACI440.1R-06 proposed an empirical method for calculating the development length of a GFRP bar (which is dictated by the concrete strength, the bar diameter and the concrete cover to the bar i.e. ACI440.1R-06 equation 11-2 and 11-3). The design approach on average “bond stress” for the bar/concrete interface along the bars can therefore be deduced with the account for equivalent factor of safety comparable with Geoguide 7.

5.2 Foundation

The intake chamber was designed to sit on top of the pre-dredged reclamation. Therefore, the settlement of the structure would not be significant. Since the internal chamber was hollow structure for receiving seawater and M&E facilities, the floatation stability of this underground structure would normally be critical. Unlike those private development with limit extent in the urban area, the base slab of the raft structure could be slightly enlarged such that the soil within the zone of influence would help to balance the uplifting force. Under the cl. 4.2.2(2) in Code of Practice for the Foundations, BD(2017), plate loading test would be necessary to verify the

design bearing capacity in submerged condition if the bearing pressure fell within one of the criteria specified. In order to comply with the code requirements, the design of the net increase in bearing pressure was controlled to be less than 50kPa. This was done by the iteration on the extent of footing enlargement, ***Figure 10***.

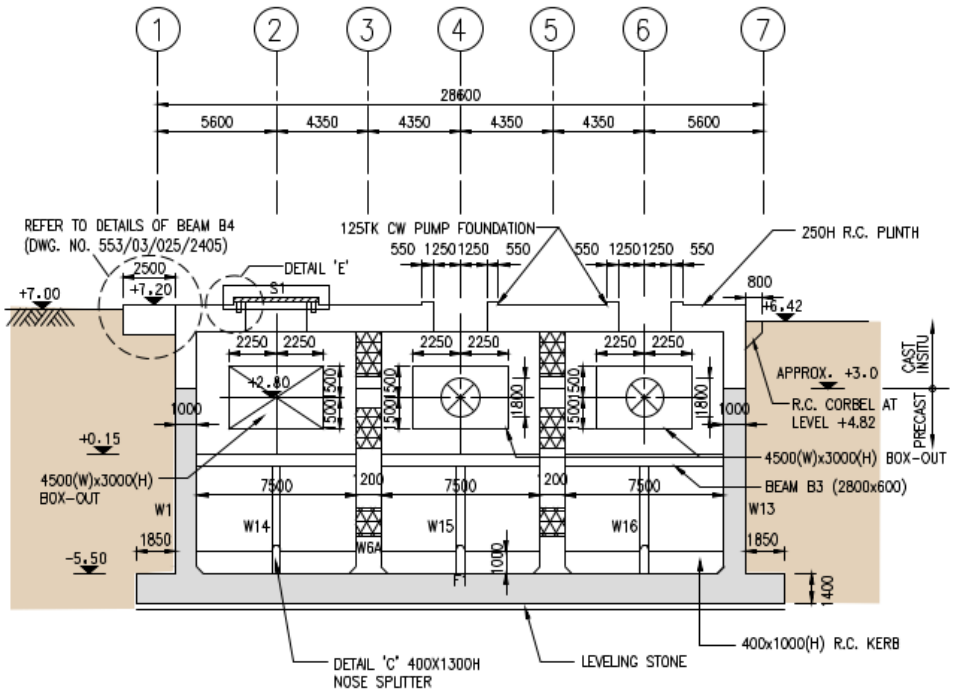

Figure 10: Typical Section for the Intake Structure

For the site supervision, BD(2009), inspection of bearing stratum was classified as one of the critical stage of works for raft and spread footing. In order to have inspection properly, chain sound survey on the completed excavation level and independent diver inspection was necessary to confirm the foundation of the bearing stratum with the present of Technical Competent Persons. The survey was carried out in grid manner such that it could be recorded the inspection properly, ***Plate 4***.

Plate 4: Confirmation of the Founding Level

6 CONCLUSIONS

The ELS design in this Lamma Island project had taken the merits between both characteristics in infrastructure and private development. Although it was common to have the marine construction and new material tie-back system for those infrastructure and rail projects, we as the Engineer responsible would advance more with hybrid consideration according to the codes and international standards. During the construction, the ELS works had faced against several typhoon attacks (such as Chaba, Mulan & Ma-on with highest typhoon signal no. 8) and remained intact when the seawall was opened. It was no doubt that the ELS was an effective and robust solution for this project. The recent update on legislative requirements in CAP 123Q Building Construction Regulation (2021) allowed the use of material in performance based. This would encourage the innovative and new material design to have simplified administration to fulfill those requirements such that we would deliver a more safe and reliable design to face the new engineering challenges.

ACKNOWLEDGEMENTS

This paper is published with the kind support and permissions of The Hongkong Electric Company Limited and the hard-work from the site supervision team as well as the contributing effort from Paul Y Construction Limited.

REFERENCES

ACI318-05. *Building Code Requirements for Structural Concrete and Commentary (ACI318-05)*, Reported by ACI committee 318

ACI440.1R-06. *Guide for Design and Construction of Structural Concrete Reinforced with FRP Bars*, Reported by ACA Committee 440

BD (2009). *Code of Practice for Site Supervision 2009(2021 Edition)*. Buildings Department, The Government of Hong Kong SAR, Hong Kong, 123p.

BD (2017). *Code of Practice for Foundations 2017*. Buildings Department, The Government of Hong Kong SAR, Hong Kong, 123p.

CEO (2002). *Port Works Design Manuel Part 4 – Guide to Design of Seawall and Breakwater*. Civil Engineering Office, Civil Engineering Department, The Government of the Hong Kong SAR

Dextra (2019). *ASTEC Soil-Nail Submission File* for BD Submission. Dextra Group

FBEL (2022). *Method Statement of Towing and Installation for the No. 5 C.W. Intake Chamber*. Friendly Benefit Engineering Limited

GEO (1993). *Guide to Retaining Wall Design, Geoguide 1, 2nd Edition*. Geotechnical Engineering Office, Civil Engineering and Development Department.

GEO (2008). *Guide to Soil Nail Design and Construction, Geoguide 7*. Geotechnical Engineering Office, Civil Engineering and Development Department.

GCO(1990). *Review of Design Methods for Excavations (1990), GCO Publication No. 1/90*. Geotechncial Control Office, Hong Kong, 192p

HKSARG (2006). *General Specification for Civil Engineering Works (2006 Edition)* (Incorporating all Amendments). The Government of Hong Kong SAR, Hong Kong, Volumes 1 and 2.

Plaxis (2019). Software and manuals of PLAXIS (Version 2019). Plaxis bv, Computerlaan 14, 2628 XK Delft, The Netherlands

A Recent Case Study of Portal Cavern Design

J. Chin, D. Shut, N. Wang & P. Wu
Aurecon Hong Kong Limited

ABSTRACT

A new dual-two lanes tunnel of about 3.8 kilometers long was constructed in Kowloon East in Hong Kong recently. It forms part of a major strategic road network to provide an express connectivity and improve the traffic condition between Kowloon East and Kowloon West.

Two portal caverns, which are at the east end of the tunnels, are the first and largest of its kind with slender pillar constructed in highly fractured volcanic rock. A competent and optimised temporary cavern support design was required with the consideration of the pillar stability and construction logistics prior to the permanent support in place. A number of design reviews were carried out to suit the highly constrained construction sequence as the excavation works of the rock-cut slopes and the caverns were carried out concurrently. Some challenges that the project team had to deal with were installation of waterproof membrane and cast-in-situ reinforced concrete (RC) permanent lining for the crown that requires propping of steel shutter. Such challenges call for a cost saving design (CSD) with the use of sprayed waterproofing membrane and fibre reinforced sprayed concrete (FRSC) lining as the permanent support system for the portal caverns.

This paper discusses the optimisation of the temporary support design, the CSD for the permanent cavern support faced by the construction works, and the design methodology of both the temporary and permanent cavern support with the details of the application of the sprayed waterproofing membrane.

1 INTRODUCTION

Located at the eastern end of the tunnels, the portal caverns are approximately 32 m high and 26 m wide with 11 m pillar separating the caverns. The purpose of constructing such large caverns at the portal (instead of further cut back of the rock slopes) was to minimise slope excavation works next to the seashore and hence reduce the environmental impact. As such, half of the ventilation building will be inside the cavern and the remaining half is outside.

The portal caverns were excavated predominantly in fine ash tuff belonging to the Mount Davis Formation. The tuff was mainly slightly to moderately decomposed with very closely- to closely spaced joints. The as-mapped Q'-value (where $Q' = RQD/J_n \times J_a/J_r$) varies from 1.22 to 2.44. The rock cover of the caverns ranges from approximately 3 m at the slope to 40 m at the end of the cavern.

2 GEOLOGICAL SETTING

Based on the available ground investigation (GI) information and the published geological maps, the portal caverns are situated predominantly in Cretaceous volcanic rocks belonging to the Mount Davis Formation (

Figure 1). Site specific GI indicates Grade II/III rock with closely spaced discontinuities. The apertures of the discontinuities are generally relatively tight with localised variations. Micro-fractures or incipient joints were observed in the core photos.

A three-dimensional (3D) geological ground model was constructed based on the available GI information (

Figure 2). Two sub-vertical NE-SW and ENE-WSW trending geological features comprising highly fractured rocks and localised Grade IV/V materials with limited extent (approximately 3 m width) were inferred at the site area. It was inferred that the rock mass quality, Q-value, in the vicinity of the caverns was expected to be better than 0.1 (where $Q = RQD/J_n \times J_a/J_r \times J_w/SRF$) with the consideration of the low rock cover and the existence of geological features.

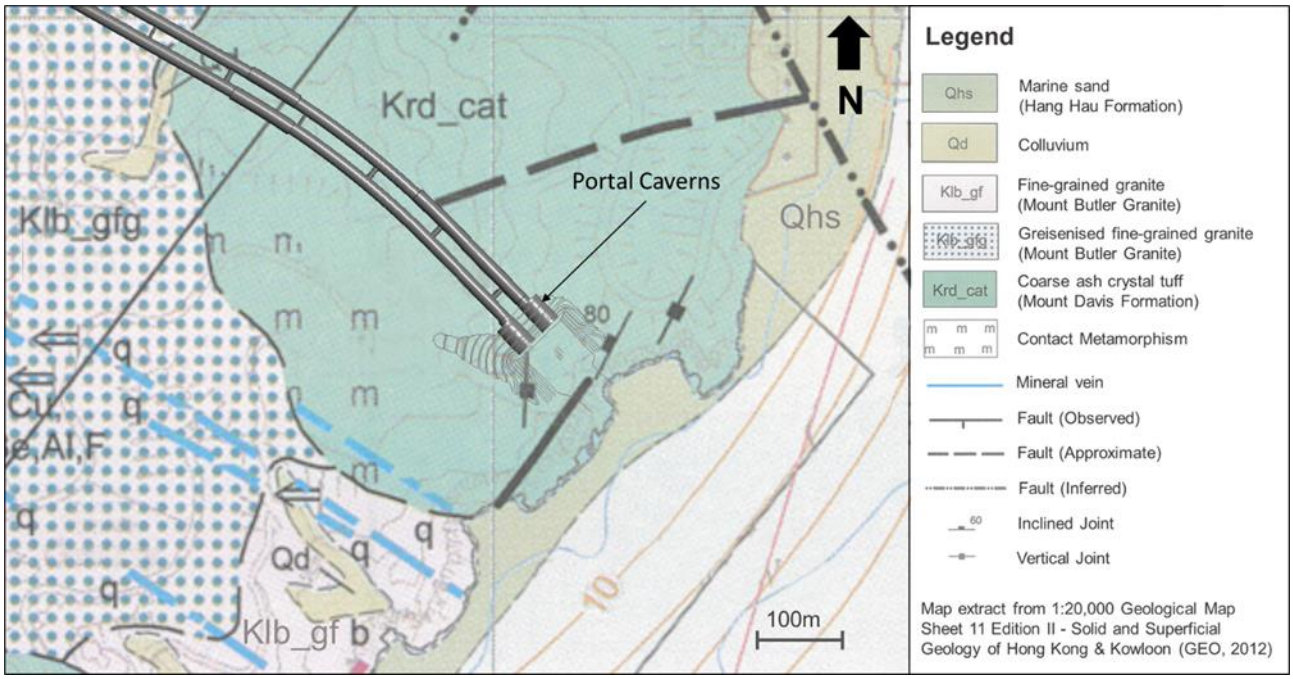

Figure 1: Geological map of the site area

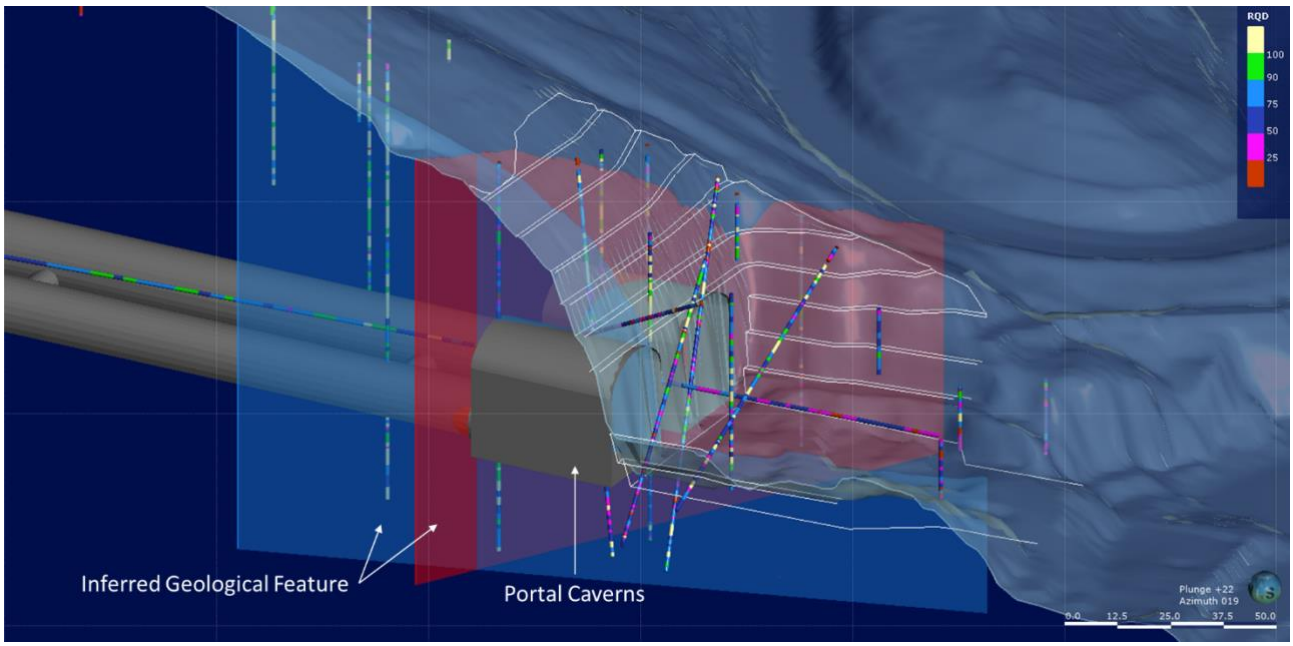

Figure 2: 3D geological model of the site area. Two geological features are shown in red and blue.

3 CAVERN TEMPORARY SUPPORT DESIGN

The span and height of the portal caverns are approximately 25.8 m and 30.2 m respectively (including the 1.5 m thick cast-in-situ RC lining as per original design). The pillar width between the two caverns is approximately 11 m.

Aurecon was employed by the Contractor and responsible for optimising the original cavern temporary support design. The original temporary support for the rock caverns generally comprises systematic bolts and fibre reinforced shotcrete. However, this original design required the pillar to be supported by pre-tensioned stitching of rock dowels penetrating the pillar and locked by face plates with nuts on both ends. It also required both caverns to be excavated concurrently (

Figure 3) so that the stitching bolts could be pre-tensioned from both caverns. These design requirements resulted in significant limitation to the overall construction program. For example, the caverns were required to excavated concurrently from the heading to the benching. Therefore, the key targets of this temporary support design were to optimise the pillar support and allow a greater flexibility of the construction sequence as preferred by the Contractor (

Figure 3).

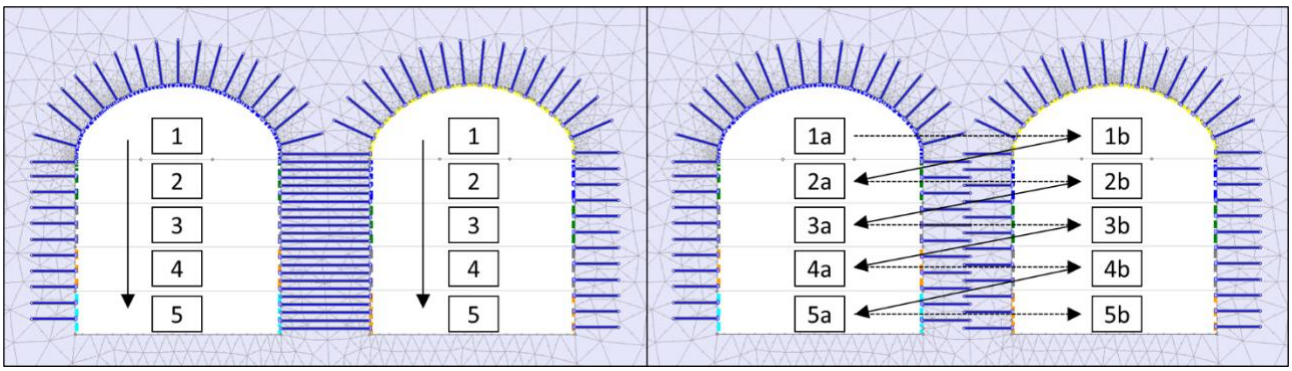

Figure 3: (left) Original concurrent and (right) Contractor's preferred flexible construction sequence of the portal caverns

3.1 Design Methodology

The cavern stability and the proposed temporary supports were assessed using continuum finite element analysis conducted by a two-dimensional (2D) numerical modelling program, *Phase2* (now *RS2*). Three support classes for Q ≥ 0.4 (Support Class 1), 0.13 ≤ Q < 0.4 (Support Class 2) and 0.02 ≤ Q < 0.13 (Support Class 3) were proposed based on the predicted ground conditions. The Q-value which is used for classifying different support classes and tunnel face mapping is converted to Geological Strength Index (*GSI*) to derive the geotechnical design parameters of rock mass using the Generalized Hoek-Brown (GHB) Failure (Hoek, 1994; Hoek et al., 1995; Hoek et al., 2002; Hoek and Brown, 2019) based on the following equations and in the numerical model.

$$\sigma_1 = \sigma_3 + \sigma_{ci}\left(m_i \frac{\sigma_3}{\sigma_{ci}} + s\right)^a$$

where σ_1 and σ_3 are the major and minor principal stresses respectively, and m_i, s and a are the rock mass material constants given by

$$m_b = m_i \exp[(GSI - 100) / (28 - 14D)]$$

$$s = \exp[(GSI - 100) / (9 - 3D)]$$

$a = 1 / 2 + 1 / 6 (e^{-GSI/15} - e^{-20/3})$

where *D* is a factor which depends upon the degree of disturbance to which the rock mass has been subjected to blast damage and stress relaxation.

A summary of the adopted geotechnical design parameters for the most possible expected ground conditions of $0.13 \leq Q < 0.4$ (Support Class 2) is presented in **Table 1**.

Table 1: Adopted geotechnical design parameters for Support Class 2 for the portal caverns

Parameters	Values	Remarks
Q-value, *Q*	0.13	$Q = RQD/J_n \times J_a/J_r \times J_w/SRF$
Joint water reduction factor, J_w	1	Dry or minor inflow
Stress reduction factor, *SRF*	5	Low rock cover condition
Q'-value, *Q'*	0.64	$Q' = RQD/J_n \times J_a/J_r$
Geological strength index, *GSI*	40	$GSI = 9 \ln(Q') + 44$
Intact rock constant, m_i	13	Recommended value for tuff
Disturbance factor, *D*	0	Mechanical excavation
Unit weight, γ (kN/m³)	27	From project-specific lab tests
Intact rock unconfined compressive strength (*UCS*), σ_{ci} (MPa)	150	From project-specific lab tests
Intact rock Young's modulus, E_i (MPa)	79,000	From project-specific lab tests
Poisson's ratio, v'	0.3	From project-specific lab tests
m_b	1.52515	Calculated from GHB Failure Criterion
s	0.001273	Calculated from GHB Failure Criterion
a	0.511368	Calculated from GHB Failure Criterion
Rock mass *UCS*, σ_c (MPa)	4.96	Calculated from GHB Failure Criterion assuming $\sigma_3 = 0$
Rock mass modulus, E_{rm} (MPa)	12,612.5	According to Hoek & Diederichs (2006)

To model the 3D effect of the progressive cavern excavation and support the installation in 2D plain strain numerical analysis, longitudinal displacement profiles (LDP) based on the method by Vlachopoulos & Diederichs (2009) and Hoek et al. (2008) were established to understand the convergence behaviour of the cavern induced by cavern advance length. Ground reaction curves (GRC) were constructed to understand the required support pressure and convergence behaviour of the cavern under gradual increase of stress relaxation in cavern (i.e. a gradual decrease of in-situ pressure or internal pressure in cavern as the excavation advances) and different ground conditions using numerical analysis. Combining the LDP and GRC, the relationship between the degree of stress relaxation in cavern and the cavern advance length could then be obtained and applied in the 2D numerical analysis.

3.2 Results

A number of numerical analyses were carried out for different pillar support and construction sequence for different ground conditions. Based on the numerical analysis results, pillar stabilization measure using 6.0 m long 25 mm diameter Grade 500 rock dowels (without pre-tension) in a staggered pattern with 1 m overlapping at the end of the rock dowels installed from the two portal caverns was adopted. This support measure also fulfilled the site constraint and preferred excavation sequence by the contractor. The results of the adopted numerical analysis of Support Class 2 are shown in

Figure 4 and

Figure 5. The results show that the maximum total deformation is approximately 17 mm at the cavern crown and the maximum shear strain of the pillar is approximately 0.3% and the cavern deformation is within the anticipated limit.

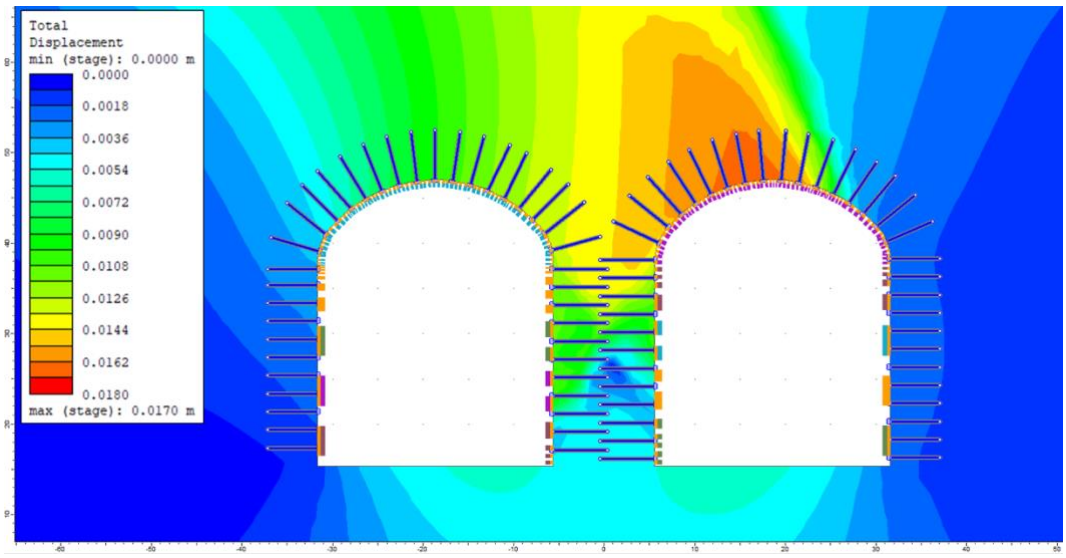

Figure 4: Total deformation of the adopted numerical model of Support Class 2

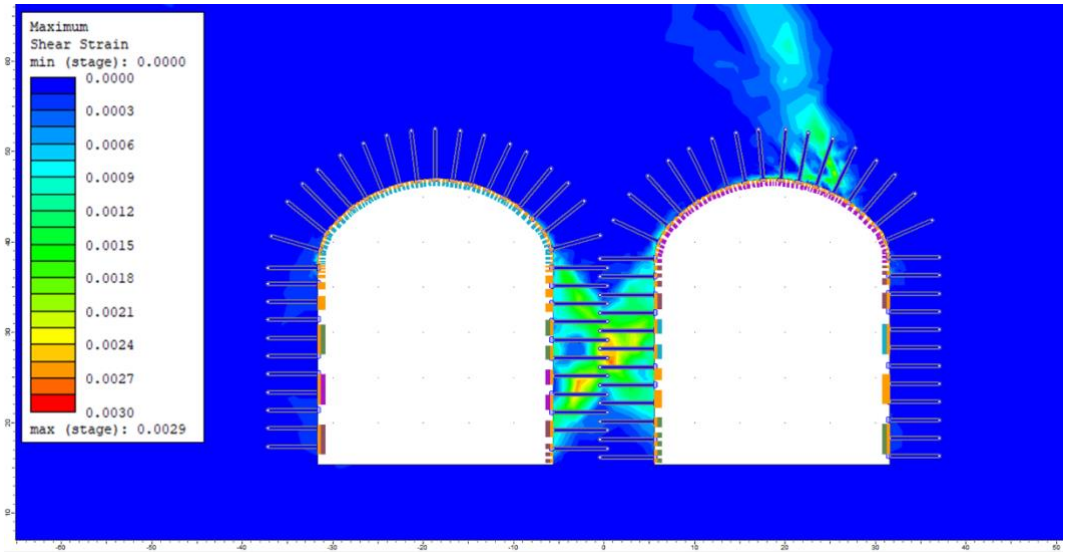

Figure 5: Maximum shear strain of the adopted numerical model of Support Class 2

The induced strain of the rock mass surrounding the opening was also assessed as suggested by Hoek (1998) and Sakurai (1983). The strain is defined by the ratio of convergence to cavern diameter. Sakurai (1983) suggested that any tunnels with strain levels exceeding approximately 1.0% could be associated with tunnel stability problems and difficulties in providing adequate support. It was further supported by Hoek (1998) based on the plot showing the field observations during construction of three tunnels in Taiwan by Chern et al. (1998) against the rock mass uniaxial strength (σ_c) (

Figure 6). The maximum strain of the portal caverns measured from the adopted numerical model of Support Class 2 is only approximately 0.1% while the rock mass uniaxial compressive strength calculated according to the Generalized Hoek-Brown Failure Criterion is 4.96 MPa. Therefore, as shown in

Figure 6, the excavation of the portal caverns with the optimised pillar support and the Contractor's preferred flexible construction sequence is stable.

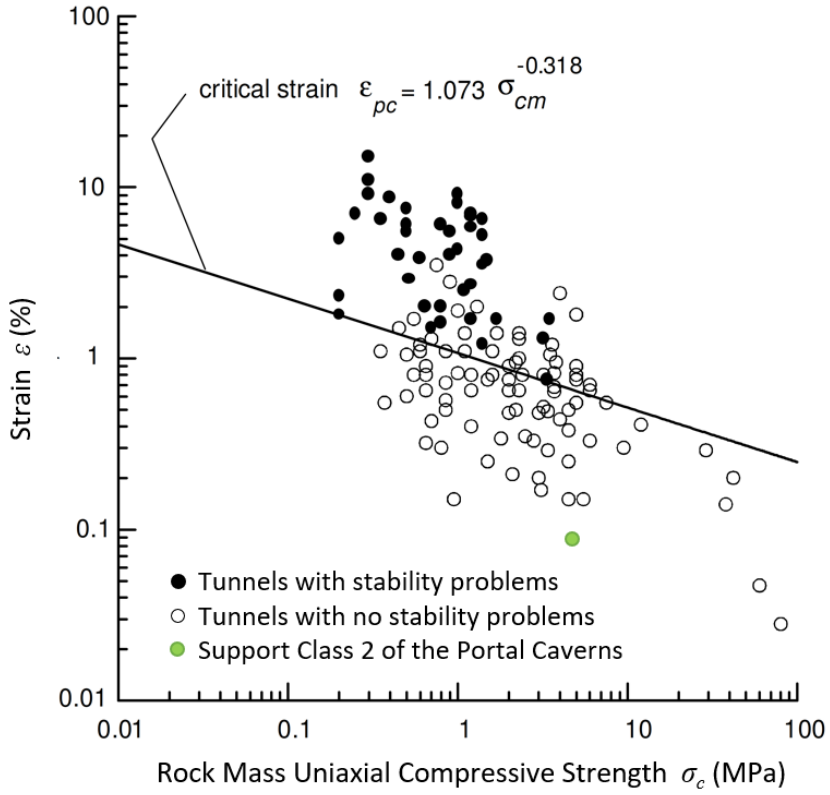

Figure 6: Total deformation of the adopted numerical model of Support Class 2 (after Hoek (1998))

4 CAVERN PERMANENT SUPPORT DESIGN

Apart from the temporary support design, Aurecon was also responsible for CSD of the permanent lining of the portal caverns. The conforming design of the caverns comprises 1.5 m thick cast-in-situ RC lining with sheet waterproofing membrane between the temporary and permanent lining for the wall and crown. However, the installations of the cast-in-situ RC lining and sheet waterproofing membrane for caverns with height up to 30 m are extremely difficult, especially at the crowns. RC lining at such height would involve a tremendous amount of scaffolding works from the crown all the way down to the invert, thus occupying the entire working space of caverns, which would seriously affect other construction works within the caverns such as the construction of the ventilation buildings. Hence it was proposed to optimise the cavern crowns from cast-in-situ RC lining and sheet waterproofing membrane to FRSC and sprayed waterproofing membrane.

4.1 Design Methodology

Numerical, non-linear analyses using finite element programme Strand7 were undertaken for the structural analysis of the permanent linings. The Strand7 programme utilises a 3D plate model (

Figure 7) with compression only support attribute whilst the surrounding soil-structure interaction medium is represented by a series of springs. The tensile capacity of these ground springs is ignored and therefore no reaction is given to the lining when the springs are in tension under the action of the loadings.

4.1.1 As-built Ground Condition

The permanent support design was commenced after the excavation of the top heading of the caverns. Therefore, the design was based on the actual ground conditions observed during the excavation of top heading. The caverns were divided into two sections with an adopted design *Q*-value of 0.22 and 0.3 (with the application of SRF of 5) and different rock cover.

4.1.2 Design Load

Different load combinations including dead load, earth load, wedge load, groundwater load, surcharge load, E&M load, earthquake load and fire load were considered in the numerical analysis.

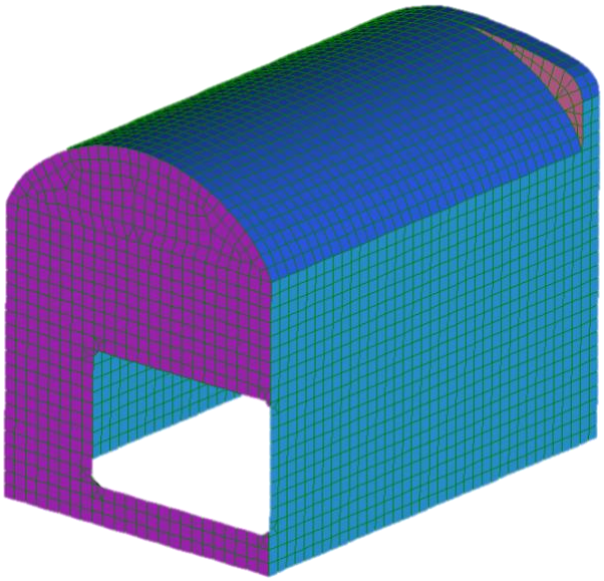

Figure 7: Strand7 model geometry

The earth load support pressure was estimated according to Grimstad & Barton (1993). This estimation often gives a conservative result. Therefore, in order to optimise the design, additional numerical analysis using Phase2 models was carried out. The model adopted the same design *Q*-values with corresponding temporary support and the preferred construction sequence, and the average contact pressures between the ground and the permanent lining extracted from the Phase 2 models were then used as input earth load in Strand7 structural model. A comparison of the earth load estimates according to Grimstad & Barton (1993) and those extracted from the Phase2 models are summarised in **Table 2**. The results show that the earth load extracted from Phase 2 models could significantly help optimise the support design while it was also considered that this load was more applicable and realistic since the numerical models considered the more realistic as-built ground and support information.

Table 2: Comparison of the earth load estimated according to (Grimstad & Barton, 1993) and extracted from the Phase 2 models

Design Q-value	**Support Pressure (P_{roof}) according to Grimstad & Barton (1993) (kPa)**	**Average Contact Pressure extracted from Phase2 Model (kPa)**
0.3	299	109
0.22	330	40

Note 1: Different rock covers of the two sections with the adopted *Q*-values of 0.3 and 0.22 were considered in the Phase2 models. The section with $Q = 0.22$ is closer to portal slope, hence rock cover and average contact pressure is lower.
Note 2: $P_{roof} = 0.2\ J_n^{1/2}\ Q^{-1/3} / 3 / J_r$ (unit in MPa)

Regarding the fire induced load, the design for the sidewalls and end walls, which would be cast-in-situ RC structure, was deemed-to-satisfy in accordance with the Hong Kong Code of Practice for Structural Use of Concrete. The nominal cover provided shall satisfy the fire limit state (FLS) design requirements.

The deemed-to-satisfy approach of the Hong Kong Code of Practice Structural use of Concrete is not applicable to FRSC because there is no steel bar reinforcement in the FRSC so cover to reinforcement is not applicable. Hence, the design of the FRSC for the crown of the caverns under fire load assumed that a certain thickness of the lining would be structurally ineffective from fire damage due to the loss of stiffness and excessive spalling under high temperature. These structurally ineffective sections, which is still attached to the remaining lining, are being treated as superimposed dead load on the remaining structurally sound lining that is not damaged by fire. This design approach followed the 500℃ isotherm method in accordance with BS EN 1992-1-2:2004.

The FRSC lining was designed for 4-hour fire resistance rating. The 4-hour ISO curve was chosen for the FLS design. The loss of strength of the FRSC lining at elevated temperatures was estimated using data for siliceous aggregates in BS EN 1992-1-2:2004. For the fire design case, the capacity reduction factor curves of the EC2 were used, and the damaged and structurally ineffective section was calculated to have an equivalent of 65 mm thickness. Another 10 mm thick of the lining was rendered ineffective on account of concrete spalling. The adequacy of the remaining lining after section reduction was analysed with the appropriate load and material factors according to the Hong Kong Code of Practice for Structural Use of Concrete.

To reduce the risk of concrete spalling for all structural concrete during fire, monofilament polypropylene fibres not less than 1.0 kg/m^3 shall be included in the concrete mix regardless of any thermal barrier to be installed. The fibres shall be 6 – 12 mm long and 18 – 32 μm in diameter, and shall have a melting point less than 180℃.

4.1.3 Ground Spring Stiffness

In the Strand7 model, the springs are located at the extrados of the shell elements to simulate elastic behaviour of lining-rock interaction. The springs represent the soil/rock medium and are modelled as "compression only" face support to the shell elements used to model the lining.

Tangential springs are applied in the crown only. These springs represent the resistance to the sliding action between the ground and the lining. These are modelled as beam elements acting as springs tangential to the lining profile. The magnitude of spring stiffness in the tangential direction is assumed to be 20% of the radial spring stiffness. This assumption is conservative and assumed to be the lower bound value suggested in "Design Recommendations for Concrete Tunnel Linings" (Paul et al., 1983).

The radial spring stiffness was calculated based on the equation suggested by Duddeck and Erdmann (1985); the spring model and the spring stiffness for straight wall were calculated based on Bowles (2001).

4.2 Results

Based on the numerical analysis results, the conforming design using 1,500 mm thick cast-in-situ RC lining for cavern crown was successfully optimised to FRSC with thickness varying from 650 mm to 1,500 mm with local steel reinforcement using wire mesh near the portal and end wall (

Figure 8).

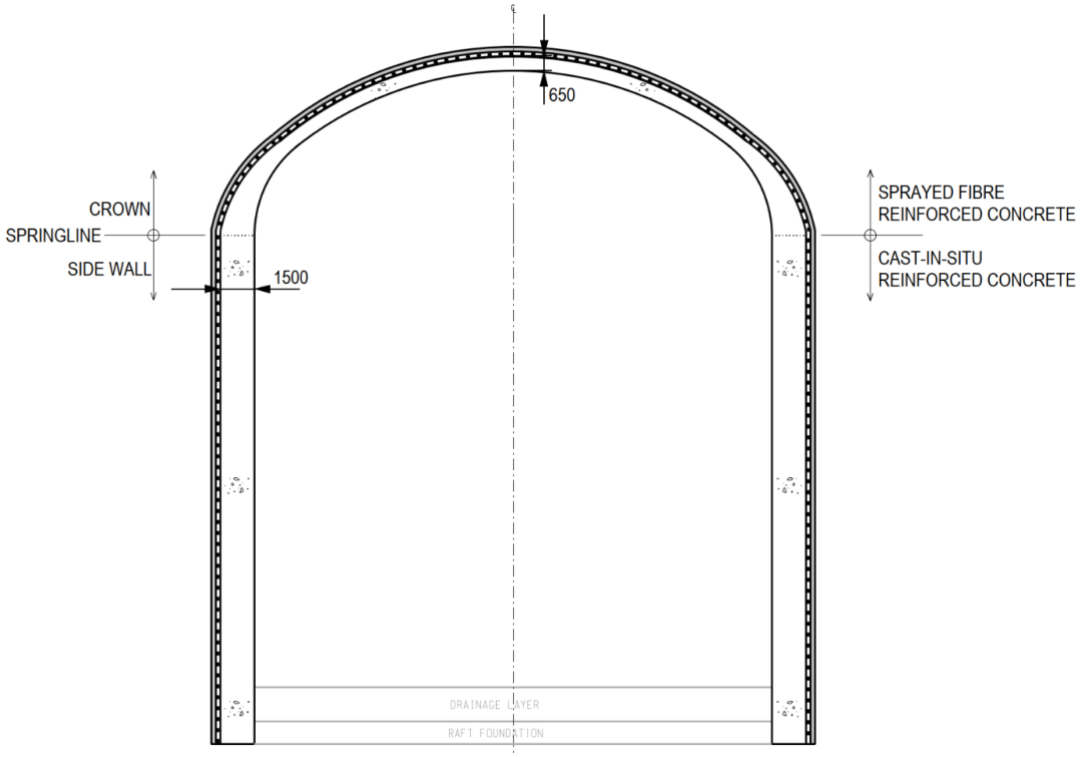

Figure 8: General arrangement of optimised permanent lining for the portal caverns

4.3 Waterproofing

Since the typical sheet waterproofing membrane applied between the temporary systematic dowel and shotcrete lining and permanent cast-in-situ concrete lining could not be used with permanent FRSC lining, it was proposed to adopt the sprayed waterproofing membrane for the cavern crown. The key requirements listed below were considered for successful spray-applied membrane installation in accordance with Geoguide 4:

- method suitable for excavation with limited water ingress;
- adequate substrate surface quality and preparation;
- adequate selection and maintenance of spraying equipment to promote adherence of membrane to the surface with minimum rebound and maximum adhesion and coverage,
- proper training and accreditation of applicators, and
- application trials, and close and systematic quality control of an in-situ produced membrane, to ensure correct thickness and coverage, and curing of the membrane under the tunnel environmental conditions.

Quality control was required throughout the membrane application process to ensure full compliance with the Particular Specification and manufacturer's instructions. A list of quality control measures was proposed as per recommendations in the ITAtech (2013) and ASTM standards (**Table 3**).

Table 3: Proposal of quality control for application of sprayed waterproofing membrane

Parameter	Test method	Frequency	Pass criteria
Coverage / continuity	Visual inspection	Visual inspection to be carried out continuously while the membrane is applied and following application	100% coverage
Thickness	Wet film thickness by depth gauge	10 tests per 100 m^2	Min. measured thickness of each course of the membrane and the entire thickness of the finished membrane shall be ≥ 2 mm or as per

Parameter	Test method	Frequency	Pass criteria
Thickness	Application quantity	Applied thickness assessed by measuring the quantity of spray membrane used for the area over which it has been applied; 1 measurement per 100 m^2.	manufacturer's recommendation, whichever thickness is greater. Average thickness over the applied area identified from the measurement of spray quantity; Thickness shall be greater than or equal to the identified average thickness.
Thickness	Cut-out inspection for 50 mm x 50 mm patches	Optional method; Patches taken randomly from all sections of the tunnel profile	Min. patch thickness shall be ≥ 2 mm or as per manufacturer's recommendation, whichever thickness is greater.
Composite	Bond tests	1 test per 200 m^2; Locations where deficient adhesion is suspected by Site Engineers or a min. of 3 tests	Min. bond strength > 0.5 MPa

7 CONCLUSION

The portal caverns are located in highly fractured tuff with rock mass quality *Q*-value in the range of 0.2 to 0.5. During the excavation works of the portal slope and caverns, the movement of the slope and caverns were monitored closely and found to be within the predicted observation levels. It showed a successful example of the construction of caverns with narrow rock pillar in Hong Kong, even in tuff with very low rock mass quality. This cavern design also demonstrated a successful adoption of permanent FRSC lining and sprayed waterproofing membrane for rock caverns which are much safer to apply while providing equally sufficient structural contribution. This successfully designed and built portal caverns can be considered as the good practice and design reference for all upcoming cavern projects in Hong Kong.

8 REFERENCES

Bowles, J. E. (2001). *Foundation Analysis and Design* (5th ed.). McGraw Hill.

Chern, J. C., Yu, C. W., & Shaiu, F. Y. (1998). Tunnelling in Squeezing Ground and Support Estimation. *Proc. Reg. Symp. Sedimentary Rock Engineering.* Taipei.

Duddeck, H., & Erdmann, J. (1985). Structural Design Models for Tunnels in Soft Soil. *Underground Space, 9: 5-6*, pp. 246-259.

Grimstad, E., & Barton, N. (1993). Updating of the Q-System for NMT. *International Symposium on Sprayed Concrete,* 46-66. Fagernes.

Hoek, E. (1994). Strength of rock and rock masses. *ISRM News Journal, 2*(2), 4-16.

Hoek, E. (1998). Tunnel Support in Weak Rock. *Keynote Address, Symposium of Sedimentary Rock Engineering.* Taipei, Taiwan.

Hoek, E., & Brown, E. T. (2019). The Hoek-Brown Failure Criterion and GSI - 2018 edition. *Journal of Rock Mechanics and Geotechnical Engineering, 11*(3), 445-463. Retrieved from https://doi.org/10.1016/j.jrmge.2018.08.001

Hoek, E., & Diederichs, M. S. (2006). Empirical Estimation of Rock Mass Modulus. *Internal Journal of Rock Mechanics and Mining Sciences, 43*(2), 203-215.

Hoek, E., Carranza-Torres, C., & Corkum, B. (2002). Hoek-Brown Failure Criterion - 2002 Edition. *NARMS-TAC Conference,* 267-273. Toronto.

Hoek, E., Carranza-Torres, C., Diederichs, M., & Corkum, B. (2008). The 2008 Kersten Lecture: Integration of Geotechnical and Structural Design in Tunneling. *56th Annual Geotechnical Engineering Conference.* Minneapolis: University of Minnesota.

Hoek, E., Kaiser, P. K., & Bawden, W. F. (1995). *Support of underground excavations in hard rock.* Rotterdam: A.A. Balkema.

Paul, S. L., Hendron, A. L., Cording, E. J., Sgouros, G. E., & Saga, P. K. (1983). *Design Recommendations for Concrete Tunnel Linings Volume II: Summary of Research and Proposed Recommendations.* University of Illinios at Urbana-Champaign, Department of Civil Engineering. Cambridge, Massachusetts: U.S. Department of Transportation - Research and Special Programs Administration.

Sakurai, S. (1983). Displacement Measurements Associated with the Design of Underground Openings. *International Symposium on Field Measurement in Geomechanics*, 1163-1178. Zurich.

Vlachopoulos, N., & Diederichs, M. S. (2009). Improved Longitudinal Displacement Profiles for Convergence-Confinement Analysis of Deep Tunnels. *Rock Mechanics and Rock Engineering*, *42*(2), 131-146.

Waterproofing, I. A.-L. (2013). *ITAtech Design Guidance for Spray Applied Waterproofing Membranes.* ITA, ITAtech Activity Group - Lining and Waterproofing. The International Tunnelling and Underground Space Association.

Digitalization, Modularisation and Sensors Application of a Deep Excavation Project in Urban District of Hong Kong

Gavin SH Toh[1], John Latter[2], Alan WL Wan[3]
Dennis TS Ho[1], Elaine CL Chan[1]
[1] *Lambeth Associates Limited, Hong Kong*
[2] *Mandarin Oriental Hotel Group*
[3] *Gammon Construction Limited*

ABSTRACT

The redevelopment of the Excelsior Hotel site included a 3-level basement that required excavation up to 17m. The design of the temporary works consisted of contiguous pipe piles braced by five layers of lateral support to provide stability to the pipe pile wall cofferdam, efficient groundwater cut-off and to control ground movement impact to the adjacent ground and buildings. The adjacent buildings comprised the World Trade Centre, five residential dwellings built in the 1960s, and an existing link bridge structure that required to be supported within the excavation area. This paper will discuss the collaborative and digital approaches in the design and planning of the method and sequence of the work, modularization of the shoring system, and the use of scanning and sensor monitoring devices – that will showcase and promote modern construction for Hong Kong deep excavation work. The collaborative and digital approach streamline the construction work process by first building in the virtual work before the real world. The buildability, safety, and quality of the actual implementation are greatly improved.

1 INTRODUCTION

With the advancement of technology, digital applications are used to design deep excavation work. Digital Information Modeling (e.g., BIM) 3-Dimension is a norm in the industry and plays an important role in the design, planning, and management of construction process. The 3D BIM model provides virtual constructability reviews in deep excavation such as construction plant/equipment access, practical sequence of work, identification and resolution of clashes, and define standardized shoring module and fabrication details.

The application of digital scanning technology to generate actual site condition and as-built alignment provide reliable and accurate information for design and planning of the next construction phase, such as, the basement and superstructure work. Digital instrumentation sensors have been in used in the industry for a few years and its monitoring data is becoming more reliable and gives confidence to the relevant stakeholders. Toh et al. (2019) outlines benefits and prospects of integrated application of modularisation, digitalization, and sensors that combines processes and people from the design and planning to construction.

This paper presents the collaborative and digital approaches of deep excavation work and how these approaches have improved safety and quality of the construction work.

1.1 Project Background

Located at the former Excelsior Hotel, a new office building will be developed in the urban district of Causeway Bay. The proposed redevelopment includes a 32-storey high building structure with a 3-level basement supported by raft foundation. A footbridge will be built to connect the office block to the World Trade Centre Hong Kong and an existing footbridge to La Foret shopping centre in Chee On building will be reconnected. Refer to Figure 1 & 2 for photo of the old Excelsior Hotel and location of the project, respectively.

Figure 1 The former Excelsior Hotel

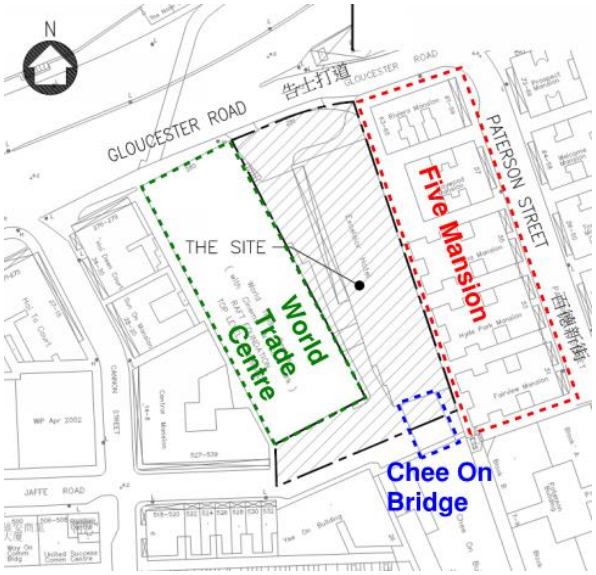

Figure 2 Site Location Plan

2 EXCAVATION DESIGN FOR THE REDEVELOPMENT OF EXCELSIOR HOTEL

2.1 Site Location and Adjacent Sensitive Structure/ Utilities

In the urban district of Causeway Bay, the site is in proximity to existing buildings and utilities. The site is approximately 110m in length and 45m in width. The minimum clear distance from the site boundary to the adjacent World Trade Centre and the closest residential block built in 1960s is 7m and 2.5m, respectively.

2.2 Excavation and Lateral Support Design

The excavation and lateral support (ELS) consisted of pipe pile wall with shear pins as the temporary vertical wall with grout curtain to provide water cut-off to the excavation. Five layers of struts were adopted for the construction of 3 levels of basement with maximum retaining height of 17m. The excavation level is generally at -12.8mPD and -15.8mPD for lift pit areas. Pre-loading of struts were applied to minimize the lateral deflection of the pipe pile, and the impact to adjacent structures and utilities. The layout plan and sections of the cofferdam with strutting arrangement are shown in Figure 3, 4 and 5, respectively.

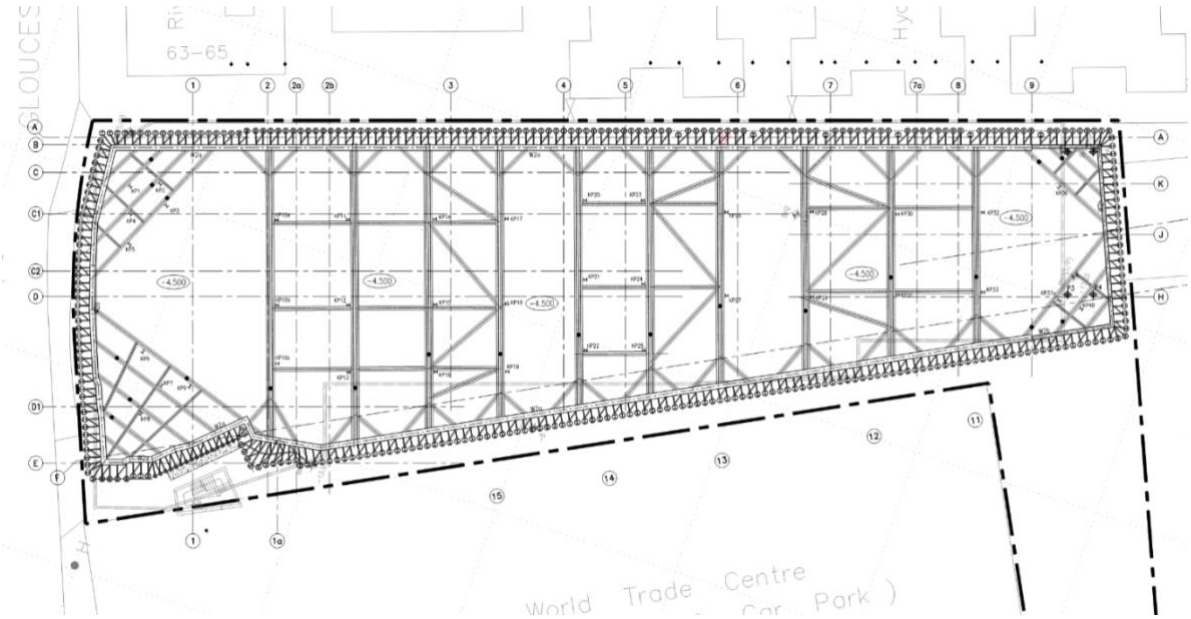

Figure 3 Layout Plan of the ELS

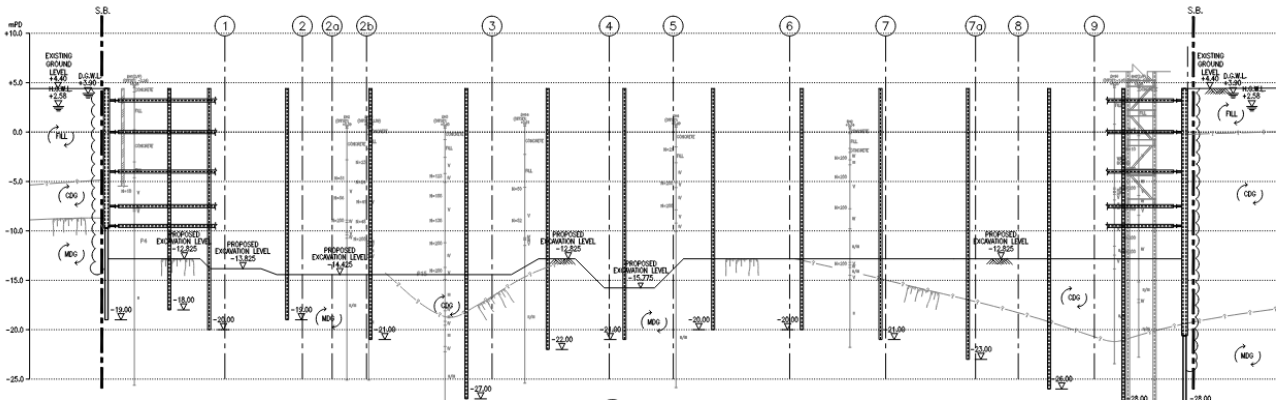

Figure 4 Longitudinal Section

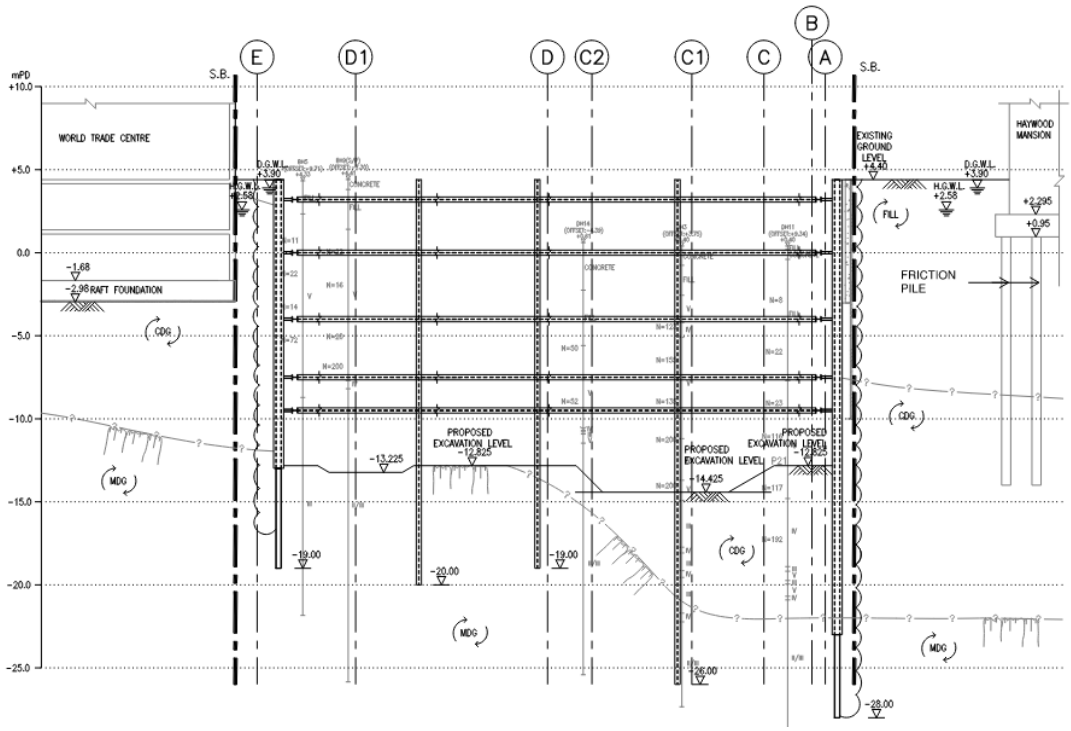

Figure 5 Cross Section

3 INSTRUMENTATION MONITORING SYSTEM

As the development is situated in a busy commercial district with adjoining operating offices and domestic buildings, a comprehensive system of instrumentation was set up to closely monitor any effect induced by the construction works. Instruments included inclinometers, vibration check points, tilting markers, standpipes and piezometers, ground and building settlement checkpoints. These were installed at all sensitive receivers, such as the 5 residential mansions and the World Trade Centre.

Gammon's GEOMON system was used as the primary means of instrumentation and monitoring data management. GEOMON is a robust web-based data monitoring and reporting system. The system comprises an instrumentation database server, web server and associated scripting engine to store, retrieve and tabulate, graph or generate PDF reports of the monitoring data. Shall any instrument reach a Response Level, the system will automatically alert all Gammon's supervisors.

Real time monitoring adopting digital instrumentation sensors included strain gauge and inclinometer were set up to monitor the performance of the deep excavation and provide confidence to the values measured. Comparison of the predicted and measured magnitude of the maximum lateral displacement of the wall had been carried out to verify model assumptions in PLAXIS. Figures 6 and 7 show cross sections with two real-

time inclinometer INC7 and INC10 readings and two conventional inclinometer INC2 and INC5 readings. For INC7 and INC10 near World Trade Centre, the predicted and measured wall deflection are comparable, implying the ELS design can resemble the actual site condition. For INC2 and INC5 near the residential mansions, the predicted wall deflection is generally larger than the measured wall deflection, which verifies the performance of the ELS. Below the final excavation level, the predicted wall deflection is much greater than the measured wall deflection, which may be attributed to a better than predicted ground condition.

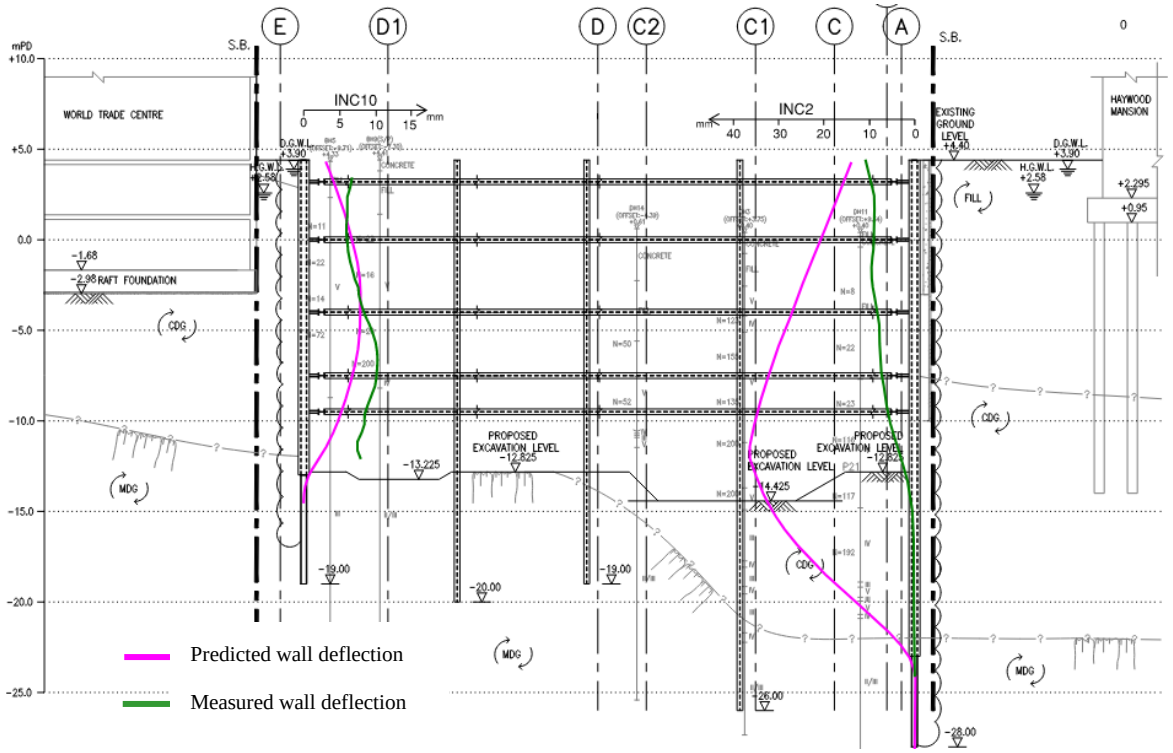

Figure 6 Section with Predicted and Measured Wall Deflection

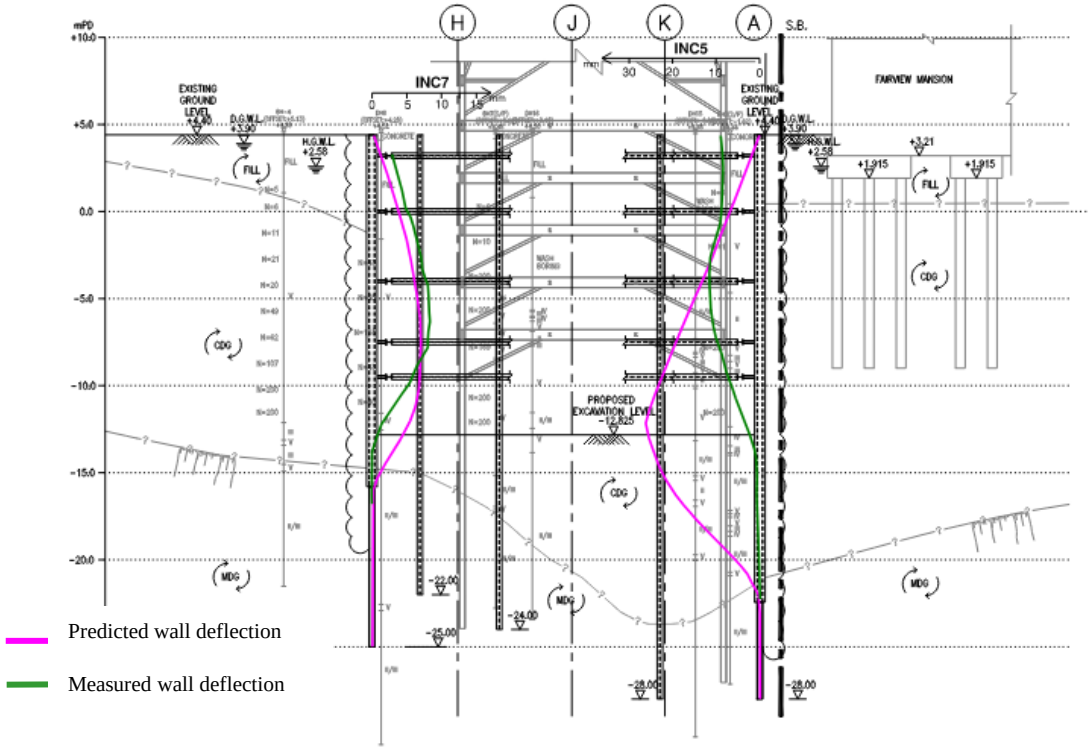

Figure 7 Section with Predicted and Measured Wall Deflection

Other real-time instrumentation included vibration monitoring of the existing Chee On Bridge that had been temporarily supported during the excavation. CCTV was installed at the bridge to monitor real time the condition of the cladding. Set up of the vibration monitoring and the CCTV at the bridge are shown in Figure 8 and 9.

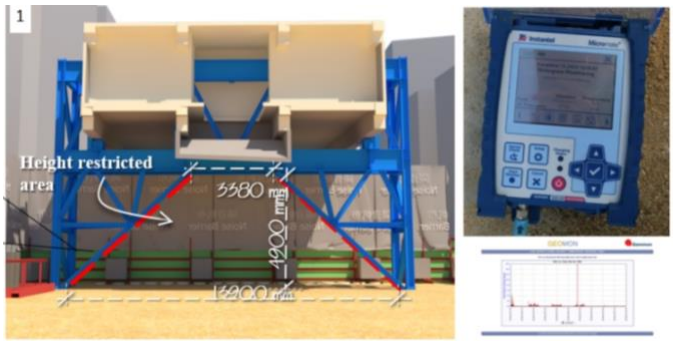

Figure 8 Real Time Vibration Monitoring for Chee On Bridge

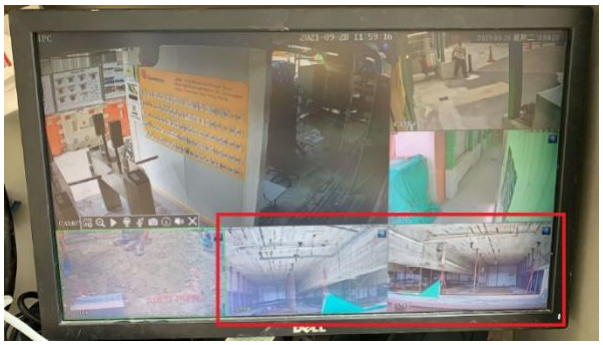

Figure 9 CCTV Monitoring on Bridge Cladding

4 DIGITAL TECHNOLOGY APPLICATIONS AND INNOVATION

4.1 Application of BIM

Three dimensional BIM digital models were utilized throughout the construction project life cycle. Steel support and temporary steel platforms were modelled using BIM for clash analysis. The model is also updated concurrently for as-built steel deck supports and ELS vertical elements to evaluate for any further clashes with permanent structures. The example of clash analysis of the model and modification implemented in the design to eliminate clashes is demonstrated in Figure 10 and 11.

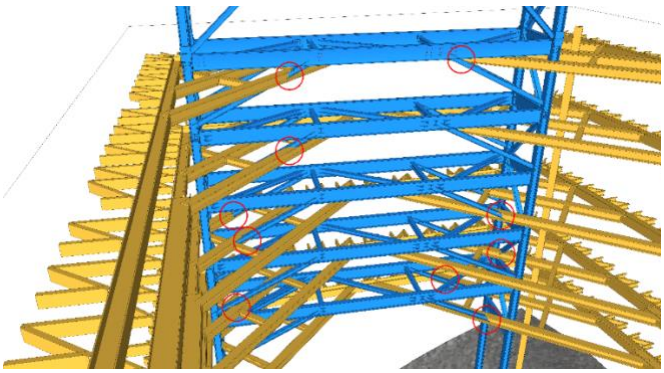

Figure 10 Clash Analysis for ELS

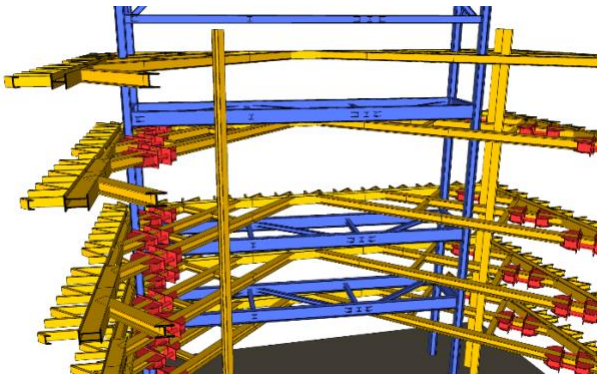

Figure 11 Revise ELS Design to Eliminate Clash

The BIM digital model provides insight into construction logistics that will greatly improve planning of plants and equipment movements and the provision of safe access routes for workers. Any construction issues can be resolved in the virtual world before the real world. The illustration shown in Figure 12 highlights the complexity of the logistic plan during the pipe piling work whereby without the digital model it would not be able to provide a realistic and practical construction work plan.

Apart from the site logistic planning, digital virtual model combined with existing and planned details help to work out a practical method and the sequence of the construction. In Figure 13 the BIM model combining with the sequence of work plan presented the construction planning with time digitally, and subsequently used for monitoring the progress during the actual work.

With the digital 3D model, step-by-step visualization of work brings significant benefits on buildability. The example shown in Figure 14, involves heavy piling plants for the pipe piling work in a congested and low headroom condition. With digital visualization, suitable piling plants, maneuvering of the plants, sequence of the work, fatal and safe zone for workers were all sorted out and communicated in the digital environment

before actual implementation. The digital imaging method prepared using formats familiar for the frontline workers were used for pre-work briefing.

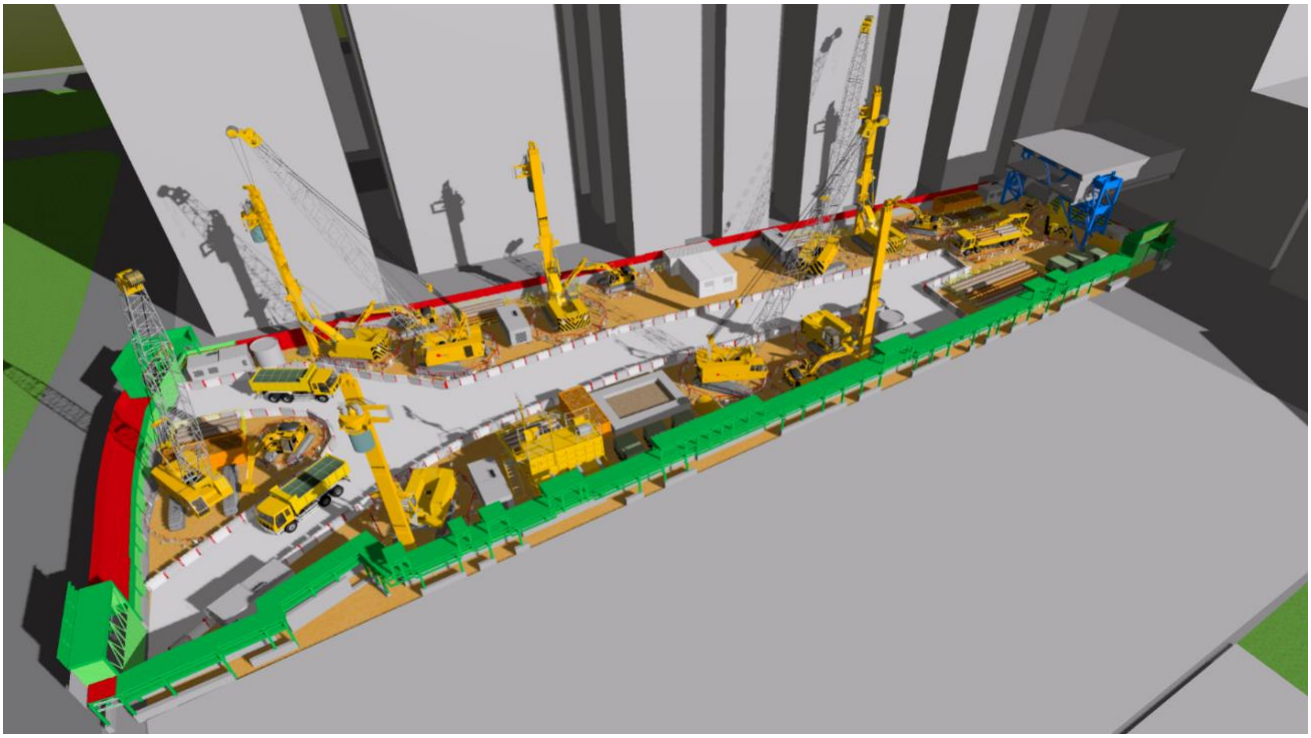

Figure 12 Digital Model on Logistic Planning

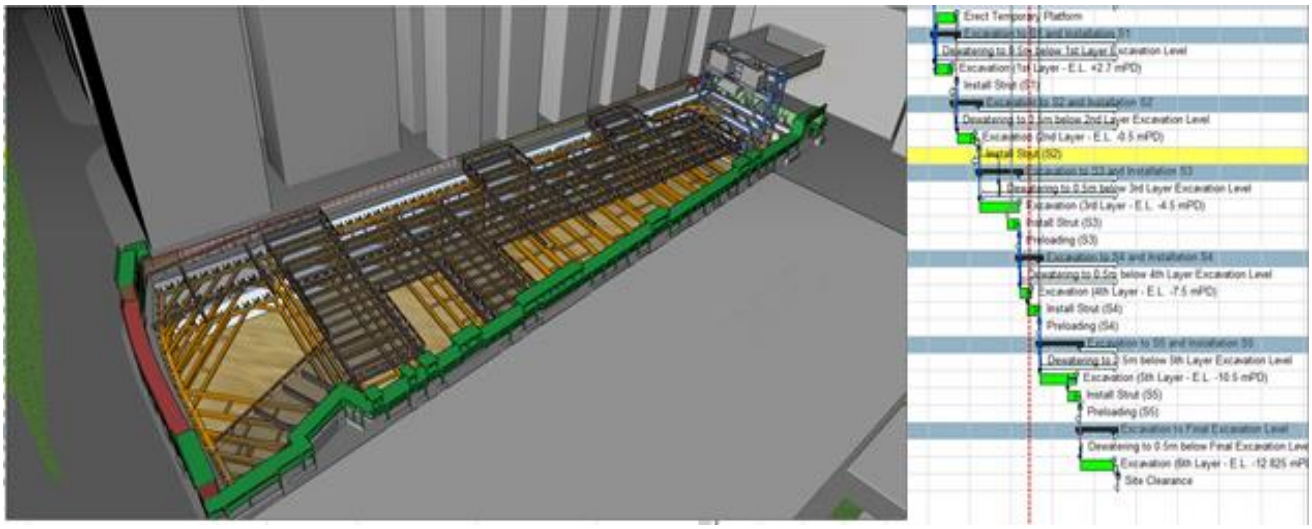

Figure 13 Combining Work Plan and Sequence in the Digital BIM Model

Figure 14 Pictorial Digital Method of Work

4.2 Laser 3D Scanning

A portable and compact handheld 3D scanner was used for monitoring site topography, progress monitoring and estimating excavation volume. Digital images shown in Figure 15 and 16. Survey points by LIDAR and colour imagery could efficiently and accurately be collected compared to conventional ground surveys. The latest ground profile of site could be obtained to verify the excavated volume of soil or rock. Apart from excavation volume, as-built structures could also be reflected from the 3D imagery. The as-built ELS vertical elements, such as pipe pile walls and steel supports were scanned on site and extracted into the BIM model for clash detection with permanent structures. This not only saved manpower as only one surveyor was required for data taking and safety was also enhanced as surveyor did not need to walk into dangerous zone on site. With 3D scanning and BIM models complementing each other, it greatly helped project planning.

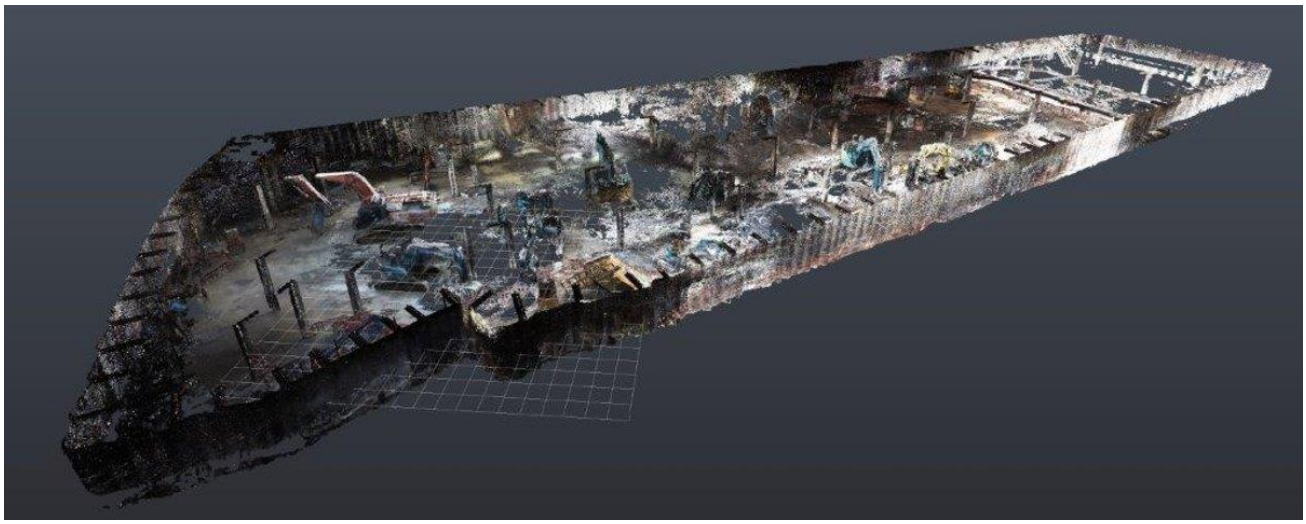

Figure 15 Laser 3D Scanning Imagery of the Construction Progress

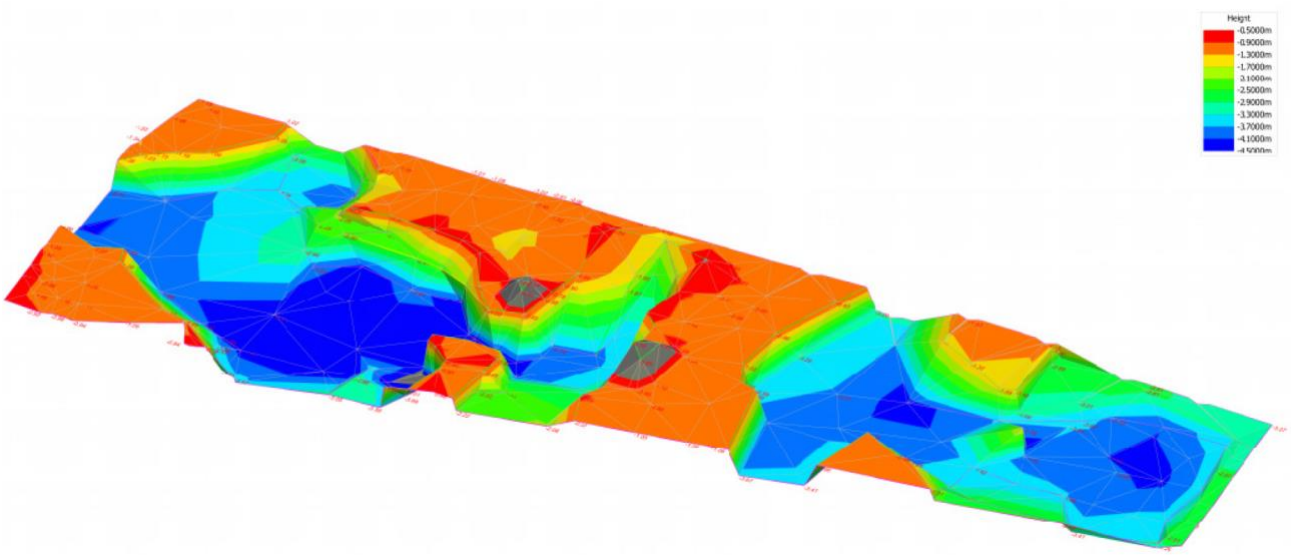

Figure 16 Topography of Excavation Profile from the Laser 3D Scan Imagery

4.3 Modularisation for ELS

An important aspect in buildability for deep excavation is modularisation of the shoring system. In modularizing the struts, integrated modules and components are planned and designed, manufacture and fabricated off-site in a factory using highly efficient machines and skilled labors under a stable and suitable environment. The modules are then logistically delivered to site for assembly – an application of DfMA (Design for Manufacture and Assembly). Other multi-functional components such as bolting arrangement, preloading brackets, lifting eyes, and provision for edge protection are integrated in the module during fabrication. This greatly reduces on-site welding.

For the Excelsior redevelopment project, to facilitate the flexibility to re-use the modules, the size of the structural steel members was strategically selected. The length of each spliced segment was also capped to a maximum of 9m as the choice of delivery trailer was limited due to the busy Gloucester Road and the narrow site gantry. Using bolt and nut connections saved a total of 580 man-days of welding as compared with fully welded connections. In addition, the installation time for each strut layer was reduced by 3 weeks with bolt and nut connections.

In the design of each module, digitization consolidates design and detailing including connection, virtual assembly. Any issue with assembly is tackled early, which greatly improves workflow for off-site fabrication and on-site assembly – illustrated in Figure 17 and 18.

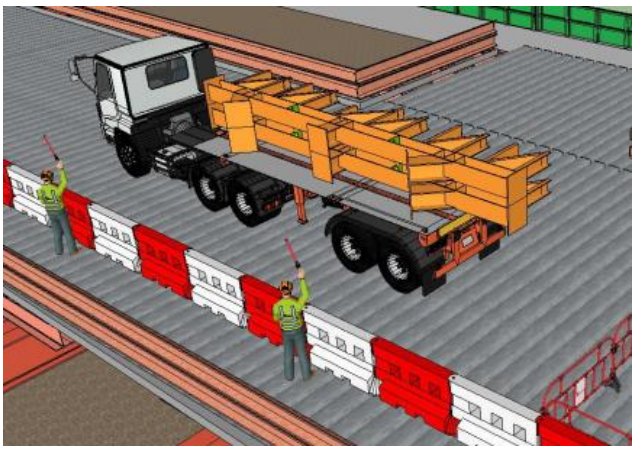

Figure 17 Digital Delivery of Modules to Site

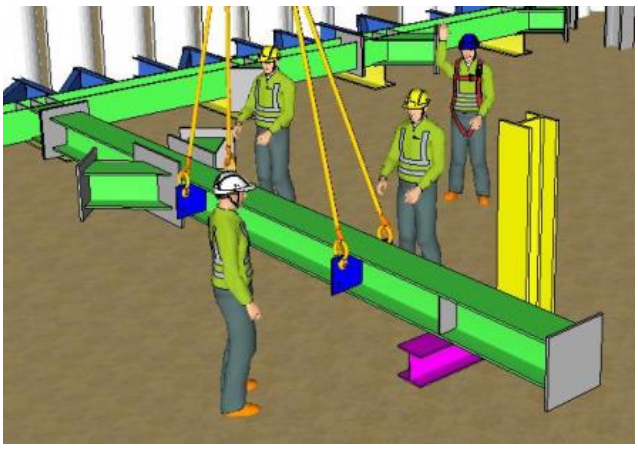

Figure 18 Digital Installation of each Module

Another application of DfMA has been implemented at the Excelsior Hotel redevelopment project is the modular steel access staircase. The steel staircase was designed and prefabricated with connections that could

be easily assembled and removed at end of the project, hence, facilitating for reuse in other projects. The digital and actual connection assemble details are illustrated in Figure 19 and 20.

Figure 19 Actual Connection of the Modular Stair

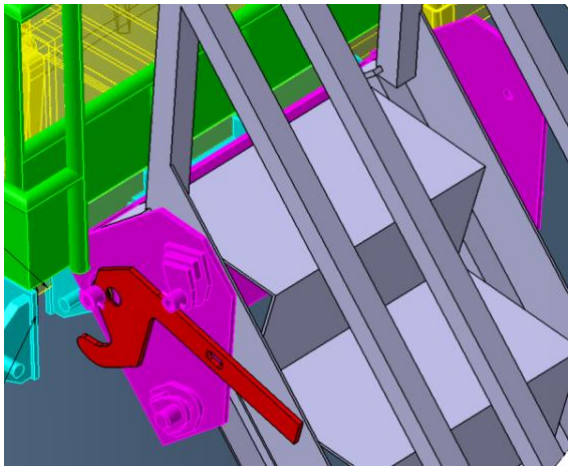

Figure 20 Digital Connection of the Modular Stair

4.5 Digital Sensor Detection

Automatic water detection sensors were installed 500mm above excavation level as in Figure 21 below. When abnormal water level is detected, automatic signals would be sent to site team and security guard at site entrance. This enabled fast remedial measures to be carried out to mitigate flooding risk on site.

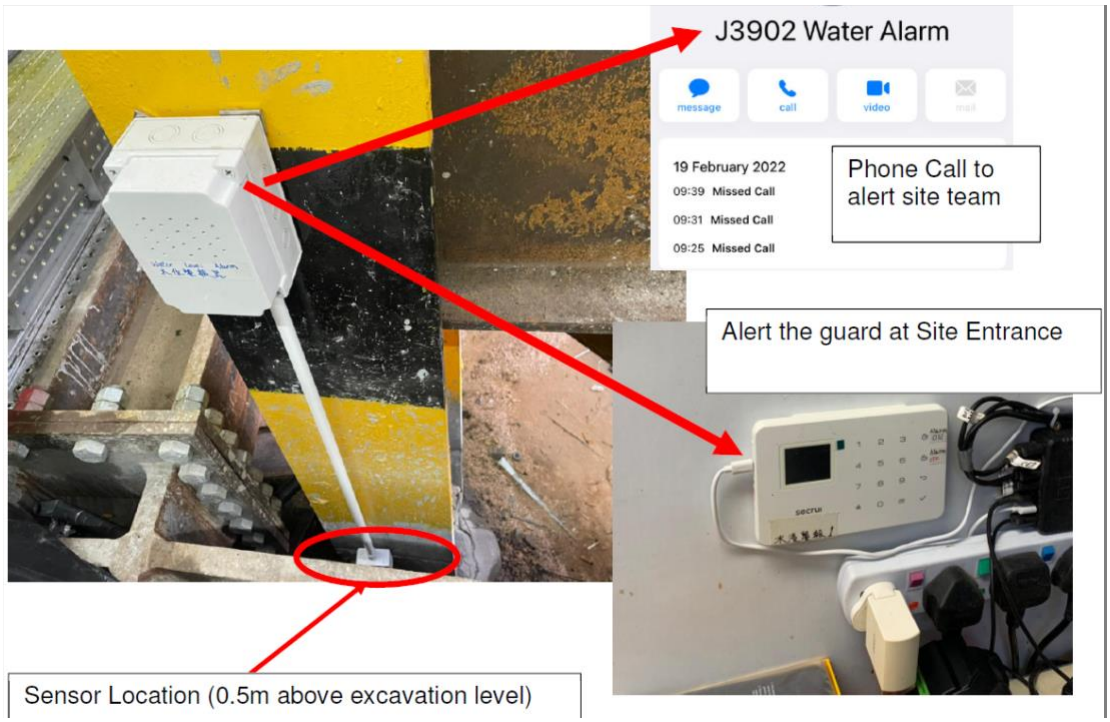

Figure 21 Water Detection Sensors

4.6 Core-bide Method for Drilling Through Underground Structure

The traditional down the hole hammer method for the pipe piling work may induce high levels of noise disturbance and vibration to surrounding area. In the Excelsior Hotel redevelopment project, the team has adopted tailor-made hybrid core bits welded with tungsten carbide to core out the existing heavily reinforced pile cap in one piece. Compared with the hard coring method, noise generated from core-bide method was

significantly reduced considerably from 90dBA to 73dBA, while vibration induced was reduced from 20ppv to 5ppv. In addition, diesel consumption for this innovative core-bide method could be reduced by more than 90%, which greatly reduced carbon emission. The details of the core-bide method of drilling and comparison of the data with traditional method are given in Figure 22 and 23. The Core-bide method has received the Merit Award (Construction Sustainability) of the CIC Construction Innovation Award 2022.

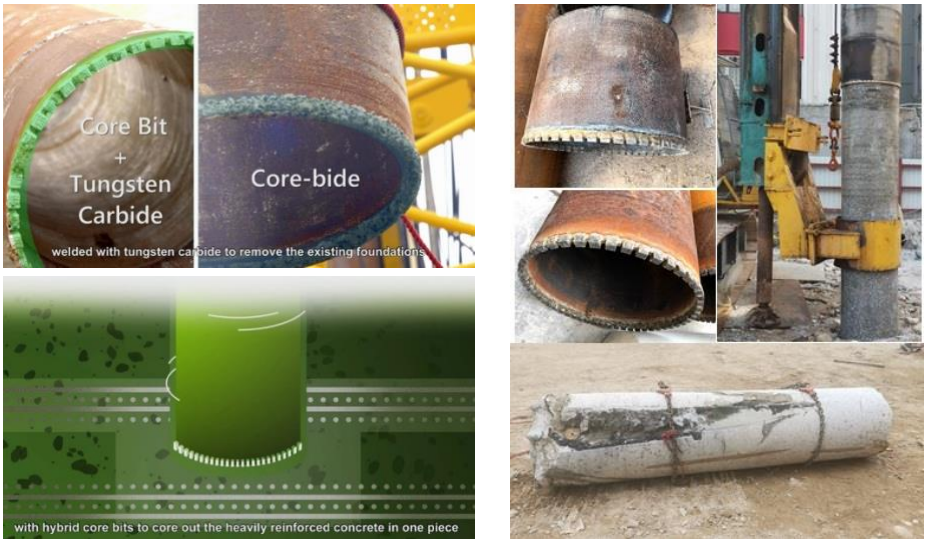

Figure 22 Core-bide Method for Drilling Through Existing Reinforced Pile Cap Underground

Description	Hard Driving Method	Sustainable Core-bide Method
Noise (dBA)	90	73
Vibration (ppv)	20	5
No. of Air Compressor	3	0
Productivity (days/pile)	4	2
Diesel Consumption (Liters)	916,800	57,300

Figure 23 Comparison Table for Core-bide Method and Hard Coring Method

5 CONCLUSIONS

The application using digitalization, modularization and sensors in the design, planning, and monitoring of the deep excavation work of the Excelsior Hotel redevelopment has been successfully implemented not just at the onset of the project, but also throughout the whole life cycle of the construction period. The continuous efforts and determination of the design and construction teams in a collaborative and digital approach is another important aspect to realize the full benefits of modern construction. The project has recorded zero safety incidents during the 850 calendar days of the construction, which has been considered as an outstanding safety performance. In addition, the project was completed ahead of the planned time.

ACKNOWLEDGEMENTS

This paper is published with the permission of Mandarin Oriental Hotel Group and Gammon Construction Limited. The support and participation of the project teams including Hong Kong Land (Project Management) Ltd, Ronald Lu & Partners (Hong Kong) Ltd and Meinhardt (C&S) Ltd are highly appreciated.

REFERENCES

Toh S.H., Ho C.N., Jenkins S.A., Tsui K.L., Lai, U.S. 2019 Integrated Application of Shoring Modularization, Digitalization and Monitoring Sensors in Deep Excavation Project. *Proc of Transformation in Geotechnical Engineering – Technology, Digital and Innovation.* The HKIE Geotechnical Division 39th Annual Seminar 2019.

A Technical Overview of Contract No. 3801 APM and BHS Tunnels on Existing Airport Island: Jacked Box Tunnels under AEL

Il. Tsaparas, R.B. Cook
AECOM, Hong Kong (formerly Benaim)
Ch. Venetz, G. Lee
VSL / Intrafor, Hong Kong
K CK Chiang, V YN Wu;
China State Construction Engineering (Hong Kong) Ltd
Tommy KY Leung, Joe YC Sam
Hong Kong Airport Authority

ABSTRACT

The provision of the new Automated People Mover (APM) tunnel connecting the expanded Terminal 2 (T2) with the Third Runway Concourse (TRC) and the new Baggage Handling System (BHS) tunnel, are key works being provided as part of the expansion of the Hong Kong International Airport (HKIA) into a Three-Runway System (3RS).The alignment of the tunnels crosses under the operational Airport Express Line (AEL) and was constructed using Jack Box tunnelling techniques. This paper presents some of the technical solutions developed for the box jacking works. Two 30m long portions of the APM and BHS tunnels were jacked as continuous precast reinforced concrete boxes under the AEL embankment within a ground improved grout block. A horizontal pipe pile canopy positioned above the tunnels was constructed using micro TBM methods to allow ground movement control and enhance face stability. The two boxes were jacked forward off a jacking slab using hydraulic jacks positioned at the rear of the boxes. An additional innovative strand jacking system was employed in combination with the canopy piles as an anti-drag system, which also supplemented the slab jacks thrust. The thrust forces on the post-tensioned prestressed jacking slab were restrained by a combination of rock friction and inclined temporary ground anchors. The two boxes were safely jacked to their final position in July 2022 without disrupting MTRC AEL operations.

1 INTRODUCTION

1.1 General

The new APM and BHS tunnels have an approximate length of 2.6km and will run between HKIA's T2 and the Third Runway Concourse (TRC) buildings. The two tunnels are vital for the successful operation of the TRC as part of the 3RS development. The section of the tunnels formed within the existing HKIA platform from the expanded T2 to the TRC which is within the newly reclaimed 3RS platform are being constructed under Contract No. 3801 (C3801). The portion of the proposed tunnels that cross under the operational AEL were constructed using Jack Box tunnelling techniques (Figure 1). Using this technique two pre-cast concrete boxes were built in a casting and jacking shaft on the south side of the AEL embankment and jacked through the embankment into a receiving shaft on the north side, whilst maintaining the operation of the AEL railway.

China State Construction Engineering Ltd (CSCE) is the Main Contractor of the works and Intrafor Ltd (ITF) is the Specialist Contractor for the Jacked Box construction. ITF was responsible for a) the ground improvement works; b) the temporary structures for the launching and jacking of the boxes; c) the structural design of the boxes in all the temporary conditions and temporary loads; and d) the construction of the two reinforced concrete boxes. ITF engaged AECOM's (AEC) legacy company, Benaim Ltd, to provide the detailed design of the box jacking works. CSCE-ITF-AEC teamed up for the second time in similar roles to successfully execute the box jacking works under C 3801, following the previous box jacking works of HKLR03 at Scenic Hill (Cook et al 2018). ITF-AEC having also worked together on the award-winning Brisbane Airport Link jacked tunnels at Toombul in Australia. The main parties involved in the C3801 project are presented in Figure 2.

Figure 1: C3801 – Project area

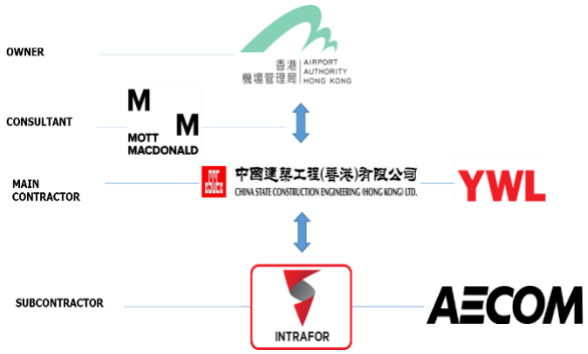

Figure 2: C3801 – Project O-chart

1.2 Structures and Construction Concept

The two permanent reinforced concrete boxes were jacked through the ground below the AEL railway well below natural groundwater level, which was tidally affected. The jacking length for both boxes was approximately 30m. Each of the two boxes were monolithically constructed as single units with an approximate length of 30m. The boxes are oversized outside their original curved alignment envelope to allow their jacking along a horizontal plane and on a straight line.

To accommodate the construction (temporary) stage the APM box had cross sectional dimensions of approximately 30.9m wide by 9.4m high and a length of 30m - (Figure 3 and Figure 4). The BHS box has cross sectional dimensions of approximately 19.8m wide by 11.8m high and a length of 30m. The front of both jacked boxes was inclined at 70 degrees from the horizontal and were equipped with a steel shield at the wall interfaces with the ground faces.

In order to enable the construction of the two jacked boxes, two temporary shafts were constructed (see Figure 1). The shaft on the southern side of the AEL embankment, was the casting and jacking shaft. The shaft on the northern side was the receiving shaft. Once formation level was reached inside the jacking shaft, the jacking slab (Figure 6) was constructed. This served initially as the casting bed for the two boxes and subsequently as the reaction system for the jacking works, transferring the jacking loads to the ground only, ensuring no load transfer to the ELS of the shafts as required under the contract

Each tunnel box was precast inside the jacking shaft, providing a higher quality of works compared to casting the tunnel in-situ beneath the AEL. The boxes were then jacked forward off the casting bed (the jacking slab) using push jacks located at the rear of the boxes which reacted against corbels stressed down to the jacking slab.

The maximum depth of overburden over the BHS box is approximately 8.5m and for the APM it is approximately 9m. The original embankment for the AEL was constructed with rockfill. Grouting of the fill material was carried out using fan array methods from the sides and extending under the AEL. The ground improvement works were an essential part of the Box Jacking works to provide a hydraulic cut-off from the tidally affected groundwater under the AEL; improve the ground properties like mass stiffness, strength and permeability; as well as limit ground settlements; and ensure face stability during excavation and jacking operations.

To provide groundwater cut-off two grout walls made by the Tube a Manchette method (TAM) were formed along the external edges of the tunnels extending from the design ground water level at +3.5mPD down to the toe which was embedded into the underlying rockhead, providing - together with the grouted cofferdam walls for the jacking and receiving shaft installed by CSCE - a sealed enclosure of the site.. The shafts perimeter grout curtains were supplemented by a mass fan grouting array pattern, extending from the jacking shaft to the receiving shaft, in order to:

a) limit ground movements during box jacking;
b) provide excavation face stability; and
c) stabilise any residual water bearing ground.

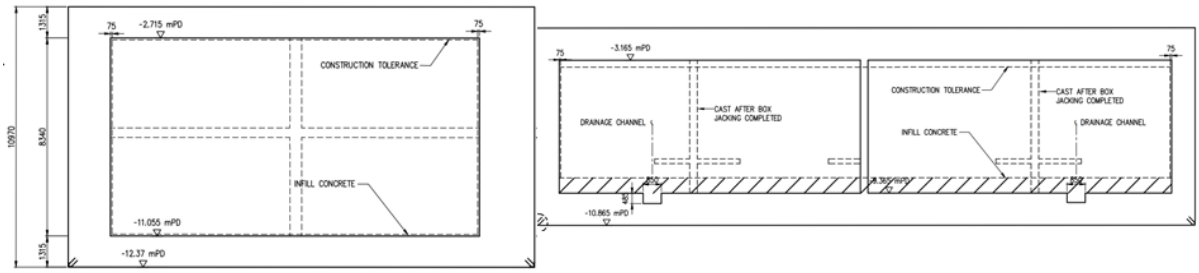

Figure 3: Typical Sections of APM & BHS Boxes

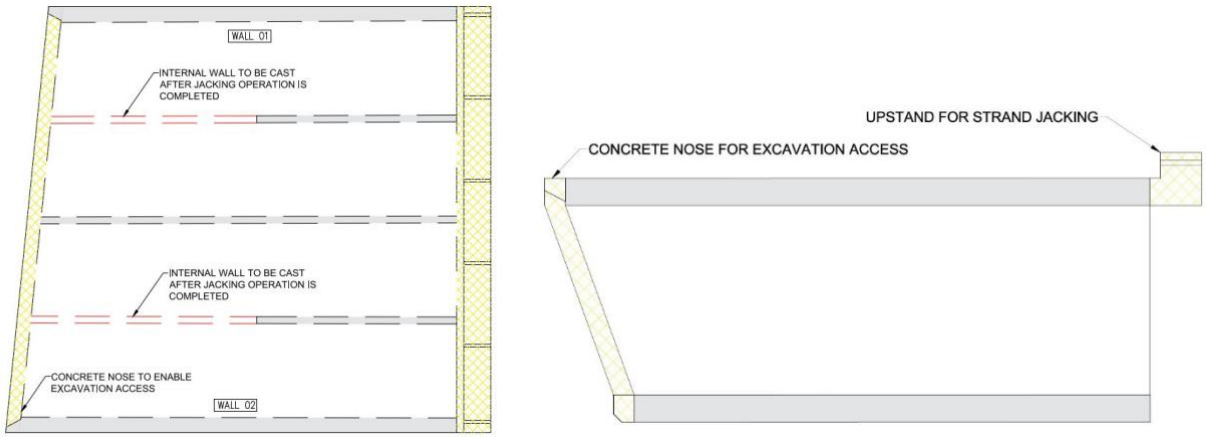

Figure 4: Plan View and elevation of APM & BHS Boxes

To enable the construction of the two jacked boxes, two temporary shafts were constructed by CSCE (see Figure 5). The shaft on the southern side of the AEL embankment was the casting and jacking shaft, while the one on the northern side was the receiving shaft. The shafts were approximately 20m deep on the BHS side and 18.5m deep on the APM side. The two shafts were formed using steel pipe piles which were supported mainly by a braced steelwork excavation and lateral support system, except for the headwall where the braced steelwork was designed out. This latter arrangement allowing the jacked boxes to enter the embankment through the pipe piles which were incrementally demolished as the boxes entered the embankment. Once formation level was reached inside the jacking shaft, the jacking slab (Figure 6) was constructed, which served initially as the casting bed for the two boxes and subsequently as the reaction system for the jacking works, transferring the jacking loads to the ground ensuring no load transfer to the ELS of the shafts by providing a sliding interface along the side faces of the jacking slab

The mass grouting under the AEL displaced the groundwater from the rockfill. This was confirmed via horizontal probing from the shafts before the headwall removal.

To limit potential AEL movements and provide excavation face stability, a pipe pile canopy was constructed prior to excavation/jacking operations. The horizontal steel pipe piles was formed using 1430mm diameter steel pipe, installed by micro TBM and then infilled with grout. These pipes extended from the jacking shaft to the receiving shaft. The canopy also acted as an anti-drag system (ADS) isolating the embankment over the boxes from horizontal displacement effects caused by the box friction under as it moved forward. The pipes themselves being restrained by prestressing strand that passed through the duct in the centre of the grouted pipes to strand jack attachment points on the top rear of the boxes. Excavation of the ground was then carried out in 1.5m steps under the canopy, followed by incremental jacking of the tunnel boxes.

An extensive instrumentation and monitoring plan was provided. This included a real time Automatic Data Monitoring System (ADMS) with instrumentation and monitoring "Alert", "Alarm" and "Action" limits for the AEL rail tracks. Vertical track movement (settlement and heave), horizontal movement, differential settlement between rails, as well as vibration were recorded and reported in real time, enabling any transgressions of AAA levels to be automatically notified to the relevant parties by SMS and email.

1.2 Main Site Constraints

The main site constraints of the project can be summarised as follow: (i) the MTRC AEL, whose regulations govern the maximum allowable ground settlement and vibrations induced by the construction activities; (ii) working restrictions due to the close proximity to AEL; (iii) existing utilities within the AEL embankment such as a fresh water main, CLP cable ducts, communication cables and a storm water drain; (v) king posts at the back of the jacking shaft supporting the temporary traffic deck which extended partially over the site; (vi) the heavy braced steelwork that provided the ELS for the jacking and receiving shafts (see Figure 1).

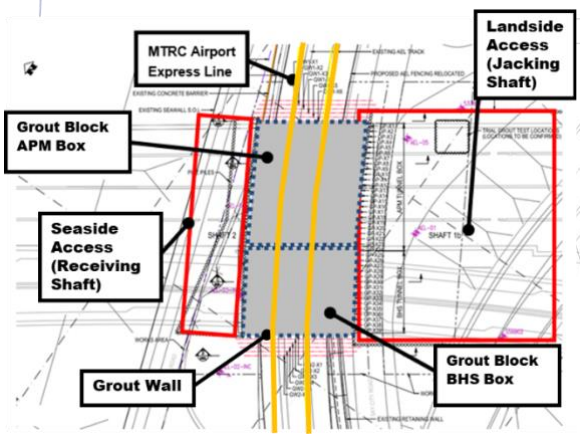

Figure 5: Footprint of Receiving and Jacking Shafts

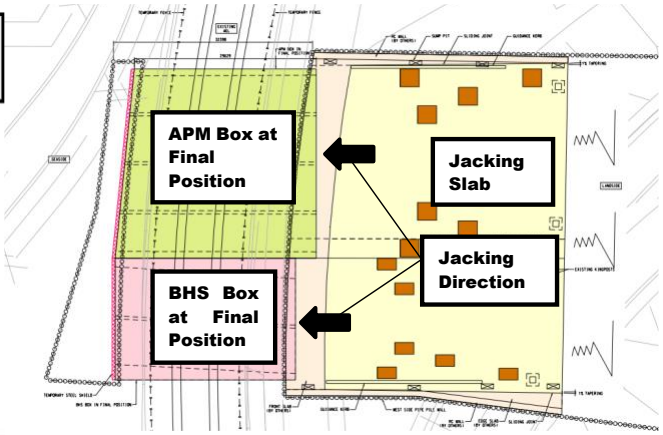

Figure 6: General Plan of Box Jacking Works

2 GROUT BLOCK UNDER AEL (GBUAEL)

2.1 In-Situ Ground Conditions

The in-situ ground conditions of the project area comprised rockfill, overlying alluvial sand lenses and saprolitic decomposed granite. The rockfill was placed during the original reclamation works for the Chep Lap Kok Airport platform and is composed of boulders, cobbles and sand. The depth of rockfill under the AEL embankment varies between 17m and 20m. The underlying granite rockhead varies significantly and generally lies between 5m and 25m lower than the final formation level of the jacking slab.

2.2 Ground Improvement Scheme - Objective

An essential element of the Box Jacking Works was the successful implementation of ground improvement over the tunnel works site zone under the AEL. To ensure the safe execution of the works and the continued safe operation of the AEL it was necessary to enhance the engineering properties of the in-situ ground. The ground improvement works aimed to enhance the following ground properties:-

a) Mass stiffness - for the control of ground deformations induced by the works and therefore limit the resulting ground settlement movements under the AEL;
b) Strength - to improve face stability during excavation underneath the AEL as well as to reduce the horizontal earth pressure imposed on the headwalls of the jacking & receiving shafts; and
c) Permeability - to control groundwater seepage into the works and the potential for adverse consolidation effects due to drawdown of the naturally occurring levels.

The target strength and stiffness properties are presented in Table 1.

Table 1: Target properties for GBUAEL

Engineering Property	Target Value
Friction Angle (ϕ')	40° (min)
Cohesion (c')	50 kPa (min)
Young's Modulus (E')	250,000 kPa (min)
Permeability (k)	1 x 10^{-6} m/s (max)

2.3 Grout Trial Block (GTRB)

For this project two trial grout blocks (TR1 and TR2) had to be formed within the Island reclamation fill at a location where they best represented the ground conditions of the future GBUAEL (see Figure 7). The testing of these GTRB was used to demonstrate the grouting quality and to verify whether the design parameters specified in the detail design were achievable before the actual grout block works under the AEL were carried out.

The GTRB were formed using permeation grouting inside of a 7.0m x 7.0m cofferdam, which was made of steel pipe piles and a grout curtain to provide a hydraulic cut off and prevent seepage below the toe of the wall. The same grouting technique was employed as for the future GBUAEL. The grout holes were done vertical with a spacing of 1.3 x 1.5m.

The same verifications tests as for the main GBUAEL had to be carried out for the trials and included: (i) Geophysical Testing to confirm the integrity of the GTRB; (ii) Plate Load Tests to confirm the Young Modulus; (iii) Angle of Response; (iv) Falling Head Tests to verify the permeability; and (v) Pressuremeter Tests to confirm the target soil properties.

Both the TR1 and TR2 confirmed that the trial grouted soil parameters met the specified target design criteria used for the detail design of the main GBUAEL.

2.4 Ground Improvement Scheme - Implementation

Firstly, the Tube a Manchette (TAM) grouted cofferdam walls for the jacking shaft and the receiving shaft were constructed. Two further grout walls were then constructed (Figure 9), one on each side of the AEL, with toe embedment into the underlying rockhead. These two grout walls provided a sealed enclosure to the site by connecting with the TAM grouted headwalls of the jacking shaft and receiving shafts. A Grout Block under the AEL was then formed within this sealed enclosure by permeation grouting. The extent of the grouting works was sufficient to effectively form 'sidewalls' to the tunnels and control the potential for lateral movements at the excavation face during the jacking/excavation works.

The grouting technique and the sequence of grouting were developed to maximise control over/limit near-surface ground movements and hence AEL impacts. The technique was detailed to ensure that the installation could be carried with a fan of inclined boreholes from outside the proposed fence line of the MTRC boundary (3m buffer from AEL) and protect the adjacent utilities in the area. The treating of similar ground by permeation grouting was previously successfully used on the Scenic Hill jack box (Cook et al 2018).

2.5 Ground Improvement Scheme – As Built Verification

After completion of the grouting works, the following verification tests were carried out for the grout block (see Figure 8):

1) 30No. constant head tests through 10No. vertical boreholes to establish the permeability;
2) 50No. pressuremeter tests through 10No. inclined boreholes for verification of the Young's Modulus and back analysis of the shear strength; and
3) Geophysical tests (cross hole seismic test) through 10No. vertical boreholes to establish the integrity of the grout block.

Based on the verification test results the minimum measured permeability of the GBUAEL was 9.2x10-7m/s, the minimum Young's modulus was 264MPa and the minimum cohesion was 217kPa. These minimum values were higher than the target properties. In addition the geophysical testing results measured wave velocity within each formation (rockfill, alluvium and CDG) indicated that the grouting works met the design intent within all formations.

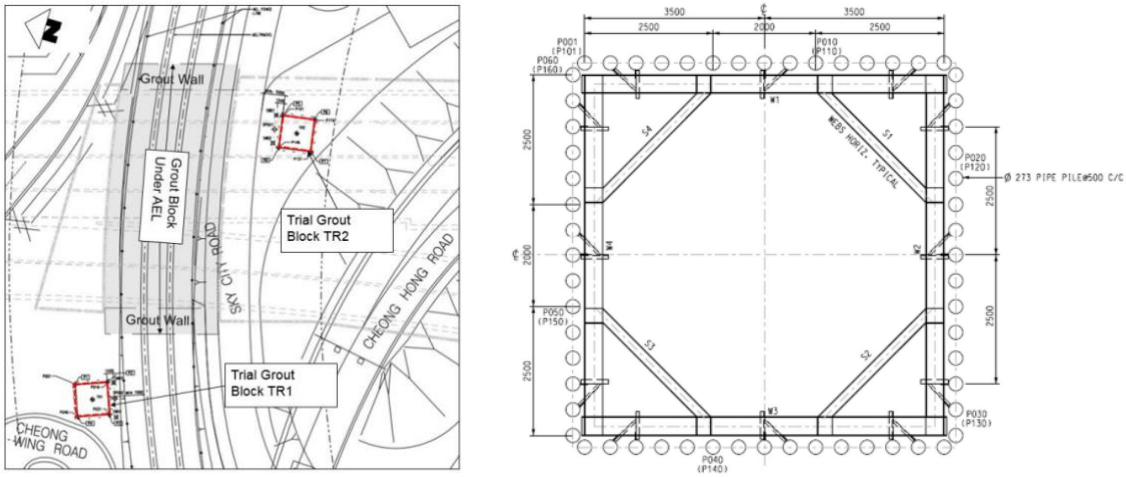

Figure 7: Location and cofferdam of Grout Trial Block (GTRB) TR1 and T2

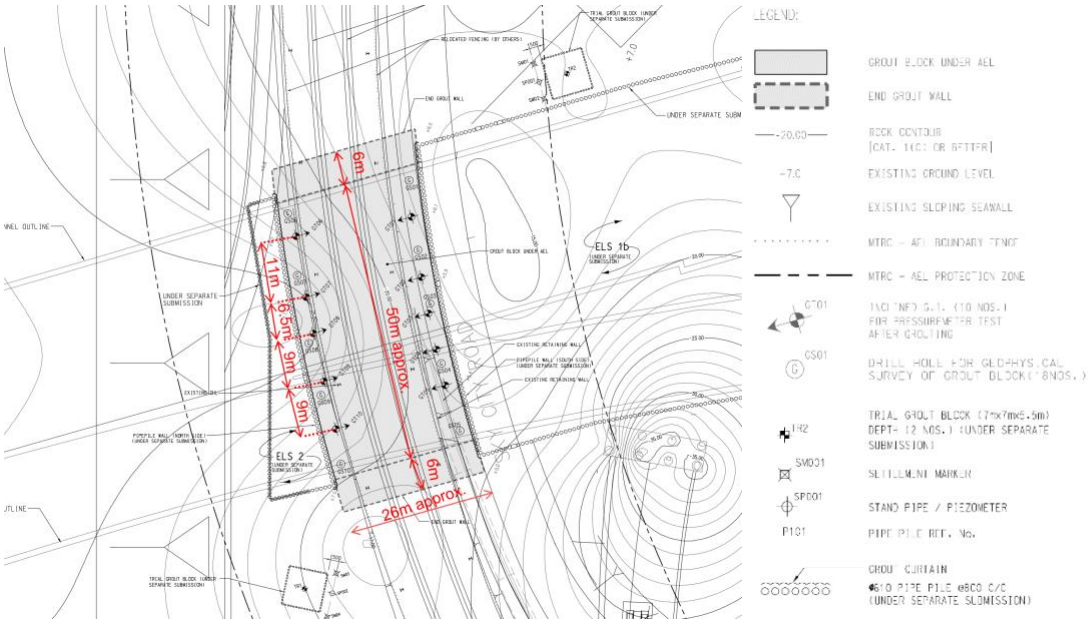

Figure 8: Layout of the executed GBUAEL verification test program

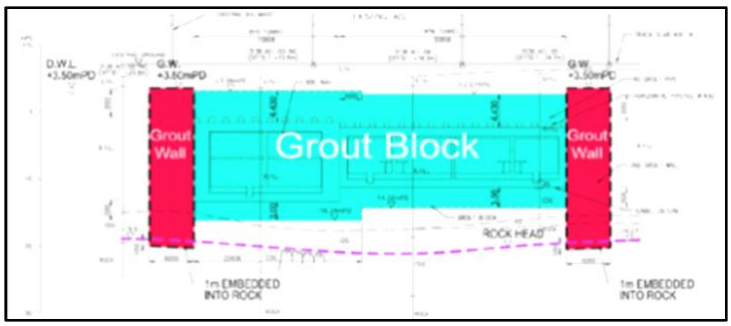

Figure 9: a) Cross section Grout Walls and GBUAEL;

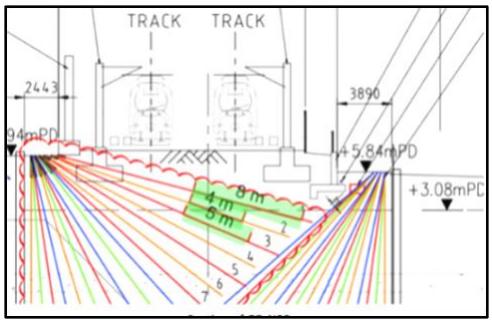

b) Typical Fan Grouting Section under AEL

3 HORIZONTAL PIPE PILES (HPP)

3.1 HPP Requirements

Grouted HPP were used to form a canopy above the crown of the APM and BHS jacked boxes, these being restrained by horizontal prestressing strands placed within centrally positioned ducts which were attached to the top rear of the boxes. The HPP were made of 1430mm diameter x 14mm thick spirally welded steel pipes spaced at 2.0m centres. The canopy was a fundamental element of the temporary works used to control ground settlements during the excavation process. The HPP provided a stiff support to the AEL embankment as they span over the excavation face, supported off the jacked box on one side and off the improved ground ahead of the excavation face on the other side.

The restrained HPP also provided the controlled sliding surface for the crown of the reinforced concrete tunnel boxes by acting as an Anti-Drag System (ADS), thus isolating/preventing horizontal ground disturbances of the AEL embankment during the jacking works.

3.2 Installation of HPP

The 26 No. HPP were installed by pipe jacking and using micro TBM's, from an intermediate formation level above the crown of each tunnel box, in advance of the jacking and receiving shafts being excavated down to their formation level (see Figure 10). The pipes were delivered in stock lengths of 6m. At the joint interface of the connecting pipe lengths a flexible temporary joint connection using a rubber seal was provided to enable a smooth control of the alignment and level. The flexible joint connection was then welded with a full butt weld after the pipe in front of the joint was fully jacked into the ground, finally forming a continuous pipe from the jacking shaft to the receiving shaft. The jacking works were typically carried out during MTRC's non-operation hours, while the welding works was done during the day off the programme critical path.

The micro TBM enabled the installation of the pipes to close tolerances in alignment and level, well within the specified +/- 100mm. The pipe jacks were secured to a temporary reaction slab and wall to resist the TBM thrust forces.

After completion of installation of a respective tube, annular grouting was carried out, where the periphery of the tube was grouted over its full length. After jacking of all HPP, the tubes were filled with grout around the central placed prestressing ducts.

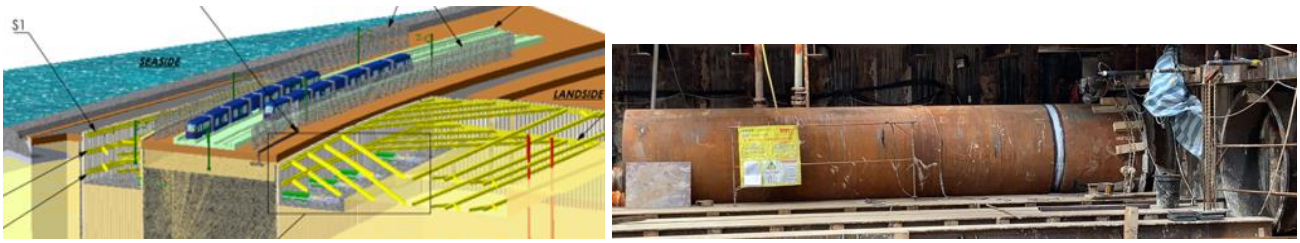

Figure 10: Installation of Canopy Tubes above Crown of Tunnel Boxes by micro TBM and pipe jacking

3 BOX JACKING SYSTEM

3.1 The Jacking Slab

Once formation level was reached inside the launch shaft, the jacking slab with its shear keys and inclined anchors(see Figure 11) was constructed, which initially served as the casting bed for the two jacked boxes, and subsequently as the reaction system that enabled the jacking of the tunnel boxes, without loading the shaft ELS. The jacking slab was a 1.2m thick post-tensioned raft with four shear keys of 2.0m depth, anchored to grade III rock with temporary ground anchors. The structurally monolithic slab was formed with two terrace levels to accommodate the different soffit levels of BHS box (top of slab -12.373mPD) and APM box (top slab -10.868mPD). For each level the surface is flat without any longitudinal gradient or crossfall. The jacking slab is separated by a movement joint from the edge infill slabs around the vertical pipe-pile wall. The movement joints along the sides were designed as sliding joints with sliding bearings at the interface, to prevent on the one hand any shear transfer to the ELS system, but also on the other hand to provide axial support to the vertical PP wall to enable the removal of the lower strutting levels S3 and S4 which would otherwise clash with the boxes construction. Towards the headwall the jacking slab was separated by the provision of an infill slab, which acted as a horizontal deep beam to provide support to the headwall, the

jacking slab being isolated from it by a 20mm joint with a compressible joint filler, but with dowel bars to prevent differentials developing across the infill/jacking slab sliding surfaces.

Concrete guide kerbs designed for accidental skew loadings were cast on top of the slab on the outer side of the BHS and APM boxes to guide the boxes during the jack boxing operation.

Each tunnel box was cast inside the launch shaft on the jacking slab (Figure 11). This ensured a safer and higher quality of works compared to casting the tunnel in-situ beneath the AEL, in the multiple stages, that would otherwise be required. In order to provide sufficient space for an excavator, the central internal wall and slab of the BHS box as well as the front part of the two outer internal walls of the APM box were omitted for the 1st stage and cast in a 2nd stage after completion of the box jacking operations (refer to Figure 4). The boxes were then jacked forward off the jacking slab (casting bed) using ram jacks located at the rear of the boxes (which jacks reacted against corbels attached to the jacking slab by tensioned stress bars).

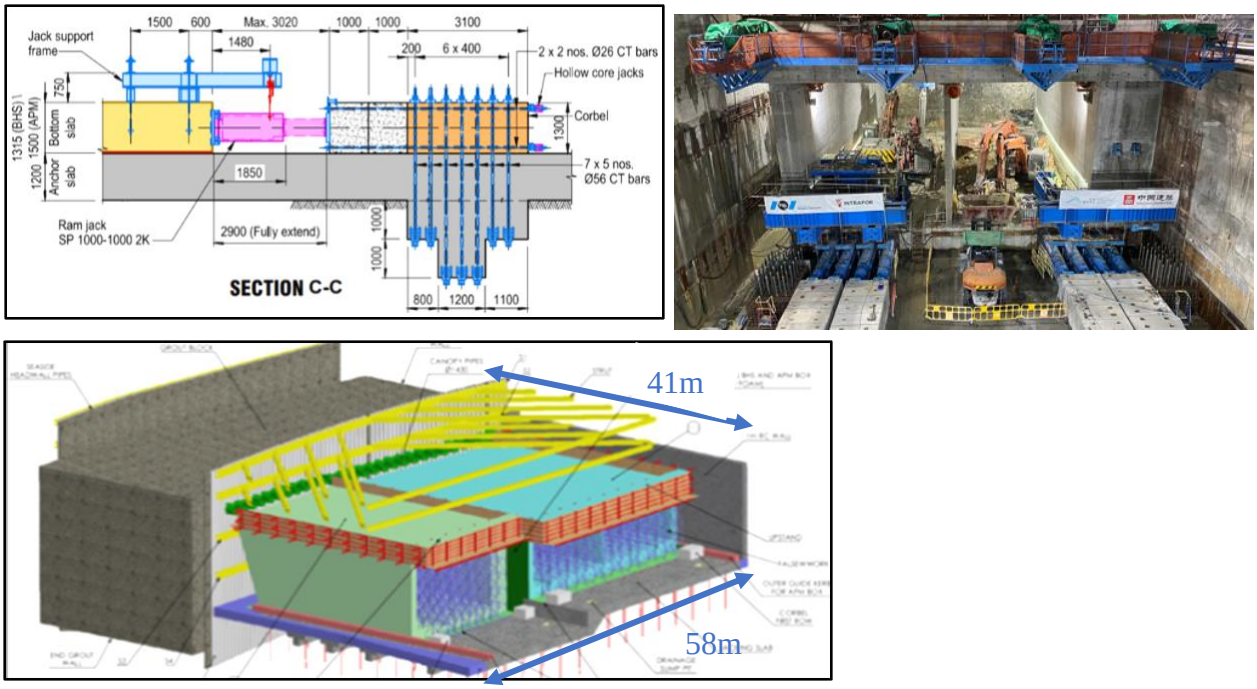

Figure 11: Construction of APM and BHS Tunnel Boxes in Jacking Shaft on top of Jacking Slab

The tunnel boxes were jacked forward across the jacking slab, spacer blocks being installed in between the tunnel boxes and corbels iteratively to fill the gap as the tunnel boxes were being jacked forward. The jacking force being transferred through the spacer blocks to the restraining corbels, and then to the shear keys and inclined anchors underneath. The anchors were embedded in CDG strata and rock strata below the jacking slab invert.

The jacking at the rear of the tunnel boxes was carried out by up to 3000mm stroke jacks with 460 tonne working loads and supplemented with short stroke ram-jacks of 2000 tonne working loads (Figure 13). The jacks were equipped with a spherical head at either end to allow some bearing geometry tolerance and were supported on a cantilevering steel hanger frame fixed to the bottom slab of the tunnel boxes. The jacks applied the forces to embedded steel plates cast into the rear of the box base plate (see Figure 12).

The required jacking forces to overcome the friction between the tunnel box and the surrounding interfaces was estimated by carrying out a sensitivity analysis using upper and lower bounds for the materials present and by considering a bentonite lubrication system to reduce the friction during jacking. “Best estimate” serviceability friction forces were estimated which were multiplied by a 1.5 safety factor to derive the “design” jacking forces. The provided total jacking capacity which was allowed for was significantly higher than the estimated design friction forces, to allow for unforeseen geotechnical variations. The highest jacking forces occurred typically during break out of a respective jacking stage, after which the forces gradually decreased as the box began moving (ref Table 2).

Table 2: Summary of estimated versus actual jacking forces

Box	Best Estimate [MN]	FoS	Design Friction [MN]	Strand Jack Capacity [MN]	Ram Jack Capacity [MN]	Total Jack Capacity [MN]	Max Actual Jacking Force [MN]
APM	141	1.5	212	48	175.5	223.5	192
BHS	95	1.5	142	32	114	146	101

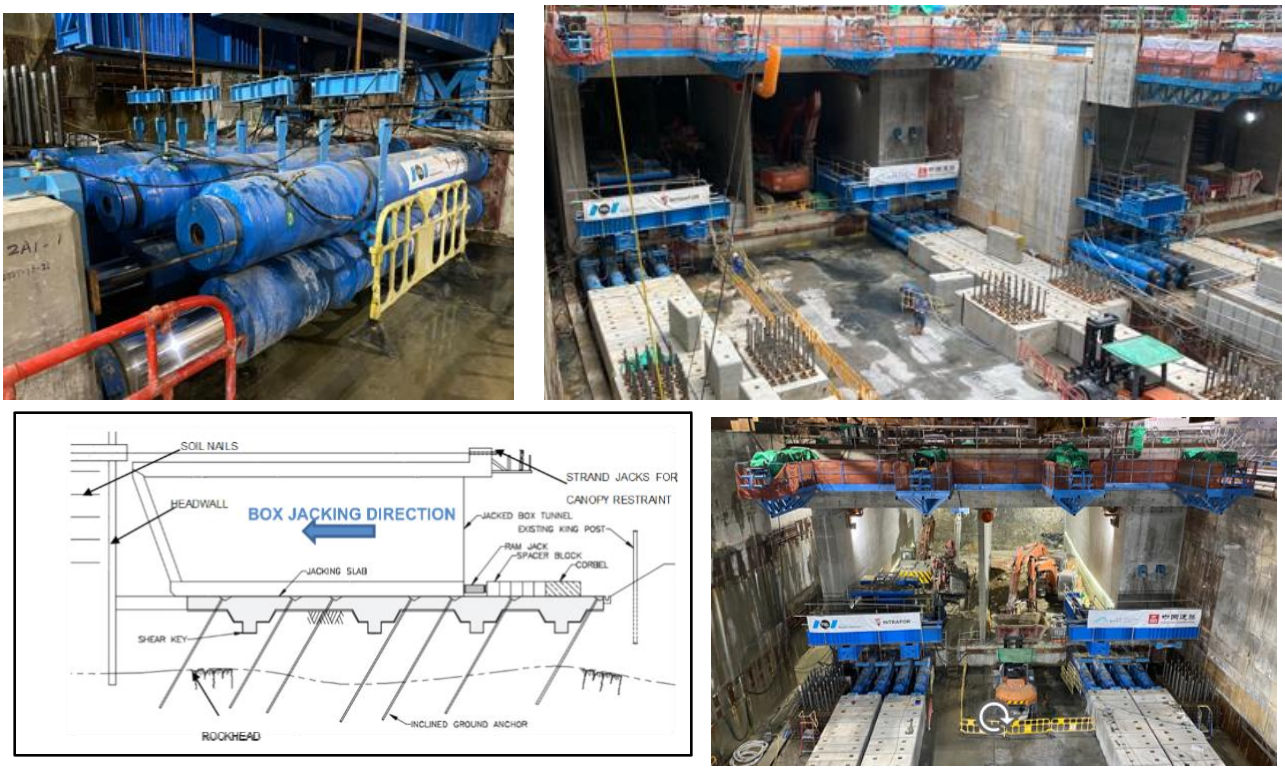

Figure 12: Typical Arrangement of Jacked Boxes on Jacking Slab

Prestressed ground anchors were installed prior to the box jacking operation at angle of 30 degrees to the vertical. The horizontal component of the anchors prestressing force being detailed so as to act against the jacking force during box jacking operations. The vertical downward force component of the ground anchors also acting as a surcharge on the soil underneath the slab enhancing the horizontal friction shear resistance. The jacking slab relied on the horizontal component of the ground anchor prestress force, as well as the soil friction under the slab and at the toes of the shear keys, to resist the horizontal jacking force during box jacking operations (Figure 14). While the horizontal anchor force and soil friction provided the primary restraint during jacking, before significant movement occurred, the passive resistance behind the shear keys was also assessed to understand the ultimate stability FOS against failure. Notwithstanding the system strain compatibility differences between these restraint types.

The above ultimate potential failure checks were undertaken first as a global stability check. Detailed checking was also undertaken using Plaxis, which allows soil/structure rigorous analysis to assess the potential of local failures, as well as the level of ground deformations/structure movements during jacking. Conventional 2-D Plaxis was first used for this assessment to comply with the expectations of the Approval Authorities.

A 3-D analysis with Plaxis 3-D was then additionally undertaken to assess the stability of the jacking slab and the induced deformation in a more realistic way (Figure 15). In addition, the 3-D analysis enabled a more accurate model of the distribution of the stress around the corbels during jacking, and hence the induced ground movements. In addition, the 3-D model enabled the assessment of the interaction between the jacking slab and the ELS system of the launching shaft through the ground. Finally, the 3-D model allowed the impact of the jacking works on the adjacent king post supports (which were supporting the temporary bridge structures over the sire) to be assessed, which supports passed through and adjacent to the jacking slab.

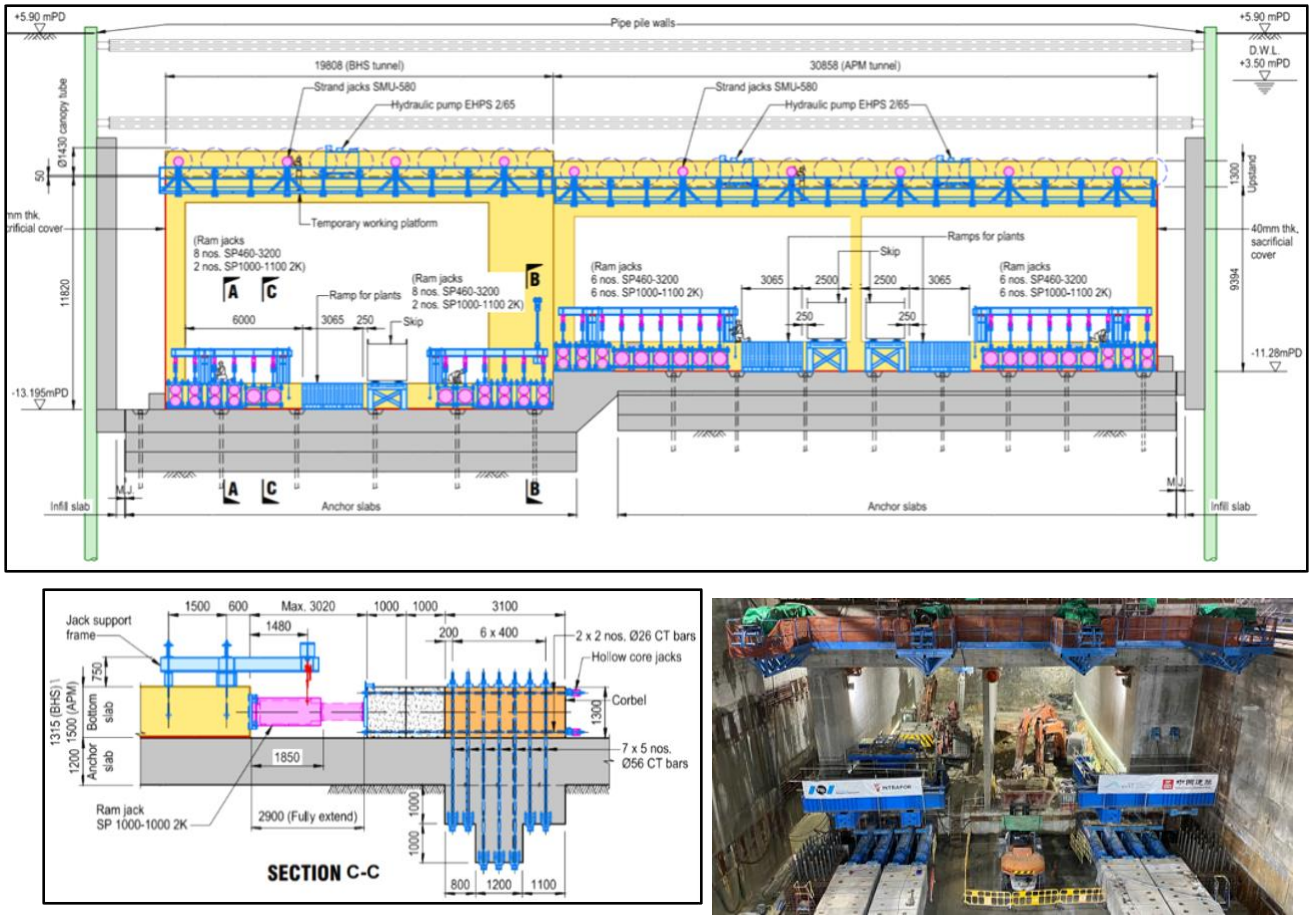

Figure 13: Typical Arrangement of push jacks at rear of APM and BHS box

3.2 Monitoring of the jacking slab and the AAA levels system that were adopted during the works.

The maximum horizontal displacement limit of the slab parallel to the jacking direction was set to only 10mm while the lateral ground deformation limits to be measured using inclinometers were ±7mm. These values were also defined as 'Alarm' values. Despite the fact the Alarm values were stringent, the monitoring of the relevant instruments did not breach them. The relevant values assessed in Plaxis 2-D were more than 50% higher than the limits adopted in construction. However the movement assessment using Plaxis 3-D showed lower limits could be achieved and thus allowed lower limits to be adopted with confidence that they would be achieved in practice. In other words the 3-D method of analysis contributed towards safety during the works, by allowing the setting of a lower allowable deformation.

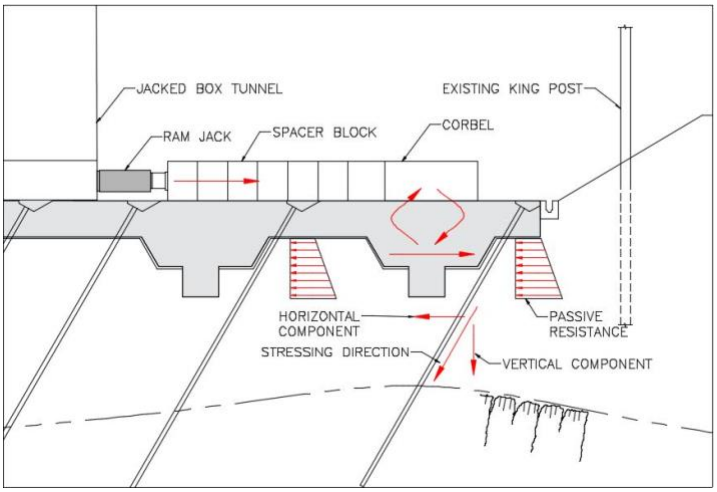

Figure 14: Jacking slab restraint load considerations

3.3- Ground Anchors Design

The ground anchors used to restrain the jacking slab were a single proprietary 14No. strand temporary ground anchor type with a working load of 2300kN (Figure 17 and Table 3). The strands were PE sheathed within their free length and bare within the bonded length and ran inside a corrugated PE duct. The design of the anchors was in accordance with BS8580 (latest version) which is also in accordance with Hong Kong's own GEOSPEC 1. The design specifications of the anchors were set to comply with the most up to date definition of loads to comply with BS8580. The design effort put into this allowed the contractor to conduct an anchor test program which was rigorous and complied with the state of the art technical requirements for prestressed ground anchors. Three suitability ground anchor tests had to be carried out in advance of the installation of the working ground anchors under the identical conditions and configuration. These suitability tests were carried out from the HPP formation level behind the temporary reaction slab for the canopy tube jacking (Figure 16).

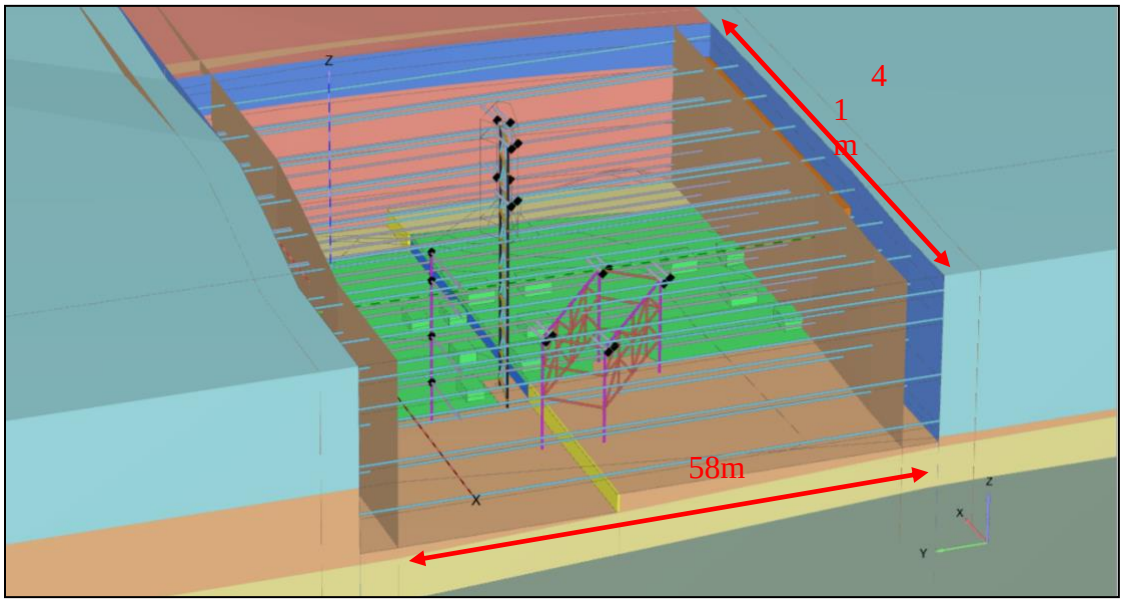

Figure 15: Plaxis 3-D model for the analysis of the jacking slab

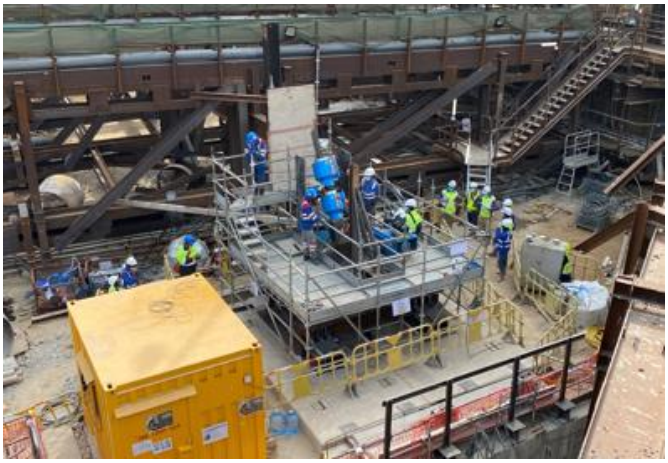

Figure 16: Ground Anchor Suitability Test Set Up

3.4 Load Paths

As noted above the friction forces acting at the sliding interface between the roof slab and the HPP were restrained by a strand jacking system attached to the top rear of the boxes (refer to the Anti-Drag System section).

The ram-jack forces were reacted by the jacking slab and the soil / structure interaction that transmitted the forces into the ground mass below the slab formation. The ram jack forces entered the slab via the thrust corbels that were positioned at discrete locations on the jacking slab to suit the ram-jack arrangement. The

slab acted as a horizontal diaphragm to transmit the thrust loads to the shear keys while resisting the out of plane bending and tension effects these induced.

Table 3: Properties of Proposed Ground Anchors

S/N	Description	Value
1	Working Load	2300 kN
2	No. of Strands per Anchor	14
3	Strand Diameter	15.7mm
4	Ultimate Breaking Load of Anchors	3906kN
5	Minimum Free Length	4000mm
6	Minimum Fixed Body Length	3000mm

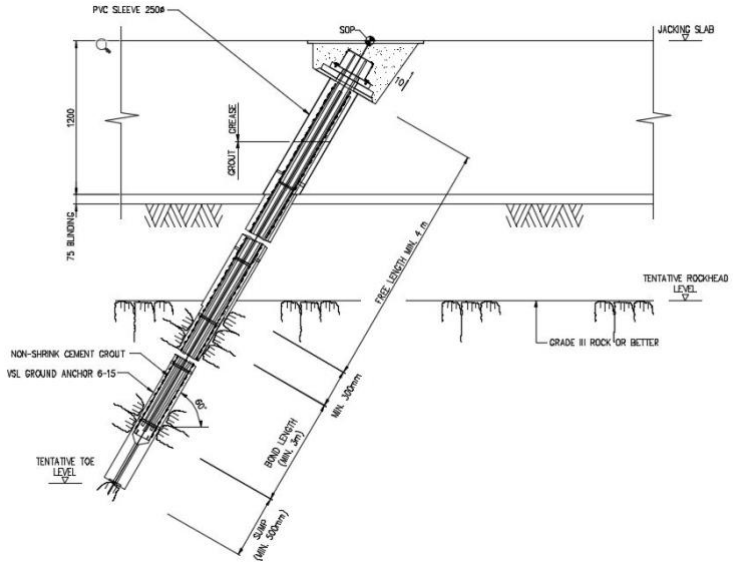

Figure 17: Typical Arrangement of Inclined Ground Anchor

The shear keys transmitted the thrust loads into the upper sections of the formation by inducing a passive reaction locally in the ground (Figure 18). The horizontal component of the prestressed 30 degrees inclined temporary ground anchors acted against the jacking force, while the vertical downwards component acted as a surcharge on the soil and thus increased the soil interface shear friction resistance.

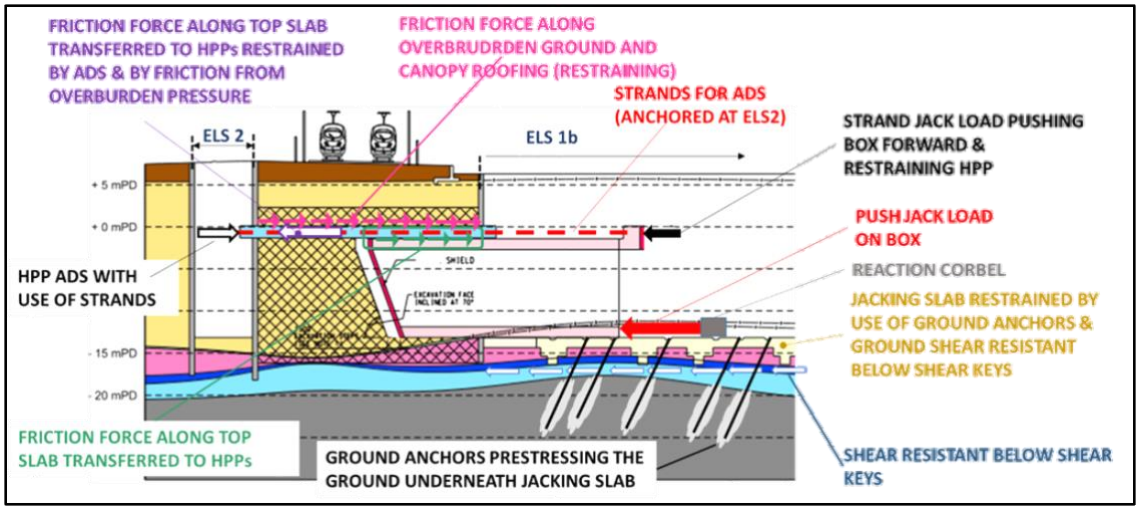

Figure 18: Load path during box jacking

3.5 Anti-Drag System

The restrained HPP provided the controlled sliding surface for the crown of the reinforced concrete tunnel boxes by acting as an Anti-Drag System (ADS). Thus preventing horizontal ground disturbances to the AEL embankment during the jacking works. The HPP were restrained by an innovative strand jacking system (Figure 19). Prestressing strand bundles ran through ducts cast into ten selected pipes and were anchored at the front receiving shaft end on waler beams bearing against the HPP and vertical pipe pile wall of the receiving shaft. At the back the strands were connected to strand jacks bearing against an upstand beam at the rear of the APM and BHS tunnel boxes. The HPP and restraint system were instrumented and monitored for load and movement. The forces in the strand jacks were linked with those of the main ram jacks allowing adjustments to be made to the strand jacks depending on the roof / canopy friction forces they experienced. The upper strand jacks used were VSL's proprietary model SLU800 with a safe working load of 8,000kN. 6 No. of strand jacks were used for APM and 4 No. for the BHS respectively.

In summary uniquely the strand jack loads which were used to move the boxes forward, were are also used to prevent the HPP from moving. Thus enabling an observational approach to be adopted where the HPP movements were monitored to ensure they were minimal. Box friction forces on the bottom of the HPP being balanced against the applied strand loads.

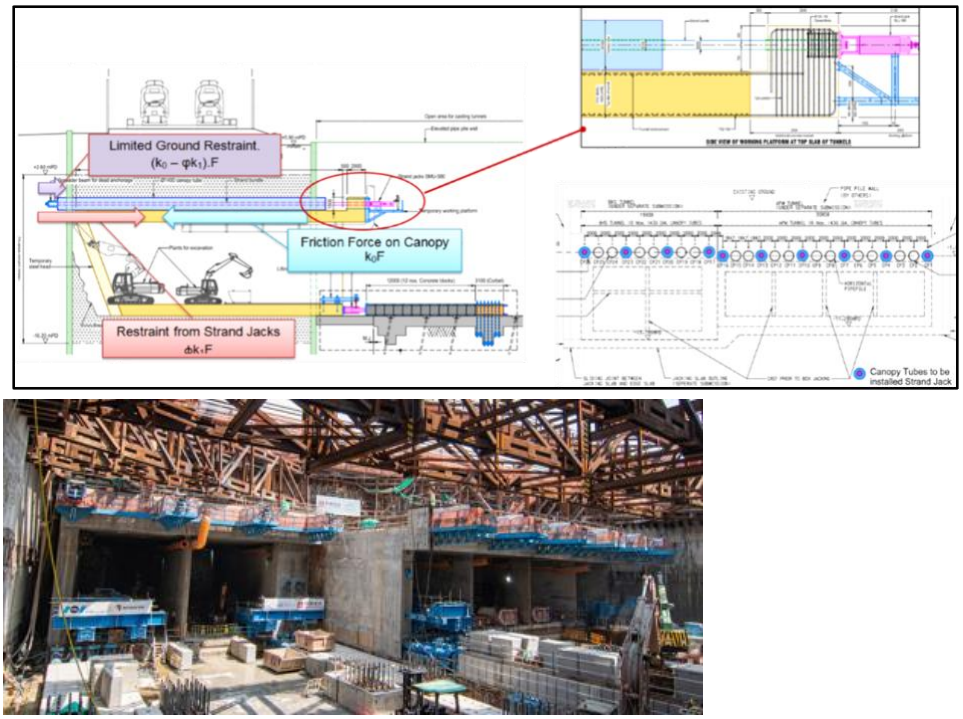

Figure 19: Anti Drag System with strand jacking restraint

Figure 20: Detail Chair Shims welded to HPP (left); view 1st chair on HPP; shot-creting of gap between HPPs.

3 TUNNEL EXCAVATION AND STABILISATION WORKS

3.1 Tunnel Excavation

An open excavation face was adopted for the boxes after taking into consideration the improved ground conditions expected after completion of ground improvement and the dewatering, i.e. a face shield was not necessary. The excavation was retained at 70 degrees to the horizontal and advanced in 1.5m increments ahead of the leading face of the tunnel boxes, which were cast to the same angle. The sloping face of the boxes were constructed of reinforced concrete including embedded couplers to allow for the subsequent stitching to the adjacent RC cut & cover sections. Steel plates with shear studs were cast into the nose to protect the couplers, concrete face and edges during tunnel excavation and box jacking.

The horizontal roof face in front of both tunnels exposed during excavation was protected from collapsing and from excessive deformations by the canopy roofing provided by the HPP (Figure 20). Following each excavation step, chair shims were welded to the HPP at 1.5m centres to compensate for the construction tolerances during the HPP installation. The chair shims bore against cast-in steel plate strips of the tunnel box roof slabs with a maximum gap of 5mm. The HPP spanned the gap between the front of the box and the ground mass and provided a skidding interface against the tunnel boxes.

Excavation was carried out by hydraulic excavator and breaker, followed by mucking out, scaling and jacking (Figure 21). The excavation and tunnel box jacking started first with the deeper BHS box so as to maintain a minimum distance of 5m to the APM box to prevent undercutting it at the interface. A typical excavation and jacking cycle of 1.5m length was carried out in 4 days (8 shifts).

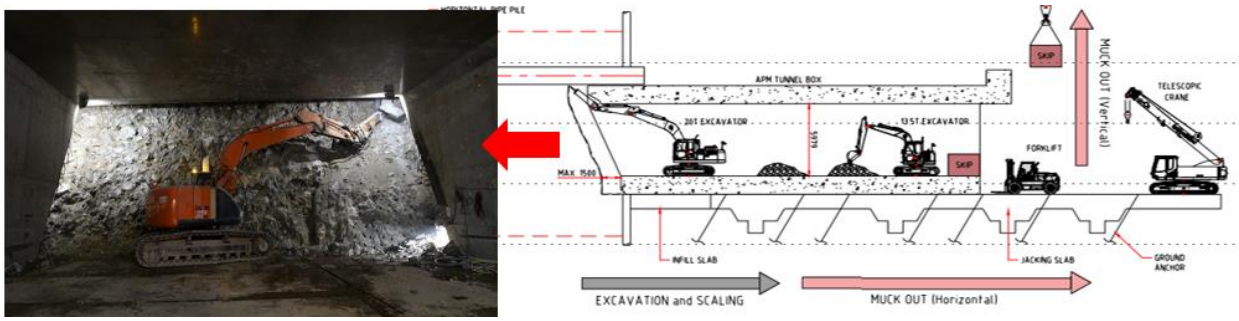

Figure 21: Excavation with the use of hydraulic excavator and breaker.

4 IMPACT ASSESSMENT ON AEL

All movements of the AEL were monitored with the use of ADMS, measuring deformations of the rail tracks in three dimensions. Figure 22 presents the ADMS instrumentation above the APM box (the arrangement for BHS box was similar).

AEL rail movement monitoring during the box jacking works of the APM was provided using ADMS measuring stations ref. 58850-, 558860- and 558870- UN, US, DN, DS, 58830 UN, US, DN, DS. Overhead Line (OHL) footings were measured using stations ref. 58840- and 58860- DA & DB.

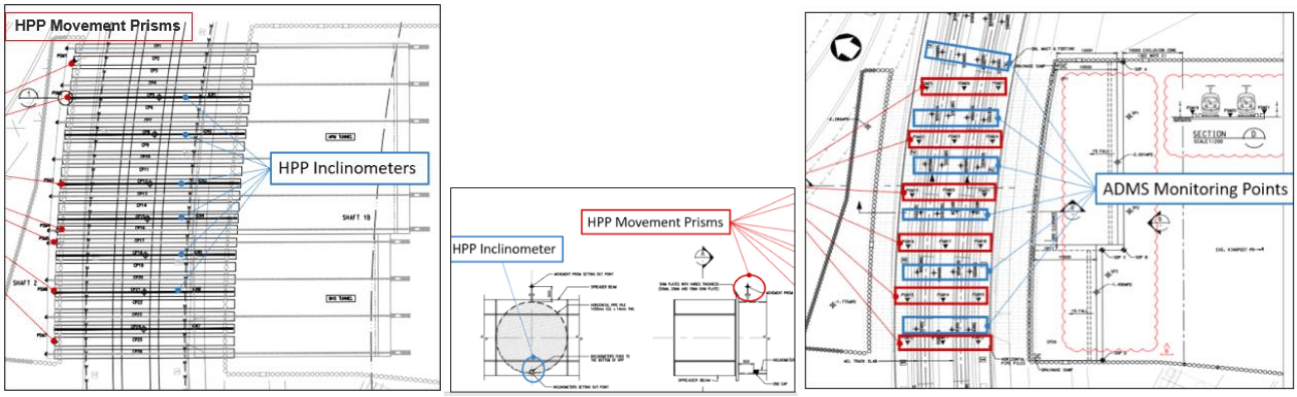

Figure 22: ADMS arrangement of AEL below APM

Table 4 presents the AEL settlements based on the ADMS readings from the instruments. The actual settlements of Table 4 were taken in February 2022 after the completion of the APM box jacking, i.e. the

completion of the box jacking works overall. As can be seen from the readings, the maximum settlement of the AEL track was 11mm which was within the design settlement of 16mm. The accurate design and the good care provided during the execution of the works resulted in uninterrupted operation of the AEL during box jacking.

Table 4: AEL movements at completion of the APM box Jacking

	ADMS Monitoring Points Reference											
	58850U		58860U		58870U		58850D		58860D		58870D	
	UN	US	UN	US	UN	US	DN	DS	DN	DS	DN	DS
Induced Settlement (mm)	-4.3	-8.2	-1.2	-3.6	-6.1	-6.2	-10.8	-9.7	-10.4	-5.8	-10.8	-8.5
Maximum Settlement (mm)	-8.2						-10.8					
Design Settlement at 100% progress (mm)	-16						-16					

5 CONCLUSIONS

The APM and BHS Tunnel section of the HKIA under the AEL was the second project in Hong Kong, after the Scenic Hill tunnels, using the jacked box tunneling technique.

The project was executed by the partnership of China State and Intrafor under the care of the Airport Authority. AECOM was the designer of the box jacking works in all temporary conditions. The works included a high quality ground improvement scheme to stabilize and improve the ground properties, and the installation of a canopy roof made of HPP. The HPP, installed using micro TBM's/pipe jacking, were instrumental to ensure that the box jacking works of the two tunnels were carried out safely, without any disruption to the operating AEL railway. The APM and BHS tunnel boxes were jacked into the ground with a launching system comprising push jacks installed at the lower tail of the two boxes and strand jacks attached to the upper rear of the boxes. The push jacking forces reacted on a system of corbels constructed on the jacking slab, which was itself restrained by high capacity ground anchors anchored in rock. An innovative Anti-Drag System was installed as a canopy to the excavation roof that prevented adverse horizontal ground movements below the AEL during jacking. At the same time the ADS also served as part of the jacking system which improved the efficiency of the system and enable an 'observational' approach to canopy movement versus strand load provision. A detailed ADMS was installed to monitor the movements of the AEL tracks during the execution of the works that could give an immediate warning on adverse movement beyond the acceptable levels.

The jacking works for the APM tunnel and BHS tunnel were successfully completed within tolerances in June 2022, with the AEL movements being kept within the design expectations. The works were ultimately performed with a high level of safety, without any effect on the regular operations of the AEL. This demonstrating that the box jacking technique in Hong Kong is an appropriate construction method for tunnel construction in a settlement sensitive environment.

ACKNOWLEDGEMENTS

The authors wish to acknowledge the valuable contribution of the large project team (designers, site team and supervision) that led to a successful project.

REFERENCES

R.B. Cook, I. Tsaparas, Ch. Venetz, (2018) - The Scenic Hill Jacked Box Tunnel Under the Hong Kong Airport Express Line. Proceeding of the 38th Annual Seminar Geotechnical Division, The Hong Kong Institution of Engineers, Hong Kong, pp 30-41.

Review of Analytical Methods and Recent Advancement in Slope Stability Analyses

S.A. Faizi, U. Majeed & R. Tse
Arup, Hong Kong
C. Matthews
Arup, Newcastle, UK

ABSTRACT

This paper covers two key aspects concerning slope analysis and design. In the first part, different analytical methods are reviewed and a method of limit equilibrium slope analysis that allows the interslice force inclinations to vary is presented. The new approach (referred to as the Arup Method), applicable on both circular and non-circular slips, is a further refinement on the popular Bishop and Janbu methods and is designed to overcome the numerical difficulties stemming from interlock. The proposed approach achieves overall horizontal, vertical and moment equilibrium of the slope, while also keeping every slice in horizontal and vertical equilibrium. Illustrative examples are presented to compare results from this method against recognized methods of analysis, including Morgenstern-Price, which employs a user-defined interslice force function. In the second part of the paper, development of a digitalised workflow for slope analyses and design is discussed and the authors demonstrate how customised coding enables optimisation of slope design involving soil nailing.

Keywords: limit equilibrium, slope stability, interslice, optimisation, automation, soil nailing

1 INTRODUCTION

Current geotechnical practice widely adopts the method of slices, such as Bishop, Janbu, Spencer and Morgenstern-Price, to analyse slope stability using limit equilibrium. These methods divide the slipping mass of slope into several vertical slices, onto which equations of static equilibrium are subsequently applied. They differ fundamentally based on the conditions of equilibrium they satisfy, and their assumptions regarding the interslice forces involved.

While the discussion on the merits and deficiencies of those methods have been made in previous publications such as GEO Report No. 208, it comes to the attention of the authors that misunderstanding have been developed over the years among some practitioners, in particular to some of the variations of the rigorous Bishop and Janbu methods. This paper will propose the use of variably inclined interslice forces that Arup has developed in Bishop and Janbu methods. This method will from hereon be referred to as the Arup method and is a refinement of the Bishop and Janbu methods for slope analysis. The mechanics behind the Arup method is subsequently explained and case examples are used to compare results using this method against other analytical approaches, including Morgenstern-Price, which employs a user-defined interslice force function instead. Implications of using this approach for the different slope scenarios are then discussed.

On the other hand, with the recent advancements in computation, streamlining of the analysis process and optimisation through rapid parametric study is also possible. The second part of this paper introduces the development of a digitalised workflow for slope analyses and describe how customised coding enables optimisation of slope design adopting soil nailing.

2 LIMIT EQUILIBRIUM ANALYSES FOR SLOPE STABILITY

In the popular method of slices using limit equilibrium, a slip surface of some geometric shape (such as a wedge, circular or log spiral) is assumed, and the slipping mass is divided into a series of vertical slices, as shown in Figure 1. Various equations of static equilibrium are then applied either to each slice or to the slipping mass as a whole.

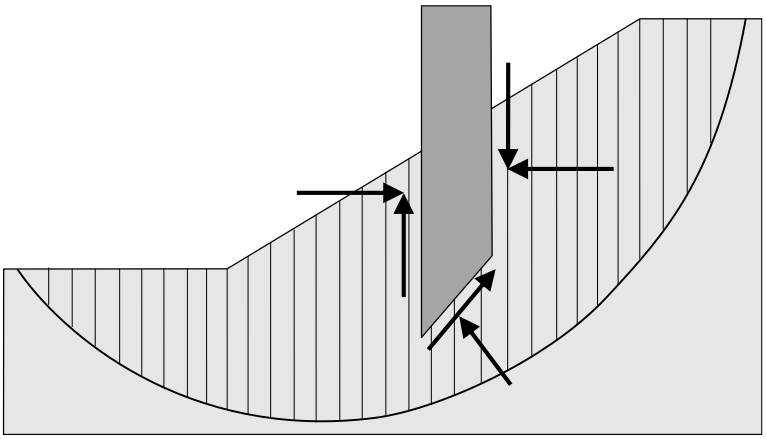

Figure 1: Method of slices in slope stability analysis

Analysing slope stability is, however, an indeterminate problem since there are more unknowns than equations. Sufficient assumptions are, hence, required to make the problem statically determinate.

Various analytical methods have been developed and adopted to evaluate slope stability. Some of the successfully adopted methods include Bishop (1955), Janbu (1957), Morgenstern-Price (1965) and Spencer (1967). All these methods differ in the conditions of equilibrium they satisfy and the assumptions they make to render the problem statically determinate. In both Bishop and Janbu methods, horizontal inter-slice force is assumed. However, the two methods differ in the conditions of equilibrium they satisfy. The Bishop method satisfies vertical force equilibrium for each slice and overall moment equilibrium, while the Janbu method satisfies vertical force equilibrium for each slice, as well as overall horizontal force equilibrium for the entire slip mass. In the Morgenstern-Price method, the inter-slice shear forces are assumed to be related to the inter-slice normal forces using an arbitrary function. The user-defined function allows the inclinations of the interslice forces to vary between successive slices, and the Morgenstern-Price method can satisfy all conditions of equilibrium for the slipping mass as well as for each slice. Despite being more complex, this method is regarded as the most accurate method of slope stability analysis and is used most abundantly. The Spencer method, on the other hand, assumes a constant for the interslice function, resulting in parallel inclined interslice forces. The Spencer method is able to satisfy all conditions of overall equilibrium for the slipping mass.

Several studies and publications have investigated the merits and deficiencies of the different limit equilibrium methods (Wright et al. 1973; GEO 2007). According to these studies, there are several fundamental limitations of the different methods, especially the simpler methods of Bishop and Janbu. One of these limitations is the inability of some analytical methods (like Bishop and Janbu) to satisfy all the conditions of equilibrium. While this is true, several studies (Bishop 1955; Whitman & Moore 1963; Whitman and Bailey 1967; Spencer 1967; Chirapuntu & Duncan 1975) have observed that despite not meeting all conditions of equilibrium, the errors in the calculated factors of safety from these simpler methods (for example, Bishop) are usually small and on the safe side. According to Chirapuntu & Duncan (1975), the Bishop method gives result well within about 5% of the results calculated by the more accurate methods that achieve all equilibrium conditions, even for effective stress analyses with high pore pressures. However, there are situations in which these relatively simple analytical methods may encounter issues. Whitman and Bailey (1967) investigated the formulation of Bishop method and its implication in various slope scenarios. They noted that the Bishop method may incur numerical difficulties and provide misleading answers, in special instances involving interlock.

2.1 Interlock and numerical errors in the Bishop method

Despite being largely useful and accurate, the Bishop method incurs numerical problems and may potentially give unreliable results when interlock is involved. The interlock arises in the case of a deep slip with a low factor of safety, where the toe of the slip surface passes steeply through a highly cohesive and/or dense granular material (Whitman and Bailey 1967; Chirapuntu & Duncan 1975).

Oasys Ltd. (2022) explains this interlock phenomenon. If a deep slip emerges at a steep angle and has a high cohesion or mobilized angle of friction, then the direction of the resultant force, R, on the base of the slice may be almost horizontal or even pointing downwards. This can be visualized when referring to Figure 2.

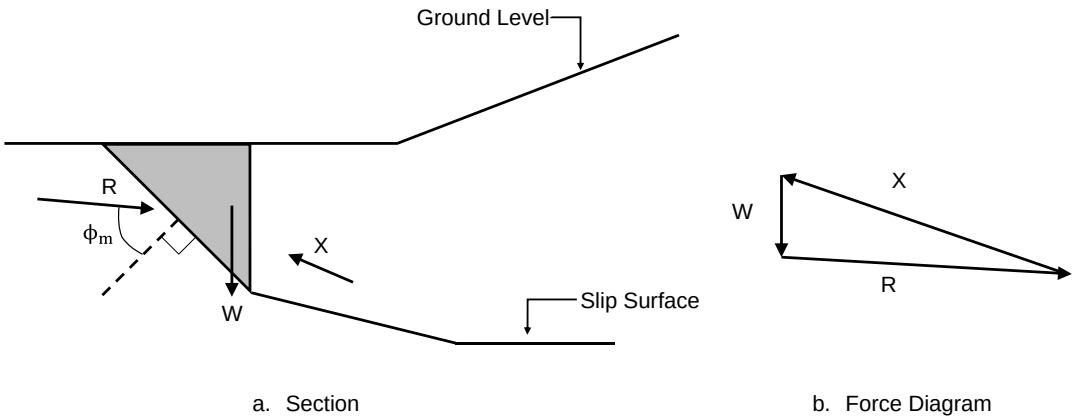

Figure 2: Interlock in slope stability analysis, shown a) on section and b) using force diagram (Oasys Ltd. 2022)

To satisfy equilibrium of this slice, the interslice force, X, must point upwards. This direction is not consistent with the assumption of either horizontal (i.e. Bishop and Janbu methods) or even parallel inclined interslice forces (i.e. Spencer method). In such cases, the inclination of the interslice forces should be allowed to vary to act in the correct direction and take interlock into account, as shown in Figure 3.

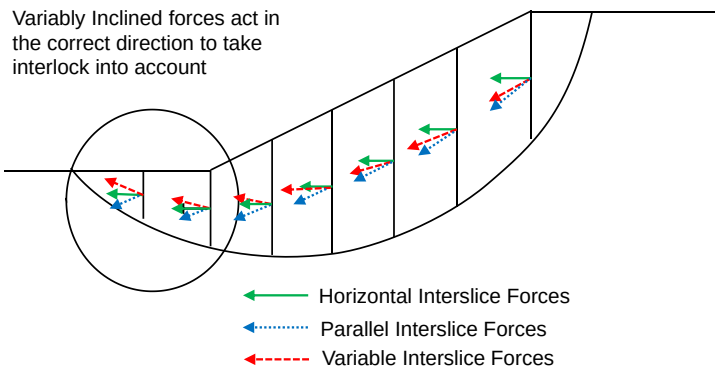

Figure 3: Inclination of interslice forces for different slope methods (Oasys Ltd. 2022)

Whitman and Bailey (1967) explained the source of the difficulty, using the expression for effective normal force at the base of the slice that is adopted in the method ($\overline{N}$), as shown in Equation (1).

$$\overline{N} = \frac{W - u\Delta x - c'\,\Delta x \tan\alpha / F}{\cos\alpha + \tan\emptyset' \sin\alpha / F} \quad (1)$$

where W = weight of the slice, u = pore pressure, Δx = length of the base of the slice, α = inclination of the base of the slice with horizontal, c' = effective cohesion, $\emptyset'$ = effective friction angle, and F = factor of safety

Referring to the above expression for $\overline{N}$, it can be observed that the denominator can possibly take on either very small or negative values towards the outward toe end of a slip circle where the angle of base inclination (α) is negative and of large magnitude. If this denominator is small, the value of $\overline{N}$ will be very large and so will the frictional component of the strength for this slice. If the denominator is negative, the normal force and frictional component of strength will also be negative. In both circumstances the Bishop method would give unreasonable values of safety factors.

Similarly, for slopes in cohesive soils, another similar numerical difficulty may arise, where the numerator in the above expression may take on a negative value if cohesion is very high. This may result in the effective normal forces on the base of the slices of the slope to be negative, which would not be reasonable, and the calculated factor of safety would be unreasonably low.

3 SLOPE STABILITY EQUATIONS WITH VARIABLE INTERSLICE FORCE INCLINATIONS – THE ARUP METHOD

The inclination of the interslice forces is a key consideration for an accurate slope stability analysis, and the assumptions made for the different methods of analysis will have impact on how the forces are calculated and how the conditions of equilibrium between slices met. To overcome the problem of interlock, the analytical methods would need to allow the inclinations of the interslice forces to vary and follow the right direction.

3.1 The Arup method

In this method developed by Arup, Bishop and Janbu methods are refined further by enabling the inclinations of the interslice forces to vary. Under this approach, the program calculates the interslice forces to maintain horizontal and vertical equilibrium of each slice first. The inclinations of the interslice forces are then varied in each iteration until overall horizontal, vertical and moment equilibrium is also achieved.

This method is currently available in Oasys Slope program as an option to choose when running Bishop or Janbu Methods for slope stability analysis. Oasys Slope is Arup's software program that is used for slope stability analysis using limit equilibrium. The program offers a variety of widely used methods for performing slope stability checks, including Ordinary (or Swedish circle (Fellenius) method), Bishop (1955), Janbu (1957), Spencer (1967) and Morgenstern-Price (1965) methods.

Since the program uses iteration to reach convergence, the interslice force is adjusted separately, for both the vertical and horizontal directions by adding the fraction of the residual values from the previous iteration. The fraction is determined by the horizontal length of the slip surface represented by that slice. The interslice force direction is, hence, free to vary through this approach, but each slice is always in equilibrium along with the slipping mass, as a whole.

The variably inclined interslice force option is available on both circular and non-circular slip surfaces, and is a useful function designed to overcome the problem of interlock when using analytical methods that restrict the direction of the interslice forces.

The variably inclined method is preferable to horizontal and even parallel inclined interslice force methods, as it keeps every slice in horizontal and vertical equilibrium at all times. However, it can exceed the soil strength along the slice interface as it does not check the vertical interslice forces against the shear strength of the material. The results should therefore be checked for this criterion.

In the following sub-section, two case examples are discussed that were previously investigated to demonstrate the limitation of using Bishop method due to interlock.

3.2 Case examples

3.2.1 Example 1 (Figure 3.4, Chirapuntu & Duncan 1975)

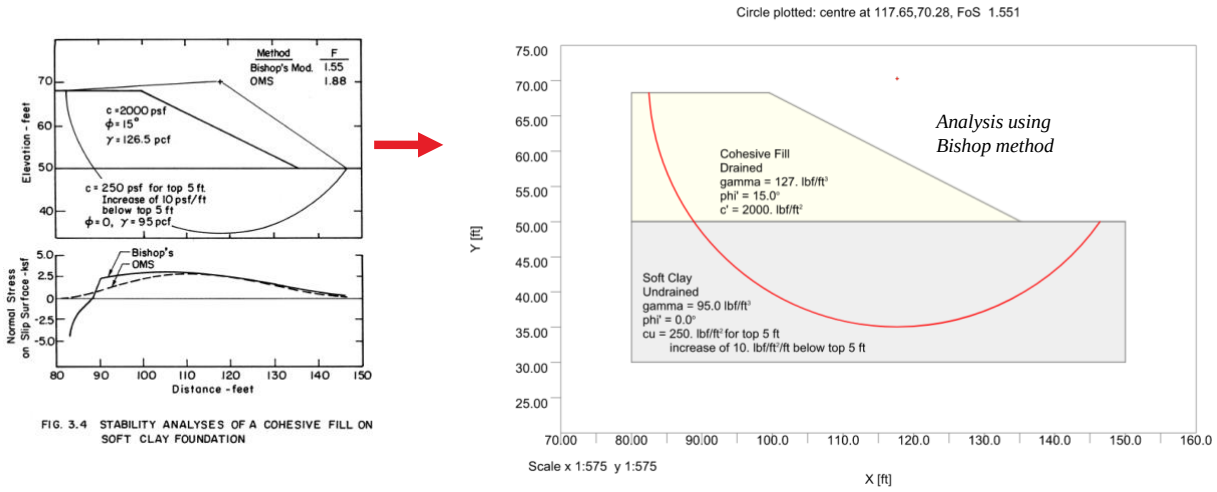

Figure 4: Reproduced model of cohesive fill embankment on soft clay foundation (From Figure 3.4, Chirapuntu & Duncan 1975)

It should be noted that an imperial system of units is used for this example for easier comparison with the original study.

Chirapuntu & Duncan (1975) exemplified the difficulty of employing the Bishop method by investigating the results of slope stability analysis for an embankment made of highly cohesive soil (Figure 4). They performed slope stability analysis, using Ordinary, Bishop and Spencer methods, and noted good agreement between the factors of safety obtained for Ordinary and Spencer methods, while a much smaller factor of safety using Bishop method. The results from the original study are summarised in Table 1.

Table 1: Summary of slope stability analysis for Example 1

Slope analysis method	Factor of safety from Chirapuntu & Duncan (1975)	Factor of safety from Oasys Slope
Ordinary	1.88	1.88
Bishop	1.55	1.55
Arup	-	1.88
Spencer	1.88	Solution did not converge
Morgenstern-Price	Solution did not converge	Solution did not converge

Referring to the formulation for effective normal force at the base of interslice above, we know that a high cohesion can result in a negative numerator, and thereby negative normal force at the base of some slices. This is not reasonable and would lead to the computation of an unreasonably low safety factor value.

This slope case was, hence, replicated and reran on Oasys Slope. The results were found to be consistent using both the Ordinary and Bishop Methods, suggesting successful replication of the model. Interestingly, both Morgenstern-Price and Spencer methods resulted in convergence issues upon rerunning this example, unlike the original study which noted convergence issue for Morgenstern-Price, but not Spencer method. However, it should be noted that the authors also acknowledged difficulty in getting solution when using both Spencer and Morgenstern-Price methods, despite trying several interslice functions. The results are summarised in Table 1.

The model was then analysed using Arup method. A similar safety factor value was noted upon using the Arup method, when compared to the Ordinary and Spencer methods from original study.

Similar trends were also observed when the normal force on slip surface was plotted for the different slope methods. As stated in Chirapuntu & Duncan (1975), the unreasonably low factor of safety from Bishop can be attributed to the fact that the effective normal force on the bases of most of the slices in the fill are negative, shown in Figure 5.

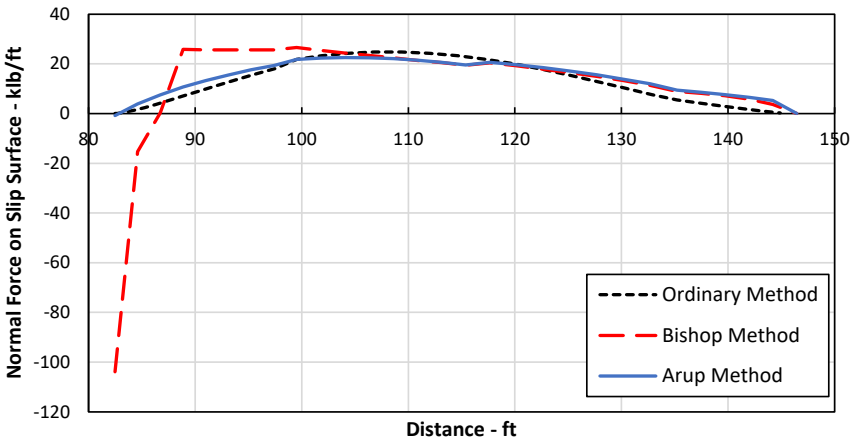

Figure 5: Normal force on slip surface against slope distance

3.2.2 Example 2 (Figure 11, Low 1989)

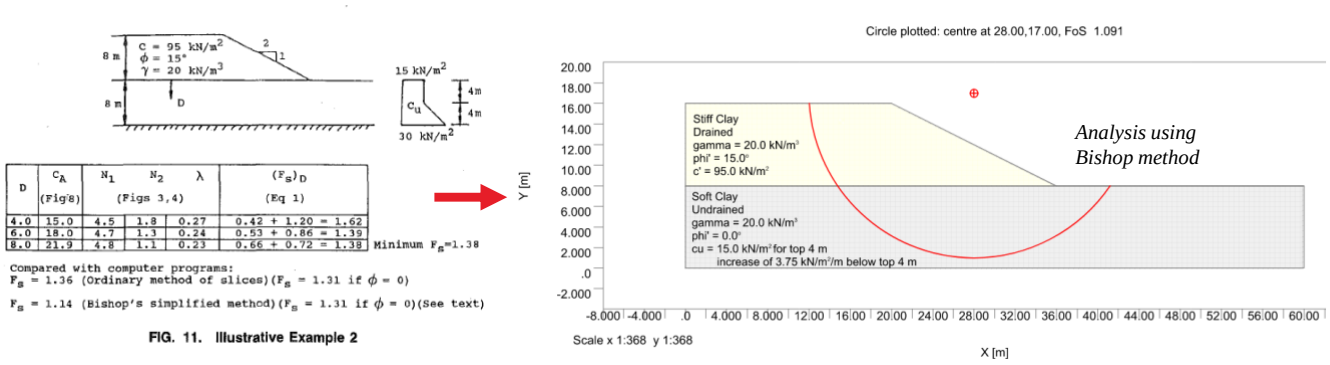

Figure 6. Reproduced model of stiff clay embankment on soft clay (From Figure 11, Low 1989)

In this 'Illustrative Example 2' from Low (1989), an embankment of stiff clay was constructed on soft clay, and the undrained shear strength of the soft clay was noted to vary with depth (Figure 6). The critical slip surface was determined using a computer program and the critical factors of safety were obtained using both Ordinary method of slices and the Bishop method.

Low (1989) noted a much lower factor of safety given by Bishop method, when compared against hand-calculated safety factor value of 1.38 and the factor of safety computed using Ordinary method. Upon performing sensitivity check of friction angle using Bishop method, an unreasonable trend of increasing safety factor with reducing friction angle was also observed, which led to the conclusion that the safety factor from Bishop method is unreliable. The cause of the error was associated with an interplay between the steeply inclined bases of the slices as well as a high cohesion of the embankment material. In such circumstances, the normal force computed on the base of some slices can be suspected to either be negative or unreasonably large. The results from the original study are summarised in Table 2.

Table 2: Summary of slope stability analysis for Example 2

Slope analysis method	Factor of safety from Low (1989)	Factor of safety from Oasys Slope

Ordinary	1.31	1.33
Bishop	1.14	1.09
Arup	-	1.36
Spencer	-	Solution did not converge
Morgenstern-Price	-	1.41

Hence, the model in this case example was replicated and reran on Oasys Slope. The model, upon rerunning, gave similar results for both the Ordinary and Bishop methods, indicating successful replication. Table 2 shows similar safety factor values of the slope model upon reanalysing using the two approaches. Additionally, the seeming paradox of the increasing safety factor upon reducing friction angle trend was also captured for the Bishop method and is shown in Figure 7.

The slope model was then analysed using the Arup, Spencer and Morgenstern-Price methods as well. Referring to the results shown in the table below, it can be seen that a factor value similar to the Ordinary Method was obtained when using Arup method, while a slightly higher safety factor was obtained when using Morgenstern-Price method. The Spencer method, however, could not converge. A sensitivity analysis was once again performed using Arup and Morgenstern-Price methods, and logical trends of safety factor against friction angle was noted for these methods, as shown in Figure 8.

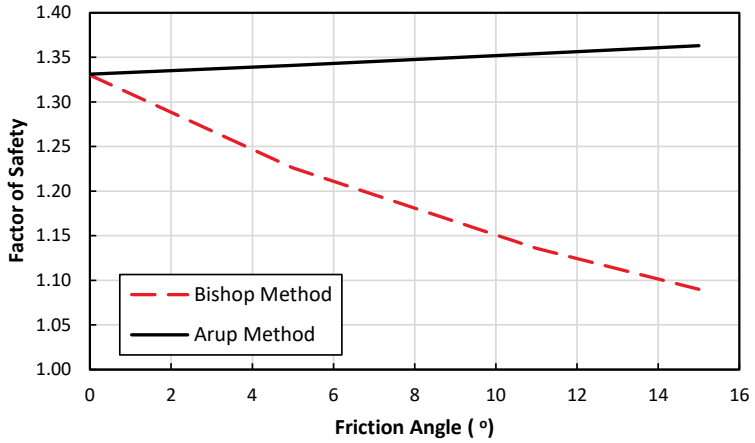

Figure 7. Computed factor of safety under various friction angle values

Hence, it is evident that the Arup method, offered by Oasys Slope, solves slope stability problems involving interlock and gives reliable results. This new feature of enabling the inclination of the interslice forces to vary is indeed a promising step forward towards performing accurate slope analyses and thereby delivering robust slope designs. Similarly, slope designs can benefit greatly if existing design procedures can be streamlined. Fortunately, Oasys Slope does offer designers the opportunity to automate using customised coding. In the following section, the authors will share their experience of developing optimisation tools using Oasys Slope and basic scripting to facilitate their design workflow involving soil nailing.

4 AUTOMATION IN SOIL NAILING DESIGN

Soil nailing is an effective slope stabilization and upgrading method that is widely adopted in Hong Kong. With recent advancements in computation, optimization is possible through rapid parametric study and a streamlining of the analysis process. This section provides a detailed description of soil nail design automation using Oasys Slope and discusses how it leads to an efficient optimization of soil nail design.

4.1 Mapping design workflow

Mapping the existing design workflow can facilitate the identification of areas that can benefit most from design automation. The typical workflow for carrying out slope upgrading design is outlined in Figure 8. The workflow is separated into different stages. First step is the selection of critical section which is obtained based on the desk study and engineering judgement. The geometry and analysis method are then defined in a limit equilibrium program (such as Oasys Slope). Design parameters are entered manually through the GUI (graphical user interface), after which, Oasys Slope performs calculations to determine the critical slip surface and factor of safety for the slope.

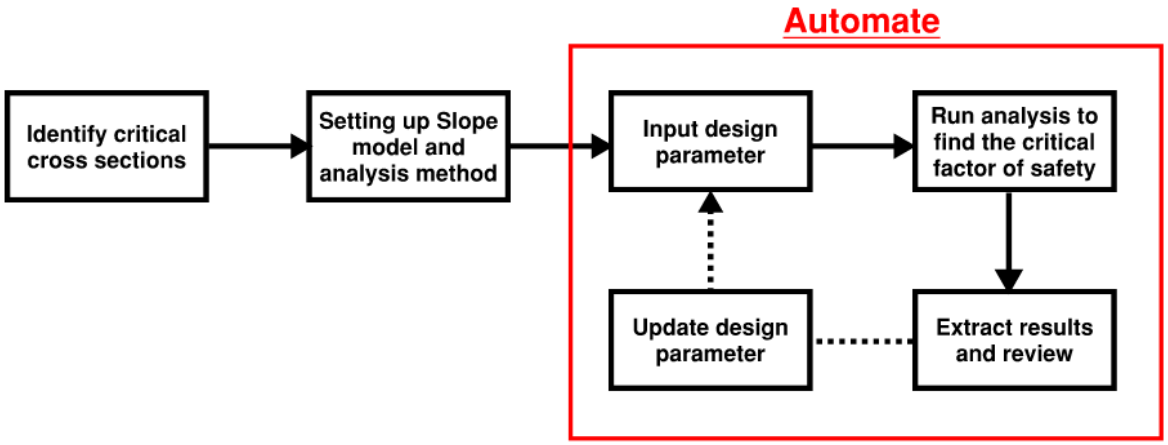

Figure 8: Typical workflow for slope upgrading design

Using the results of the initial analysis, an engineer can determine whether the existing slope stability meets the required safety standards or requires upgrading or stabilization via soil nailing. It is important to note that the process of soil nail design involves several key parameters. For example, there can be multiple combinations for soil nail lengths, diameter, spacing and soil nail angle. In addition, the critical slip surface may change depending on the arrangement, length and other parameters. When soil nails are designed based on analytical approach, involving detailed calculation of bond strength based on specific slip surface, several manual calculations are required and have to updated whenever the soil nail parameters are modified or slip surface changes. Automating this crucial part of the design workflow can greatly assist an engineer and minimize chances of errors due to manual handling.

In Oasys Slope program, a single critical factor of safety is obtained per analysis setup and finding the optimal soil nail arrangement is an iterative process to test different patterns. The developed automation tool provides a way to do this iterative process automatically, through creating data sets in Excel and integrating it with Oasys Slope using scripts to control and run the analyses until an optimal design is found.

4.2 Reinforcement calculation in Oasys Slope

Oasys Slope allows the user to define several different types of reinforcement, including ground anchors, soil nails, geotextiles, and rock bolts. For active reinforcements specified, the forces in the reinforcement are calculated and applied in the analysis in slightly different ways depending on the selected analysis method. The soil nail function in Oasys Slope allows the specifications of the geometry of the soil nail systems, including the lengths, levels, inclinations, and out-of-plane spacing. The tensile capacity of the soil nails can also be specified. The bond strength of each soil nail is derived from the available bond length and the effective overburden stress of the current slip surface. The available capacity of each soil nail is then resolved into vertical and horizontal components, which are applied as surface loads in the calculations of the factor of safety.

Details on how reinforcement calculations are performed in Oasys Slope can be found in Oasys Ltd. (2022).

4.3 Automation with Oasys Slope

Oasys Slope 21.0 includes an API (Application Programming Interface) that allows the user to interact with the program using external VBA or Python scripts instead of going through the GUI (Graphical User Interface). Once the API has been setup, users can pass relevant data to Oasys Slope and remotely run analysis through calling its built-in COM functions. The full list of API COM functions can be found in the program manual (Oasys Ltd. 2022).

This section presents a tool to automate the iterative design process using Visual Basic (VBA) programming language. VBA is complimentary and built into Microsoft Office, thus Excel is chosen as an intermediary to store data and act as a control interface for Oasys Slope through VBA scripts.

Key advantage in using Excel is that design information can be inputted and stored in an accessible and familiar format, RANGE functions within VBA scripts can be used to specify the data input area within each worksheet and feed the data to Oasys Slope through COM functions in the VBA scripts. The same COM functions can be used to extract the output from Oasys Slope once each analysis is completed and pass the data back to Excel, where additional processing, such as applying factors or comparing between the last results, can be done from within Excel easily.

The Oasys Slope analyses are setup to loop within the VBA scripts until the termination criterion is reached. This can be set within excel using a "switch cell", which is an IF statements that compares the analysis result and ends the loop if the conditions are met, for example, if the minimum factor of safety falls below 1.

An optimization function is made for soil nails using VBA, which sequentially modifies each soil nail length by a user-specified interval until the required factor of safety is achieved. Using more rigorous optimization algorithms, by adding additional boundary conditions checks, for e.g., applying soil nail length constraints, or using more advanced search method altogether, such as the gradient descent method, can produce greater accuracy in soil nail design and allow more flexibility in soil nail optimization by allowing alternating nail lengths. Other boundary conditions, such as water table height or surcharge can similarly be manipulated and ran successively by implementing their respective COM functions in the VBA scripts and modifying the termination criteria switch cell within Excel to include their consideration. This enables rapid parametric study to better understand the influence of each factor on the nail design separately.

Outputs can also be extracted by calling the COM functions, which will save the data to sets of variables (e.g. FOS1, FOS2 etc.) to be printed in the user desired format in Excel. The results can then be used for further analysis or presentation of results. For checking of model analysis, COM functions can command Oasys Slope to save a new .sbd file after each iteration in the loop as record.

An outline of the automation framework is shown in Figure 9.

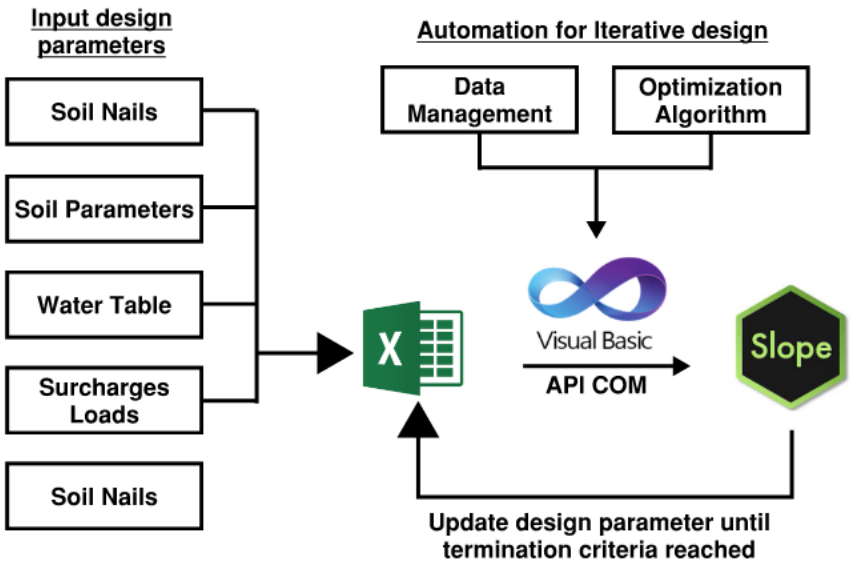

Figure 9: Oasys Slope automation framework

4.4 Benefits of automation

By enabling data to be passed automatically to and from Oasys Slope, efficiency in carrying out analyses is substantially increased. This allows a large number of design scenarios to be analysed through iterative looping and setting different termination criteria.

Increased model output allows a more comprehensive understanding of the slope's condition to be visualized, an example is demonstrated below with the relationship between soil nail length and critical factor of safety. This also serves as a sensitivity check and similar reference data can be extracted from each iteration of the model to lend more confidence to the engineer's design.

Designers can create a data set of parameters from envisioning the possible design conditions and quickly analyse all of them through the automation tool. The tool can automatically find solutions that satisfies multiple design constraints with high precision, in addition, the automation also removes the need to manually input data into each model through the GUI, reducing the chance of human error, resulting in overall higher accuracy.

Optimization algorithms can be implemented within the automation framework, allowing the engineer to refine their designs automatically. However, it should be noted for soil nail design, various nail patterns can give the same factor of safety. Having a good understanding in the selected optimization algorithm as well as exercising engineering judgement to determine a reasonable nail pattern will be required to produce more feasible design.

Nevertheless, the automation is still capable in producing, if not exact, then a very close first estimate of slope upgrading works required, streamlining the soil nail design process. The framework can also quickly produce updated results in the event of design parameter changes, promoting flexibility.

Ultimately, using the automation for slope design is expected to produce optimized and high-quality designs in less time.

4.5 Demonstration of Soil Nail optimization using automation

An example is shown in Figure 10 below to demonstrate the automation's capability to optimize soil nail design and produce large number of models for sensitivity checking.

The given feature is part of a project to assess the effects of varying soil nail lengths on slope factor of safety. The feature's geometry and design parameters were reviewed from desk study and setup in Oasys Slope.

The procedure to carrying out the soil nail optimization was as follows:

1. The material and surcharges were tabulated in Excel and passed to Oasys Slope through COM functions.

2. Two base versions of the Slope model, one with a design water table and the other with a worst ground water table was created to check for both cases.

3. Specified slip surfaces were setup to distinguish the critical slip more clearly and to reduce the run time, though it is possible to use grid and radius method with the automation.

4. The soil nails were optimized through reducing each nail's length incrementally by 1m using WHILE loops in VBA until required factor of safety is reached.

5. The Factor of safety for each of the soil nail patterns tested in the analysis loop are extracted to Excel and plotted to generate a full relation between soil nail length and the critical factor of safety for each of the water table cases, shown in Figure 11 and 12.

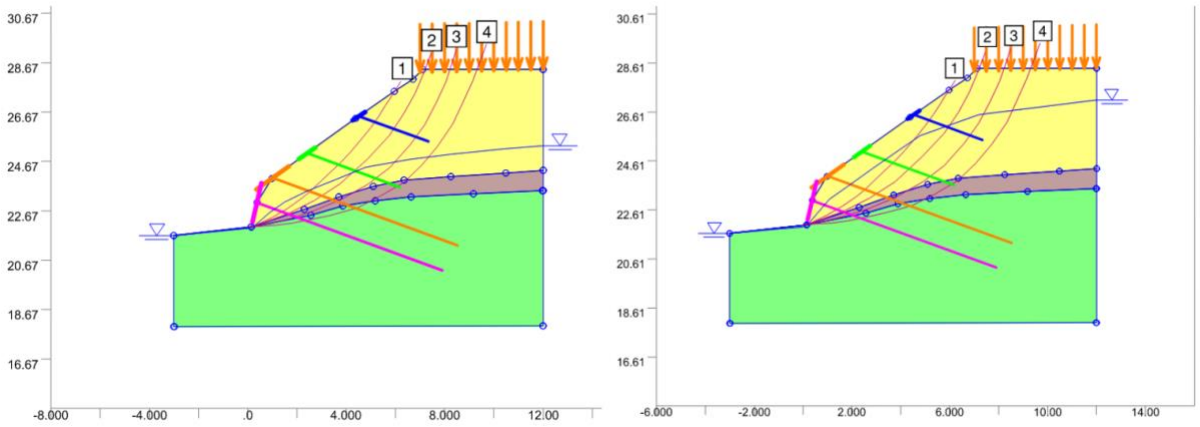

Figure 10: Feature with soil nails setup in Oasys Slope

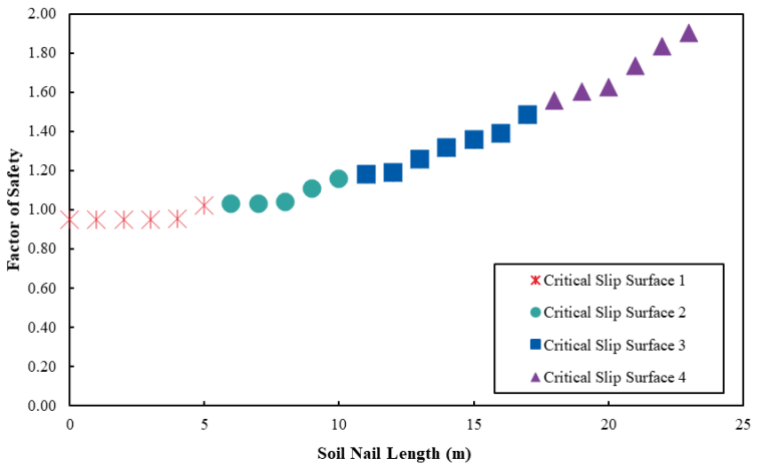

Figure 11: Soil nail length against factor of safety (1-in-10 design ground water table condition)

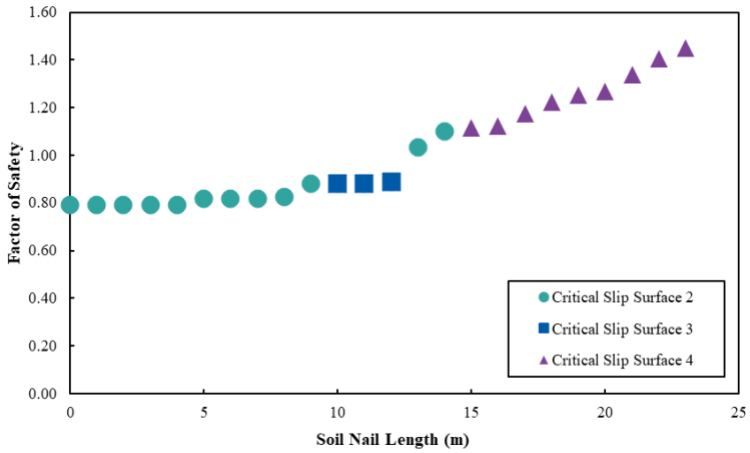

Figure 12: Soil nail length against factor of safety (predicted worst ground water table condition)

A total of 48 combinations of soil nails were analysed with the automation. A complete behaviour can be obtained from plotting the data, it can be observed that for the 1-in-10 design water table case, the factor of safety increases linearly with increasing soil nail length. For the predicted worst ground water table case, there is a gap around FOS = 1, attributed to the higher water table and its proximity to those slip surfaces, the automation thus allows us to know if there are sensitive ranges to be avoided during design.

5 CONCLUSION

The use of variably inclined interslice forces in the slope stability analysis (i.e. Arup method) based on limit equilibrium method is presented. Its computer implementation solves slope stability problems involving interlock and gives reasonable results. It is, however, imperative to check the details of a slope stability analysis results to ensure that the solution does not violate the assumptions made in the analysis procedure used. A simple reliance on the computed safety factor alone to a slope problem without scrutinizing other details of a solution should be avoided under all circumstances.

This paper also presented our development of a digitalised workflow for slope analyses that allows streamlining of the analysis process and optimisation through rapid parametric study. The use of Oasys Slope software along with customised coding enables automation of the design workflow and optimisation of soil nailing design.

REFERENCES

Bishop, A.W. 1955. The use of the slip circle in the stability analysis of earth slopes. Géotechnique, 5(1): 7-17.

Chirapuntu, S. & Duncan, J. M. 1975. The role of fill in the stability of embankments on soft clay foundations. Geotechnical Engineering Report No. TE 75-3, University of California, Berkeley.

GEO. 2007 Review of limit equilibrium methods for soil nail design. GEO Report No. 208

Janbu, N. 1957. Earth pressures and bearing capacity calculations by generalized procedure of slices. Proc. 4th International Conference Soil Mech. Fdn. Engng., 2: 207-212.

Low, B.K. 1989. Stability analysis of embankments on soft ground. Journal of Geotech. Engng., 115(2): 211-227.

Morgenstern, N.R. & Price, V.E. 1965. The analysis of the stability of general slip surfaces. Geotechnique, 15: 79-93.

Oasys Ltd. 2022. Slope 21.0 Manual.

Spencer, E. 1967. A method of analysis of embankments ensuring parallel interslice forces. Géotechnique, 77: 11-26.

Whitman, R.V. & Bailey, W.A. 1967. Use of computers for slope stability analysis. International Soil Mech. Fdns. Div. Am. Soc, Civ. Engrs., 93(4): 475-498.

Whitman, R.V. & Moore, P.J. 1963. Thoughts concerning the mechanics of slope stability analysis. Proc. 2nd Pan American Conference on Soil Mech. and Fdn. Engng., Brazil, 1: 391-411.

Wright, S.G., Fred H.K. & James, M.D. 1973. Accuracy of equilibrium slope stability analysis. Journal of the Soil Mech. and Fdn. Div., ASCE, 99(10): 783-791.

Advancement in Geotechnical Practice for Smarter and Greener Projects Delivery

Sammy PY CHEUNG, Lawrence KW SHUM, Raymond CH KOO
Civil Engineering and Development Department, Geotechnical Engineering Office, Government of Hong Kong SAR

ABSTRACT

The disastrous landslides in 1972 proved to be the turning point in the evolution of geotechnical engineering in Hong Kong, as the Government decided to establish the Geotechnical Engineering Office (GEO) to manage the geotechnical hazards. Geotechnical profession in Hong Kong has prospered ever since and over the years, local geotechnical practice has been subtly put together with the collaborating efforts from the Government, academia and practitioners. Geotechnical engineering is a challenging discipline, as it deals with natural material that are highly variable in their compositions, characteristics and engineering properties. Many methodologies and analyses in geotechnical engineering are not exact sciences and have been developed based on experience, simplifications and assumptions. Inevitably, geotechnical practice is embedded with some degree of conservatism to allow for the uncertainties. On the other hand, developments in Hong Kong have always been squeezed into a tight construction programme and are subject to a highly regulatory framework. These constraints may have impeded the advancement of geotechnical practice from innovative perspective. In recent years, the Government has made significant investments on infrastructural developments to compete with other international financial centres. There are increasing demands for the industry to boost the productivity whilst enhancing safety, quality and sustainability in the delivery of construction projects. Maintaining normalcy in geotechnical practice cannot meet the infrastructural investments and demands of society. Innovation in practice has always been a priority in the GEO and this always calls for a paradigm shift to our understanding of the geotechnical practice. The GEO has been working with practitioners, academia and other Government authorities in materialising advancements that would enable a smarter, leaner and greener project delivery portfolio. This paper discusses the rationale and considerations behind some of the advancements that have important benefits in realising leaner and greener construction when executing geotechnical works in site formation, excavation and foundation.

1 INTRODUCTION

Land is valuable commodity and it has long been the Government major revenue. Unfortunately, Hong Kong has a mountainous topography and the scarcity of flat land had plagued Hong Kong since the mid-nineteenth century. In the early days, reclamation on the central harbourfront provided the much-needed land for commercial activities. Hillsides on the Hong Kong Island were also terraced for buildings and roads to provide dwellings for people. The population bloom started in 1950s when Hong Kong began to develop as a manufacturing centre. There was an immense pressure for making more land to support the rapid economic growth and accommodate the population. The rapid surge of population in the 1960s and 1970s had resulted in intense urbanization on the fringes of the hillsides in many parts of Hong Kong. Many new migrants were living in flimsy squatter structures erected illegally on the hillsides. Inevitably, many slopes were formed in association with these hillside developments.

Unlike today geotechnical standards, little attention was given to the nature of soils when filling the valleys or cutting the hillsides in the old days. Slope design was simply a matter of constructing them in accordance with standard details based on experience, which were considered acceptable in most cases. Eves (1913) described road cutting as steep as 75 degree as the practice at that time. The steep cutting had the advantage of having a very small surface exposed to rain, although landslides were frequent. However, as there was little wheeled traffic at that time, landslides did not cause much damage and delay. Pedestrian could climb over the debris, which were often left for weeks. The slope design practice had changed starting from 1950s (Lumb, 1972), as steep cutting behind terraced building sites produced a change in the consequence of a slope failure. Landslide was no longer a matter of inconvenience and there was a real danger of loss of life for dwellers

living at the toe of the steep cutting. Around the post-war years, cut slope was commonly formed to a batter of 10:6 with a berm of 1 to 2 m wide added at every 7.5 m interval in height. If failure occurred during construction, the batter was reduced to 1:1 giving an average slope angle of 40 degree. Fill embankment was formed by end-tipping without much compaction. Chunam plaster was usually applied to the slope surface for preventing infiltration of rainwater into the soils. Weep holes were added in subsequent practice, which allowed groundwater to seeping out of the slope.

Given the rugged topography, seasonal heavy rainfall and slope formation practice in the past, landslides are common in Hong Kong. Records show that more than 470 people have been killed in fatal landslides since 1948. The disastrous landslides occurred in 1972 and 1976 had resulted in more than 160 fatalities and that galvanised the Government's determination to tame the landslide problem in Hong Kong. Thus, the Geotechnical Engineering Office (GEO) was established in 1977 as the centralised regulating body and has been given the mandate to manage the landslide risk. The Slope Safety System formulated by the GEO comprises three main strategies, including (a) regulating the design and construction of new geotechnical works; (b) retrofitting substandard slope and undertaking slope maintenance; and (c) reducing the consequence of landslides. The GEO faced many challenges upon its establishment, as there was an absence of geotechnical community to provide adequate input to the geotechnical works, let alone the sets of acceptable standards to follow. It was, therefore, an important task to set geotechnical standards that best suit local condition and environment. The GEO has a dedicated team with specific role of technical development for production of guidance documents. They include the authoritative series of Geoguides, Technical Guidance Notes, GEO publications and technical circulars, etc. The guidance documents cover a wide variety of pertinent subjects, encompassing geology, ground investigation, slope engineering, excavation and lateral support, foundation and landscaping. Practitioners follow these guidance documents in the design and construction of geotechnical elements which are subject to the regulatory control exercised by the GEO. Besides technical considerations, other administrative matters (e.g. land use planning and zoning) may also influence the technical solutions. Over the years, geotechnical practice has been subtly put together that is unique to Hong Kong.

The construction cost in Hong Kong is amongst the highest in the world, especially when compared with other cities of similar economic scale. The situation is expected to be worsen in the coming years, as the Government is committed to invest heavily on infrastructures and housing developments; and the local construction industry faces many problems such as an aging labour force and escalating inflation. The Government has pushed for the transformation of the construction industry to survive the productivity crush. New digital construction methods are promoted to improve project delivery capability and facilitate offsite construction that reduces reliance on manual labour. Besides these initiatives, there is a narrative that changes in the regulatory control could significantly leverage the productivity gains from leaner construction and catalyze productivity improvement. There is no dispute that construction works are subject to a highly regulatory framework in Hong Kong, which involves the enforcement of the Buildings Ordinance for private developments and the administrative instructions imposed on public works projects. The GEO is certainly part and parcel of this regulatory framework, for the role as the technical advisor to the Building Authority and other Government project offices on geotechnical matters.

The GEO always embraces innovations that can bring advancement to the geotechnical engineering. Whilst most people view innovations as applying novel technologies for new services, innovations also mean implementing new ideas and processes to existing services that leads to productivity enhancement and financial gains. This is particularly relevant to the prevailing geotechnical practice that have different degree of conservatism and perception on safety margin on the design. It is well recognised that not only the geotechnical standards drafted by the GEO but also the interpretation of them by practitioners, including those in regulatory authorities, have profound influence on shaping the local geotechnical practice. The GEO sees that maintaining normalcy in geotechnical practice is not sustainable to satisfy the expectation of society and the productivity gains necessitated for the huge infrastructural investment. It has been opportune that the GEO has been working with practitioners, academia and other Government authorities in recent years, and made advancements in the geotechnical practice that greatly benefit the execution of site formation, excavation and foundation. Some advancements call for paradigm shift on the understanding and rationale of the prevailing practice; and some rest on readjusting the perception on safety margins.

2 RECENT ADVANCEMENT IN SITE FORMATION PRACTICE

2.1 Control of moisture content of fill material at time of deposition

In projects involving substantial filling works, fill compaction is typically controlled by product specifications in accordance with the General Specification (GS) on Civil Engineering Works (CEDD, 2020), where special or general fill material are available and specified by the Engineer. The GS places a restriction, as a compliance condition, on the moisture content (MC) of the fill material to be controlled within ±3% of optimum moisture content (OMC) during deposition. Samples should be collected and delivered to designated laboratory for determining the MC within one hour after deposition. Practitioners raised the concern that the collection of samples and testing the MC at deposition has a great implication on the filling process. In addition, this procedure brings significant workload to the Public Works Laboratory (PWL), which is the only authorised laboratory for conducting compliance tests in public works projects. In the event that the MC at deposition is not determined, the MC obtained in the subsequent sand replacement test (SRT) is sometimes used as a substitute for checking the compliance requirement. Some engineers decided to remove the compacted layer when receiving a non-compliance report based on the MC obtained in the SRT, despite the fact that it did not equate to the MC of the fill material at deposition.

The GEO has taken the initiative to study the effect of the MC on the engineering properties of the fill material compacted to the requirements. Four selected types of fill material were compacted to a target relative compaction (RC) of 95% at different MCs. Triaxial tests were then carried out to study the strength properties (Chung & Chu, 2020). Figure 1 shows the particle size distribution of the four types of fill material used in the study. They were compacted with MC beyond the tolerance of ±3% from OMC. The test results show no evidence that there is appreciable difference on the strength and stiffness of the fill material which is compacted to a target RC of 95% with MC beyond the tolerable range of ±3% OMC. Figure 2 shows the results of the triaxial tests conducted on the compacted samples. The peak friction angles achieved are generally greater than the strength parameters of compacted fill commonly used in the design. Besides, a review of widely adopted local and international specifications on the control of filling works has been conducted. It is found that only the GS for Civil Engineering Works specifies the MC of fill material at deposition as a compliance requirement.

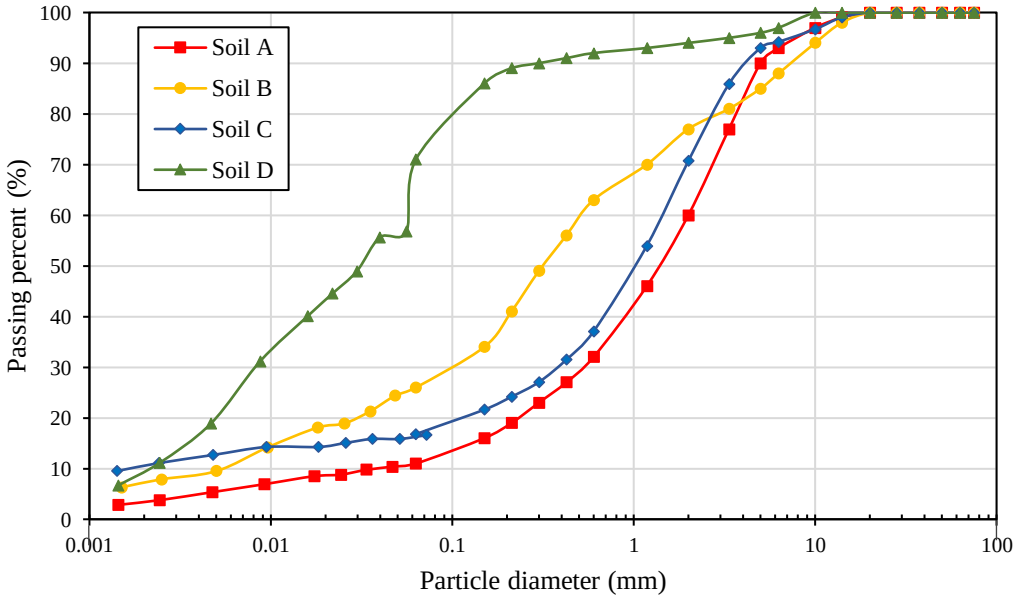

Figure 1 - Particle size distribution curves of the four soils tested

After benchmarking with local and international specifications as well as reviewing the laboratory test results of the selected fill material, it is considered that the compliance criterion on the MC of fill material at deposition is not essential to forming a stabilized fill. Arrangement has been made to remove such specific requirement from the GS.

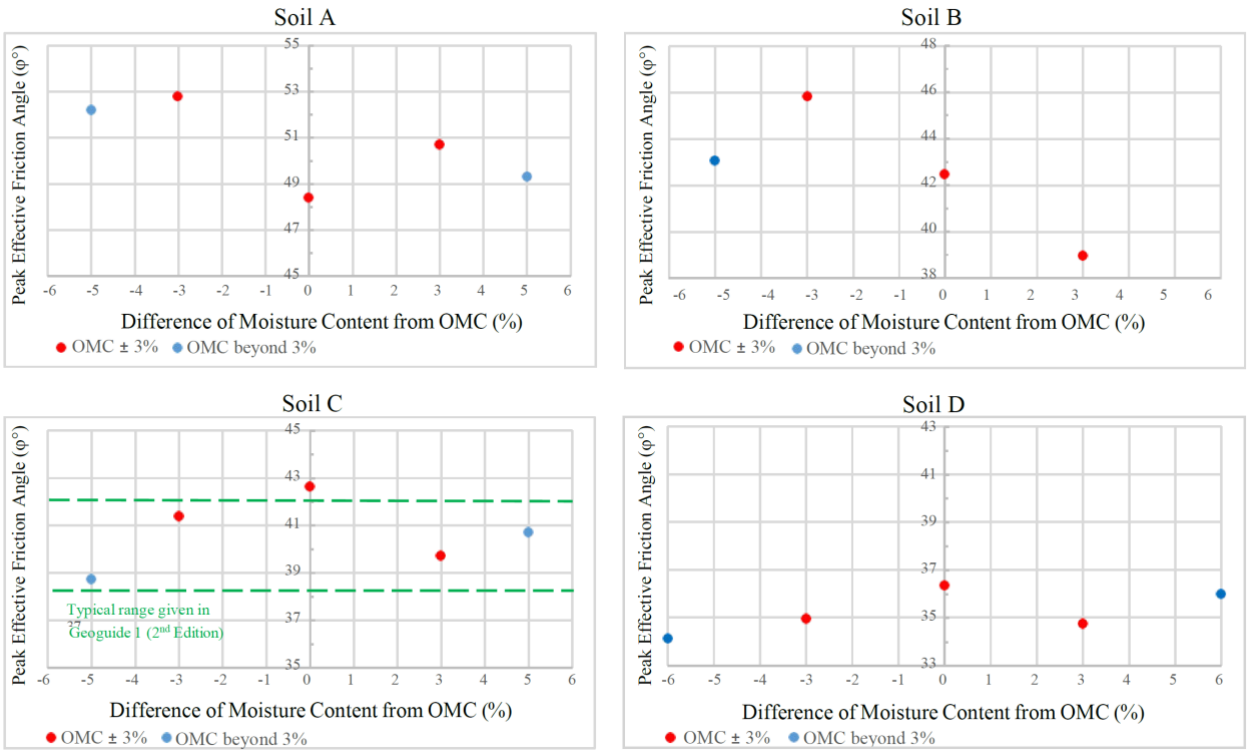

Figure 2 - Variation of effective peak friction angle (φ°) at different moisture content

2.2 Slope with soil nails installed on Government land

In recent years, more sites on hillsides are earmarked for public and private developments, which always necessitate substantial site formation works. It has been the customary obsession by practitioners that all engineering works should be restricted within the site boundary and that has been cast in stone. Permission to install structural support elements (e.g. soil nails) outside the site will rarely be granted by relevant authorities. Such constraint always results in the adoption of costly and extensive bored pile walls along the peripheral of the site.

In fact, such perception is not unique to site formation works for new developments. It has also plagued many slope owners who have been served with Dangerous Hillside Order (DHO) to investigate and upgrade their man-made slopes. In majority of these DHO cases, the slopes are formed along the peripheral of the site boundary to maximize the building areas. Upon completion of the buildings, there is practically no access or space for constructing massive bored pile walls (Figure 3). Installation of soil nails is considered as the only plausible and affordable solution. However, obtaining approval for installing the soil nails outside the lot boundary had deterred many geotechnical professional to pursue this sensible solution. Such problems have profound implications on public safety, as the slope owners or the geotechnical professional engaged would have much difficulty in overcoming these hurdles. The statutory order has specific time limit that requires the slope owner to comply with and it is undesirable to allow the order be extended for a long period of time.

In view of the practical difficulty, the GEO has reached out to relevant Government departments, including Lands Department (LandsD) and Highways Department (HyD), and worked out the principles that could facilitate slope owners to pursue slope remedial scheme with soil nails installed outside the site. In gist, on the advice of the GEO, LandsD would consider positively for applications involving DHO and proactive action by the owner to improve the stability of their slope. On the other hand, the GEO drafted relevant lease clauses to indemnify the Government's right and liability in the event of any damages caused by the lot owner installing soil nails in Government land. In addition, the lease clauses also have provisions on the scenario when the adjoining areas are to be developed and the liability and impact of the construction on the installed soil nails.

Figure 3 – Congested space and access available for upgrading substandard slope

Soil nailing technique has been introduced to Hong Kong since 1980s and the experience suggests that there is little or no maintenance required for soil nails installed in the soil mass. In the newly drafted "Soil Nailing Works Clause", it no longer imposes any maintenance responsibility to the owners regarding any additional area occupied by the soil nails. This relieves the worries of the slope owner on any additional liability, particularly where the land above the soil nails is natural hillside. Similar principle is also acceptable to situation where soil nails are to be installed underneath the public road maintained by HyD. In fact, GEO helped owners and Buildings Department to resolve seven DHO cases that had been held in abeyance for some years, since approval to install soil nails underneath the public road were difficult to obtain. HyD took the same sympathetic attitude on slope upgrading works that would improve slope safety. A general principle has been established that a 3m deep exclusion zone measuring from the road surface is provided in the slope design, where no soil nails should be installed. Figure 4 shows the conceptual stabilisation scheme that was used in slope upgrading works at a Kwun Tong site. The primary objective of the exclusion zone is to provide adequate space for installing and maintaining services and utilities underneath the road pavement.

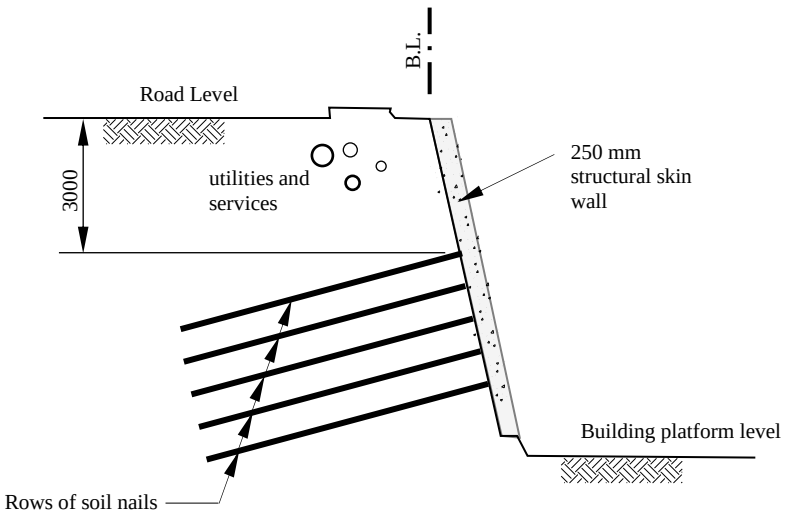

Figure 4 – Stabilization scheme for cut slope abutting public road
with soil nails installed outside lot boundary at Kwun Tong

The same concept has been extended to public works projects, particularly the site formation works for public housing developments, as this involves the public coffers. Substantial saving in cost and time could be achieved if soil nailed slopes, instead of bored pile walls, are used to form the building platforms. The land authority, on the advice of the GEO, will incorporate suitable clauses in the land instrument to define the responsibility for damages and problems associated with the soil nailing works in the Government land. A vivid example of applying this concept involved the site formation works for a public housing at Fanling. With the collaborative efforts from the project office, policy bureau, consultants and the GEO, soil nailed slopes were adopted in lieu of bored pile walls for forming the building platforms. Such optimisation had resulted in 50% saving in cost and 6 months advancement in the programme of the formation works.

In fact, a forward-looking mindset in the planning of development site in hillside can help minimising many geotechnical works. Where new site is identified for development, particularly on the hillside, the proposal is circulated to Government departments for comment and advice. The GEO is usually asked on the views of applicable geotechnical clauses to be included in the land instrument and any geotechnical constraints on developing the site. Besides the usual advice, the GEO now takes a proactive approach to postulate the scenario of geotechnical works that are likely needed for the development and identify any improvement on the site layout that could minimise the geotechnical works. Such consideration should be made even at the planning stage when the zoning proposal is being circulated. Any planning constraint (e.g. rezoning of green belt) should be resolved earlier which, otherwise, may limit the practicality of revising the boundary at a later stage. Figure 5 shows the initial circulation of a proposed land sale site that would be carved from existing hillside. The planner intended to align the lot boundary of the site along the ridgeline of the man-made slope adjoining a public road. However, this would leave a truncated slope that needs to be supported by either a retaining wall or a substantial cut slope within the proposed site. There was no reason for leaving a portion of this slope from technical consideration. Hence, on GEO's advice, the site boundary was moved further southwest to align with the public road. This gives more flexibility on the site formation works to form the platform levels that match the road level and eliminate the need for any retaining structure. Such concept is equally important to engineers when planning the project boundary and the works area required for the project. In determining the land requirement, the engineer should also optimise the site layout, with the focus on minimising the geotechnical works, especially for hillside development where the substantial cutting is always necessary.

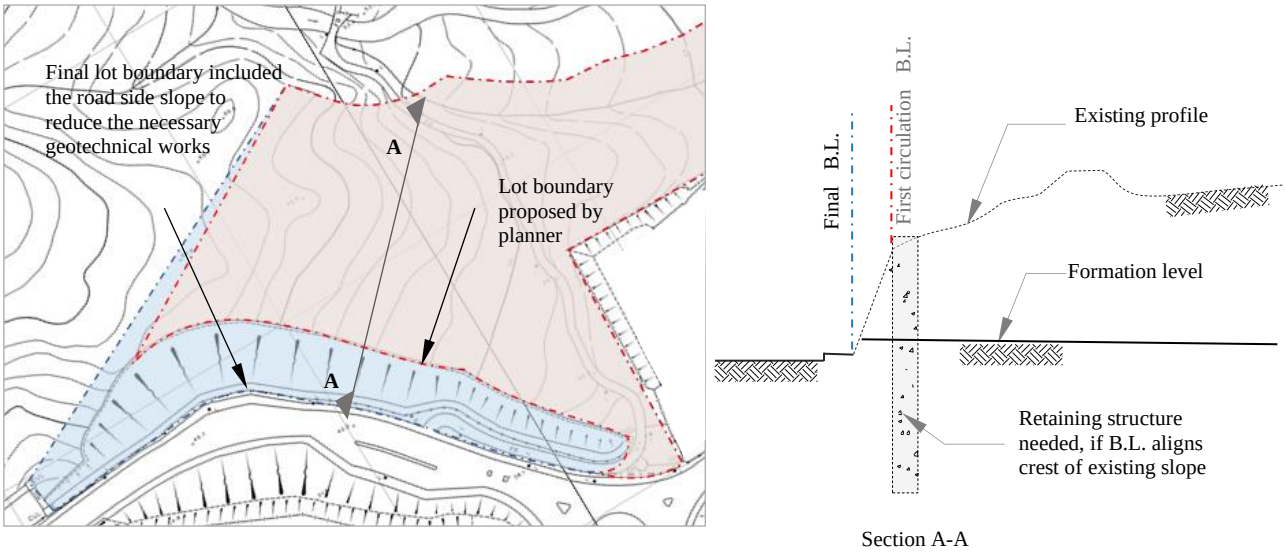

Figure 5 – Smarter planning of the site layout and lot boundary to minimize the geotechnical works necessary for the development

2.3 Soil nails with sustained load

While preference is given to use soil nailed slope in site formation works, there is a need to review the requirements for soil nails subjected to sustained load, in order to facilitate the wider adoption of such scheme. The use of soil nails as structural support to excavation is common in overseas practice. Unlike stabilising existing slope, soil nail that is installed in tandem with slope excavation, is considered to have been mobilised with sustained load during its service life. Concerns on soil nails with sustained load relate to the durability, deformation and creep behaviour. Geoguide 7 (GEO, 2007) transpires these into additional provisions which, amongst other requirements, include the need for monitoring the movement of the soil nails for at least two wet seasons after construction. Some practitioners hesitate on such requirement, as it will bring uncertainty at the completion stage of the project. Any remedial works after the project completion would have huge implication to the users of the land. There was a case in which the engineer decided to form the slope to its final profile and installed the soil nails as a stabilisation measure to an existing slope. As such, it was presumed that the soil nails were installed for stabilizing an existing slope and therefore, the soil nails did not carry any sustained load. The construction sequence was peculiar, as it involved forming the slope at a reduced safety factor and erecting temporary platforms for installing the soil nails. These were riskier operations that could be prevented.

The need for post-construction monitoring was debated when the GEO was preparing the Geoguide 7 (GEO, 2007) in 2005. It was considered at that time that local volcanic and granitic soils generally behave as granular material, but limited data has shown that the plasticity index (PI) of the fine portion of the weathered soils could be higher than 20. This PI threshold has been adopted in overseas design guidelines for fine-grained soils that would exhibit creep displacement in soil grout interface under sustained load. As there was little information on the creep behaviour of local soils, it was decided to include creep test as part of the pull-out test in the construction of soil nails in Hong Kong. The intention was to obtain enough data for further review at a later time. In general, creep potential is considered unlikely when the creep displacement is less than 2 mm per log cycle of time in 6 to 60 minutes period when the soil nail is subject to a constant load.

A review of the creep tests conducted in slope upgrading works under the Landslip Prevention and Mitigation Programme (LPMitP) was carried out. Altogether, 286 no. of tests in different types of soils were reviewed and analysed. Figure 6 shows the distribution of the slopes from which the results of the pull-out tests were collected. The creep tests followed the procedures as stipulated in the Geoguide 7 (GEO, 2007) and creep extension was measured between 6 to 60 min with the nail force maintained at T_{DL2}. T_{DL2} is the design load of the soil nail with a safety factor on bond friction. Figure 7 depicts the extension of 143 soil nails at the creep test stage. The observed maximum creep displacement over this period is less than 0.1 mm, which is well below the 2 mm extension as the creep potential threshold. All creep tests reviewed so far do not show any creep potential of concern.

In the control framework for soil nails with sustained load, deformation analysis is required to investigate the effect of movement caused by the slope engineering works when there are sensitive receivers in adjoining ground, such as buildings and utilities. This is similar to other construction activities, e.g. excavation and lateral support works and foundation works, to ensure that the movements induced are within the tolerable limit of the sensitive receivers. Monitoring the deformation of the soil nails is reasonable within the construction stage but long-term monitoring is considered not necessary for the creep behaviour.

Given the preliminary finding on the review of creep tests, it appears plausible to dispense with the post-construction monitoring. In fact, pull-out tests and creep tests are usually carried out prior to the construction of the working soil nails. Therefore, there is an opportunity to identify any creep potential of the soil nails and implemented precautionary measures to address this problem, e.g., increasing the number or the bonded length of the soil nails to reduce the bond friction, or installing the bonded section at different type of soils where possible. The GEO will complete the review with more creep tests on different types of soils before concluding on the requirement of this post-construction monitoring. As a simple clarification, this post-construction monitoring should not be applicable to soil nails socketed in rock.

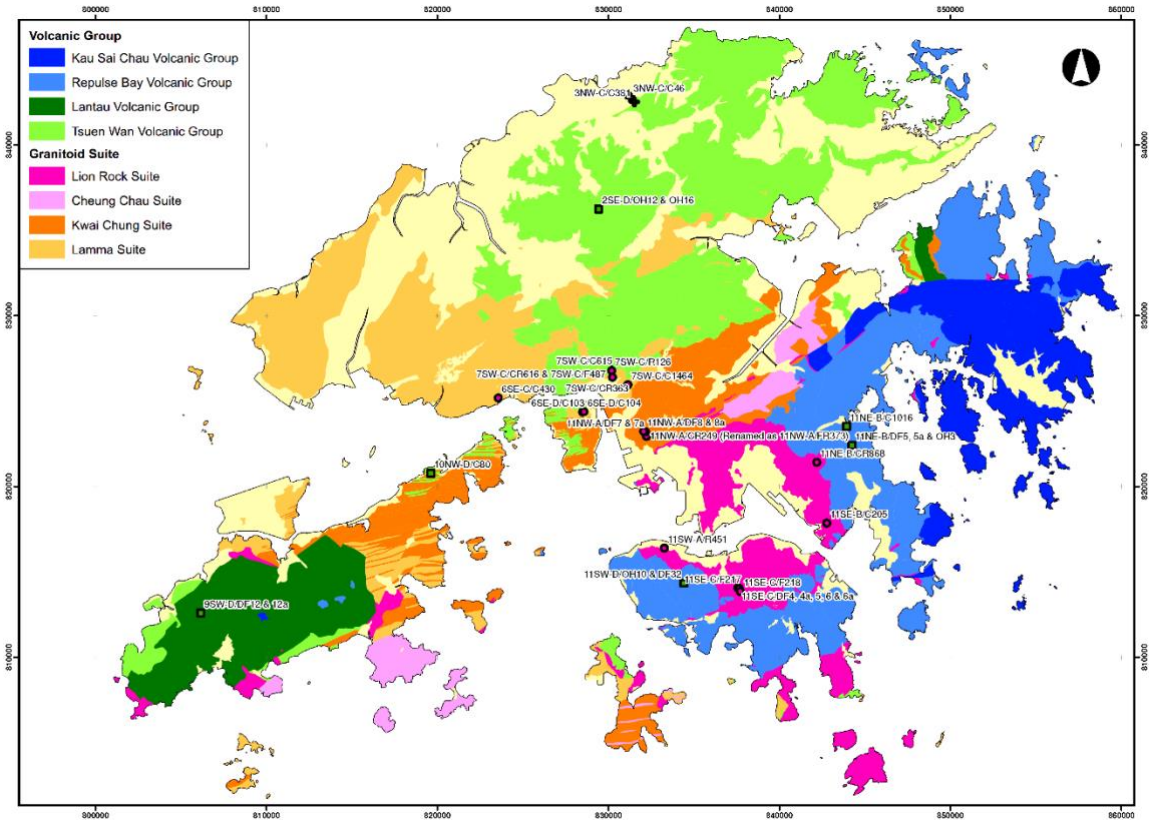

Figure 6 – Review of pull-out tests of soil nails installed in slope upgrading works

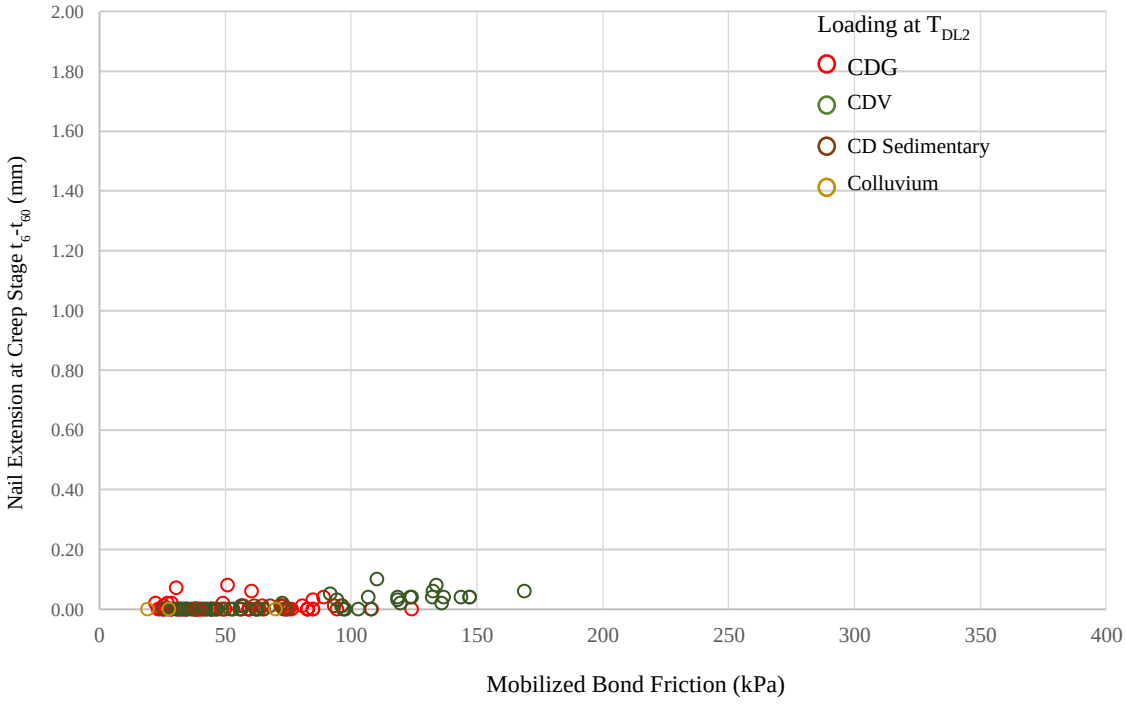

Figure 7 – Creep extension of soil nails at T_{DL2} loading stage between t_6 and t_{60}

3 RECENT ADVANCEMENT IN DEEP EXCAVATION PRACTICE

GCO Publication No. 1/90 (GEO, 1990) provides a review of the state-of-the-art practice of the design methods for excavation. Since its promulgation in 1990, it has been used by practitioners as a key reference document in excavation design. However, there have been much advance in the design and construction of excavation methods since then, notably the application of Partial Factor Method (PFM) as stipulated in the CIRIA Report No. C580 on Embedded Retaining Wall – Guidance on Economic Design (Gaba et al. 2003) published by the Construction Industry Research & Information Association (CIRIA C580). The Buildings Department has imposed additional provisions for using the guidance given in CIRIA C580 to suit local setting and limited experience at that time (BD, 2012). In 2017, a review of the excavation practice was carried out by a task force led by the Geotechnical Division of the HKIE, which made explicit recommendations for the advancement of practice in excavation design and construction. The GEO is currently revising the GCO Publication No. 1/90 and will take cognizance of the recommendations. The revision is supported by a working group comprising practitioners and representatives from relevant government departments. The revised publication is scheduled for completion in 2023. The debate and rational on some of the advancements and improvements that would be promulgated in the revised publication are documented below.

3.1 Additional provisions on application of partial factor method

The new publication will incorporate the application of the PFM in the design of excavation works, which are largely based on the experience of using CIRIA C580 with additional provisions as given in the Practice Notes No. PNAP APP-57 (BD, 2012). This will also incorporate relevant recommendations given in the updated version of the guidance (Gaba et al, 2017). Having gained much experience in the application of PFM since 2011, practitioners and the GEO generally agreed that certain additional provisions as stipulated in Practice Notes APP-57 could be dispensed with. These include the requirements for a post-construction performance review, sensitive analysis of collapse or excessive deformation caused by incorrectly installed strut.

When executing geotechnical works, a fundamental principle is that their performance should be continuously monitored during the construction stage and compared with the design assumptions, especially any variation to the ground conditions. Precautionary and remedial measures should be implemented timely where necessary. The regular review is usually undertaken by the senior professional of the designer's firm under the qualified supervision system. Thus, post-construction review of the temporary ELS works does not provide any value-added benefit in safeguarding public safety.

A high standard of quality supervision is put in place in local construction projects to ensure that the works are carried out in accordance with the approved construction sequences. The risk of incorrectly installed strut should be managed by proper site supervision, rather than relying on the tolerance provided in the design. Similarly, better site management should be imposed to guard against any accidental removal of struts. In recent years, it has been common to adopt innovative solutions to manage construction risks, e.g. sensors and alarm system that could provide warning to the operator of the possibility of hitting nearby person and other machinery. In fact, such worries on irregularity should not be applied to design method based on PFM only.

3.2 Rock socket design

Geoguide 1 (GEO, 1994) stipulates that, where no adverse rock discontinuities are identified in the ground investigation, the rock socket depth should be designed based on preventing bearing failure of the rock mass. However, in practice, discontinuity-controlled failure is often considered by assuming the presence of the most adversely oriented discontinuity. It is mainly because rock discontinuity survey is seldom conducted at the ground investigation stage and designer is indifferent to the missing of such important piece of information. In some cases, even rock discontinuity survey is conducted and major joint sets identified, some practitioners and regulating authority still question the possibility of the presence of individual yet adversely oriented discontinuity that could be missed by the survey. Such perception often resulted in excessively conservative design of rock socket length.

In the revised publication, the importance of conducting rock discontinuity survey at the ground investigation stage is reiterated, when it is anticipated that the embedded wall will penetrate the rock formation for stability. Without such information, it would be difficult to make a proper engineering judgement as to the presence of any adverse discontinuity that would affect the stability of the embedded wall. A high concentration of discontinuities in a stereo plot should be the evidence indicative to the potential of persistence of that joint set (Figure 8). The rock cores should be inspected and the weathering condition of the discontinuity also tells the likelihood of its persistence.

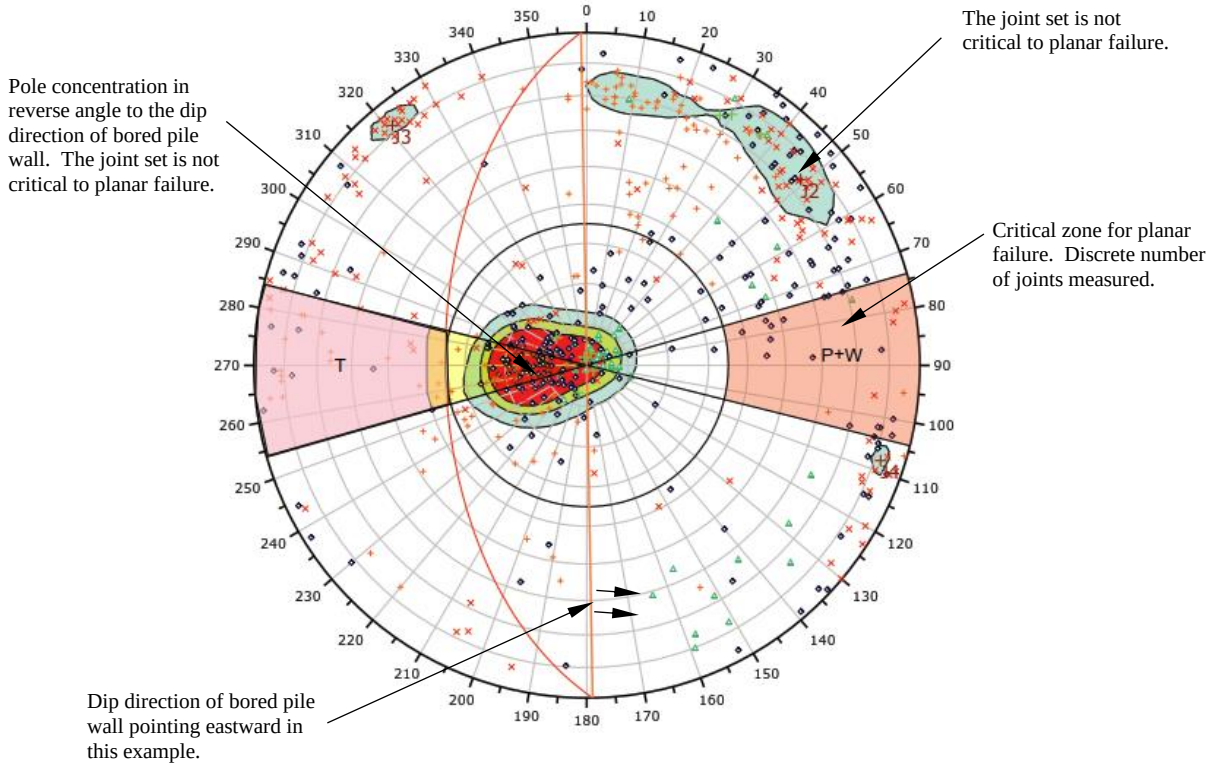

Figure 8 – Rock discontinuity survey to identify critical discontinuities for assessing the likelihood of discontinuity-controlled failure

In a recent site formation project involving the use of bored pile walls socketed into slightly and moderately decomposed tuff, the initial design assumed the presence of the most adverse joint at an inclination of about 16 degree to horizontal, although there were results of rock joint survey. The design included a discontinuity-controlled failure analysis following the recommendation of Geoguide 1 (GEO, 1994) and a socketed length of about 20 m was proposed for a 15 m cantilevered bored pile wall. It is interesting, yet difficult to comprehend, to note that the length of this assumed persistent discontinuity would run into more than 150 m in horizontal distance for a 6-degree discontinuity plane, which was considered as an exceptional joint set. In assessing the likelihood of such failure mechanism and its stability subject to the horizontal load from the embedded wall, the building load or foundation piles will certainly give confidence on whether such a discontinuity-controlled planar failure is plausible. Figure 9 shows the section of the bored pile wall scheme that could help the engineer in making sound engineering judgement on the potential of such individual persistent rock discontinuity-controlled failure. A holistic assessment of the likelihood of such failure is important to derive a sensible and cost-effective solution. In this project, the GEO has proactively engaged the designer to revisit the assumptions and review the rock discontinuities pattern. The collaborative effort has resulted in reduction of the rock socket lengths of the bored pile wall.

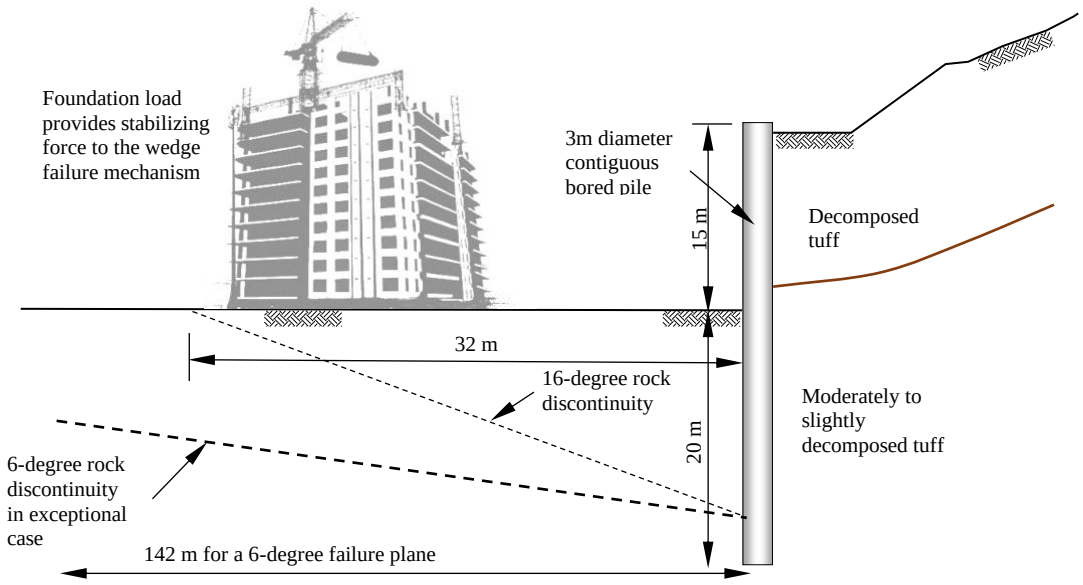

Figure 9 – Holistic assessment of the likelihood of wedge failure due to presumed adverse rock discontinuity plane

3.3 Pumping test for deep excavation

Full-scale pumping test is often specified with the presumption that it is used for validating the permeability of the soil mass assumed in the groundwater seepage analysis prior to bulk excavation. However, majority of the pumping test was, in fact, used to conclude the insignificant effect caused to adjoining area by the dewatering, rather than review the assumption of the soil mass permeability. A major disadvantage of such arrangement is that dewatering would induce significant lateral deflection to the embedded retaining wall, particularly for deep excavation projects. In urban setting where excavation is commonly surrounded by sensitive structures and utilities, e.g. old buildings on shallow foundations, MTR facilities, gas mains etc., it is more desirable and prudent to adopt construction sequences that would minimise any ground deformation. However, there is currently no clear guidance on when such a field validation is necessary and full-scale pumping test is conducted indiscriminately, even for ELS works that are primarily designed as a 'dry' excavation, for which the design intent is to cut-off water seepage into the excavation. There seems to be no real benefit of conducting pumping test to prove the permeability and seepage quantity for such a 'dry' excavation system. For ELS works, it is almost mandatory to implement an instrumentation and monitoring scheme to ensure that the excavation works will not cause any damage or adverse effect on adjoining ground, facilities and structures. Therefore, any adverse effects due to dewatering would be safeguarded by the monitoring and action plan at the bulk excavation stage. Dewatering carried out in tandem with the strut installation can reduce the lateral deformation of the embedded retaining wall. The necessity of conducting a full-scale pumping test prior to bulk excavation should be carefully assessed and is not preferred in excavation system where it is designed to be fully enveloped with an impermeable barrier.

Where the engineer considers desirable to conduct a full-scale pumping test, there is a potential saving by streamlining the test procedures. At present, the procedures in pumping tests for excavation works involve holding the steady state seepage condition for a 72-hour period, before allowing the recovery of the groundwater table. A review of 24 pumping tests conducted in recent deep excavation projects was conducted to explore the necessity of holding the steady stage seepage for such a long period. Figure 10 shows the normalised dewatering curves extracted from the reports of these pumping tests. The steady state seepage condition, once achieved, remained stable for the entire steady state seepage to 72 hours. Unlike the purpose of water yield test, the pumping test is not meant to determine the continuous extraction rate for a prolonged period. Therefore, it has been proposed in the revised publication that the holding period for steady state seepage could be reduced to 24 hours. This allows the commencement of recovery stage at an earlier time.

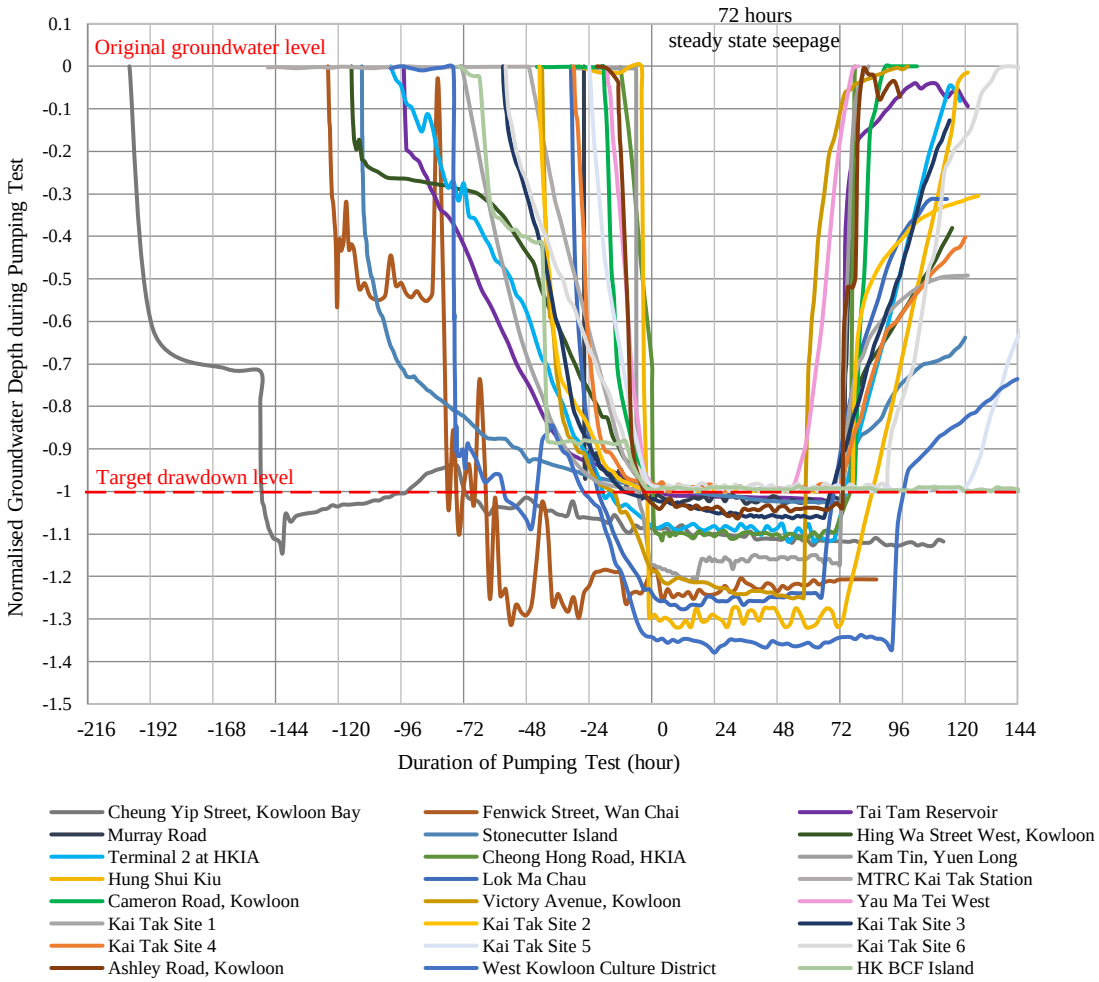

Figure 10 – Consolidated plot for performance of dewatering during pumping test results

3.4 Response and control mechanism on ground settlement

ELS works need to be cautiously carried out to ensure that the induced impact on the nearby sensitive receivers is kept within an acceptable level. A three-tier triggering control mechanism, i.e. Alert-Alarm-Action (AAA) Levels, with corresponding response actions is usually specified to forewarn any excessive ground movement and safeguard the sensitive receivers during construction. At Action Level, the control mechanism usually calls for suspension of all site works. Works suspension is very disruptive on the construction programme and always produce a negative impression to the public on the engineers and the project proponent.

A performance review of recent deep excavation projects was conducted. The projects were selected based on the availability of quality monitoring data. It is found that the ground settlement induced by the ELS works generally varied from 0.3% to 0.5% of the maximum excavation depth, depending on the compactness of the soils, excavation system and construction sequences. In recent years, private developments always include a basement for the benefit of concession in gross floor area. Hence, it is common to find development projects with a 2 to 3-level basement that typical involve 20 m excavation. If the empirical value of 25 mm is still adopted as the Action Level for ground settlement, there is a high possibility that this Action Level would be breached at certain stage of excavation. Some designers took the risk and looked for negotiating with relevant stakeholders and authority when this Action Level was reached. However, it is highly undesirable to have an excavation with active dewatering maintained for an extended period of time, which will prolong the risk of affecting the nearby facilities. Also, it would bring uncertainty to the construction programme, as there were many cases that it took months, if not years, to get approval to recommence the project. On the other hand, the

relaxation of the Action Level is often accused by the public of moving the goalposts and this has a definite negative impact on the professional image of all parties involved in the project.

Some designs strengthened the support systems (e.g., using preload of more than 1,500 ken/m or putting strut layers at every 1.5 m vertical intervals) to meet the empirical limit. However, this will not only give rise to overdesign and end up with increased construction cost and time, it may even result in a counterproductive design that will bring constructability and safety issues. For example, the installation of longer or larger pipe piles involves the use of compressed air, which could pose construction risks to workers or the public, if the boring operation is not properly controlled. There are few incidents that were caused by deep excavation works as documented in GEO (2020). The preloading of the strut would induce reverse deformation of the embedded retaining wall and there had been reported cases of breakage of welding connections for those struts and walings installed at the earlier stages and at higher levels.

Based on past records, many excavations were suspended due to the exceedance of the Action Level for ground settlement of 25 mm, rather than the building structures which are commonly supported on deep foundations. Carriageway, pavement, footpath and playground surface can be readily repaired in case there are serviceability concerns (e.g. cracks or uneven surface). Therefore, it is sensible to understand the serviceability limit of road and pavement and the recommended repair strategy, such that a reasonable response could be formulated.

The Guidance Notes for Road Inspection Manual (Report No. RD/GN/016C) (HyD, 2016) recommend that depression larger than 20 mm may pose a safety hazard to pedestrians and repair works should be carried out if necessary. On the other hand, there may be concern on the integrity of the paving material when there is significant ground settlement. The National Standards of the People's Republic of China published the Specifications for Design of Highway Subgrades (JTG D30-2015) (MOT, 2015) and recommend the allowable differential settlement between bridges and road abutment to be 100 mm and total settlement of 300 mm for general road pavement for carriageway. These guidance documents provide the basis for proposing a more representative value on when repair to the road and pavement is considered necessary.

In fact, the control mechanism can be devised to address two separate issues. One is primarily related to the serviceability issue, e.g. driving comfort and pedestrian safety, distorted utilities. Repairing the ups and downs of the road or pavement could be easily completed at affordable time and cost. It takes few hours to open up the road and repair any leakage of drains and water mains. A smarter arrangement for addressing these concerns is to put in place a good communication with the relevant stakeholder (e.g. HyD maintenance party) to agree the actions necessary (e.g. repaving the pavement or readjusting the distortion of settled services) when the serviceability limit (e.g. 20mm) has been reached.

The other issue comes to play when the estimated ground movement has been exceeded, which cast doubt on the design assumption and the overall stability of the ELS works. Usually this limit will be higher and is comparable to the value of 0.3% of the excavation depth; or when the tolerable limit of the ground settlement has been reached. Under such circumstance, no further construction activities that will aggravate the ground settlement should be carried out near the identified safety hazard area. Investigation and design review should be carried out to find out the cause, estimate further movements and assess the impact to the nearby sensitive receivers based on the performance of ELS works. Such investigation should also look for the presence of any underground voids and cavities caused by the excavation works. However, it is important to note that works that are contributing to the stability or performance of the excavation system, should be continued. There were many cases where all works were suspended at the stage where the walings and struts were yet to be properly installed. They were important to safely transfer the load across the excavation.

Such control mechanism is more practical and sensible. It should avoid setting an unrealistic Action Level on ground settlement that is bound to be triggered. The repair work would be carried out anyway, but at a much-controlled manner, rather than under a situation where the site works are suspended and public announcement made.

4 RECENT ADVANCEMENT IN FOUNDATION PRACTICE

GEO Publication No. 1/2006 gives technical guidance on the design and construction of foundations and some recommendations were based on the Code of Practice for Foundation (CoPF) (BD, 2004). In 2017, Buildings Department published the second edition of the CoPF and as a consequential change, the GEO considers that there is a need to update the publication to align the technical standards for private and public projects. In addition, it is also opportune to enhance the guidance to improve the productivity and economy of foundation works, as the industry has carried out many studies and instrumented pile loading tests since 2006.

4.1 Presumed bearing capacity on igneous rocks

The publication gives recommendations on the presumed allowable bearing capacity and bond friction for foundations rest on different categories of igneous rocks, which follows the CoPF (BD, 2004). Practitioners always question whether higher allowable presumed bearing capacities could be adopted, which are used in other places with similar geological formations and foundation practice, particularly for competent rocks such as Category 1(a), 1(b) and 1(c) igneous rocks. The prevailing guidelines given in the publication for the presumed allowable bearing capacity are 10,000 kPa, 7,500 kPa and 5,000 kPa, respectively.

In order to explore the feasibility of enhancing the bearing capacity, the instrumented pile loading tests that were conducted since 2006 were collected and consolidated into the pile database documented in the publication. The pile database now comprises more than thirteen cases of instrumented pile loading tests founded on igneous rocks. Figure 11 presents the proven bearing capacity from these instrumented pile loading tests versus with the uniaxial compressive strength (UCS) of the rock mass underneath the founding level of piles. In addition, the instrumented piles that were founded on Cat 1(b) and Cat 1(c) rocks are also labelled for reference.

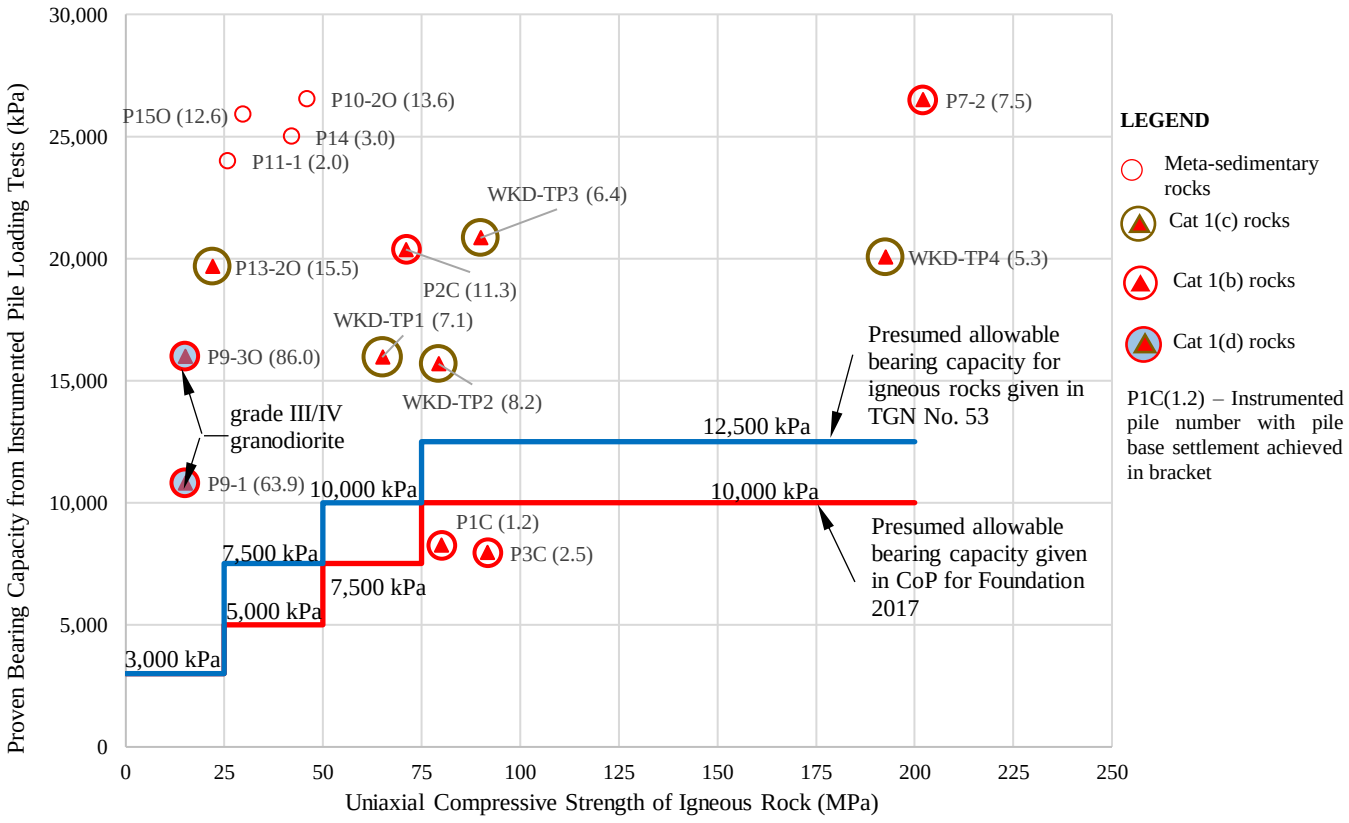

Figure 11 – Presumed allowable bearing capacity for foundations on igneous rocks (TGN No. 53, (GEO, 2022))

Based on the instrumented pile loading test data and the interpretation reports of these pile loading tests, the measured settlements at the pile base ranged from 1.2 mm to 15.5 mm for piles founded on Cat 1(c) or better rock, with the maximum pile base settlement less than 1% of the base diameter. Most of these pile tests indicates a low mobilisation of the bearing capacity, that were attributed mostly to the limits of the kentledge load or the capacity of the Osterberg load cell set up for the tests. For example, pile loading test Nos. P1C and P3C only recorded 1.2 mm and 2.5 mm base settlement when the maximum kentledge load had reached. It is anticipated that much higher bearing capacity would be proven, should a larger kentledge load be provided. Most of the proven bearing capacity for piles founded on Cat 1(c) or better rock was well above 15,000 kPa, except pile test Nos. P1C and P3C as explained above. It is obvious that there is still a significant margin for increasing the presumed bearing capacity for foundations rested on competent igneous rocks.

The settlement of foundation founded on Cat 1(b) and Cat 1(c) rocks has been estimated with the circular loaded area ranging from 1 m to 4.5 m in diameter, which covers the common dimensions of bored piles used in Hong Kong. The settlement computed for applying 7,500 kPa on Cat 1(c) is about 21 mm for a pile with a base dimension of 4.5 m. This corresponds to a mobilisation ratio of only 0.46% of the width of the foundation. The maximum settlement computed for applying 10,000 kPa on Cat 1(b) rock is about 8 mm for the same dimension of loaded area. In the estimation, it is assumed that rock within 600 mm from the founding level should not be non-intact (i.e., the rock cores are not fragmented). Highly decomposed materials are assumed to be existed at the top of each 1 m core length. The settlements computed are the upper-bound values, as the most unfavourable distribution of weaker material and the lower bound rock modulus of 5 GPa for igneous rocks based on Geoguide 1 (GEO, 1994) are adopted in the computation. The settlements estimated are less than 1% of the foundation width, for the increased bearing pressure of 7,500 kPa and 10,000 kPa on Cat 1(c) and Cat 1(b) rocks, respectively.

For foundations founded on fresh rock satisfying the Cat 1(a) rock that composes of strong to very strong igneous rock with 100% TCR of rock with UCS greater than 75 MPa, there is hardly any base settlement needed to be assessed. An allowable presumed bearing capacity of 12,500 kPa is proposed for foundations founded on Cat 1(a) rock in the revised guidelines. The consideration is mainly to have a comparable compressive stress on the shaft of the concrete piles, which usually adopts Grade 60 concrete. The revision of the presumed allowable bearing capacity is promulgated in the Technical Guidance Notes No. 53 (TGN No. 53) (GEO, 2022) and summaries in Table 1.

Table 1 – Presumed allowable bearing pressure and bond friction of igneous rock given in TGN No. 53 (GEO, 2022)

Category	Description of Igneous Rock	Presumed Allowable Bearing Pressure (kPa)	Presumed Allowable Bond Friction (kPa)
1(a)	Fresh to slightly decomposed strong to very strong granite or volcanic rock of material weathering grade II or better, with 100% TCR of the designated grade which has a minimum UCS of rock material not less than 75 MPa (or an equivalent point load index strength PLI50 not less than 3 MPa)	12,500	1,000 (under compression or transient tension) 500 (under permanent tension)
1(b)	Fresh to slightly decomposed strong granite or volcanic rock of material weathering grade II or better, and with not less than 95% TCR of the designated grade, which has a minimum UCS of rock material not less than 50 MPa (or an equivalent point load index strength PLI50 not less than 2 MPa)	10,000	
1(c)	Slightly to moderately decomposed moderately strong granite or volcanic rock of material weathering grade III or better, and with not less than 85% TCR of the designated grade, which has a minimum UCS of rock material not less than 25 MPa (or an equivalent point load index strength PLI50 not less than 1 MPa)	7,500	700 (under compression or transient tension) 350 (under permanent tension)

4.2 Presumed bond friction on igneous rocks

The current guidelines only provide the presumed allowable bond friction for pile socketed into Cat 1(d) and Cat 1(c) or above rocks. It is evident that saving can be further achieved by differentiating the presumed allowable bond friction for Cat 1(c) and Cat 1(d), as the later has a higher uniaxial compressive strength (UCS). The instrumented pile loading tests conducted for the railway projects had also investigated the bond friction in the rock socket. Figure 12 presents the proven bond friction for piles socketed into various rock formations. The bond friction on majority of the pile loading tests was not fully mobilized. It can be observed that the proven bond frictions are generally greater than 1,800 kPa for piles socketed into rocks with UCS greater than 50 MPa.

ICE (2012) documented a number of correlations between the UCS of the rock and bond friction based on load test data on socketed piles in overseas projects. Horvath and Kennedy (1979) gives the lower bound values amongst the reported correlations. This is largely consistence with the bond friction obtained from the instrumented pile loading tests conducted in Hong Kong. By applying a mobilisation factor of 1.5 on the proven bond friction, a higher presumed allowable bond friction of 1,000 kPa could be adopted for pile socketed into Cat 1(b) or better rock, which should have UCS greater than 50 MPa. The tension capacity under permanent load case is likewise taken as 500 kPa accordingly. The recommended changes are also promulgated in TGN No. 53 and given in Table 1.

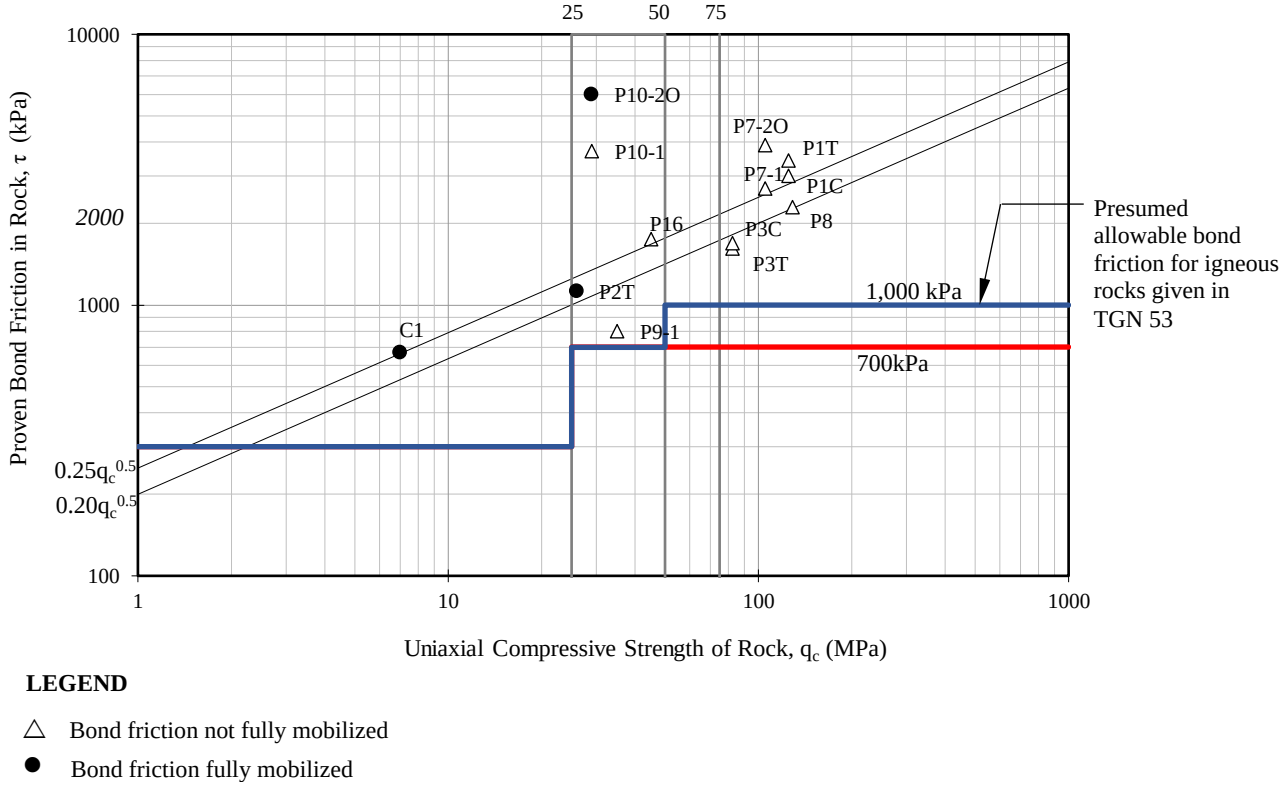

Figure 12 – Presumed allowable bond friction for foundations on igneous rocks (TGN No. 53, (GEO, 2022))

Although there are thirteen instrumented pile loading test cases carried out in different projects, it is important to note that the foundations of all these private and public projects were constructed based on the higher bearing capacity as a result of the instrumented pile loading tests. There had been no report of defects or excessive settlement arising from the use of the increased bearing capacity.

4.3 Presumed bearing capacity on marble and marble bearing rocks

The CoPF published in 2017 (BD, 2017) includes a new Category 2 rock that is described as

moderately decomposed, moderately strong to moderately weak meta-sedimentary rock of material weathering grade III or better, and with not less than 85% TCR of the designated grade. A presumed allowable bearing capacity of 3,000 kPa is specified for foundations founded on such rock. Since its promulgation, practitioners interpreted that marble was also a type of meta-sedimentary rock and therefore, the recommended presumed value for Category 2 rock is also applicable to the design of piles founded on marble rock formation. The consequence of this interpretation had reduced the presumed allowable bearing capacity and bond friction for piles founded on marble formation to 3,000 kPa and 300 kPa (friction under compressive), respectively. It was quite a frustration to practitioners as the foundation design used to accept the presumed bearing capacity of 7,500 kPa and 5,000 kPa for competent marble rocks prior to this interpretation.

Marble is a metamorphic rock composed largely of recrystallized carbonate minerals and their engineering properties are very different from meta-sedimentary rocks. GEO Publication No. 2/90 (GEO, 1990) documents the foundation and engineering properties of marble and other rocks in Yuen Long Formation. Figure 13 was reproduced from the publication which shows the engineering classification of marble in terms of elastic modulus (E) and UCS. This figure is also supplemented with the strength properties (E and UCS) of Grade II and III igneous rocks based on the laboratory tests conducted in the PWL and tabulated in Irfan & Powell (1991) and Lee, Y.W. (2019). It provides a comparison and illustrates that the elastic modulus of marble and marble bearing rocks are stronger than that of igneous rocks and generally have high moduli.

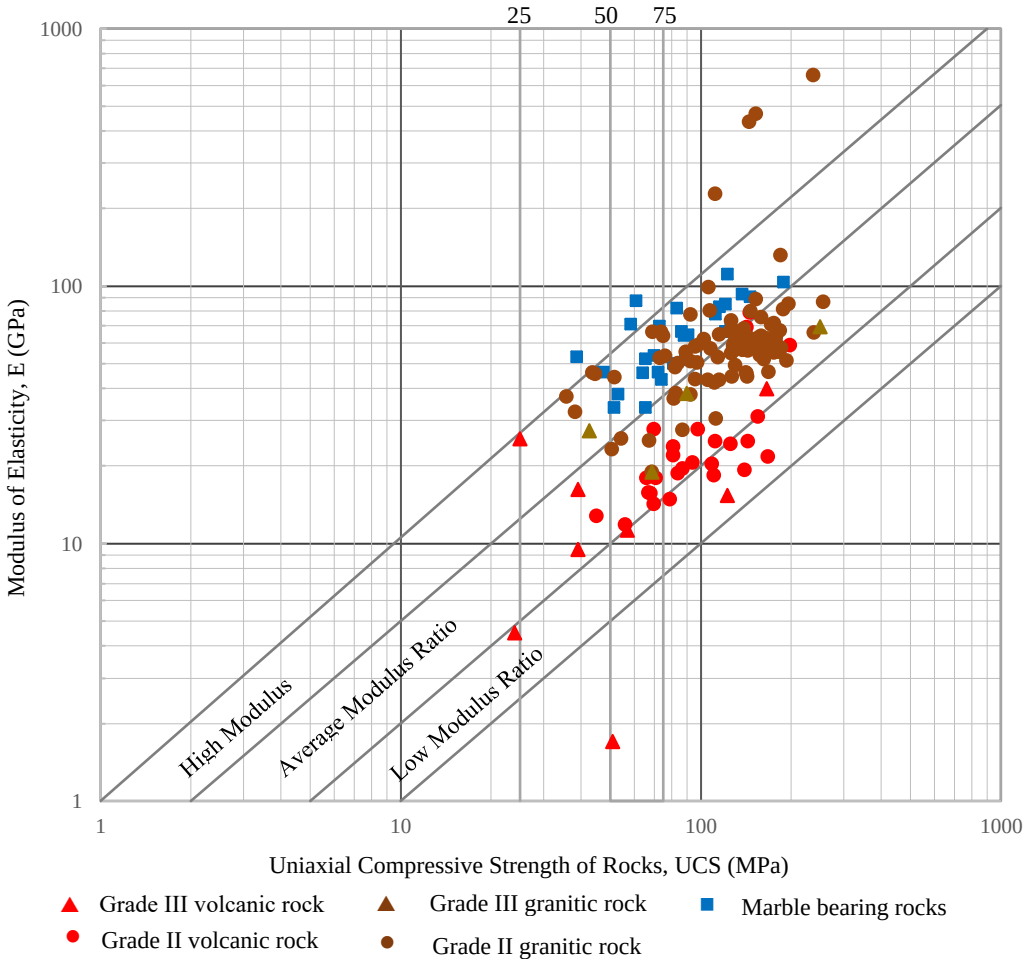

Figure 13 – Engineering classification of igneous rocks and marble in terms of modulus of elasticity and uniaxial compressive strength

The GEO saw that the misunderstanding had caused significant impact on the foundation design in Scheduled Areas underlain by marble. Not only the number of bored piles is increased, so is the construction risk associated with the piling works. In 2020, GEO clarified and the BD published an addendum to exclude

marble and marble-bearing rock from the Category 2 rock. However, the industry was still not given any presumed values for the design of piles on marble rock. Practitioners continued to adopt allowable bearing capacity of 3,000 kPa, which could avoid the need for instrumented pile tests and lengthy approval process.

High-rise buildings exceeding twenty storeys constructed in Scheduled Areas underlain by marble rock formation with cavities are subject to long-term building settlement monitoring. Table 2 tabulates those Yuen Long projects that were carried out between 2010 and 2017 and the presumed bearing pressure adopted in the foundation design. No undue building settlement have been observed for these high-rise buildings and the performance of the foundations are considered satisfactory. The end bearing pressures adopted in these projects ranged from 5,000 kPa to 7,500 kPa.

Table 2 – Long term building settlement monitoring for selected buildings at Yuen Long

Project Site	Type of Pile Foundation	Founding Criteria	Date of Approval	Adopted Presumed Values	Building Settlement Monitoring (after OP)
Building at Tai Tong Road	Bored piles with bell out	Class II Marble or better, UCS > 50MPa and TCR > 95%	April 2010	End-bearing 7,500 kPa	4mm (4/2014 – 8/2021)
Building at Fung Cheung Road	2.75m and 3m dia. Bored piles with bell out	Class II Marble, UCS > 25MPa and TCR > 85%	December 2010	End-bearing 5,000 kPa	9mm (9/2014 – 8/2021)
Building at Long Ping	2.5m dia. Bored piles with bell out	Class II Marble, UCS > 25MPa and TCR > 85%	July 2013	End-bearing 5,000 kPa	8mm (2/2018 – 8/2021)
Building at On Ning Road	2.5m and 3m dia. Bored piles with bell out	Class II Marble, UCS > 25MPa and TCR > 85%	June 2012	End-bearing 5,000 kPa	2mm (6/2021 – 8/2021)

For piles founded on rock formation, the settlement of the rock mass can be estimated based on the elastic theory (GEO, 2006). Assuming a bored pile with a bell-out diameter of 4.95 m and applying a bearing pressure of 7,500 kPa to the rock mass with a lower bound elastic modulus of 5 GPa for Grade III igneous rock, the cumulative settlement in the rock mass is only about 4 mm. The typical elastic modulus of marble and marble bearing rocks is in fact higher than 30 GPa from Figure 13 and is certainly greater than the assumed 5 GPa used in the estimation. Hence, it is comfortably to conclude that the settlement for piles found on sound marble (i.e., Class I and II) with UCS and TCR comparable to the igneous rocks are considered capable of taking 7,500 kPa.

Given that the engineering properties of sound marble is comparable or better than igneous rocks, and the experience of using presumed values similar to igneous rocks, it is considered plausible to provide clear guidance on the presumed values and founding criteria for piles founded on sound marble rocks. There would be substantial saving in terms of cost and time in the construction of the foundation in marble area. GEO has updated the TGN No. 26 that clarifies that piles founded on sound marble (i.e. Marble Class I or II) are considered acceptable and provides the presumed allowable bearing capacity that can be used. With the revision of the presumed allowable bearing capacity of igneous rocks as given in TGN No. 53, there are scope for further revising the same for marble and marble bearing rocks. The GEO would further examine the suitability of aligning the recommended capacity between igneous rocks and marble rocks.

5 PARADIGM SHIFT ON EXERCISING GEOTECHNICAL CONTROL

In recent years, the GEO emphasizes adopting proactive approach in managing requests for

geotechnical advice, whether these are formal submissions of detailed design by consultants and registered geotechnical engineer, circulation of land instruments and planning documents; and feasibility and technical studies by other project offices. Whilst public safety remains the primary objective of the regulatory control exercised by the GEO, consciousness of practicality and cost benefits of the geotechnical works are equally important and ought to be exercised. The GEO is committed to continue the journey of promoting the role of regulator and facilitator for the betterment of our society. Practitioner also plays an important role in shaping the geotechnical practice. There are too many occasions that designers substantially revise the design when confronted by the regulating authority, without arguing and defending the design intent, which they have spent months in developing the scheme and design. Rationale based on sound engineering judgement is the best defense and it does not hurt to bring the matters to the appropriate levels of authority for resolution. The GEO has promoted openness with fellow practitioners in recent years. In fact, pre-submission meeting mechanism has been well documented in the Practice Notes No. ADM-19, BD (2023) and encouraged by the GEO. An Expert Checking Panel mechanism has also been set up in the GEO that allows practitioners to propose innovative ideas and methods to be adopted in geotechnical works. The mechanism aims to provide in-principle agreement to the proposal and give directive on auditing the critical issues at detailed design stage. This gives more rooms for practitioners to discuss and justify their innovative proposals.

The advancements in geotechnical practice achieved in the recent endeavors as encapsulated in this paper are the collaborative efforts by all relevant parties, including practitioners in the industry and regulating authority. From innovative perspective, the progressive mindset helped breaking new ground on geotechnical practice that have significant benefits. There is no magic in these efforts, most issues are tackled from basic principles, engineering judgement and the determination to solve problems. A final concluding remark on advancement in geotechnical practice rests on the perception of "how safe is safe" and the risk aversion nature of fellow practitioners, regardless of which organizations they serve. This is a phycological barrier for many people and makes practicing in the geotechnical discipline even more interesting and challenging. Rather than taking them for granted, confronting the practice that are adopted as routine is the beginning of any advancement.

6 ACKNOWLEDGEMENT

This paper is published with the permission of the Head of the Geotechnical Engineering Office and the Director of Civil Engineering and Development, the Government of the Hong Kong Special Administrative Region.

7 REFERENCES

BD (2004). *Code of Practice for Foundations (2004 Edition)*. Buildings Department, Hong Kong Government of Special Administrative Region, 64 p.

BD (2012). *Requirements for an Excavation and Lateral Support Plan Building (Administration) Regulation 8(1)(bc), Practice Notes for Authorized Person, Registered Structural Engineers and Registered Geotechnical Engineers, (APP-57)* , Buildings Department, The HKSAR Government, Hong Kong, 7 p.

BD (2017). *Code of Practice for Foundations (2017 Edition)*. Buildings Department, Hong Kong Government of Special Administrative Region, 111p.

BD (2023). *Building Approval Process, Practice Notes for Authorized Person, Registered Structural Engineers and Registered Geotechnical Engineers, (ADM-19).* Buildings Department, The HKSAR Government, Hong Kong, 35 p.

Chung, P. W. K and Chu, F. L. F. (2020). Review of quality control of fill compaction works in Hong Kong. *Proceeding of HKIE Geotechnical Division Annual Seminar 2020,* Hong Kong Institution of Engineers – Geotechnical Division, pp 18-27.

Eves, G.W. (1913). The Canton-Kowloon Railway: British Section. *Proceedings of Institution of Civil Engineering*, vol 192, pp 190-246.

Gaba, A., Hardy, S., Doughty, L., Powrie, W. & Selematas, D. (2017). *Guidance on Embedded Retaining Wall Design (CIRIA C760)*, Construction Industry Research & Information Association, London. 285 p.

Gaba, A., Simpson, B., Powrie, W. & Beadman, D.R. (2003). *Embedded Retaining Walls: Guidance for Economic Design (CIRIA C580)*, Construction Industry Research & Information Association, London. 390 p.

GEO (1990). *Review of Design Methods for Excavations*, Geotechnical Engineering Office, GCO Publication No. 1/90, Civil Engineering and Development Department, HKSAR Government, 187 p.

GEO (1994). *Geoguide 1: Guide to Retaining Wall Design* (Second Edition). Geotechnical Engineering Office, Civil Engineering and Development Department, HKSAR Government, 258 p.

GEO (2006). *Design and Construction for Foundation*, Geotechnical Engineering Office, GCO Publication No. 1/2006, Civil Engineering and Development Department, HKSAR Government, 376p.

GEO (2007). *Geoguide 7: Guide to Soil Nailing Design*, Geotechnical Engineering Office, Civil Engineering and Development Department, HKSAR Government, 97 p.

GEO (2020). Technical Guidance Notes No. 26. *Supplementary Guidelines on Foundation Design in Areas Underlain by Marble and Marble Bearing Rocks*. Geotechnical Engineering Office, Civil Engineering and Development Department, HKSAR Government, 5 p.

GEO (2022). Technical Guidance Notes No. 53. *Supplementary Guidelines on Design and Construction of Foundation.* Geotechnical Engineering Office, Civil Engineering and Development Department, HKSAR Government, 4 p.

Horvarth, R. G. and Kenney, T. C. (1979). Shaft resistance of rock socketed drilled piers. *Proceedings of the ASCE Annual Convention*, Atlanta, Georgia. Pre-print No. 3698.

HyD (2016). *Guidance Notes - Road Inspection Manual (Report No. RD/GN/016C)*, Research and Development Division, Highways Department, HKSAR Government, 31 p.

ICE (2012). *ICE manual of geotechnical engineering, Geotechnical Design, Construction and Verification,* Institution of Civil Engineers, 1508p.

Irfan T.Y. & Powell G.E. (1991). *Foundation Design of Caissons on Granitic and Volcanic Rocks (1991)*, Geotechnical Engineering Office, Civil Engineering and Development Department, HKSAR Government, 212 p.

Lee, W.Y. (2019). *A study of brittleness of granitic rocks in Hong Kong.* Thesis for MSc in Applied Geology, The University of Hong Kong, 121 p.

Lumb, P (1972). Slope Failures in Hong Kong. *Quarterly Journal of Engineering Geology and Hydrogeology*, Vol. 8, Pages 31 – 65.

MOT (2015). *Specifications for Design of Highway Subgrades, JTG D30-2015*, Ministry of Transport of the People's Republic of China, 226 p.

Exploratory Study of Using Artificial Intelligence for Landslide Predictions

R.W.M. Cheung, H.W.M. Li & E.K.H. Chu
Geotechnical Engineering Office, Civil Engineering and Development Department, Government of HKSAR, Hong Kong SAR, China

ABSTRACT

Riding on the comprehensive inventories of landslide-related data maintained by the Geotechnical Engineering Office (GEO) over the years, the GEO has initiated an exploratory study to enhance the existing landslide prediction models (i.e. Model A – landslide susceptibility model for natural terrain, and Model B – rainfall-landslide correlations for reported landslides on man-made slopes) with the application of machine learning (ML) and big data analytics. Model A adopted seven common ML algorithms to correlate the multitude of features (e.g. rainfall, geology, and some terrain-related features) with landslide in the natural terrain on the Lantau Island non-linearly. Domain knowledge of geotechnical and geological engineering was incorporated in the course of developing the ML model. The training and testing of the ML models used most of the available data as an approach to acquire realistic prediction of landslide probabilities out of an inherently acutely-imbalanced dataset. The applicability of some common evaluation metrics to this approach, and grid size effect were examined. Promising results with about three orders of magnitude enhancement to the model resolution were achieved. The use of ML on Model B is ongoing based on the knowledge and experience gained from Model A. This paper presents the latest progress of the exploratory study.

1 INTRODUCTION

Landslide prediction models estimate the likelihood of landslide occurrence in an area based on a collection of landslide contributory factors. Over the years, the Geotechnical Engineering Office (GEO) has been continuously enhancing two territory-wide landslide prediction models which constitute the crucial parts of the slope safety system in Hong Kong (Cheung, 2021). The natural terrain landslide susceptibility model (Model A) predicts the spatial likelihood of the landslide occurrence of the natural terrain over the territory. It provides a rational and scientific basis to the formulation of the landslide risk management strategy including the spatial assessment of landslide risk and prioritisation of mitigation works, as well as land use planning. On the other hand, the rainfall-landslide correlation model for man-made slopes (Model B) provides real-time prediction of spatial landslide frequency and hence the total number of landslides over the territory in a rainstorm. It serves as the backbone of the Landslip Warning System (LWS) in Hong Kong, which was established in 1977 and is the first territory-wide early landslide warning system in the world (Chung et al., 2023; Kong et al., 2020). The LWS is intended to prompt the public to take precautionary measures to reduce their exposure to risk posed by landslide. It also supports the government's landslide emergency system. Both of the models were developed through data-driven analysis based on conventional statistical approach adopting predefined functions.

Recently, with the significant advancement of artificial intelligence (AI) which serves a highly capable yet readily accessible and cost-effective means for data driven analysis, the GEO has initiated an exploratory study of applying AI for landslide predictions. Focus is placed on enhancing the accuracy and resolution of the existing landslide prediction models with the use of machine learning (ML) technology coupled with big data analytics, which rides on the comprehensive inventories of territory-wide landslide-related data (e.g. landslide database, LiDAR data, rainfall data and geological maps) maintained by the GEO over the years.

2 LANDSLIDE RELATED DATA INVENTORIES

Good quality data with sufficient spatial and temporal resolutions are fundamental to data-driven analysis. In the past 40 years, the GEO has been collecting, and maintaining in light of technological advancement, a spectrum of landslide-related datasets in Hong Kong in a continuous manner. The geotechnical, geological and meteorological database pertinent to landslide prediction modelling that are maintained by the GEO are summarised in Table 1.

Table 1: Summary of Geotechnical Database Pertinent to Landslide Prediction Modelling

Geotechnical Database	Available Information	Temporal and Spatial Resolution
LiDAR-based Digital Terrain Model (DTM)	Digital terrain models which can be converted into maps of various topographic information (e.g. gradient, curvature, aspect, catchment, etc.)	On average 4 data points/m^2 or 0.5m-grid for the territory-wide LiDAR survey undertaken in 2010
Geological Maps	Geological data (e.g. solid geology, superficial geology and faults) based on a large amount of borehole logs, tunnel logs, cut slope exposures and geophysical survey records since 1980s.	Map scale = 1:20,000
Rainfall	Spatial and temporal records of rainfall intensity of various durations	Average density of 1 rain gauge /10km^2 Readings taken at 1 min interval
Enhanced Natural Terrain Landslide Inventory (ENTLI)	Records of natural terrain landslides (including the unreported ones) identified from high-flight and low-flight aerial photographs (more than 100,000 landslide records)	Aerial photos temporal resolution = 1 year ENTLI Database = update every 3 years
Reported Landslides	Records of landslides reported to the GEO since 1984 (about 10,000 records)	Annual review of reported landslides
Catalogue of Slopes	Details (e.g. location, geometry, geology, formation and failure history, maintenance responsibility, etc) of about 60,000 nos. registered man-made slopes	Continuous update when needed

2.1 Digital Terrain Model (DTM)

The Airborne Light Detection and Ranging (LiDAR) technique can overcome the problem of views being obscured by dense vegetation, thereby obtaining the 'bare-earth' profile of the city and identifying geomorphological features more accurately. High resolution digital terrain model (DTM) as generated by multi-return LiDAR survey technique which can 'see through' vegetation in a territory-wide scale contains good quality topography-related information. The 0.5m-grid DTM was developed based on the 2010 territory-wide LiDAR survey. The DTM could be resampled into different grid sizes and converted into various topographic indices including gradient, plan and profile curvature, upslope catchment area and topographic position for landslide prediction modelling.

2.2 Geological Map

The GEO maintains a well-documented geological database of Hong Kong, which was developed based on extensive geological studies on a large amount of available borehole data (more than 300,000 ground investigation stations over the territory), tunnel logs, cut slope exposures, geophysical survey records and other available geological information over the years. For the purpose of landslide prediction modelling, the lithology of the territory was categorised into three main groups (namely intrusive, volcanic, and sedimentary) based on the 1:20,000 solid and superficial geology maps so as to relate the engineering properties and thus landslide potential of the soil to their parent rocks. Other geological information e.g. distance to fault is also available but they were not adopted in the modelling further to assessment (see Section 3.2.3).

2.3 Rainfall Data

The landslides in Hong Kong are primarily induced by rainfall, which is highly correlated with the rainfall intensity and duration. In this regard, the GEO has been operating an extensive network of automatic rain

gauge stations to collect real-time rainfall data at one-minute interval, which have been using for supporting the Landslip Warning System (Chung et al., 2023; Kong et al., 2020). Currently, the GEO Rain-gauge System consists of 90 automatic rain gauge stations in the network. Together with 31 automatic rain gauges managed by the Hong Kong Observatory (HKO) and the Drainage Services Department (DSD), the available real-time rainfall measurement at one-minute interval covers the whole territory of Hong Kong with an average density of one rain gauge per 10 km^2. With the data, spatial and temporal distributions of rainfall with different durations for a given rainstorm can be readily determined for subsequent analyses.

2.4 Enhanced Natural Terrain Landslide Inventory (ENTLI)

The ENTLI provides a comprehensive Geographic Information System (GIS)-based inventory of natural terrain landslides of the territory. It was firstly developed by identifying landslides from aerial photographs interpretation based on high-flight aerial photographs (taken at 2,400 m altitude or above) since 1945, and later supplemented with the results from the mapping of historical natural terrain landslides using low-flight aerial photographs (taken at lower than 2,400 m altitude) for an improved accuracy. Currently, over 100,000 landslides are recorded in the inventory. The ENTLI provides comprehensive and important data for landslide prediction modelling since landslides that occurred on natural hillsides and remote areas without affecting the public would have been missed otherwise, biasing the predictive model with the accessibility of the landslide locations. On the other hand, with its temporal resolution limited by the frequencies of aerial photo-taking and interpretation, the analysis of Model A adopting this database is bounded to be year-based as a result.

2.5 Reported Landslides

The GEO has been collecting landslide data through a reporting mechanism and conducting annual reviews of landslides and rainfalls in Hong Kong since 1984. On average, about 300 landslides are reported to the GEO every year. In general, most of the reported landslides are of a relatively small scale (i.e. less than 50 m^3 in volume), but some of them are sizeable (500 m^3 or more) (Ho & Cheung, 2021). To facilitate data management and manipulation, a computerised dataset of landslide records since 1984 has been established (Ho & Lau, 2008 & Mak et al., 2001). To date, about 10,000 landslides are recorded in the landslide database.

2.6 Catalogue of Slopes

All sizeable man-made slopes in Hong Kong (i.e. cut slopes, fill slopes and retaining walls) have been systemically identified from interpretation of historical aerial photographs and field inspections, and they are registered in a comprehensive Catalogue of Slopes (Ho & Cheung, 2021 and Lam et al., 1998). The Catalogue of Slopes (the Catalogue) contains a wide range of useful information of the man-made slopes, such as geometry, geology, formation history, landslide records, maintenance responsibility and photographs, and the information contained in the Catalogue has been continuously updated. It provides the essential information of about 60,000 registered man-made slopes for landslide risk management.

3 NATURAL TERRAIN LANSLIDE SUSCEPTIBILITY MODEL (MODEL A)

3.1 Existing landslide susceptibility model for the natural terrain of Hong Kong

A landslide susceptibility model predicts the spatial distribution of the landslide likelihood in an area with reference to its local terrain conditions (Brabb, 1984). The resulted susceptibility map enables the hazard zoning and the assessment the landslide risk of the area quantitatively, providing useful information for the decision makers to better understand and mitigate the landslide risks. The latest territory-wide landslide susceptibility model for the natural terrain of Hong Kong is given in Lo et al. (2015). This model discretised the natural terrain of Hong Kong into 5m x 5m grids (c.f. the total natural terrain area of Hong Kong is about 660 km^2), which were categorised into 144 classes and correlated to landslide susceptibility using conventional statistical approach. The classification of the grids was based on three landslide contributory factors (features), namely 1) eight classes of slope gradient, 2) three classes of lithology and 3) six classes of rainfall anomalies. A total of 24 years of landslide and rainfall data as recorded between year 1985 and 2008 were considered. Rainfall anomalies were characterised in terms of year-based normalised maximum rolling

rainfall (NMRR) with rolling durations of 4-hour and 24-hour. NMRR is determined as the maximum rolling rainfall at a location normalised with the mean annual rainfall of the same location of a 30-year period from year 1977 to 2006. This model has an overall resolution of 4-5 orders of magnitude in terms of landslide density (no./km^2) (Figure 1). Based on this susceptibility model, a terrain-based landslide frequency map which predicts the annual theoretical number of landslides that would likely occur in a year for a given the mean annual frequency of rainfall occurrence was generated in Ko (2018).

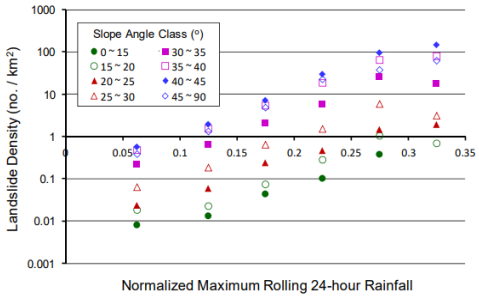

Figure 1: Year-based Rainfall Landslide Correlation in Lo et al. (2015) for Combined Geology

3.2 Machine learning-based natural terrain landslide susceptibility model

In order to explore the potential of applying ML in analysing the landslide susceptibility of natural terrain in Hong Kong, the GEO has undertaken a pilot study of Model A since 2021. This pilot study was carried out in two phases, with the first phase reported in Li et al. (2021). Further enhancement to the first phase ML model through reviewing the suitability of other algorithms and features was conducted in the second phase of the study. This paper reports the combined findings of the two phases of the study.

The study considered a pilot study area (Section 3.2.1) for the same period of year 1985-2008 as in Lo et al. (2015). The analysis was treated as grid-based binary classification problem (Section 3.3) with seven ML and deep learning algorithms considered (Section 3.2.2). A total of seven pertinent features were selected to train the ML model based on a tailor-made feature selection framework (Section 3.2.3). An optimal grid size of 5m x 5m was considered further to a review of the grid size effect (Section 3.2.4).

3.2.1 Pilot Study Area

The pilot study selected a 130 km^2 natural terrain on and around the Lantau Island (the pilot study area), which constitutes about one-fifth of the natural terrain area in Hong Kong (Figure 2). The pilot study area was selected for its high variability in topography-related and rainfall data, and the plentiful historical landslides available. Among the 24 years (i.e. 1985-2008) considered in the study, the study area experienced the most intense rainfall in 1993 and 2008, with the 24-hour maximum rolling rainfall of over 500 mm and 600 mm, respectively. The ENTLI recorded over 6,100 recent natural terrain landslides within this area.

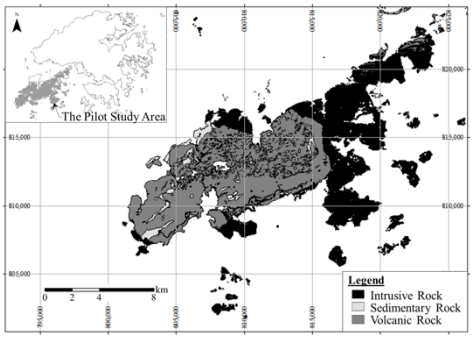

Figure 2: The pilot Study Area

3.2.2 Machine Learning Algorithms

The pilot study considered seven machine learning and deep learning algorithms which are commonly adopted for landslide susceptibility analysis. The key features of these algorithms are summarised in Table 2.

In each of the study phases, the algorithms were applied to the same feature set to identify the best performing one(s). The assessment of the algorithms' performance was based on evaluation matrices as elaborated in Section 3.5.1. XGBoost was found to be the best performing algorithm in the Phase 1 study and it was tested again in Phase 2 to compare with the remaining algorithms.

Table 2: Key Features of the Machine Learning/Deep Learning Algorithms Considered

Algorithm*	Phase studied	Characteristics	Remarks	Computational Efficiency**
DT	1	• Tree-based algorithm which partition data recursively to yield maximum information gain	• Less robust and is sensitive to the predictive data • The patterns used to link the training datasets are highly interpretable	Very High
RF	1	• Tree-based algorithm • Ensembles by the bagging method to lower variance and avoid model overfitting	• One of the best performing algorithms in ML competition before the introduction of XGBoost	Moderate
XGB	1,2	• Tree-based algorithm • Ensembles by boosting to improve robustness and generalizability • Grows level-wise	• Introduced in 2016 • One of the best performing algorithms in ML competition	High
LGBM	2	• Tree-based algorithm • Ensemble by boosting • Grows leaf-wise to enhance computation efficiency	• Introduced in 2017 • Techniques to improve efficiency: o Gradient-based One-side Sampling (GOSS); o Exclusive Feature Bundling (EFB)	Moderate to High
ANN	2	• Deep learning algorithm • Combines the activation functions in nodes through transformation with weight and bias applied	• Application not limited to structured data but also text, images, video and audio input	Moderate to High
SVM	2	• Works by maximizing the margin between decision boundary and data points	• Commonly adopted in ML-based LSA in literatures • Determination of probability is highly resource demanding	Very Low
LR	2	• Model optimized based on maximum likelihood considering log(odds)	• Monotonic relationship between feature and probability assumed • Cannot handle highly correlated features	Very High

* DT = Decision Tree (Breiman et al., 1984); RF = Random Forest (Breiman, 2001); XGB = XGBoost (Chen & Guestrin, 2016); LGBM = LightGBM (Ke et al., 2017); ANN = Artificial Neural Network (Rosenblatt, 1958); SVM = Support Vector Machine (Cartes & Vapnik, 1995); LR = Logistic Regression (Cox, 1958)

** the efficiency of computation was assessed specific to the dataset and approach taken in this pilot study

3.2.3 Feature Selection

While ML is often used in a way of maximizing the accuracy of predictions with the data mechanism behind unknown (Breiman, 2001), the GEO places much emphasis on ensuring the ML models remain physically meaningful for its prediction to be explainable without compromising prediction accuracy through critically incorporating domain knowledge to the model throughout the study. This is essential for model debugging and bias detection (Ma et al., 2021), and the necessary understanding of the model based on which sensible decision can be made. In particular, a tailor-made framework was used to ensure potential features which are physically significant to landslide occurrences are selected for modelling only. This framework comprises the three criteria as follows:

1) the availability of quality dataset for the feature in terms of spatial and temporal coverage, resolution and accuracy;
2) the existence of a reasonable degree of statistical correlation between the feature and landslide occurrence; and

3) the above statistical correlation being explainable and consistent with the existing engineering principles (i.e. domain knowledge) on landslide occurrence.

Big data analytics techniques were adopted in compiling the suitable data for assessment against the framework, as well as for the ML model development. The characteristics of the features selected based on the above framework, and their physical significance to landslides are summarised in Table 3.

Table 3: Characteristics of the Selected Features and Physical Significance to Landslides

Feature	Description	Physical Significance to Landsides
Slope Gradient	Inclination of slope	Affects the balance of stabilizing and destabilizing forces and thus the overall stability of a slope
Plan Curvature	The rate of change of slope gradient on horizontal plane	Influences the convergence and divergence of surface runoff and subsurface groundwater flow
Profile Curvature	The rate of change of slope gradient on vertical plane	Considered as a proxy to the break in slope that is assumed to be landslide related
Geology	Bedrock geology classified into three groups: Intrusive, Volcanic and Sedimentary	Related to the engineering properties of the soils derived from the parent rocks
Rainfall	Anomalies of rainfall characterised as normalised maximum rolling rainfall (NMRR)	Natural terrain landslides in Hong Kong were rainfall-induced; destabilising forces
Upslope Catchment Area	Contributory area of potential flow accumulating to the location	Indicates the degree of potential erosion of the area
Topographic Position Index	The difference in elevation of the grid and the average elevation of the surrounding ones	Indirectly reflects the terrain morphology and thus the susceptibility of landslide of the area

Features commonly considered in literatures e.g. elevation, aspect, distance to drainage line, distance to fault, vegetation cover, etc were reviewed but eventually discarded for not fulfilling the selection framework.

3.3 Approach and workflow of modelling

The analysis was treated as grid-based binary classification problem in ML, which means the derived ML classifier predicts the landslide occurrence of a grid as a binary-dependent variables of positive or negative values (i.e. with and without landslide). This is a very commonly adopted approach among similar studies in Hong Kong (e.g. Ng et al., 2021; Wang et al., 2021). Since positive grids always constitute a very scarce portion of the data, the dataset for LSA is inherently acutely-imbalanced. Data sampling, while biasing the predicted probabilities of the classifier, is often used to achieve a more balanced dataset. However, in order to obtain a more realistic prediction of the landslide probability of the grids, this technique is not used in the pilot study. The alternative approach adopted enhances the overall resolution of the model and enables the prediction of the total number of landslides with simple mathematics.

The overall workflow of the modelling is illustrated in Figure 3. Geographical information system (GIS) software was used to prepare the feature datasets and they were then converted from raster to structured format for modelling, and vice versa for visualisation of the model output. All ML processing tasks including data pre-processing, model training and model performance evaluation were carried out with python coding. These tasks were carried out on a cloud platform given the enormous amount of data to be handled. The resampling of data for model training, validation and testing is also shown in the same figure.

The ML models are trained with the input dataset comprising all the available data except those that were reserved for testing. The hyperparameters of the ML models were tuned using five-fold cross validation (CV), with the training data randomly split to 7:2 to serve as the training and validation data in each fold. Stratified sampling based on landslide occurrence (i.e. landsliding or non-landsliding) was adopted such that same ratio of landsliding to non-landsliding data was maintained.

As for the model performance evaluation, this pilot study adopted an additional set of testing data (TD1) for evaluating model performance as compared with literatures. It comprises the data from Year 1993 and 2007 data which correspond to a high and a moderate rainfall scenarios, respectively. This testing data TD1 mimics future data that were unseen by the models to test their abilities in making forward prediction. On the other hand, testing dataset TD2 randomly extracted from the remaining 22 years of data was of nature similar to those considered in literatures. It is adopted to enable meaningful comparison and benchmarking of the model performance with literatures.

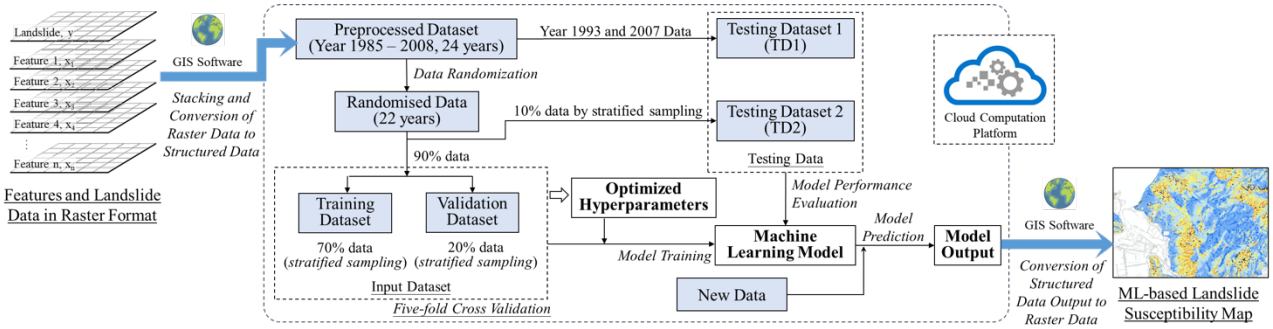

Figure 3: Overall Workflow and Resampling of Data of the Pilot Study

3.4 Grid size effect

An optimal grid size improves the predictive power of the ML model through effectively capturing the morphological conditions affecting the stability of the slopes (Martinello et al., 2022). In order to study the appropriateness of the adopted grid size of 5m in this pilot study, the performance of a 5m-grid XGB model (the best performing algorithm in Stage 1 study) is compared with that of a 10m-grid XGB model adopting the same feature set in Table 4. Grid size of 10 m was considered since it covers about 80% of the landslide scars according to ENTLI. ROC AUC to be discussed in Section 3.5.1 is used to measure the performance of the model. It is evident from Table 4 that 5m-grid gives a better model performance and hence it is considered more effective in capturing the landslide-related morphological conditions.

Table 4 ROC AUC of the XGB Models based on Different Grid Sizes (5m vs 10m)

Grid Size	Testing Data 1 (TD1)	Testing Data 2 (TD2)
5 m x 5 m	0.915	0.973
10 m x 10 m	0.896	0.961

3.5 Results and discussion

The performance of the ML models was assessed in respect of (1) classification accuracy, (2) accuracy of the predicted landslide probability and (3) the degree of enhancement to model resolution.

3.5.1 Classification accuracy

The performance of the ML models in respect of classification accuracy is measured using the Area Under Curve (AUC) of the Receiver Operating Characteristic Curve (ROC), which is the most commonly used index for assessing the performance of a ML model (Spackman, 1989). Table 5 summarizes the results of the seven ML algorithms being tested in this pilot study. The predicted class of a grid is determined based on its predicted probability of the positive class with reference to a classification threshold. An ROC curve plots the true positive rate (TPR, i.e. the proportion of the truly classified actual positive data) against the false positive rate (FPR, i.e. the proportion of falsely classified actual negative data) for the full range of classification threshold from 0 to 1 (Figure 4). The concept of TPR and FPR for a given threshold is illustrated in a confusion matrix in the same figure. A higher ROC AUC value indicates a better model performance in classification accuracy.

Table 5: Summary of the ROC AUC Values Achieved by ML Models Adopting Different Algorithms

Data*	DT	RF	XGB	LGBM	ANN	LR	SVM
TD1	0.876	0.908	0.915	0.910	0.913	0.865	0.796
TD2	0.944	0.967	0.973	0.973	0.964	0.953	0.829

* see Section 3.3 for the discussion on the characteristics of the testing datasets TD1 and TD2

The overall ROC AUC achieved by the models is comparable to the range of values reported in the literature (see Figure 4). LR and SVM had the lowest ROC AUC amongst the studied algorithms. The relatively low ROC AUC of LR is probably attributable to its intrinsic property which correlates data in a monotonic manner, and thus limits the model's predictive capability. On the other hand, as compared with the other algorithms, SVM required significantly longer running time under the adopted approach which makes it

the least competitive model. The reliability of predicted landslide probability by models achieving the highest classification accuracy, including XGB, LGBM and ANN, were further assessed in the next section.

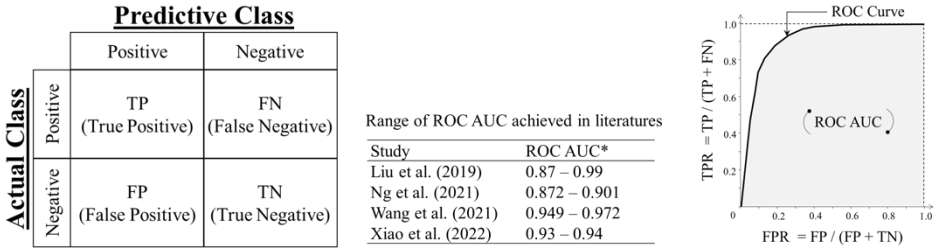

Figure 4: Confusion Matrix and Receiver Operating Characteristic (ROC) Curve

Other available evaluation metrics for the evaluation of classification accuracy includes accuracy, sensitivity, specificity and precision, etc. Most of them combines the distribution of these true positive (TP), false positive (FP), true negative (TN) and false negative (FN) data in various manner. A threshold of 0.5 is often considered for models trained with sampled data. Nonetheless, the present review indicates that the use of these metrics which are based on a single classification threshold for assessing model performance can be misleading for models derived from an imbalanced dataset and therefore they were not used in this study. On the other hand, accuracy of the predicted probability of the ML models were examined in the next section in lieu of using metrics e.g. brier's score or log-loss for a more detailed assessment.

3.5.2 Landslide probability prediction

The approach adopted in this study is considered to enable a more realistic prediction of the landslide probability, which can be directly taken as the probability of the positive class of individual grids. This is validated by comparing the values of the probability of the positive class as predicted by the model and the actual landslide probability of the grids. Figure 5 compares the two values of the XGB, LGBM and ANN models accordingly, with a linear relationship with a gradient of unity indicating good agreement among the two quantities. It is noted that XGB and ANN models give quite a reasonable prediction of landslide probability for values higher than $5x10^{-6}$, while LGBM model basically under predicts in all cases. Neither XGB nor LGBM models are able to differentiate data points with predicted probability of landslide beyond $5x10^{-6}$. While ANN model gives landslide probability predictions beyond $5x10^{-6}$, those are under predictions. Nonetheless, differentiating areas with P(LS) lower than $5x10^{-6}$ is seldom pursued in applications.

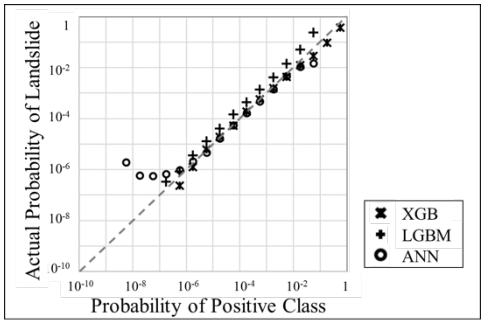

Figure 5: Predicted Probability of Positive Class vs Actual Landslide Probability of the XGB, LGBM and ANN Models

3.5.3 Degree of enhancement to model resolution

The resolution of the susceptibility model is dependent on the relative landslide susceptibility among grids, while the susceptibility of a grid is determined with reference to the predicted probability of landslide in this study. With the inclusion of multitude of features to the model enabled by the use of ML, this section looks at the enhancement to the resolution of the model as a result through assessing the range of the landslide

probability of the entire pilot study area as predicted by the ML models. XGB model is considered since it provides the most reliable landslide probability predictions according to Section 3.5.2. The resolution of the models accounting for seven selected features in five different classes of the 24-hour NMRR is compared to that of a reference model in Figure 6. This reference model is an XGB model considering the three features adopted in the Lo et al. (2015) study (i.e. gradient, lithology and rainfall anomalies) for benchmarking purpose. The resolution of the model is found to be enhanced by two to three orders of magnitude, attributing to the introduction of four additional terrain-related features. The resulted spatial distribution of the predicted landslide probability in the Tai O area subject to 24h-NMRR of 0.275 produced by the 2022 XGB model is given in Figure 6 for visual illustration.

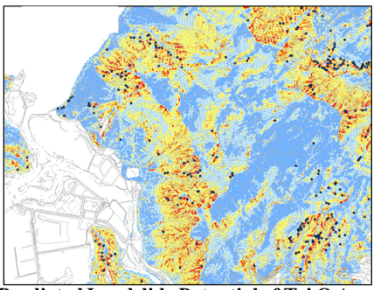

Predicted Landslide Potential of Tai O Area

Range of Predicted Landslide Probability of the Pilot Study Area

ML Model		RF Class I (0.025 – 0.10)*	RF Class II (0.10 – 0.15)	RF Class III (0.15 – 0.20)	RF Class IV (0.20 – 0.25)	RF Class V (0.25 – 0.30)
Reference Model	Min	2.12×10^{-7}	2.54×10^{-7}	6.35×10^{-7}	3.45×10^{-6}	9.61×10^{-6}
	Max	2.04×10^{-5}	3.36×10^{-5}	2.10×10^{-4}	2.68×10^{-3}	2.56×10^{-3}
2022 XGB Model	Min	2.80×10^{-7}	2.97×10^{-7}	4.64×10^{-7}	7.89×10^{-7}	9.02×10^{-7}
	Max	2.74×10^{-3}	2.20×10^{-3}	7.76×10^{-3}	3.70×10^{-2}	5.84×10^{-1}

* *values in bracket denote the range of 24-hour NMRR represented by the rainfall (RF) class*

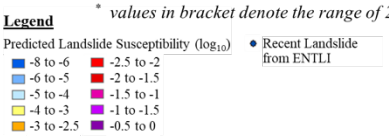

Figure 6 – Range of Predicted Landslide Probability of the Pilot Study Area and an Extract of Predicted Landslide Potential of the Tai O Area

4 CORRELATION MODEL FOR RAINFALL AND REPORTED LANDSLIDES ON MAN-MADE SLOPES (MODEL B)

4.1 Landslide prediction for Landslip Warning System

As one of landslide risk management tools in the Slope Safety System in Hong Kong, a territory-wide Landslip Warning System has been established and implemented, with an aim to alerting the public of possible landslide risk due to heavy rainstorms and supporting the landslide emergency system within the government to deal with landslide incidents. Landslide prediction models have been developed to the operation of the Landslip Warning System during heavy rainstorms. A Landslip Warning may be issued when the prediction of landslides reaches the threshold level.

It is recognised that a significant number of landslides at remote areas, such as natural hillsides at country parks, may not be found and reported, so the number of reported landslides in a rainstorm may only reflect a portion of the full figure of landslides occurred. However, as these landslides at remote areas may not have significant impacts on public safety, the prediction models for the Landslip Warning System thus only focus on predicting the number of reported landslides in a rainstorm, instead of covering all landslides occurred.

Rainfall is the major trigger of landslides in Hong Kong. Rainfall severity of a given rainstorm could be characterised in different ways, such as maximum rolling rainfall and antecedent rainfall with different durations, and considered into a landslide prediction model. As different types of man-made slopes may perform differently under the same rainfall conditions, characteristics of the man-made slopes, such as slope geometry, slope forming materials and level of geotechnical input, are potential contributory factors of landslide occurrence and are commonly incorporated into the prediction model.

4.2 Current prediction models for reported landslides on man-made slopes

Four generations of landslide prediction models have been developed for the GEO Landslip Warning System since 1977 (Chung et al., 2023; Kong et al. 2020). Along with the development of the GEO Raingauge System and the establishment of the Catalogue of Slopes since the 1980s, the prediction models have been continuously reviewed and updated based on the available datasets of landslides, rainfall and man-made slopes, to reflect the changing of landslide risk through urban development in Hong Kong. In the latest model, spatial distributions of registered man-made slopes and reported landslides, as well as spatial and temporal variations of rainfall intensities were adopted to develop bi-linear correlation models between landslide

frequency and maximum rolling 24-hour rainfall for four types of man-made slopes (i.e. soil cut, rock cut, fill slope and retaining wall) to predict the number of landslides. The latest correlation models were updated in 2012 based on the data for the period of 1996 to 2010, followed by another review in 2018 with no further update to the correlations using the data up to 2016. Figure 7 shows the current correlation models between landslide frequency and maximum rolling 24-hour rainfall for four types of man-made slopes.

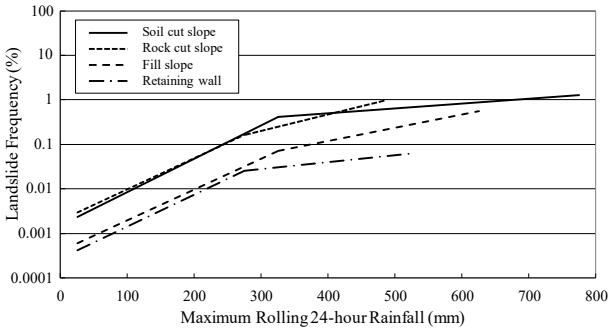

Figure 7: Correlations between landslide frequency and max. rolling 24-hour rainfall for four types of man-made slopes

4.3 Opportunities of machine learning

The GEO has launched an exploratory study to apply ML to revisit the relationship between rainfall and reported landslides on man-made slopes and seek opportunities to enhance the current capability in landslide prediction. Alternative ways of characterising rainfall severity and additional landslide contributory factors will be explored using ML in this study, with a view to improving the performance of the prediction models.

The maximum rolling 24-hour rainfall was adopted in the current landslide prediction models, as being a parameter strongly correlating failures of man-made slopes (Yu, 2004 and Pun et al., 1999) as well as a convenient parameter to characterise the intensity of rainfall in a given rainstorm. It was noted that maximum rolling 24-hour rainfall might not be a good indicator of landslide potential in some occasions (Yu, 2004). To gain more insight, it is worth exploring ways of characterising rainfall severity in correlating the landslide frequency of man-made slopes in a given rainstorm using ML tools. Maximum rolling rainfall with durations other than 24-hour and antecedent rainfall with different durations are examples to be explored whether or not they have statistical links with the landslide frequency in a given rainstorm.

Furthermore, additional potential landslide contributory factors that have not been considered before could be introduced to enhance the capability in landslide prediction model using the ML tools, which enable non-linear and multivariate analyses. The high-quality inventories of territory-wide landslide-related data established and maintained since the 1980s could be utilised for identifying potential landslide contributory factors. Apart from slope types and slope forming materials considered in the current prediction model, incorporating other slope information, such as slope angle and level of geotechnical input, into a ML model may give higher prediction accuracy. Although a wide range of data in various inventories are available, particular attention should be paid in selecting suitable features with due considerations of their physical meaning, reliability and accuracy. Careful feature engineering process should be carried out to make sure that selected features are consistent with our domain knowledge on landslide occurrence.

4.4 On-going development work

The work plan of the exploratory work of applying ML in the prediction of landslides on man-made slopes has been formulated. A slope-based binary classification analysis is conducted to formulate a ML model of a storm-based prediction of the reported landslides on the man-made slopes. Similar approach as in Model A is adopted to handle the highly imbalanced data of the reported landslides under a rainstorm event.

To develop the ML-based landslide prediction model for man-made slopes, the datasets of reported landslides, rainfall and man-made slopes have been compiled, extracted and pre-processed, and are ready for model construction. An assessment for feature selection is being conducted to select pertinent features with high quality and statistical and physical relevance for inclusion in the ML model. As a first attempt, a ML model incorporating the features considered in the current bi-linear correlation models for landslide prediction (i.e. maximum rolling 24-hour rainfall, slope types and slope forming materials) is being developed using

some tree-based ensemble ML algorithms, such as Random Forest and XGBoost. The dataset resampling for model training and testing is presented in Figure 8. The datasets of about 200 rainstorm events from 1996 to 2010 are extracted and pre-processed. The dataset is resampled into a training dataset, a validation dataset, and two testing datasets, which comprise the data of 10% of rainstorm events (i.e. Testing Dataset 1), and 10% of the data randomly selected from the remaining rainstorm events in a stratified manner (i.e. Testing Dataset 2), respectively. Currently, model training using the ML algorithms with cross validation and optimising their hyper-parameters are in progress. The performance of the trained ML models will be evaluated using model metrics, such as ROC AUC and Brier Score to compare the accuracy of the ML algorithms using Testing Dataset 2, and performance metrics, such as R^2 and Root Mean Squared Error to compare predicted numbers of reported landslides using the ML models and bi-linear correlation models with actual numbers of reported landslides using Testing Dataset 1.

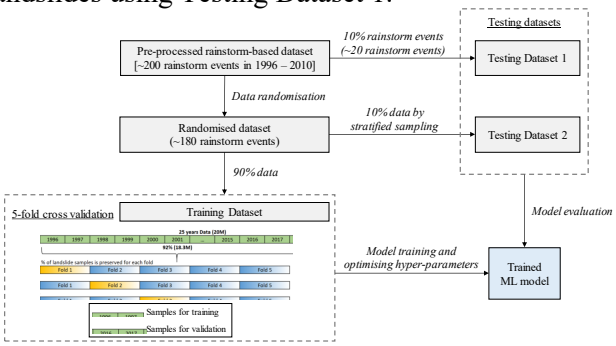

Figure 8: Dataset resampling for model training and testing

5 CONCLUSIONS

Riding on the comprehensive landslide-related data inventories collected and maintained over the years, the GEO has been exploring the potential of improving the current landslide prediction models with the use of artificial intelligence. Promising progress and outcome are obtained from the exploratory study of the two existing landslide prediction models so far.

The pilot study of the natural terrain landslide susceptibility model (Model A) suggests the use of ML technique coupling with big data analytics could bring about a 2-3 orders of magnitude enhancement to the resolution of the natural terrain landslide susceptibility model without compromising the prediction accuracy of the model. In this study, various aspects of ML including the workflow, characteristics of algorithms, feature selection as well as methods of model performance evaluation had been thoroughly investigated with respect to the modelling approach adopted. Emphasis was placed in each step on the importance of understanding the model and introducing sound domain engineering knowledge to ensure the derived ML model to remain physically meaningful. It is believed that the discussed approach and methodology can be extended to the development of Model A to a territory-wide scale for it to better facilitate the formulation of the slope safety management strategy and land use planning.

With reference to the above, the GEO has kick-started another exploratory study to apply ML to enhance the prediction model of landslides on man-made slopes. It is expected to gain insight into the relevance of various factors to the landslide occurrence, while the consistency with our domain knowledge on the landslide occurrence would be carefully assessed throughout the study. The upcoming technical development work would indubitably uncover the potential of ML in landslide prediction, to make a remarkable contribution to the slope safety system in Hong Kong.

ACKNOWLEDGEMENTS

This paper is published with the permission of the Head of the Geotechnical Engineering Office and the Director of Civil Engineering and Development, the Government of the Hong Kong Special Administrative Region, China.

REFERENCES

Brabb, E.E. 1984. Innovative approaches to landslide hazard mapping. *Proceedings of 4th International Symposium on Landslides*, 1, 307-324.

Breiman, L., Friedman, J.H., Olshen, R.A.& Stone, C.J. (1984). *Classification and Regression Tree.* Wadsworth, New York.

Breiman, L. (2001). Random Forest. *Machine Learning*, Volume 45, pp. 4-32 (2001).

Cox, D. R. (1958). The regression analysis of binary sequences. *Journal of the Royal Statistical Society: Series B (Methodological)*, 20(2), 215–232.

Chen, T. & Guestrin, C. (2016). XGBoost: A Scalable Tree Boosting System. *Proceedings of the 22nd ACM SIGKDD International Conference on Knowledge Discovery and Data Mining*. San Francisco, CA, pp. 785-794.

Cheung, R.W.M. (2021). Landslide risk management in Hong Kong. *Landslides*. 18, pp 3457-3473.

Chung, P.W.K., So, S.T.C. & Chu, E.K.H. 2023. Landslip Warning System in Hong Kong – Over 40 years of evolution, *Current Chinese Science 3(2)*, pp 123-140.

Cortes, C., & Vapnik, V. (1995). Support-vector networks. *Machine Learning*, 20(3), 273–297.

Ho, K.K.S. & Cheung, C. 2021. Human fingerprints in landslides the importance of strategic landslide risk management, *Proceedings of 13th International Symposium on Landslides*, Cartagena, Colombia, 2021, 1-40.

Ho, K.K.S. & Lau, T.M.F. 2008. The systematic landslide investigation programme in Hong Kong, *Landslides and Engineered Slopes, from the past to the future*, CRC Press, 243-248.

Ke, G., Meng, Q., Finley, T., Wang, T., Chen, W., Ma, W., Ye, Q. & Liu, T. (2017). Lightgbm: A highly efficient gradient boosting decision tree. *Advances in Neural Information Processing Systems*, 30, 3146–3154.

Ko, F.W.Y. (2018). *Terrain-based Landslide Frequency Map for Natural Terrain in Hong Kong (GEO Report No. 340)*. Geotechnical Engineering Office, Civil Engineering and Development Department, Hong Kong, 18 p.

Kong, V.W.W., Kwan, J.S.H. & Pun, W.K. (2020). Hong Kong's landslip warning system – 40 years of progress. *Landslides*. 17, pp 1453-1463.

Lam, C.C.L., Mak, S.H., & Wong, A.H.T. 1998. A new slope catalogue for Hong Kong. In *Slope engineering in Hong Kong, Proceedings of 17th Annual Seminar of Geotech. Division*, Hong Kong Institution of Engineers, Hong Kong, pp. 235-242.

Li, H.W.M., Lo, F.L.C., Wong, T.K.C. & Cheung, R.W.M. (2022). Machine Learning-Powered Rainfall-Based Landslide Predictions in Hong Kong – An Exploratory Study. *Appl. Sci.* 2022, 12, 6017. https://doi.org/10.3390/app12126017.

Lo, F.L.C., Law, R.P.H. & Ko, F.W.Y. (2015). *Territory-wide Rainfall-based Landslide Susceptibility Analysis (Special Project Report No. SPR 1/2015)*. Geotechnical Engineering Office, Civil Engineering and Development Department, Hong Kong, 27 p.

Ma, Z.; Mei, G.; Piccialli, F. Machine Learning for Landslides Prevention: A Survey. *Neural Computing and Applications 2021*. 33(17), 10881–10907.

Mak, S.H., Ma, T.M., Chan, T.P. & Chan, D.C. 2001. Slope Information System – An indispensable tool for Hong Kong slope safety management, Proceedings of the fourteenth Southeast Asian Geotechnical Conference – Geotechnical Engineering Meeting Society's Needs, 1, 855-861.

Martinello, C., Cappadonia, C. & Rotigliano, E. (2022). Investigating the effects of cell size in statistical landslide susceptibility modelling: a test for different landslide typologies in central-northern Sicily. *Remote Sens*. Not yet published.

Ng, C.W.W., Yang, B., Liu, Z.Q., Kwan, J.S.H., Chen, L. (2021). Spatiotemporal modelling of rainfall-induced landslides using machine learning. *Landslides*, 18: 2499-2514.

Pun, W.K., Wong, A.C.W. & Pang, P.L.R. 1999. *Review of Landslip Warning criteria 1998/1999 (Special Project Report No. SPR 4/99)*, Geotechnical Engineering Office, Civil Engineering and Development Department, Hong Kong, 77 p.

Rosenblatt, F. (1958). The perceptron: a probabilistic model for information storage and organization in the brain. *Psychological Review*. 65 (6): 386–408.

Spackman, K.A. (1989). Signal detection theory: Valuable tools for evaluating inductive learning. *Proceedings of the Sixth International Workshop on Machine Learning*. San Mateo, CA, pp. 160-163.

Wang, H., Zhang, L., Lau, H., He, J., Cheung, R.W.M. (2021). AI-powered landslide susceptibility assessment in Hong Kong. *Engineering Geology*, 288, 106103.

Yu, Y.F. 2004. *Correlations between rainfall, landslide frequency and slope information for registered man-made slopes, GEO Report No. 144*. Geotechnical Engineering Office, Civil Engineering and Development Department, Hong Kong, 109 p.

Model Deep Cement Mixing Specification for Hong Kong

Sunny TC SO, Leo CY SHU, Linda YW IU and Lawrence KW SHUM
Geotechnical Engineering Office, Civil Engineering and Development Department,
The Government of Hong Kong SAR

ABSTRACT: Reclamation outside Victoria Harbour is one of the multi-pronged approaches of increasing land supply in Hong Kong and tops the agenda of the current-term Government of HKSAR in order to build up a land reserve in the long run to solve the housing problem. The Government has been proactively pressing forward studies for such new reclamation projects as in Lung Kwu Tan and Ma Liu Shui, in addition to those for Kai Yi Chau Artificial Islands and North Lantau. This calls for cost-effective planning, design and construction practices of reclamation works in Hong Kong in order to expedite land production in meeting the vision set in the Hong Kong 2030+. The Geotechnical Engineering Office (GEO) of the Civil Engineering and Development Department (CEDD) has taken steps to work hand in hand with practitioners, academia and relevant government departments to consolidate the experience gained from the recent reclamation projects in the territory to enhance the design and construction practices. Focus has been put not only on enhancing the quantity, speed, efficiency and quality of reclamation works, but also promoting the adoption of the latest smart technologies and green construction materials to set a new norm for sustainable development. The first deliverable is the model specification for deep cement mixing (DCM), a prevailing ground improvement technique used in non-dredged reclamation. This paper discusses the rationales and considerations behind the enhancements on the DCM construction specification that could benefit future reclamation projects, and moreover, the planning of and actions taken by the GEO in developing a state-of-the-art while practical local design and construction guide for different reclamation methods and ground improvement techniques.

1 INTRODUCTION

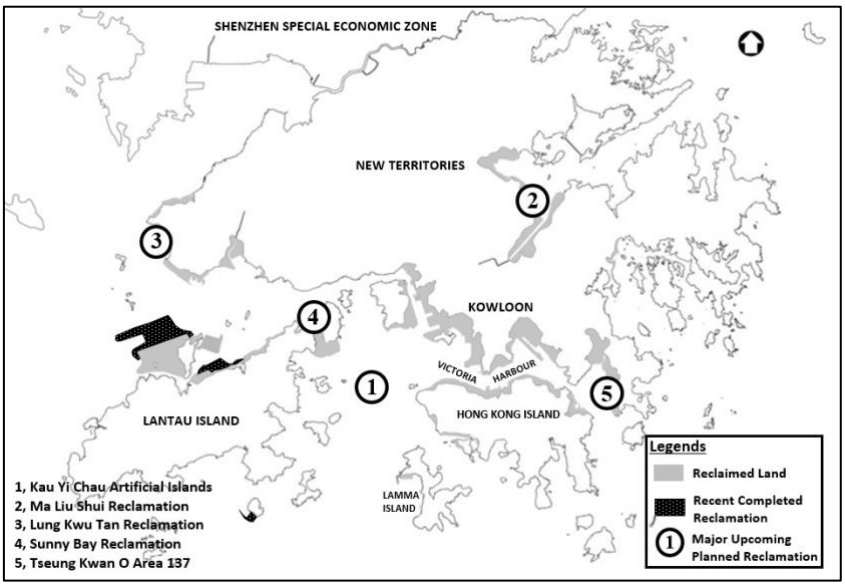

Figure 1: Major upcoming reclamation projects (PlanD 2021; CEDD 2019, 2020)

Hong Kong had undergone a series of reclamation operations along the shorelines of Victoria Harbor since the 1850s to expand the Hong Kong Island and Kowloon Peninsula for accommodating a growing population, where these reclaimed lands underwent fast urbanisation. Reclamation has added about 6,500 hectares of land to the original land area of Hong Kong. Since the enactment of the Protection of the Harbour Ordinance in 1996,

the pace of reclamation has been substantially slowed. In a bid to meet the ever-growing housing needs of society, the Government revives reclamation as an important strategy for the long-term land supply, as it can provide vast tracts of new land for development. Figure 1 summarises the reclamation works done in the past and the planned reclamation projects in the coming years. Moving on from the conventional dredged reclamation method, the reclamation techniques have evolved significantly over time, with new technologies and methods being developed to improve the sustainability and efficiency of land reclamation. The DCM method adopted in Tung Chung East Reclamation project, for instance, advanced the completion of reclamation by about 6 months when compared with the conventional drained method using prefabricated vertical drains and surcharging; saved around 6 million tonnes of fill material due to reduced replenishing settlement; and reduced 3,000 vessel trips passing through the north Lantau water channel near Brothers Marine Park which in turn resulted in less energy consumption, noise and air impacts as well as disturbances to marine habitats (HKIE 2022). Extensive use of DCM in reclamation started in around 2016-2017 for the Three Runway System and Tung Chung East Reclamation projects. At that time, the design and construction specifications were largely based on overseas practice and inevitably, conservative and cautious approaches were adopted by the designers and the authority. The experience gained in these large-scale reclamation projects provides an excellent opportunity for Hong Kong practitioners to obtain the domain knowledge in the application of DCM and pave the way for developing a local guidance document that would best suit the Hong Kong setting. As the first step, the GEO is currently developing a model specification and technical guidance notes for DCM works in Hong Kong through joint efforts with practitioners, academia and relevant government departments, which will improve the quality, cost and time required of DCM works. The DCM model specification will form part of the interim Design and Construction Guide with a particular focus on DCM method, which will be available tentatively by the end of 2023. The complete Guide covering broader ground improvement and reclamation techniques is tentatively scheduled for promulgation in mid-2025. In the following sections, key enhancement measures which are to be incorporated into the model DCM specification are briefly discussed.

2 IDENTIFYING AREAS FOR IMPROVEMENT IN DCM SPECIFICATION AND BEYOND

With the local experience from the recent local reclamation projects consolidated, several aspects of the use of DCM that could be improved have been identified. In addition to the model DCM specification, guidance notes are also produced to supplement the model specification, covering suggestions on key areas in the planning, design, construction and testing stages. The recommendations are prepared in consultation with local practitioners, academia and relevant government departments, with due consideration of the experience and lessons learnt from recent DCM applications in Hong Kong. Moreover, the guidance notes not only detail the rationales of the enhancements, but also aid in setting directions for the GEO to develop the technical guidelines.

The following key areas extracted from the model DCM specification and guidance notes are presented in the remaining parts of the paper.

a) Planning stage: Ground investigation strategy
b) Design stage: Requirement on coring and sampling frequency
c) Construction stage: Use of green binder materials, reuse of heaved materials, smart construction monitoring (digitalisation and automation)
d) Testing stage: Performance-based testing plan

3 APPROACH TO PLANNING AND DESIGN

3.1 Ground Investigation Strategy

Issue identified: For a large-scale reclamation project involving DCM construction, sufficient ground investigation (GI) data for design is essential for smooth and fast construction. However, project delivery schedule is always tight and resources for carrying out marine GI works are usually limited. The designer often faces challenges in producing a robust design scheme with limited GI data. Moreover, some DCM projects in

Hong Kong relied on electric current response of mixing rig and adopted post-construction GI works (i.e. performing cone penetration tests (CPTs) after completion of DCM elements) as quality control methods of confirming the sufficient embedment length of DCM element into the competent stratum (i.e. a soil layer that can provide sufficient support for the DCM element without excessive settlement). However, the challenges of this practice were that rig current readings could be easily affected by various site conditions and installation parameters (i.e. workmanship of DCM rig operator and local small obstructions below seabed level) and there could be risk of late revelation of problem by the post construction verification works; any remedial works required would result in a delay in site progress, especially when manoeuvring of marine plants in very often congested site condition was not easy.

Way forward: Sufficient time and resources should be secured in the project planning stage. Together with a proper GI strategy, e.g. phased marine GI as suggested in Port Works Design Manual (CEDD 2002), acquaintance of sufficient GI information to pre-determine the toe level would be possible with minimal geotechnical risk, thus eliminating the late revelation of abrupt change in geology by post-construction GI works which may have time and cost implications. Nevertheless, it is still prudent to maintain real-time monitoring of the rig current during DCM installation which should only serve as a reference for the engineer on site to verify the pre-determined design toe level. The engineer should intervene only when obvious deviation from expected rig current profile is observed. The concept of pre-determination of DCM element toe levels will be incorporated into the model DCM specification.

The GEO is undertaking studies to explore the use of data-driven tools to leverage on existing geological knowledge and to develop a cost-effective GI strategy by using "machine learning" approach to adaptively optimise locations and quantity of GI works to determine the subsurface geology with minimal stratigraphic uncertainty through the most effective spatial distribution of borehole locations before construction. This concept, which could lead to substantial savings in both time and resources throughout the marine GI works at different phases before commencement of construction works, would later be incorporated into the guidance documents when the "machine learning" approach is developed through a series of hypotheses testing and verification. Should this AI-assisted approach be adopted in the future, this would mean GI planning would shift from "empirically specified" to "statistically based" which is more efficient with higher reliability. The reliance of post-construction verification works such as coring, CPTs and rig current readings could therefore be further minimised and more rational decisions could be made by the engineer in selecting the location of post-construction GI for verification.

3.2 Requirement on Coring and Sampling Frequency

Issue identified: In the absence of local guidelines and experience, the design of DCM works in recent projects was based on overseas guidelines and practices and the construction works were carried out in a more conservative approach to ensure the quality. With reference to recent local DCM projects, approximately 3% to 6% of DCM elements constructed along seawall area in a project were selected for coring. The frequency certainly tops amongst other international practices. Similar situation was also observed in sampling. A comparison between overseas practices and local experiences is given in Tables 1 and 2. As such, the specified coring and sampling frequencies are one of the many examples that designers should focus on to avoid excessive works.

Table 1: Recommended/Adopted Coring Frequency in Overseas and Hong Kong

Reference	Recommended/Adopted Coring Frequency
Federal Highway Administration Design Manual	2% to 4% of DCM elements constructed. At a minimum, five DCM elements should be cored, even for small projects (FWHA 2013).
JTS 147-2017 Code for Foundation Design on Port and Waterway Engineering – Clause 9.3.4.6(3)	Minimum 3 cores or 0.5% to 1% of DCM elements constructed, whichever is greater (MTPRC 2017).

Overseas publications	3% of DCM elements constructed (Li et al. 2015)
	1 core per 1,000 linear meters of DCM elements constructed, where linear meter means depth along a DCM element (equivalent to 2% of DCM elements constructed*) (Daramalinggam et al. 2019).
	1 core is generally conducted for every 10,000m^3 of treated soil (i.e. volume of DCM elements). When the total volume exceeds 100,000m^3, 1 additional core should be conducted for every further 50,000m^3 (equivalent to approximately 0.2% to 0.9% of DCM elements constructed*) (Kitazume and Terashi 2013).
Local projects	Approximately 3% to 6% of DCM elements constructed.

* Conversion is made by assuming each DCM element constructed is 20m in length and has a cross sectional area of 4.6m^2.

Table 2: Recommended/ Adopted Sampling Frequency in Overseas and Hong Kong

Reference	Recommended/Adopted Sampling Frequency
Federal Highway Administration Design Manual	At least 5 test specimens from each full-depth continuous core (FWHA 2013).
Overseas publications	Samples from 5 representative depths (Daramalinggam et al. 2019).
	Core run returned from 3 representative depths and 3 samples from each core run (Kitazume and Terashi 2013).
Local projects	1 sample per metre core-run along the full-depth continuous core or 10 tests per full depth core sample.

Way forward: A project-specific coring and sampling plan should be determined based on the following key considerations:

a) Project size and complexity;
b) Nature of supporting structures and magnitude of loading after completion;
c) Variability of sub-surface conditions;
d) Variability of deep mixing performance with respect to the level of control and detailing of specifications;
e) Variability of operational parameters and mix design;
f) Workmanship;
g) Confidence level of deep mixing performance; and
h) Economic consequence for subsequent rectification.

It is also worth noting that by plotting the strength test results of cored DCM samples against depth, the general strength characteristics of DCM material in relation to a geological profile can be observed as illustrated in Figure 2.

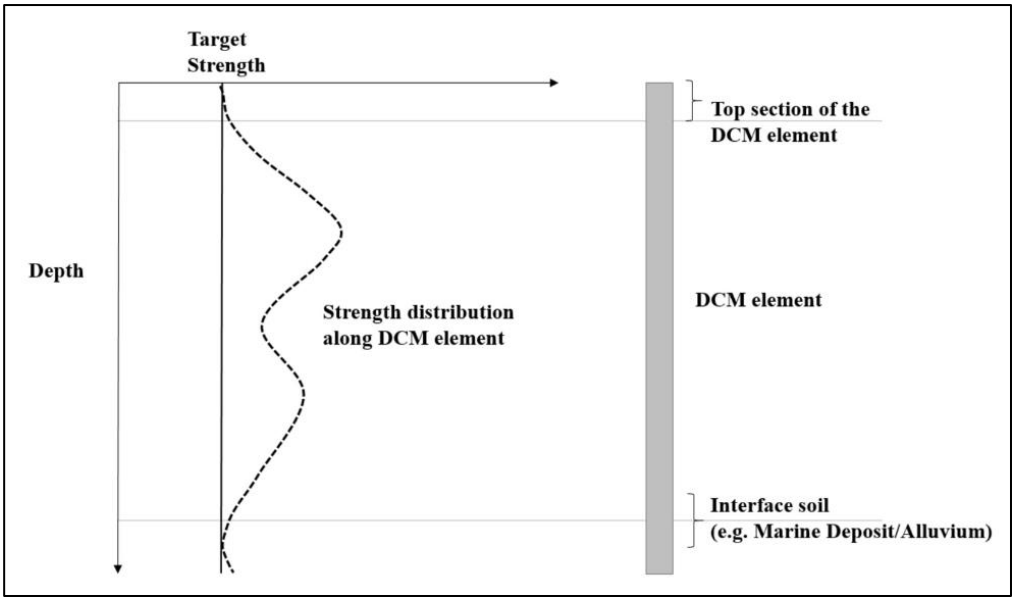

Figure 2: Example variation of unconfined compressive strength of DCM material with depth

With reference to HKIE's Interim Guidelines on Testing of UCS of Cement Stabilised Soil Cores in Hong Kong (HKIEGD 2017), only the correction factors for UCS test results of specimens with a length-to-diameter ratio (L/D) of 1.5 to 2.0 are adopted. The GEO thus carried out further study in collaboration with the HKU (Chung et al. 2022) and extended the L/D range to cover 1.0 to 1.5. With such findings, it is envisaged that greater flexibility will be allowed for engineers on site to select cored DCM samples for UCS testing.

Based on the international norm as shown in Table 1 and 2, general DCM material behaviors shown in Figure 2 and together with a more flexible sample dimension ratio available for strength compliance testing, the location and frequency of coring, as well as the depth and frequency of sampling should be carefully determined to cost-effectively uphold the quality of DCM works. The GEO would continue to study this subject with a view to optimise the coring and sampling frequencies and later incorporate recommendations into the guidance documents.

4 APPLICATION OF SUSTAINABLE MATERIALS AND SMART CONSTRUCTION TECHNOLOGY

4.1 Use of Green Binder Materials

Issue identified: Ordinary Portland Cement (OPC) is a typical binder for strengthening of in-situ soils. Its performance and application have no doubt been verified by the construction industry across the globe and is widely adopted, particularly in concrete production. Due to its innate versatility and strength gaining characteristics as a binder material, OPC has been adopted as a binder material to mix with in-situ marine soils to form DCM elements.

However, in view of the large quantity of OPC required for DCM works and the associated high carbon footprint during OPC production, the sustainability of future DCM works should be reviewed. Moreover, the performance of OPC as a binder with in-situ marine soils at different ranges of pH values and organic contents are well documented in the literature (Kitazume and Terashi 2013). In general, the strengths of soils treated by OPC at high acidity or high organic content tend to be low (see Figure 3).

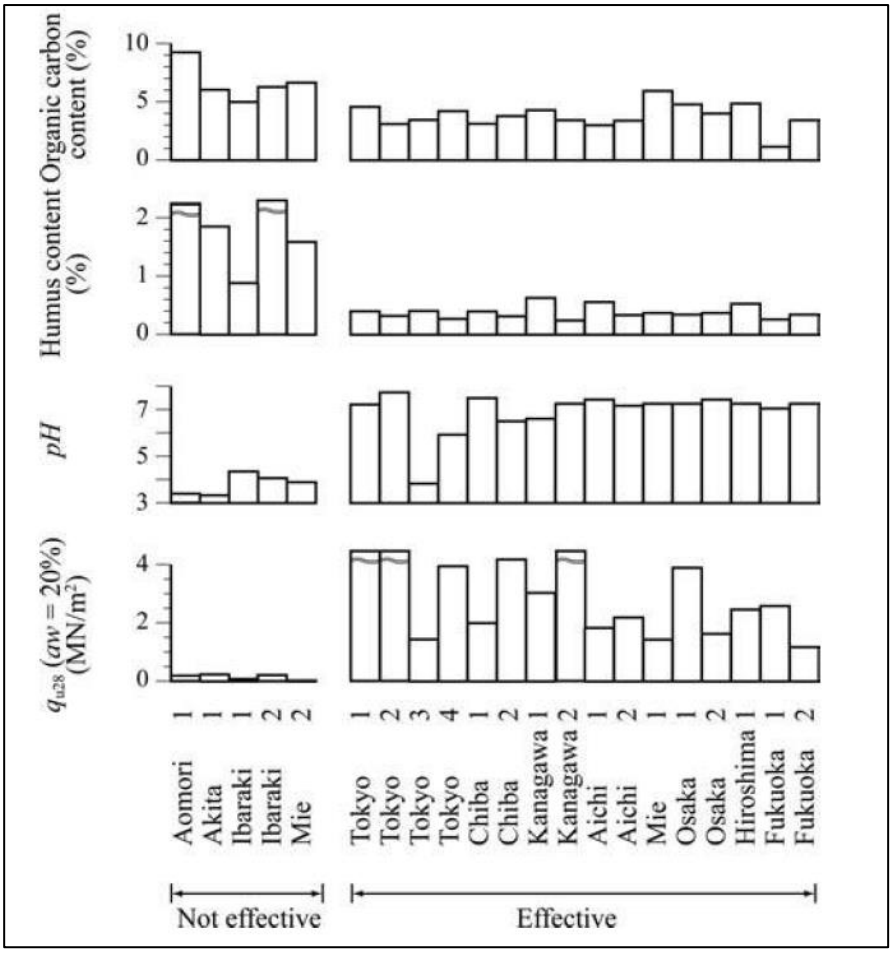

Figure 3: Extract of findings on influence of soil pH and organic carbon contents on strength of cement stabilised soil (Kitazume and Terashi 2013)

Way forward*:* Portland Blast-furnace Cement (PBFC), which has been available in the market for a while, is a solution to this problem. PBFC is a homogeneous blend of OPC and Ground Granulated Blast-furnace Slag (GGBS). From the engineering perspective, the good performance of PBFC as a binder mixed with marine deposits or alluvium clay in Hong Kong has been proven in recent reclamation projects. Its performance even surpassed that of OPC (see Figure 4). PBFC because of GGBS is more resistant to acid and organic matters when compared with OPC (Lang et al. 2020). From the sustainability point of view, GGBS, practically "carbon emission free", substitutes a portion of OPC in PBFC. The typical CO_2 emissions arising from the production of GGBS is approximately one sixteenth that of OPC only (Seymour 2007). In the Tung Chung East Reclamation project, the use of PBFC with 60% GGBS content reduced CO_2 equivalent carbon greenhouse gas emission by around 600,000 tonnes (HKIE 2022).

In view of the above advantages, adoption of PBFC in DCM works is recommended in the guidance notes. The GEO would also be looking into the possibilities of optimising the dosages of GGBS in PBFC as well as adopting other commonly available sustainable binder materials to replace OPC with an aim to further lowering carbon emission while keeping the required design strength achievable. Findings and recommendations on green binder materials would be duly incorporated into the guidance documents.

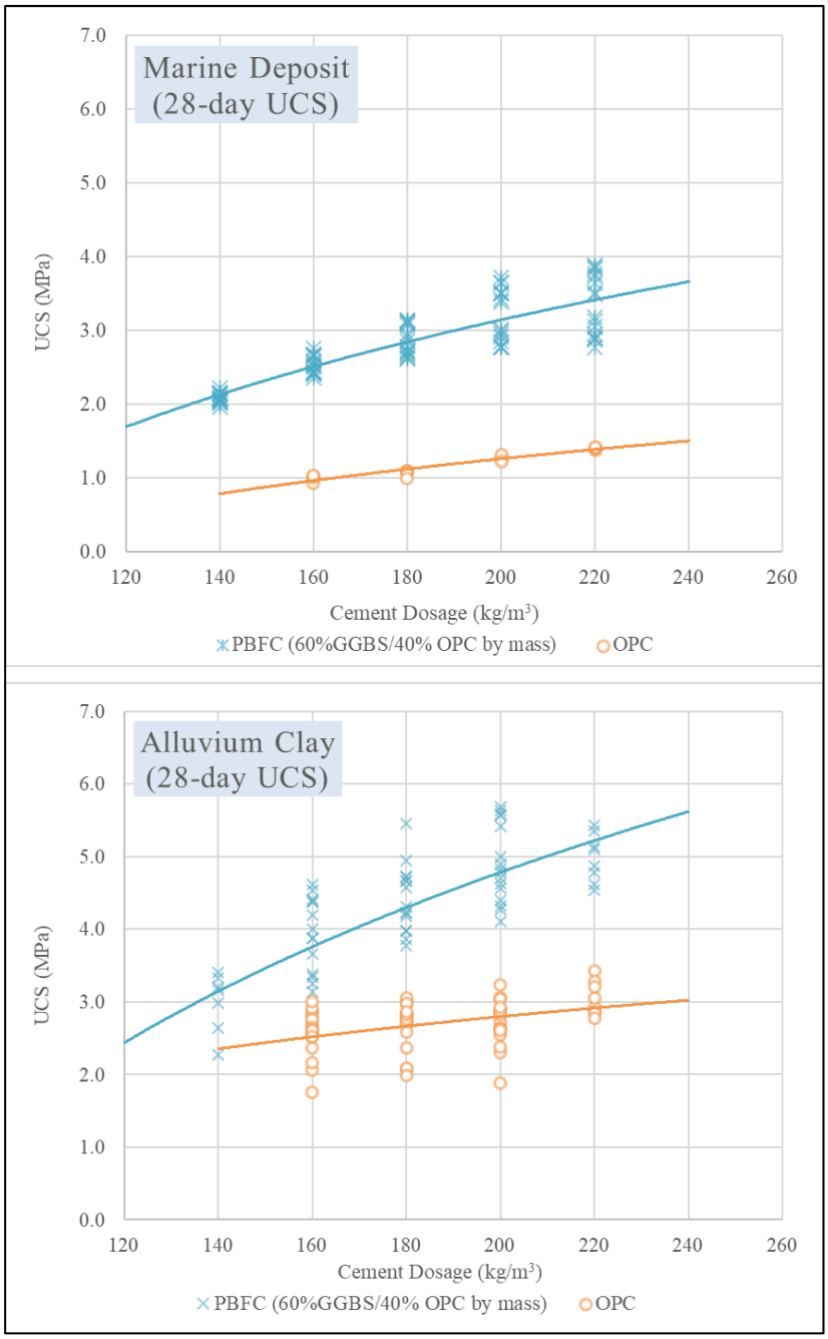

Figure 4: Comparison of 28-day UCS of OPC and PBFC treated marine deposits and alluvium clay at different binder dosage (Cheung et al. 2021)

4.2 Reuse of Heaved Materials

Issue identified: Heaved materials, a mixture of marine clay, sand and cement formed at the top of DCM clusters after DCM clusters installation, is unavoidable. While the volume of the heaved materials accounts for approximately 70% of the injected cement slurry volume (Kitazume and Terashi 2013), the volume of heaved materials could be substantial in large-scale DCM works. Typically, heaved materials are removed to prevent the formation of a weak layer in the seawall foundation because of its lower strength. However, the additional cost and time incurred from levelling of the seabed and removal of heaved materials off site are undesirable. Figure 5 illustrates the formation of heaved materials.

Way forward: The first step is to minimise heaving. In the previous projects, DCM cluster top level was terminated at 1m below the top of sand blanket as stated in the contract specification. However, heaving will raise the top level of the sand blanket resulting in getting the DCM cluster top termination level higher and higher. The requirement will be revised in the model DCM specification to terminating the DCM cluster top at a certain distance from a fixed datum, not necessarily the original seabed level, as specified in the drawing. Notwithstanding this, heaving is inevitable and removal of the heaved materials may be necessary in critical location, e.g. beneath the seawall structure. Appropriate treatment (e.g. mixed with suitable fill and/or binder) of the heaved materials can make them suitable for reuse as a fill material in the same main reclamation area. Such a treatment option will be desirable and thus incorporated in the DCM model specification. Chen et al. (2022) reported a full-scale test that had demonstrated the performance of the reused heaved materials resulting from high cement dosage, low water/cement ratio, low injection pressure and low blade rotation number near the top of the DCM elements could meet the design requirement as a fill material.

Further study would also be carried out by the GEO to investigate the type of green binder materials that are suitable for turning heaved materials into a suitable fill material. Findings and recommendations would be duly incorporated into the guidance documents.

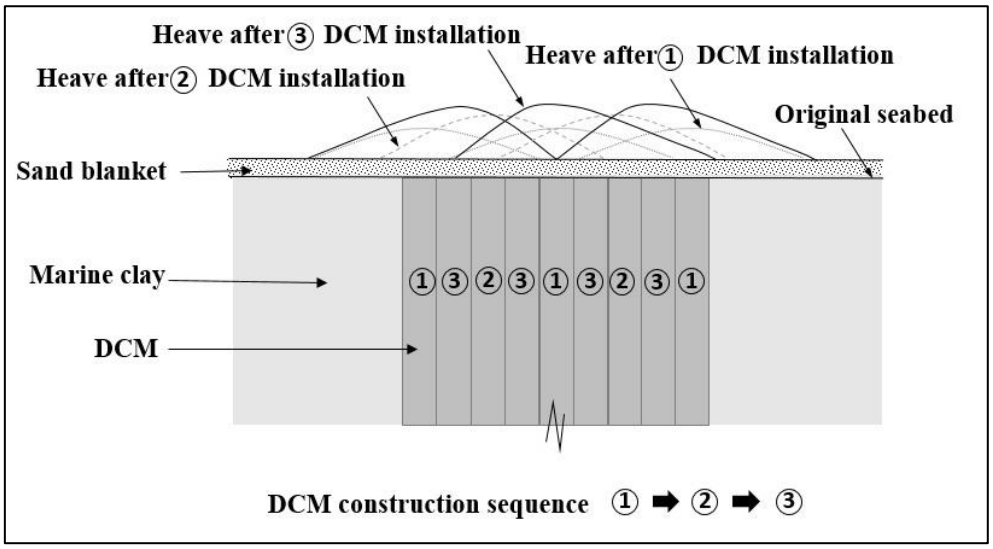

Figure 5: Formation of heaved material above DCM clusters

4.3 Smart Construction Monitoring (Digitalisation and Automation)

Issue identified: In a large-scale DCM project, effective data management and communication between the front line and the engineer in site office is often difficult. As such, delays are inevitable and hinder the engineer from providing timely responses to any non-conformity on site, leading to a situation that the quality of DCM works carried out at that instance heavily relies on the experience of the DCM contractor. With a substantial time lapse between DCM installation and data analysis by the engineer, additional maneuvering of DCM plants and time are therefore required in case additional or remedial works are identified. Moreover, without centralising the DCM installation data and analysis results, more resources and manpower from both the contractor and the engineer are expected for continuous monitoring to maintain the high quality of DCM works.

Way forward: With the aim of enhancing the efficiency and the quality of works, it is desirable to provide a project specific digital platform (PSDP) to serve as a common data environment to facilitate seamless and dynamic information exchange on DCM works between the contractor and the engineer. The concept is illustrated in Figure 6. The PSDP should have the following functions:

a) To serve as a hub for the real-time management of DCM works construction records and to facilitate the analysis of the quality of works;

b) To serve as a common data environment to facilitate seamless and dynamic information exchange between the engineer and contractor. In this regard, compatibility with the BIM model specified in the contract is recommended;
c) To monitor the progress of DCM works;
d) To quickly identify some suspicious non-compliance cases for those installed DCM elements not meeting the installation parameters;
e) To provide information to facilitate the engineer and contractor to make decision on the need for any necessary remedial actions; and
f) To support the development of digital twins for the project, if any.

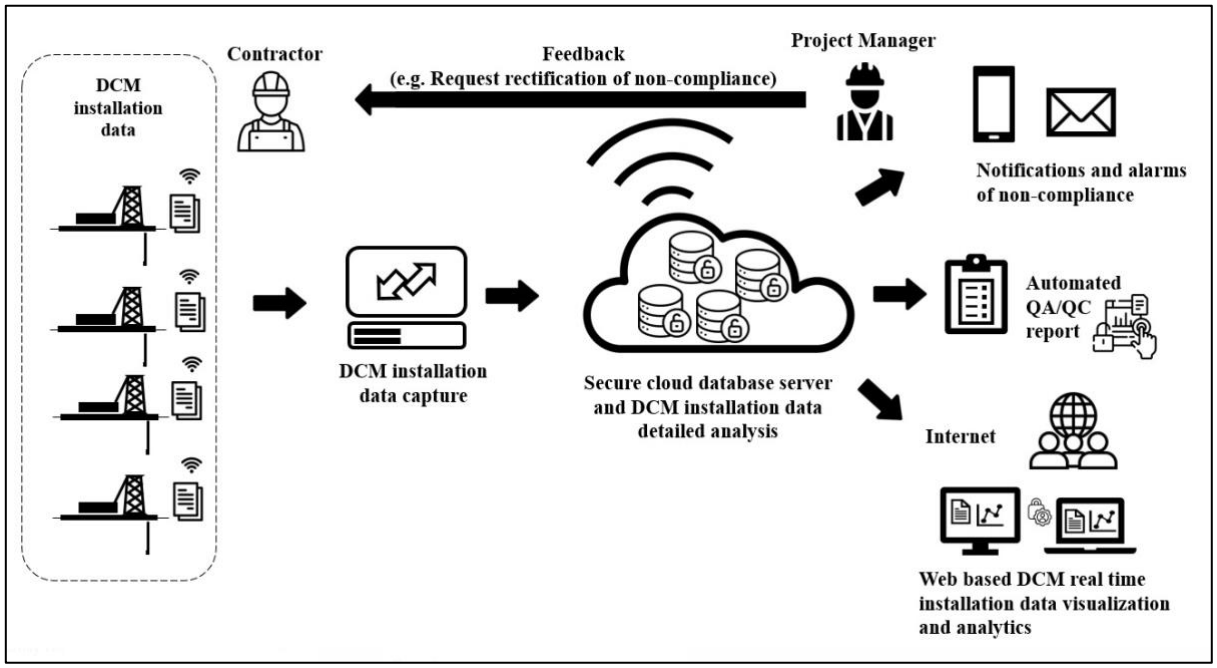

Figure 6: Real-time monitoring of DCM installation data and feedback

It is recommended that a set of detailed specifications and requirements on digitalisation (e.g. details on data handling and format standardisation, appropriate computer hardware, system software, servers, security, data backup system, power supply system, fixed broadband internet network communication services, testing requirements and all other necessary equipment, staffing and infrastructures to meet the functional requirements of the PSDP) should be formulated and included in the contract specification. If the situation permits, such PSDP should be developed during the detailed design stage to enable early setup and identification of any follow up actions to be included in the specification. The designer is recommended to work out the implementation plan as soon as the specifications are developed. The employer may also consider the procurement of supporting services to facilitate early establishment of PSDP, and collocating users' requirements for enhancing construction management.

The detailed specifications and requirements on digitalisation would be further elaborated in the model DCM specification and guidance documents.

5 INCORPORATING THE MATERIAL BEHAVIOR ON DCM TREATED SOIL

5.1 Performance-based Testing Plan

Issue identified: With reference to Federal Highway Administration Design Manual on Deep Mixing for Embankment and Foundation Support (FWHA 2013) and the experience in local projects, the design shear strength of DCM treated soil is derived from 28-day UCS with factors applied to cater for different scenarios, applications, strength variability and risk level. On the other hand, it has been well understood that the strength

of the DCM continues to increase beyond the 28-day. To arrange the tests to be carried out on the 28-day, coring is recommended to be carried out from the 20th to 25th day for higher core recovery (FWHA 2013). Under this rigid 28-day design requirement, the contractor always faced the difficulties of planning and maneuvering the coring plants and DCM plants to allow for the coring at the specified day. Moreover, the contractor may tend to, for instance, provide a conservative binder dosage in order to meet the target strength specified in the contract, resulting in a higher construction cost (reflected as a higher tender price).

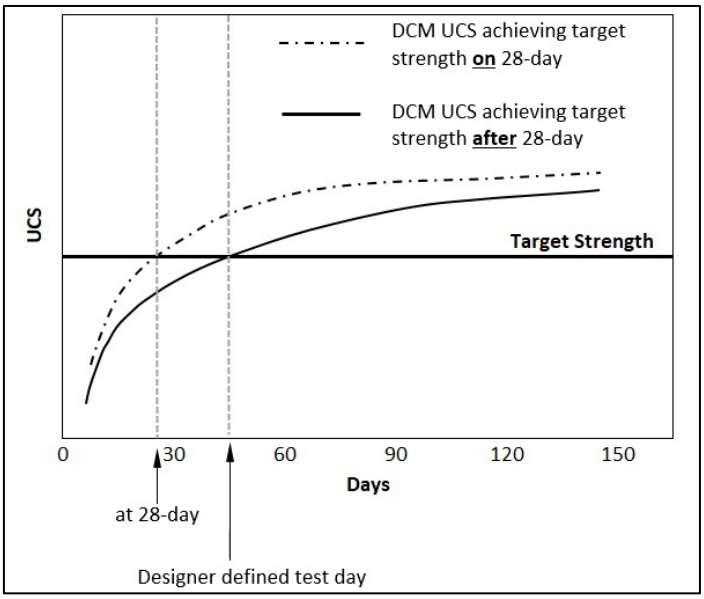

Figure 7: Designer defined UCS test day

Way forward: The effect of curing time on strength gain is well documented in the literature and local projects. Whilst the 28-day UCS is adopted in general, the designer may alternatively consider the curing time effect to enhance the cost-effectiveness of design. From the quality control perspective, it is preferable to assess the mixing performance as soon as practicable. In case of non-compliance, corrective measures can be executed and QA/QC system can be reviewed immediately. On the other hand, the tests may not necessarily be conducted on the 28-day from the geotechnical design perspective, unless the construction sequence warrants.

In essence, the periodical DCM plant site trial for performance verification and the associated selected cores could be tested for the 28-day strength as a quality control. The designer may specify the range of curing time and allow the tests to be carried out within a specified period as the design verification. Notwithstanding the above, it should be reiterated that the specified period should not be unreasonably early or late that renders core recovery being infeasible or any defect not recoverable. As an example, if the design shear strength is derived from 1MPa and the subsequent critical activity (e.g. construction of seawalls, reclamation filling, etc.) is anticipated for commencement in 2 months after the completion of DCM works, 1MPa could be taken as the target UCS and the testing period may be specified as from the 28-day to 40-day. The proposed approach not only allows flexibility in construction, but also provides an opportunity for cost savings in relation to the mix design. Figure 7 illustrates the concept with strength-time curves of DCM samples with different binder dosages. The concept will be incorporated into the model DCM specification and guidance documents.

6 CONCLUSIONS

The model DCM specification and guidance notes are just the beginning of an effort to enhance the DCM design and construction works in Hong Kong and the first milestone of the GEO to develop a comprehensive local reclamation design and construction guide. Despite these suggestions would only offer modest improvement to the DCM works, it is believed that significant cost and time savings and further reduction in environmental impacts would result in the upcoming mega-scale reclamation works.

7 ACKNOWLEDGEMENTS

This paper is published with the permission of the Head of the Geotechnical Engineering Office and the Director of Civil Engineering and Development, the Government of the Hong Kong Special Administrative Region.

8 REFERENCES

American Concrete Institute (ACI) Committee 233. 2019. Slag Cement in Concrete and Mortar. ACI 233R-03. American Concrete Institute. (Available at https://ksaravind.yolasite.com/resources/P.K.Metha%20 CONCRETE%20-%20microstructure%20properties%20and%20materials.pdf)

Chen, J., Chen, L.T. and Chan, Y.P. 2022. A study of Heaving Material Resulted from Deep Cement Mixing Construction. In Toh, S.H.G. Editor(ed.) and Lee, S.W. (ed.), *Proc. of The HKIE Geotechnical Division 41st Annual Seminar: Adapt to Challenges, Create to Thrive, 18 May 2021*. The Hong Kong Institution of Engineers. (Available at https://books.aijr.org/index.php/press/catalog/book/126/chapter/1526)

Civil Engineering and Development Department, The Government of the HKSAR (CEDD). 2002. *Port Works Design Manual*. Civil Engineering and Development Department, The Government of the HKSAR. (Available at https://www.cedd.gov.hk/eng/publications/ceo/pwdm/index.html)

Civil Engineering and Development Department, The Government of the HKSAR (CEDD). 2019. *Role of Reclamation in Hong Kong Information Sheet (3)*. Civil Engineering and Development Department, The Government of the HKSAR. (Available at https://www.cedd.gov.hk/filemanager/eng/content_954/Info_ Sheet3.pdf)

Civil Engineering and Development Department, The Government of the HKSAR (CEDD). 2020. *Executive Summary on Strategic Environmental Assessment for Reclamation*. Civil Engineering and Development Department, The Government of the HKSAR. (Available at https://www.cedd.gov.hk/ filemanager/eng/content_961/4/Executive_Summary_on_Strategic_Environmental_Assessment_for_Reclama tion_-_Figures.pdf)

Cheung, K.W.C, Wong, H.K.A., Cheung, K.T.H and So, T.C.S. 2021. Design of Deep Cement Mixing Treatment for Non-dredged Seawall in Hong Kong. *Proc. Of Deep Mixing 2021 Online Conference, Hawthorne, US, 17 June 2021.* Deep Foundation Institute.

Chung, P., Chu, F., Cheung, H., Yan, C.H., Cheung, C. and Wong, A. 2022. Technical Developments Related to Deep Cement Mixing Method in Hong Kong. In Lee, S.W. Editor(ed.) and Leung, Y.F.A. (ed.), *Proc. of The HKIE Geotechnical Division 42nd Annual Seminar: A New Era of Metropolis and Infrastructure Developments in Hong Kong, Challenges and Opportunities to Geotechnical Engineering. Hong Kong, 13 May 2022*. The Hong Kong Institution of Engineers. (Available at https://books.aijr.org/index.php/press/catalog/book/133/ chapter/1724)

Daramalinggam, J. and Yohannes, M.M. 2019. Specifications, Sampling Methods and Correlations of Engineering Properties for Deep Soil Mixing and Jet Grouting in Malaysia. *International Conference on Case Histories and Soil Properties, Singapore, 5-6 December 2019.* Geotechnical Society of Singapore. (Available at https://www.researchgate.net/publication/337830284_Specifications_sampling_methods_and correlations_of_engineering_properties_for_Deep_Soil_Mixing_and_Jet_Grouting_in_Malaysia)

Federal Highway Administration (FWHA). 2013. *Federal Highway Administration Design Manual: Deep Mixing for Embankment and Foundation Support, Report No. FHWA-HRT-13-046, October 2013*. U.S. Department of Transportation, Federal Highway Administration.

Kitazume, M. and Terashi, M. 2013. *The Deep Mixing Method*. CRC Press.

Lang, L., Song, C., Xue, L. and Chen, B. 2020. Effectiveness of Waste Steel Slag Powder on the Strength Development and Associated Micro-mechanisms of Cement-stabilised Dredged Sludge. Construction and Building Materials 240 (2020): 117959.

Li, M., Williams, R., Wilson, B. and Filz, G. 2015. Effective Sampling, Testing and Specification Approaches for Deep Mixing at Kitimat LNG, BC. *Proc. Deep Mixing 2015 Conference. San Francisco, 2-5 June 2015*. Deep Foundation Institute. (Available at https://www.geosystemsbruce.com/v20/biblio/305%20-%20Kitimat%20LNG%20DM%20paper%202-QAQC.pdf)

Ministry of Transport of the People's Republic of China (MTPRC). 2017. *Code for Foundation Design on Port and Waterway Engineering.* Ministry of Transport of the People's Republic of China.

Planning Department, The Government of the HKSAR (PlanD). 2021. *Towards a Planning Vision and Strategy Transcending 2030*. Planning Department, The Government of the HKSAR. (Available at https://www.pland.gov.hk/pland_en/p_study/comp_s/hk2030plus/document/2030+_booklet.pdf)

Seymour, P. 2007. Sustainable Cement. Passive House + Sustainable Building, https://passivehouseplus.ie/articles/sustainable-building-technology/sustainable-cement (accessed on 5 April 2023).

The Hong Kong Institution of Engineers (HKIE). 2022. Tung Chung New Town Extension – Tung Chung East Reclamation, *Journal of The Hong Kong Institution of Engineers*, Volume 50 (March 2022): 08-14. (Available at http://www.hkengineer.org.hk/issue/vol50-mar2022/cover_story/)

The Hong Kong Institution of Engineers Geotechnical Division Task Force on Testing Unconfined Compressive Strength of Cement Stabilised Soil in Hong Kong, Geotechnical Division of HKIE (HKIEGD). 2017. *Interim Guidelines on Testing of Unconfined Compressive Strength of Cement Stabilised Soil Cores in Hong Kong*. The Hong Kong Institution of Engineers.

Monitoring of Flexible Barrier For Slope Safety Against Potential Rockfall Using IoT Sensors

Dr. Tim CHUK T. Y., Ringo SZE W. H.
Amain Engineering Development Ltd., Hong Kong
Mike FUNG S. H.
Hong Kong RFID Limited, Hong Kong
Simon NG P. H., Frankie YEUNG H. W.
Mannings (Asia) Consultants Ltd., Hong Kong

ABSTRACT

Flexible barrier is one of the widely used geotechnical features to mitigate/minimize open hillslope landslide (OHL) hazards affecting roads/existing development for natural terrain. While routine maintenance of flexible barrier may identify early signs of minor rockfall/landslide through visual inspection of any accumulation of rock/soil at toe, the actual happening of such event and/or the duration cannot be assessed/determined which may cause time lag for any necessary follow-up actions.

This can be overcome through the fixing of IoT sensors to flexible barrier posts with a non-destructive metal "mounting clamp" to measure the movement with data then transfer to a cloud platform for analytical process. Data is presented in an easy-to-understand heat map format showing the movement patterns of the entire flexible barrier system. This method helps to detect any large movements of the barriers. In time, through learning the movement patterns especially during adverse weather conditions, can provide valuable reference to Geotechnical/Civil engineers.

INTRODUCTION

1.1 Attributes of Flexible Barrier

Flexible barrier is one of the defense measures adopted in Hong Kong in recent years against landslide debris or boulder fall from natural hillside terrain with the aim to strike a balance between risk mitigation, cost effectiveness and disturbance to the natural environment.

A flexible barrier typically consists of components such as chain wire meshes, steel ring nets, longitudinal steel wire ropes, steel posts, bracing steel wire ropes and energy dissipation devices (Figure 1 and Plate 1). The interval of steel posts is typically at 10.0m c/c.

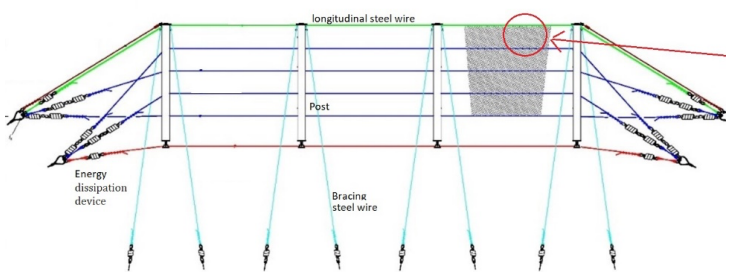

Figure 1: schematic arrangement of flexible barrier

Plate 1: Photo of chain wire meshes and teel ring nets

With Reference to Geotechnical Engineering Office Technical Guidance Note 37 (TGN37), empirical approach can be adopted for the selection of flexible barriers based on the relationship between the open hillside catchment and downhill facilities. The flexible barrier types for selection:

R1: 3,000 kJ flexible rock fall barrier with minimum height of 4 m
R2: 2,000 kJ flexible rock fall barrier with minimum height of 3 m.
R3: 1,000 kJ flexible rock fall barrier with minimum height of 3 m.

For a 3,000 kJ flexible barrier, it is typically assumed that the flexible barrier to have a ceiling velocity of 9.0 m/s under a landslide volume of approx. 200m^3.

1.2 Routine Inspection Practices for Flexible Barrier

In Hong Kong, large majority of flexible barriers were constructed under Landslip Prevention and Mitigation Programme (LPMitP) by the Civil Engineering and Development Department (CEDD). The number of flexible barriers constructed is continuously increasing and CEDD detailed the minimum requirement for inspection and maintenance of flexible barrier in Guide to Slope Maintenance (Geoguide 5).

Under Geoguide 5, the routine maintenance inspection frequency for flexible barrier is governed by the Consequence-to-life (CTL). For CTL Category 1 and Category 2 slopes, the routine inspection frequency is once every year while it is once every two years for Category 3 slopes. It is noted that Geoguide 5 does not require the routine maintenance inspection of flexible barrier be conducted by professional grade personnel with geotechnical knowledge.

For Government Departments, the inspection officer to conduct the routine maintenance inspection for flexible barrier is typically a supervising level staff such as work supervisor or technical officer.
In conducting the routing maintenance inspection, the inspection officer is required to complete the record sheet in Geoguide 5 and identify the need for maintenance works including:

- trim/remove undesirable vegetation from the barrier
- remove accumulated debris from the barrier,
- and other general maintenance actions such as drainage channel clearance.

In addition, the inspection officer is also required to identify, if applicable, whether the barrier has been affected by landslide/rockfill/hill fire with estimation of the volume of debris generated. This would then trigger a special follow-up review by professional engineers and/or barrier manufacturers. Nevertheless, an Engineer's Inspection (EI) by professional engineer is required in 5 years or 10 years intervals depending on the CTL Category of the slope.

Given the routine maintenance inspection covers mainly general maintenance and conducted by non-professional staffs but the flexible barrier is aimed to be, in some circumstance, the last line of defense to facilities against openhill landslide hazard (OHL), therefore the use of internet of thing (IoT) sensors to enhance the monitoring of flexible barrier can provide a solution in an innovative and creative ways.

1.3 This Project

This paper presents the development of tailor-made remote sensor for long term monitoring of flexible barriers in Hong Kong. The sensors are fixed to the flexible barrier steel post(s) near the based supports and measure the acceleration in g (m/s^2) and transfer the measured data directly to a cloud server.

Measured data is then processed to give the movement of steel post in velocity (m/s) to produce a real-time graph at the online cloud platform. The movement of steel posts at the pinned-joint base can be recorded and then be statistically analyzed individually and/or as a whole to "learn" the movement trends with the aim to

produce a baseline movement data during normal and adverse weather condition. In time, with sufficient measured data, this baseline can be used as on-going reference with the aim give alert signal when abnormal movement against baseline is recorded which may indicate the likelihood of a potential landslide/rockfall events that enable relevant parties to trigger a proactive inspection and necessary follow-up action.

2 USE OF IoT SENSORS FOR MONITORING OF FLEXIBLE BARRIER

2.1 Information of IoT Sensors

Development of tailor-made IoT sensor was required with the following conditions:

- accurate measurement of movement/motion and its directions
- ability to transmit measured data wirelessly to cloud platform
- ability to remotely monitor and amend the sensor settings
- minimize power consumption to run minimum 3 months
- not easily notifiable by public and small in size

The team was able to deliver a IoT sensor with Wireless Sensor Network (WSN) that can fulfill the technological difficulties with reliability and productivity (see Figure 2).

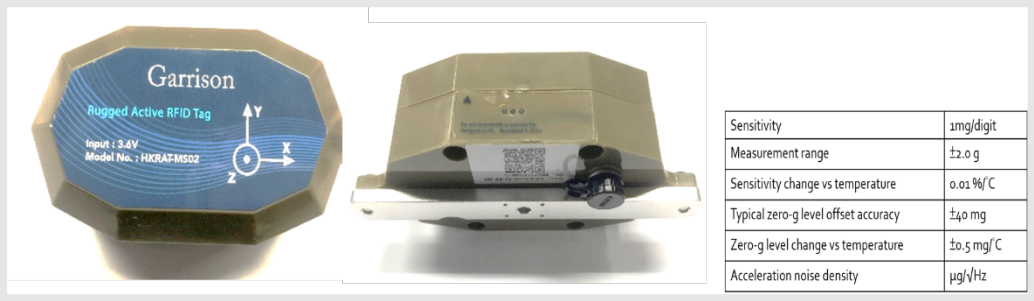

Sensitivity	1mg/digit
Measurement range	±2.0 g
Sensitivity change vs temperature	0.01 %/°C
Typical zero-g level offset accuracy	±40 mg
Zero-g level change vs temperature	±0.5 mg/°C
Acceleration noise density	μg/√Hz

Figure 2: Tailor-made IoT Sensor

2.2 Sensors Components

Within this, there are the sensor, power source and micro-controller all connected to the main board. Another core element is the transceiver which is a chip of Nordic nRF905 to handle data processing in each node. It has an inbuilt proprietary media access control that supports data packets up to 32B and required only an SPI-bus connection to the sensor.

This transceiver does not provide radio function but used to control modulation scheme making it compatible with NB-IoT and battery control.

The sensor just one small part of a complex system that includes internet links from the sensor to a cloud platform that enables real-time access of measured data (see Figure 3).

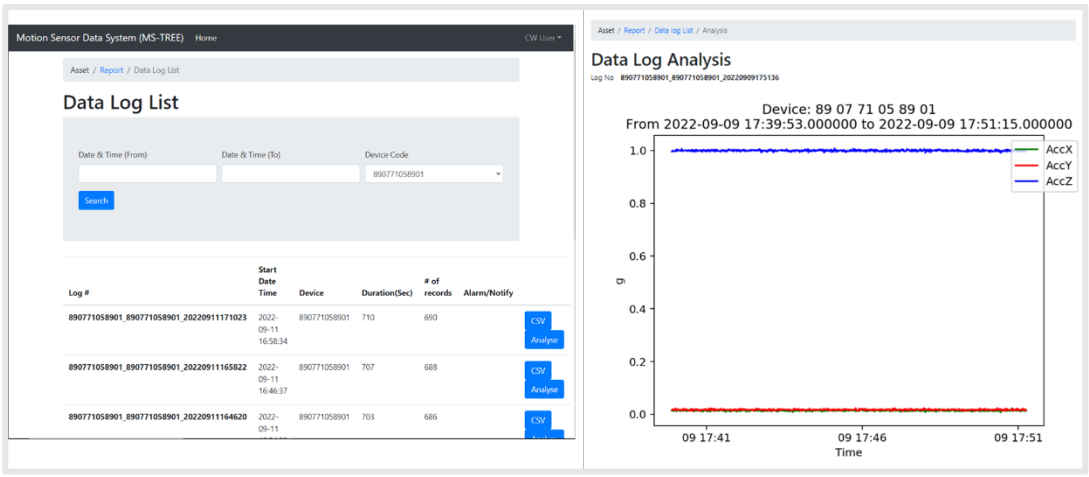

Figure 3: Remote access of real-time measured data from cloud platform

Each of these components is critical for successful environmental monitoring. The internet link from a sensor network to the server assumes that an internet endpoint exists but this is not always the case. Communication of NB-IoT is ideal in principle but sometimes problematic in practice. It is common to naively presuppose that servers are always connected, but the truth is that network connectivity infrastructure is unable to guarantee always up. During the connectivity down moment, those servers are inaccessible from the outside world and its live environmental data.

Accuracy and calibration are critically important which must reflect accurate data of environment state. Sensor calibration and detecting stuck values from broken transducers are critical too.

2.2 Information of Selected Flexible Barrier for This Project

Selected flexible barrier is located near the downhill side of Sai Wan Shan at Pamela Youde Nethersole Eastern Hospital Staff Quarters was selected for this project (see Figure 4).

Figure 4: Map of Selected Flexible Barrier

At crest of Sai Wan Shan (~ at 190mPD), it is the transposer station that can be accessed through Lei Yue Mun Park. It is estimated the Sai Wan Shan has a gradient of 35° and since the uphill was excavated/distributed, there is a possibility of landslide/rockfill in time after adverse weather condition and therefore flexible barriers were provided at downhill (Figure 5).

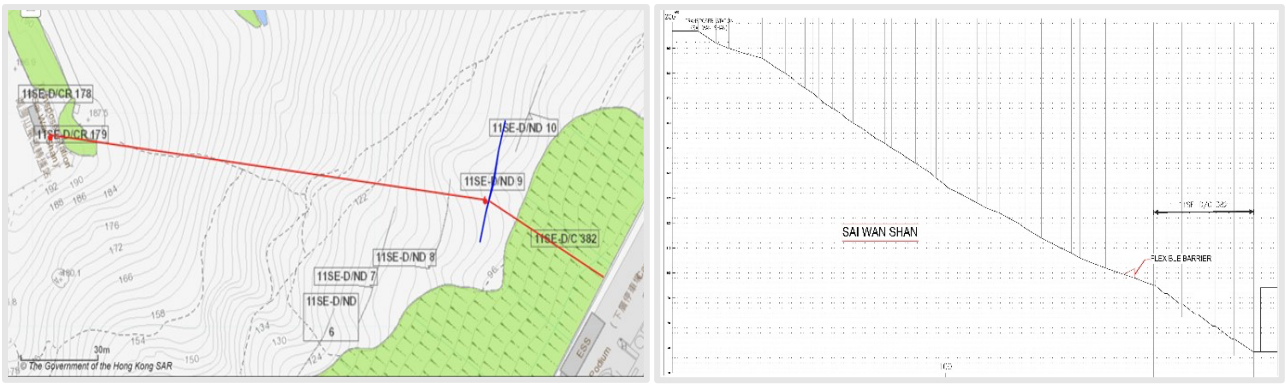

Figure 5 : Site Plan and Section

This flexible barrier (slope number: 11SE-D/ND9) is one of flexible barriers located at downhill of Sai Wan Shan along the hospital facilities with a man-made slope in-between. The concerned barrier is located about 50m from hospital facilities at +90mPD with 40m in length and 4.0m in height, consisting of 5nos steel posts at 10m intervals. Based on the information available, this flexible barrier has absorbing capacity of 3000 kJ.

2.3 IoT Sensors Installation to Flexible Barrier

To securely fix the IoT sensor onto the flexible barrier without affecting its structural integrity, a tailor-made steel "clamp" was designed to fix the sensor onto the steel post without the need to form any drillhole /weld (Figure 6). Then the sensor together with its mounting can be fixed onto the steel clamp and facing the downhill side of the steel post (Plate 2).

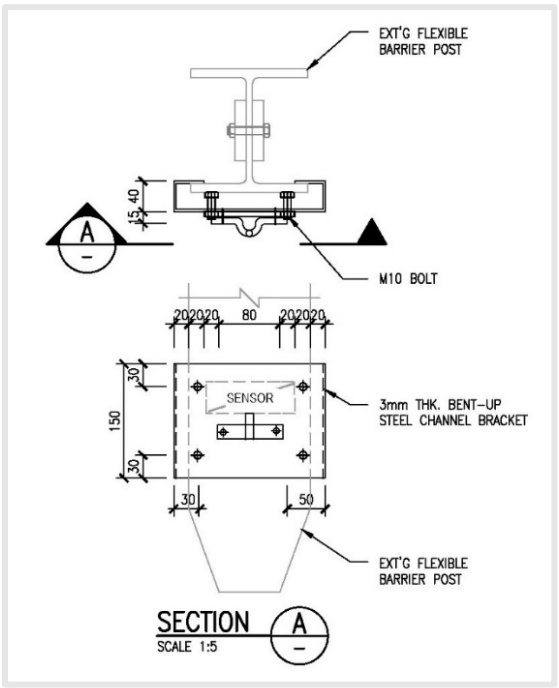

Figure 6: Schematic Details of Steel Clamp for Sensor Fixing

Plate 2: Photo of Sensor Fixing to Steel Post

In addition, an external weatherproof USB cable is prefixed to the sensor for recharging of battery without the need to direct-in-touch the sensor body (see Plate 3).

Plate 3: Photo of Sensor Charging using power bank

3 Processing of Measured Data from IoT Sensor

3.1 Data Collection and Pre-processing

Over two months continuously measured data starting from 26 Nov 2022 to 18 Feb 2023 on the movement of flexible barrier posts was collected by the IoT motion sensors. The primary data used for analysis was the maximum level of displacement in gravity (m/s^2) unit each day. Pre-processing steps were conducted to ensure that the data was in a suitable format for time series analysis. The pre-processing steps included removing any missing or invalid data points through data cleaning, and scaling the data to ensure it had a mean of zero and a standard deviation of one through data normalization.

Next, the data was plotted as a heatmap, with the sensors displayed on the Y-axis and time on the X-axis. The heatmap showed the maximum velocity (m/s) recorded for the sensor on each day (Figure 7).

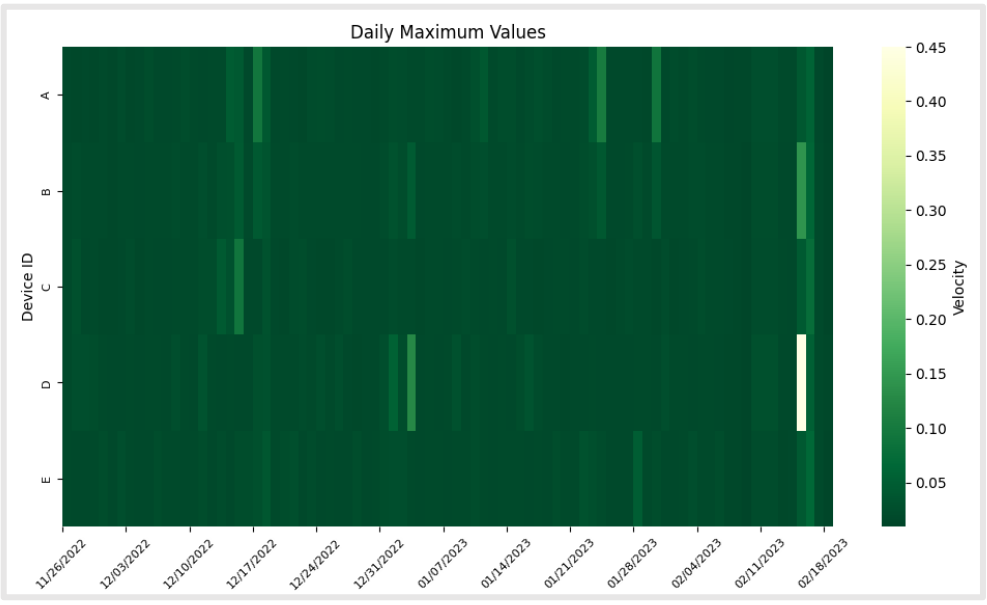

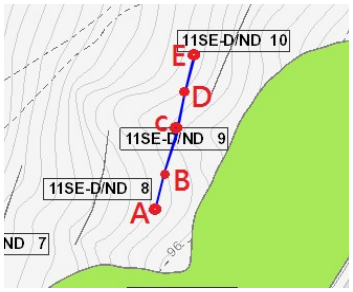

Figure 7: Heat Map of Sensor Movement

This heatmap showing the velocity of each IoT sensors at the flexible barrier is accessible through the cloud platform (see Figure 8).

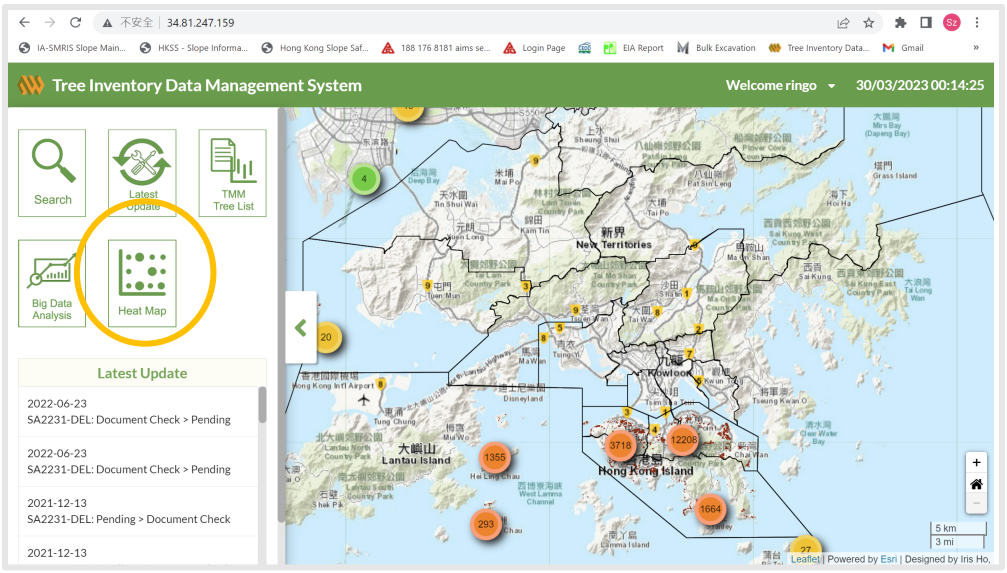

Figure 8: Heat Map at the Cloud Platform

3.2 Methodology of Data Analysis Using Time Series Analysis

To analyze the daily maximum displacement recordings, data was segmented in weeks and two time series models were utilized. The first model was based on the Singular Spectrum Analysis (SSA) approach which is a decompositional approach that involves transforming data into a series of principal components. SSA is particularly useful for time series that exhibit complex patterns, such as nonlinear, trends or cyclical variations. The second model was based on the Vector Autoregression (VAR) approach, which helps to analyze the relationships between multiple time series. VAR was used to investigate the relationships between the weekly time series of daily maximum displacement data.

The stationarity of the time series was evaluated using both methods. With SSA, the trend component was extracted from the time series and tested for stationarity using the Kwiatkowski-Phillips-Schmidt-Shin (KPSS) test. VAR was also applied to model the relationship between multiple time series, with the data segmented into weeks to create a time series for each week. Both SSA and VAR were employed to provide a comprehensive approach to analyze for stationarity.

SSA is able to better capture complex trend patterns, while VAR can identify correlations among trends over different time periods. Alert signal will be generated when stationarity is likely violated.

3.2 Further Analysis on Alert Signal with Stochastic Processes

To analyze alert signals generated in the previous step, the Hidden Semi-Markov Model (HSMM) approach was employed. The likelihood of instability was estimated for each post, and the likelihoods were subsequently normalized into probabilities using HSMM. By providing a precise assessment of potential instability based on the observed patterns in the time series data, this approach enables effective identification of safety risks and guidance of targeted interventions to mitigate those risks.

3.3 Data Analysis for This Study

The graphs below show the moving average of the five sensors (see Figure 8 to 12 for Sensor A to E respectively) over the measured period.

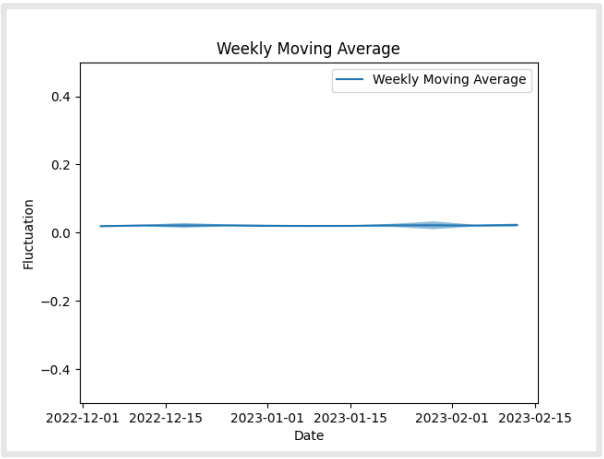

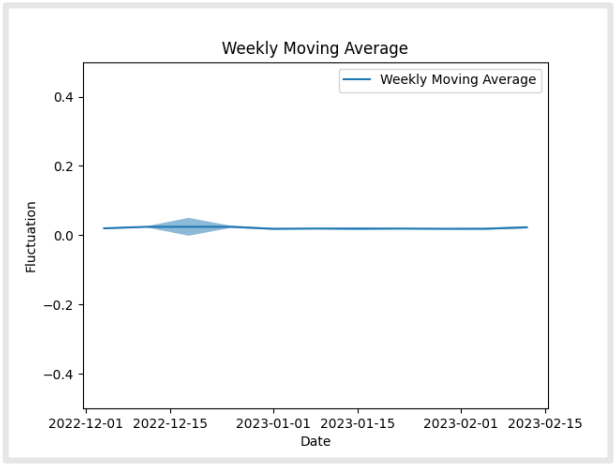

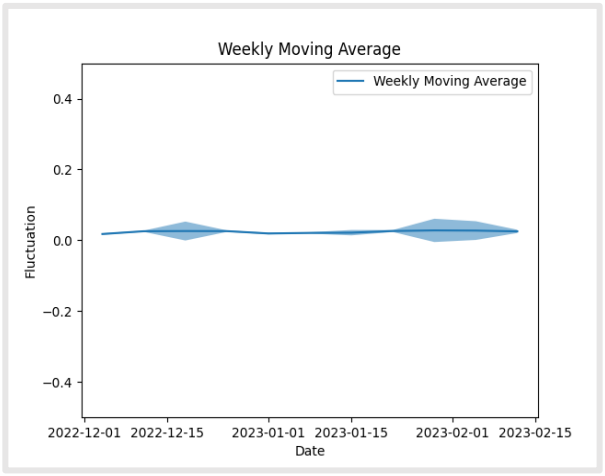

Figure 10: Sensor C

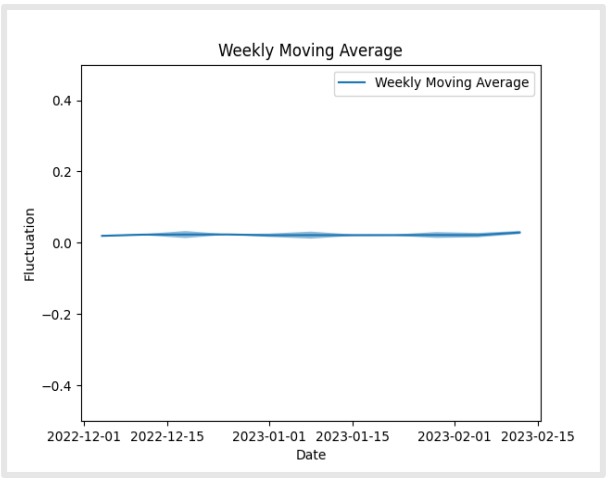

Figure 11: Sensor D

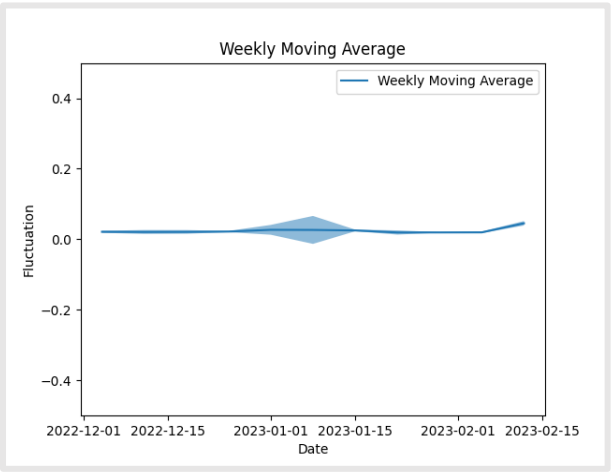

Figure 12: Sensor E

The moving average of the sensors seem smooth, but the analysis of the maximum displacement gave a different finding.

SSA and VAR were used to analyze the daily maximum displacement recordings by weekly segment. To examine the stationarity of the time series, the trend component was extracted from the time series using SSA, and the Kwiatkowski-Phillips-Schmidt-Shin (KPSS) test was used to evaluate the extracted trend component. Then the data was segmented into weeks so that each week became a time series, and VAR was applied to model the relationships between multiple time series.

The analysis of the weekly time series of daily maximum displacement data revealed that, on average, 9 trends were noted for Post "A" using both SSA and VAR approaches. No trend was noted for Post "B", while 4 trends were noted for Post "C", and 5 trends were noted for both Post "D" and Post "E". These trends signals spanned over a total of 12 weeks.

Then, Stochastic Processes based on the Hidden Semi-Markov Model (HSMM) approach was used to analyze the occurrence of these trends yielded from the previous step analysis. Based on the transition pattern for each post, the estimated likelihood of the post being potentially unstable and normalized the likelihoods into probabilities using HSMM is presented (Table 1)

Post Mark	Probabilities p
A	0.03
B	0.01
C	0.18
D	0.17
E	0.17

Table 1: Result of probabilities on alert occurrence using HSMM

The analysis indicated Post "A" had a significantly longer duration being in a trendy state, indicating that Post "A" was at higher risk of being potentially recording higher movement. Yet no trend was observed for Post "B" could indicate that notifiable object(s) causing these movements between Post "A" and Post "B" occurred more towards Post "A".

Site inspection conducted in 2 March 2023 and no abnormality was observed from to the flexible barrier. The measured data will be compared again after Typhoon Season from June to October 2023 so as to get a more comprehensive benchmark data on the movement of flexible barrier during normal and adverse weather condition.

This benchmark data will continuously be enhanced with the aim to improve the effectiveness in using IoT sensors for monitoring the movement flexible barrier.

3. CONCLUSION

In this study, through the installation of IoT sensors onto the flexible barrier steel posts, and present the measured data real-time on a cloud platform, with a two-step time series to further analyze the data. While the accuracy on monitoring of movement or deformation of flexible barrier under actual situation is not available, the monitoring of flexible barrier is enhanced and, in time when making reference with the benchmark data under normal and adverse weather condition, if any large movement to the flexible barrier in comparison to the benchmark data, then this finding can be a valuable reference to the Geotechnical/Civil engineers in considering a proactive inspection and any follow-up actions if necessary.

ACKNOWLEDGEMENTS

The authors would like to express our gratitude to Mr. Liu Lam Fung, Xavier and Mr. Wong Hoi Hong, both graduates from Thei for their supports in IoT sensors management and Mr. Hui Ka Chun for his expertise in building the Cloud Platform.

REFERENCES

GEO, (updated in 2021). Guide to Slope Maintenance, Geoguide 5. Geotechnical Engineering Office, Civil Engineering and Development Department, HKSAR.

J.S.H. Kwan & R.C.H. Koo. Enhanced Technical Guidelines for Design of Debris-resisting Barriers, GEO Report No.333. Geotechnical Engineering Office, Civil Engineering and Development Department, HKSAR.

GEO, (2014). Guidelines on Empirical Design of Flexible Barriers for Mitigating Natural Terrain Open Hillslope Landslide Hazards. Technical Guidance Note No. 37 (TGN37). Geotechnical Engineering Office, Civil Engineering and Development Department, HKSAR.

Golyandina, N., & Zhigljavsky, A. (2018). Singular spectrum analysis for time series. Springer.

Lütkepohl, H. (2005). New introduction to multiple time series analysis. Springer Science & Business Media.

Kwiatkowski, D., Phillips, P. C., Schmidt, P., & Shin, Y. (1992). Testing the null hypothesis of stationarity against the alternative of a unit root: How sure are we that economic time series have a unit root?. Journal of econometrics, 54(1-3), 159-178.

Peng, Y., & Dong, M. (2011). A prognosis method using age-dependent hidden semi-Markov model for equipment health prediction. Mechanical Systems and Signal Processing, 25(1), 237-252.

Effects of curing temperature and stress on the mechanical behaviour of cemented Hong Kong marine clay

K.F. Jiao & C. Zhou

The Hong Kong Polytechnic University, Hong Kong

ABSTRACT

Deep cement mixing (DCM) is an important method for treating soft clay. In the field, cemented soils are usually subjected to various temperatures and stresses during the curing process. The influence of curing conditions, including the curing temperature and stress, on the mechanical behaviour of cemented soil has not been well understood. In this study, the effects of cement content, curing temperature and curing stress on the strength of cemented soil were studied by unconfined compression tests. Hong Kong marine clay with an initial water content of 65% was used. Cemented specimens were prepared at different temperatures (20 °C, 30 °C, 40 °C), vertical stresses (0 kPa, 300 kPa) and with various cement contents (15%, 25%, 35%). Specimens were tested after 28 days of curing under constant temperature and pressure conditions. This paper will present and analyses the influence of cement content, curing temperature and stress on the unconfined compressive strength (UCS) and secant Young's modulus E_{50}.

Keywords: Cemented soil; unconfined compression test; curing temperature; curing stress

1 INTRODUCTION

DCM is considered an environmentally friendly and fast construction method for land reclamation (Chung et al. 2022). This technique generally has less disturbance to the marine ecological system than conventional reclamation methods. Moreover, it can form DCM columns in a shorter time to support the seawall and filling materials, reducing the construction time.

Cemented soils are usually subjected to various temperatures and stresses during curing in the field. According to the field data from Japan (Enami et al. 1985), Singapore (Lu 2013) and Norway (Fiskvik et al. 2022), the temperature inside DCM columns can be as high as 40 degrees and last for a month, which is around 20°C higher than that of laboratory conditions. Furthermore, the length of DCM columns is generally above 10 meters, and the effective confining pressure can reach several hundred kPa. Therefore, it is important to understand the influence of curing temperature and stress on the properties of cement-treated soils.

So far, some studies in the literature have investigated the effects of curing temperature (Kido et al. 2009; Ju 2019; Fiskvik et al. 2022) and curing stress (Rabbi et al. 2011; Fernandez and Santamarina 2001) on the mechanical behaviour of cemented soils, but they mainly focus on the cement contents lower than that of DCM practices. Furthermore, the previous studies mostly focus on UCS but not soil stiffness. E_{50} is a commonly used stiffness parameter in engineering, which is often estimated from the value of UCS. In the U.S. design guideline (Kitazume and Terashi 2013), the ratio of E_{50} and UCS is 300 and 150 for the wet and dry mixing methods, respectively. So far, the effects of curing temperature and curing stress on E_{50} have not been investigated.

This study conducted unconfined compression tests to investigate the mechanical behaviour of cemented Hong Kong marine clays, including the stress-strain relation, UCS and E_{50}. Particular attention was paid to the

effects of cement content, curing temperature and curing stress. A new temperature and stress-controlled curing equipment for cemented soil was developed.

2 TEST PROGRAM AND MATERIALS

A series of unconfined compression tests were carried out to study the effects of cement content, curing temperature and curing stress on the mechanical behaviour of cemented Hong Kong marine clay. Three cement contents were used: 15%, 25%, and 35%, which refer to the mass ratio of the dry cement and dry soil. Three curing temperature levels were used based on the results of field monitoring (Enami et al. 1985; Lu 2013; Fiskvik et al. 2022), namely 20°C, 30°C, and 40°C. The curing vertical stresses at the 1D condition are 0, 150 and 300 kPa. Details of the test programme are summarized in Table 1.

Table 1 Testing programme

Test ID	Cement content (%)	Curing stress (kPa)	Curing temperature (°C)
1	15	0	20
2	25		
3	35		
4	25	0	30
5	25	300	
6	15	0	40
7	25		
8	35		
9	25	300	

The materials used are Hong Kong marine clay and ordinary Portland cement. The initial moisture content of Hong Kong marine clay is 65%, and its engineering properties are summarized in Table 2. The wet mixing method was simulated in which the cement is mixed with water before mixing with marine clay. Referring to the test methods of Wang et al. (2019), the water/cement ratio of the cement slurry was kept at 1:1. This study considered three different cement contents (15%, 25% and 35%), which is defined as the ratio of cement to the mass of dry of Hong Kong marine clay. Given each cement content, specimens were cured at different temperatures (20 °C, 30 °C, 40 °C) and vertical stresses (0 kPa, 300 kPa). Unconfined compression tests were conducted after 28 days of curing.

Table 2 Basic properties of Hong Kong marine clay

	Specific Gravity	Liquid Limit (%)	Plastic Limit (%)	Plasticity Index (%)	Particle Size Distribution (%)		
					Sand content	Silt content	Clay content
HKMD	2.62	63.9	28.2	35.7	63.69	18.62	17.69

3 Test apparatuses

Figure 1 shows a newly developed system for curing cemented specimens at different stress and temperature conditions. It has two main modifications: the overburden pressure application system and the heating system. The curing stress application method used in this study is K_0 loading, which is applied by the cylinder above the specimens. Some studies show that curing stress is applied in a triaxial chamber via isotropic stress. The shortage is the cemented soil has a large compressibility before the initial setting time of the cement, which may lead to a large volume change. The experimental results may be affected by the size effects. Two kinds of moulds were used for curing, that is, 50 mm in diameter and 100 mm in height for zero stress curing and 50 mm in diameter and 150 mm in height for stress curing. The mould used in stress curing is higher to ensure a specimen length larger than 100 mm after curing. The excess length was cut by a cutting machine.

Figure 2 shows the experimental setup for unconfined compression tests. To well capture the stress-strain relationship of cemented soil in the whole process of compression, three kinds of sensors are used to measure the specimen strain, including two vertical strain gauges, two local LVDTs and one global LVDT. After 28

days of curing, the specimens are cut to a standard size using a cutting machine with a diameter of 50±0.5 mm and a length of 100±1 mm. The stress and strain are determined according to ASTM (2017) standard D2166.

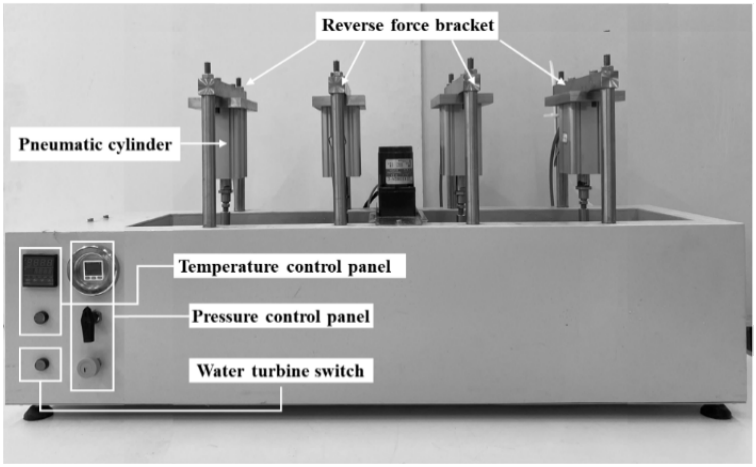

(a) external structure

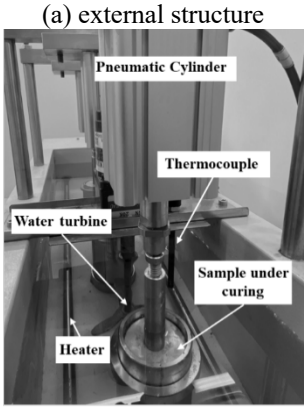

(b) internal structure

Figure 1 Specimen curing equipment

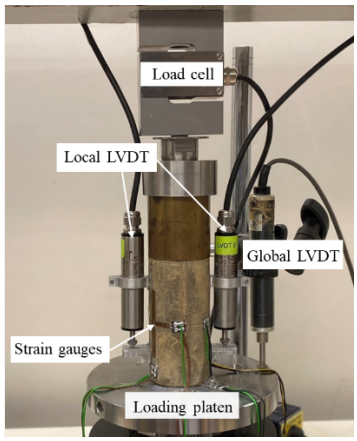

Figure 2 Photos of unconfined compression test setup

4 INTERPRETATIONs OF EXPERIMENTAL RESULTs

4.1 Effects of cement content

Figure 3 shows the stress-strain curves of the specimens with different cement contents. The results at two different curing temperatures (20°C and 40°C) are presented. All specimens show similar stress-strain relations at a qualitative level. The specimen usually reaches its peak strength at 1-2% strains, followed by a significant softening.

Consistent with the results of previous studies (Chang and Woods, 1992, Yin 2001, Nafisi et al. 2020, Ho et al. 2021), the strength of cemented soil increases significantly with an increase in cement content. The peak strength doubles as the cement content increases from 15% to 35% because the hydration of cement increases the cohesion between soil particles. The chemical mechanism of cement hydration and its influence on soil behaviour were discussed in detail by some previous researchers (e.g. Xiao 2009).

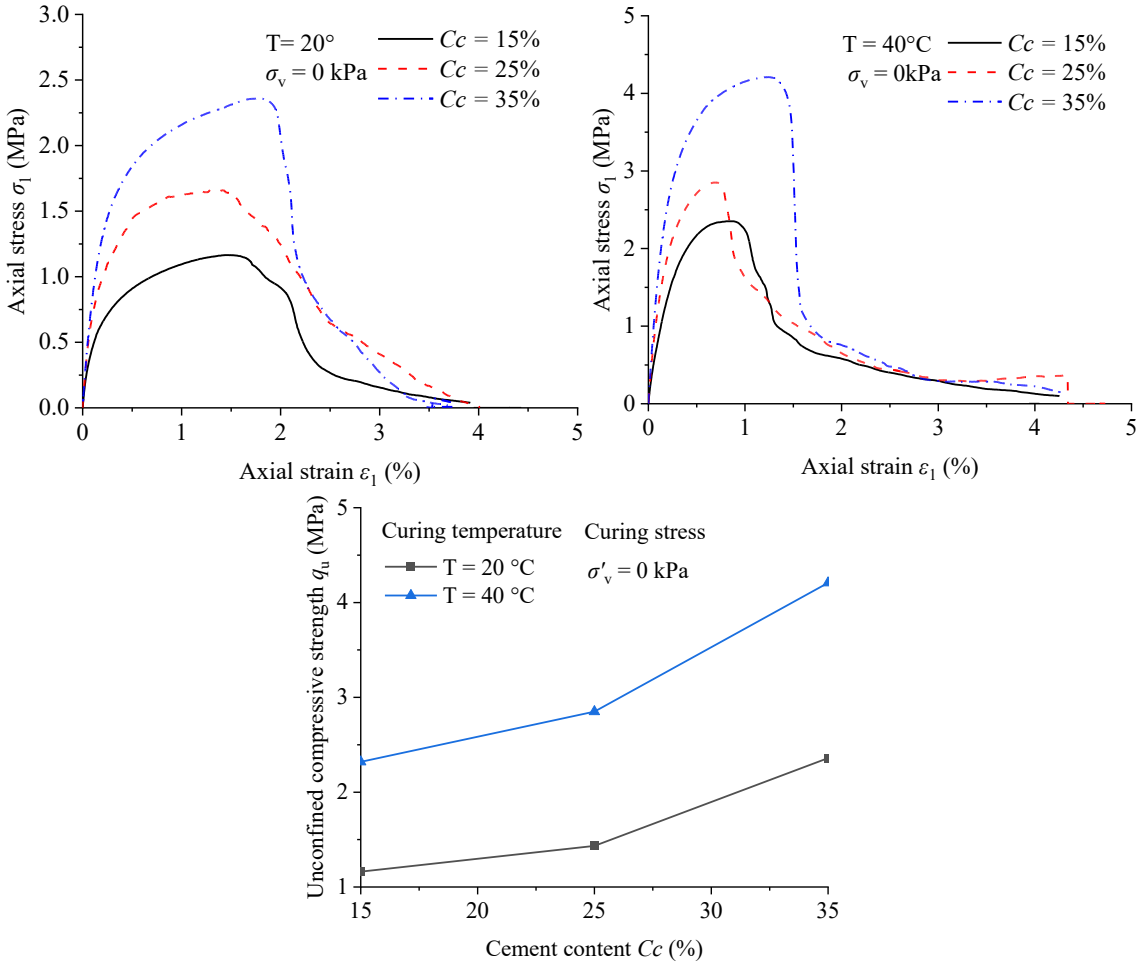

Figure 3 Effects of curing temperature on cemented soil

4.2 Effects of curing temperature

Figure 4 shows the unconfined compression behaviour of the specimens at different curing temperatures of 20°C and 40°C. When the curing temperature increases from 20 to 40 degrees, the UCS increases by about 75%. The increase is at least partially because, with increased curing temperature, the cement hydration rate is higher, producing more hydration products and enhancing the bonding between soil particles. Figure 5 shows the scanning electron microscope photomicrographs of the specimens under different curing temperatures. Soil pores are more effectively filled with cementation products at a higher curing temperature.

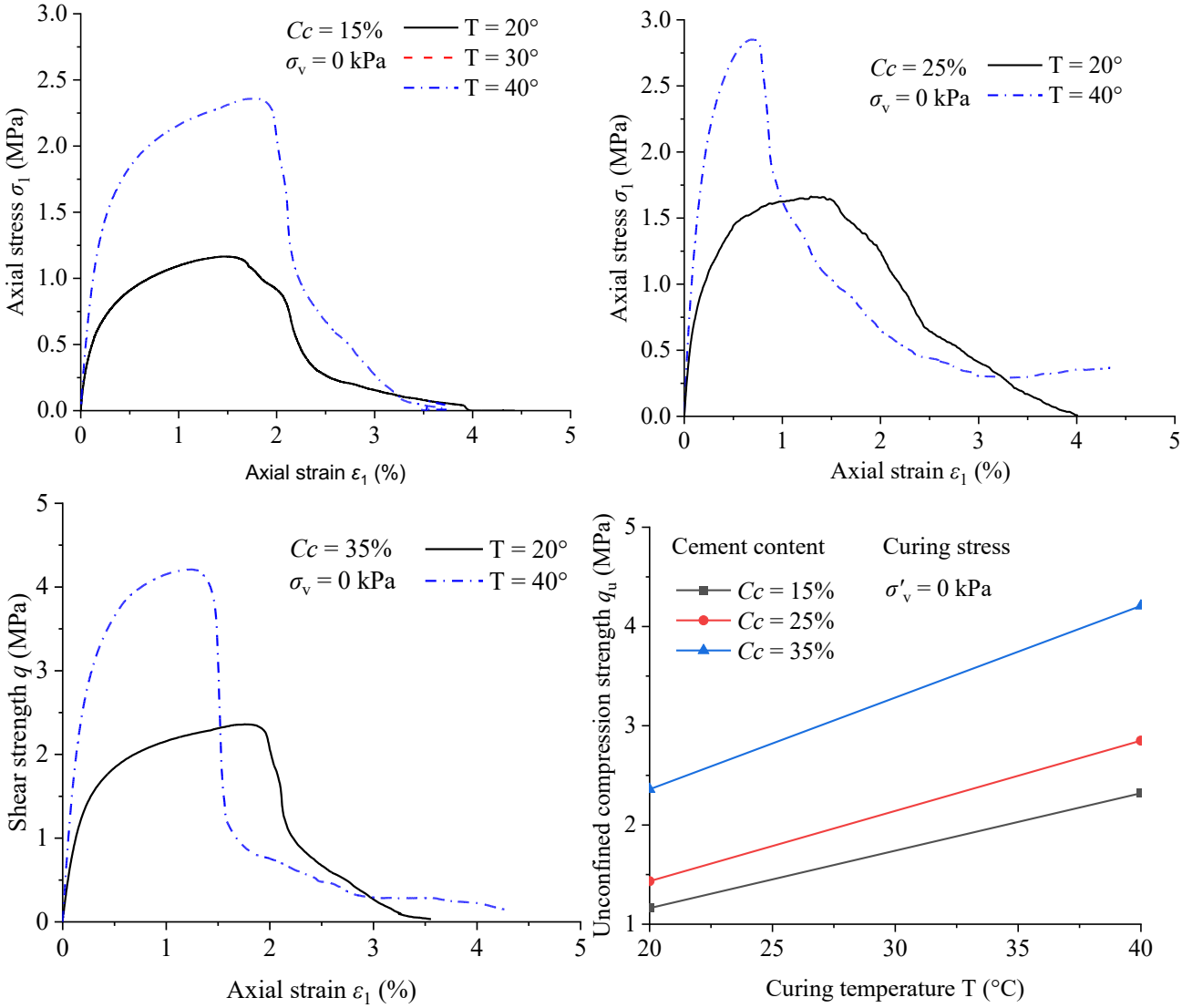

Figure 4 Effect of curing temperature on strength

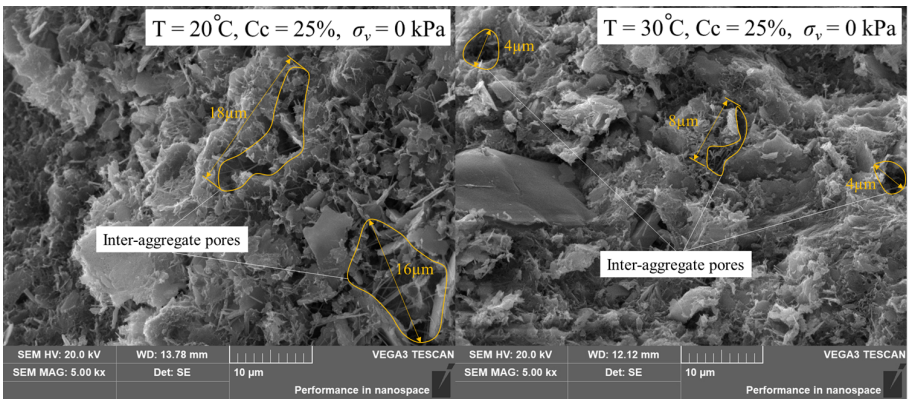

Figure 5 SEM photomicrographs of specimens with different curing temperatures

4.3 Effects of curing stress on cemented soil

Figure 6 shows the effects of curing stress on UCS. As the curing stress increases from 0 to 300 kPa, UCS increases by about 2 times. This is likely because a denser cemented structure is formed when the curing stress increases. For example, the void ratio decreases from 1.73 to 1.24 when the curing increases from 0 to 300 kPa at 30°C. SEM photomicrographs under different curing stresses provide better evidence. Scanning electron microscopy photomicrographs in Figure 7 shows that the specimen exhibits a denser structure under

stress curing. The pore size in the specimen under stress curing is smaller than the specimen without curing stress. The stress-strain curves of cemented soil exhibited a similar pattern with increased strain. For all the specimens, the strain softening ends at 3% strain.

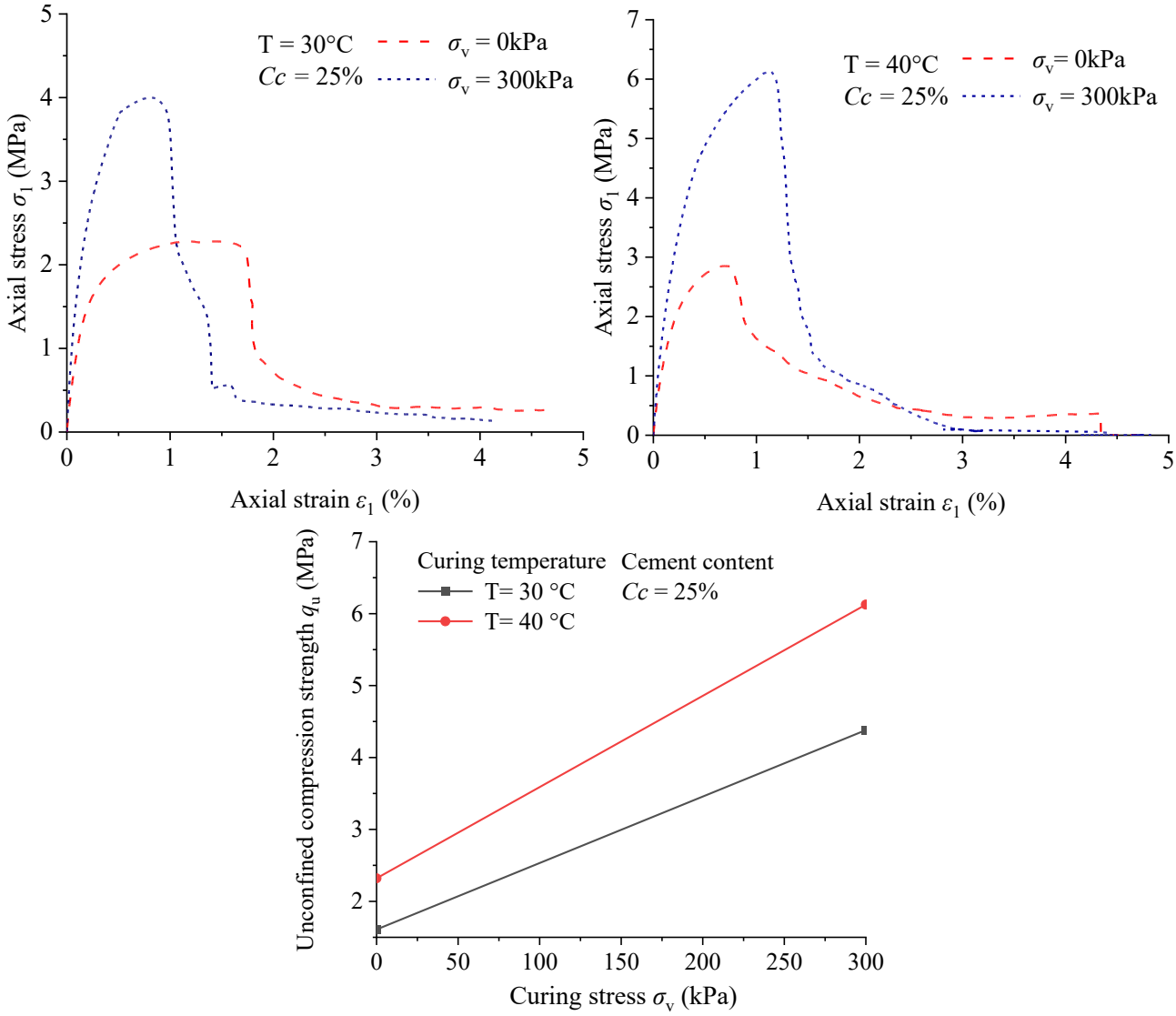

Figure 6 Effects of curing stress on strength

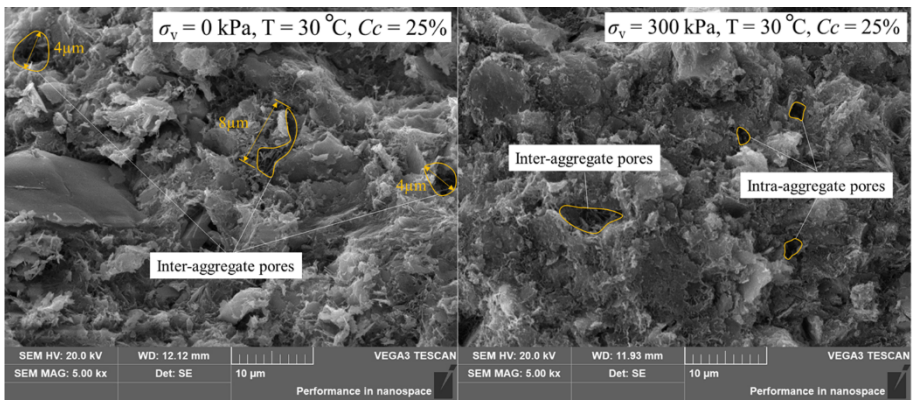

Figure 7 SEM photomicrographs of specimens with different curing stress

4.4 Relationship between UCS and E50 under different curing conditions

Figure 8 is a summary of the relationship between UCS and E_{50}. Curing temperature and curing stress can significantly increase UCS and E_{50}. However, their ratio does not change much. For cemented Hong Kong marine clay, the ratio UCS and E_{50} is close to 320, close to the value (300) suggested by the guideline (Bruce et al. 2013) for the wet mixing method.

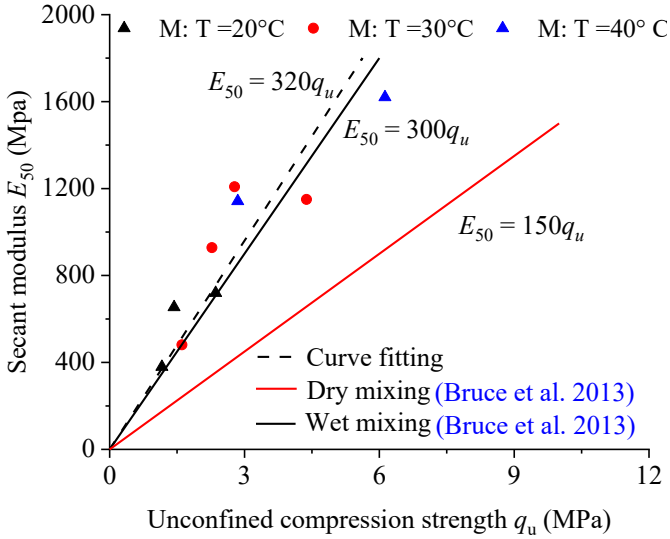

Figure 8 The relationship between q_u and E_{50}

5 CONCLUSION

This research studied the curing condition effects on the cemented Hong Kong marine clay. A series of unconfined compression tests were carried out. A temperature and stress-controlled equipment for specimen curing was developed. The works may contribute to improving deep cement mixing engineering design and reduce engineering investment. The main conclusions are as follows:

(a) Increased temperature and stress significantly improved the strength and modulus of cemented Hong Kong marine clay. The increase in curing temperature enhances the hydration reaction rate of cement, while the overlying pressure mainly affects the structure of cement soil.

(b) The increase in curing temperature and curing stress did not change the relationship between UCS and E_{50} much.

ACKNOWLEDGEMENTS

The National Science Foundation of China supports this work through research grant 52022004. The authors also would like to thank the HKSAR Research Grants Council (RGC) for providing financial support through grant 15205721.

REFERENCES

ASTM D2166-00. 2017. Standard Test Methods for Unconfined Compressive Strength of Cohesive Soils. *Annu. Book ASTM Stand.* 4, 163-167.

Bruce, M.E.C, Berg, R.R., Collin, J.G., Filz, G.M., Terashi, M. & Yang, D.S. 2013. *Deep mixing for embankment and foundation support.* In: FHWAHRT-13-046. Federal highway administration design manual, Washington, DC

Chang, T.S. & Woods, R.D. 1992. Effect of particle contact bond on shear modulus. *Journal of geotechnical engineering* 118(8):1216-1233.

Chung, P. Chu, F. Cheung, H. Yan, C. Cheung, C. & Wong, A. 2022. Technical Developments Related to Deep Cement Mixing Method in Hong Kong. *AIJR Proceedings*:249-259.

Enami, A. Yoshino, M. Hibino, S. Takahasi, M. & Akiya, K. 1985. In-situ measurement of temperature in soil cement columns and influence of curing temperature on unconfined compressive strength of soil cement. *In Proc. the 20 th Nat. Conf. Japan Soc. Soil Mech. and Found. Engrg*, pp. 1737-1740.

Fernandez, A. & Santamarina, J. (2001) Effect of cementation on the small-strain parameters of sands. *Can. Geotech. J.* 38(1):191-199.

Fiskvik, B.B.K., Wiersholm, P., Paniagua, P. & Emdal, A. 2022. Effect of Temperature on the Strength of Lime–Cement Stabilized Norwegian Clays. *J. Geotech. Geoenviron. Eng.* 148(3):04021198.

Ho, T.O., Chen, W.B., Yin, J.H., Wu, P.C. & Tsang, D.C. 2021 Stress-strain behaviour of cement-stabilized Hong Kong marine deposits. *Constr. Build. Mater.* 274:122103.

Ju, H. 2019. Influence of Curing Temperature on Strength of Cement-treated Soil and Investigation of Optimum Mix Design for the Wet Method of Deep Mixing. Virginia Tech.

Kido, Y., Nishimoto, S., Hayashi, H. & Hashimoto, H. 2009. Effects of curing temperatures on the strength of cement-treated peat. *In Proceedings of International Symposium on Deep Mixing and Admixture Stabilization*.

Kitazume, M. & Terashi, M. 2013. *The deep mixing method.* CRC press London.

Lu, Y., Tan, T. & Phoon, K. 2012. Accelerated testing of cement treated Singapore marine clay cured under elevated temperature. *In GeoCongress 2012: State of the Art and Practice in Geotechnical Engineering*, pp. 920-929.

Nafisi, A., Montoya, B.M. & Evans, T.M. 2020. Shear strength envelopes of biocemented sands with varying particle size and cementation level. *J. Geotech. Geoenviron. Eng.* 146(3):04020002.

Rabbi, A.T.M.Z., Kuwano, J., Deng, J. & Boon, T.W. 2011. Effect of curing stress and period on the mechanical properties of cement-mixed sand. *Soils and foundations* 51(4):651-661.

Wang, Y., Xie, G. & Dou, H. 2019. Stabilization of Soft Clay by Deep Cement Mixing (DCM) Method–A Case Study.". HKIE Transactions 26(3):115-125.

Xiao, H.W. 2009. "*Yielding and failure of cement treated soil*. National University of Singapore.

Yin, J.H. 2001. Stress-strain-strength characteristics of soft Hong Kong marine deposits without or with cement treatment. *Lowland Technology International* 3(1):1-13.

Yitan, L. 2013. *Early Strength Development of Cement Mixed Singapore Marine Clay*. National University of Singapore.

Integrated Use of GNSS and InSAR Techniques for Movement Monitoring under Trunk Road T2 and Cha Kwo Ling Tunnel

Tommy C W Wong
East Development Office, Civil Engineering and Development Department, Hong Kong SAR, China
Dr. T O Ishola
Asia Infrastructure Solutions Limited
Stephen T M Mak
Meinhardt Infrastructure and Environment Limited

ABSTRACT

In the Trunk Road T2 and Cha Kwo Ling Tunnel (collectively "the T2") project, a number of innovative techniques have been employed successfully. In particular, the Global Navigation Satellite System (GNSS) and Interferometric Synthetic Aperture Radar (InSAR) have proven to be beneficial in enhancing productivity and site safety for movement monitoring of sensitive receivers during the course of tunnel works in the T2 project. This paper reports the site application of these two innovative techniques in this tunnel project and the results of the GNSS and InSAR monitoring works. GNSS monitoring was applied to monitor the movement of the existing Public Works Central Laboratory (PWCL) Building due to the Tunnel Boring Machine (TBM) launching shaft construction works in close proximity and the movement of the seawalls and breakwater due to the crossing of TBMs underneath these marine structures, whereas InSAR monitoring was used to monitor the settlement of the existing structures in Cha Kwo Ling Village due to the T2 tunnel works. It is demonstrated that both GNSS and InSAR monitoring can effectively supplement the conventional survey monitoring.

1 INTRODUCTION

With the recent advancement in satellite technology and data analytics, a remarkable opportunity to employ innovative solutions in construction projects has been unleashed in recent years. Both GNSS and InSAR are innovative techniques for monitoring purpose, involving the use of satellites for movement or deformation monitoring with high precision and accuracy, for application under different site scenarios or site constraints. GNSS can offer accurate real-time 3D movement monitoring at specific locations on site, whilst InSAR is a remote sensing technology which is suitable for monitoring deformation over large areas owing to its large spatial coverage.

In the T2 project, the GNSS-based monitoring system was established to achieve real-time and fully automatic monitoring of 3D movements of various sensitive receivers, which include the PWCL Building, the Kwun Tong Typhoon Shelter breakwater and seawalls in the former South Apron and Cha Kwo Ling (CKL) areas, where they are located directly above or in close proximity to the TBM launching shaft or along the tunnel alignment. The GNSS receivers installed at these sensitive receivers can be located as a unique point on Earth by using trilateration technique. With the addition of the Chinese BeiDou Satellite System and advancements in computing algorithms, improved accuracy and reliability for precise positioning of the GNSS receivers can be achieved, with an accuracy of one to two millimetres, which is on a par with conventional surveying methods.

In addition, the remote sensing technique of InSAR was employed for mapping ground deformation, using satellite radar images acquired for every 11 days of a satellite's orbiting cycle, at the CKL Village where the closely annexed houses and narrow alleys in the village rendered conventional survey monitoring extremely

difficult and time consuming. The InSAR technique identifies ground deformation based on the phase differences between high-resolution satellite radar images taken when the radar satellite revisits the exact same location. Compared with GNSS, the InSAR technique does not require any pre-installed receiver or power supply on the ground surface making it extremely suitable for deformation monitoring of areas with restricted access. Details of the site application of these two techniques are presented in the following sections.

2 GLOBAL NAVIGATION SATELLITE SYSTEM (GNSS) MONITORING

2.1 Working Principle

GNSS rover stations installed on the ground surface can continuously and automatically receive microwave signals emitted from the operating satellites travelling above Hong Kong for which the signals carry positioning and timing data, and record the time taken for the signals emitted from each satellite in space to calculate the distance from the satellite. With the use of GNSS base stations, the accuracy and precision of the system can be further enhanced.

In principle, a minimum of 3 nos. of satellite is sufficient to determine the position (i.e. x, y, z-coordinates in 3-dimensional space) of the GNSS rover station on the Earth's surface by trilateration algorithm (as illustrated in Figure 1 below). However, by employing all available satellite systems orbiting above Hong Kong, including Beidou (China), GPS (US), Galileo (Europe) and Glonass (Russia), a total of up to 33 nos. of satellite can be adopted by the GNSS system for precise positioning with an accuracy of ± 1 to 2 mm, which is practically on a par with the conventional survey system.

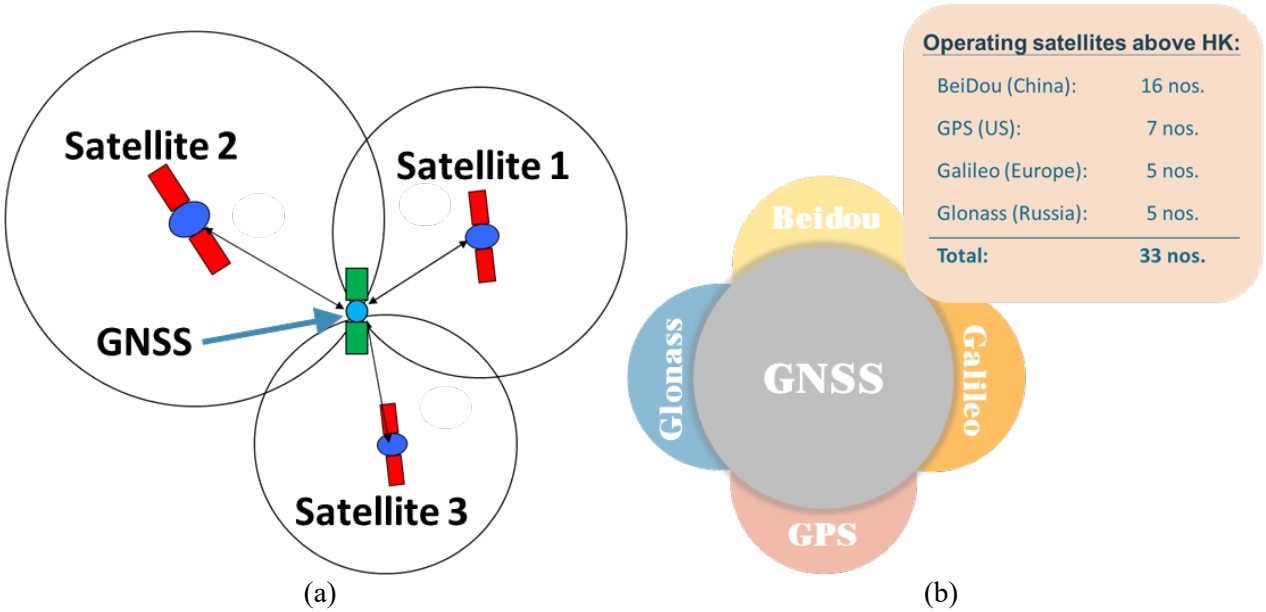

Figure 1: (a) Locating GNSS rover stations on Earth by trilateration with minimum 3 nos. of satellite and (b) Operating satellites above Hong Kong for GNSS monitoring

All real-time data collected at the GNSS rover stations is relayed to the cloud server in Hong Kong via 5G mobile network, where data processing will take place in the server using the proprietary computing algorithm. The output movement monitoring data will then be posted to the dedicated web portal via internet, from which the real-time movement monitoring data can be viewed graphically in the web portal.

2.2 Field Installation and Monitoring

In T2 project, the GNSS monitoring was implemented in two phases. The phase 1 GNSS rover stations were installed at the rooftop of the PWCL Building and along the South Apron seawall to monitor the induced

movement due to the bulk excavation of the adjacent TBM launching shaft and due to the TBM crossing underneath the South Apron seawall respectively. As for phase 2, the GNSS rover stations were installed on Kwun Tong Typhoon Shelter breakwater and along CKL seawall to monitor the induced movement due to TBM crossing underneath the breakwater and CKL seawall. The two-phase installation is illustrated in Figures 2 and 3 below.

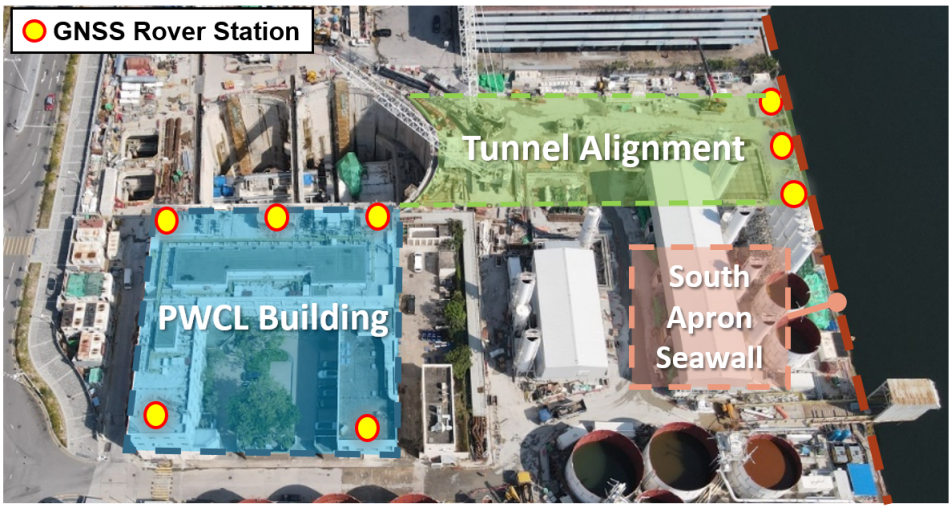

Figure 2: Phase 1 GNSS monitoring: at rooftop of PWCL Building (left) and along South Apron seawall (top right)

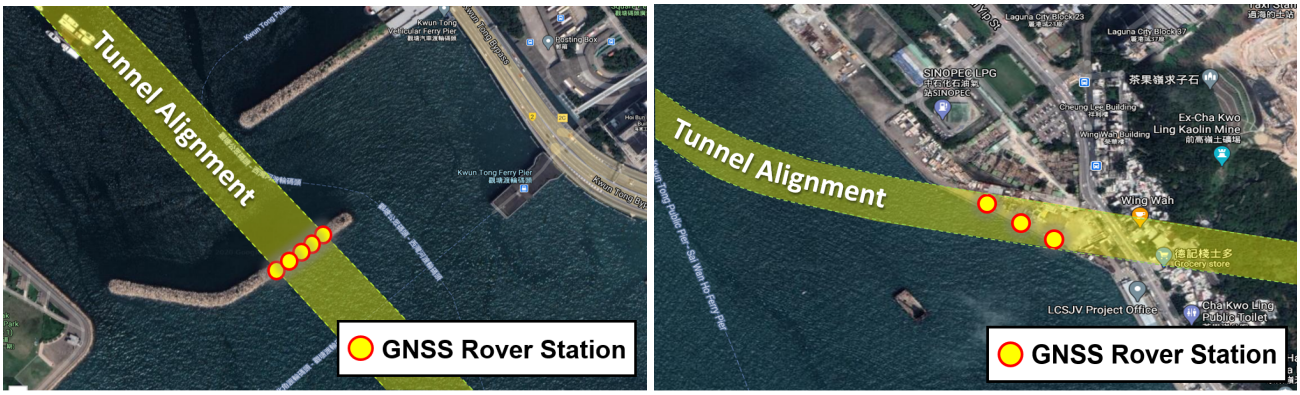

(a) (b)

Figure 3: (a) Phase 2 GNSS monitoring: at Kwun Tong Typhoon Shelter breakwater and (b) along Cha Kwo Ling seawall

Construction of the TBM launching shaft is the critical element in this project, with specific considerations to its deep excavation works (38 m depth) and close proximity – only 2.5 m from the existing foundations of the PWCL Building, which is a sensitive structure in which the laboratory equipment is sensitive to vibration and the government's public laboratory testing services must be maintained and uninterrupted during the construction of the TBM launching shaft and the subsequent launching of both TBMs. Hence, stringent monitoring requirements are imposed on the PWCL Building. Apart from conventional manual survey, GNSS is also adopted to supplement the monitoring of building movement of the PWCL Building during the works period.

The typical set-up of GNSS rover stations at the PWCL Building is shown in Figure 4(a) below. A minimum of 70% sky visibility is recommended by the GNSS service provider to ensure that sufficient satellite signals are received to produce reliable monitoring data and this requirement is achievable at the rooftop of the PWCL Building.

As for the Kwun Tong Typhoon Shelter breakwater, it is an isolated breakwater surrounded by sea and without an electrical power supply, each GNSS rover station installed on the breakwater was equipped with a solar panel to provide electrical power to the receiver of the rover station, as shown in Figure 4(b).

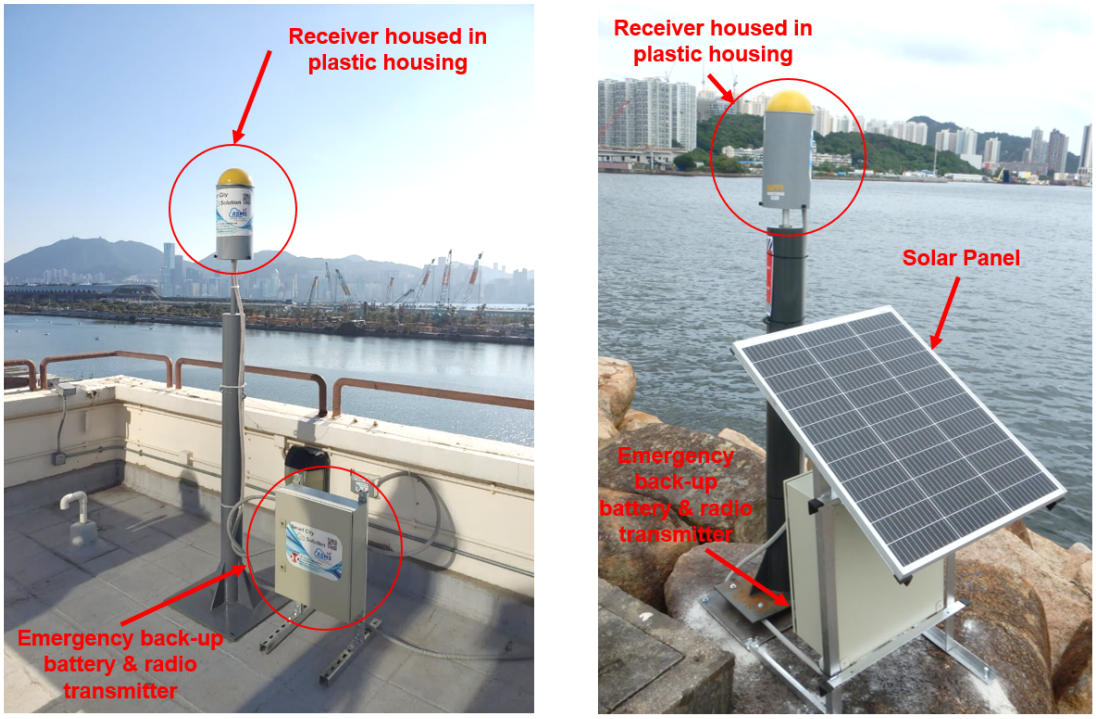

(a) (b)

Figure 4: (a) Typical setup of GNSS rover station at rooftop of PWCL Building and (b) at Kwun Tong Typhoon Shelter breakwater with solar panel

2.3 Monitoring Results

All real-time GNSS monitoring data can be viewed via the dedicated web portal, as indicated in Figure 5 below.

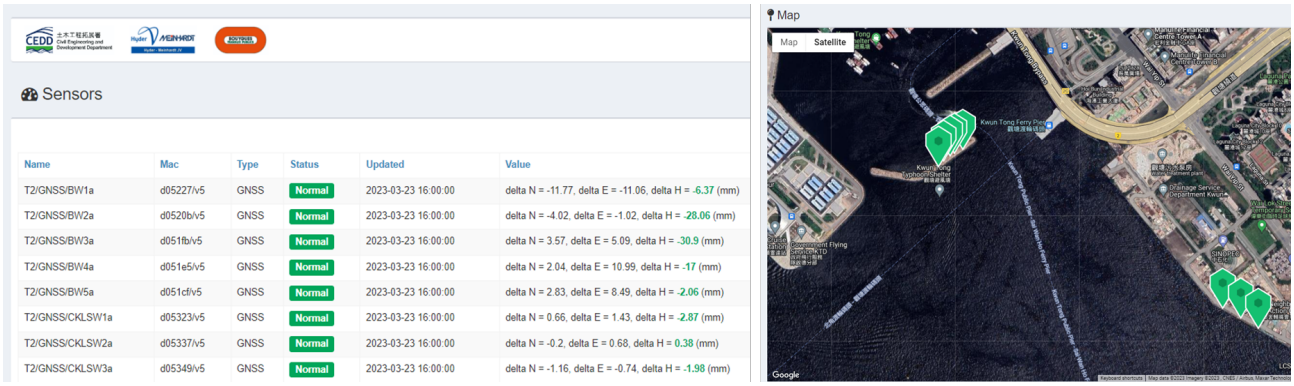

(a) (b)

Figure 5: (a) Dedicated web portal for real-time reporting of monitoring data and (b) Location plan of rover stations at Kwun Tong Typhoon Shelter breakwater and Cha Kwo Ling seawall as view in web portal

In this paper, the GNSS settlement monitoring data collected at the PWCL Building and the South Apron seawall in phase 1 monitoring were compared with those settlement data surveyed by conventional methods, viz a survey marker on the rover station at the PWCL Building and ground settlement markers along the South Apron seawall.

For the PWCL Building, GNSS monitoring covered the whole works period of bulk excavation at the TBM launching shaft which is located at only 2.5m away from the piles of the PWCL Building, and the works period of the subsequent base slab construction and assembly of the two TBMs. Based on the monitoring results for the GNSS rover station located at the northeast of the building (see Figure 6), it is shown that the settlement monitoring records were generally consistent for those taken by GNSS and manual survey.

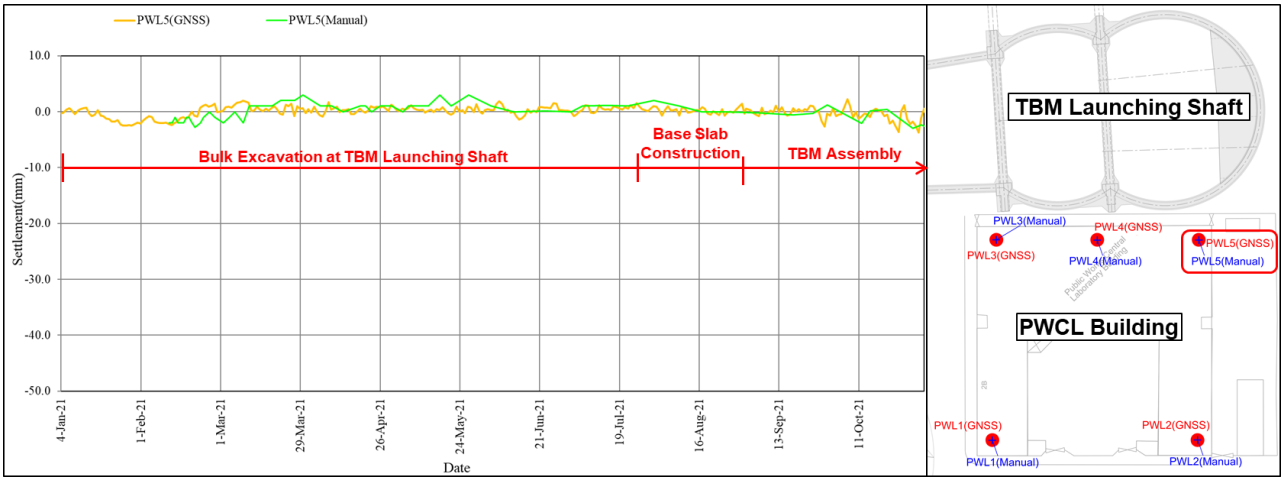

Figure 6: Comparison of settlement monitoring data by GNSS and manual survey at rooftop of PWCL Building

For the South Apron seawall, GNSS monitoring covered the period of TBM crossing underneath the seawall for the excavation of the Westbound Tunnel. According to the monitoring results for the GNSS rover station located at the seawall coping (see Figure 7), it is shown that the ground settlement monitoring records were in good consistence for those taken by GNSS and manual survey.

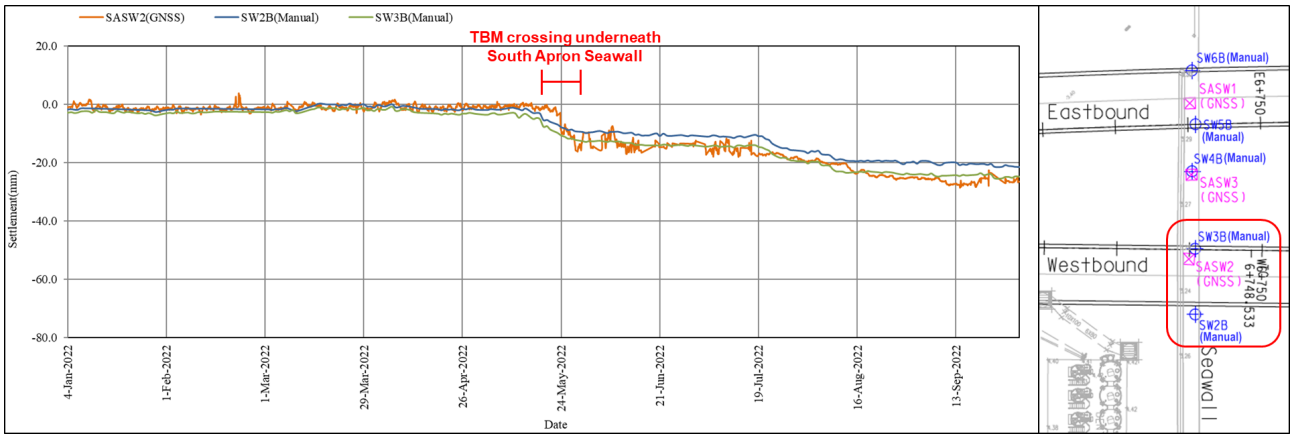

Figure 7: Comparison of ground settlement monitoring data by GNSS and manual survey at South Apron Seawall

Based on the above results, it is observed that a similar trend of settlement was demonstrated by both GNSS and manual survey at the PWCL Building and the South Apron seawall. Hence, it is considered that GNSS monitoring can effectively supplement the conventional survey monitoring, for close monitoring of sensitive / important structures during critical construction periods.

2.4 Merits and Limitations

For the merits, the GNSS technique can provide continuous monitoring readings at 15-minute intervals over a 24-hour/7-day continuous period, which is far more frequently than the commonly adopted daily monitoring using conventional surveying methods, hence it is an ideal monitoring method for sensitive / important structures requiring close monitoring during critical construction periods. Additionally, GNSS monitoring is not affected by adverse weather conditions. With respect to eco-friendly efficiency, the GNSS rover stations can be powered by solar panels, which is advantageous for monitoring in areas with difficult and/or remote access, such as the sea-locked Kwun Tong Typhoon Shelter breakwater.

As for limitations, when installing GNSS rover stations in the urban area, the engineers should pay attention to the presence of the adjacent buildings with glass curtain walls, which will create multipath signals and may cause errors in the GNSS monitoring data. Also, 70% of sky visibility is required for the GNSS rover station to receive sufficient satellite signals to produce reliable monitoring data, so the rover stations should not be installed near objects which may cause sky invisibility, such as near the wall of buildings or under trees or other vegetation.

By knowing the merits and limitations of the GNSS technique, engineers can make the best use of this technique to facilitate monitoring of sensitive / important structures or remote areas with difficult access.

2.5 Site Consideration for Cha Kwo Ling Village

The T2 project team has considered to extend the use of GNSS monitoring to the settlement monitoring of the existing structures in CKL Village. However, the GNSS rover stations require a flat and firm surface for installation and the corrugated rooftop of the existing village houses do not provide suitable locations to install the rover stations, as shown in Figure 8 below. Therefore, the InSAR technique was adopted as an alternative for settlement monitoring in CKL Village.

(a) (b)

Figure 8: (a) Corrugated rooftop unsuitable for installation of GNSS rover station in CKL Village and (b) Rooftop occupied by antennas & prior consent from resident required for installing GNSS rover station

3 INTERFEROMETRIC SYNTHETIC APERTURE RADAR (InSAR) MONITORING

3.1 Working Principle

In T2 project, the InSAR monitoring data was based on the satellite images provided by the TerraSAR-X satellite, which is a commercial German Synthetic Aperture Radar (SAR) Earth observation satellite launched in 2007 with operation altitude at 514 km above the ground surface, as shown in Figure 9 below.

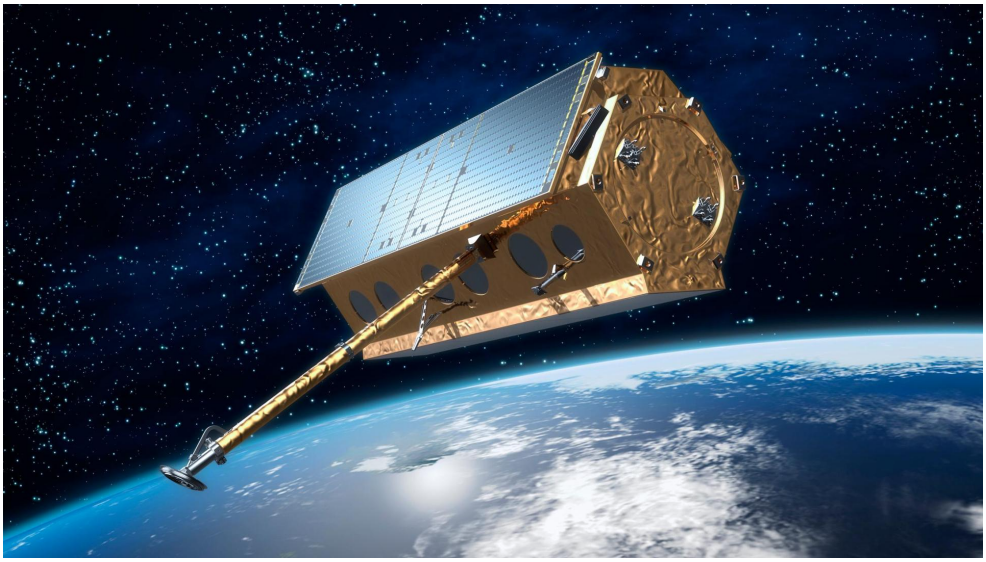

Figure 9: Computer image of TerraSAR-X satellite with X-band radar antenna (bottom left)
(Source of image: German Aerospace Center (www.dlr.de))

The X-band radar emitted by the satellite to the ground surface, with typical frequency of 9.65 GHz and wavelength of 3.1 cm within the electromagnetic spectrum of microwave, can achieve higher sensitivity in detecting small change on the ground surface when the radar signal is reflected back to the satellite. Hence, the X-band radar is commonly adopted for creating high resolution satellite images for terrestrial movement measurement purposes. The satellite makes an orbit around the Earth with a repeat period of 11 days and therefore the satellite images taken at the same location on Earth will have an interval of 11 days.

Measurement of ground deformation is made possible by measuring the phase difference of two radar images taken 11 days apart when the satellite revisits the exact same location. By detecting the phase difference using the latest radar technology to form interferogram, the ground deformation (i.e. the change in ground level) can be measured accurately, as illustrated in Figure 10 below.

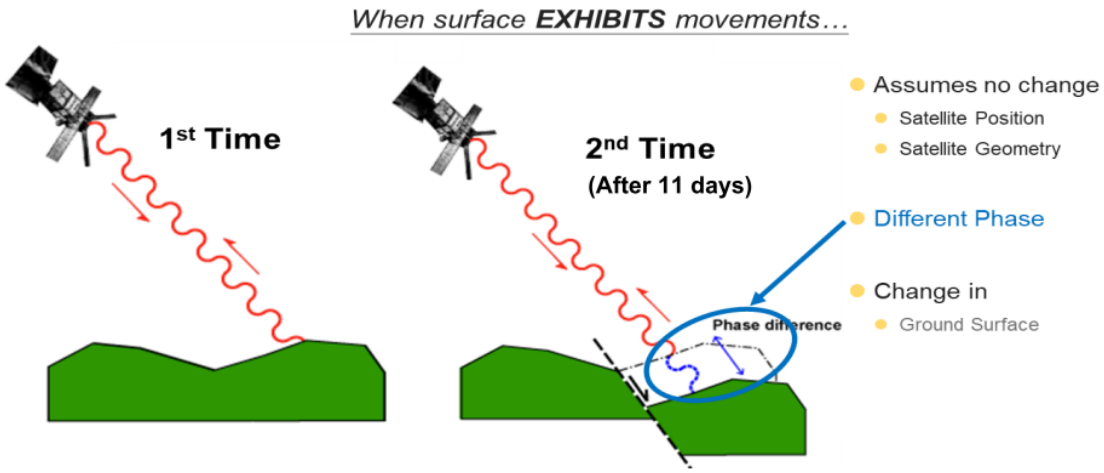

Figure 10: Measurement of ground movement by measuring phase difference of radar signals emitted at different times

Each TerraSAR-X satellite image can cover an area of 30 km x 50 km (width x length) on the ground (see Figure 11), with spatial resolution (i.e. pixel size) of 3 m x 3 m on plan and vertical accuracy of ± 2 mm. For CKL Village, the angle of incidence (α) of the acquired satellite images is 37°, with descending satellite orbit over the Hong Kong's sky.

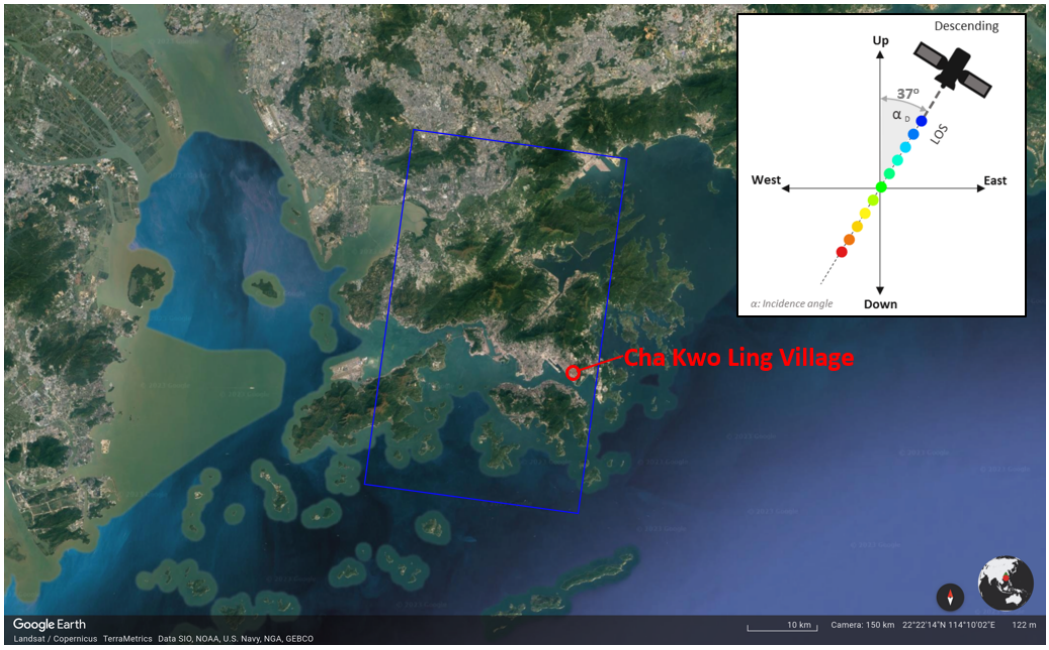

Figure 11: Coverage of one TerraSAR-X satellite image (30 km x 50 km, in blue rectangle) over Hong Kong including the CKL Village

3.2 Site Coverage by InSAR under T2 Project

In T2 project, there are a total of 840 nos. of InSAR monitoring points in CKL Village, as shown in Figure 12 below. Due to the closely annexed village houses or squatter dwellings with narrow alleys in CKL Village, most of the InSAR monitoring points are located on the roof of the structures which can reflect radar signals to form observable monitoring points under InSAR, whereas a small portion of the monitoring points are located on the ground surface of hard pavement.

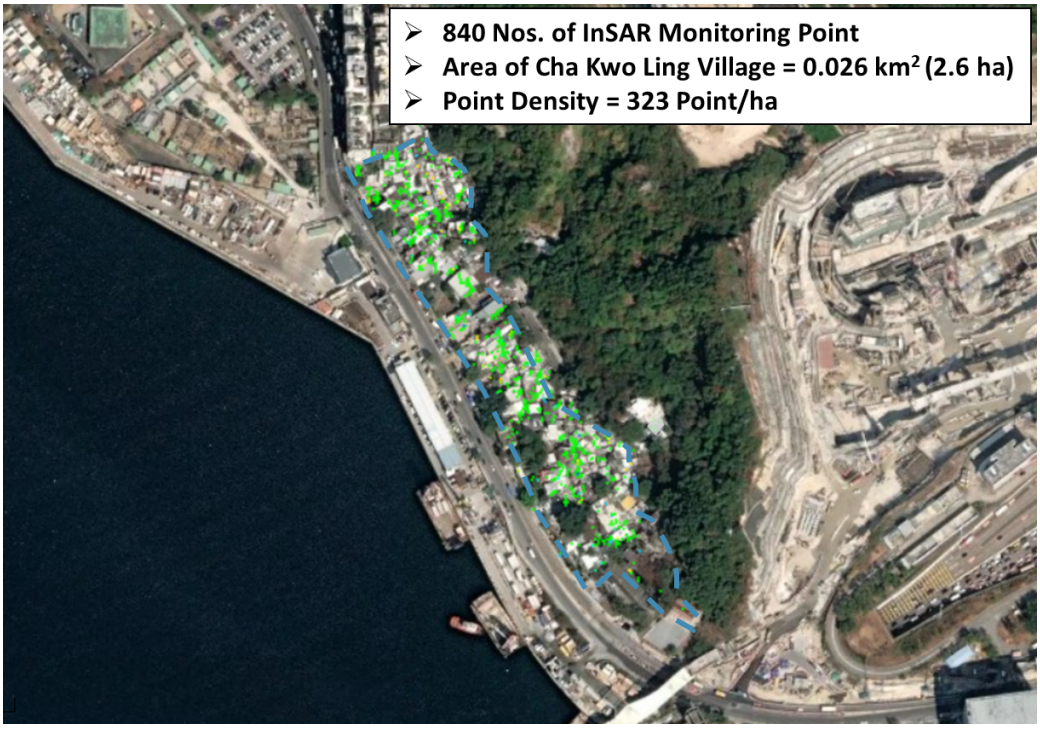

Figure 12: InSAR monitoring points (green dots) inside CKL Village (bounded by blue dotted line)

Under the InSAR monitoring exercise, the satellite images and the associated ground deformation monitoring data, can be acquired as far back as November 2017, which is approximately three years before the commencement of CKL tunnel works under the T2 project. It means that sufficient historical monitoring records at the concerned works area can be retrieved and studied well before the commencement of works to facilitate the review of monitoring data during the works.

3.3 Monitoring Results

The remote sensing of InSAR technique was used to supplement the monitoring of building settlement of the village houses and ground settlement within the CKL Village during the T2 tunnel works period, in which the drill-and-blast and drill-and-break works for both Eastbound and Westbound tunnels were directly underneath the Village. InSAR monitoring was particularly useful during the period of COVID-19 pandemic, in which there was restricted access to the village houses and dwellings for conventional manual survey, and InSAR could provide monitoring data to allow continuous settlement monitoring of the houses and the surrounding ground.

Like GNSS, the InSAR monitoring data can also be readily accessible for review at any time via a dedicated web portal, as shown in Figure 13 below.

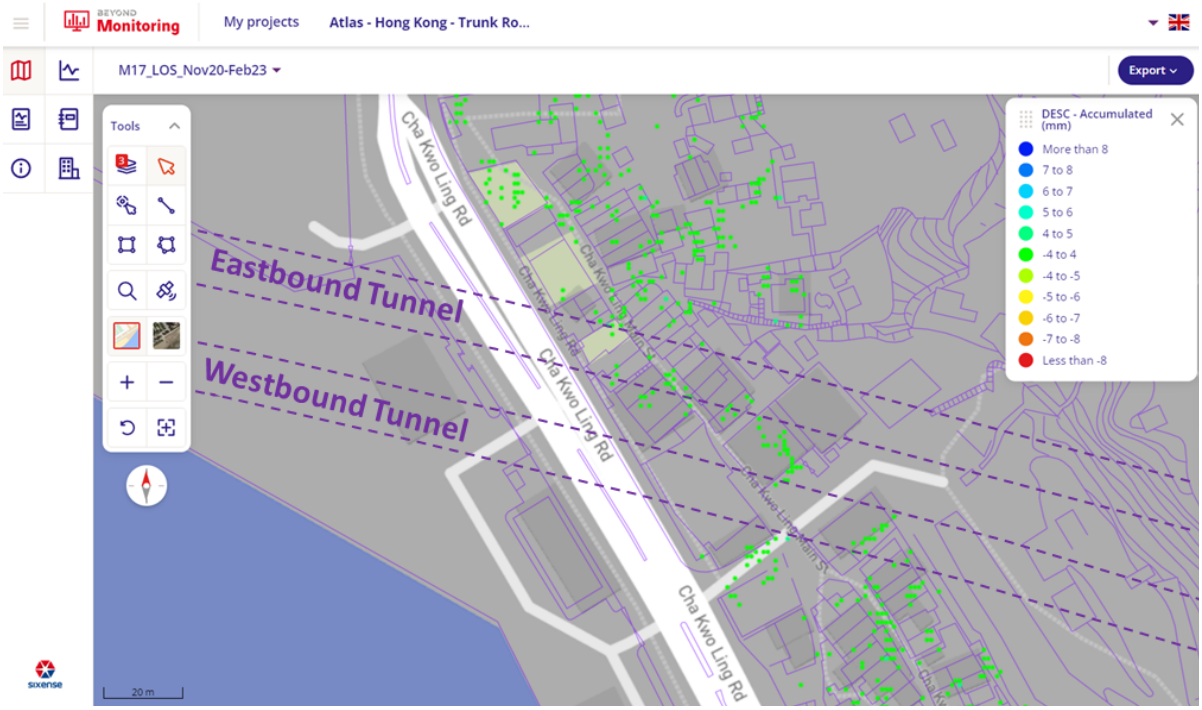

Figure 13: View of the dedicated web portal of InSAR for monitoring of CKL Village, with green dots representing InSAR monitoring points

After review of both conventional settlement monitoring data and InSAR monitoring data in the CKL Village during the T2 works period, it is observed that both sets of monitoring data show consistent trends of movement. Therefore, it is considered that InSAR monitoring can be a reliable means of monitoring to supplement conventional manual survey.

3.4 Merits and Limitation

The merits of the InSAR technique include availability of historical monitoring data for review, monitoring unaffected by adverse weather conditions due to the high penetration power of the X-band radar through

moisture and no need for installation of any instrument or physical presence of any surveyor, thereby enhancing site safety for the surveying works and making it ideally applicable for monitoring works in inaccessible or remote areas. During the outbreak of COVID-19, any close contact between the surveyors and residents in the narrow alleys of CKL Village could also be eliminated.

As for the limitation, due to the orbiting period of 11 days for the TerraSAR-X satellite, the InSAR monitoring data could only be obtained for every 11 days. However, this limitation can be resolved easily by deploying additional InSAR satellites with different visiting timeframe to Hong Kong, such that the monitoring data can be obtained with closer intervals.

By understanding the above merits and limitation of the InSAR technique, engineers can maximize the use of this technique under the various challenging scenarios of instrumentation monitoring.

4 CONCLUSIONS

In the T2 project, both GNSS and InSAR monitoring techniques have been employed very successfully. All monitoring data collected by these techniques was easily accessible through their associated dedicated web portals. Both monitoring techniques are unaffected by adverse weather conditions. In future, it is envisaged that these monitoring techniques will have huge potential for wider geotechnical applications involving movement monitoring in remote and/or restricted areas.

ACKNOWLEDGEMENTS

This paper is published with the permission of the Project Manager of the East Development Office of Civil Engineering and Development Department.

REFERENCES

Bjorndahl, F., Lofgren, J. 2008. Tropospheric correction for InSAR using interpolated ECMWF data and GPS zenith total delay measurements from the southern California integrated GPS network.

Adoption of New and Green Construction Materials in the Landslip Prevention and Mitigation Programme

Chris C.W. Chan, Rex L.Y. Ip, Jackie C.K. Leung & Terry K.F. Luk
Geotechnical Engineering Office, Civil Engineering and Development Department,
The Government of the Hong Kong Special Administrative Region

ABSTRACT

As technology advances, the Geotechnical Engineering Office of the Civil Engineering and Development Department has endeavoured to take every opportunity to improve our geotechnical standards and services through technical development and innovation. It is also our policy to seek continuous improvement in the Landslip Prevention and Mitigation Programme, our long-term rolling programme in reducing systematically the landslide risks of man-made slopes and natural hillsides affecting existing facilities. One of the key areas of technical development is the adoption of new and green construction materials for use in the design and construction of our landslip prevention and mitigation works. This paper summarises our work on the technical development and application of self-compacting backfill material and ground granulated blastfurnace slag grout mixes as part of our contribution in shaping a safe, green and sustainable city.

1 INTRODUCTION

The Geotechnical Engineering Office (GEO) of the Civil Engineering and Development Department (CEDD) has devoted its effort to tackle landslide problems in Hong Kong. One of the key elements of the Hong Kong Slope Safety System is the implementation of the Landslip Prevention and Mitigation Programme (LPMitP) with a view to reducing systematically the landslide risks in Hong Kong. The Programme has also provided ample opportunities for technical development and innovation in the slope engineering field, as well as in geotechnical engineering from a wider perspective.

Recently, we have explored the use of self-compacting backfill material (SCM) in slope works with a view to improving productivity and enhancing site safety. The trials completed at selected sites under the LPMitP revealed that the use of SCM had resulted in notable improvement in site progress and significant reduction in manual handling required for the backfilling operations when compared with conventional fill replacement methods. Following the successful pilot applications, we have documented the relevant findings in the GEO Technical Note No. 1/2023 (Chan & Ip, 2023) and issued a standard material specification with a view to promoting a wider use of the material in slope and retaining wall works.

In addition, noting the continuous improvement in quality control and supply of ground granulated blastfurnace slag (GGBS), a by-product of the iron manufacturing industry, for concrete production in the past few years, we have explored the use of GGBS for partial replacement of Ordinary Portland Cement (OPC) in grout mixes for soil nailing works with a view to reducing the carbon footprint of LPMit works. GGBS is a supplementary cementitious material, of which its production requires less additional energy as compared to the production of OPC, and thus a relatively green construction material. We have arranged laboratory testing at the Public Works Central Laboratory (PWCL) for identifying possible grout mixes which satisfy the relevant technical requirements. Field trials of the preferred GGBS-cement grout mixes are being arranged. Upon successful laboratory and field trials, a standard material specification will be prepared to promote the use of GGBS-cement grout in LPMit works.

2 USE OF SELF-COMPACTING BACKFILL MATERIAL

2.1 Background

In Hong Kong, the stabilisation of loose fill slopes is usually challenging in terms of constructability and construction time. The replacement or re-compaction of the top 3 m layer of loose fill is one of the options for the slope upgrading works. The current practice for the replacement of loose fill typically involves re-compaction of the existing fill, replacement by cement-soil, replacement by no-fines concrete or replacement by mass concrete. To address the concern on slope stability during the construction stage and for preservation of existing trees on the slopes, the fill replacement is usually undertaken by pit-by-pit construction method. However, it is usually difficult and time consuming to carry out fill replacement and the necessary quality assurance test with such limited working space at steep terrain, not to mention the site safety hazards in connection with manual handling and working in those pits.

With this background, the GEO has identified the opportunity of using a SCM developed by Nano and Advanced Materials Institute Ltd. (NAMI) in lieu of the conventional soil backfill materials in slope and retaining wall works with a view to enhancing constructability and site safety. A pilot study with site trials for use of the SCM was launched in late 2020 as a continuous improvement initiative under the LPMitP.

2.2 The self-compacting backfill material

The SCM developed by NAMI (SCM-NAMI), with a material formulation named as "NAMI DM-4" as referred to by NAMI, is originally designed for trench backfilling for the Highways Department (HyD) (Nissinen, 2021, HyD, 2022, Kwong et al, 2022). SCM-NAMI is a mix of (i) cementitious material; (ii) fine aggregate; (iii) crushed rock fines; (iv) water; and (v) admixtures, with necessary optimisation in the mix formula to achieve a balance between workability and strength, while maintaining homogeneity. As the SCM-NAMI was originally developed for its intended use in backfilling of trenches and voids in road works, the mix was designed for a target maximum compressive strength of less than 1 MPa to allow future re-excavation while achieving high flowability, as well as self-levelling and self-consolidating properties.

Considering the composition and properties of the SCM-NAMI, it could be categorised as a kind of "Controlled Low-Strength Material (CLSM)" (ASTM, 1998, Hitch, 1998, ACI, 2013), which is a collective term to describe a family of mixtures that compose of a self-consolidating cementitious material used primarily as a backfill as an alternative to compacted fill. The SCM-NAMI with a target maximum compressive strength of less than 1 MPa is classified as a lower-strength CLSM mix. Typical lower-strength CLSM mixes exhibits soil-like performance with negligible liquefaction potential. As the SCM-NAMI exhibits self-compacting properties, the conventional compaction control requirements for fill material as laid down in Section 6 of the General Specification for Civil Engineering Works (GS) (HKSAR Government, 2020) are not applicable.

2.3 Site trials and key findings

After a preliminary review on the feasibility of using SCM-NAMI in LPMit works including initial laboratory tests conducted by the PWCL to verify the properties and suitability of SCM-NAMI for slope applications, a series of site trials was arranged. Pilot applications, involving the use of over 1,300 m^3 of SCM-NAMI, had been carried out at a total of eight trial sites. The pilot applications involved the replacement of about top 3 m of existing loose fill on slope or behind retaining wall by SCM-NAMI as part of the slope upgrading works under the LPMitP. Both ready-mixed SCM-NAMI produced by concrete batching plants and mixed-on-site SCM-NAMI using pre-packed materials by adding water and admixture, were under trial. A list of the pilot sites is shown in Table 1.

Table 1: List of pilot sites

Feature no.	Location	Type of mix	Volume applied (m^3)
7SW-D/C454	Lei Uk Tsuen, Sha Tin	Ready-mixed	166
15NE-A/F116	Tai Tam Road, Southern	Ready-mixed	22
7SE-C/F110	Sha Tin Road, Sha Tin	Ready-mixed	179
6NE-C/R45	Shug Shan New Village, Yuen Long	Ready-mixed	50
8SW-A/R16	Tso Wo Hang, Sai Kung	Mixed on site	50
14NW-D/FR53	Kwun Yam Wan Road, Cheung Chau	Mixed on site	30
14NW-D/FR54	Kwun Yam Wan Road, Cheung Chau	Mixed on site	10
11NW-D/FR141	King's Park, Yau Ma Tei	Ready-mixed	855

The key findings from the site trials are summarised below:

(a) General - The SCM-NAMI produced by the concrete batching plant or by mixing on site has demonstrated self-compacting properties, and the respective material properties, including wet density and flowability, were largely consistent among the samples collected from the trial sites. In general, the ready-mixed SCM-NAMI demonstrates better consistency in material properties than SCM-NAMI mixed on site as expected. After placement and setting of the SCM-NAMI, no noticeable ground subsidence was observed.

(b) Strength - The SCM-NAMI at 28 days achieved an unconfined compressive strength of at least 0.2 MPa consistently.

(c) Flowability and density - The fresh SCM-NAMI exhibited high flowability (i.e. slump greater than 200 mm) consistently at the trial sites. The self-levelling, self-consolidating and void-fillable characteristics enhanced the efficiency of the fill replacement operations significantly. The wet density of the fresh SCM-NAMI ranges from 1.9 Mg/m^3 to 2.3 Mg/m^3. The bulk density of hardened SCM-NAMI is about 1.8 Mg/m^3 to 2.2 Mg/m^3.

(d) Constructability - The SCM-NAMI allows horizontal pumping of over 250 m and vertical pumping of over 30 m by using typical concrete pumps, thus facilitating placement of the SCM-NAMI at sites with difficult access. There was also no observable excessive ingress of the SCM-NAMI into the surrounding loose fill materials. The setting time of SCM-NAMI was about 8 hours. The key quality control tests, i.e. checking of wet density and flowability, to be carried out on site are simple and straight-forward. The ease in placement and simple quality control of the material also led to a remarkable shortening of construction duration.

(e) Permeability - The SCM-NAMI is relatively impermeable, with a mass permeability between 5.2 x 10^{-6} m/s and 7.4 x 10^{-9} m/s, which is close to the lower bound value of the compacted soil fill.

According to the pilot study (Chan & Ip, 2023), the SCM-NAMI or equivalent is found to be a feasible alternative to compacted fill (or other typical backfill material such as cement-soil, no-fines concrete, and mass concrete) for backfilling of pits, trenches and voids in slope and retaining wall works. Photographs of the site trials are presented in Plates 1 to 4.

(a) Delivery of ready-mixed SCM by concrete truck

(b) Discharge of ready-mixed SCM to concrete pump

(c) Use of pipelines for transportation of SCM within the site

(d) Placement of SCM by chutes

Plate 1: Delivery and placement of ready-mixed self-compacting backfill material

(a) Production of SCM using screw mixer on site

(b) SCM discharged from the screw mixer

Plate 2: Production of self-compacting backfill material mixed on site

(a) Placement of SCM for fill replacement in a pit

(b) Loose fill replaced by SCM

Plate 3: Application of self-compacting backfill material on site

(a) Flowability test in accordance with ASTM D6103-17

(b) Sampling and preparation of cylindrical sample for laboratory testing

Plate 4: Field testing and sampling of self-compacting backfill material on site

2.4 Benefits and limitations

The most significant benefits about the use of SCM are the major reduction of manual handling and the remarkable shortening of construction duration due to the elimination of compaction operations. As compared with conventional soil re-compaction or replacement by cement-soil, the use of SCM, which exhibits self-levelling, self-consolidating and void-filling properties, eliminates the need for compaction operations and necessary compaction tests required. The use of SCM is also less affected by inclement weather, bringing further improvement of the overall site progress. As compared with replacement of loose fill by no-fines concrete or mass concrete, the use of high pumpability of SCM without the need of in-situ vibration during placement can minimise the manual operations in connection with the transportation and placement of replacement material. It expedites the backfilling process and helps to overcome access constraints. Besides, on some special occasions, e.g. maintenance of underground utilities is required, use of SCM with limited strength would facilitate future excavation.

Overall speaking, the site trials completed revealed that the use of the ready-mixed SCM had resulted in a notable improvement in site progress, with over 75% time saving and 50% labour reduction for the backfilling operation as compared with the conventional fill replacement methods. The use of SCM to be mixed on site provide similar benefits on labour reduction but with less time saving as production rate of SCM on site is limited. Last but not least, the use of SCM in fill replacement operations was also observed to have enhanced

the overall constructability and minimised the construction operations at the congested environment on steep slopes, which improved construction site safety as a whole.

Currently, the material cost of SCM in Hong Kong is higher than that of re-compaction of the existing fill or replacement by cement-soil, no-fines concrete or mass concrete, likely due to limited demand at the current stage. At the time being, the SCM developed by NAMI has been licensed to four companies for commercial scale production and supply locally. It is believed that the cost of SCM-NAMI or equivalent can be reduced through market competition among suppliers and with wider application of the material in the future.

2.5 Wider uses in slope and retaining wall works

With the observations and findings of the site trials, a set of particular specification (PS) for the use of SCM-NAMI or equivalent in slope and retaining wall works was prepared with a view to facilitating the wider use of the material. The PS sets out the quality requirements, standards of workmanship, testing methods and acceptance criteria of using SCM for backfilling of pits, trenches and voids in slopes and retaining walls. The PS supplements Section 7 – Geotechnical Works of the GS (HKSAR Government, 2020). The GEO issued the PS to government departments and geotechnical practitioners in September 2022 to facilitate the general use of the SCM in backfilling of pits, trenches and voids in slope and retaining wall works (GEO, 2022).

For quality control requirements of the SCM, the key tests rest on the field checking of flowability and wet density to verify the consistency of the SCM mix without segregation. For the compliance test of minimum strength level, UCS tests for cylindrical specimens has been specified with due consideration on the use of the SCM for geotechnical works. The method of testing shall be in accordance with Appendix B of the "Interim Guidelines on Testing of Unconfined Compressive Strength of Cement Stabilised Soil Cores in Hong Kong" published by Geotechnical Division of The Hong Kong Institution of Engineers in October 2017 (HKIE, 2017). In the PS, the flowability of the SCM is specified to be at least 200 mm without segregation according to ASTM D6103-17. The minimum compressive strength of the SCM at 28 days is specified to be 0.2 MPa.

The SCM, which has been demonstrated as a feasible alternative in fill replacement operations, provides opportunities for streamlining site operations in suitable projects in enhancing the project performance in terms of productivity, safety and sustainability.

3 USE OF GROUND GRANULATED BLASTFURNACE SLAG IN CEMENT GROUT

3.1 Background

Cement-based grout is widely used in slope engineering works in particular for grouting of soil nails, rock bolts and rock dowels. Traditionally, a simple and standardised cement grout mix, involving OPC and water with a water cement ratio not exceeding 0.45 has been referred to in standard specifications in the past decades. To promote a green and sustainable slope engineering practice and to support the carbon neutrality initiative, the potential incorporation of supplementary cementitious material for partial replacement of OPC in grout mixes has been explored. In addition to the reduction of carbon footprint, the use of supplementary cementitious material, such as pulverised fuel ash (PFA) and GGBS, usually means the incorporation of potential waste for production use.

PFA, which is the ash resulting from the burning of pulverised coal in coal-fired electricity power stations, has been widely used as supplementary cementitious material locally. However, there may be a shortage of supply of PFA in the near future due to the reduced use of coal for power generation locally. GGBS, which is a by-product of the iron manufacturing industry, is another supplementary cementitious material which may be used for replacement of OPC in concrete production. Granulated blastfurnace slag is obtained by quenching molten iron slag from a blastfurnace in water to produce a granular product, which is then dried and ground to become GGBS.

For concrete, Section 16 the General Specification for Civil Engineering Works (HKSAR Government, 2006) was amended in 2012 to allow the general use of GGBS as supplementary cementitious material. For cement grout in geotechnical works, there are provisions for the use of PFA in cement grout in Section 7 of the GS but not GGBS. In view of the foreseeable decline of local PFA supply and the continuous improvement in quality control and supply of GGBS for concrete production in the past few years, we have launched a study to review the use of GGBS for partial replacement of OPC in grout mixes for soil nailing works under the LPMitP.

3.2 Key issues on the use of GGBS in cement grout and past experience

With due consideration on the material properties and supply of GGBS, as well as the past experience of the GEO on the use of GGBS in concrete and in cement grout (Wong & Chi, 2016), key issues on the use of GGBS in cement grout are summarised below:

(a) Sustainability - The production of one tonne of GGBS would generate about 0.083 tonne of CO_2 equivalent, as compared to 0.95 tonne for cement and the energy consumption for one tone of GGBS and cement are 1,600 MJ and 5,500 MJ respectively (BSRIA, 2011). Therefore, using GGBS as a partial replacement of cement can significantly reduce the carbon footprint in concrete and cement grout production.

(b) Physical and chemical properties - Section 16 of the GS (HKSAR Government, 2020) requires that the GGBS should comply with BS EN 15167-1 (BSI, 2006). Generally speaking, the physical and chemical properties of GGBS are similar to those of OPC, and this makes partial replacement of cement with GGBS technically feasible. Notwithstanding this, the fineness of GGBS typically adopted in concrete production is higher than that of OPC.

(c) Setting time and strength development - Generally speaking, since the hydration property of GGBS is latent when compared to that of OPC, GGBS-cement grout requires more time for setting than conventional cement grout. Moreover, the GGBS-cement grout may have a slower early strength development as compared with that of conventional cement grout.

(d) Workability and bleeding - Due to the higher fineness of GGBS as compared with OPC, the replacement of OPC by GGBS may reduce the workability of the cement grout. In theory, the bleeding of GGBS-cement grout is related to the fineness of GGBS, the water to cementitious materials ratio and the amount of any admixture used.

(e) Quality control and supply - There are continuous improvement in the quality control and supply of GGBS for concrete production. In particular, GGBS produced by plants with internationally recognised quality assurance system which fulfils BS EN 15167-1 are available locally. The material cost of GGBS is in the same order of OPC.

In view of the above, we have arranged laboratory testing at the PWCL for identifying possible grout mixes which satisfy the relevant technical requirements with a view to seeking considerable replacement of OPC by GGBS with an optimal addition of admixtures. Particular attention is given to the use of admixture and the performance of GGBS-cement grout mixes in terms of workability and bleeding.

3.3 Laboratory trials

With the technical support of GGBS / cement / concrete suppliers, a series of laboratory trial mixing using different grout formulas, cementitious materials and admixtures was arranged. In addition, four control mixes with GGBS replacement ratio of 50% and one control mix using pure OPC were arranged. No admixtures were used in the control mixes. A list of the grout mix formulas is shown in Table 2.

Table 2: List of grout mix formulas

Mix ID.	Cementitious content (kg/m^3)	GGBS replacement ratio	w/c ratio	Admixture	Cement brand	GGBS manufacturer	Mixing sequence
E1AA	1420	65%	0.36	Retarder + Superplasticiser + Water retaining agent	A	A	Adding water to dry cement and GGBS
E1AB						B	
E1BA					B	A	
E1BB						B	
E2AA	1365	50%	0.39		A	A	
E2AB						B	
E2BA					B	A	
E2BB						B	
G1AA	1305	69%	0.41	Superplasticiser + Retarder and expansion agent	A	A	Adding cement to water first and then adding GGBS to the grout mix
G1AB						B	
G1BA					B	A	
G1BB						B	
G2AA	1320	73%	0.40		A	A	
G2AB						B	
G2BA					B	A	
G2BB						B	
CMAA	1365	50%	0.40	-	A	A	
CMAB						B	
CMBA					B	A	
CMBB						B	
CMA	1365	-	0.40		A	-	

A number of compliance tests were carried out on the trial mixes in accordance with the GS:

(a) Flow cone test in accordance with ASTM C939;
(b) Bleeding tests in accordance with ASTM C940; and
(c) Compressive strength tests on grout cubes at 3, 7, 14 and 28 days in accordance with CS1:2010.

3.4 Observations from laboratory test results

The test results of the compliance tests on the trial mixes are summarised below:

(a) General and workability - The GGBS-cement grout mixes with various replacement ratios ranging from 50% to 73%, using different brands of raw materials and with the addition of admixtures (i.e. mixes under E1, E2, G1 and G2 series) meet flow cone efflux time requirement of not less than 15 seconds as stipulated in the GS as shown in Figure 1 and the limiting maximum time of 35 seconds as recommended in the relevant testing standard. The four control mixes using 50% GGBS replacement but without the use of admixtures demonstrated poor workabilility as expected.

(b) Bleeding - For all mixes, the 3-hour bleeding results are the same as the final bleeding results. The mixes under the E1 series, which have the lowest w/c ratio of 0.36, as well as the control mixes under the CM series satisfy the 3-hour bleeding requirement (< 0.5%) as specified in the GS. All the mixes under E2, G1 and G2 series with a higher w/c ratio of 0.39 to 0.41, except the G2AB mix, demonstrated 3-hour bleeding results of 0.5% to 1%. All mixes satisfy the maximum bleeding requirement (< 1%). The test results are summarised in Figure 2. In addition, all mixes were observed to have absorbed the bled water within 24 hours.

(c) Strength - All samples achieved the compressive strength requirement of 30 MPa as stipulated in the GS. Mixes under the E1 and E2 series exhibited higher compressive strengths when compared to mixes under the G1 and G2 series as shown in Figures 3 and 4 and this may be due to the lower w/c ratios (0.36 & 0.39) adopted in the former series. In addition, it is observed that for the E2AA mix, the 28-day compressive strength result is lower than the 14-day compressive strength result as shown in Figure 3(b).

This may be due to the poor uniformity of the mix as observed inside the crushed sample. Such uniformity of the mix may be attributed to the adopted method of mixing as listed in Table 2.

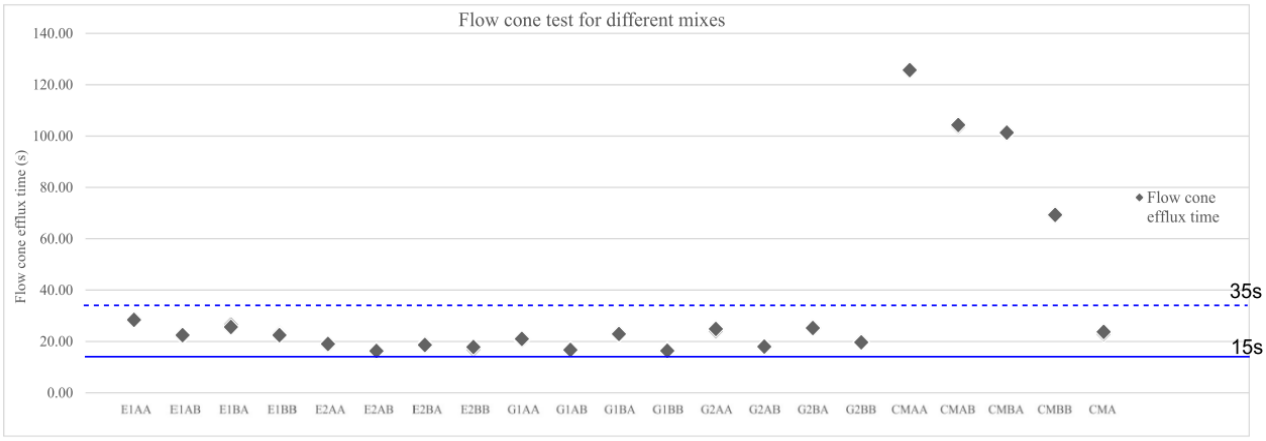

Figure 1: Flow cone test results

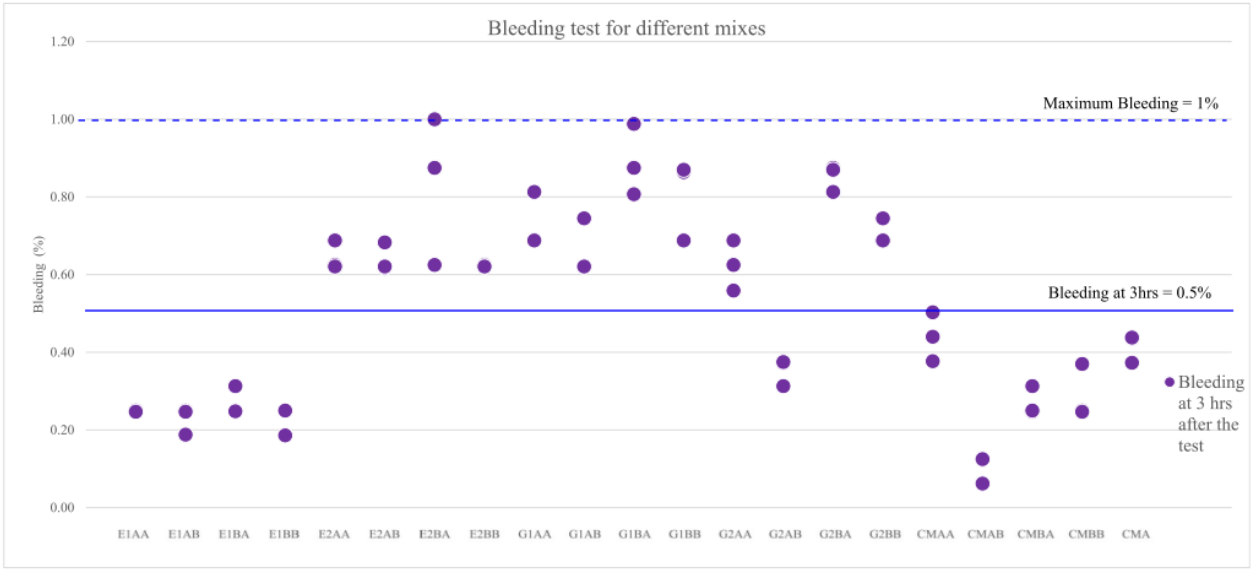

Figure 2: Bleeding test results

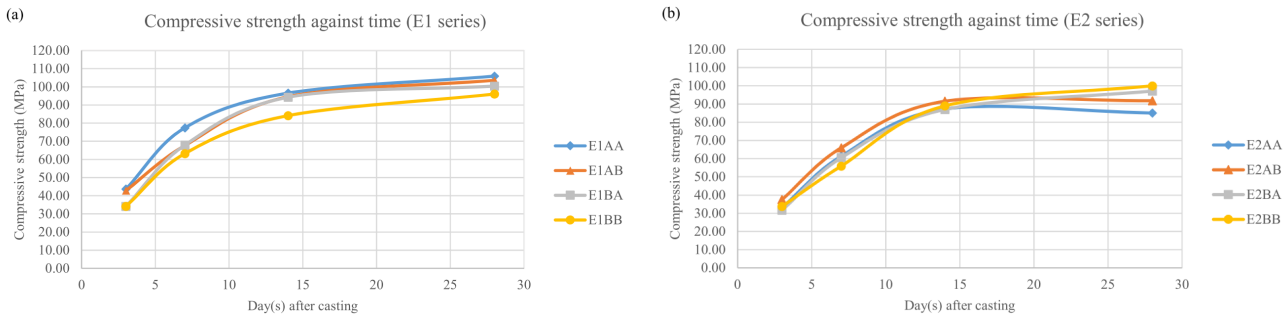

Figures 3(a) and (b): Compressive test results for E1 and E2 series grout mixes

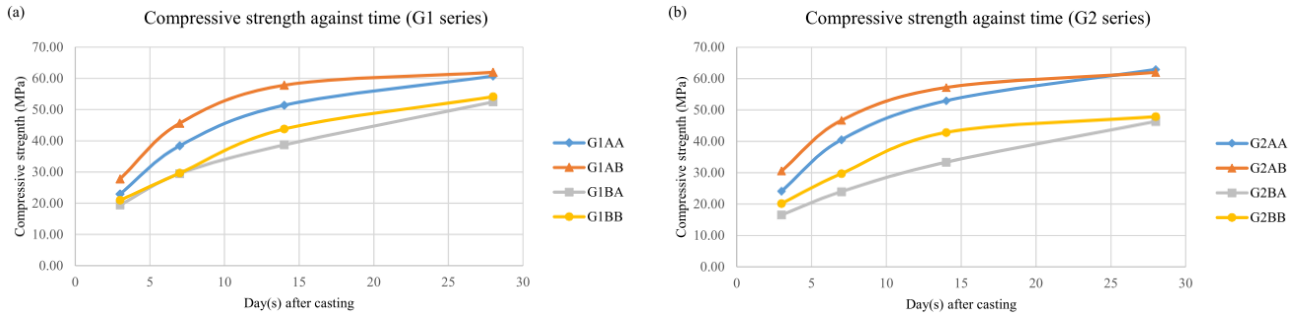

Figures 4(a) and (b): Compressive test results for G1 and G2 series grout mixes

With due consideration of the test results, further trials are being undertaken to review the potential use of mixes with different w/c ratio and the respective bleeding performance and the recommended grout mixing sequence.

3.5 Further work

The GEO are now arranging field trials of the preferred GGBS-cement grout mixes at sites under the LPMitP. The findings from the initial field trial conducted in March 2023 are also promising. Specific review shall be carried out on the field mixing operations of the GGBS-cement grout mixes. In parallel, the GEO and the consultants are reviewing the anticipated order of overall OPC replacement by GGBS in slope engineering works, with an intention to encourage supply of pre-packed GGBS in bags to facilitate storage, transportation and field mixing of GGBS-cement grout. Upon successful laboratory and field trials, a standard material specification will be prepared to promote the use of GGBS-cement in LPMit works.

4 CONCLUSIONS

While the ongoing LPMitP has brought about major improvement to slope safety in Hong Kong, it is necessary to seek continuous improvement in the LPMitP in overcoming the challenge of potentially increasing landslide risks due to climate change and in decarbonising our LPMit works. Technical development and innovation in the slope engineering field in the past decades have also led to advances in knowledge and technology in reducing landslide risks. The recent work of the GEO in the two pilot projects involving the adoption of new and green construction materials in the LPMitP has been highlighted in this paper. Further technical development and innovation as part of the ongoing LPMitP will continue, which can open up more opportunities for practical applications and advances in geotechnical engineering practice, for the development of a safer, greener and sustainable city.

ACKNOWLEDGEMENTS

This paper is published with the permission of the Head of the Geotechnical Engineering Office and the Director of Civil Engineering and Development, the Government of the Hong Kong Special Administrative Region of the People's Republic of China. The technical advice from Nano and Advanced Materials Institute Ltd. on the pilot use of the self-compacting backfill materials, the technical support from Excel Concrete Ltd., Greentex Construction Materials Ltd. and K. Wah Construction Materials Ltd. in the trials of GGBS-cement grout are gratefully acknowledged. The input and support from the participating LPMitP consultants, namely AECOM Asia Company Ltd., C M Wong and Associates Ltd., Fugro (Hong Kong) Ltd. and Halcrow China Ltd., and the participating LPMitP contractors, namely Chi Wo Contractors Ltd., China Geo-Engineering Corporation, Geotech Engineering Ltd. and U-Win Construction and Engineering Company Ltd., on the two pilot projects are also acknowledged.

REFERENCES

ACI. 2013. *ACI 229R-13 Report on Controlled Low-Strength Materials.* Reported by ACI Committee 229. American Concrete Institute.

ASTM. 1998. *The Design and Application of Controlled Low-strength Materials (Flowable Fill).* American Society for Testing and Materials.

BSI. 2006. *Ground Granulated Blastfurnace Slag for Use in Concrete, Mortar and Grout. Definitions, Specifications and Conformity Criteria.* BS EN 15167-1: 2006. British Standards Institution, London.

BSRIA. 2011. A BSRIA Guide. Embodied Carbon: The Inventory of Carbon and Energy (ICE).

Chan, C.C.W. & Ip, R.L.Y. 2023. Pilot Study on the Use of Self-compacting Backfill Material in Slope and Retaining Wall Works. GEO Technical Note No. 1/2023, 57p.

Highways Department. 2022. *Particular Specification for Use of Self-compacting Backfill Material for Backfilling Utility Trenches and Voids.* Research and Development Division, Highways Department, The Government of the Hong Kong Special Administrative Region.

Geotechnical Engineering Office. 2022. *Particular Specification for Use of Self-compacting Backfill Material in Backfilling of Pits, Trenches and Voids in Slope and Retaining Wall Works.* Geotechnical Engineering Office, Civil Engineering and Development Department, The Government of the Hong Kong Special Administrative Region.

Hitch, J.L. 1998. *Test Methods for Controlled Low-Strength Material (CLSM): Past, Present, and Future.* The Design and Application of Controlled Low-strength Materials (Flowable Fill), ASTM STP 1331, A.K. Howard and J.L. Hitch, Eds., American Society for Testing and Materials.

HKIE. 2017. *Interim Guidelines on Testing of Unconfined Compressive Strength of Cement Stabilised Soil Cores in Hong Kong.* Geotechnical Division of The Hong Kong Institution of Engineers.

HKSAR Government. 2006. *General Specification for Civil Engineering Works (2006 Edition).* The Government of the Hong Kong Special Administrative Region.

HKSAR Government. 2020. *General Specification for Civil Engineering Works (2020 Edition).* The Government of the Hong Kong Special Administrative Region.

Kwong, M.M.K., Zhu, H.G., Chen, E.X.R., Sham, I.M.L., Chan, I.H.H., Chan, C.C.W. & Goh, S.N. 2022. Novel Cementitious Materials for Geotechnical Applications – Vibration Resistant Sprayed Concrete for Rock Tunnel Lining and Self-compacting Backfill for Slope Upgrading Works. In Proceedings of the 42nd Annual Seminar, Geotechnical Division, The Hong Kong Institution of Engineers. Hong Kong, 13 May 2022, pp. 239-251.

Nissinen, T. 2021. *Innovative Self-Flow Low Strength Concrete Materials for Pavement Backfill in Hong Kong.* Annual Concrete Seminar 2021. Standing Committee on Concrete Technology, The Government of the Hong Kong Special Administrative Region.

Wong, H.D. & Chi, R.C.Y. 2016. Use of Ground Granulated Blastfurnace Slag in Cement Grout for Geotechnical Works. GEO Technical Note No. 2/2016, 34p.

Integration of BIM and Other Innovative Technologies to Enhance the Sustainable Design of Geotechnical Works

Raymond W K Cheng, David C W Mak, Again Q J Wei,
Joe J P Yan & Quentin H Q Pan
AECOM Asia Company Limited, Hong Kong

ABSTRACT

Recent advancements in smart technologies, such as building information modeling (BIM) and digital twin systems, offer promising opportunities to enhance geotechnical practices. The integration of smart technology in geotechnical engineering has provided innovative and sustainable solutions to the challenges faced by engineers, geologists and construction professionals. For example, Dynamo visual programming is used to develop scripts within Civil 3D and Revit software for modeling subsurface conditions and proposed soil nailing works for slope upgrading projects, as well as to facilitate data exchange in tunnel projects. Handheld laser scanning devices are utilized to generate 3D point clouds of the existing conditions, which are then converted into BIM-compatible models through photogrammetry. The use of these tools and technologies provides many benefits, including improved accuracy and efficiency, as well as reduced costs. The integration of BIM, digital twins, and tools such as Dynamo scripts, handheld LiDAR scanning, and UAV photogrammetry has proven to be a game-changer in the field of geotechnical engineering, providing new and innovative solutions to the challenges faced by engineers, geologists and construction professionals.

1 INTRODUCTION

Building Information Modeling (BIM) has become a popular digital design and management tool in the construction industry, offering a unified platform for the design, construction, and maintenance of infrastructure assets. To improve the sustainability of geotechnical works, BIM can be integrated with other innovative technologies such as UAV photogrammetry, handheld LiDAR scanning, and automation tools with visual programming scripts for parametric design. These integrations can enhance the accuracy and efficiency of sustainable design for geotechnical works.

2 UAV PHOTOGRAMMETRY AND HANDHELD LIDAR SCANNING

UAV photogrammetry and handheld LiDAR scanning are two innovative technologies that can improve the accuracy and efficiency of geotechnical design and construction. UAV photogrammetry involves using unmanned aerial vehicles (UAV) to capture high-resolution images of the construction site, which can be used to create 3D models of the site. Handheld LiDAR scanning involves using a portable LiDAR scanner to capture accurate 3D data of the site. These technologies can be used to improve the accuracy of site surveys, reduce the risk of accidents and injuries, and enable more efficient and effective design and construction.

2.1 UAV Photogrammetry

Traditional topographic survey methods can be physically demanding and time-consuming when conducting topographic surveys at areas with steep slopes, dense vegetation, or areas obscured by debris. The process of setting up total stations and surveying points in such environments can be challenging, which can lead to

errors and bias in manual processing. However, innovative technologies such as UAV photogrammetry can overcome these challenges and improve the accuracy and efficiency of topographic surveys.

UAV photogrammetry can be used to create a 3D model of the construction site that can be used for site analysis, visualization, and planning. UAV can quickly capture high-resolution aerial images and access hard-to-reach areas such as landslide scars, making it possible to create accurate 3D models of the terrain. These models can be used for a variety of purposes, including analyzing the site's topography, identifying potential hazards, and designing effective solutions for geotechnical engineering projects.

Furthermore, UAV photogrammetry can be used to track changes in the construction site over time, enabling construction teams to monitor progress and identify potential issues before they become major problems. This can lead to more efficient and effective project management and ultimately result in cost savings.

Plate 1: Unmanned Aerial Vehicle (UAV) equipped with Light Detection and Ranging (LiDAR) systems for digital terrain modelling and landslide mapping applications

2.2 Handheld LiDAR Scanning

Handheld LiDAR scanning technology can capture accurate data of existing structures, terrain, and underground utilities for more precise design and construction. A scan-to-BIM approach can be adopted for rapid and accurate on-site point cloud data capturing. Handheld LiDAR scanning captures and produces various types of data, including colorized point cloud data points, digital terrain model, and digital surface model.

The integrated scan-to-BIM approach offers several benefits, including better site characterization for hard-to-reach areas, enhanced safety for workers and the public, and reduced costs due to more efficient and accurate design and construction processes. In addition to landslip prevention and mitigation works, the scan-to-BIM approach can be used for digital terrain modeling, landslide debris mapping, and as-built modeling for heritage sites.

Utilizing handheld LiDAR scanning technology for geotechnical engineering works offers significant benefits in terms of efficiency, accuracy, cost savings, and safety. The technology can improve efficiency and accuracy

by up to ten times compared to traditional surveying methods, while cutting the bulk of traditional surveying costs by around 80%. Moreover, using this technology can save up to 50% of staff hours and eliminate safety hazards associated with accessing challenging terrain.

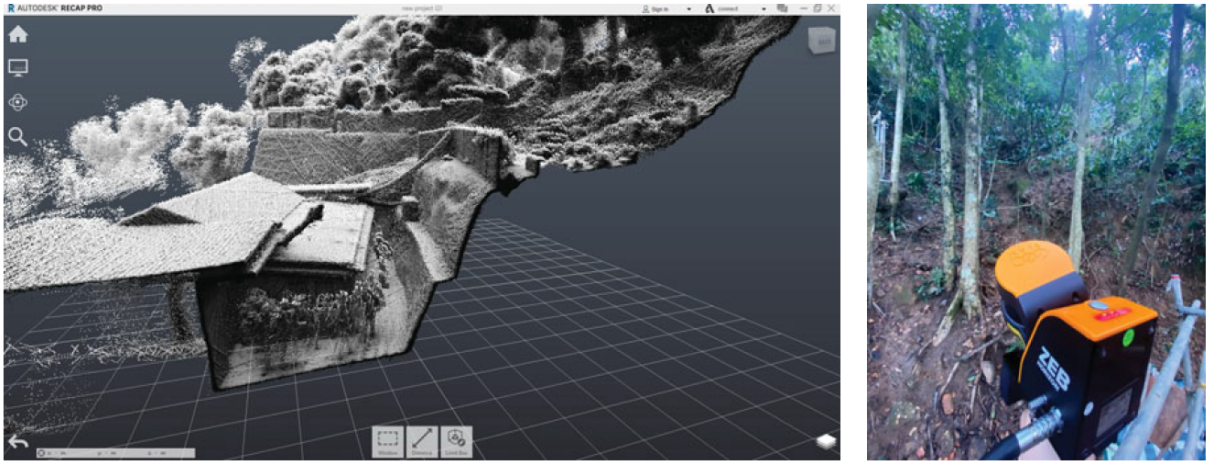

Plate 2: Handheld LiDAR scanner for rapid generation of digital surface model with unprecedented level of details

3 BUILDING INFORMATION MODELLING (BIM) AND DYNAMO VISUAL PROGRAMMING

BIM and Dynamo visual programming are innovative technologies that can improve the accuracy and efficiency of geotechnical design and construction. BIM involves creating a digital 3D model of the construction project, which can be used to simulate construction activities, detect clashes, and optimize design and construction processes. Dynamo is a visual programming tool for BIM that enables the creation of custom scripts to automate design and construction tasks.

3.1 Dynamo scripts for slope upgrading works

Dynamo scripts can be used to automate geotechnical design and construction tasks such as slope upgrading works, site formation projects, and parametric design for tunnel projects. The benefits of using BIM and Dynamo for geotechnical design and construction include improved accuracy and efficiency of design and construction processes, reduced errors and rework, and more effective collaboration between stakeholders.

Designers can create parametric models that can be easily modified to test different design options and evaluate their impact on project objectives. This can help to identify the optimal design solution that best meets the project requirements. Moreover, the use of scripting can help to optimize the design process for factors such as time, cost, productivity, quality, safety, and sustainability. This can be achieved by creating scripts that automate repetitive tasks, enable faster iteration of design options, and provide real-time feedback on the impact of design changes.

One of the main advantages of using Dynamo is that it allows designers to easily include repetitive objects into the model. This can save time and reduce errors by automating tasks that would otherwise be done manually. For instance, scripts can be created to generate repetitive elements in slope upgrading work projects, such as the placement of soil nails, tree rings and hoarding layout. This can help the designer to optimize the layout of the proposed slope upgrading works and avoid clashing of different objects on slope. By using this streamlined design workflow, the needs for future design review can be minimized and hence the time and cost required for the project can be reduced.

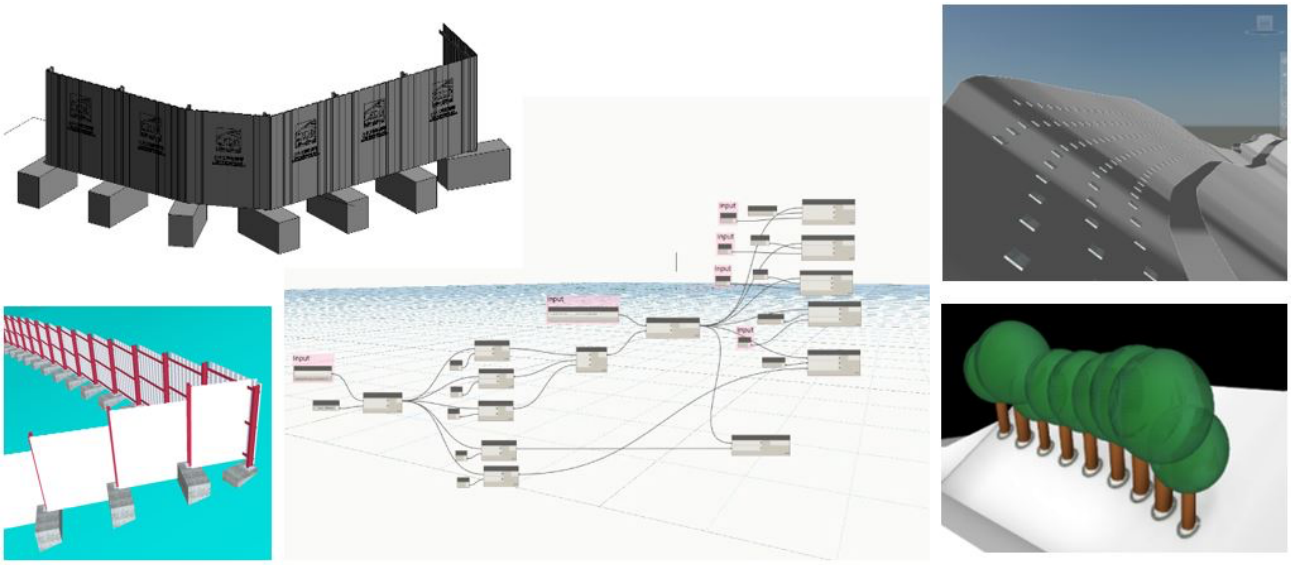

Figure 1: Dynamo scripts developed to streamline the design workflow of slope upgrading works

3.2 Automation for the design of site formation projects

Site formation projects can benefit significantly from the use of automation tools. In particular, LiDAR data can be used to create accurate terrain models that can help to plan and optimize the site formation level and platform area. Better coordination between different utility undertakers for underground utilities can also be achieved using automation tools to provide better integration between Geographic Information System (GIS) and BIM. This can help to reduce conflicts and rework. Real-time updating of 3D ground models and clear visualisation of soil-rock interface can help to identify potential adverse geological issues early on and allow for adjustments to be made quickly upon the completion of site-specific ground investigation works.

BIM models can be used to fine-tune and optimize the site formation level and platform area based on a pre-defined set of design criteria. Programming scripts such as Python can be used to quickly enhance the detailing of the site formation project such as adding retaining walls, soil nails, surface drainage channels and maintenance access, ensuring optimal design with minimal errors. Automation tools can also be used to measure and estimate the quantity of works required for a site formation project, as well as estimating cut-and-fill volume. This can help to ensure completion on time and within budget.

Additionally, automation tools can produce design drawings quickly and accurately, reducing time and effort for the preparation of plans, cross-sections and elevations drawings. Effective communication with draughtsmen can also be facilitated using automation tools, minimizing revisions and ensuring everyone understands the project requirements. Overall, the use of automation in site formation projects can improve efficiency, accuracy, and quality, while reducing waste and costs.

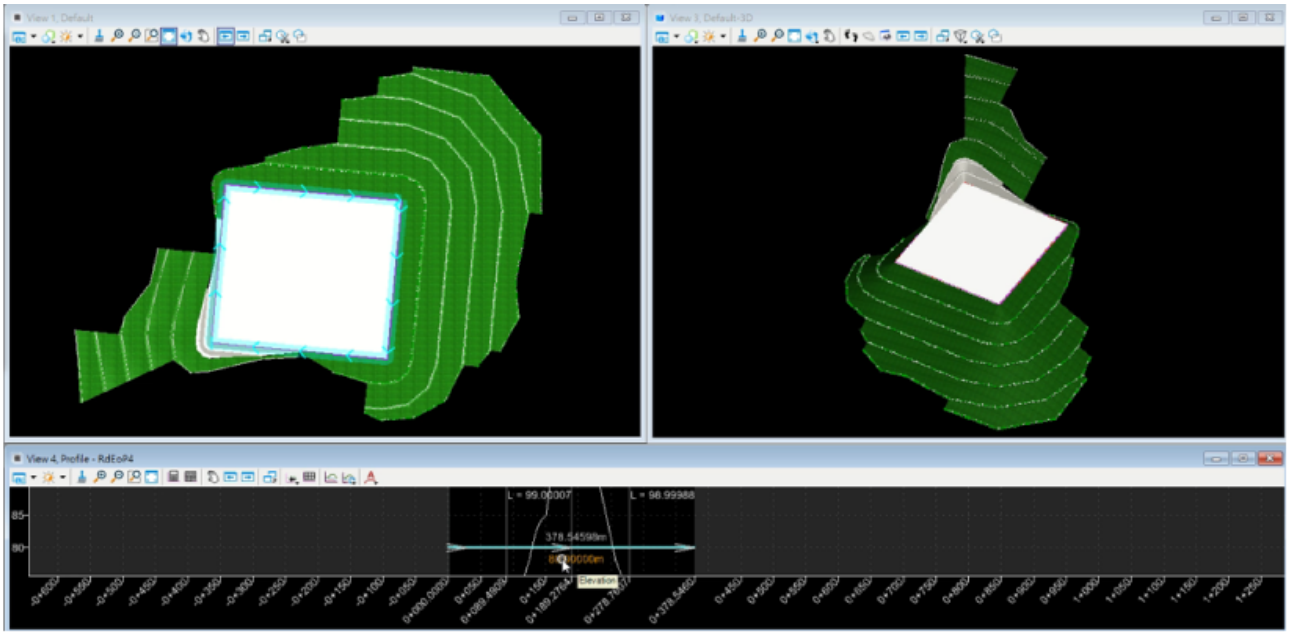

Figure 2: Use of BIM model to fine-tune and optimize the site formation level and platform area

3.3 Parametric design for tunnel projects

Parametric design is a method of design that uses a set of defined parameters to generate a range of design options. In the context of tunnel projects, parametric design can be used to generate multiple design options for tunnel alignment, cross-section, and support systems. This can help to optimize the design for a range of factors such as cost, constructability, safety, and environmental impact.

One of the main benefits of parametric design for tunnel projects is that it enables rapid iteration and evaluation of design options. By adjusting the defined parameters, designers can generate a range of design options and evaluate them against a set of criteria such as cost, constructability, safety, and environmental impact. This can help to identify the optimal design option that best meets the project requirements.

Parametric design can also help to improve the efficiency of the design process by automating repetitive tasks such as generating cross-sections and performing finite element analysis for different configurations. This can reduce design time, minimize errors, and improve the accuracy and consistency of the design. Furthermore, parametric design can enhance collaboration and communication between different stakeholders involved in the design process.

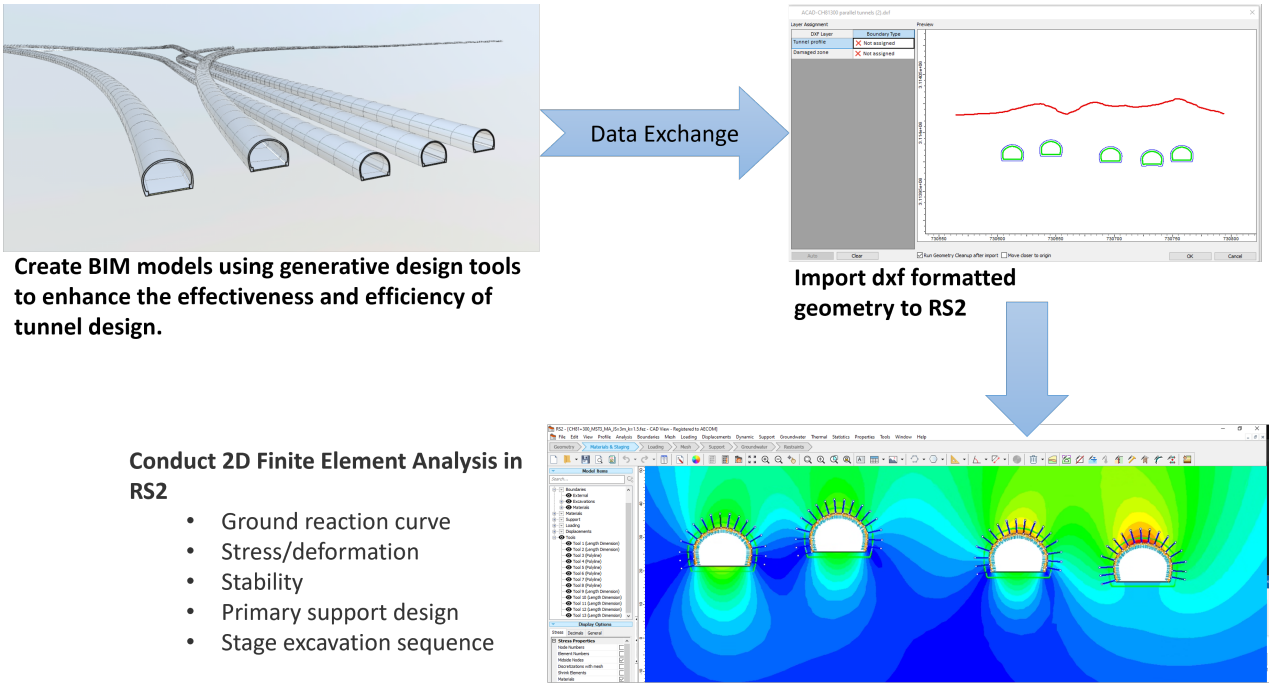

Figure 3: Sample workflow of using BIM models as generative design tools in a tunnel project

Dynamo scripts can be used to create data exchange workflows, which can be implemented into the project management plan. The workflows can include importing and exporting data between different software applications between commonly used BIM software. These data exchange workflows can be tested and refined to ensure that they are working correctly. The use of Dynamo scripts to automate data exchange workflows can save time and reduce errors associated with manual data exchange. It also ensures that all stakeholders have access to the most up-to-date information, enabling effective decision-making.

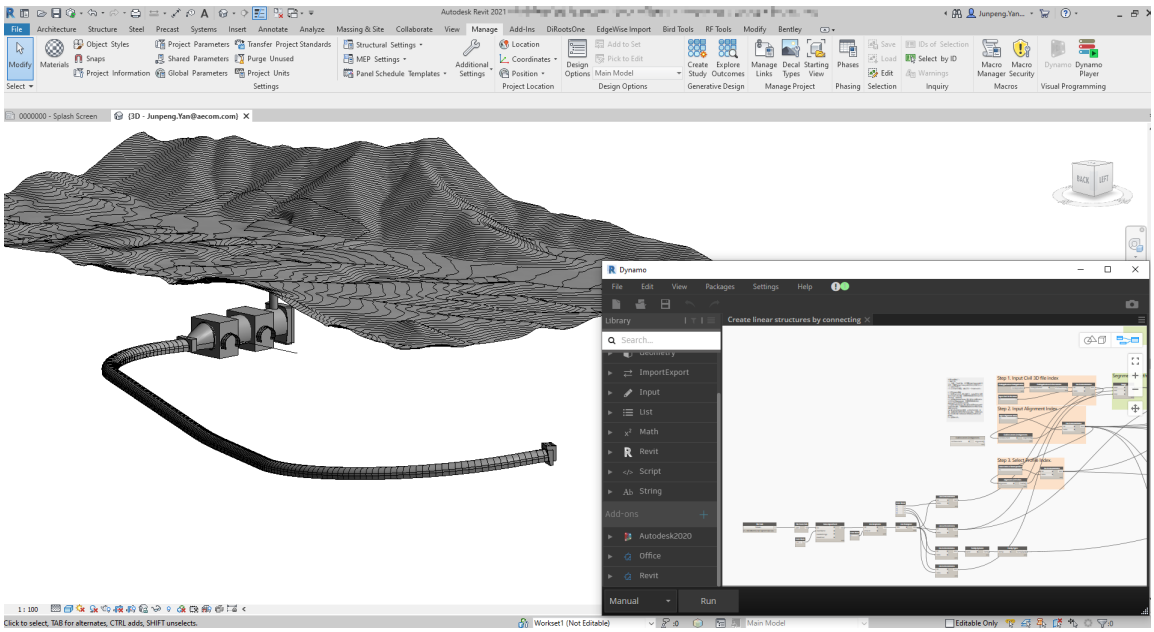

Figure 4: Use of Dynamo scripts to facilitate data exchange in a tunnel project

4 DIGITAL TWIN SYSTEMS AND AS-CONSTRUCTED BIM MODELS

Digital twin systems and as-constructed BIM models are innovative technologies that can improve the accuracy and efficiency of maintenance and repair tasks, reduce downtime and costs, and enable more effective collaboration between stakeholders. As-constructed BIM models involve creating a digital model of the construction project that accurately reflects its as-built condition.

4.1 As-constructed BIM Models using openBIM

Digital twin systems and as-constructed BIM models using openBIM can provide a comprehensive and accurate representation of geotechnical works, enable real-time monitoring and analysis of their performance. As-constructed BIM models can be used as the basis for creating digital twins of geotechnical works, providing a detailed and accurate representation of the physical asset. The use of openBIM format ensures that the as-constructed BIM models can be easily integrated with other data sources, such as sensor data, to create a digital twin that accurately reflects the current state of the asset.

Digital twin systems and as-constructed BIM models using openBIM can also help to streamline the design review process for geotechnical works. The use of digital twin systems and as-constructed BIM models can also enhance collaboration and communication between different stakeholders involved in the design review process. The 3D models and simulations can be easily shared and reviewed by all stakeholders, which can help to identify potential issues and enable timely and effective decision-making.

The as-constructed BIM models can be used to compare the design intent with the actual construction and identify any discrepancies or issues that need to be addressed. This helps to improve the accuracy and completeness of the design and ensures that the constructed asset meets the design intent. Furthermore, digital twin systems can be used to simulate the performance of the geotechnical works under different conditions, such as changes in loading or environmental factors. This can help to identify potential issues and optimize the design to ensure that the asset meets the required performance criteria.

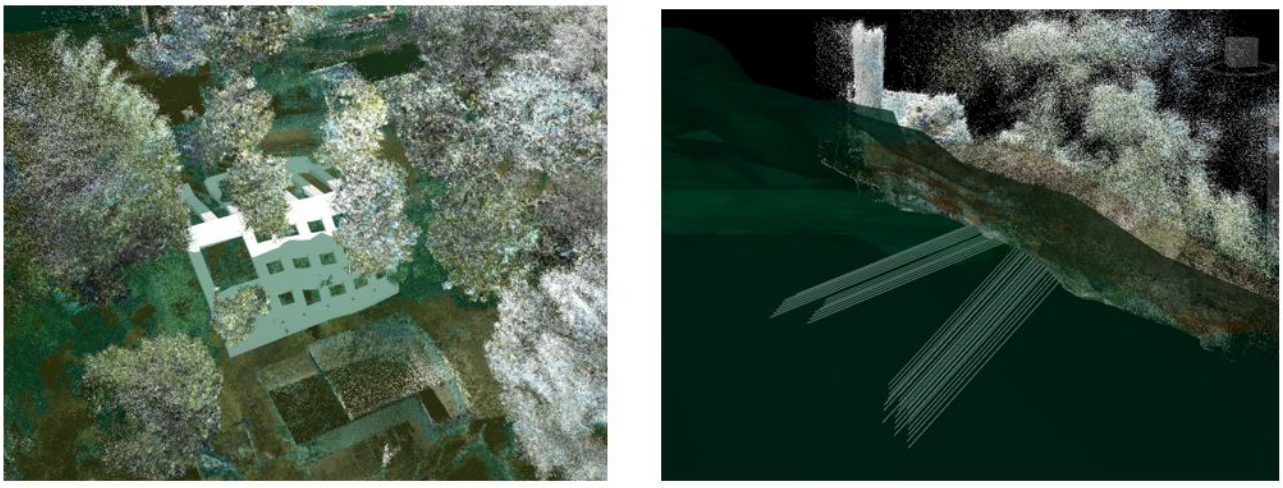

Figure 5: BIM models created using point cloud data from handheld LiDAR scanner to facilitate the design review process and production of as-built drawings

4.2 Data exchange and asset management

As-constructed BIM models created in openBIM format can facilitate information exchange in Common Spatial Data Infrastructure (CSDI) and future asset management by maintenance departments. CSDI is a platform for sharing spatial information across different organizations and government departments. It is crucial for effective asset management and maintenance of geotechnical works. As-constructed BIM models

in openBIM format can provide a standardized and interoperable platform for sharing spatial information between different organizations and government departments.

The use of openBIM format ensures that information can be easily exchanged between different software programs and platforms, regardless of their proprietary formats. This means that maintenance departments can access and use the information from the as-constructed BIM models without the need for specialized software or data conversion. The openBIM format also enables the integration of other relevant data such as geospatial and environmental information, which can enhance the accuracy and completeness of the asset management system.

The as-constructed BIM models can provide a comprehensive and accurate representation of the geotechnical works, including their location, shape, size, and condition. This information can be used for a range of asset management activities such as condition assessment, maintenance planning, and cost estimation. The use of BIM-based asset management can also help to improve the efficiency and effectiveness of maintenance operations by providing timely and accurate information to the maintenance agencies for better planning and prioritization of resources.

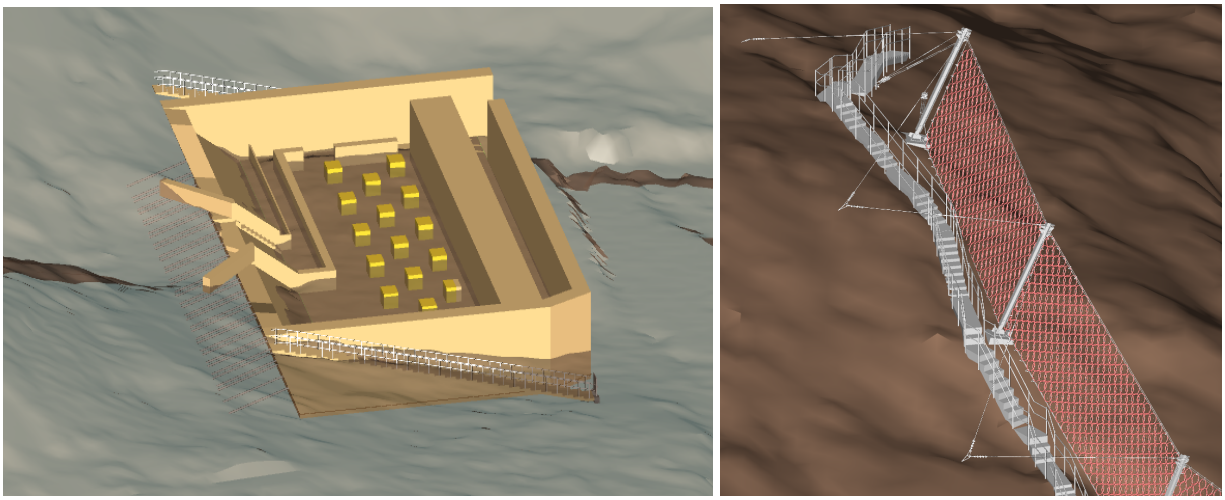

Figure 6: As-constructed BIM models created in openBIM format to facilitate information exchange in Common Spatial Data Infrastructure (CSDI) and future asset management by maintenance department

5 SUSTAINABLE DESIGN OF GEOTECHNICAL WORKS

5.1 Design for safety

Design for safety is a method of designing products, systems, or structures with the goal of minimizing or eliminating safety hazards. It involves considering potential safety hazards during the design process and implementing measures to prevent or mitigate those hazards. The design for safety approach is based on the principle that it is easier and more cost-effective to design safety features into a product or system from the beginning rather than trying to address safety concerns after the design is completed. The goal of design for safety is to ensure the safety of workers and the public, reduce the risk of accidents and injuries, and comply with safety standards and regulations.

BIM models and automated scripts can improve the design for safety of geotechnical works by providing a more accurate and detailed representation of the construction site, identifying potential safety hazards, and developing effective solutions to mitigate these risks. Comprehensive site analysis is possible using BIM models, incorporating data on the site's topography, geology, and other features. This allows engineers and construction teams to identify potential safety hazards and problematic areas in the early stage of the project

and develop effective solutions to mitigate these risks. Automated scripts can be used to analyze complex data quickly and accurately, reducing the risk of errors and improving the efficiency of the design process.

Simulating construction processes is another application of BIM models. These models can be used to simulate the construction process, identifying potential safety hazards and developing effective solutions to mitigate these risks. Real-time monitoring is also possible with BIM models and automated scripts. These technologies can be used to monitor the construction site in real-time, identifying potential safety hazards and taking action to prevent accidents and injuries. This can include using sensors to monitor the stability of excavations and temporary slope cuttings, detecting the presence of hazardous materials, and alerting workers to potential hazards.

5.2 Enhanced sustainability

Sustainable design is an important aspect of geotechnical works, and BIM and other innovative technologies can be utilized to promote sustainable design by enabling more accurate and efficient design and construction processes. For example, BIM can simulate construction activities and optimize design and construction processes, which can help reduce waste and energy consumption. Other innovative technologies, such as UAV photogrammetry, handheld LiDAR scanning, and digital twin systems, can also enhance the accuracy and efficiency of sustainable design for geotechnical works.

In addition to BIM and other technologies, parametric and generative design can be utilized to explore a wide range of design options quickly and efficiently, thus promoting sustainability in geotechnical design. Generative design has several benefits, including optimizing material usage, reducing energy consumption, enhancing safety, improving resilience, and reducing carbon footprint. By using generative design, engineers and geologists can identify optimal solutions that are not only safe and efficient but also sustainable, contributing to the achievement of the United Nations Sustainable Development Goals (UNSDGs). Generative design can help optimize the placement of structures and infrastructure, reduce the amount of material used in construction projects, design infrastructure that is more resilient to natural disasters and climate change, and identify solutions with a lower carbon footprint.

5.3 Promoting the use of BIM within the company

Promoting the use of BIM and other innovative technologies within the company is essential to promote digital transformation within a company and thus achieving sustainable design for geotechnical works. Strategies for promoting the use of BIM and other innovative technologies include training and education, collaboration with stakeholders, and integration of BIM into company standards and procedures.

To foster a BIM culture within the company, it is important to provide training and education on BIM and other innovative technologies. This can be achieved through various methods, such as promoting in-house BIM training programmes, webinars, and technical knowledge sharing sessions. By providing these training opportunities, engineers and geologists can become more familiar with BIM and its applications, leading to increased adoption of BIM technologies and embedded design for safety and sustainability from the preliminary design process. Providing basic training to graduates and developing Dynamo scripts for BIM applications can also help reduce the learning curve of preparing BIM models, encouraging more engineers and geologists to use BIM in their work.

Another way to promote the use of BIM within the company is to integrate BIM into company standards and procedures. This can help ensure that BIM is used consistently and effectively across projects, leading to improved collaboration and efficiency.

Finally, it is important to collaborate with stakeholders, such as contractors, consultants, and clients, to promote the use of BIM and other innovative technologies throughout the project lifecycle. This can help ensure that BIM is used effectively and efficiently, leading to more sustainable geotechnical design and construction. Accreditation and certification of training programs such as Construction Industry Council's (CIC) Certified BIM Managers (CCBM) and BIM Coordinators (CCBC) also help promote the use of BIM

and other innovative technologies among stakeholders, leading to increased collaboration and a more sustainable design process.

5.4 Potential areas for further development

Digital transformation can enhance workflows, promote automation, handle repeatability, improve collaboration, and support knowledge transfer. The shortage of resources, such as geotechnical engineers, geologists, and BIM modellers, can be addressed through investment in BIM education and training programmes.

The design process can be optimized using tools and techniques to ensure cost-effectiveness, buildability and constructability, sustainability, and compliance with relevant codes and standards. Pre-fabrication and modular construction, including 3D printing, offer opportunities for greater efficiency and cost savings. The development of advanced materials can improve the sustainability, durability, and performance of geotechnical engineering projects, while also reducing their environmental impact.

The use of autonomous construction technologies, such as drones and robots, can improve efficiency and safety. Augmented reality and virtualization technologies can improve visualization, communication, and collaboration. Big data and predictive analytics, including AI, can enable more accurate and efficient decision-making. Wireless monitoring and IoT sensors can improve safety, efficiency, and maintenance.

Cloud-based tools and real-time collaboration can improve communication and coordination between different stakeholders. Overall, the use of automation tools and digital technologies can improve the efficiency, quality, and sustainability of geotechnical engineering projects.

6 CONCLUSIONS

BIM and other innovative technologies have the potential to enhance sustainability and promote design for safety right from the preliminary design process, thus contributing to the achievement of the UNSDGs. For instance, the use of UAV photogrammetry and handheld LiDAR scanning can improve the accuracy and efficiency of topographic surveys, which can help reduce the environmental impact of construction activities. BIM and Dynamo visual programming can automate design and help to visualize complex site settings, which can enhance safety and improve the efficiency of construction activities. Digital twin systems and as-constructed BIM models can improve the effectiveness of design review and scheduled maintenance for asset management, which can contribute to the sustainability and lower long-term recurrent costs of the projects.

The use of generative design and machine learning algorithms can be explored in the design of geotechnical works. For instance, machine learning algorithms can be used to optimize the design of soil nailing works, which can help reduce material waste and energy consumption. Generative design can be used to explore a wide range of design options quickly and efficiently, which can help identify optimal solutions that are safe, efficient, and sustainable.

To achieve these sustainability goals, companies can adopt Industry 4.0 and Construction 2.0 strategies that leverage the power of digital technologies such as BIM, IoT, and AI. These strategies can enhance collaboration, improve efficiency, reduce waste, and promote sustainability in the design and construction of geotechnical projects, contributing to a more sustainable and resilient future.

REFERENCES

BuildingSMART (2012). Industry foundation classes (IFC) for data sharing in the construction and facility management industries. BuildingSMART.

Chen, Y., et al. (2018). UAV-borne LiDAR for topographic surveying and its accuracy analysis. Remote Sensing, 10(10), 1557.

Construction Industry Council (2021a). CIC BIM Standards - General (Version 2.1 - 2021)

Construction Industry Council (2021b). Construction Digitalisation Roadmap for Hong Kong.

Dey, T. K., et al. (2017). Automated design of earth retaining structures using building information modeling. Journal of Computing in Civil Engineering, 31(2), 04016051.

Gudipudi, R. B., et al. (2020). BIM-based slope stability analysis: A case study of a highway project. Journal of Computing in Civil Engineering, 34(1), 04019047.

Han, K., et al. (2018). Development of a BIM-based foundation design system using parametric modeling. Journal of Computing in Civil Engineering, 32(6), 04018033.

Kim, H., & Lee, G. (2015). A BIM-based framework for sustainable building design. Sustainability, 7(9), 12087-12104.

Kim, S. J., et al. (2019). BIM-based parametric design of a retaining wall for road infrastructure. Advances in Civil Engineering, 2019, 1-9.

Lin, Y., et al. (2019). A review of handheld and mobile laser scanning for geoscience applications. Earth-Science Reviews, 196, 102873.

Lu, Y., et al. (2019). BIM-based geotechnical design for deep excavation projects. Journal of Computing in Civil Engineering, 33(6), 04019025.

Rieke, M., et al. (2020). UAV-based vegetation mapping using LiDAR and photogrammetric techniques. Remote Sensing, 12(2), 291.

Vignesh, R., et al. (2017). BIM-based design and analysis of retaining walls with soil nailing. Journal of Computing in Civil Engineering, 31(6), 04017033.

Yan, H., et al. (2018). BIM-based design of a deep excavation support system using a parametric approach. Journal of Computing in Civil Engineering, 33(1), 04018069.

Design and Construction for the First Semi-Cavern Building in Hong Kong – A Case Study in Tseung Kwan O – Lam Tin Tunnel

Clayton Y. K. Chan, Billy W. L. Siu & Franklin K. L. To
AECOM Asia Company Limited, Hong Kong

ABSTRACT

The Tseung Kwan O – Lam Tin Tunnel (TKO-LTT) has been commissioned since December 2022, which is a new truck road linking Tseung Kwan O and Kowloon urban area, with about 2.2 km long rock tunnels. This tunnel connects the Cross Bay Link in the east, and the Trunk Road T2 in the west, forming the integrated part of future Route 6, servicing the second tunnel for TKO residents to Kowloon with shortened travelling time.

At the TKO Portal, two large-span caverns were designed and constructed to accommodate a semi-cavern tunnel ventilation buildings. This idea was proposed to reduce the surface footprint of ventilation building by placing its significant portion into the caverns. With this innovative semi-cavern building scheme, the slope cutting and stabilization works have been minimised, the disposal of excavated materials and tree felling have been reduced, it also improves the visual impact of the ventilation building and enhanced the construction programme. With portion of ventilation building inside the caverns, it could provide stable environment for E&M equipment with regard to weather protection, steady temperature and humidity.

The challenges in terms of geology, hydrogeology and geotechnical engineering have been overcome successfully throughout the project implementation. This innovative engineering solution also provided significant benefits to the project in terms of cost effectiveness, sustainability and energy efficient aspects in the construction and operation stages of the project. This semi-cavern building scheme is a perfect example that the industry is utilising underground space and promoting rock cavern development in Hong Kong.

This paper presents a successful case study for the rock semi-cavern works in TKO-LTT from the planning, detailed design to construction stages.

1 INTRODUCTION

1.1 The Project

Before the commissioning of Tseung Kwan O – Lam Tin Tunnel (TKO-LTT), the existing Tseung Kwan O Tunnel (TKO Tunnel) constructed in 1990 was the main connection between TKO and East Kowloon. The TKO Tunnel was operating at its maximum capacity at peak hours and unable to cope with the future traffic demand arising from further developments in TKO. Therefore, the construction of TKO-LTT serving as an additional highway was required to relieve the existing traffic congestion in order to meet the future traffic demands arising from the planned population in TKO area.

In September 2013, AECOM Asia Company Limited was commissioned by the Civil Engineering Development Department (CEDD) of the HKSAR Government to provide the design and construction services for the TKO-LTT. It is a 4.2 km dual two-lane highway involving the construction of tunnels, viaducts, at grade roads, reclamation, building facilities, landscaping and environmental protection works.

The overview of TKO-LTT is presented in **Figure 1**. It has been successfully commissioned since December 2022. It is a new truck road linking Tseung Kwan O and Kowloon urban area, the main tunnel is an approx. 2.2 km long rock tunnels connecting the Cross Bay Link and the Trunk Road T2, forming the integrated part of future Route 6, servicing the second road tunnel for TKO residents to Kowloon with shortened travelling time.

Figure 1: Tseung Kwan O – Lam Tin Tunnel (TKO-LTT)
(CEDD project website: https://www.tko-ltt.hk/)

1.2 General Site Descriptions and Ground Conditions

The main tunnel is within slightly to moderately decomposed rock, the western and central portions of TKO-LTT is underlain predominantly by Mount Butler Granite (Klb), whereas the eastern portion is underlain by tuff belonging to Mount Davis Formation (Krd). The superficial geology generally comprises deposits and fill materials. These include fill, colluvium, alluvium, residual soil and saprolite of highly to completely decomposed granite and tuff. The thickness of these stratums varies along the main tunnel alignment.

A number of weakness zones, fault zones and geological contacts were inferred within the project area. These include weathered seams, core loss, dyke intrusion and mineralization, greisenized zone and minor weak zones associated with the topographic depression lines. The Rennie's Mill Fault zone indicated on the published geological map was encountered during the construction works of Harbour Area Treatment Scheme (HATS) Tunnel Stage 1 in the 1990s. A geological granite-volcanic contact was also identified where zone of high permeability and alteration may be anticipated.

1.3 Rock Semi-Caverns Works at TKO Portal

At the eastern Tseung Kwan O Portal of the main tunnel, two large-span caverns were designed and constructed to accommodate part of the East Ventilation Building (EVB). This idea was proposed to reduce the surface footprint of ventilation building by placing part of the building underground. The photomontage in **Figure 2** was prepared during the design stage to illustrate the general arrangement of the semi-cavern ventilation building at TKO Portal, it provides stable environment for E&M equipment with regard to weather protection, steady temperature and humidity.

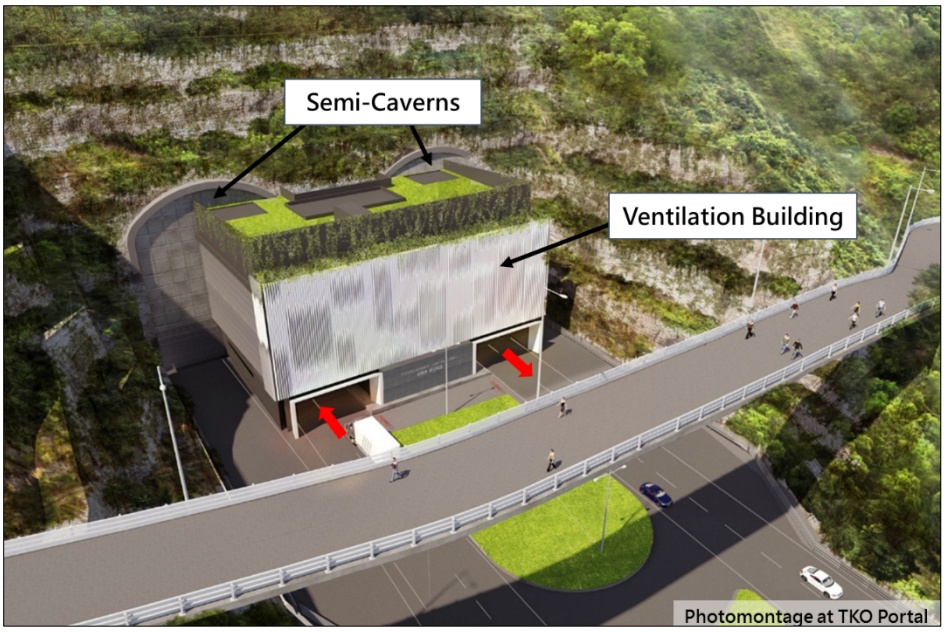

Figure 2: Photomontage at TKO Portal

2 PLANNING AND DESIGN

2.1 Geological Setting at TKO Portal

The TKO Portal is located at the western shoreline of Junk Bay in TKO. It is adjacent to the Junk Bay Chinese Permanent Cemetery. One of the particular highlights for the semi-cavern scheme is that, these two caverns were not proposed and constructed within the current Strategic Cavern Areas (SCVAs) under the Cavern Master Plan (CMP). Therefore, more challenges in terms of geology, hydrogeology and geotechnical engineering were expected and encountered during the course of design and construction stages of the project.

The area is underlain by tuff belonging to Mount Davis Formation (Krd). The rockhead level varies between approximately +60mPD and +85mPD, with the highest level at the northwest and the lowest at the southwest. Two isolated outcrops of the Krd formation, surrounded by granite, are located between Yau Tong and TKO. Much of the rock has been thermally metamorphosed by the granite. The Krd Tuff is typically described as fine to coarse ash Tuff locally intruded by brecciated quartz veins. Chloritized and silicified Tuff and coarse ash lithic Tuff are encountered in places as well. Iron and manganese staining are commonly observed on the joint surfaces. Calcite, chlorite, kaolin and epidote coatings at the joint surfaces are also recorded locally in some boreholes. Chlorite, quartz and silicified pyrite infillings are identified locally in some of the boreholes.

In addition, localized dyke rocks such as aplite, basalt, and quartz syenite were identified from the published geological map and localized borehole records. Extremely weak to weak zones containing Grade III/IV, IV and V materials were found in Tuff. Various weathering grades of localized dyke such as Aplite and Basalt were occasionally observed. The superficial geology generally comprises Quaternary Deposits and fill materials, with varying thickness in the onshore and offshore areas.

2.2 Ground Investigation and Geological Model

Multi-staged consultancy agreement is commonly adopted for medium to mega-scale government infrastructure projects in Hong Kong. For the TKO-LTT project, these multi-stages since 2009 included the feasibility study stage, investigation & preliminary design stage, and finally the design & construction stage. Ground investigation works in each of these stages were carried out for different purposes and requirements. During the early planning stage, the ground investigation works aimed to assess the planning and selection of different tunnel alignment options. It also tried to identify any potentially problematic ground and minimized the geotechnical risks conditions along the tunnel alignment. After the confirmation of tunnel alignment by

consolidating multi-disciplined aspects, further ground investigation works were carried out to focus at specific locations and depths, to obtain geotechnical information for subsequent detailed design.

At the TKO portal, two caverns for the construction of a semi-cavern ventilation building were planned in highly fractured volcanic tuff with complicated geological conditions. This was an ambitious design that required a thorough study to ensure its constructability in the planning and design stage.

Extensive ground investigation works including vertical boreholes, inclined boreholes and horizontal directional coring (HDC) were carried out and interpreted into a three-dimensional geological model as illustrated in **Figure 3**. The ground investigation results assisted the interpretation of the locations for the two inferred geological features, and revealed that the both features dip sub-vertically. Different dipping scenarios from angle of 70 to 85 degree for both features were incorporated into the three-dimensional geological model for assessing the geological impact on the subsequent cavern construction.

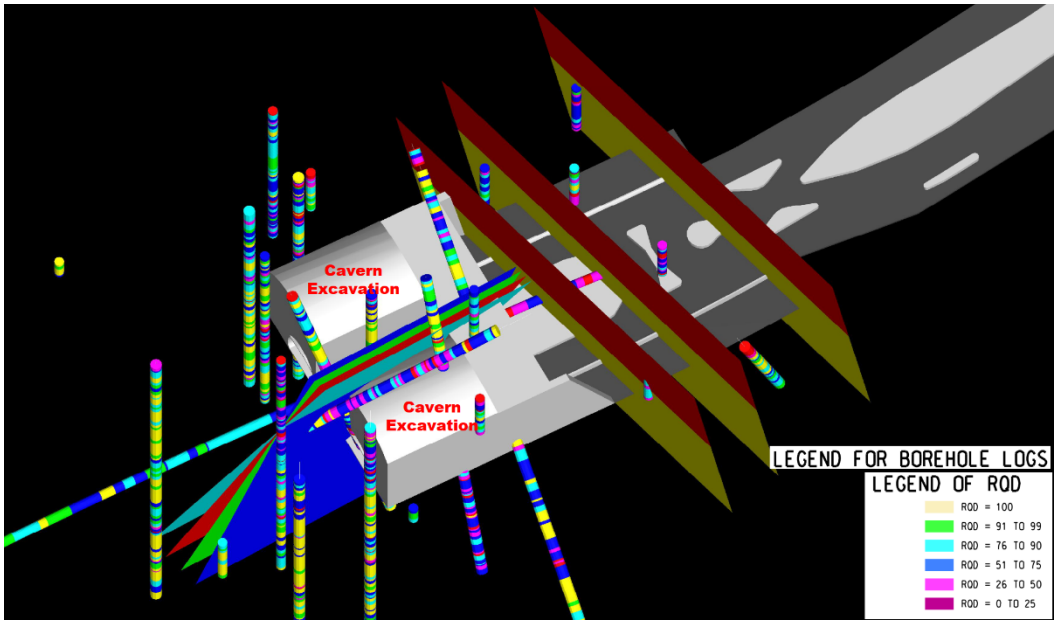

Figure 3: Three-Dimensional Geological Model for the Caverns at TKO Portal

2.3 Engineering Parameters

Throughout the assessment using the relevant field and laboratory test data from the ground investigation information, the engineering properties for the volcanic tuff at TKO portal area were summarized in **Table 1**.

Table 1: Summary of Engineering Properties

Rock	Unit Weight, (kN/m^3)	Poisson's Ratio ν	Intact Modulus, E_i (MPa)	Permeability k (m/s)	Uniaxial Compressive Strength, UCS (MPa)
MDT/V	27	0.25	45000	2.00E-07	150
SDT/V	27	0.25	50000	4.00E-07	170

Over 8,100 rock discontinuity readings were obtained from boreholes using Borehole Acoustic Televiewer surveys from the project-specific ground investigation works. The data of dip and dip direction from the televiewer survey was contoured by rock types and stereographic plot results of the joint sets of tuff are summarized in **Table 2**.

Table 2: Summary of Major Joint Sets

Joint Set	Dip Direction	Dip Angle

Set 1	101°	23°
Set 2	213°	72°
Set 3	305°	70°
Set 4	052°	77°

2.4 Development of the Innovative Semi-Cavern Scheme

The East Ventilation Building (EVB) was required at the TKO Portal to maintain the ventilation (air exchange and smoke extraction system) for the main tunnel for satisfying the environmental and fire engineering requirements. In order to create the site formation area for EVB, extensive soil and rock slope cutting with an excavation volume of approximately 440,000m^3 was previously proposed in the preliminary design stage.

To shorten the construction period, the exposed EVB footprint was significantly reduced by adopting an innovative underground rock cavern to partially house the EVB part embedded into the hillside as illustrated in **Figure 4**. The exposed part of EVB is still required to maintain effective ventilation, facilitate maintenance and equipment delivery and minimise fire safety provisions for some major plants/rooms. This arrangement significantly reduced approx. 180,000m^3 of excavated materials and hence 470,000 tons of inert construction waste has been reduced.

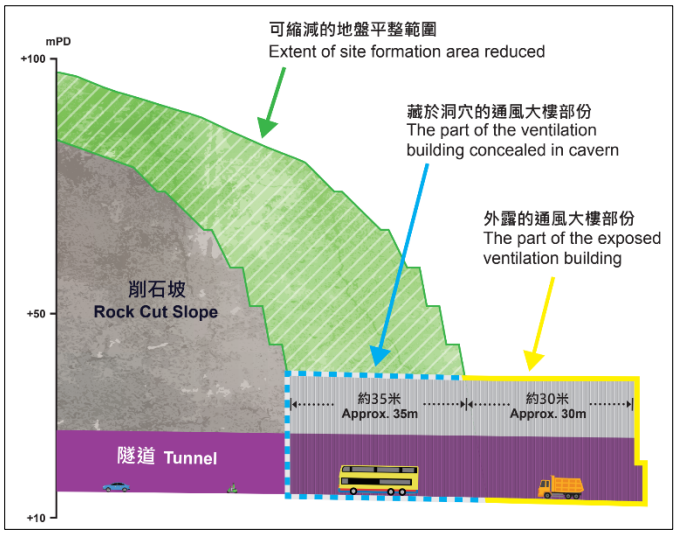

Figure 4: Reduced Site Formation Works at TKO Portal
(Project Newsletter: https://www.tko-ltt.hk/document/Newsletter%20(Construction)%20No.%2015.pdf)

The semi-cavern approach results in a building seamlessly integrated with the natural and built setting as shown in **Figure 5,** enhancing the sustainable design approach this project has adopted throughout the various stages of the works. With this innovative semi-cavern building scheme, the slope cutting and stabilization works have been minimised, the disposal of excavated materials and tree felling have been reduced, it also improve the visual impact of the ventilation building and enhanced the construction programme.

The preservation of vegetation and habitat was also enhanced by greatly reducing the tree felling area by approximately 46%. Environmental and visual enhancement was achieved by reducing the exposed EVB structure, while maintaining the same building height such that the impact of views from nearby residential buildings were minimised.

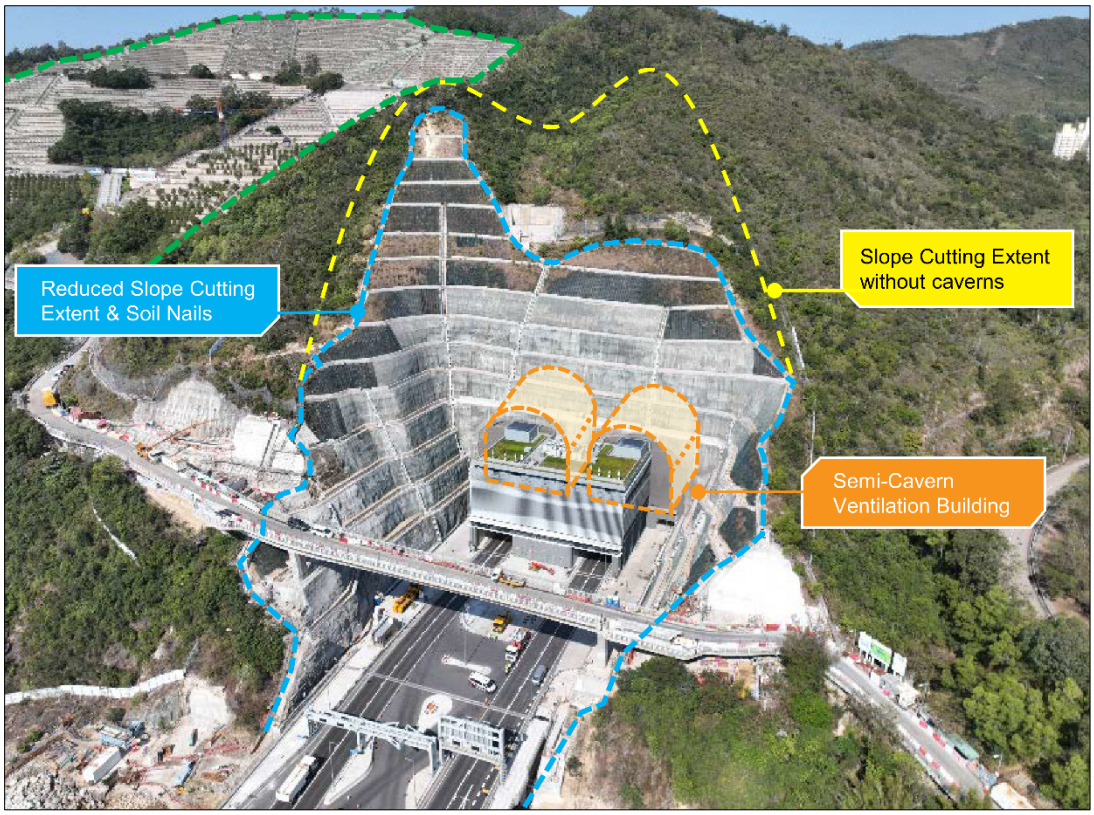

Figure 5: Seamless Integration of EVB with the Natural Environment

2.6 Cavern Profile and Geometry

The cavern internal profile was developed to meet the functional requirements of both the ventilation building and the main tunnel, such as the ventilation facilities, E&M equipment and utility services within the ventilation building, maintenance requirements, carriageway, structural gauge, sightline, ventilation area, traffic control and surveillance system (TCSS) and emergency walkway. The external profile was further determined based on the rock mass quality and support installation requirements.

An arched shape was designed as the geometric setting for the crown of semi-cavern. After excavation, the stresses surrounding the excavation profile will be re-distributed. The arched structural form utilises the rock arching as well as development of hoop stress along the concrete lining. The earth pressure at cavern crown is then effectively transferred through the arch to the cavern sidewalls. This arrangement increases the overall structural robustness which greatly reduces the cavern support requirements.

Based on the above-mentioned design requirements, the cavern profile and geometry were further developed. The excavation span and height for the caverns were about 26m and 31m respectively. The cavern height includes 7m depth of arch roof and 24m of straight wall. Cross section and longitudinal section showing the general arrangement of the semi-cavern EVB are indicated in **Figure 6** and **Figure 7** respectively.

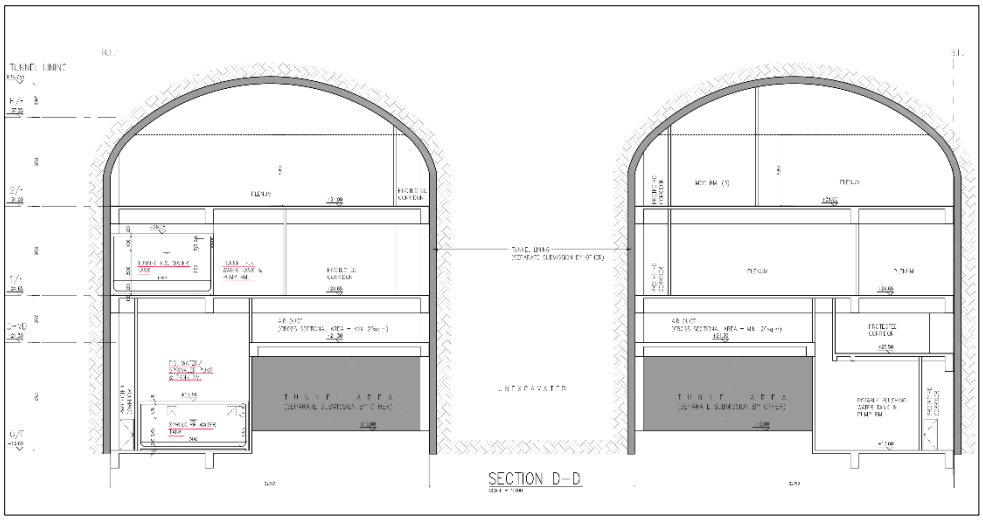

Figure 6: Cross Section of Semi-caverns and EVB Facilities

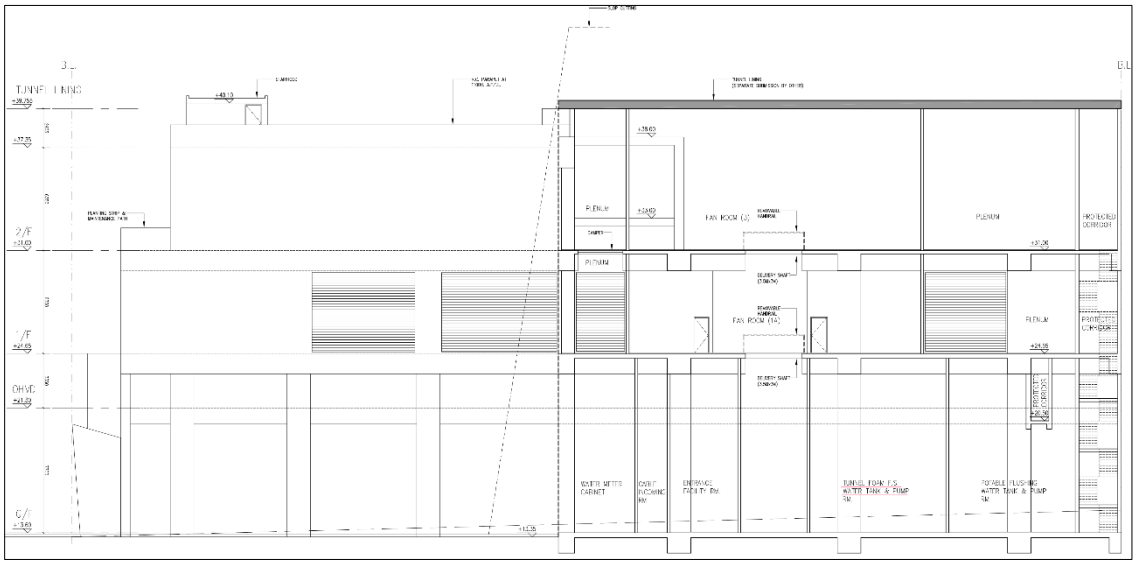

Figure 7: Longitudinal Section of Semi-caverns and EVB Facilities

2.7 Design and Analysis of Rock Supports

The caverns were designed to be self-supported. No ground loadings shall be transferred on to the EVB structures.

Computational software was used for the design and analysis of rock supports. Kinematic analysis was carried out using UNWEDGE V3.0 (BD Ref. No. G0137) with the rock joint sets interpreted from the ground investigation data as shown in **Figure 8**. Finite Element Model (FEM) Phase^2 (now re-named as RS2) V8.0 (BD Ref. No. G0179) was adopted to study the earth load act on the lining and rock pillar stability using the Generalized Hoek-Brown (GHB) failure criterion as presented in **Figure 9**.

The permanent support of the caverns was designed to withstand the induced rock supporting pressure from the surrounding ground after excavation. For the portion of caverns where the rock cover is less than one span of cavern, permanent support was designed to withstand the pressure from full overburden above the cavern.

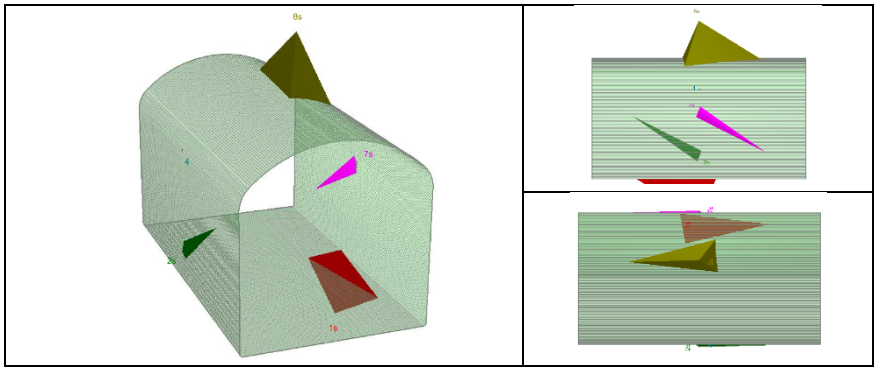

Figure 8: Kinematic Analysis for Support Design and Analysis

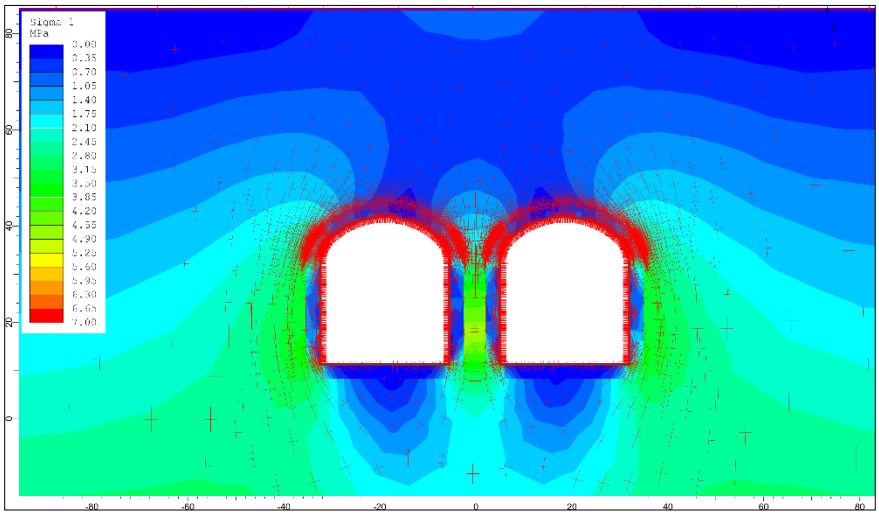

Figure 9: Finite Element Model for Support Design and Analysis

3 CONSTRUCTION

The excavation works commenced in August 2018. The two caverns are located in moderately and slightly decomposed volcanic tuff with three to four numbers of identified rock joints sets. Although the UCS values of volcanic tuff obtained from the laboratory tests were in general larger than 100 MPa, the volcanic tuff are highly fractured in nature. The cavern excavation was carried out by mechanical method using hydraulic breakers, top-down synchronizing with the site formation works as shown in **Figure 10**.

Figure 10: Top-heading Excavation by Mechanical Method

The design of temporary cavern supports was carried out based on the empirical approach and further verified by numerical modelling. At shallow rock cover, the excavated ground was temporarily supported by a combination of steel canopy tube, lattice girder and shotcrete; where after reaching ground with sufficient rock cover, the temporary supports comprised the installation of rock bolts, fibre-reinforced shotcrete and steel bars as rock pillar reinforcement.

Figure 11: Installation of Lattice Girder Segment

The progressive nature of mechanical excavation allowed a close monitoring of ground movement throughout the excavation, enabling timely strengthening works to ensure the stability of the caverns under such challenging ground conditions.

Following the completion of top-heading excavation, the subsequent cavern bench excavation and portal slope site formation works were carried out as shown in **Figure 12**. The excavation sequence was well-planned to overcome the major challenges including interfacing issues, machinery movement, logistic arrangement, and the handling of excavated materials in order to complete the works within the tight schedule.

Figure 12: Cavern Bench Excavation and Portal Slope Site Formation Works

The excavation works was completed in March 2020. The permanent works for the caverns and semi-cavern EVB commenced after the completion of rock excavation works. The permanent lining works included fibre-reinforced sprayed concrete at the crown and cast-in-situ reinforced concrete for side walls and end wall. **Figure 13** shows the installation of waterproofing system and casting of reinforced concrete lining at side walls. The construction of the semi-cavern East Ventilation Building was eventually completed in July 2022.

Figure 13: Waterproofing and Reinforced Concrete Lining at Side Walls

Figure 14: The completion of Semi-Cavern and EVB works

4 CONCLUSION

The TKO-LTT project has achieved the commissioning target by 2022, and the operation of the tunnel has been successful in alleviating traffic congestion in the TKO area, existing TKO tunnel and eastern Kowloon major roads approaching the Eastern Harbour Crossing.

The two large-span caverns for ventilation building integration were successfully constructed. The surface footprint of ventilation building was significantly reduced, and achieved a great construction time and cost saving in extensive slope cutting and stabilization works, avoid huge among of tree felling, minimize visual impacts and reduce the rock excavation period to minimize the nuisance to public during the construction stage.

This innovative engineering solution provided significant benefits to the project in terms of cost effectiveness, sustainability, environmentally friendly and energy efficient aspects in the construction, operation & maintenance stages of the project.

The semi-cavern EVB at TKO-LTT will serve as a good model to promote the use of underground space and rock cavern development in Hong Kong.

ACKNOWLEDGEMENT
The authors gratefully acknowledge the Civil Engineering and Development Department, the Government of the Hong Kong Special Administrative Region, for permission to publish this paper.

REFERENCES

AECOM. 2015. *Tseung Kwan O – Lam Tin Tunnel – Design and Construction, Geotechnical Engineering Report.*

AECOM. 2015. *Tseung Kwan O – Lam Tin Tunnel – Design of Permanent Lining for Caverns at Tseung Kwan O Portal.*

GEO. 2018. *Geoguide 4: Guide to Cavern Engineering, Second Edition (2018)*. Geotechnical Engineering Office, Hong Kong SAR.

To F. K. L., Tsang I. H. K., Chan C. Y. K., Lo S. S. P., Lee P. K.F. & Tsang S. N. F. 2020. *Geotechnical Aspects of Rock Tunnel and Semi-Cavern Works for Tseung Kwan O - Lam Tin Tunnel in Hong Kong*. Proceedings of the World Tunnel Congress 2020: Innovation and Sustainable Underground Serving Global Connectivity. Kuala Lumpur, Malaysia, May 2020.

Machine learning-powered landslide forecasting: from initiation to mobility

Te Xiao & Li-Min Zhang
The Hong Kong University of Science and Technology, Hong Kong

ABSTRACT

Prompt prediction of landslide occurrence and movement in a future rainstorm is one of the most effective manners to cope with the increasing landslide risk in a changing climate. Despite the rapid development of many machine learning algorithms, most studies stay on landslide susceptibility mapping because of the challenging time-unknown and terrain-unmatched issues in landslide forecasting. This study proposes two novel machine learning strategies to predict the spatio-temporal distribution of landslides considering both initiation and mobility. Hong Kong is taken as an example to demonstrate the capacity of city-scale landslide forecasting using machine learning. The spatio-temporal evolution of both man-made slope failures and natural terrain landslides in a rainstorm can be well predicted using machine learning models, which can provide a powerful real-time decision-making tool for landslide early warning and risk management.

1 INTRODUCTION

Hong Kong has long struggled with landslides, because of its rainy climate, hilly terrain, and dense urban development (Cheung 2021). According to the records of the Geotechnical Engineering Office (GEO), over ten major storms have occurred every year and have triggered approximately 380 natural terrain landslides and 230 man-made slope failures annually. A severe rainstorm can impact a large area and trigger thousands of landslides in a short time, wreaking havoc on urban systems and causing enormous fatalities. For example, the record-breaking rainstorm on 6-9 June 2008 alone triggered about 2400 natural terrain landslides and 200 man-made slope failures over the territory of Hong Kong, most of which occurred within the critical four hours; the 18 June 1972 rainstorm triggered two catastrophic landslides on Po Shan Road and Sau Mau Ping that caused 138 deaths in a single day.

To manage landslide risk in a changing climate, in addition to structural landslide mitigation programmes that augment the capacity of slope safety system (e.g., Landslip Preventive Measures Programme (1977-2010) and Landslip Prevention and Mitigation Programme (2010-present) implemented by the GEO), non-engineering measures such as early warning and emergency management will be more effective in minimising the consequences of landslides. The GEO has operated a territory-wide landslide early warning system for 40 years (Kong et al. 2020), the latest version of which is based on statistical rainfall-landslide correlations (Xiao and Zhang 2020). The most critical question in landslide early warning concerned by decision-makers is "where and when would landslides occur amid a rainstorm?" This requires the prediction of spatio-temporal distribution of landslide occurrence. After initiation, landslides may travel certain distances downstream (e.g., hundreds of metres), threatening more people and properties along larger runout areas. For example, on 7 June 2008, massive landslide debris travelled over 600 m from its source to Yu Tung Road (Figure 1), resulting in the closure of westbound lanes for two months. The prediction of landslide mobility is thus another important issue in landslide forecasting.

Figure 1: The Yu Tung Road landslide on 7 June 2008

Physically-based methods (Baum et al., 2010; Shen et al. 2018; Kwan et al. 2021) can predict both the initiation and post-failure movement of landslides but are less suitable for real-time applications because of the high computational costs. By contrast, data-driven methods such as statistical correlation and machine learning (Finlay et al. 1999; Dai and Lee 2002; Merghadi et al. 2020; Wang et al. 2021) can make real-time predictions. Machine learning has emerged as a powerful alternative to traditional statistical methods, with the availability of larger amounts of landslide data and the advancement of computer technologies. Despite the rapid development of many algorithms, most machine learning-related landslide studies stay on susceptibility mapping that identifies landslide-prone areas from the spatial distribution of historical landslide records. The absence of time-related elements in landslide susceptibility mapping makes it fail to fully leverage the high efficiency of machine learning and fail to forecast landslide occurrence and movement in a future rainstorm.

This study will first overview the challenges in machine learning-powered landslide forecasting and then develop novel machine learning strategies to predict the spatio-temporal distribution of landslides considering both initiation and mobility. Hong Kong will be taken as an example to demonstrate the capacity of city-scale landslide forecasting using machine learning. The machine learning models can provide a powerful real-time decision-making tool for landslide early warning and risk management.

2 CHALLENGES IN LANDSLIDE FORECASTING

In the literature, spatio-temporal landslide occurrence prediction and post-landslide runout prediction are rarely investigated using machine learning techniques. This is mainly because (1) most landslide databases collected are not qualified for such purposes, particularly missing records of landslide times and paths; and (2) landslide initiation and mobility involve more complicated dynamic processes, thus requiring more advanced task-specific machine learning strategies than general algorithms. Specifically, the time-unknown issue and terrain-unmatched issue are the most challenging problems hindering the predictions of landslide initiation and mobility, respectively.

2.1 Time-unknown issue in landslide initiation forecasting

To develop a machine learning model that can predict landslide occurrence in a future rainstorm, it is vital to link historical landslides with their triggering rainstorms through the recorded failure times, known as storm-based data integration (Xiao et al. 2022). By this means, dynamic rainfall features of different rainstorms can be utilised for temporal prediction, in addition to various static slope and geo-information features as used in landslide susceptibility mapping.

Notably, the failure time is available for man-made slope failures but not for natural terrain landslides. Man-made slope failures in urban areas can be promptly reported by the public so that the failure time can be accurate to a day. By contrast, natural terrain landslides in remote areas are usually identified through post-event geological surveys or interpretation from remote sensing images over a certain period (e.g., once in a year or even less frequent), from which only the range of landslide time (i.e., within several possible rainstorms) can be determined. Conventional data processing cannot handle such time-unknown landslide data well. One straightforward choice that limits training data to a small portion regarding time-known data will underestimate the predicted number of landslides undoubtedly. On the contrary, another common method that assigns all time-unknown landslides to the largest storm in a given period will lead to over-prediction. In a simple scenario with known years of landslides, Ko and Lo (2016) proposed a practical year-storm adjustment approach according to the rainfall frequency to approximately transform the year-based statistical rainfall-landslide correlations into storm-based ones. This adjustment approach has not been rigorously verified and may not be extensible to more complex scenarios.

2.2 Terrain-unmatched issue in landslide mobility forecasting

Regarding landslide mobility prediction, previous studies have established some region-specific statistical relationships between the fall height and travel distance, two key parameters describing a landslide runout path. As a matter of fact, both variables are unknown before the stop of landslide mass movement. With the unknown fall height, a trial-and-error terrain matching process is required to construct a 3-D runout path. Specifically, the longitudinal profile of a possible runout path starting from the landslide source (e.g., the steepest path) is first extracted from a 3-D digital terrain model (DTM), and all cells along the path are then visited one by one to determine where the landslide should terminate, namely the best location whose fall height and travel distance to source on the DTM satisfy the statistical correlation of the database. For statistical models, such a terrain matching process can be adopted for path prediction after the model training but is hardly involved during the model training. The inconsistency in terrain matching may reduce the accuracy of landslide runout path prediction (Ju et al. 2022), despite a strong correlation between the fall height and travel distance.

3 MACHINE LEARNING-POWERED LANDSLIDE FORECASTING

3.1 Comprehensive databases for Hong Kong

Hong Kong is a society rich in landslide-related data, which provides an ideal opportunity to release the potential of machine learning in landslide forecasting. Fundamental databases for this task should cover rainstorms (Figure 2(a)), slopes (Figure 2(b)), and landslides (Figure 2(c)). In the period of 1984–2017, 419 major rainstorms are identified, and the hourly rainfall amounts of 50 Hong Kong Observatory (HKO) rain gauges and 91 GEO rain gauges are collected. The slope information system managed by the GEO had registered more than 60,000 man-made slopes of cut slopes, fill slopes, and retaining walls.

Past landslides in Hong Kong have been compiled into two databases. One is the Enhanced Natural Terrain Landslide Inventory (ENTLI) (https://www.geomap.cedd.gov.hk/GEOOpenData/eng/ENTLI.aspx), including 90,000 relict natural terrain landslides and over 21,000 recent natural terrain landslides in 1924–2019. These landslides are interpreted from annual aerial photos so that the failure time is only accurate to a year. The ENTLI takes points and polylines to represent the landslide sources and paths, respectively, and records four key geometric features, namely travel distance, fall height, and length and width of the landslide source.

The catalogue of landslide incidents (https://www.geomap.cedd.gov.hk/GEOOpenData/eng/Incident.aspx) is another major landslide database, which records a few reported natural terrain landslides and about 8000 man-made slope failures in 1984–2017. Prompt reporting from the public makes the failure time accurate to a day in most incidents. The tabular catalogue of landslide incidents contains the time, location, type, scale, and consequences of landslides.

In addition to rainfall, slope, and landslide databases, geographic databases of terrain, geology, land cover, and infrastructure are also utilised in machine learning in this study. Given such rich data, the abovementioned time-unknown issue and terrain-unmatched issue can be properly addressed through new machine learning strategies developed as follows.

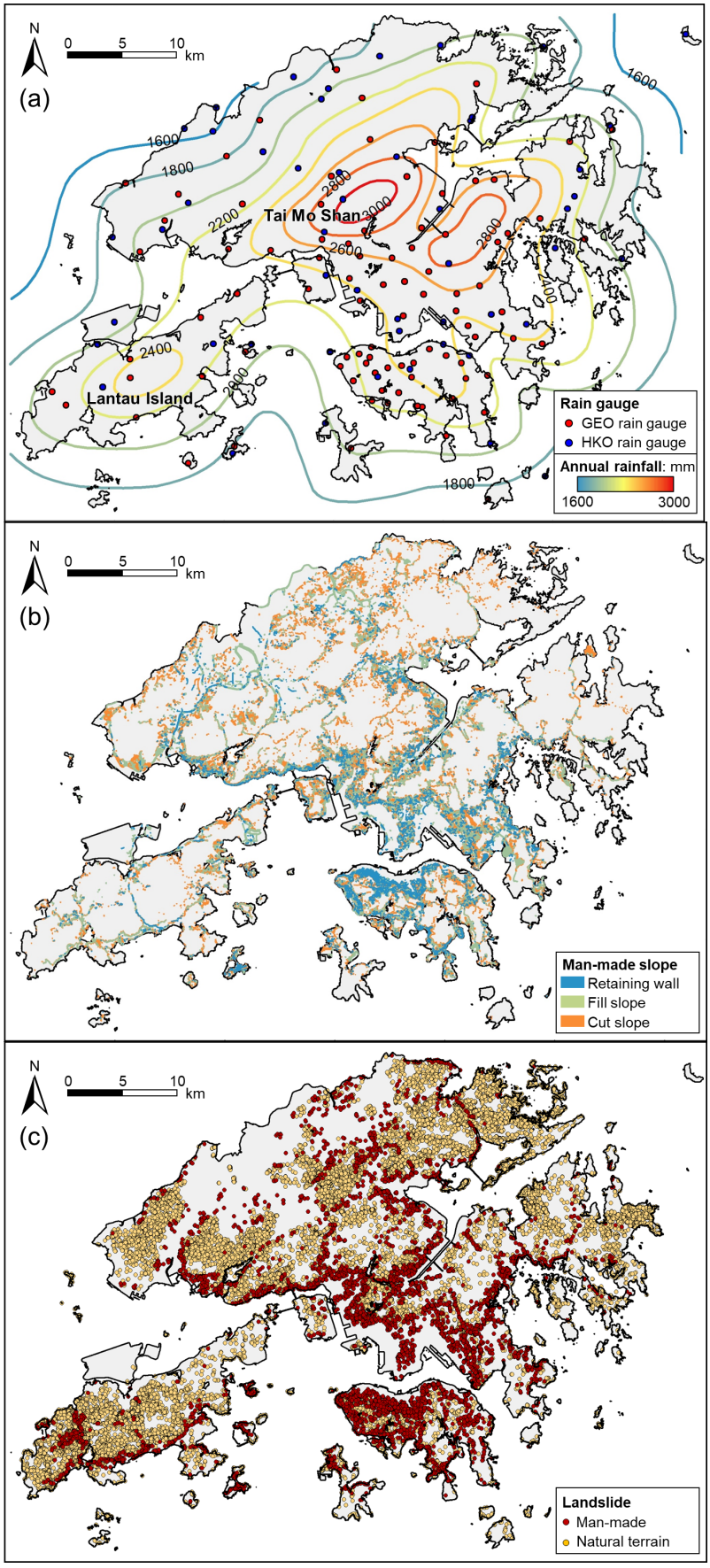

Figure 2: Comprehensive databases for Hong Kong: (a) rainstorm; (b) slope; (c) landslide

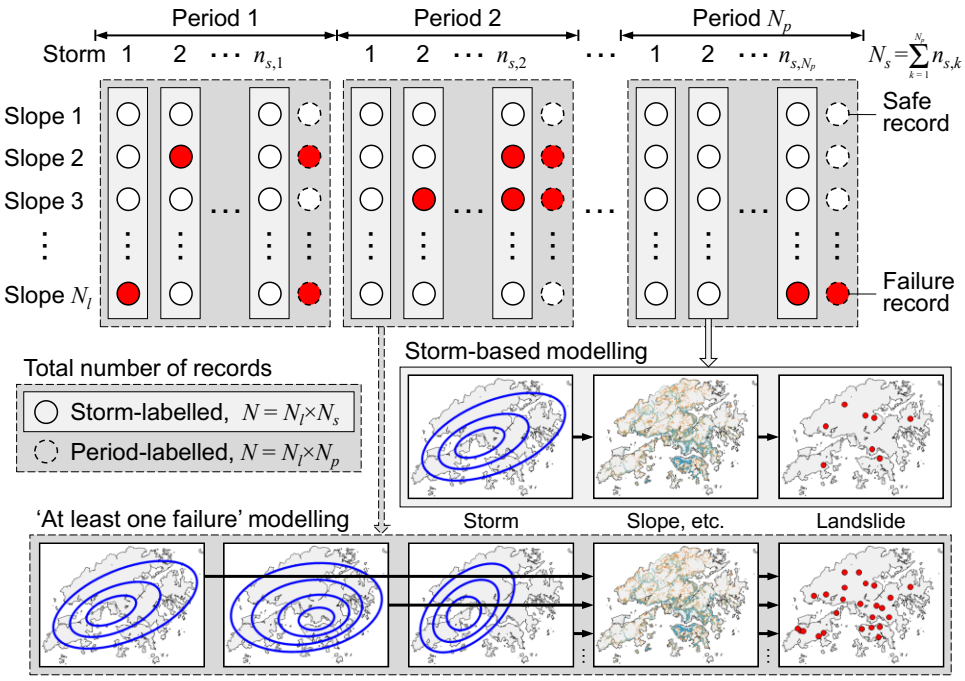

Figure 3: Probabilistic modelling strategy for landslide initiation forecasting

3.2 Probabilistic modelling strategy for landslide initiation forecasting

If landslide times are known (i.e., storm-labelled landslides as shown in Figure 3), a storm-based landslide forecasting model can be directly established using any machine learning algorithm (Xiao et al. 2022), similar to the procedure of landslide susceptibility mapping but involving dynamic rainfall features such as the maximum rolling 24-h rainfall amount to achieve temporal prediction.

If landslide times are unknown but labelled over a consistent period (e.g., one year for year-labelled landslides in ENTLI), it is conservative to claim that, for a particular landslide, the slope has at least one failure triggered by storms in this period. Therefore, N_l slopes after N_p-period observations produce a total of $N = N_l \times N_p$ records (Figure 3). For each record, the probability P of observing at least one failure for a slope, after suffering n_s storms in a period, can be evaluated as (Xiao and Zhang 2023a):

$$P = 1 - \prod_{s=1}^{n_s} (1 - p_s) \tag{1}$$

where p_s = failure probability of a slope in the sth storm, estimated by a storm-based landslide forecasting model. Equation (1) is referred to as probabilistic modelling strategy of 'at least one failure' for time-unknown landslides. Consequently, the cost function $J(\boldsymbol{\theta})$ of the machine learning model given a set of model parameters $\boldsymbol{\theta}$ can be written as:

$$J(\boldsymbol{\theta}) = -\frac{1}{N} \sum_{i=1}^{N} \left[y_i \ln P_i + (1 - y_i) \ln (1 - P_i) \right] \tag{2}$$

where y_i = period-based observation of the ith record: y_i = 0 for a non-landslide record and 1 for a landslide record; and P_i = predicted failure probability of the ith record using Equation (1).

Equation (2) is similar to the cost function used in storm-based forecasting for time-known landslides, but the landslide observation frequency has changed from every storm to a period consisting of several storms. Through the 'at least one failure' strategy, the storm-based failure probabilities are transformed into period-based failure probabilities to match the period-based observations. In other words, although only $N_l \times N_p$ observations are available, Equation (2) still computes $N_l \times N_s$ failure probabilities (where N_s is the total

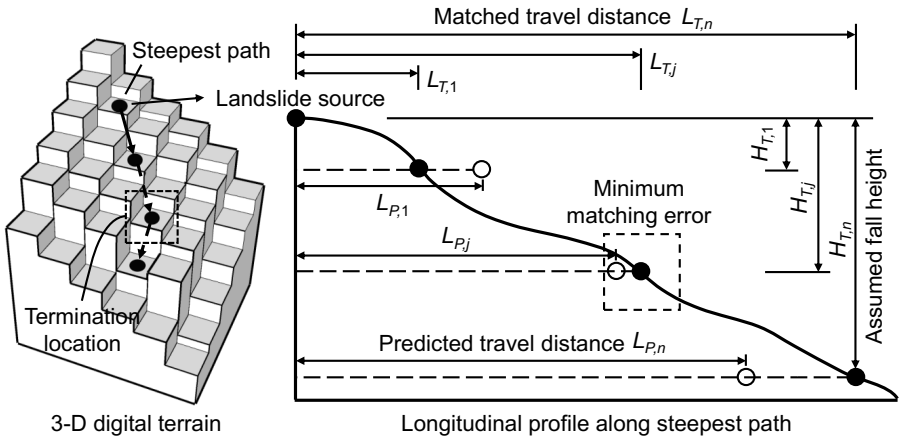

Figure 4: Trial-and-error terrain matching for landslide runout path prediction

number of storms in all periods), consistent with that in a storm-labelled scenario. This enables storm-based landslide forecasting using time-unknown landslide data.

The realistic landslide database is more often a mixture of both time-known and time-unknown landslides, and the observation period may vary from one slope to another. In such a case, an integrated machine learning model can be established using the proposed 'at least one failure' strategy, and the cost function is a weighted combination of time-known and time-unknown landslides (Xiao and Zhang 2023a).

During the landslide initiation forecasting, it is also possible to simultaneously incorporate the prediction of landslide scale (Xiao et al. 2022), by re-formulating the binary classification problem (i.e., non-landslide and landslide) as a multiclass classification problem according to various landslide scales (e.g., non-landslide, and very minor, minor, major, and very major landslides). The landslide scale will have a great impact on the subsequent prediction of landslide mobility.

3.3 Terrain matching strategy for landslide mobility forecasting

Traditionally, a statistical model (e.g., multivariate linear regression) only predicts the landslide travel distance; hence, a trial-and-error terrain matching process is required to convert the distance into a path. As shown in Figure 4, it requires a 3-D DTM and a landslide runout analysis model that predicts a travel distance (L) from a given fall height (H) and other factors. A possible runout path starting from the source is identified first on the DTM by assuming that the landslide moves along the steepest path to an adjacent position. If the landslide stops at the jth cell along the path (j = 1, 2, …, n), the actual fall height and travel distance on the DTM from the landslide source to the termination location are $H_{T,j}$ and $L_{T,j}$, respectively, while the runout analysis model predicts another travel distance $L_{P,j}$ from the given $H_{T,j}$. The two distances (i.e., $L_{T,j}$ and $L_{P,j}$) may not be identical. After going through all cells on the path, the cell with a minimum matching error between $L_{T,j}$ and $L_{P,j}$ can be taken as the termination location, and the runout path is accordingly determined. Note that the targets of model training and path prediction are inconsistent in a statistical model. For model training, the target is to fit the predicted travel distance (L_P) to the one recorded in the landslide database (L), while it is to match the predicted travel distance to the one derived from the DTM (L_T) in path prediction.

A consistent terrain matching strategy in both model training and prediction is proposed for machine learning-based landslide runout path prediction (Ju et al. 2022), as shown in Figure 5. Unlike conventional machine learning models, an additional step for determining the most probable termination location is inserted between the forward runout prediction and backward parameter estimation. The explanatory variables of each cell along the possible path are fed separately into the machine learning model to predict multiple travel distances $L_{P,j}$ (i.e., Step II). Afterwards, the cell k with a minimum matching error between $L_{P,j}$ and the actual distance $L_{T,j}$ on the DTM is regarded as a temporary termination cell (i.e., Step III), and the actual distance $L_{T,k}$ is then fed back into the machine learning model to estimate model parameters (i.e., Step IV). These procedures are iteratively repeated until the optimal model parameters $\boldsymbol{\theta}$ are obtained. The cost function to be minimised can be written as:

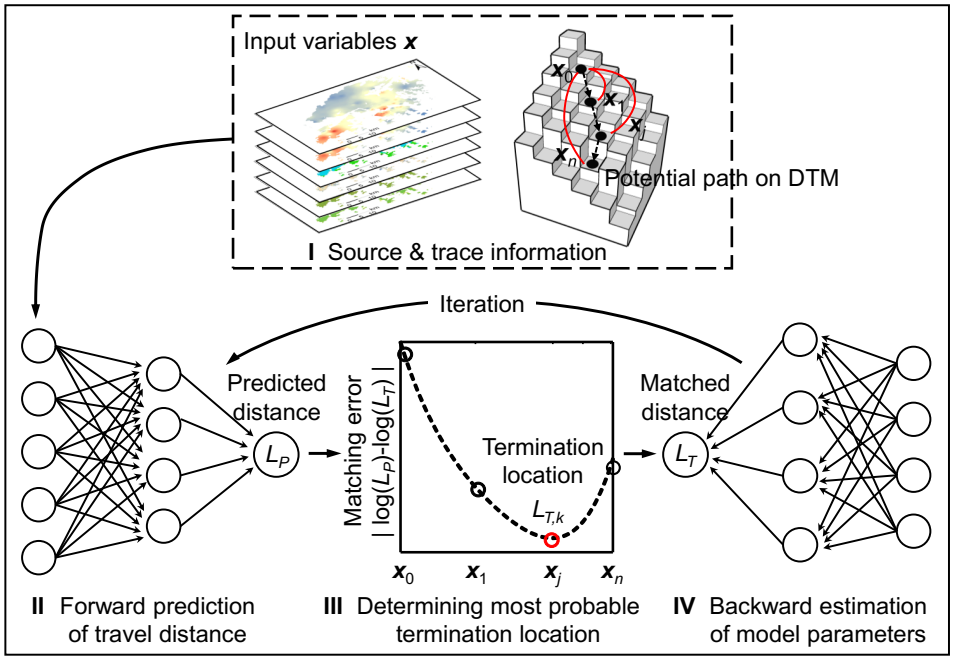

Figure 5: Terrain matching strategy for landslide mobility forecasting

$$J(\boldsymbol{\theta}) = \frac{1}{N}\sum_{i=1}^{N}\left[\log\left(L_{T,k,i}\right) - \log\left(L_i\right)\right]^2 \tag{3}$$

where $L_{T,k,i}$ = the most probable travel distance at location k on the DTM for the ith landslide and the termination location k can be determined according to the fitness of terrain as:

$$k = \underset{j=1,2,\ldots,n_i}{\arg\min}\left|\log\left(L_{P,j,i}\right) - \log\left(L_{T,j,i}\right)\right| \tag{4}$$

where $L_{P,j,i}$ = predicted travel distance at the jth cell on the ith landslide path.

Combining Equations (4) and (3) makes the predicted travel distance (L_P) first fit the one on the DTM (L_T) and then the one recorded in the landslide database (L). Such a pseudo bi-objective optimization makes the predicted landslide path more comparable with the terrain reality. Another advantage of the terrain matching iteration is that: it can easily consider the variable trace features from the landslide source to the jth cell when visiting all possible termination locations.

It should be highlighted that the proposed machine learning strategies to address the time-unknown issue in initiation forecasting and terrain-unmatched issue in mobility forecasting can be flexibly applied with various basic machine learning algorithms, such as logistic regression, neural network, or even deep learning techniques, as they only need the updating of cost functions. The validation and comparison of the proposed machine learning strategies against historical landslide data and statistical models can be referred to Xiao and Zhang (2023a) and Ju et al. (2022). The following section will take Hong Kong as an example to demonstrate the capacity of city-scale landslide forecasting using machine learning.

4 CASE STUDIES FOR HONG KONG

4.1 Spatio-temporal landslide forecasting

Applying the probabilistic modelling strategy, regardless of whether the landslide time is known or not, two landslide initiation forecasting models can be developed for the 60,000 registered man-made slopes (Xiao et al. 2022) and 26 million natural terrain hillslope cells (5 m × 5 m) (Xiao and Zhang 2023b), respectively. Logistic regression is adopted as the basic machine learning classifier in both models.

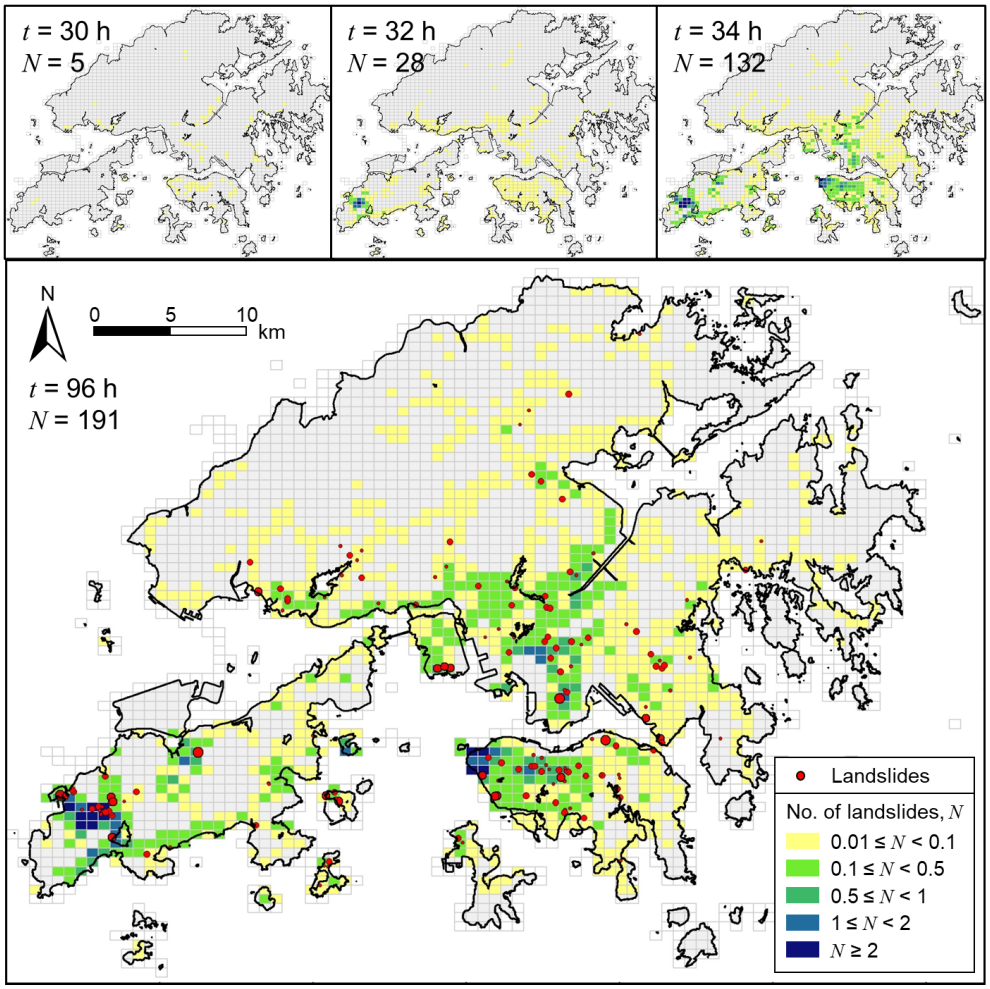

Figure 6: Predicted evolution of man-made slope failures during the 6-9 June 2008 storm

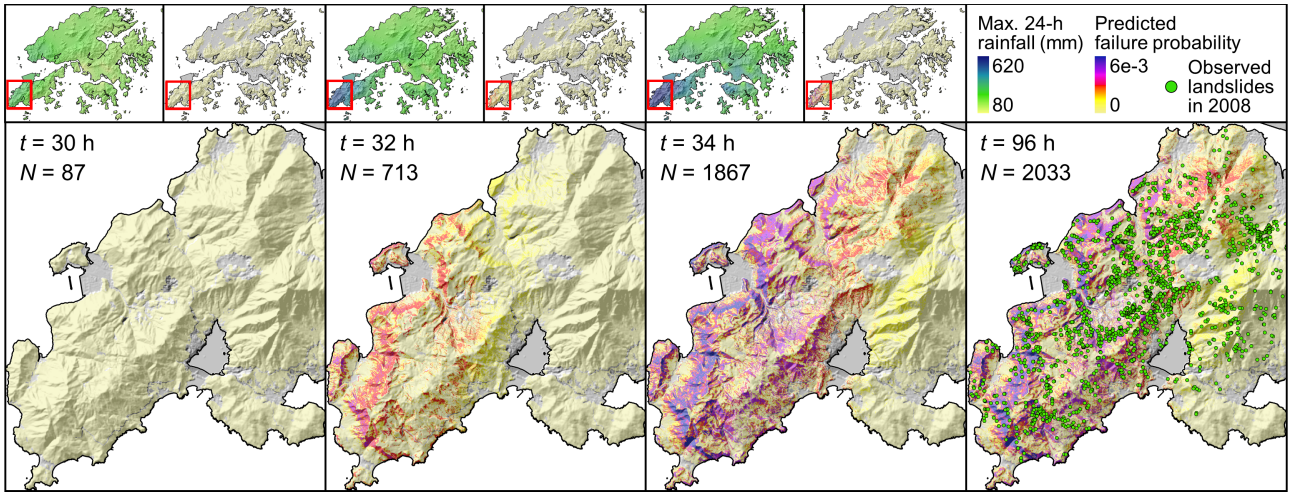

Figure 7: Predicted evolution of natural terrain landslides during the 6-9 June 2008 storm

The 6-9 June 2008 storm is one of the most severe rainstorms in the history of Hong Kong, with 1-h, 4-h, and 24-h rainfall amounts all falling in the top five rainstorms ever recorded. The storm triggered 162 confirmed failures of registered man-made slopes and about 2400 natural terrain landslides (estimated). The

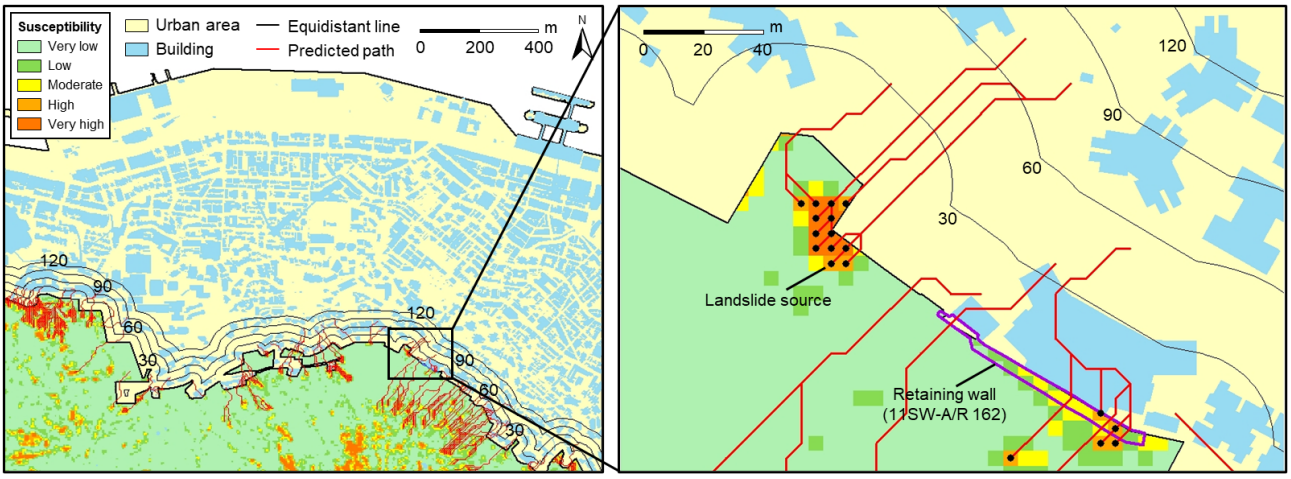

Figure 8: Predicted landslide-affected areas in the Mid-Levels

spatio-temporal evolutions of man-made slope failures (Figure 6) and natural terrain landslides (Figure 7) during the 6-9 June 2008 storm can be predicted using the two machine learning model with nearly real-time efficiency. For man-made slopes, hardly any landslides occur before time t = 30 h; the western Lantau Island is the first area to witness many landslides at t = 32 h; afterwards, there is a rapid outbreak of landslides on the north-western Hong Kong Island and western Kowloon. The predicted number of natural terrain landslides experiences a similar temporal escalation, from less than 100 at t = 30 h to more than 1800 at t = 34 h, but almost all concentrate on western Lantau Island in space. Both the predicted numbers of landslides and landslide-prone areas agree well with the observations.

4.2 Identification of landslide-affected urban areas

Applying the terrain matching strategy, the performance of the machine learning-powered landslide mobility forecasting model can be significantly improved from less than 0.4 to higher than 0.7, even though a very simple neural network is adopted (Ju et al. 2022). The proposed machine learning model can not only provide rapid regional runout path predictions like a statistical model does, but also reasonably incorporate complex geographic characteristics along landslide traces and 3-D terrain reality like in a 3-D numerical simulation.

With the developed prediction model of landslide runout paths, it is possible to identify potential landslide-affected urban areas and high-risk landslide-bearing elements. Consider the Mid-Levels at the foot of Victoria Peak on Hong Kong Island as an example (Figure 8). The Mid-Levels is a landslide-prone area with various buildings densely packed near the steep natural hillsides. One of the most severe rainstorms hitting the Mid-Levels in history is the storm on 16-21 August 2005, with the maximum rolling 4-h and 24-h rainfall amounts being 171 mm and 567.5 mm, respectively. Integrated with landslide susceptibility mapping results, 2238 landslide travel paths can be predicted in the investigated area, among which 1268 landslides rush into the urban area, as shown in Figure 8. About 72% of these landslides stop within 30 m to the mountain foot, and only a few travel a long distance (e.g., 0.5% over 90 m to the mountain foot). The building at the lower right corner of Figure 8 is at the highest risk of being attacked by several potential landslides and demands necessary slope stabilization measures. In fact, an 8 m high concrete retaining wall (11SW-A/R 162) has been constructed between the building and the mountain for safety reasons.

4.3 Future application to prompt quantitative risk assessment

The ultimate application target of the machine learning-powered landslide forecasting models will be the prompt quantitative risk assessment (He et al. 2023), which requires real-time predictions of both landslide initiation (i.e., occurrence probability) and mobility (i.e., spatial impact probability) under a full probabilistic framework (Figure 9).

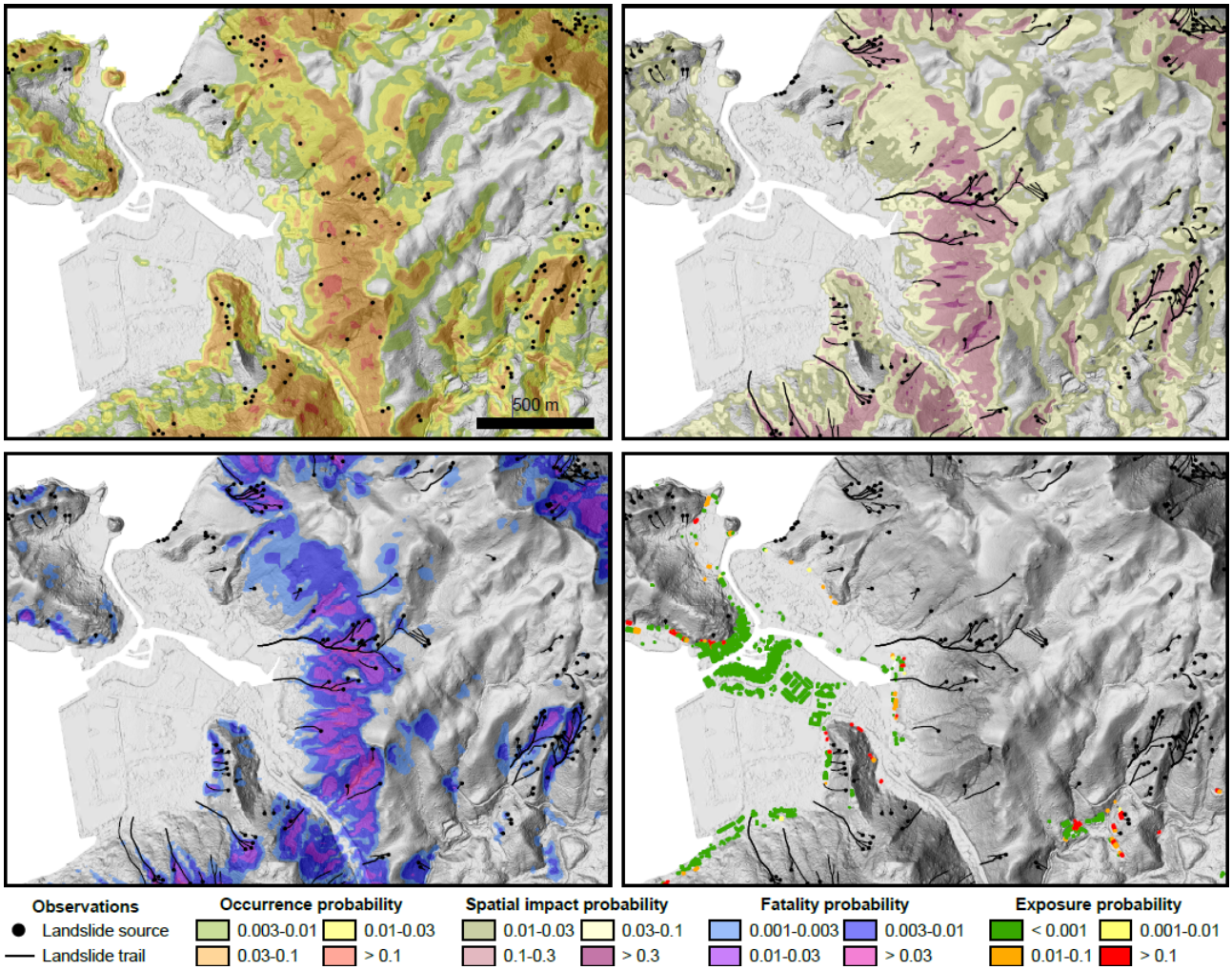

Figure 9: Example of quantitative landslide risk assessment

The current statistical version only assesses the risk of natural terrain landslides. Considering that man-made slope failures occurring in densely populated urban regions (e.g., Hong Kong Island and Kowloon) will pose much higher risk than natural terrain landslides occurring in sparsely populated remote regions (e.g., Lantau Island), it is crucial to assess the risk of man-made slope failures simultaneously. As demonstrated in the previous two applications, machine learning models have already achieved the initiation prediction of both natural terrain landslides and man-made slope failures. Future work should focus on the mobility prediction of man-made slope failures. A possible solution is to discretize man-made slopes into the same cells as the natural terrain does. By this means, the post-failure movement of man-made slopes can be modelled in a consistent probabilistic manner.

The GEO is operating two landslide early warning systems for man-made slope failures and natural terrain landslides separately. Due to the difference in safety levels and covering areas of these two types of landslides, different quantity-based warning criteria are adopted, namely 15 for man-made slope failures and [500, 1000, 2000] for natural terrain landslides. The landslide risk as an integration of both occurrence probability and consequence would be a better indicator than the landslide quantity to unify man-made slope failures and natural terrain landslides. The next-generation risk-informed landslide early warning system will benefit a lot from machine learning-powered landslide forecasting.

5 CONCLUSIONS

Machine learning-related landslide studies stay on landslide susceptibility mapping for decades. Moving towards the prediction of landslide occurrence and movement, the time-unknown issue and terrain-unmatched

issue should be addressed primarily. For such a purpose, this study proposes two novel machine learning strategies of probabilistic modelling and terrain matching for forecasting landslide initiation and mobility, respectively. It is found that even simple machine learning algorithms can have significant improvements than conventional statistical methods, as long as well-designed task-specific machine learning strategies can be developed.

Hong Kong is taken as an example to demonstrate the capacity of city-scale landslide forecasting using machine learning. The spatio-temporal evolution of both man-made slope failures and natural terrain landslides in a rainstorm can be well predicted using machine learning models, which can provide a powerful real-time decision-making tool for landslide early warning and risk management.

ACKNOWLEDGEMENTS

This work was supported by the Research Grants Council of the Hong Kong SAR (Nos. 16205719, 16203720, N_HKUST620/20, and AoE/E-603/18). The authors would like to thank the Geotechnical Engineering Office of the Civil Engineering and Development Department, the Government of the Hong Kong SAR, for providing the landslide data.

REFERENCES

Baum, R.L., Godt, J.W., & Savage, W.Z. 2010. Estimating the timing and location of shallow rainfall-induced landslides using a model for transient, unsaturated infiltration. *Journal of Geophysical Research: Earth Surface*, 115: F03013.

Cheung, R.W.M. 2021. Landslide risk management in Hong Kong. *Landslides*, 18(10): 3457-3473.

Dai, F.C., & Lee, C.F. 2002. Landslide characteristics and slope instability modeling using GIS, Lantau Island, Hong Kong. *Geomorphology*, 42(3-4): 213-228.

Finlay, P.J., Mostyn, G.R., & Fell, R. 1999. Landslide risk assessment: prediction of travel distance. *Canadian Geotechnical Journal,* 36(3): 556-562.

He, J., Zhang, L., Xiao, T., Wang, H., & Luo, H. 2023. Prompt quantitative risk assessment for rain-induced landslides. *Journal of Geotechnical and Geoenvironmental Engineering*, 149(5): 04023023.

Ju, L.Y., Xiao, T., He, J., Wang, H.J., & Zhang, L.M. 2022. Predicting landslide runout paths using terrain matching-targeted machine learning. *Engineering Geology*, 311: 106902.

Ko, F.W., & Lo, F.L. 2016. Rainfall-based landslide susceptibility analysis for natural terrain in Hong Kong-A direct stock-taking approach. *Engineering Geology*, 215: 95-107.

Kong, V.W.W., Kwan, J.S.H., & Pun, W.K. 2020. Hong Kong's landslip warning system—40 years of progress. *Landslides*, 17(6): 1453-1463.

Kwan, J.S.H., Sze, E.H.Y., Lam, C., Law, R.P.H., & Koo, R.C.H. 2021. Development and applications of debris mobility models in Hong Kong. *Proceedings of the Institution of Civil Engineers-Geotechnical Engineering*, 174(5): 593-610.

Merghadi, A., Yunus, A.P., Dou, J., et al. 2020. Machine learning methods for landslide susceptibility studies: A comparative overview of algorithm performance. *Earth-Science Reviews*, 207: 103225.

Shen, P., Zhang, L., Chen, H., & Fan, R. 2018. EDDA 2.0: integrated simulation of debris flow initiation and dynamics considering two initiation mechanisms. *Geoscientific Model Development*, 11(7): 2841-2856.

Wang, H., Zhang, L., Luo, H., He, J., & Cheung, R.W.M. 2021. AI-powered landslide susceptibility assessment in Hong Kong. *Engineering Geology*, 288: 106103.

Xiao, T., & Zhang, L. 2020. Evaluation of performance of engineered slopes under extreme rainstorms. In *Geo-Congress 2020: Engineering, Monitoring, and Management of Geotechnical Infrastructure*. pp. 737-743. Reston, United States: ASCE.

Xiao, T., & Zhang, L.M. 2023a. Data-driven landslide forecasting: Methods, data completeness, and real-time warning. *Engineering Geology*, 317: 107068.

Xiao, T., & Zhang, L.M. 2023b. Storm-based forecasting of natural terrain landslides. In *Geo-Risk 2023: Advances in Theory and Innovation in Practice*. pp. 1-10. Reston, United States: ASCE.

Xiao, T., Zhang, L.M., Cheung, R.W.M., & Lacasse, S. 2022. Predicting spatio-temporal man-made slope failures induced by rainfall in Hong Kong using machine learning techniques. *Géotechnique*, 1-17. DOI: 10.1680/jgeot.21.00160

A Strategy to Estimate & Optimise Carbon Footprint for Foundations

Tim M T Wong & Charmaine Leung

Arup, Hong Kong

ABSTRACT

In response to the Paris Agreement with its Climate Action Plan 2030+, The Hong Kong government aims at 26% to 36% absolute carbon reduction by 2030 and achieve carbon neutrality by 2050. As the construction industry accounts for a significant amount of carbon emission, engineering practitioners have begun searching for ways to reduce the industry's impacts through greener construction processes. Understanding and assessing the carbon footprint of the construction process enables benchmarking how "green" currently our works are. It provides insights on areas for improvement including reducing carbon emissions. While the methodology of carbon footprint assessment has been developed and adopted for superstructure, the same for underground elements such as foundations have yet been discussed and proposed. This is due to the great variety of substructure, the uniqueness of geological and geotechnical conditions in different regions, as well as the influence of local practices and regulations. The above makes the standardization and benchmarking of carbon emissions for substructure a challenge.

In this paper, the authors attempt to develop a strategy for the assessment of embodied carbon on substructures in Hong Kong. Current obstacles and difficulties, as compared to those for other structures and structural elements are discussed. A strategy to look into the carbon footprint systematically and logically for foundations is then proposed and explained. The authors discuss possibilities to reduce and optimise carbon footprint of foundation works through careful decisions in early-stage planning, design, and construction control.

1 INTRODUCTION

1.1Greenhouse Gases and CO2e

According to the Kyoto Protocol, there are seven types of greenhouse gases (GHG) found to have effects on our climate system, including carbon dioxide (CO2), methane (CH4), nitrous oxide (N2O), hydrofluorocarbons (HFCs), perfluorocarbons (PFCs), sulphur hexafluoride (SF6), and nitrogen trifluoride (NF3). CO2 and N2O are emitted during fossil fuel combustion, while CH4 would be generated from decomposition of organic materials, e.g., paper waste. HFCs and PFCs mainly come from leakage from refrigeration / air-conditioning plants which is not common if there is proper maintenance of the systems, while SF6 and NF3 mainly come from industrial processes.

Emissions of the direct greenhouse gases are calculated as carbon dioxide equivalent (CO2e), which is a quantity that describes, for a given mixture and amount of greenhouse gas, the amount of CO2 that would have the same global warming potential (GWP). The carbon dioxide equivalent for a gas is obtained by multiplying the mass and the GWP of the gas. It is a normalised term for accounting the carbon emission from a source with different GHG generation.

1.2 Objective

Several studies have addressed the issue of embodied carbon for superstructures, while excluding foundations. This is because foundation design is heavily influenced by the unique ground conditions of each site. (Chau, Hui, Ng& Powell, 2012; Hart, *D'Amico & Pomponi, 2021)* This paper aims to develop a strategy for the assessment of embodied carbon on substructures in Hong Kong. Current obstacles and difficulties, as compared to those for other structures and structural elements are discussed. A strategy to investigate the carbon footprint systematically and logically for foundations is then proposed and explained.

1 CURRENT METHODLOGY FOR CARBON MANAGEMENT

2.1 Modular Approach for Whole Lifecycle Carbon Assessment

The quantification of GHG emissions for an infrastructure or building asset can be undertaken using a modular structure which is consistent with the principles set out in BS EN 15978:2011 (Sustainability of construction works – Assessment of environmental performance of buildings – Calculation method) and BS EN 15804:2012 (Sustainability of construction works - environmental product declarations). Such approach can be visually illustrated as shown in Figure 1.

Figure 2 illustrates the general trend of carbon emissions of an infrastructure or building asset during its whole life cycle. It can be clearly seen that the construction products and processes stage accounts for a significant proportion of carbon emissions. Also known as Upfront Carbon as shown in Figure 1, this stage can be divided into sub-categories as follows:

A1-A3: This accounts for raw materials of substructure and superstructure for the carbon emissions associated with the "cradle to gate" processes: raw material supply, transportation and manufacturing processes.

A4-A5: Construction stage process – accounting for the carbon emissions associated with the transportation of the materials to site and the construction itself (material wastes, construction plant and machineries). The term transportation also includes all movement of equipment and materials from intermediate storage to site. Waste management activities (transport, processing, final disposal) associated with waste arising from the construction site should also be accounted for.

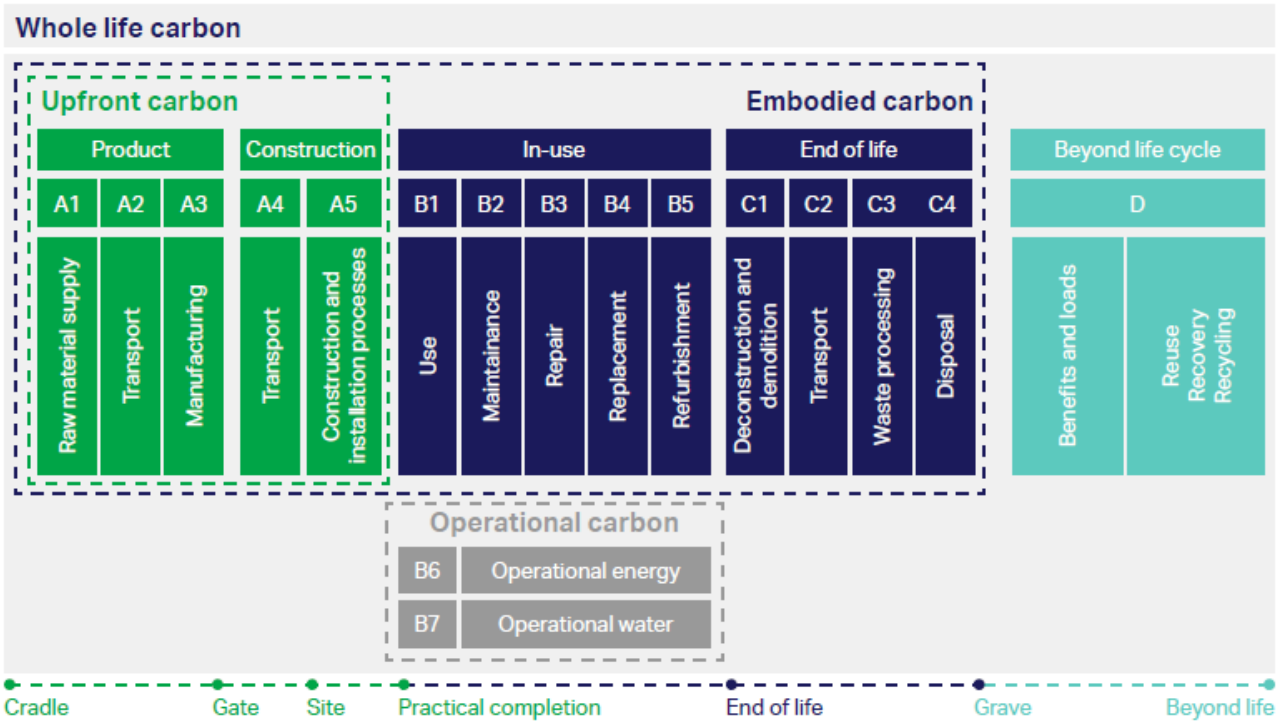

Figure 1 Modular approach in Whole life cycle stages, EN15978 (2011)

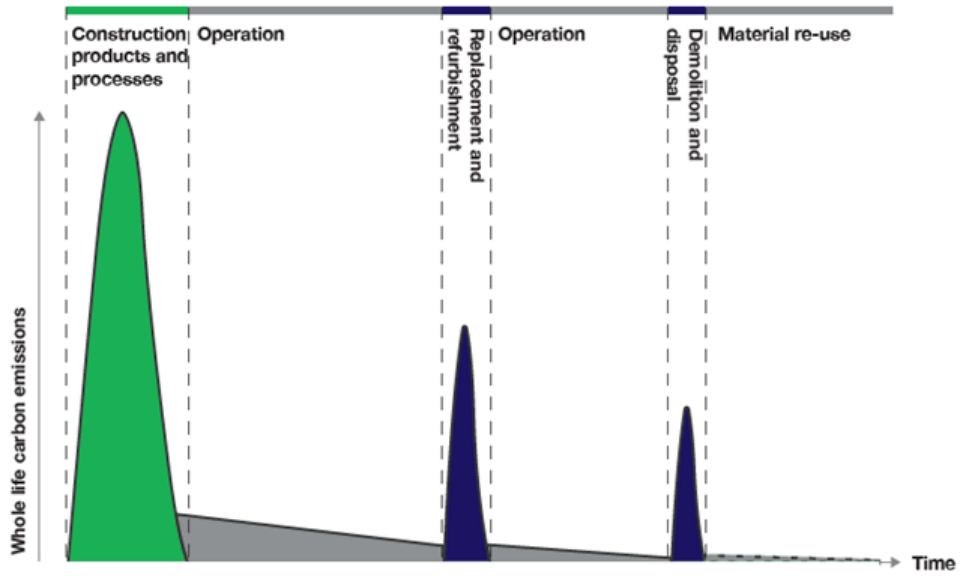

Figure 2 Whole Life cycle stages Carbon Emissions

2.2 Upfront Carbon Quantification and Benchmarking

In general, the GHG emission can be calculated using the following formula:

*Emission = Activity Rate * Emission Factor*

In Hong Kong, the Construction Industry Council (CIC) Carbon Assessment Tool (CAT) (Figure 3) can be adopted for estimating upfront carbon emissions. It is a platform to evaluate the carbon accounting for construction works (i.e. A1 to A5) into different attributes as defined as permanent works, temporary works, site impacts. The CAT is currently providing two platforms for design and construction stages namely, "Design Tool" and "Construction Tool".

"Design Tool" accounts for A1-A3, while "Construction Tool" also accounts for site impact activities to cover for A1-A5. CAT provides most of the emission factors data for major materials in the CIC Green Product Certification scheme. Additional research work will have to be undertaken when emission factors are not available in CAT database.

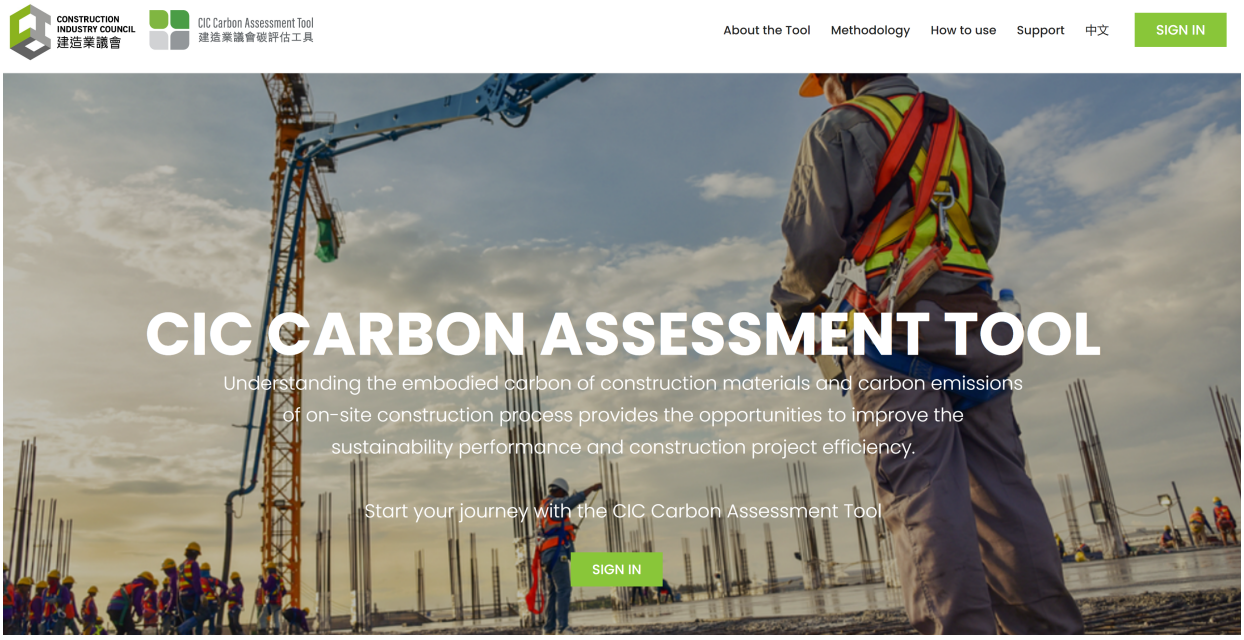

Figure 3 CIC Carbon Assessment Tool (CAT) Platform for Embodied Carbon A1-A5

By quantifying the upfront carbon emission of different infrastructure or structure assets, benchmarks and databases can be developed to allow designers to assess the performance of their design in terms of anticipated carbon footprint. Such information enables designers to find ways to improve their design and deliver embodied carbon efficiency. It is an important step towards the goal of net zero building, as only when such data are available, suitable and appropriate carbon offsetting plans can be planned, designed and implemented.

3 LIMITATIONS ON CARBON ASSESSMENT FOR FOUNDATIONS

3.1 Carbon Emissions Generated by Foundation Works

Substructure, including foundations, ground bearing slab and basement retaining walls, typically contributes to approximately 20-30% of embodied carbon emission in whole building. *(LETI, 2021)*. From the authors' previous studies, substructure contributes 25 % of total embodied carbon emission in our local project and results in 191kgCO2e/GFA. The rule of thumb on embodied carbon distribution in selected types of structures is illustrated in Figure 4. Within the category of substructure, it is considered that foundations (including pile cap and piling) contain the largest proportion of the embodied carbon.

A worked sample on substructure embodied carbon is given in Table 1 for a 30-storey residential building, which is supported by 2.5m diameter Bored Piling and site area at 15,000m^2 located in in New Territories, HKSAR. This sample shows the embodied carbon quantification assessment during the design stage for the proposed foundation with the defined category, activities, materials, quantity and unit as tabulated. These data are taken from the building information modelling, then integrated with the CIC CAT for quantification.

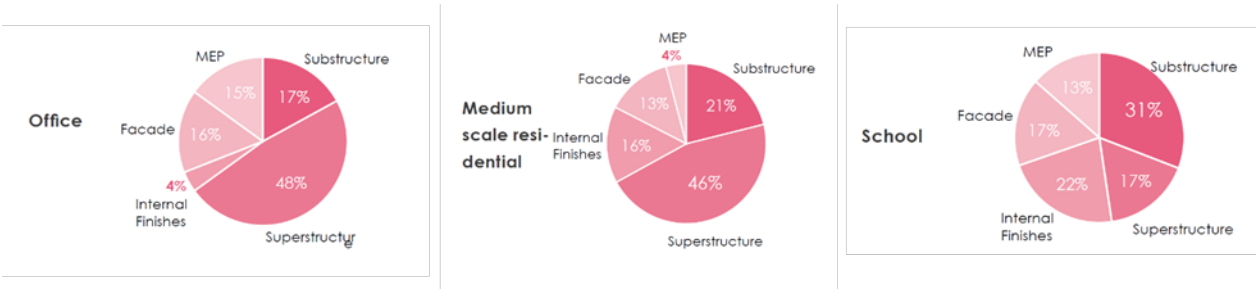

Figure 4 Rule of Thumb on Embodied Carbon Distribution in Buildings *(LETI, 2021)*

Category	Activities	Material	Quantity	Unit	Tonnes CO2e
A1-3	Bored Piling	Concrete grade C45, OPC	2983	m3	1275
A1-3	Bored Piling	Reinforcement Bar, General Reinforcement Bar	144586	kg	310
A1-3	Sheet Piling	Structural Steel, General Structural Steel	35067	kg	90
A1-3	Pile Cap	Concrete grade C45, OPC	385	m3	165
A1-3	Pile Cap	Concrete grade C60, OPC	6	m3	3
A1-3	Pile Cap	Reinforcement Bar, General Reinforcement Bar	475458	kg	1020
A1-3	Pile Cap	Timber	1172	m2	5
				Total	2868

Table 1 Sample of foundation quantity and embodied carbon quantification

3.2 Difficulties in Baselining Carbon Emissions in Foundations

Figure 4 demonstrates that the substructure accounts for the second largest carbon emissions impact in embodied carbon, hence, it shall be considered during planning and design stage to assess the reduction measures. Although carbon auditing and estimate for foundation can be done in similar fashion as the superstructure elements of an infrastructure or structure asset, baselining on carbon emissions for foundations have not been undertaken. This hinders designers from reaching the goal of moving towards net zero or carbon neutrality target.

The calculated embodied carbon on substructure, particularly the foundation, is more complicated to set out the baseline when comparing with superstructure with typical floor function space and per area. The major obstacle is that the choice of foundation and its scale are not only influenced by the superstructure type and height, but also highly influenced by the geological condition as well as the groundwater table. For instance, the same commercial building will have an entirely different foundation scheme when it is located on a newly reclaimed land with substantial thickness of soft deposits as compared to located in an ex-quarry site where competent engineering rockhead can be encountered at shallow depth from the existing ground level.

4 CARBON STRATEGY FOR FOUNDATIONS

4.1 Alternative Way of Assessment

Ideally, in order to have a meaningful comparison on carbon emissions for foundations, designers should consider baselining their proposed schemes against shortlisted samples with superstructures with similar functionality as well as similar geological condition. However, this could be difficult to achieve in the short term as there may not be enough data with such categorisations. Prior to such database becoming mature, it is suggested that effort should be made on treating carbon reduction as one of the targets in value-engineering activities. For a particular type of foundation, for example in-situ cast concrete bored piles, there would be a common range of carbon emission per unit volume of the pile structure. Focus should then be put on ways to achieve a lower CO2e per unit volume, or in other words, a higher embodied carbon efficiency.

4.2 Carbon Reduction Initiatives

A majority of substructure elements including foundations are reinforced concrete product and will remain prominent over the next decade, there are several ways to reduce the carbon impact of reinforced concrete structures whereas most effective to reduce embodied carbon is to use less of the heaviest polluting elements, for instance, less cement and less reinforcing steel. The breakdown of the reinforced concrete material carbon impact breakdown is presented in Figure 5.

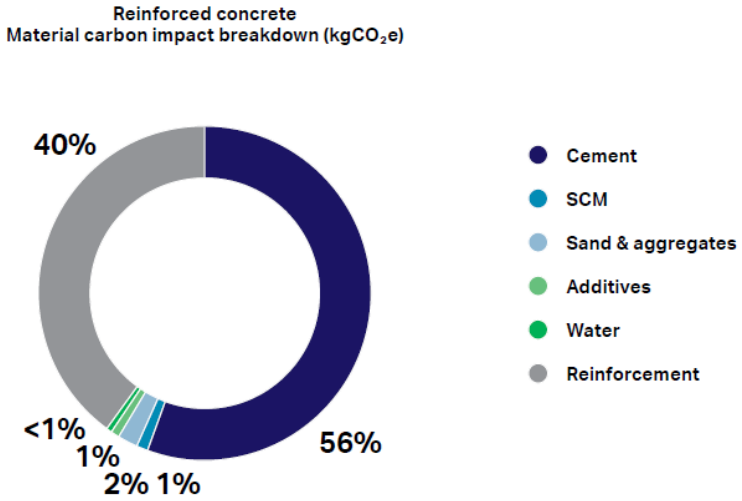

Figure 5 Reinforced concrete Material carbon impact breakdown (kgCO_2e). *(L.E.T,2020)*

4.2.1 Green Concrete

Use of GGBS (Ground Granulated Blast Furnace Slag) could be one of the ways to reduce embodied carbon in structural components in both substructure and superstructure, which have been recently adopted in recent projects. Several research suggests that GGBS can replace up to 70% of cement while PFA can only replace up to 35% of cement. These substitutes can contribute to further CO2 reduction. According to the Carbon Assessment Tool established by CIC and as illustrated in Figure 6, 63.8% of CO2 reduction can be achieved by using 65% GGBS concrete mixture to replace Portland Cement.

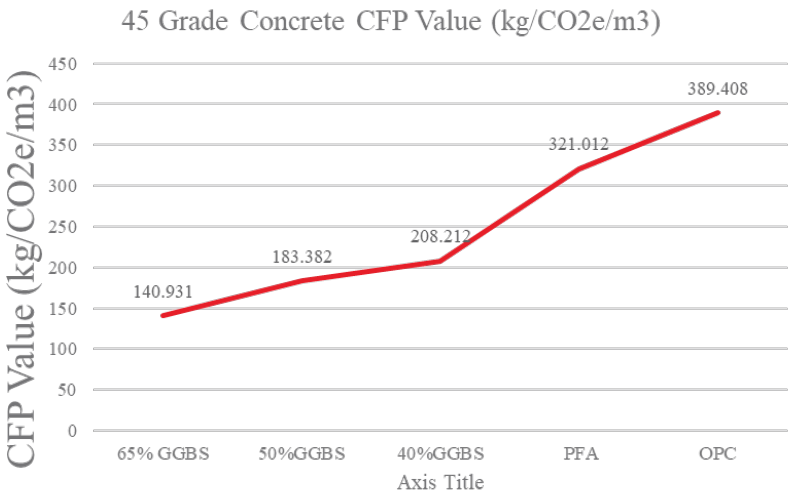

Figure 6 Carbon Footprint Value (CFP) in 45 Grade Concrete

4.2.2 Recycled Steel Supplier

With the advancement of Electric-arc-furnace (EAF) technology, the rate of recycling of steel scrap has increased to 94%, reducing the environmental effects of iron mining without compromising social or economic development. For instance, O-PARK2 is an example of making use of rebar that is 100% recycled, and it has a 67% potential to reduce carbon emissions.

4.2.3. Improvement in Design Approaches and Methodologies

The overall carbon emissions of foundation are generally proportional to the construction material e.g. concrete, rebars, steel, etc. Therefore, improvements in design approaches and methodologies that results in reduction of construction materials used would have a significant impact on the embodied carbon efficiency of the foundation system. For example, the recent enhancement of allowable bearing capacity of Category 1(c) rock as per Code of Practice for Foundations potentially enables the same structures to be supported by smaller size or fewer numbers of piles, hence providing the opportunity for substantial reduction in carbon emissions. It is suggested that the industry should collaborate with the statutory bodies and look into the possibilities of adopting more technological advanced foundation solutions in local projects.

5 CONCLUSION

This paper has presented the carbon management process, standards, methodology, boundary setting and carbon accounting tools for embodied carbon on infrastructure and structure asset. Its applicability on substructures, in particular foundations, is studied and discussed. The study shows despite the limitations on providing benchmarking for assessing carbon footprint for foundations, immediate improvements can be achieved with the use of greener construction material and better design approaches & methodologies. In the longer-term baselines can be developed for foundations with the consideration of geological conditions and groundwater conditions.

6 REFERENCES

Chau, C. K., Hui, W. K., Ng, W. Y., & Powell, G. (2012). Assessment of CO2 emissions reduction in high-rise concrete office buildings using different material use options. *Resources, conservation and recycling*, *61*, 22-34.

Sandanayake, M., Zhang, G., & Setunge, S. (2016). Environmental emissions at foundation construction stage of buildings–Two case studies. Building and Environment, 95, 189-198.

McAlinden, B. (2016, August). PAS 2080: world first specification for cutting carbon dioxide emissions in infrastructure. In Proceedings of the Institution of Civil Engineers-Civil Engineering (Vol. 169, No. 3, pp. 99-99). Thomas Telford Ltd.

Hart, J., D'Amico, B., & Pomponi, F. (2021). Whole-life embodied carbon in multistory buildings: Steel, concrete and timber structures. Journal of Industrial Ecology, 25(2), 403-418.

John W H Chung, Robert Y K Chan, Gloria Y Y Tang, Raymond W M Au, CM Tsang, Hong Kong Institution of Engineers. 2022. High-performance low-carbon GGBS concrete for sustainable development: a case study in Hong Kong - Facing forthcoming OPC & PFA shortage and carbon neutral challenges

London Energy Transformation Initiative., 2020. LETI Embodied Carbon Primer, Supplementary guidance to the Climate Emergency Design Guide

The Institution of Structural Engineers, 2020. How to calculate embodied carbon.

World Business Council for Sustainable Development, Arup. 2023. Net-zero buildings Halving construction emissions today.

Chapa, J. (2019). Bringing embodied carbon upfront. *Built Environment Economist: Australia and New Zealand*, 38-41.

Evaluation of the Performance of GGBS Concrete Used in Civil and Geotechnical Works

Jack Y. KWOK and Jackie C.K. LEUNG

Geotechnical Engineering Office, Civil Engineering and Development Department,

The Government of the Hong Kong Special Administrative Region

ABSTRACT

The use of supplementary cementitious materials (SCM) such as Pulverised Fly Ash (PFA) and Ground Granulated Blastfurnace Slag (GGBS) has been proven effective in reducing the total carbon emission of the concrete production process by lowering the use of Ordinary Portland Cement (OPC). The general specifications published by the Government of the Hong Kong Special Administrative Region have allowed the use of PFA as SCM in concrete production for public work projects in the past three decades. From 2012 onwards, the use of GGBS as SCM has also been permitted. In recent years, the local electricity companies have been reducing their reliance on coal-fired plants for electricity generation. The local supply of PFA has been declining and is expected to deplete by the 2030s. Through the management of the concrete mix ID database, the Public Works Central Laboratory (PWCL) noted the trend of using GGBS concrete in public works contracts has been on the rise in the past two years.

The PWCL has recently conducted an in-house technical study on the performance of GGBS concrete mixes recently adopted in public works contracts. Based on the original concrete mix formulas and sources of materials, fresh concrete batches were made in laboratory environment. Furthermore, additional concrete test cubes were obtained from available on-going public works construction sites adopting GGBS concrete. Various performance aspects of the concrete mixes, such as the early strength development and shrinkage properties were evaluated. PWCL has also obtained the results of the recent "Low Carbon Concrete Trophy Competition 2022" initiated by the Standing Committee on Concrete Technology and organised by HKIE for comparison purposes. In view of the improved quality of GGBS available in the market in the past few years, PWCL is also planning to conduct a further study on the performance of GGBS concrete, focusing on the recent technological advancement in this area, and the feasibility of achieving higher replacement levels, higher grade strengths with the use of locally available raw materials.

This paper summarises our current work on evaluation of the performance of GGBS concrete used in recent public works contracts with the aim of facilitating the industry's consideration for wider adoption of GGBS concrete in civil and geotechnical engineering works.

1 INTRODUCTION

1.1 Use of Supplementary Cementitious Materials (SCM)

Cement is one of the major constituent materials for the production of concrete. To produce cement, limestone, clay and other materials are heated in large kilns to high temperatures (about 1500 °C). During the process, greenhouse gases (e.g. carbon dioxide, nitrous oxides, sulphur dioxide) are emitted. Carbon dioxide (CO_2) accounts for the majority of the gas emissions, which comes from the calcination of limestone (breaking down into CO_2 and calcium oxide) and the combustion of fossil fuels for heating the kilns. The cement industry accounts for about 8% of the global CO_2 emission.

The use of supplementary cementitious materials (SCM) such as Pulverised Fly Ash (PFA) and Ground Granulated Blastfurnace Slag (GGBS) has been proven effective in reducing the total carbon emission of the concrete production process by lowering the use of Ordinary Portland Cement (OPC). The General Specification for Civil Engineering Works published by the Government of the Hong Kong Special

Administrative Region has allowed the use of PFA as SCM in concrete production for public work projects in the past three decades. From 2012 onwards, the use of GGBS as SCM has also been permitted. In recent years, the local electricity companies have been reducing their reliance on coal-fired plants for electricity generation. The local supply of PFA has been declining and is expected to deplete by the 2030s.

1.2 Low Carbon Concrete Trophy Competition 2022

The "Low Carbon Concrete Trophy Competition 2022" (LCCTC) initiated by the Standing Committee on Concrete Technology and organised by HKIE was completed in November 2022. The objective of the competition was to arouse the awareness and interest of stakeholders in the construction industry towards the benefits of low carbon concrete produced using GGBS. The competition had two categories, viz. the Students Category and the Practitioners Category. Each participating team was required to design a concrete mix using GGBS as SCM to achieve the target strength. The teams were later required to produce their designed concrete mix in laboratory environment. Strength tests and durability tests were conducted on the produced concrete specimens and scores were given based on a set of pre-defined criteria. Under the Students Category (with a total 10 teams), most of the teams prepared concrete mixes with GGBS content from 70% to 75% for a target strength of 45MPa. Under the Practitioners Category (with a total 12 teams), most of the teams prepared concrete mixes with GGBS content from 80% to 85% for a target strength of 60MPa. From the results of the competition, it was observed that the ratio of 7-day strength / 28-day strength and 56-day strength / 28-day strength ranged from 0.65 to 0.81 and 1.05 to 1.13 respectively.

1.3 In-house Technical Study on GGBS

Through the management of the concrete mix database, the Public Works Central Laboratory (PWCL) noticed that the trend of using GGBS concrete in public works contracts has been on the rise in the past two years. The PWCL has recently conducted an in-house technical study on the performance of GGBS concrete mixes adopted in public works contracts in 2022. Based on the original concrete mix formulas and sources of materials, fresh concrete batches were made in laboratory environment. Furthermore, additional concrete test cubes were also obtained from available on-going public works construction sites adopting GGBS concrete. Various performance aspects of the concrete mixes, such as the early strength development and shrinkage properties were evaluated.

This paper summarises the above recent work conducted by the PWCL and presents some observations obtained thereby regarding the performance of GGBS concrete used in Hong Kong.

2 IN-HOUSE TECHNICAL STUDY

2.1 Concrete Samples prepared by PWCL

PWCL identified the GGBS concrete mixes adopted in public works contracts in 2022 through the management of the concrete mix database. Amongst the GGBS concrete mixes from the database, the grade strengths and GGBS replacement ratios range from Grade 25 to Grade 60 and 35% to 65% respectively. It was observed that Grade 45 was the most common grade used. PWCL replicated 13 of these GGBS concrete mixes using the same cementitious content, aggregate content and W/C ratio in laboratory environment from December 2022 to March 2023. The selected mixes cover various grade strengths and GGBS replacement ratios. Strength tests and shrinkage tests were conducted in laboratory conditions in accordance with Hong Kong Construction Standard CS1:2010 and BS EN 12390-16 respectively. For each of the replicated GGBS mix, a control OPC mix with the same W/C ratio was also prepared for comparison purpose.

In all concrete mixes, superplasticizer was added to achieve the target slump of each mix. In the preparation of the concrete mixes, OPC with strength class 52.5N in accordance with BS EN 197-1 and GGBS in accordance with BS EN 15167-1 with fineness between 400 and 500 m^2/kg were used. A summary of the concrete mixes is shown in Table 1. The grade of concrete mixes ranged from Grade 25 to Grade 60. The total cementitious content ranged between 406 to 480 kg/m^3. The concrete mixes with higher grade strengths generally have lower W/C ratios.

Table 1 – Summary of Concrete Mixes prepared by PWCL

Mix Number	Grade	Total Cementitious Content, kg/m^3	GGBS Content %	A/C Ratio	W/C Ratio
1	25	410	60%	4.09	0.49
2	30	406	35%	4.26	0.45
3	30	450	60%	3.61	0.46
4	40	410	50%	4.44	0.38
5	45	450	35%	3.83	0.41
6	45	480	40%	3.52	0.36
7	45	450	60%	3.80	0.42
8	45	450	65%	3.91	0.36
9	45	410	65%	4.41	0.38
10	50	450	65%	3.91	0.36
11	55	430	65%	4.20	0.35
12	55	460	65%	3.76	0.35
13	60	460	50%	3.83	0.35

2.3 Concrete Cubes Obtained from Available On-going Public Works Construction Sites

In addition to the concrete specimens prepared by PWCL, extra GGBS concrete cubes were also obtained from available on-going public works construction sites for carrying out strength tests for comparison purpose. The concrete mixes include 5 GGBS concrete and 2 PFA concrete. A summary of the concrete mixes is shown in Table 2.

Table 2 – Summary of Concrete Samples obtained from Available On-going Public Works Construction Sites

Mix Number	Grade	Total Cementitious Content, kg/m^3	SCM %	A/C Ratio	W/C Ratio
14	40	410	50% GGBS	4.44	0.38
15	45	480	40% GGBS	3.52	0.36
16	45	450	65% GGBS	3.91	0.36
17	45	450	65% GGBS with Shrinkage Reducing Agent	3.91	0.36
18	45	450	35% PFA + PP Fibre	3.83	0.35
19	60	500	40% GGBS + 8% CSF	3.35	0.32
20	60	450	35% PFA + 8% CSF	3.85	0.32

3. RESULTS AND DISCUSSION

3.1 Concrete Samples prepared by PWCL – Concrete Strength

A total of 13 GGBS mixes and 13 OPC control mixes were prepared in this study. Concrete cube samples (100mm x 100mm x 100mm) were made for each mix. All cube samples were water cured at 27 +/- 3 ºC after demoulding at 1 day after casting until strength tests were carried out. Concrete cube strength tests were carried out at ages of 3, 7, 14, 28 and 56 days. While majority of the results at 56 days were not yet available

at the time of writing, the results of the tests at 3, 7, 14 and 28 days are summarised in Table 3 and Figures 1 to 4.

Table 3 – Concrete Samples prepared by PWCL – Concrete Strength

Mix Number		Grade	GGBS Content %	3-Day Strength, MPa	7-Day Strength, MPa	14-Day Strength, MPa	28-Day Strength, MPa	Ratio of 28-Day Strength (GGBS) / 28-Day Strength (Control), %
1	GGBS	25	60%	19.2	32.1	39.0	46.5	85%
	Control			34.6	44.0	47.6	54.5	
2	GGBS	30	35%	31.7	43.6	53.7	61.2	95%
	Control			43.1	54.1	59.7	64.7	
3	GGBS	30	60%	23.9	35.9	46.3	57.7	104%
	Control			36.1	45.7	51.1	55.5	
4	GGBS	40	50%	36.4	57.7	71.6	84.2	123%
	Control			49.9	58.6	65.5	68.6	
5	GGBS	45	35%	39.1	56.8	68.4	76.3	110%
	Control			49.9	60.2	65.7	69.2	
6	GGBS	45	40%	43.2	62.9	78.6	83.4	106%
	Control			55.9	67.4	74.4	78.4	
7	GGBS	45	60%	31.1	48.9	62.2	73.3	97%
	Control			51.4	62.0	69.8	75.5	
8	GGBS	45	65%	33.1	50.7	65.8	77.7	105%
	Control			54.4	63.3	71.4	73.9	
9	GGBS	45	65%	31.7	48.9	60.7	69.7	102%
	Control			49.9	58.6	65.5	68.6	
10	GGBS	50	65%	37.2	56.2	70.6	82.4	96%
	Control			64.8	76.9	81.2	85.9	
11	GGBS	55	65%	33.4	59.7	71.6	79.1	91%
	Control			62.6	76.8	79.9	87.0	
12	GGBS	55	65%	33.7	50.1	61.0	71.9	97%
	Control			53.9	65.1	71.4	74.1	
13	GGBS	60	50%	40.4	56.2	75.4	86.2	114%
	Control			53.8	62.0	71.6	75.9	

Figure 1 – 3-Day Strengths

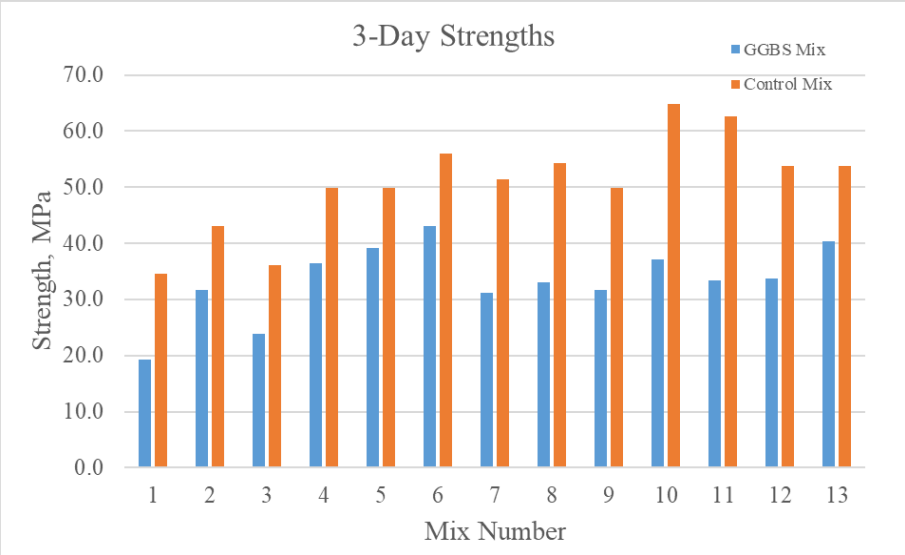

Figure 2 – 7-Day Strengths

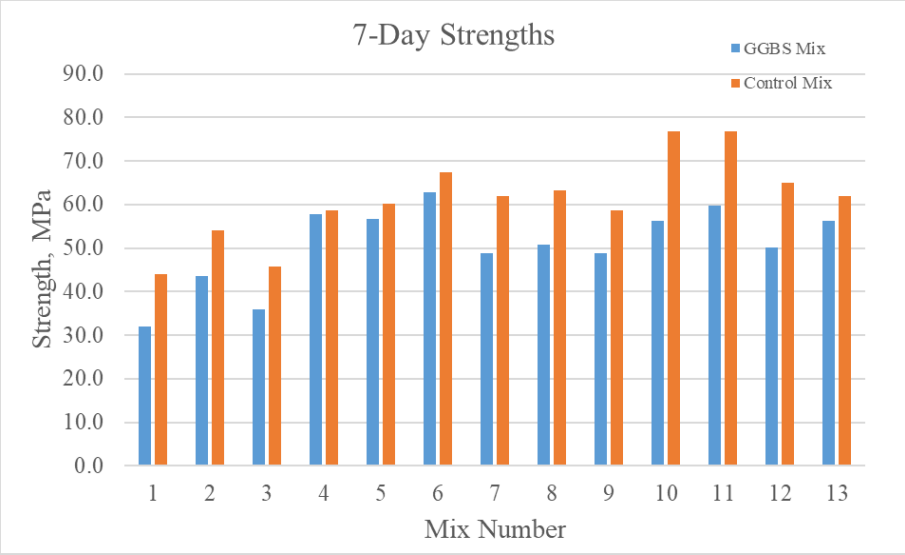

Figure 3 – 14-Day Strengths

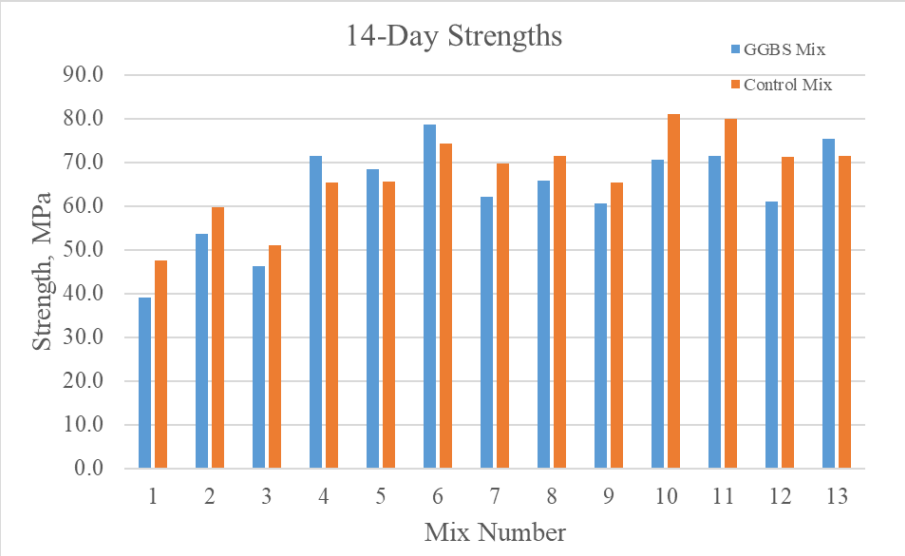

Figure 4 – 28-Day Strengths

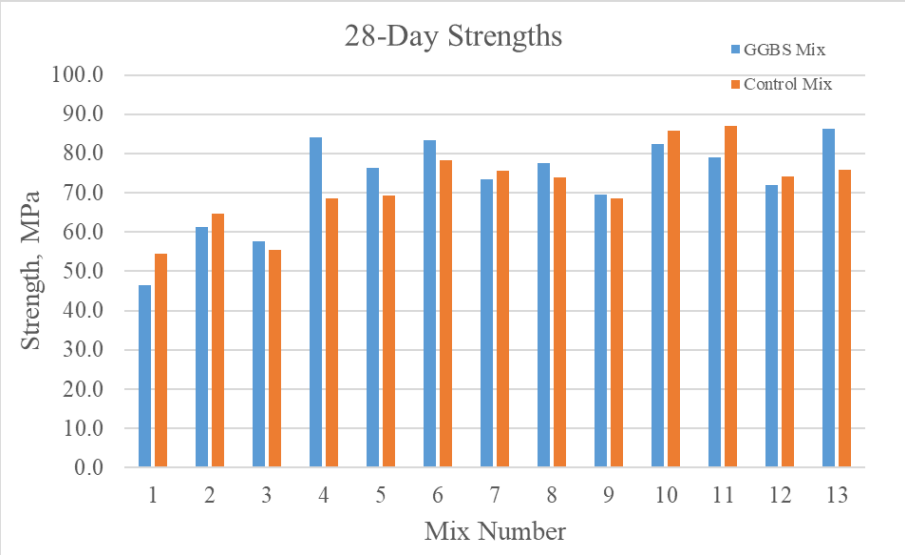

To better illustrate the strength development of each mix, the results of tests were further computed in two ways: (1) as a percentage of the 28-day strength, as shown in Table 4 and (2) as a percentage of the grade strength, as shown in Table 5. The graphical representations of the results are shown in Figures 5 and 6.

The results show that all GGBS mixes have achieved greater than 40% of the 28-day strength at 3 days and greater than 60% of the 28-day strength at 7 days. When compared with the grade strengths, all GGBS mixes have achieved greater than 60% of the grade strength at 3 days and 90% at 7 days. The 7-day strength / 28-day strength of the GGBS mixes ranged from 0.62 to 0.76. The early strengths at 3 days and 7 days of all GGBS mixes were consistently lower than the control OPC mixes. Notwithstanding this, the actual strengths achieved by all GGBS mixes at 3 days and 7 days are considered sufficient for general civil and geotechnical engineering works.

The results show that 9 out of 13 GGBS mixes have lower 14-day strengths when compared to the corresponding control mixes. The remaining 4 GGBS mixes (Mix. Nos. 4, 5, 6 and 13) have higher 14-day strengths and the GGBS contents of such mixes range from 35% to 50%. Mix No. 2 with 35% GGBS content did not show the same trend. All GGBS mixes have comparable 28-day strengths when compared to the control mixes. The 4 mixes (Mix. Nos. 4, 5, 6 and 13) showing higher 14-day strengths also have higher 28-day strengths when compared to the corresponding control mixes (approximately 6% to 23% higher).

The following observations on the 28-day strengths of the GGBS concrete mixes, categorised by the GGBS replacement ratios, were made:

(a) When compared to the corresponding control mix, Mix No. 5 with 35% GGBS content has higher 28-day strength while Mix. No. 2 also with 35% GGBS content has a lower 28-day strength.

(b) All mixes with 40% to 50% GGBS content (Mix Nos. 4, 6 and 13) have higher strengths at 28 days when compared to the corresponding control mix (6% to 23% higher).

(c) Mix Nos. 1, 7, 8, 9, 10, 11 and 12 with 60% to 65% GGBS content have 85% to 105% of the 28-day strength of the corresponding control mix.

The authors noted the above observations were made based on small sample sizes only and might not reflect the actual characteristics of the various GGBS replacement ratios.

Table 4 – Concrete Samples prepared by PWCL – Comparison against 28-day Strength

Mix Number		Grade	GGBS Content %	3-Day Strength, %	7-Day Strength, %	14-Day Strength, %	28-Day Strength, %
1	GGBS	25	60%	41%	69%	84%	100%
	Control			63%	81%	87%	100%
2	GGBS	30	35%	52%	71%	88%	100%
	Control			67%	84%	92%	100%
3	GGBS	30	60%	41%	62%	80%	100%
	Control			65%	82%	92%	100%
4	GGBS	40	50%	43%	69%	85%	100%
	Control			73%	85%	96%	100%
5	GGBS	45	35%	51%	74%	90%	100%
	Control			72%	87%	95%	100%
6	GGBS	45	40%	52%	75%	94%	100%
	Control			71%	86%	95%	100%
7	GGBS	45	60%	42%	67%	85%	100%
	Control			68%	82%	92%	100%
8	GGBS	45	65%	43%	65%	85%	100%
	Control			74%	86%	97%	100%
9	GGBS	45	65%	45%	70%	87%	100%
	Control			73%	85%	96%	100%
10	GGBS	50	65%	45%	68%	86%	100%
	Control			75%	89%	94%	100%
11	GGBS	55	65%	42%	76%	91%	100%
	Control			72%	88%	92%	100%
12	GGBS	55	65%	47%	70%	85%	100%
	Control			73%	88%	96%	100%
13	GGBS	60	50%	47%	65%	87%	100%
	Control			71%	82%	94%	100%

Table 5 – Concrete Samples prepared by PWCL – Comparison against Grade Strength

Mix Number		Grade	GGBS Content %	3-Day Strength, %	7-Day Strength, %	14-Day Strength, %	28-Day Strength, %
1	GGBS	25	60%	77%	128%	156%	186%
	Control			138%	176%	190%	218%
2	GGBS	30	35%	106%	145%	179%	204%
	Control			144%	180%	199%	216%
3	GGBS	30	60%	80%	120%	154%	192%
	Control			120%	152%	170%	185%
4	GGBS	40	50%	91%	144%	179%	211%
	Control			125%	146%	164%	171%
5	GGBS	45	35%	87%	126%	152%	170%
	Control			111%	134%	146%	154%
6	GGBS	45	40%	96%	140%	175%	185%
	Control			124%	150%	165%	174%

7	GGBS	45	60%	69%	109%	138%	163%
	Control			114%	138%	155%	168%
8	GGBS	45	65%	74%	113%	146%	173%
	Control			121%	141%	159%	164%
9	GGBS	45	65%	70%	109%	135%	155%
	Control			125%	146%	164%	171%
10	GGBS	50	65%	74%	112%	141%	165%
	Control			130%	154%	162%	172%
11	GGBS	55	65%	61%	109%	130%	144%
	Control			114%	140%	145%	158%
12	GGBS	55	65%	61%	91%	111%	131%
	Control			98%	118%	130%	135%
13	GGBS	60	50%	67%	94%	126%	144%
	Control			90%	103%	119%	127%

Figure 5 – GGBS Mix Strength Development – 35% to 50% Replacement

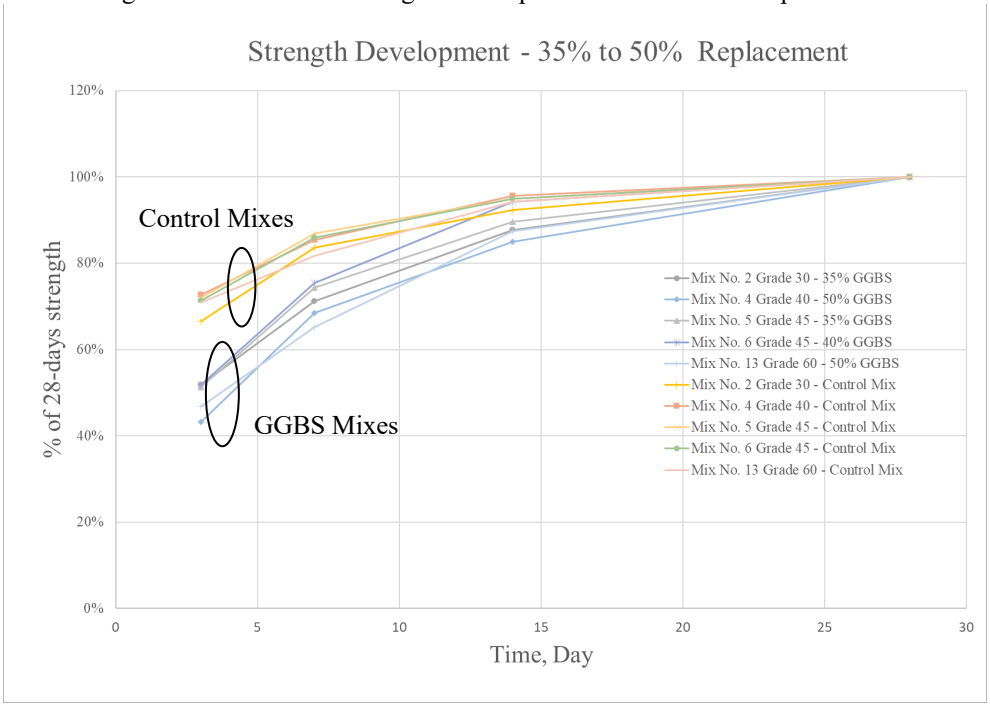

Figure 6 – GGBS Mix Strength Development – 60% to 65% Replacement

3.2 Concrete Samples prepared by PWCL – Shrinkage

Two numbers of 75mm x 75mm x 285 mm specimens for each GGBS mix and control mix were also prepared for evaluating their shrinkage performance at 20+/-2ºC and 60+/-5% relative humidity. The total shrinkage of the specimens was determined in accordance with BS EN 12390-16. The results of the total shrinkage at 7 days, 14 days and 28 days as compared with the value at demoulding 1 day after casting are shown in Table 6. As observed from the results, 9 out 13 GGBS mixes (Mix Nos. 1, 2, 3, 5, 8, 10, 11, 12, 13) showed less total shrinkage than the corresponding control mixes, while the remaining mixes (Mix Nos. 4, 6, 7 and 9) showed the opposite result. No consistent trend on the influence of GGBS on shrinkage performance could be observed in this exercise. Further study on the influence of GGBS on the autogenous shrinkage and drying shrinkage, as well as to cover longer measurement periods is recommended.

Table 6 – Concrete Samples prepared by PWCL – Total Shrinkage

Mix Number		Grade	GGBS Content %	7-Day Shrinkage, microstrain	14-Day Shrinkage, microstrain	28-Day Shrinkage, microstrain
1	GGBS	25	60%	210	317	406
	Control			226	340	459
2	GGBS	30	35%	237	319	420
	Control			221	326	430
3	GGBS	30	60%	264	408	456
	Control			249	394	480
4	GGBS	40	50%	155	247	357
	Control			222	284	307
5	GGBS	45	35%	288	348	418
	Control			322	441	574
6	GGBS	45	40%	276	319	409
	Control			274	326	409
7	GGBS	45	60%	300	370	434
	Control			167	263	395

8	GGBS	45	65%	260	356	398
	Control			259	350	467
9	GGBS	45	65%	235	287	328
	Control			222	284	307
10	GGBS	50	65%	250	312	388
	Control			256	362	504
11	GGBS	55	65%	223	256	295
	Control			245	316	388
12	GGBS	55	65%	299	361	404
	Control			260	373	462
13	GGBS	60	50%	242	284	306
	Control			243	334	406

3.3 Additional Concrete Samples obtained from On-going Public Works Construction Sites

Additional concrete cube samples were obtained from available on-going public works construction sites for testing at PWCL. The exercise involved a total of 7 mixes including 5 GGBS mixes and 2 PFA mixes. All concrete involved were ready-mix concrete produced by concrete batching plants. Cube strength tests were conducted at 3, 7, 14, 28 and 56 days, where applicable. The results available at the time of writing are summarised in Table 7. Similar to the previous exercise (PWCL mix replication exercise), the strength results were normalised as a percentage of the 28-day strengths and grade strengths, which are summarised in Table 8 and 9 respectively.

The formulas for Mix Nos. 14, 15 and 16 (produced by concrete batching plants) are similar to those of Mix Nos. 4, 6 and 8 (prepared in laboratory scale by PWCL) respectively. The results of the tests on these mixes are extracted and shown in Table 10. The results of strength tests from the two exercises at 3, 7, 14 and 28 days for the various mixes are found generally aligned, providing the authors confidence with the consistency of the results.

The PFA mixes (Mix Nos. 18 and 20) exhibit relatively high early strength gain (3-day) when compared to the GGBS mixes. However, it should be noted that for Mix. No. 20, this was possibly due to the use of 8% Condensed Silica Fume (CSF). The results of this mix was also found comparable to GGBS Mix. No. 19, which also involves the use of 8% CSF. Also, Mix No. 18 with 35% PFA involves the use of 1.5 kg/m^3 polypropylene fibre. The effect of the addition of fibres to the strength behaviour of concrete is outside the scope of this study.

The 7-day strength / 28-day strength of GGBS mixes range from 0.60 (Mix No. 17) to 0.88 (Mix No. 15), while the 56-day strength / 28-day strength ranged from 1.05 (Mix No. 17) to 1.20 (Mix No. 15).

Table 7 – Concrete Samples obtained from On-going Public Works Construction Sites – Results of Tests

Mix Number	Grade	SCM %	3-Day Strength, MPa	7-Day Strength, MPa	14-Day Strength, MPa	28-Day Strength, MPa	56-Day Strength, MPa
14	40	50% GGBS	32.6	50.5	65.7	74.7	80.6
15	45	40% GGBS	-	66.1	71.7	75.1	90.2
16	45	65% GGBS	34.2	55.0	65.8	79.7	87.5
17	45	65% GGBS with Shrinkage Reducing Agent	29.3	40.7	51.8	67.3	70.7
18	45	35% PFA + PP Fibre	49.8	68.5	78.6	87.9	-

19	60	40% GGBS + 8% CSF	50.0	77.1	92.8	97.4	103.6
20	60	35% PFA + 8% CSF	48.7	74.4	91.5	91.2	101.6

Table 8 – Concrete samples obtained from On-going Public Works Construction Sites – Comparison by 28-Day strength

Mix Number	Grade	SCM %	3-Day Strength, %	7-Day Strength, %	14-Day Strength, %	28-Day Strength, %	56-Day Strength, %
14	40	50% GGBS	44%	68%	88%	100%	108%
15	45	40% GGBS	-	88%	96%	100%	120%
16	45	65% GGBS	43%	69%	83%	100%	110%
17	45	65% GGBS with Shrinkage Reducing Agent	44%	60%	77%	100%	105%
18	45	35% PFA + PP Fibre	57%	78%	89%	100%	-
19	60	40% GGBS + 8% CSF	51%	79%	95%	100%	106%
20	60	35% PFA + 8% CSF	53%	82%	100%	100%	111%

Table 9 – Concrete samples obtained from On-going Public Works Construction Sites – Comparison by Grade Strength

Mix Number	Grade	SCM %	3-Day Strength, %	7-Day Strength, %	14-Day Strength, %	28-Day Strength, %	56-Day Strength, %
14	40	50% GGBS	81%	126%	164%	187%	201%
15	45	40% GGBS	-	147%	159%	167%	200%
16	45	65% GGBS	76%	122%	146%	177%	194%
17	45	65% GGBS with Shrinkage Reducing Agent	65%	90%	115%	149%	157%
18	45	35% PFA + PP Fibre	111%	152%	175%	195%	-
19	60	40% GGBS + 8% CSF	83%	128%	155%	162%	173%
20	60	35% PFA + 8% CSF	81%	124%	152%	152%	169%

Table 10 – Comparison of tests on samples prepared by PWCL vs samples obtained from on-going public works construction sites

Mix Number		Grade	GGBS Content %	3-Day Strength, MPa	7-Day Strength, MPa	14-Day Strength, MPa	28-Day Strength, MPa
4	GGBS Mix	40	50%	36.4	57.7	71.6	84.2
14	GGBS Mix			32.6	50.5	65.7	74.7
6	GGBS Mix	45	40%	43.2	62.9	78.6	83.4
15	GGBS Mix			-	66.1	71.7	75.1
8	GGBS Mix	45	65%	33.1	50.7	65.8	77.7
16	GGBS Mix			34.2	55.0	65.8	79.7

4 OBSERVATIONS AND RECOMMENDATION

4.1 Key Observations

The key observations of the recent in-house study are summarised below: -

(a) In terms of the 28-day strength and total shrinkage, the performance of the GGBS mixes considered in this study are similar to the corresponding OPC control mixes. For certain ranges of GGBS replacement, the 28-day strengths even performed better than the corresponding OPC control mixes.

(b) The early strength development (3-day and 7-day strengths) of the GGBS mixes are slower than the OPC control mixes. Notwithstanding this, the actual strengths achieved at such early stages are considered sufficient for general civil and geotechnical engineering works.

(c) The 7-day strength / 28-day strength of the GGBS mixes ranged from 0.60 to 0.88, which are in line with the results of the LCCTC (0.65 to 0.81).

(d) The 56-day strength / 28-day strength of the GGBS mixes ranged from 1.05 to 1.20, which are in line with the results of the LCCTC (1.05 to 1.13).

(e) Some of the GGBS mixes exhibited smaller total shrinkage than the corresponding OPC control mixes, while the remaining mixes produced opposite results. No definitive relationship could be observed.

4.2 Recommendation and further work

The purpose of this study is to evaluate the performance of GGBS concrete used in recent public works contracts. Through testing of concrete specimens made by replication of the concrete mixes in laboratory environment and additional specimens collected from on-going public works construction sites, the performance of the GGBS concrete mixes considered were found to be on-par with OPC concrete mixes and are suitable for general civil and foundation works.

The scale of this study was relatively confined and its scope only covered strength tests and total shrinkage tests. More verification / study on the performance, including but not limited to the durability (e.g. chloride resistance) and heat evolution, is therefore recommended. A more focused study on the early strength development of GGBS concrete, with due consideration on the construction cycles of building works, is also recommended. PWCL is planning to conduct a further study on the performance of GGBS concrete, focusing on the recent technological advancement in this area, and the feasibility of achieving higher replacement levels, higher grade strengths with the use of locally available raw materials.

ACKNOWLEDGEMENTS

This paper is published with the permission of the Head of the Geotechnical Engineering Office and the Director of Civil Engineering and Development, the Government of the Hong Kong Special Administrative Region of the People's Republic of China. The input and support from the various public works contracts in providing additional concrete specimens for this study are gratefully acknowledged.

REFERENCES

Rodgers L, 2018. *Climate change: Themassive CO^2 emitter you may not know about*. BBC News. <https://www.bbc.com/news/science-environment-46455844>

BSI. 2006. *Ground Granulated Blastfurnace Slag for Use in Concrete, Mortar and Grout. Definitions, Specifications and Conformity Criteria.* BS EN 15167-1: 2006. British Standards Institution, London.

BSI. 2011. *Cement – Part 1: Composition, specifications and conformity criteria for common cements*. BS EN 197-1:2011. British Standards Institution, London.

BSI. 2019. *Testing hardened concrete Part 16: Determination of the shrinkage of concrete.* BS EN 12390-16:2019. British Standards Institution, London.

HKSAR Government. 2006. *General Specification for Civil Engineering Works (2006 Edition)*. The Government of the Hong Kong Special Administrative Region.

HKSAR Government. 2020. *General Specification for Civil Engineering Works (2020 Edition)*. The Government of the Hong Kong Special Administrative Region.

HKSAR Government. 2010. *Construction Standard – Testing Concrete (2010 Edition)*. The Government of the Hong Kong Special Administrative Region.

Peter W.C. Leung & H. D. Wong, 2011. *Final Report on Durability and Strength Development of Ground Granulated Blastfurnage Slag Concrete*. GEO Report No. 258. HKSAR